Regulation of Stability and Copy Number of Tandem Repeats in *Saccharomyces cerevisiae*

Thesis

Regulation of stability and copy number of tandem repeats in *Saccharomyces cerevisiae*

A thesis by

Devika Salim

submitted to

The School of Life, Health, and Chemical Sciences

in partial fulfilment of the requirement for the degree of

Doctor of Philosophy

The Stowers Institute for Medical Research

an Affiliated Research Centre of The Open University

August 2019

ABSTRACT

Tandem repeats are inherently unstable and exhibit extensive copy number polymorphisms. Despite mounting evidence for their adaptive potential, the mechanisms associated with regulation of the stability and copy number of tandem repeats remain largely unclear. To study copy number variation at tandem repeats, I used two well-studied repetitive arrays in the budding yeast genome, the ribosomal DNA (rDNA) locus, and the copper-inducible *CUP1* gene array. I developed powerful, highly sensitive assays to measure repeat instability and copy number and used them in multiple high-throughput genetic screens to define pathways involved in regulating rDNA copy number variation. These screens revealed that rDNA stability and copy number are regulated by DNA replication, transcription, and histone acetylation. Through parallel studies of the *CUP1* array, I showed that instability at both tandem arrays can be induced by DNA replication stress and altered transcription of the locus. Importantly, while changes in instability in response to stress are observed within a few cell divisions, a change in steady state repeat copy number requires selection. Further, H3K56 acetylation is required for regulating transcription and transcription-induced instability at the *CUP1* array, and, importantly, it restricts transcription-induced amplification of the *CUP1* array. My work suggests that the modulation of replication and transcription is a simple, reversible strategy to alter instability at tandem repeats in response to environmental stimuli, which provides cells rapid adaptability through copy number variation. Additionally, histone acetylation may function to promote the normal adaptive program in response to transcriptional stress. Given the ubiquity of DNA replication, transcription, and chromatin marks like histone acetylation, the mechanisms I have characterized could significantly advance our understanding of the behavior of other tandem repeats and their role in shaping eukaryotic genomes.

Director of Studies: Jennifer L. Gerton, Ph.D.

To my parents,

the original Dr. Salim and the honorary Dr. Salim.

ACKNOWLEDGEMENTS

First and foremost, I would like to thank my supervisor, Dr. Jennifer Gerton, for believing in me and encouraging me to go back to graduate school, for allowing me total intellectual and creative freedom in the lab, and for always being unconditionally supportive of my career aspirations. Jen, I am so grateful for our shared, deep love for repetitive DNA biology, and the relationship we have developed over the last few years. I could not have asked for a better PhD mentor; I can only hope to emulate you throughout my career.

Next, I would like to thank the members of my dissertation committee – Dr. Scott Hawley, Dr. Joan Conaway, and Dr. Kausik Si. Scott, your commitment to students is inspiring. I am humbled by your deep involvement in my thesis work, for always having my best interests in mind, and for always making time for me when I reached out for advice. Joan and Kausik, I am grateful for your commitment to my projects, for always offering thoughtful comments and asking profound questions that significantly improved my experiments and ideas. The three of you made my committee meetings thoroughly enjoyable. Dr. Matt Gibson, who first recruited me to Stowers, and eventually joined my mentoring team, and always offered his unbiased perspective and advice on science, careers and life. I would also like to thank my examination committee – Dr. Ron Conaway (Chair), Dr. Brian McStay (external examiner), and Dr. Paul Trainor (internal examiner). I am grateful for your time and efforts in making my dissertation defense a memorable experience. I am also thankful to Dr. Leanne Wiedemann, for making it so easy for me to go through the Open University program, for deeply caring about every one of us, for routinely monitoring my progress and keeping me on track, for always offering support and a unique perspective on everything. Lisa Hodges, for keeping all my paperwork and records organized, and making scheduling meetings effortless.

I would like to express my gratitude to my collaborators at Stowers, without whom my projects would not have been possible. Dan Bradford, for his enthusiasm and commitment to my multiple high-throughput screens, and for always prioritizing my projects. Jin Zhu and Dominic Heinecke, for sharing strains, reagents, and their invaluable experience and advice so generously as I was developing my own assays. Dr. Boris Rubinstein, for developing critical mathematical formulae, for his incredible patience in helping me understand basic mathematics, and for our long discussions on koala bears. María Bravo Núñez, for being a wonderful collaborator and friend, for critical reading of my thesis chapters and for teaching me so much about meiosis and fission yeast among other things. Andrew Box, for always being enthusiastic and helpful in developing new tools. Willie McDowell, for helping us develop our first ddPCR assays. All members of the Cytometry and Molecular Biology cores, for helping me with instrument usage, data analysis, and troubleshooting.

I would like to thank the Gerton lab members for making the lab an incredible place to learn and grow. Bethany and Geetha, for being so welcoming when I first moved to Kansas City, and making it so easy for me to settle into the lab and Stowers. Kobe, for our discussions about science, life, and careers. Musinu, Dong-Hwan and Mark, for making our side of the lab a fun place to be in. Karthik, for all the career advice and for making travel to conferences enjoyable. Vijay and Wei-ting, for teaching me some murine biology, and always offering helpful suggestions and constructive criticism. Tamara, for always being generous with her time and advice. Carolyn, for effortlessly managing our lab's administrative needs. Sirma and Xengie, thank you for making sure I left the lab occasionally, I deeply cherish our friendship and would not have survived graduate school without you.

Most importantly, I am forever indebted to my family. My parents, for teaching me everything I know about science and life, for unconditionally supporting my dreams, even when it took me halfway across the world from them, and for always being there to pick me up when I made mistakes. My in-laws, for their unwavering support in everything I do. Poorna, for her unconditional love and friendship. Rahul, my husband and best friend, he makes it so easy for me to follow my ambitions, none of my accomplishments would have been possible without his unconditional love, support and belief in my abilities and aspirations.

TABLE OF CONTENTS

LIST OF FIGURES

LIST OF TABLES

CHAPTER 1

Tandem repeats and the adaptable genome

Parts of this chapter are excerpts from Salim, D., & Gerton, J. L. (2019). Ribosomal DNA instability and genome adaptability. *Chromosome Res, 27*(1-2), 73-87. doi:10.1007/s10577-018-9599-7

1 CHAPTER 1

1.1 List of Figures

1.2 Introduction

Repetitive DNA sequences are an integral part of all eukaryotic genomes. Repeats can be classified broadly as interspersed repeats or tandem repeats. Interspersed repeats encompass individual repeat units distributed throughout the genome (for example, transposable elements). In contrast, tandem repeats comprise multiple repeat units arranged in a head-to-tail configuration (for example, ribosomal DNA repeats). Of these, tandem repeats have remained largely undercharacterized because of the difficulties in sequencing, assembling, and identifying them. With the advent of cheaper whole genome sequencing technologies and sophisticated computational tools, copy number polymorphisms at tandem repeats have emerged as a significant source of genetic diversity in populations. However, despite increasing evidence linking these polymorphisms with phenotypic variation and adaptation, the mechanisms associated with regulation of copy number variation at tandem repeats remain largely unclear.

My thesis work focuses on the identification and characterization of basic principles underlying the ability of tandem repeats to undergo extensive copy number variation – regulation of their inherent instability, and the stable maintenance of normal repeat copy number in unperturbed conditions. In my studies, I used two well-studied tandem arrays in the budding yeast, *Saccharomyces cerevisiae*, the tandem array of ribosomal RNA genes (ribosomal DNA), and the copper-resistance *CUP1* gene array. In this chapter, I will introduce the budding yeast ribosomal DNA (rDNA) locus and review existing literature that provides evidence for the role of rDNA copy number variation beyond ribosomal RNA (rRNA) production for ribosome biogenesis. I will also briefly discuss new tools to measure rDNA copy number. I will then introduce the *CUP1* array, and highlight key design and regulatory features that are shared with the rDNA array that enable the use of the two arrays to study tandem repeat behavior. Following this, I discuss the unique adaptive potential conferred by a highly unstable, tandemly repeated array of genes in light of more recent evidence implicating rDNA and *CUP1* copy number variation in cellular response to the environment. I conclude this chapter

by proposing a model for the regulation of copy number variation at tandem repeats through modulation of DNA replication and transcription at these loci.

1.3 Copy number variations at tandem repeats have functional relevance

Tandem repeats are unstable by design. The presence of multiple identical repeat units in a head-to-tail arrangement makes them susceptible to copy number variation resulting from polymerase slippage during DNA replication and/or unequal exchange events during recombination-mediated repair. While large, cytogenetically recognizable structural alterations and single nucleotide polymorphisms (SNPs) have been observed for many decades, the widespread prevalence of copy number variations in eukaryotic genomes is only just beginning to be appreciated. Early comparative genomic hybridization-based attempts identified copy number variations at over a 1000 regions, covering nearly 400Mb of the human genome (Redon et al., 2006). More recently, a computational attempt to discover tandem repeats in the human genome identified 25,000 arrays between 600bp and 10kb in length, with 503 arrays larger than 10 kb (Warburton et al., 2008). Furthermore, extreme variation in copy number has been reported for tandemly repeated genes in the human genome (Brahmachary et al., 2014). In fact, copy number variations are now recognized as the most significant source of genetic diversity in human populations (Iafrate et al., 2004; Redon et al., 2006; Sebat et al., 2004; Zarrei et al., 2015). Moreover, there are approximately 235 copy number variants that have been associated with either well-established or emerging human chromosomal syndromes (Wyandt et al., 2017). However, copy number polymorphisms are not always detrimental, and could confer a wide range of adaptative phenotypes (reviewed in (Beckmann et al., 2007; Hurles et al., 2008)). Analysis of the mutational landscape in wine strains of *S. cerevisiae* revealed that these strains had very low levels of SNP diversity, but exhibited significant copy number variations at loci relevant for adaptation to specific fermentation environments (Steenwyk & Rokas, 2018). A recent

genome-wide association study of 1,011 natural isolates of *S. cerevisiae* showed that copy number variations not only contributed the most to genetic variation, but also had the most significant effect on phenotype (Peter et al., 2018). These data suggest that copy number polymorphisms make significant contributions to genome function. While the potential functional impact of copy number variations is beginning to be appreciated, the extent of copy number variation in the human genome remains far from fully determined because of technical difficulties in sequencing, assembling, and identifying repetitive genomic regions. As a result, fundamental principles governing the behavior of tandem repeats critical to their ability to undergo copy number variations, and the impact of variation on cellular function remain largely uncharacterized.

1.4 Ribosomal DNA as a model to study tandem repeats

Ribosomes are large, multi-subunit macromolecular machines essential for protein synthesis. Ribosome composition is largely conserved across all eukaryotes, comprising of large (60S) and small (40S) ribosomal subunits, each made up of rRNAs and several ribosomal proteins. Eukaryotic ribosomes contain four RNA components that play critical structural and catalytic roles – the 25-28S, 5.8S, and 5S rRNAs (in the 60S ribosomal subunit), and the 18S rRNA (in the 40S ribosomal subunit) (Figure 1.1A). Ribosomes are the most abundant cellular macromolecules, with over 60% of total cellular transcription devoted to their biosynthesis (Warner, 1999). To meet the high cellular demand for ribosomes, the genes encoding rRNAs, the ribosomal DNA (rDNA), are present in numerous copies and arranged in clusters of tandem arrays in all eukaryotes. rDNA loci are missing from genome assemblies owing to difficulties in the sequencing and assembly of large stretches of tandem repeats. Moreover, the rDNA loci are difficult to manipulate genetically, given their repetitive nature and essential role in cellular viability. As a result, the rDNA remained “the dark matter” (McStay, 2016) of the genome for many decades. Regardless, because of their essential role in cell physiology,

relatively high sequence homogeneity between repeats within species, ubiquity, and conservation of key structural and regulatory elements across species, the rDNA repeats are the most well characterized tandem repeat family.

1.4.1 Structural organization of the rDNA is conserved

Remarkably, the organization of the rDNA is largely conserved in the vast majority of eukaryotes studied. rDNA genes are arranged in clusters of tandem repeats that form the nucleolus, the site of rRNA transcription, processing and ribosome assembly. In all eukaryotes studied, the 25-28S, 18S, and 5.8S rRNAs are transcribed by RNA Polymerase I (RNAPI) as a single precursor rRNA transcript from several copies of a single gene (ranging from 35S in the budding yeast, *Saccharomyces cerevisiae* to 47S in mammals). Copy number of the 35-47S rDNA repeat units per haploid genome ranges from ~100-200 copies in *S. cerevisiae* (Salim et al., 2017), *Schizosaccharomyces pombe* (Wood et al., 2002), mice and humans (Gibbons et al., 2015; Xu et al., 2017) to several thousand copies in some plants (Rosato et al., 2016). While the 35-47S rDNA repeats are always arranged in tandem, in a head to tail fashion, the number of clusters and their chromosomal locations vary widely across species. For example, in *S. cerevisiae*, the 35S rDNA repeats are arranged in a single cluster on the long arm of chromosome XII (Petes, 1979a), whereas in the human genome, the 47S (also referred to as 45S) rDNA repeats are found on 5 acrocentric chromosomes, 13, 14, 15, 21, and 22 (Henderson et al., 1972) (Figure 1.1B-C). The 5S rRNA is transcribed by RNA Polymerase III (RNAPIII) from a separate gene. Typically, the 5S rDNA is organized as a single cluster of tandem repeats physically separated from the 35-47S rDNA repeats in all eukaryotes. Notable exceptions to this organization are *S. cerevisiae*, where the 5S rDNA is part of the repeat unit containing the 35S rDNA, and *S. pombe*, where

the ~30 5S rDNA genes are dispersed throughout the genome (Mao et al., 1982; Wood et al., 2002).

The conservation of structural organization of the rDNA loci is illustrated in figure 1.1 using the budding yeast and human rDNA loci as examples. Each rDNA repeat unit has coding sequences for the 35-47S precursor rRNA separated from the adjacent repeat by intergenic spacers (IGS). Additionally, while the rRNA coding sequences are highly conserved, the IGS regions exhibit a relatively high degree of variation, in both, size and sequence (Gonzalez & Sylvester, 1995, 2001). These spacers also contain important regulatory elements, as illustrated in figure 1.1. In *S. cerevisiae*, the IGS is separated into two spacers by the 5S rDNA. IGS2 contains an rDNA origin of replication (rARS), and a cohesin associating region (CAR). IGS1 contains a replication fork barrier (RFB) site to which Fob1 binds; the binding of Fob1 inhibits DNA replication in the direction opposite to 35S rDNA transcription, preventing head-on collisions between transcription and replication machinery (Brewer et al., 1992; Kobayashi, 2003). IGS1 also contains a bi-directional, non-coding RNA polymerase II dependent promoter, E-pro, whose activity is normally suppressed by the binding of Sir2, an NAD-dependent histone deacetylase (Kobayashi & Ganley, 2005).

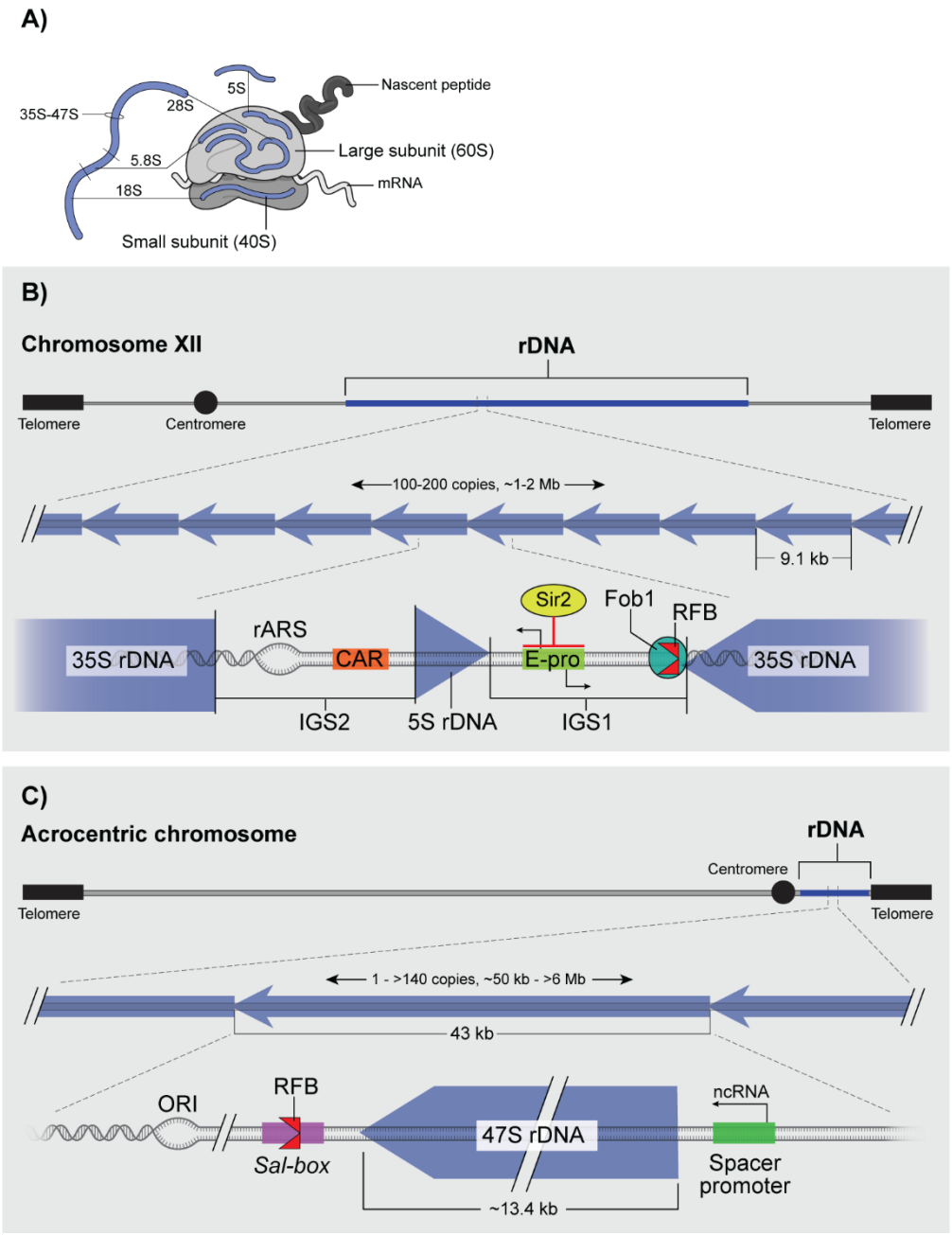

Figure 1.1. rDNA loci in budding yeast and human cells. A) Structure of the eukaryotic ribosome showing the large and small ribosomal subunits and rRNA components. B) Structure of the budding yeast rDNA locus. 100-200 repeating units (~9.1kb each) are arranged in tandem on the long arm of Chromosome XII. The 35S and 5S rDNA genes within each repeat are separated by two intergenic spacers (IGS1 and IGS2). Direction of arrows indicates direction of rRNA transcription. rARS – rDNA origin of replication. CAR – Cohesin associating region. E-pro – bidirectional RNAPII promoter whose activity is suppressed by Sir2 binding. RFB – Replication fork barrier, Fob1 binding blocks replication forks moving from left to right in the figure, in the direction opposite to 35S rDNA transcription by RNAPI. (C) Structure of the human rDNA locus. 1- >140 repeating units (~43kb each) are arranged in tandem on the short arm of 5 acrocentric chromosomes. Direction of arrows indicate direction of rRNA transcription. Adjacent 47S rDNA genes are separate by a large intergenic spacer. ORI – origin of replication. *Sal-box* – RNAPI transcription terminator elements. RFB - replication fork barrier, located within the *Sal-box*. Spacer promoter – non-coding promoter. 5S rDNA genes are located in a separate cluster on Chromosome I (not shown).

Several of these features are conserved in the human 47S rDNA repeat unit, which consists of a large, ~30kb IGS separating the ~13.4kb 47S rRNA coding sequences of adjacent repeats. ~2kb upstream of the rRNA transcription start site is a spacer promoter whose transcription has been shown to play a role in silencing of rDNA repeats by enabling establishment and maintenance of heterochromatin (Mayer et al., 2006; Santoro et al., 2010). The IGS also contains origin(s) of replication (ORI) (Little et al., 1993) and a cluster of RNAPI transcription termination elements collectively called a *Sal-box*. The *Sal-box* motifs function as RFBs, with different *Sal-box* motifs causing either polar, or bidirectional arrest of replication forks when bound by the RNAPI termination factor TTF-1 (Akamatsu & Kobayashi, 2015; Little et al., 1993).

Besides the organization of the rRNA coding sequences, several elements within the intergenic spacers have also been shown to be remarkably conserved in a variety of eukaryotes studied. For example, in addition to budding yeast and humans, DNA replication origins within the IGS and RFB activity at the 3' end of rDNA genes have been identified in *Tetrahymena thermophila* (MacAlpine et al., 1997), *S. pombe* (Sanchez et al., 1998), frogs (Wiesendanger et al., 1994), plants (Hernández et al., 1993), and mice (Diermeier et al., 2013; Gerber et al., 1997) (also reviewed in (Dalgaard et al., 2011)). While RFB activity is independent of RNAPI transcription in *S. cerevisiae* (Brewer et al., 1992), the regulation of RFB activity within the rDNA genes is coupled to RNAPI transcription in higher eukaryotes. For example, in mice and *S. pombe* RFB activity also depends on the RNAPI transcription termination factor TTF-1 (Reb1 in *S. pombe*) and causes polar arrest of replication forks in the direction opposite to RNAPI transcription (Gerber et al., 1997; Sanchez-Gorostiaga et al., 2004; Sanchez et al., 1998). While the strength of the RFB and the mechanism and polarity of replication fork arrest vary, the role of the RFB in maintaining mostly unidirectional DNA replication co-oriented with RNAPI transcription in the highly

transcribed rDNA appears to be conserved across eukaryotes. The observation that RFB activity in human rDNA repeats is restricted to actively transcribed rDNA repeats, with activity coinciding with the replication of these active repeats early in S-phase (Akamatsu & Kobayashi, 2015) also supports this idea.

Additionally, the rDNA contains binding sites for several proteins like cohesin, condensin, CTCF, and DNA replication and transcription factors, which play important roles in organization of the rDNA chromatin (reviewed in (Potapova & Gerton, 2019)). Disproportionate binding of these proteins to rDNA arrays of varying size or chromatin states could result in altered concentrations of these proteins throughout the rest of the genome, affecting chromatin environments and transcription genome-wide. In fact, human population genome sequencing data analysis has revealed correlations between rDNA copy number and the expression of several genes, notably *CBX1* (*HP1β*), *CTCF*, *CDYL2*, *MYST1*, *RASL11A*, *CENPA*, *KTI12*, *INO80C* and *KDM4B* (Gibbons et al., 2014), all of which are known chromatin-modifying factors. Such a correlation between rDNA copy number variation and gene expression has also been demonstrated in *Drosophila melanogaster* (Paredes et al., 2011). Additionally, variation of rDNA copy number modulates the expression of *SIR2* and cellular pools of Sir2 in budding yeast, which in turn affects Sir2-dependent silencing of specific loci in the rest of the genome (Michel et al., 2005). This supports the idea that the rDNA locus could titrate genome-wide levels of various factors. The demonstration of the importance of specific sequence elements within rDNA loci in the organization of nucleolus and the nuclear genome and the importance of these contacts in regulation of rRNA transcription, rDNA stability, and rDNA copy number (Cahyani et al., 2015; Mayan & Aragon, 2010; O'Sullivan et al., 2009; Yu & Lemos, 2018) in a variety of model systems, and the conservation of these functionally relevant elements of the rDNA across eukaryotes further supports

the idea that the extra-ribosomal functions of the rDNA arrays in modulating genome dynamics may also be conserved across eukaryotes.

1.4.2 rDNA instability and copy number variation may confer adaptability

The rDNA array is the most highly transcribed genomic locus. The high rates of transcription at the rDNA combined with its repetitive nature makes the locus highly prone to replication-transcription conflicts. While DNA replication encounters many obstacles on the template DNA, transcription remains one of the most mutagenic obstacles to the replisome, particularly at highly transcribed genes (reviewed in (Kim & Jinks-Robertson, 2012)). In *S. cerevisiae,* the RFB, when bound by Fob1, serves to prevent head-on collisions between the replisome and RNAPI by stalling replication forks that progress in a direction opposite to RNAPI transcription (Kobayashi, 2003). These stalled forks eventually collapse and are processed into double-stranded breaks, which are likely repaired through one of many homologous recombination-dependent repair pathways (Kobayashi et al., 2004). Recombination has been shown to require RNAPI transcription (Kobayashi et al., 1998), and is further enhanced by non-coding transcription from E-pro, which is thought to clear cohesin from the rDNA repeats, promoting unequal sister chromatid exchange (Kobayashi & Ganley, 2005). Given the presence of many identical repeats that can serve as a template for homologous recombination, the rDNA is highly susceptible to unequal recombination-mediated repeat copy number changes at every cell division (reviewed in (Kobayashi, 2014)). This makes the rDNA one of the most unstable and hypervariable genomic regions. Despite this relatively high instability, repeat copy number at the rDNA locus is stably maintained in every species studied. The regulation of this inherent instability and the somewhat paradoxical, stable maintenance of normal repeat copy number have remained areas of intense scientific investigation. The last two decades have witnessed

the discovery of many genes involved in the regulation of instability and maintenance of rDNA copy number, mainly through high-throughput genetic screens in *S. cerevisiae* (Ide et al., 2013; Iida & Kobayashi, 2019; Mansisidor et al., 2018; Saka et al., 2016; Salim et al., 2017; Smith et al., 1999). These genes generally fall into three broad categories – i) regulation of DNA replication, ii) regulation of RNAPI transcription, and iii) regulation of recombination/repair (reviewed in (Kobayashi & Sasaki, 2017)). While most of this work was done in budding yeast, recent years have seen the discovery of many orthologous factors that control rDNA stability and copy number in mammalian cells (reviewed in (Tsekrekou et al., 2017)). Given the conservation of key regulatory elements controlling replication and transcription of the rDNA repeats from yeast to humans, it is likely that at least some basic principles of the maintenance of this locus are conserved.

For many years, the extensive copy number variation at the rDNA was thought to be the inevitable consequence of the inherent instability at the locus. This was confounded by the observation that “normal” rDNA copy number was stably maintained under normal growth conditions. Further, while rDNA copy number and stability could be altered under stress, or in mutant genetic backgrounds, there seemed to be no apparent correlation between rDNA stability and copy number. While it was known that multiple copies of rDNA repeats are required for the high rates of rRNA biosynthesis observed in actively growing cells, the reason for the maintenance of rDNA repeats in over 2-fold excess of the requirement for rRNA biogenesis also remained unclear (French et al., 2003). The first hints suggesting the importance of the extra, untranscribed rDNA repeats came from early studies in budding yeast showing that rDNA copy number could be reduced significantly without affecting rRNA output or cell growth (French et al., 2003; Kobayashi et al., 1998). These studies also showed that while only a fraction of the rDNA repeats is transcribed in a strain with normal

(~150 copies) copy number, in the low (~40 copies) copy strain, both, the number of transcribed repeats, as well as RNAPI load per transcribed repeat increased. In fact, it had been observed that loss of extra copies of rDNA could rescue yeast temperature-sensitive mutants of the Origin Recognition Complex, the key replication initiation complex (Ide et al., 2007), suggesting that under certain conditions, the highly repetitive rDNA could be a burden on cellular machinery. Work from Ide et al. (2010), also in budding yeast, subsequently established the importance of the extra, untranscribed rDNA repeats for efficient DNA damage repair in the highly transcribed array (Ide et al., 2010). This group showed that cells with low rDNA copy number were sensitive to DNA damaging agents, and DNA damage sensitivity was dependent on RNAPI transcription (Ide et al., 2010), suggesting that while the extra copies of rDNA are not essential to meet cellular rRNA demands, they may serve to reduce transcriptional load on the rDNA, and allow replication-coupled repair, maintaining the integrity of this essential locus, especially under conditions of stress.

Subsequently, several studies showed that changes in rDNA copy number were frequent adaptive responses to stress. Kwan et al. (2013) identified a naturally occurring polymorphism in the budding yeast rDNA origin of replication (rARS) that results in a weakly replicating rDNA array. This “weak rARS” was shown to cause a contraction of the rDNA array and promote DNA replication in the rest of the genome (Kwan et al., 2013). Loss of regulation of rARS firing resulting from deletion of *RIF1* was also shown to be rescued by a contraction of the rDNA array (Shyian et al., 2016). These findings suggest that control of the replication program at the rDNA is critical not only to rDNA stability, but also for replication of the rest of the genome. More recently a screen of temperature-sensitive mutants of 787 essential yeast genes revealed that mutants with compromised DNA replication often had smaller rDNA arrays (Salim et al., 2017). More importantly, data from this study showed that under

conditions of DNA replication stress, loss of rDNA repeats allowed timely completion of DNA replication, allowing adaptation to replication stress (Salim et al., 2017). Work from Foss et al. (2017) provided direct evidence to support the idea that, in yeast, repetitive rDNA competes for origin firing factors with unique genomic sequences (in yeast, the rest of the genome). Foss et al. showed that tipping the balance in favor of the rDNA can lead to replication gaps, or underreplicated regions, throughout the rest of the genome (Foss et al., 2017). Taken together, data from these studies suggest that while extra, untranscribed rDNA repeats are essential for maintaining rDNA stability under normal conditions, they become detrimental to cells under conditions of DNA replication stress.

Such adaptive rDNA copy number changes are not restricted to challenges to DNA replication. Early studies in budding yeast showed that loss of the Rpa135 subunit of RNAPI led to disintegration of nucleolar structure and a loss of rDNA repeats (Kobayashi et al., 1998; Oakes et al., 1993). Subsequently, Albert et al. (2011) reported similar phenotypes in yeast strains lacking the Rpa49 subunit unique to RNAPI. Interestingly, loss of rDNA repeats partially restored nucleolar organization in these mutants (Albert et al., 2011). Given the decrease in RNAPI loading rate in the *rpa49*Δ mutants, it was proposed that interaction between RNAPI subunits in a highly transcribed rDNA array is critical to nucleolar assembly (Albert et al., 2011). This suggests that a loss of repeats would increase RNAPI density at the rDNA, allowing interaction between RNAPI subunits, and promote nucleolar assembly. The dependence of nucleolar organization on RNAPI transcription supports this idea. While loss of rDNA repeats seems more frequent, expansions of the rDNA array have also been reported. For example, Ide et al. (2013) showed that loss of Rtt109, the key histone H3 lysine 56 (H3K56) acetyltransferase in yeast, was critical to maintain normal rDNA copy number, and loss of control of rDNA amplification in *rtt109*Δ

mutants led to hyper-amplification of the rDNA array (Ide et al., 2013). Mutations which affect RNAPI transcription factors, for example, *rrn9*Δ, *rrn10*Δ, have also been shown to result in expansion of the rDNA array, presumably to compensate for the decrease in rRNA production (Ide et al., 2013; Oakes et al., 1999). Therefore, the rDNA locus may be designed to be a plastic array, whose size can be determined by selective cues from the environment.

rDNA copy number changes that could confer adaptive potential are also being discovered in mammalian systems. Xu et al. (2017) and Wang and Lemos (2017) showed through bioinformatic analyses of whole genome sequencing data from various cancers that 45S arrays are often lost in cancer (Wang & Lemos, 2017; Xu et al., 2017). Mutational analyses of these cancer genomes showed correlations of the rDNA copy number changes with a hyperactive mechanistic target of rapamycin (mTOR) pathway (Xu et al., 2017) and somatic inactivation of the tumor suppressor gene, *TP53* (Wang & Lemos, 2017). Xu et al. further showed that mouse hematopoietic stem cells (HSCs) lacking PTEN, a negative regulator of mTOR, also had contracted 45S rDNA arrays, and like yeast cells with reduced rDNA copy number, these cells were more sensitive to DNA damaging agents such as bleomycin, MMS, and X-rays. Interestingly, this DNA damage sensitivity was independent of mTOR activity, and mainly attributed to low rDNA copy number. Although PTEN is a phosphatase widely known for its role as a tumor suppressor, nuclear PTEN is essential for maintaining genome stability by dephosphorylating MCM2, and modulating replication fork progression under conditions of DNA replication stress (Feng et al., 2015). DNA replication stress resulting from reduced MCM expression was also shown to cause accumulation of phosphorylated histone H2AX (γH2AX) at the nucleolus and drive functional decline in aging mouse HSCs (Flach et al., 2014). These data suggest that the loss of 45S rDNA repeats observed in the *Pten*$^{-/-}$ mouse HSCs could be attributed to DNA replication stress. Work on the

effect of DNA replication stress on the yeast rDNA predicts that persistent DNA replication stress would select for a loss of rDNA repeats in mammalian systems as well, and this is in fact what was observed in thymic tumors derived from MCM2-deficient mice (Salim et al., 2017). Consistent with this, mouse embryonic fibroblasts derived from these MCM2-deficient mice also show increased levels of DNA damage at the 45S rDNA repeats and sensitivity to UV (Kunnev et al., 2010). Additionally, despite increased DNA damage sensitivity, the *Pten*$^{-/-}$ HSCs exhibited increased proliferation, rRNA production, and protein synthesis, suggesting the selective advantage of loss of rDNA repeats.

More recently, Udugama et al. (2018) showed that ATRX (alpha thalassemia/mental retardation X-linked)-mutated ALT (alternative lengthening of telomeres) positive human cancer cells also had low 45S rDNA copy number (Udugama et al., 2018). Through work in mouse embryonic stem cells, this group also showed that loss of ATRX affected chromatin assembly at the rDNA. The loss of ATRX was characterized by an increase in γH2AX levels at the rDNA, a loss of rDNA repeats, decreased binding of RNAPI and the key RNAPI transcription factor UBF (Upstream Binding Factor), and reduced rRNA transcription (Udugama et al., 2018). Further, cells that had lost ATRX were also sensitive to RNAPI inhibition. A recent study by Malinovskaya et al. (2018) showed a loss of rDNA repeats and a decrease in the fraction of methylated (transcriptionally inactive) rDNA repeats in cultured human fibroblasts with replicative senescence (Malinovskaya et al., 2018). In light of the observation that budding yeast cells with low rDNA copy number have a higher fraction of actively transcribed repeats relative to cells with higher rDNA copy number (French et al., 2003), it is tempting to speculate that in the face of stress that selects for a loss of rDNA repeats, transcriptionally inactive repeats may be eliminated. However, it is impossible to distinguish between preferential loss of inactive, hypermethylated rDNA repeats and changes in transcriptional status of

rDNA repeats based on existing evidence. Nevertheless, these results have very interesting implications for diagnosis and treatment of human diseases. rDNA copy number may be indicative of the history of the cell, and thus be used to diagnose past stress. Additionally, the differential sensitivity of cells with altered rDNA copy number to various drugs may aid in the selection of more effective chemotherapeutic strategies. Altogether, these data, along with the discovery of the role of rDNA stability in a variety of diseases (Diesch et al., 2014; Hallgren et al., 2014) suggest that rDNA copy number may prove to be an important indicator in human disease.

1.4.3 rDNA and the nucleolus

Ribosome biogenesis in all eukaryotes occurs in a non-membrane-bound sub-nuclear compartment called the nucleolus. Nucleoli were first observed in the nuclei of cells over two centuries ago (Fontana, 1781; Valentin, 1836, 1839; Wagner, 1835), and by the end of the nineteenth century, nucleolar morphology in a large variety of biological samples had been extensively documented, mainly in a broad cytological context (Montgomery, 1898). While nucleoli were known to be associated with heterochromatin, it was only in the 1930s that work by E. Heitz and Barbara McClintock established that nucleoli form around distinct chromosomal loci (Heitz, 1931; McClintock, 1934), termed the nucleolar-organizing body by Barbara McClintock and later called nucleolar-organizing regions (NORs). In the decades that followed, a large body of work from several groups served to demonstrate that nucleoli are the sites of rRNA transcription, processing, modification, and nascent ribosome assembly. These studies, and the discovery that NORs contained the tandemly repeated rDNA genes established the nucleolus as the “ribosome factory” of the cell (reviewed in (Pederson, 2011)). However, it has more recently been demonstrated that nucleoli are also involved in a variety of cellular processes including the

biogenesis of most cellular ribonucleoproteins, organization of the nuclear genome, regulation of growth, gene expression, and cell cycle progression, and coordination of the response to DNA damage and cellular stress (reviewed in (Iarovaia et al., 2019)).

The number of NORs and the number and morphology of nucleoli in eukaryotic cells vary widely. For example, the budding yeast, *S. cerevisiae*, has a single NOR on chromosome XII, and a single crescent-shaped nucleolus that occupies roughly one-third of the nuclear volume (Molenaar et al., 1970; Petes, 1979b; Smitt et al., 1972). The fission yeast, *S. pombe*, has two NORs, one located at each end of chromosome III, and a single nucleolus that occupies approximately half of the nucleus (Barnitz et al., 1982; Robinow & Hyams, 1989). *Drosophila melanogaster* also has two NORs, one located on each of the two sex chromosomes, and a single round nucleolus (Ritossa et al., 1966). Mammalian cells, on the other hand, have multiple NORs located on different autosomes (ex., 5 NORs in human cells and up to 6 NORs in mouse cells), and multiple nucleoli whose number and size vary even within a population of cells (Henderson et al., 1972; Kurihara et al., 1994).

Electron microscopy of nucleoli in animal cells has revealed that it has a tripartite organization, comprised of three distinct ultrastructural compartments – the fibrillar center (FC), surrounded by the dense fibrillar component (DFC) and the peripheral granular component (GC) (reviewed in (Thiry & Lafontaine, 2005)). Substantial evidence suggests that ribosome biogenesis is a vectorial process beginning in the NOR-containing FCs (reviewed in (Thiry & Lafontaine, 2005)). rDNA transcription is believed to occur at the FC-DFC interface. Co-transcriptional pre-rRNA modification and pre-rRNA processing occurs in the DFC. rRNA are then assembled into the 40S and 60S ribosomal subunits in the GC before the ribosomal subunits are exported to the cytoplasm for final maturation. This tripartite nucleolar organization has been reported in many

eukaryotes. However, the existence of a tripartite organization has remained somewhat controversial in less complex eukaryotes like *S. cerevisiae* and insects like *Drosophila melanogaster*, where a bipartite nucleolar organization lacking FCs has been observed (Sirri et al., 2008; Thiry & Lafontaine, 2005). Analysis of rDNA gene structure and nucleolar organization across many species suggests that a bipartite organization is typically observed in organisms where the transcription unit of the rDNA gene is larger or similar in size to the intergenic spacer region. In organisms with a tripartite nucleolar organization, the intergenic spacer region was found to be much larger than the transcription unit, suggesting that a tripartite organization evolved with the evolution of large non-coding spacer regions (Thiry & Lafontaine, 2005).

Nucleolar morphology, organization and function are intimately dependent on and modulated by rDNA transcription. In *S. cerevisiae*, it has been demonstrated that the normal crescent-shaped nucleolar morphology and nucleolar organization depends on transcription of rDNA by RNAPI and the tandem organization of rDNA genes in the genome. (Oakes et al., 1998; Oakes et al., 1993; Trumtel et al., 2000). Yeast like *S. cerevisiae* have a “closed mitosis”. In these cells, the nuclear envelope remains intact throughout the cell cycle, and the nucleoli do not disassemble during mitosis. rDNA are transcribed throughout the cell cycle except for a brief period in anaphase, when RNAPI transcription is inhibited by Cdc14, a protein phosphatase required for subsequent rDNA condensation, segregation, and mitotic exit (Clemente-Blanco et al., 2009; Girke & Seufert, 2019). Interestingly, ongoing RNAPI transcription during mitosis was recently also shown to be required for proper segregation of nucleolar components between mother and daughter cells (Girke & Seufert, 2019). In animal cells, on the other hand, rDNA transcription is shut off at the onset of mitosis, in prophase. Nuclear membranes break down, nuclei and nucleoli disassemble, following which chromosomes are condensed and

segregated into daughter cells. In telophase, RNAPI transcription resumes, and multiple, small nucleoli reform around individual NORs. This is followed by nucleolar fusion, which results in the formation of mature nucleoli containing multiple NORs that are observed in the interphase nucleus (reviewed in (McStay, 2016; Sirri et al., 2008)).

As expected from the dependence of nucleolar assembly and organization on rDNA transcription and ribosome biogenesis, nucleoli are remarkably dynamic organelles that exhibit responses to numerous cellular stresses that perturb RNAPI transcription as well as ribosome biogenesis. In *S. cerevisiae*, repression of rDNA transcription and ribosome biogenesis, for example, by inhibition of the TOR pathway, has been shown to result in a dramatic, reversible reorganization of the nucleolus and condensation of the rDNA (reviewed in (Matos-Perdomo & Machin, 2019)). Similarly, in human cells, inhibition of RNAPI transcription results in a rapid reorganization of the nucleolus, characterized by migration of the rDNA and associated FC and DFC components to form “caps” at the nucleolar surface, and retention of the GCs in the interior (reviewed in (Potapova & Gerton, 2019)). In human cells, stresses that perturb RNAPI transcription or ribosome biogenesis may result in the accumulation of unincorporated ribosomal protein subunits and 5S rRNA, both of which can cause accumulation of p53, which induces cell-cycle arrest and apoptosis ((Donati et al., 2013; Onofrillo et al., 2017) and reviewed in (Russo & Russo, 2017)). Changes in nucleolar morphology with age have also been reported in both yeast and human cells, and current evidence suggests that these changes are also associated with changes in rDNA transcription and ribosome production (Buchwalter & Hetzer, 2017; Lewinska et al., 2014; Tiku et al., 2017). Finally, nucleolar number, size, and morphology have been used by pathologists for decades as prognostic markers in cancer cells (Derenzini et al., 2009), which are also often characterized by altered RNAPI transcription (Lu et

al., 2009; Udugama et al., 2018; Xu et al., 2017). Therefore, nucleoli may serve not only as a sensor and source of response to genomic stresses, but also as a useful indicator of the physiological state of the cell.

Nucleolar morphology and rDNA copy number have both emerged as potentially useful indicators in health and disease. However, the relationship between rDNA copy number and nucleolar structure and function remains to be clarified. Work in *S. cerevisiae* suggests that rDNA copy number does not always correlate with cellular ribosome biogenesis or growth rate. *S. cerevisiae* strains with rDNA copy number ranging from 20-200 were shown to have similar rRNA outputs and growth rate (French et al., 2003; Ide et al., 2010). Further, it was demonstrated that yeast cells can modulate the number of transcriptionally active rDNA genes as well as RNAPI transcription rate per gene with variation in rDNA copy number so as to ensure adequate rRNA output (French et al., 2003). Given the similarity in growth rates between yeast strains that have rDNA copy number ranging from 20-200, it had been assumed that these strains also have similar nucleoli and nucleolar function. However, a recent study revealed that yeast with 25 copies of rDNA have a slightly larger nucleolus than a strain with 190 copies of rDNA (Dauban et al., 2019). Given the increase in the number of transcribed rDNA repeats and RNAPI transcription rate per gene, these data suggest that the increase in nucleolar size in the 25-copy strain is due at least in part to increased rDNA transcription. These data suggest that stability and copy number of the rDNA array has the potential to influence nucleolar structure and function independent of growth rate. In two recent studies carried out in human cells and mouse oocytes, nucleoli were observed to get larger with age, and these larger nucleoli exhibited increased rRNA and ribosome biogenesis (Buchwalter & Hetzer, 2017; Duncan et al., 2017). In a complementary study, it was shown that smaller nucleoli were associated with decreased rRNA transcription, ribosome production, and extended lifespan in worms and mice

(Tiku et al., 2017). However, rDNA copy number changes in these models of aging have not been examined thus far. rDNA copy number changes are now known to occur frequently in a variety of human cancers (Udugama et al., 2018; Wang & Lemos, 2017; Xu et al., 2017). Some of these cancers have been shown to exhibit increased rRNA transcription, protein translation, and proliferation despite a decrease in rDNA copy number (Lu et al., 2009; Xu et al., 2017), while some other cancers exhibit decreased rRNA production (Udugama et al., 2018). Nucleolar hypertrophy has been used as a marker for poor prognosis of tumors for decades – the larger the nucleoli, the worse the clinical outcome (Derenzini et al., 2009). Given the relationship between rRNA transcription and nucleolar structure, and the recent emergence of RNAPI as a promising therapeutic target for cancer (Hannan et al., 2013), the study of rDNA stability and copy number variation and their effects on nucleolar function will greatly improve our understanding of the use of this organelle as a biomarker in human health and disease.

1.4.4 New tools to measure rDNA copy number

Rising interest in the relevance of copy number variations at the rDNA loci has led to the rapid evolution of tools to measure rDNA copy number. Early studies in budding yeast relied on the estimation of rDNA copy number from the size of chromosome XII as determined by pulsed-field gel electrophoresis (PFGE) of whole chromosomes and subsequent Southern Blotting using an rDNA-specific probe (Kobayashi et al., 1998). Given the limitations of PFGE in resolution of DNA fragments larger than ~6Mb, estimation of rDNA array sizes in mammalian systems required restriction digests that liberated intact rDNA arrays (Stults et al., 2008). Despite the usefulness of PFGE in observing allelic variation and size of individual rDNA clusters from different chromosomes, this technique is time-consuming, tedious, requires considerable starting material, and offers limited

accuracy and resolution for arrays larger than ~6Mb. Additionally, interpretation of PFGE results is complicated by conditions that alter migration of DNA on the gel (for example, DNA replication/recombination intermediates) and/or affect instability at the rDNA.

Array-based comparative genomic hybridization methods were instrumental in the identification of copy number variations genome-wide at a resolution significantly greater than that offered by cytogenetic approaches (reviewed in (Carter, 2007)). However, these methods do not provide the resolution or sensitivity required for detection of relatively small copy number changes in repetitive regions like the rDNA. More recently, real-time PCR (qPCR) has been used to measure rDNA copy number (Jack et al., 2015), where fluorescent probes are used to monitor the progression of PCR amplification of the target of interest at each cycle. However, DNA copy number measurement by qPCR requires a standard curve for each experiment, and is only useful to detect relatively large changes in copy number. This makes qPCR difficult to adapt to high-throughput experiments, and limits detection of smaller rDNA copy number changes that are more common and may be functionally relevant. The last decade witnessed the revolutionization of quantitative PCR by the development of droplet digital PCR (ddPCR). The idea of “digital PCR” was developed in the 1980s and involved diluting DNA samples to a “limiting dilution” and partitioning the diluted DNA sample into different wells in a plate such that each well contained 1-2 molecules of the target of interest (Saiki et al., 1988). Early pioneers of digital PCR combined limiting dilutions with PCR amplification of the DNA to end-point, quantification using fluorescent probes, and Poisson statistics to achieve absolute nucleic acid quantification (Saiki et al., 1988; Vogelstein & Kinzler, 1999). However, despite its usefulness, particularly in the detection of rare targets, digital PCR in its early form was very labor-intensive, expensive, and therefore was quickly replaced by qPCR.

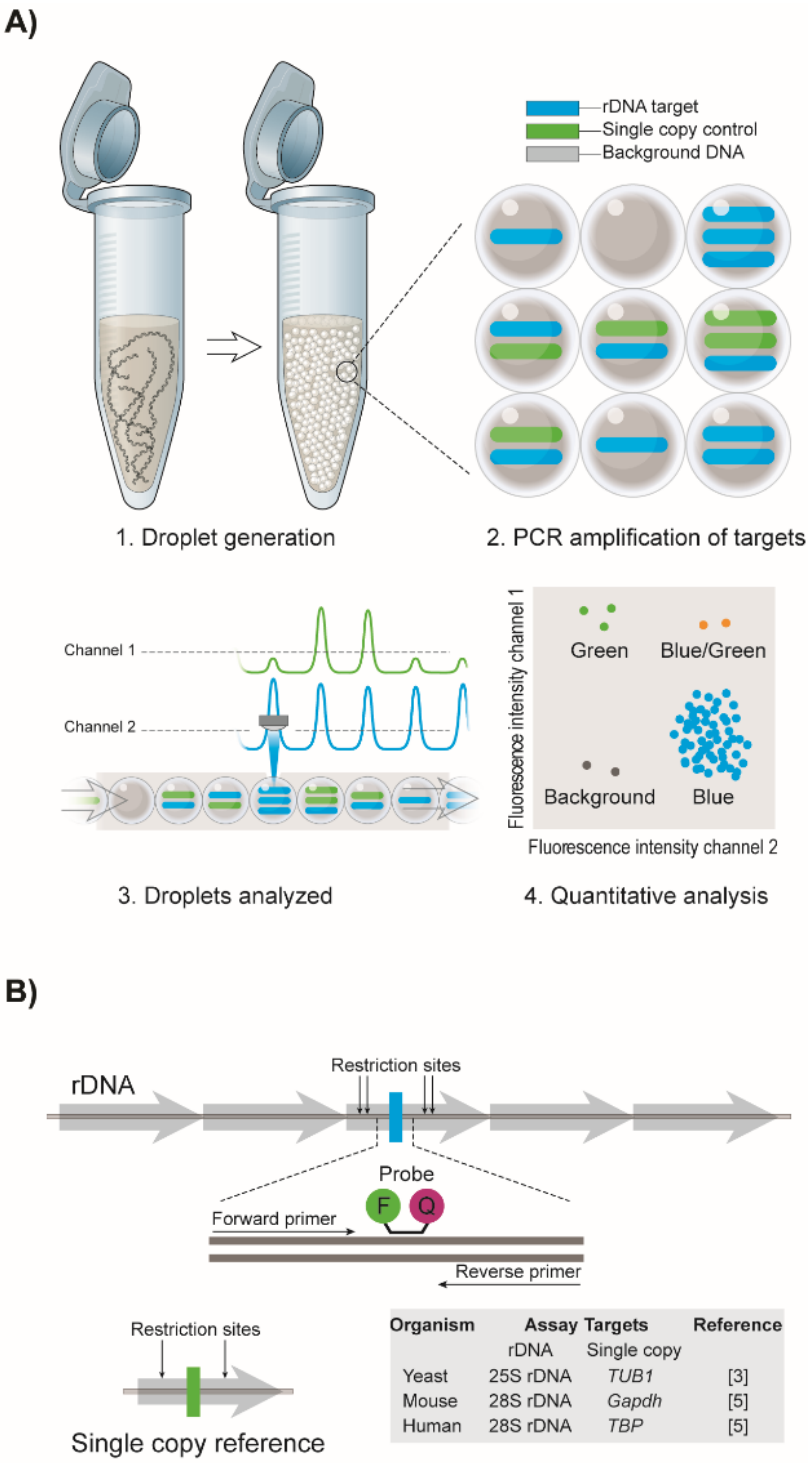

Organism	Assay Targets		Reference
	rDNA	Single copy	
Yeast	25S rDNA	*TUB1*	[3]
Mouse	28S rDNA	*Gapdh*	[5]
Human	28S rDNA	*TBP*	[5]

Figure 1.2. ddPCR to measure rDNA copy number. A) ddPCR workflow. 1. Reaction mixtures containing template DNA and rDNA (blue) and single copy reference (green) specific primers and probes are partitioned into ~20,000 nano-droplets in a single well. 2. Targets in droplets are PCR amplified to end-point. 3. Droplets are analyzed individually, and number of fluorescently positive and negative droplets are measured for each fluorophore (blue and green). 4. Fraction of fluorescently positive droplets is used to calculate the absolute number of copies of each target in the starting sample using Poisson statistics. B) Design of assays to measure rDNA copy number. Targets within the rDNA repeat (blue bar) and single copy reference gene (green bar). Arrows indicate restriction enzyme binding sites. Relative binding positions of primers and probe within one amplicon is shown. F – Fluorophore, Q – Quencher. Inset table summarizes ddPCR assay targets used to measure rDNA copy number in budding yeast, mice and humans.

In the last few years, digital PCR has been revolutionized by a combination of microfluidic chambers and the automation of sample partitioning into thousands of nanoliter sized droplets that can be PCR amplified in a single well (Hindson et al., 2011). In ddPCR, targets of interest are partitioned into ~20,000 nano-droplets and amplified to end-point with TaqMan probes as in qPCR. The concentrations of the targets are then determined by counting the number of fluorescently positive and negative droplets in the sample (Fig 1.2A). Thus, the fluorescence signal in a qPCR is converted from an analog signal into a digital one in ddPCR, eliminating the need for standard curves and allowing the determination of target copy number on an absolute scale with high precision. Additionally, partitioning the reaction mixture into droplets enables PCR amplification using homogeneous assay chemistries and workflows similar to those widely used for qPCR, considerably reducing the labor and cost involved (Hindson et al., 2011). The amount of template required is generally 1ng or less, enabling the technology to be used in situations in which starting material is limiting.

ddPCR has been increasingly used to measure rDNA copy number in a variety of model systems (Salim et al., 2017; Xu et al., 2017). In a typical assay, primers and fluorescent probes specific to a small region of the rDNA repeat, and to a stable, single copy control gene are designed. Amplicons for the rDNA target, and single copy reference gene are chosen so that they are flanked by recognition sites for one restriction enzyme; restriction enzyme digestion of the genomic DNA allows separation of tandem copies of rDNA, reduces sample viscosity and improves template accessibility. This ensures that target DNA is randomly partitioned into the ~20,000 droplets. The use of probes with different fluorophores for the rDNA and single copy reference targets allows absolute quantification of both targets in a single, duplexed ddPCR reaction. rDNA copy number per haploid genome can then be calculated from their ratio (Fig 1.2B).

Since each reaction is partitioned into ~20,000 droplets, technical error in an individual reaction can be calculated based on the droplet data from that well. Technical error in ddPCR comes mainly from errors due to sub-sampling, and partitioning into droplets. In a good assay, this total technical error should be close to the standard error of the mean, and is typically within 5-10%, which eliminates the requirement for multiple technical replicates per sample. While biological replicates are critical due to natural biological variability in rDNA copy number, ddPCR allows rapid, accurate, and sensitive detection of rDNA copy number changes.

While data from some studies suggest that rDNA copy number measurements in human DNA samples with PCR based methods may be confounded by a variety of factors including reduced amplification efficiency of the rDNA, particularly in damaged DNA, sequence polymorphisms at the rDNA, and heterogeneity in methylation status of various rDNA repeats (Chestkov et al., 2018; Zafiropoulos et al., 2005), the increasing relevance of copy number variation in diagnostics and therapeutics and the need for obtaining accurate copy number measurements in a quick, sensitive and high-throughput manner from very small amounts of samples makes ddPCR an attractive choice. In fact, the potential application for ddPCR in clinical settings was demonstrated through its use in accurate measurement of germline copy number variation in breast cancer, detection of rare mutant alleles, and in the absolute quantification of circulating DNA from cell-free plasma (Hindson et al., 2011). Therefore, ddPCR could facilitate the accurate characterization of copy number variations at repetitive regions of the genome and serve as an invaluable tool in this new era of molecular diagnostics.

1.5 *CUP1*, an inducible system to study copy number variation

While the yeast rDNA array has been used almost exclusively to model the behavior of tandem repeats, rDNA genes are constitutively transcribed, and their transcription is essential for cell viability. This makes it impossible to study copy number variation independent of transcription, and also confounds the evaluation of adaptive phenotypes. The budding yeast genome contains a second tandem array comprised of the copper-resistance *CUP1* genes. *CUP1* encodes a metallothionein that sequesters environmental copper and cadmium, although cadmium resistance is only observed at high concentrations of Cup1 (Ecker et al., 1986). Importantly, *CUP1* is only transcribed in the presence of copper in the medium, and requires the transcription factor, Cup2 (Ace1) (Welch et al., 1989). Further, *CUP1* copy number correlates directly with copper resistance (Fogel & Welch, 1982), allowing the evaluation of adaptive phenotypes by monitoring copper resistance.

The *CUP1* array shares design features with the rDNA array. It comprises 2-20 copies of a ~2kb repeat unit, arranged in tandem at a single locus on chromosome VIII. Each repeat unit contains the *CUP1* coding sequence and an origin of replication (ARS). The *CUP1* promoter, like the E-pro promoter within the rDNA, has been shown to be bidirectional, with sense and antisense transcription producing *CUP1* mRNA and a cryptic unstable transcript (CUT) respectively (Hull et al., 2017). At the rDNA, recombination is initiated from the sites of replication fork stalling at the RFB. E-pro transcription clears cohesin from rDNA repeats, and further enhances non-allelic homologous recombination, which generates copy number variation (Kobayashi & Ganley, 2005). Similarly, copper-induced transcription of *CUP1* has been shown to significantly increase the rate of mitotic recombination at the array (Zhao et al., 2017). These data suggest that transcription in the context of DNA replication can promote fork stalling, recombination and copy number variation at both, the rDNA and *CUP1* arrays. In fact, Hull et al. (2017) showed enrichment of phosphorylated serine 139 of histone H2A (γH2A) upstream of the *CUP1* ORF, suggesting that replication fork stalling and

associated double-stranded break generation occurs upstream of the *CUP1* promoter. Promoter induction was also shown to be sufficient to enhance copy number variation at the *CUP1* array (Hull et al., 2017), further supporting this idea. Finally, Hull et al. (2017) also showed that *CUP1* copy number variation was regulated by H3K56 acetylation, a chromatin mark well known for its role in maintaining rDNA copy number (Ide et al., 2013). These data suggest conservation of the basic principles of copy number variation at the rDNA and *CUP1* arrays and justify the use of the *CUP1* array to study them.

1.6 Replication, transcription, and inducible copy number variation

The traditional view of evolution states that adaptive mutations occur at random under stress and are selected for during growth under that stress. However, several studies in bacteria have shown that the genome may be designed to direct mutations to loci that require rapid evolution. Analysis of several bacterial species has revealed that while a majority of essential genes are encoded on the leading strand, such that replication of these genes is co-oriented with their transcription, a small but significant fraction of genes is encoded on the lagging strand, where, presumably, the more mutagenic head-on collisions between the replisome and transcription machinery are more frequent ("head-on genes") ((Merrikh & Merrikh, 2018), reviewed in (Lang & Merrikh, 2018)). Further, work in *Bacillus subtilis* showed that these head-on genes exhibit a higher mutation rate independent of gene sequence and chromosomal location, in a transcription dependent manner (Paul et al., 2013; Sankar et al., 2016). Moreover, it was observed that head-on genes are typically genes involved in stress response, antibiotic resistance and virulence, which are rarely expressed during growth in rich media (Merrikh & Merrikh, 2018). These data suggest that bacterial genomes have evolved to be plastic such that they are able to tune the rates of mutation at relevant loci in the face of stress.

Directing mutations to specific genomic regions is by no means restricted to bacteria. Elegant work by Hull et al. demonstrated that in budding yeast, mutagenesis could be directed to the tandemly repeated array of *CUP1* genes in a transcription dependent manner (Hull et al., 2017). Hull et al. showed that yeast cells exposed to copper exhibited extensive copy number variation at *CUP1,* which allowed for selection of copper-resistant cells with amplified *CUP1* arrays. Further, they demonstrated that this copy number variation could be induced by transcription at the locus, near sites of replication fork stalling, which accelerated the evolution of amplified *CUP1* alleles. This work suggests that transcription at sites of natural replication fork stalling could destabilize replication forks, inducing recombination-mediated repair. At repetitive loci, such recombination-mediated repair could generate increased copy number variation through unequal sister chromatid exchange events, that would allow for generation of variants in the population. Under selective pressure, variants with favorable copy number changes would prevail, thus accelerating the evolution of advantageous and reproducible environment-specific alleles (Fig 1.3).

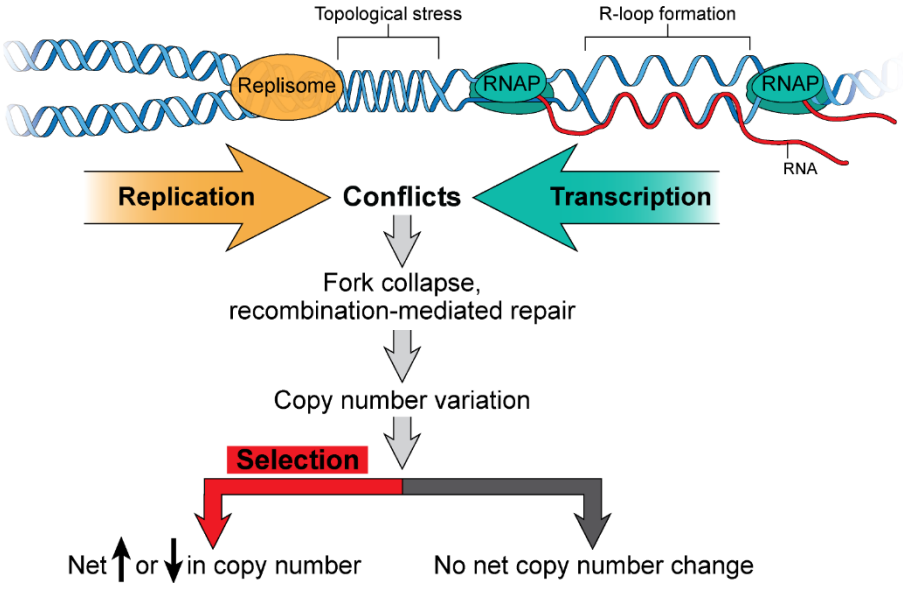

Figure 1.3. Replication and transcription may drive adaptive copy number variation. Cartoon depicting how transcription and replication can serve as sources of instability at tandem repeats. These sources include 1) topological stress created by transcription, relieved by topoisomerases, which can create nicks or breaks, 2) R-loops, a result of transcription, which can create conflicts with the replication machinery, producing breaks, and 3) replisome-RNA polymerase collisions, which may lead to replication fork collapse and double-stranded breaks. Recombination-mediated repair of breaks at repetitive loci produce copy number variation, which allows for the selection of advantageous copy number variants under stress.

Similar to the *CUP1* array, transcription and replication fork stalling are critical to recombination and copy number variation at the rDNA array, suggesting that replication-transcription conflicts and their resolution are a major source of instability at the rDNA. Further, modulating these conflicts and regulating mechanisms of their resolution could be one way of regulating instability at the locus. Additionally, several factors whose loss/gain result in more stable rDNA arrays have also been identified (reviewed in (Kobayashi & Sasaki, 2017)), suggesting that cells may have evolved to optimize instability levels, rather than minimize them.

Such mechanisms are not restricted to budding yeast. In fact, mounting evidence suggests that despite the presence of elaborate mechanisms to avoid them, secondary structures produced by transcription, and the transcription machinery itself could frequently hinder replisome progression and are a major source of genomic instability in mammalian genomes as well (reviewed in (Hamperl & Cimprich, 2016)). For example, the rDNA repeats in both prokaryotes and eukaryotes have been shown to be hotspots for the formation of unusual nucleic acid structures called R-loops, which consist of a nascent RNA-template DNA hybrid and the displaced non-template, single-stranded DNA (El Hage et al., 2010; Ginno et al., 2012; Masse et al., 1997; Nadel et al., 2015). A recent study reported that the coding regions of the rDNA repeats in human cells are strongly enriched for R-loops relative to the rest of the genome (Nadel et al., 2015). R-loops are natural by-products of transcription, particularly at GC-rich DNA sequences, which is likely why the GC-rich, highly transcribed rDNA repeats may be particularly prone to their formation. Collisions between R-loops and the DNA replication machinery are thought to be a major source of the replication-transcription conflicts that result in genomic instability (Aguilera & Garcia-Muse, 2012; Gaillard & Aguilera, 2016; Garcia-Muse & Aguilera, 2016; Skourti-Stathaki & Proudfoot, 2014), suggesting that R-loop formation and resolution contributes significantly to the inherent instability at the rDNA.

Importantly, transcription itself is mutagenic, irrespective of DNA replication, because torsional stress created by transcription is relieved by topoisomerases, which creates

nicks and breaks in the template DNA. Therefore, transcription associated mutagenesis (reviewed in (Kim & Jinks-Robertson, 2012)) may be particularly high at the highly transcribed rDNA. Significant portions of mammalian genomes are made up of repetitive elements; while many repeats are yet to be identified, it has been established that copy number variation at the rDNA is a significant source of genetic diversity in populations (Gibbons et al., 2015; Gibbons et al., 2014; Stults et al., 2008). Moreover, given the conservation of the structural organization of the rDNA repeats, particularly the tandem arrangement of repeats, the presence of a RFB, high rates of transcription, and pathways involved in maintenance of the locus, mechanisms of regulation of instability of the rDNA in budding yeast may be conserved in mammals.

1.7 Summary

Tandem repeats are common in eukaryotic genomes, and while their variability may confer phenotypic consequences, they are poorly understood. The budding yeast rDNA array has been used extensively to study the behavior of tandem repeats. The large body of work in budding yeast has provided many insights into the structural features of the rDNA locus and the mechanisms controlling these repeats. Recent studies have built on this work, providing new insights into how changes in rDNA repeat copy number may aid adaptation to stress. The essential nature of the rDNA array, its constitutive transcription, and the lack of quantitative assays to accurately measure and distinguish repeat instability and steady state repeat copy number have all hindered our progress towards gaining a comprehensive understanding of the maintenance of tandem repeats. As a result, the role of variation at tandem repeats in response and adaptation to the environment has also remained understudied. In my thesis work, I developed two highly sensitive assays to quantify repeat instability and steady state repeat copy number. Applying these assays in parallel to the rDNA array and the inducible *CUP1* array, I have characterized some of the fundamental processes that regulate tandem repeats.

In Chapter 2, I describe the development and validation of a droplet digital PCR (ddPCR) based assay to measure rDNA copy number and its use in a high-throughput genetic screen to identify pathways involved in the maintenance of normal rDNA copy number. I also present data to show that the loss of rDNA repeats facilities adaptation to DNA replication stress. In Chapter 3, I present the development and validation of a quantitative, single cell-based assay to measure repeat instability (qRIN) and demonstrate its use in a quantitative and unbiased high-throughput screen to identify genetic factors that regulate rDNA stability. Together with data from a second screen to identify additional factors involved in the maintenance of rDNA copy number, I show that instability and maintenance of rDNA copy number are regulated by DNA replication, transcription and histone acetylation. I also describe parallel studies on the rDNA and *CUP1* arrays that directly show that instability at tandem repeats can be modulated by DNA replication stress and transcription of the locus. Further, I demonstrate the distinction between instability and copy number changes through experiments showing that instability is induced rapidly in response to a variety of stresses, but a change in steady state repeat copy number requires prolonged propagation under selective conditions. In Chapter 4, I describe the characterization of the role of histone acetylation in modulating repeat stability and copy number amplification in response to transcription. Finally, in Chapter 5, I summarize the key findings from my thesis work, present important future directions, and speculate on the broad relevance and implications of my work in advancing our understanding of tandem repeat behavior and genome plasticity in higher eukaryotes. Altogether, my studies of rDNA and *CUP1* repeats may serve as a touchstone for understanding the principles of regulation of additional tandem repeats and the important functional and evolutionary roles they play in genome biology.

1.8 References

Aguilera, A., & Garcia-Muse, T. (2012). R loops: from transcription byproducts to threats to genome stability. *Mol Cell, 46*(2), 115-124. doi:10.1016/j.molcel.2012.04.009

Akamatsu, Y., & Kobayashi, T. (2015). The Human RNA Polymerase I Transcription Terminator Complex Acts as a Replication Fork Barrier That Coordinates the Progress of Replication with rRNA Transcription Activity. *Mol Cell Biol, 35*(10), 1871-1881. doi:10.1128/MCB.01521-14

Albert, B., Leger-Silvestre, I., Normand, C., Ostermaier, M. K., Perez-Fernandez, J., Panov, K. I., . . . Gadal, O. (2011). RNA polymerase I-specific subunits promote polymerase clustering to enhance the rRNA gene transcription cycle. *J Cell Biol, 192*(2), 277-293. doi:10.1083/jcb.201006040

Barnitz, J. T., Cramer, J. H., Rownd, R. H., Cooley, L., & Söll, D. (1982). Arrangement of the ribosomal RNA genes inSchizosaccharomyces pombe. *FEBS Letters, 143*(1), 129-132. doi:10.1016/0014-5793(82)80288-3

Beckmann, J. S., Estivill, X., & Antonarakis, S. E. (2007). Copy number variants and genetic traits: closer to the resolution of phenotypic to genotypic variability. *Nat Rev Genet, 8*(8), 639-646. doi:10.1038/nrg2149

Brahmachary, M., Guilmatre, A., Quilez, J., Hasson, D., Borel, C., Warburton, P., & Sharp, A. J. (2014). Digital genotyping of macrosatellites and multicopy genes reveals novel biological functions associated with copy number variation of large tandem repeats. *PLoS Genet, 10*(6), e1004418. doi:10.1371/journal.pgen.1004418

Brewer, B. J., Lockshon, D., & Fangman, W. L. (1992). The arrest of replication forks in the rDNA of yeast occurs independently of transcription. *Cell, 71*(2), 267-276. doi:10.1016/0092-8674(92)90355-g

Buchwalter, A., & Hetzer, M. W. (2017). Nucleolar expansion and elevated protein translation in premature aging. *Nat Commun, 8*(1), 328. doi:10.1038/s41467-017-00322-z

Cahyani, I., Cridge, A. G., Engelke, D. R., Ganley, A. R., & O'Sullivan, J. M. (2015). A sequence-specific interaction between the Saccharomyces cerevisiae rRNA gene repeats and a locus encoding an RNA polymerase I subunit affects ribosomal DNA stability. *Mol Cell Biol, 35*(3), 544-554. doi:10.1128/MCB.01249-14

Carter, N. P. (2007). Methods and strategies for analyzing copy number variation using DNA microarrays. *Nat Genet, 39*(7 Suppl), S16-21. doi:10.1038/ng2028

Chestkov, I. V., Jestkova, E. M., Ershova, E. S., Golimbet, V. E., Lezheiko, T. V., Kolesina, N. Y., . . . Kostyuk, S. V. (2018). Abundance of ribosomal RNA gene copies in the genomes of schizophrenia patients. *Schizophr Res, 197*, 305-314. doi:10.1016/j.schres.2018.01.001

Clemente-Blanco, A., Mayan-Santos, M., Schneider, D. A., Machin, F., Jarmuz, A., Tschochner, H., & Aragon, L. (2009). Cdc14 inhibits transcription by RNA polymerase I during anaphase. *Nature, 458*(7235), 219-222. doi:10.1038/nature07652

Dalgaard, J. Z., Godfrey, E. L., & MacFarlane, R. J. (2011). Eukaryotic Replication Barriers: How, Why and Where Forks Stall. In *DNA Replication-Current Advances* (pp. 269-304).

Dauban, L., Kamgoue, A., Wang, R., Leger-Silvestre, I., Beckouet, F., Cantaloube, S., & Gadal, O. (2019). Quantification of the dynamic behaviour of ribosomal DNA genes and nucleolus during yeast Saccharomyces cerevisiae cell cycle. *J Struct Biol*. doi:10.1016/j.jsb.2019.08.010

Derenzini, M., Montanaro, L., & Trere, D. (2009). What the nucleolus says to a tumour pathologist. *Histopathology, 54*(6), 753-762. doi:10.1111/j.1365-2559.2008.03168.x

Diermeier, S. D., Nemeth, A., Rehli, M., Grummt, I., & Langst, G. (2013). Chromatin-specific regulation of mammalian rDNA transcription by clustered TTF-I binding sites. *PLoS Genet, 9*(9), e1003786. doi:10.1371/journal.pgen.1003786

Diesch, J., Hannan, R. D., & Sanij, E. (2014). Perturbations at the ribosomal genes loci are at the centre of cellular dysfunction and human disease. *Cell Biosci, 4*, 43. doi:10.1186/2045-3701-4-43

Donati, G., Peddigari, S., Mercer, C. A., & Thomas, G. (2013). 5S ribosomal RNA is an essential component of a nascent ribosomal precursor complex that regulates the Hdm2-p53 checkpoint. *Cell Rep, 4*(1), 87-98. doi:10.1016/j.celrep.2013.05.045

Duncan, F. E., Jasti, S., Paulson, A., Kelsh, J. M., Fegley, B., & Gerton, J. L. (2017). Age-associated dysregulation of protein metabolism in the mammalian oocyte. *Aging Cell, 16*(6), 1381-1393. doi:10.1111/acel.12676

Ecker, D. J., Butt, T. R., Sternberg, E. J., Neeper, M. P., Debouck, C., Gorman, J. A., & Crooke, S. T. (1986). Yeast metallothionein function in metal ion detoxification. *J Biol Chem, 261*(36), 16895-16900.

El Hage, A., French, S. L., Beyer, A. L., & Tollervey, D. (2010). Loss of Topoisomerase I leads to R-loop-mediated transcriptional blocks during ribosomal RNA synthesis. *Genes Dev, 24*(14), 1546-1558. doi:10.1101/gad.573310

Feng, J., Liang, J., Li, J., Li, Y., Liang, H., Zhao, X., . . . Yin, Y. (2015). PTEN Controls the DNA Replication Process through MCM2 in Response to Replicative Stress. *Cell Rep, 13*(7), 1295-1303. doi:10.1016/j.celrep.2015.10.016

Flach, J., Bakker, S. T., Mohrin, M., Conroy, P. C., Pietras, E. M., Reynaud, D., . . . Passegue, E. (2014). Replication stress is a potent driver of functional decline in ageing haematopoietic stem cells. *Nature, 512*(7513), 198-202. doi:10.1038/nature13619

Fogel, S., & Welch, J. W. (1982). Tandem gene amplification mediates copper resistance in yeast. *Proc Natl Acad Sci U S A, 79*(17), 5342-5346. doi:10.1073/pnas.79.17.5342

Fontana, F. (1781). *Traité sur le venin de la vipère avec des observations sur la structure primitive du corps animal*. Florence.

Foss, E. J., Lao, U., Dalrymple, E., Adrianse, R. L., Loe, T., & Bedalov, A. (2017). SIR2 suppresses replication gaps and genome instability by balancing replication between repetitive and unique sequences. *Proc Natl Acad Sci U S A., 114*(3), 552-557. doi:10.1073

French, S. L., Osheim, Y. N., Cioci, F., Nomura, M., & Beyer, A. L. (2003). In exponentially growing Saccharomyces cerevisiae cells, rRNA synthesis is determined by the summed RNA polymerase I loading rate rather than by the number of active genes. *Mol Cell Biol, 23*(5), 1558-1568. doi:10.1128/mcb.23.5.1558-1568.2003

Gaillard, H., & Aguilera, A. (2016). Transcription as a Threat to Genome Integrity. *Annu Rev Biochem, 85*, 291-317. doi:10.1146/annurev-biochem-060815-014908

Garcia-Muse, T., & Aguilera, A. (2016). Transcription-replication conflicts: how they occur and how they are resolved. *Nat Rev Mol Cell Biol, 17*(9), 553-563. doi:10.1038/nrm.2016.88

Gerber, J. K., Gogel, E., Berger, C., Wallisch, M., Muller, F., Grummt, I., & Grummt, F. (1997). Termination of mammalian rDNA replication: polar arrest of replication fork movement by transcription termination factor TTF-I. *Cell, 90*(3), 559-567. doi:10.1016/s0092-8674(00)80515-2

Gibbons, J. G., Branco, A. T., Godinho, S. A., Yu, S., & Lemos, B. (2015). Concerted copy number variation balances ribosomal DNA dosage in human and mouse genomes. *Proc Natl Acad Sci U S A, 112*(8), 2485-2490. doi:10.1073/pnas.1416878112

Gibbons, J. G., Branco, A. T., Yu, S., & Lemos, B. (2014). Ribosomal DNA copy number is coupled with gene expression variation and mitochondrial abundance in humans. *Nat Commun, 5*, 4850. doi:10.1038/ncomms5850

Ginno, P. A., Lott, P. L., Christensen, H. C., Korf, I., & Chedin, F. (2012). R-loop formation is a distinctive characteristic of unmethylated human CpG island promoters. *Mol Cell, 45*(6), 814-825. doi:10.1016/j.molcel.2012.01.017

Girke, P., & Seufert, W. (2019). Compositional reorganization of the nucleolus in budding yeast mitosis. *Mol Biol Cell, 30*(5), 591-606. doi:10.1091/mbc.E18-08-0524

Gonzalez, I. L., & Sylvester, J. E. (1995). Complete sequence of the 43-kb human ribosomal DNA repeat: analysis of the intergenic spacer. *Genomics, 27*(2), 320-328. doi:10.1006/geno.1995.1049

Gonzalez, I. L., & Sylvester, J. E. (2001). Human rDNA: evolutionary patterns within the genes and tandem arrays derived from multiple chromosomes. *Genomics, 73*(3), 255-263. doi:10.1006/geno.2001.6540

Hallgren, J., Pietrzak, M., Rempala, G., Nelson, P. T., & Hetman, M. (2014). Neurodegeneration-associated instability of ribosomal DNA. *Biochim Biophys Acta, 1842*(6), 860-868. doi:10.1016/j.bbadis.2013.12.012

Hamperl, S., & Cimprich, K. A. (2016). Conflict Resolution in the Genome: How Transcription and Replication Make It Work. *Cell, 167*(6), 1455-1467. doi:10.1016/j.cell.2016.09.053

Hannan, R. D., Drygin, D., & Pearson, R. B. (2013). Targeting RNA polymerase I transcription and the nucleolus for cancer therapy. *Expert Opin Ther Targets, 17*(8), 873-878. doi:10.1517/14728222.2013.818658

Heitz, E. (1931). Nukleolen und Chromosomen in der Gattung Vicia. *Planta, 15*(3), 495-505. doi:10.1007/bf01909065

Henderson, A. S., Warburton, D., & Atwood, K. C. (1972). Location of ribosomal DNA in the human chromosome complement. *Proc Natl Acad Sci U S A, 69*(11), 3394-3398. doi:10.1073/pnas.69.11.3394

Hernández, P., Martín-Parras, L., Martínez-Robles, M. L., & Schvartzman, J. B. (1993). Conserved features in the mode of replication of eukaryotic ribosomal RNA genes. *The EMBO Journal, 12*(4), 1475–1485.

Hindson, B. J., Ness, K. D., Masquelier, D. A., Belgrader, P., Heredia, N. J., Makarewicz, A. J., . . . Colston, B. W. (2011). High-throughput droplet digital PCR system for absolute quantitation of DNA copy number. *Anal Chem, 83*(22), 8604-8610. doi:10.1021/ac202028g

Hull, R. M., Cruz, C., Jack, C. V., & Houseley, J. (2017). Environmental change drives accelerated adaptation through stimulated copy number variation. *PLoS Biol, 15*(6), e2001333. doi:10.1371/journal.pbio.2001333

Hurles, M. E., Dermitzakis, E. T., & Tyler-Smith, C. (2008). The functional impact of structural variation in humans. *Trends Genet, 24*(5), 238-245. doi:10.1016/j.tig.2008.03.001

Iafrate, A. J., Feuk, L., Rivera, M. N., Listewnik, M. L., Donahoe, P. K., Qi, Y., . . . Lee, C. (2004). Detection of large-scale variation in the human genome. *Nat Genet, 36*(9), 949-951. doi:10.1038/ng1416

Iarovaia, O. V., Minina, E. P., Sheval, E. V., Onichtchouk, D., Dokudovskaya, S., Razin, S. V., & Vassetzky, Y. S. (2019). Nucleolus: A Central Hub for Nuclear Functions. *Trends Cell Biol, 29*(8), 647-659. doi:10.1016/j.tcb.2019.04.003

Ide, S., Miyazaki, T., Maki, H., & Kobayashi, T. (2010). Abundance of ribosomal RNA gene copies maintains genome integrity. *Science, 327*(5966), 693-696. doi:10.1126/science.1179044

Ide, S., Saka, K., & Kobayashi, T. (2013). Rtt109 Prevents Hyper-Amplification of Ribosomal RNA Genes through Histone Modification in Budding Yeast. *PLoS Genet, 9*(4). doi:10.1371/journal.pgen.1003410.g001

Ide, S., Watanabe, K., Watanabe, H., Shirahige, K., Kobayashi, T., & Maki, H. (2007). Abnormality in initiation program of DNA replication is monitored by the highly repetitive rRNA gene array on chromosome XII in budding yeast. *Mol Cell Biol, 27*(2), 568-578. doi:10.1128/MCB.00731-06

Iida, T., & Kobayashi, T. (2019). RNA Polymerase I Activators Count and Adjust Ribosomal RNA Gene Copy Number. *Mol Cell, 73*(4), 645-654 e613. doi:10.1016/j.molcel.2018.11.029

Jack, C. V., Cruz, C., Hull, R. M., Keller, M. A., Ralser, M., & Houseley, J. (2015). Regulation of ribosomal DNA amplification by the TOR pathway. *Proc Natl Acad Sci U S A, 112*(31), 9674-9679. doi:10.1073/pnas.1505015112

Kim, N., & Jinks-Robertson, S. (2012). Transcription as a source of genome instability. *Nat Rev Genet, 13*(3), 204-214. doi:10.1038/nrg3152

Kobayashi, T. (2003). The replication fork barrier site forms a unique structure with Fob1p and inhibits the replication fork. *Mol Cell Biol, 23*(24), 9178-9188. doi:10.1128/mcb.23.24.9178-9188.2003

Kobayashi, T. (2014). Ribosomal RNA gene repeats, their stability and cellular senescence. *Proc Jpn Acad Ser B Phys Biol Sci, 90*(4), 119-129. doi:10.2183/pjab.90.119

Kobayashi, T., & Ganley, A. R. (2005). Recombination regulation by transcription-induced cohesin dissociation in rDNA repeats. *Science, 309*(5740), 1581-1584. doi:10.1126/science.1116102

Kobayashi, T., Heck, D. J., Nomura, M., & Horiuchi, T. (1998). Expansion and contraction of ribosomal DNA repeats in *Saccharomyces cerevisiae*: requirement of replication fork blocking (Fob1) protein and the role of RNA polymerase I. *Genes Dev, 12*(24), 3821-3830. doi:10.1101/gad.12.24.3821

Kobayashi, T., Horiuchi, T., Tongaonkar, P., Vu, L., & Nomura, M. (2004). SIR2 Regulates Recombination between Different rDNA Repeats, but Not Recombination within Individual rRNA Genes in Yeast. *Cell., 117*(4), 441-453.

Kobayashi, T., & Sasaki, M. (2017). Ribosomal DNA stability is supported by many 'buffer genes'-introduction to the Yeast rDNA Stability Database. *FEMS Yeast Res, 17*(1). doi:10.1093/femsyr/fox001

Kunnev, D., Rusiniak, M. E., Kudla, A., Freeland, A., Cady, G. K., & Pruitt, S. C. (2010). DNA damage response and tumorigenesis in Mcm2-deficient mice. *Oncogene, 29*(25), 3630-3638. doi:10.1038/onc.2010.125

Kurihara, Y., Suh, D. S., Suzuki, H., & Moriwaki, K. (1994). Chromosomal locations of Ag-NORs and clusters of ribosomal DNA in laboratory strains of mice. *Mamm Genome, 5*(4), 225-228. doi:10.1007/bf00360550

Kwan, E. X., Foss, E. J., Tsuchiyama, S., Alvino, G. M., Kruglyak, L., Kaeberlein, M., . . . Bedalov, A. (2013). A natural polymorphism in rDNA replication origins links origin activation with calorie restriction and lifespan. *PLoS Genet, 9*(3), e1003329. doi:10.1371/journal.pgen.1003329

Lang, K. S., & Merrikh, H. (2018). The Clash of Macromolecular Titans: Replication-Transcription Conflicts in Bacteria. *Annu Rev Microbiol, 72*, 71-88. doi:10.1146/annurev-micro-090817-062514

Lewinska, A., Miedziak, B., Kulak, K., Molon, M., & Wnuk, M. (2014). Links between nucleolar activity, rDNA stability, aneuploidy and chronological aging in the yeast Saccharomyces cerevisiae. *Biogerontology, 15*(3), 289-316. doi:10.1007/s10522-014-9499-y

Little, R. D., Platt, T. H., & Schildkraut, C. L. (1993). Initiation and termination of DNA replication in human rRNA genes. *Mol Cell Biol, 13*(10), 6600-6613. doi:10.1128/mcb.13.10.6600

Lu, Y., Chang, Q., Zhang, Y., Beezhold, K., Rojanasakul, Y., Zhao, H., . . . Chen, F. (2009). Lung cancer-associated JmjC domain protein mdig suppresses formation of tri-methyl lysine 9 of histone H3. *Cell Cycle, 8*(13), 2101-2109. doi:10.4161/cc.8.13.8927

MacAlpine, D. M., Zhang, Z., & Kapler, G. M. (1997). Type I elements mediate replication fork pausing at conserved upstream sites in the Tetrahymena thermophila ribosomal DNA minichromosome. *Mol Cell Biol, 17*(8), 4517-4525. doi:10.1128/mcb.17.8.4517

Malinovskaya, E. M., Ershova, E. S., Golimbet, V. E., Porokhovnik, L. N., Lyapunova, N. A., Kutsev, S. I., . . . Kostyuk, S. V. (2018). Copy Number of Human Ribosomal Genes With Aging: Unchanged Mean, but Narrowed Range and Decreased Variance in Elderly Group. *Front Genet, 9*, 306. doi:10.3389/fgene.2018.00306

Mansisidor, A., Molinar, T., Jr., Srivastava, P., Dartis, D. D., Pino Delgado, A., Blitzblau, H. G., . . . Hochwagen, A. (2018). Genomic Copy-Number Loss Is Rescued by Self-Limiting Production of DNA Circles. *Mol Cell, 72*(3), 583-593 e584. doi:10.1016/j.molcel.2018.08.036

Mao, J., Appel, B., Schaack, J., Sharp, S., Yamada, H., & Soll, D. (1982). The 5S RNA genes of Schizosaccharomyces pombe. *Nucleic Acids Res, 10*(2), 487-500. doi:10.1093/nar/10.2.487

Masse, E., Phoenix, P., & Drolet, M. (1997). DNA topoisomerases regulate R-loop formation during transcription of the rrnB operon in Escherichia coli. *J Biol Chem, 272*(19), 12816-12823.

Matos-Perdomo, E., & Machin, F. (2019). Nucleolar and Ribosomal DNA Structure under Stress: Yeast Lessons for Aging and Cancer. *Cells, 8*(8). doi:10.3390/cells8080779

Mayan, M., & Aragon, L. (2010). Cis-interactions between non-coding ribosomal spacers dependent on RNAP-II separate RNAP-I and RNAP-III transcription domains. *Cell Cycle, 9*(21), 4328-4337. doi:10.4161/cc.9.21.13591

Mayer, C., Schmitz, K. M., Li, J., Grummt, I., & Santoro, R. (2006). Intergenic transcripts regulate the epigenetic state of rRNA genes. *Mol Cell, 22*(3), 351-361. doi:10.1016/j.molcel.2006.03.028

McClintock, B. (1934). The relation of a particular chromosomal element to the development of the nucleoli in Zea mays. *Zeitschrift für Zellforschung und Mikroskopische Anatomie, 21*(2), 294-326. doi:10.1007/bf00374060

McStay, B. (2016). Nucleolar organizer regions: genomic 'dark matter' requiring illumination. *Genes Dev., 30*(14), 1598-1610. doi:10.1101/gad.283838

Merrikh, C. N., & Merrikh, H. (2018). Gene inversion potentiates bacterial evolvability and virulence. *Nat Commun, 9*(1), 4662. doi:10.1038/s41467-018-07110-3

Michel, A. H., Kornmann, B., Dubrana, K., & Shore, D. (2005). Spontaneous rDNA copy number variation modulates Sir2 levels and epigenetic gene silencing. *Genes Dev, 19*(10), 1199-1210. doi:10.1101/gad.340205

Molenaar, I., Smitt, W. W. S., Rozijn, T. H., & Tonino, G. J. M. (1970). Biochemical and electron microscopic study of isolated yeast nuclei. *Experimental Cell Research, 60*(2), 148-156. doi:10.1016/0014-4827(70)90500-8

Montgomery, T. S. H. (1898). Comparative cytological studies, with especial regard to the morphology of the nucleolus. *Journal of Morphology, 15*(2), 265-582. doi: https://doi.org/10.1002/jmor.1050150204

Nadel, J., Athanasiadou, R., Lemetre, C., Wijetunga, N. A., P, O. B., Sato, H., . . . Greally, J. M. (2015). RNA:DNA hybrids in the human genome have distinctive nucleotide characteristics, chromatin composition, and transcriptional relationships. *Epigenetics Chromatin, 8*, 46. doi:10.1186/s13072-015-0040-6

O'Sullivan, J. M., Sontam, D. M., Grierson, R., & Jones, B. (2009). Repeated elements coordinate the spatial organization of the yeast genome. *Yeast, 26*(2), 125-138. doi:10.1002/yea.1657

Oakes, M., Aris, J. P., Brockenbrough, J. S., Wai, H., Vu, L., & Nomura, M. (1998). Mutational analysis of the structure and localization of the nucleolus in the yeast Saccharomyces cerevisiae. *J Cell Biol, 143*(1), 23-34. doi:10.1083/jcb.143.1.23

Oakes, M., Nogi, Y., Clark, M. W., & Nomura, M. (1993). Structural alterations of the nucleolus in mutants of Saccharomyces cerevisiae defective in RNA polymerase I. *Mol Cell Biol, 13*(4), 2441-2455. doi:10.1128/mcb.13.4.2441

Oakes, M., Siddiqi, I., Vu, L., Aris, J., & Nomura, M. (1999). Transcription factor UAF, expansion and contraction of ribosomal DNA (rDNA) repeats, and RNA polymerase switch in transcription of yeast rDNA. *Mol Cell Biol, 19*(12), 8559-8569. doi:10.1128/mcb.19.12.8559

Onofrillo, C., Galbiati, A., Montanaro, L., & Derenzini, M. (2017). The pre-existing population of 5S rRNA effects p53 stabilization during ribosome biogenesis inhibition. *Oncotarget, 8*(3), 4257-4267. doi:10.18632/oncotarget.13833

Paredes, S., Branco, A. T., Hartl, D. L., Maggert, K. A., & Lemos, B. (2011). Ribosomal DNA deletions modulate genome-wide gene expression: "rDNA-sensitive" genes and natural variation. *PLoS Genet, 7*(4), e1001376. doi:10.1371/journal.pgen.1001376

Paul, S., Million-Weaver, S., Chattopadhyay, S., Sokurenko, E., & Merrikh, H. (2013). Accelerated gene evolution through replication-transcription conflicts. *Nature, 495*(7442), 512-515. doi:10.1038/nature11989

Pederson, T. (2011). The nucleolus. *Cold Spring Harb Perspect Biol, 3*(3). doi:10.1101/cshperspect.a000638

Peter, J., De Chiara, M., Friedrich, A., Yue, J. X., Pflieger, D., Bergstrom, A., . . . Schacherer, J. (2018). Genome evolution across 1,011 Saccharomyces cerevisiae isolates. *Nature, 556*(7701), 339-344. doi:10.1038/s41586-018-0030-5

Petes, T. D. (1979a). Meiotic mapping of yeast ribosomal deoxyribonucleic acid on chromosome XII. *J Bacteriol, 138*(1), 185-192.

Petes, T. D. (1979b). Yeast ribosomal DNA genes are located on chromosome XII. *Proc Natl Acad Sci U S A, 76*(1), 410-414. doi:10.1073/pnas.76.1.410

Potapova, T. A., & Gerton, J. L. (2019). Ribosomal DNA and the nucleolus in the context of genome organization. *Chromosome Res, 27*(1-2), 109-127. doi:10.1007/s10577-018-9600-5

Redon, R., Ishikawa, S., Fitch, K. R., Feuk, L., Perry, G. H., Andrews, T. D., . . . Hurles, M. E. (2006). Global variation in copy number in the human genome. *Nature, 444*(7118), 444-454. doi:10.1038/nature05329

Ritossa, F. M., Atwood, K. C., Lindsley, D. L., & Spiegelman, S. (1966). On the chromosomal distribution of DNA complementary to ribosomal and soluble RNA. *Natl. Cancer Inst. Monograph, 23*, 449–472.

Robinow, C. F., & Hyams, J. (1989). General Cytology of Fission Yeasts. In A. Nasim, P. Young, & B. F. Johnson (Eds.), *Molecular Biology of the Fission Yeast* (pp. 273–331). San Diego: Academic Press, Inc.

Rosato, M., Kovarik, A., Garilleti, R., & Rossello, J. A. (2016). Conserved Organisation of 45S rDNA Sites and rDNA Gene Copy Number among Major Clades of Early Land Plants. *PLoS One, 11*(9), e0162544. doi:10.1371/journal.pone.0162544

Russo, A., & Russo, G. (2017). Ribosomal Proteins Control or Bypass p53 during Nucleolar Stress. *Int J Mol Sci, 18*(1). doi:10.3390/ijms18010140

Saiki, R. K., Gelfand, D. H., Stoffel, S., Scharf, S. J., Higuchi, R., Horn, G. T., . . . Erlich, H. A. (1988). Primer-directed enzymatic amplification of DNA with a thermostable DNA polymerase. *Science, 239*(4839), 487-491. doi:10.1126/science.2448875

Saka, K., Takahashi, A., Sasaki, M., & Kobayashi, T. (2016). More than 10% of yeast genes are related to genome stability and influence cellular senescence via rDNA maintenance. *Nucleic Acids Res, 44*(9), 4211-4221. doi:10.1093/nar/gkw110

Salim, D., Bradford, W. D., Freeland, A., Cady, G., Wang, J., Pruitt, S. C., & Gerton, J. L. (2017). DNA replication stress restricts ribosomal DNA copy number. *PLoS Genet, 13*(9), e1007006. doi:10.1371/journal.pgen.1007006

Sanchez-Gorostiaga, A., Lopez-Estrano, C., Krimer, D. B., Schvartzman, J. B., & Hernandez, P. (2004). Transcription termination factor reb1p causes two replication fork barriers at its cognate sites in fission yeast ribosomal DNA in vivo. *Mol Cell Biol, 24*(1), 398-406. doi:10.1128/mcb.24.1.398-406.2004

Sanchez, J. A., Kim, S. M., & Huberman, J. A. (1998). Ribosomal DNA replication in the fission yeast, Schizosaccharomyces pombe. *Exp Cell Res, 238*(1), 220-230. doi:10.1006/excr.1997.3835

Sankar, T. S., Wastuwidyaningtyas, B. D., Dong, Y., Lewis, S. A., & Wang, J. D. (2016). The nature of mutations induced by replication-transcription collisions. *Nature, 535*(7610), 178-181. doi:10.1038/nature18316

Santoro, R., Schmitz, K. M., Sandoval, J., & Grummt, I. (2010). Intergenic transcripts originating from a subclass of ribosomal DNA repeats silence ribosomal RNA genes in trans. *EMBO Rep, 11*(1), 52-58. doi:10.1038/embor.2009.254

Sebat, J., Lakshmi, B., Troge, J., Alexander, J., Young, J., Lundin, P., . . . Wigler, M. (2004). Large-scale copy number polymorphism in the human genome. *Science, 305*(5683), 525-528. doi:10.1126/science.1098918

Shyian, M., Mattarocci, S., Albert, B., Hafner, L., Lezaja, A., Costanzo, M., . . . Shore, D. (2016). Budding Yeast Rif1 Controls Genome Integrity by Inhibiting rDNA Replication. *PLoS Genet, 12*(11), e1006414. doi:10.1371/journal.pgen.1006414

Sirri, V., Urcuqui-Inchima, S., Roussel, P., & Hernandez-Verdun, D. (2008). Nucleolus: the fascinating nuclear body. *Histochem Cell Biol, 129*(1), 13-31. doi:10.1007/s00418-007-0359-6

Skourti-Stathaki, K., & Proudfoot, N. J. (2014). A double-edged sword: R loops as threats to genome integrity and powerful regulators of gene expression. *Genes Dev, 28*(13), 1384-1396. doi:10.1101/gad.242990.114

Smith, J. S., Caputo, E., & Boeke, J. D. (1999). A genetic screen for ribosomal DNA silencing defects identifies multiple DNA replication and chromatin-modulating factors. *Mol Cell Biol, 19*(4), 3184-3197. doi:10.1128/mcb.19.4.3184

Smitt, W. W. S., Vermeulen, C. A., Vlak, J. M., Rozijn, T. H., & Molenaar, I. (1972). Electron microscopic autoradiographic study of RNA synthesis in yeast nucleus. *Experimental Cell Research, 70*(1), 140-144. doi:10.1016/0014-4827(72)90191-7

Steenwyk, J. L., & Rokas, A. (2018). Copy Number Variation in Fungi and Its Implications for Wine Yeast Genetic Diversity and Adaptation. *Front Microbiol, 9*, 288. doi:10.3389/fmicb.2018.00288

Stults, D. M., Killen, M. W., Pierce, H. H., & Pierce, A. J. (2008). Genomic architecture and inheritance of human ribosomal RNA gene clusters. *Genome Res, 18*(1), 13-18. doi:10.1101/gr.6858507

Thiry, M., & Lafontaine, D. L. (2005). Birth of a nucleolus: the evolution of nucleolar compartments. *Trends Cell Biol, 15*(4), 194-199. doi:10.1016/j.tcb.2005.02.007

Tiku, V., Jain, C., Raz, Y., Nakamura, S., Heestand, B., Liu, W., . . . Antebi, A. (2017). Small nucleoli are a cellular hallmark of longevity. *Nat Commun, 8*, 16083. doi:10.1038/ncomms16083

Trumtel, S., Leger-Silvestre, I., Gleizes, P. E., Teulieres, F., & Gas, N. (2000). Assembly and functional organization of the nucleolus: ultrastructural analysis of Saccharomyces cerevisiae mutants. *Mol Biol Cell, 11*(6), 2175-2189. doi:10.1091/mbc.11.6.2175

Tsekrekou, M., Stratigi, K., & Chatzinikolaou, G. (2017). The Nucleolus: In Genome Maintenance and Repair. *Int J Mol Sci, 18*(7). doi:10.3390/ijms18071411

Udugama, M., Sanij, E., Voon, H. P. J., Son, J., Hii, L., Henson, J. D., . . . Wong, L. H. (2018). Ribosomal DNA copy loss and repeat instability in ATRX-mutated cancers. *Proc Natl Acad Sci U S A, 115*(18), 4737-4742. doi:10.1073/pnas.1720391115

Valentin, G. (1836). *Repertorium für Anatomie und Physiologie* (Vol. 1). Berlin: Verlag von Veit und Comp.

Valentin, G. (1839). *Repertorium für Anatomie und Physiologie* (Vol. 4). Berlin: Verlag von Veit und Comp.

Vogelstein, B., & Kinzler, K. W. (1999). Digital PCR. *Proc Natl Acad Sci U S A, 96*(16), 9236-9241. doi:10.1073/pnas.96.16.9236

Wagner, R. (1835). Einige Bemerkungen und Fragen über das Keimbläschen (vesicular germinativa). *Müller's Archiv Anat Physiol Wissenschaft Med*, 373–377.

Wang, M., & Lemos, B. (2017). Ribosomal DNA copy number amplification and loss in human cancers is linked to tumor genetic context, nucleolus activity, and proliferation. *PLoS Genet, 13*(9), e1006994. doi:10.1371/journal.pgen.1006994

Warburton, P. E., Hasson, D., Guillem, F., Lescale, C., Jin, X., & Abrusan, G. (2008). Analysis of the largest tandemly repeated DNA families in the human genome. *BMC Genomics, 9*, 533. doi:10.1186/1471-2164-9-533

Warner, J. R. (1999). The economics of ribosome biosynthesis in yeast. *Trends Biochem Sci, 24*(11), 437-440.

Welch, J., Fogel, S., Buchman, C., & Karin, M. (1989). The CUP2 gene product regulates the expression of the CUP1 gene, coding for yeast metallothionein. *EMBO J, 8*(1), 255-260.

Wiesendanger, B., Lucchini, R., Koller, T., & Sogo, J. M. (1994). Replication fork barriers in the Xenopus rDNA. *Nucleic Acids Res, 22*(23), 5038-5046. doi:10.1093/nar/22.23.5038

Wood, V., Gwilliam, R., Rajandream, M. A., Lyne, M., Lyne, R., Stewart, A., . . . Nurse, P. (2002). The genome sequence of *Schizosaccharomyces pombe*. *Nature, 415*(6874), 871-880. doi:10.1038/nature724

Wyandt, H. E., Wilson, G. N., & Tonk, V. S. (2017). *Human Chromosome Variation: Heteromorphism, Polymorphism and Pathogenesis*.

Xu, B., Li, H., Perry, J. M., Singh, V. P., Unruh, J., Yu, Z., . . . Gerton, J. L. (2017). Ribosomal DNA copy number loss and sequence variation in cancer. *PLoS Genet, 13*(6), e1006771. doi:10.1371/journal.pgen.1006771

Yu, S., & Lemos, B. (2018). The long-range interaction map of ribosomal DNA arrays. *PLoS Genet, 14*(3), e1007258. doi:10.1371/journal.pgen.1007258

Zafiropoulos, A., Tsentelierou, E., Linardakis, M., Kafatos, A., & Spandidos, D. A. (2005). Preferential loss of 5S and 28S rDNA genes in human adipose tissue during ageing. *Int J Biochem Cell Biol, 37*(2), 409-415. doi:10.1016/j.biocel.2004.07.007

Zarrei, M., MacDonald, J. R., Merico, D., & Scherer, S. W. (2015). A copy number variation map of the human genome. *Nat Rev Genet, 16*(3), 172-183. doi:10.1038/nrg3871

Zhao, Y., Dominska, M., Petrova, A., Bagshaw, H., Kokoska, R. J., & Petes, T. D. (2017). Properties of Mitotic and Meiotic Recombination in the Tandemly-Repeated CUP1 Gene Cluster in the Yeast Saccharomyces cerevisiae. *Genetics, 206*(2), 785-800. doi:10.1534/genetics.117.201285

CHAPTER 2

DNA replication stress restricts ribosomal DNA copy number

Salim, D., Bradford, W. D., Freeland, A., Cady, G., Wang, J., Pruitt, S. C., & Gerton, J. L. (2017). DNA replication stress restricts ribosomal DNA copy number. *PLoS Genet, 13*(9), e1007006. doi:10.1371/journal.pgen.1007006

2 CHAPTER 2

2.1 List of Figures

2.2 List of Tables

2.3 Abstract

Ribosomal RNAs (rRNAs) in budding yeast are encoded by ~100-200 repeats of a 9.1kb sequence arranged in tandem on chromosome XII, the ribosomal DNA (rDNA) locus. Copy number of rDNA repeat units in eukaryotic cells is maintained far in excess of the requirement for ribosome biogenesis. Despite the importance of the repeats for both ribosomal and non-ribosomal functions, it is currently not known how “normal” copy number is determined or maintained. To identify essential genes involved in the maintenance of rDNA copy number, we developed a droplet digital PCR based assay to measure rDNA copy number in yeast and used it to screen the yeast conditional temperature-sensitive mutant collection of essential genes. Our screen revealed that low rDNA copy number is associated with compromised DNA replication. Further, subculturing yeast under two separate conditions of DNA replication stress selected for a contraction of the rDNA array independent of the replication fork blocking protein, Fob1. Interestingly, cells with a contracted array grew better than their counterparts with normal copy number under conditions of DNA replication stress. Our data indicate that DNA replication stresses select for a smaller rDNA array. We speculate that this liberates scarce replication factors for use by the rest of the genome, which in turn helps cells complete DNA replication and continue to propagate. Interestingly, tumors from mini chromosome maintenance 2 (MCM2)-deficient mice also show a loss of rDNA repeats. Our data suggest that a reduction in rDNA copy number may indicate a history of DNA replication stress, and that rDNA array size could serve as a diagnostic marker for replication stress. Taken together, these data begin to suggest the selective pressures that combine to yield a “normal” rDNA copy number.

2.4 Author summary

Eukaryotic genomes contain many copies of ribosomal DNA (rDNA) genes, usually far in excess of the requirement for cellular ribosome biogenesis. rDNA array size is highly variable, both within and across species. Although it is becoming increasingly evident that the rDNA locus serves extra-coding functions, and several pathways that contribute to maintenance of normal rDNA copy number have been discovered, the mechanisms that determine optimal rDNA array size in a cell remain unknown. Here we identify DNA replication stress as one factor that restricts rDNA copy number. We present evidence suggesting that DNA replication stress selects for cells with smaller rDNA arrays, and that contraction of the rDNA array provides a selective advantage to cells under conditions of DNA replication stress. Loss of rDNA copies may be a useful indicator of a history of replication stress, as observed in a mouse model for cancer.

2.5 Introduction

Ribosomal RNAs (rRNAs) in budding yeast are encoded by ~100-200 repeats of a 9.1kb sequence arranged in tandem on the long arm of chromosome XII, the ribosomal DNA (rDNA) locus. Each 9.1kb unit is composed of a region encoding a pre-35S rRNA that gives rise to 25S, 18S and 5.8S rRNAs (transcribed by RNA polymerase I), a small 5S rRNA (transcribed by RNA polymerase III), and two intergenic spacers (IGS1 and IGS2). IGS2 contains an rDNA origin of replication, rARS, and a cohesin associating sequence (CAR). IGS1 contains a replication fork barrier site (RFB) to which Fob1 binds; the binding of Fob1 inhibits DNA replication in the direction opposite to 35S rDNA transcription, preventing the head on collision of transcription and replication machinery (Kobayashi, 2003). IGS1 also contains a bi-directional RNA polymerase II promoter, E-pro, whose activity is normally suppressed by the binding of Sir2, an NAD-dependent histone deacetylase (Ide et al., 2013).

Two major features of the rDNA locus give it the unique potential to sense the environment and tune cellular response – high instability, and the wide range of copy number variation it can accommodate. Both features have been extensively studied, particularly in budding yeast, however molecular mechanisms of regulation of instability and copy number and their dependence on one another are not well understood. Because of the tandem nature of the repeats in the rDNA array, the high rates of transcription it needs to accommodate, and the difficulty of replicating repetitive sequences, the rDNA array is highly prone to double stranded breaks (DSBs) and homologous recombination, which leads to loss of repeats at a rate as high as 1 copy per cell division (Ganley & Kobayashi, 2011; Ide et al., 2010). In order to maintain rDNA copy number, the cell has at least two independent mechanisms to restore lost rDNA copies by amplification of repeats. These include unequal sister chromatid exchange, which occurs as a result of clearance of cohesin from rDNA by RNA polymerase II mediated transcription, and rolling circle replication (Ide et al., 2013; Kobayashi, 2006; Kobayashi et al., 1998).

Copy number of rDNA repeat units in eukaryotic cells is maintained far in excess of the requirement for ribosome biogenesis. In yeast, only about half of the ~150 rDNA repeats are actively transcribed to meet the translational needs of the cell (French et al., 2003). Although only about half of these repeats are actively transcribed, it is known that in budding yeast, reduced copy number makes cells more sensitive to DNA damage (Ide et al., 2010).The extra, untranscribed copies are thought to contribute to stability and integrity of the locus by acting as a 'foothold' for repair enzymes and for contacts with other regions of the genome (Cahyani et al., 2015; Ide et al., 2010; Mayan & Aragon, 2010; O'Sullivan et al., 2009). Human population genome sequencing data analysis has revealed correlations between rDNA copy number and the expression of several genes encoding chromatin-modifying proteins (Gibbons et al., 2014), further supporting the idea that the effects of rDNA copy number go well beyond rRNA production for ribosome biogenesis. These could involve, for example, differential recruitment of chromatin-modifying proteins to rDNA arrays with variable copy number. Disproportional binding of chromatin-modifying proteins to the rDNA locus could result in altered concentrations of these proteins throughout the rest of the genome, affecting chromatin environments and transcription genome-wide (Gibbons et al., 2015; Michel, 2005; Paredes et al., 2011).

The hypervariablity of the rDNA locus combined with its ability to titrate various factors gives it the potential to act as a sensor of various conditions or stresses and in response, be a rapid and reversible source of variation for adaptation at the cellular and organismal levels. Several genetic factors have been identified that affect copy number. Of these, some, for example, Rtt109, a histone acetyltransferase, regulate rolling-circle replication of rDNA repeats (Ide et al., 2013), and others, like Rrn10, may act by regulating RNA polymerase I transcription (Oakes et al., 1999). On the other hand, some proteins like Sir2 and Fob1 are part of the pathway that senses loss of rDNA repeats and feeds back into regulation of recombination and replication, thereby ensuring that the array does not contract beyond a certain size (Kobayashi et al., 1998; Kobayashi et al., 2004). Although the advantages of having additional copies of rDNA repeats, and

the existence of mechanisms to regulate the amplification of rDNA repeats are becoming evident, very few studies have focused on the factors that determine “normal” copy number. Ide et al. (Ide et al., 2007) first reported that the rDNA array is hypersensitive to perturbations in initiation of DNA replication, and that rDNA array size could modulate cellular response to such perturbations. A more recent study by Kwan et al. (Kwan et al., 2013) also showed that rARS activity affects rDNA copy number as well as genome-wide DNA replication dynamics. Although these studies support the idea that the rDNA array could act as a sensor and source of adaptive response to stress, identification of the mechanisms that determine normal rDNA array size requires an unbiased screen for factors that affect rDNA copy number.

To measure rDNA copy number in an accurate manner that is easily adaptable to high-throughput methods, we developed a droplet digital PCR (ddPCR) based assay to measure rDNA copy number in yeast and used it to identify essential genes involved in the maintenance of rDNA copy number. We screened the 787 mutants of the yeast conditional temperature-sensitive (ts) mutant collection of essential genes (Li et al., 2011) for mutants with altered rDNA copy number. Our data revealed that low rDNA copy number is associated with compromised DNA replication. Consistent with this, we found that subculturing yeast under two separate conditions of DNA replication stress causes a contraction of the rDNA array independent of the replication fork blocking protein, Fob1. Additionally, we show that a smaller rDNA array enables cells to complete DNA replication in a timely manner, likely by freeing scarce replication factors for use by the rest of the genome, thereby allowing cells to survive and adapt to DNA replication stress. Finally, the loss of rDNA repeats in thymic tumors derived from mice with reduced expression of mini chromosome maintenance 2 (MCM2), a key component of the MCM2-7 DNA replicative helicase, also suggests that rDNA copy number may be used as an indicator of past stress, and that past replication stress may be diagnosed by a contracted rDNA array. Taken together, these data begin to suggest the selective pressures that combine to yield a “normal” rDNA copy number.

2.6 Results

2.6.1 Development and validation of a ddPCR assay to measure rDNA copy number in yeast

Rapid and accurate high-throughput characterization of the genetic determinants of rDNA copy number has thus far been impeded by the lack of simple, sensitive assays to measure copy number. Previous methods of determining rDNA copy number involved measuring changes in the size of chromosome XII by pulsed-field gel electrophoresis (PFGE) and subsequent Southern blotting (Saka et al., 2016). More recently, qPCR has been used to measure copy number (Bose et al., 2012; Jack et al., 2015). However, adapting qPCR to high-throughput experiments is difficult because of the requirement for a standard curve for each experiment, and its ability to detect only relatively large changes in copy number. ddPCR is a DNA molecule-counting technique that directly counts the absolute number of DNA molecules in a sample. In ddPCR, targets of interest are partitioned into ~20,000 nano-droplets and amplified to endpoint with TaqMan probes as in qPCR. The concentrations of the targets are then determined by counting the number of fluorescently positive and negative droplets in the sample. Thus, the fluorescence signal in a qPCR is converted from an analog signal into a digital one in ddPCR, eliminating the need for standard curves and allowing the determination of target copy number on an absolute scale with high precision (Hindson et al., 2011). In our assay, primers and fluorescent probes specific to the 25S coding sequence of the rDNA repeat, and to a stable, essential, single copy control gene, *TUB1* were designed (Figure 2.1A). Absolute copy numbers of each target in the sample are obtained by a duplexed ddPCR reaction, and rDNA copy number per haploid genome calculated from their ratio.

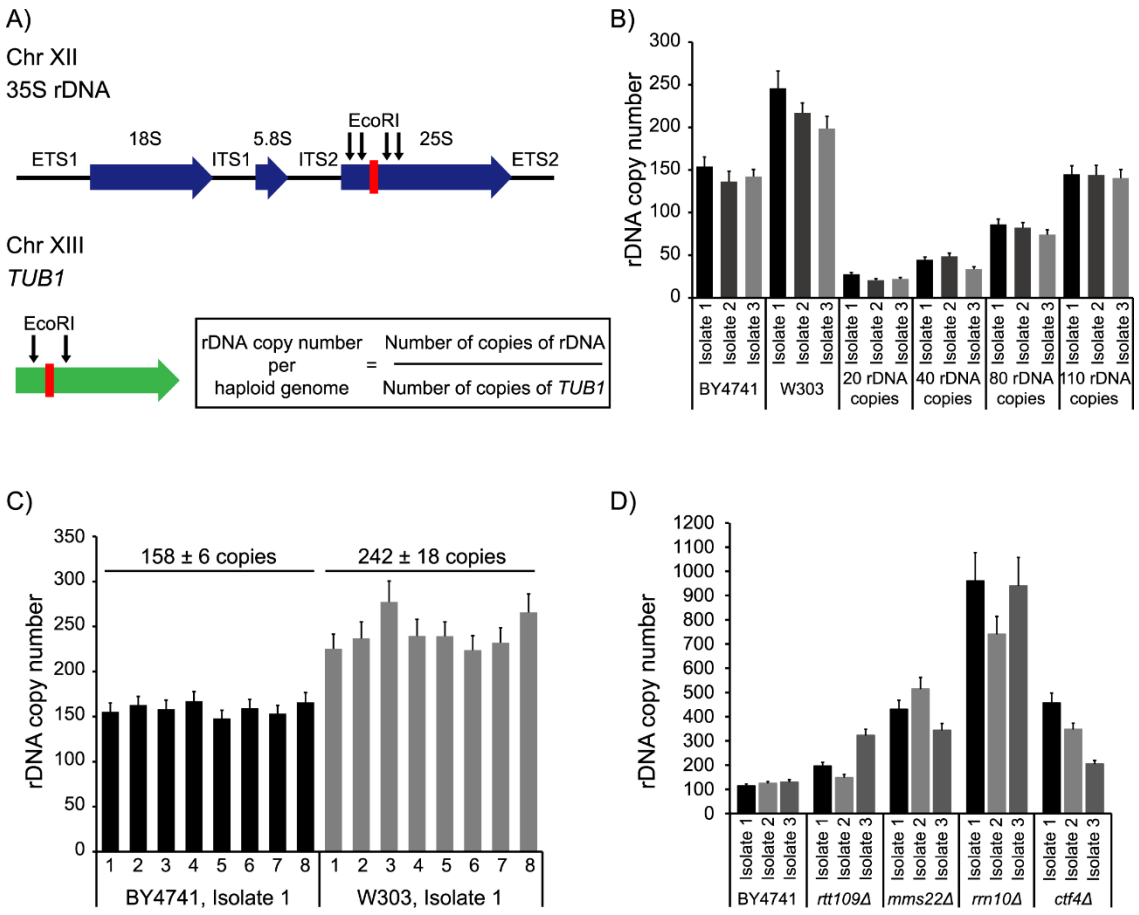

Figure 2.1. Design and validation of a ddPCR assay for rDNA copy number measurement. (A) Targets (red bars) within the rDNA and single copy reference (*TUB1*) loci in yeast. (B) rDNA copy number in 3 independent isolates each of 2 different wild-type laboratory yeast strains, BY4741 and W303, and 4 isogenic strains with varying rDNA copy number generated by Ide et al. (Ide et al., 2010). (C) rDNA copy number in 8 technical replicates each of BY4741 and W303. (D) rDNA copy number in 3 independent isolates each of mutants with expanded rDNA arrays. Error bars represent standard deviation for each individual reaction.

The assay was validated by measuring rDNA copy number in multiple independent isolates of two wild-type laboratory yeast strains, BY4741 and W303, and strains with 20-110 rDNA copies, in which rDNA copy number has been previously measured using PFGE (Ide et al., 2010). BY4741 has ~150 rDNA copies, and W303 has ~250 rDNA copies, and the strains with 20-110 rDNA copies were also easily distinguishable (Figure 2.1B). To estimate the range of technical error, we measured rDNA copy number in 8 technical replicates each of both wild-type strains, BY4741 and W303. In our assay, technical error is within 10%, and often within 5% (Figure 2.1C). Since each reaction is partitioned into ~20,000 droplets, technical error in an individual reaction can be

calculated based on the droplet data from that well. Technical error in ddPCR comes mainly from errors due to sub-sampling, and partitioning into droplets. In a good assay, this total technical error should be close to the standard error of the mean, and in our assay, closely matches the error from true technical replicates (Figure 2.1C). Therefore, we use the errors calculated for each individual reaction as an estimate of technical error, which eliminates the requirement for multiple technical replicates per sample. Biological replicates, however, are critical due to natural biological variability in rDNA copy number. Finally, we also used our ddPCR assay to confirm an increased rDNA copy number in 3 independent isolates each of *rtt109*Δ, *mms22*Δ, *rrn10*Δ, and *ctf4*Δ strains, which were previously reported to have expanded rDNA arrays (Ide et al., 2013) (Figure 2.1D).

2.6.2 Identification of essential genes involved in maintaining rDNA copy number

To screen for essential genes involved in the maintenance of rDNA copy number, we used the ddPCR assay to measure rDNA copy number in high-throughput format in the yeast ts mutant collection of essential genes (Li et al., 2011). This collection contains 787 ts strains, covering 497 (~45%) of the 1,101 essential yeast genes, with ~30% of the genes represented by multiple alleles. The mutants, along with wild-type controls, were grown at the permissive temperature (room temperature), and then shifted to the restrictive temperature (37°C) for 3 hours. Following this, genomic DNA was isolated for ddPCR. A distribution of rDNA copy number across the ~1200 strains screened is shown in Figure 2.2A (Appendix A.1). The mean rDNA copy number of wild-type strains was 95 ± 12.175. Mutants with significantly higher or lower rDNA copy number were identified based on thresholds set by variation in rDNA copy number in wild-type controls (Figure 2.2A). Of the ~1200 strains screened, 288 had significantly altered copy number ($p < 0.05$). The top 89 hits in each category, low and high copy number, were further validated by measuring rDNA copy number in two additional biological replicates

(Appendices A.2 and A.3). These top hits were also tested for aneuploidies in chromosomes XII and XIII, on which the ddPCR targets reside (Appendices A.2 and A.3). Only 5 hits, YDR311W (*tfb1-1*), YGR002C (*swc4-4*), YIL126W (*sth1-2*), and YLR186W (*emg1-1*), and YNR053C (*nog2-1*) had a ratio of Chromosome XII to Chromosome XIII that may be representative of aneuploidies that could affect rDNA copy number measurements, and these mutants were excluded from all further analyses. Additionally, rDNA copy number was also measured at the permissive growth temperature to ensure that the restrictive temperature itself did not confound our results. In fact, we found that the hits with altered rDNA copy number after growth at the restrictive temperature also had similarly altered copy number even at the permissive temperature (Appendices A.2 and A.3), suggesting that the effects on rDNA array size are likely a result of prolonged propagation in the mutant background.

Gene Ontology (GO) enrichment analyses revealed a striking difference in the pathways associated with low or high copy number. Most of the hits with high copy number were mutants in transcription and RNA processing genes, however none of these GO terms were significantly enriched in our hits relative to their background frequencies in the ts mutant collection. On the other hand, the hits with low rDNA copy number were significantly enriched for DNA replication mutants ($p<0.001$) (Figure 2.2B). Further examination of the “low copy number” hits revealed that the most significantly enriched hits were mutants in subunits of DNA polymerases α, δ, and ε, and various replication initiation complexes, such as the Mini chromosome maintenance 2-7 (Mcm2-7) complex, the Origin Recognition Complex (ORC), and the Cdc7-Dbf4 complex. The “low copy number” hits were also significantly enriched for mutants in subunits of the cohesin complex, well known for its multiple roles in maintaining chromosome integrity, including DNA replication and repair (Lu et al., 2014; Nasmyth & Haering, 2009; Villa et al., 2016). Therefore, this data suggested that compromised DNA replication may select for contraction of the rDNA array.

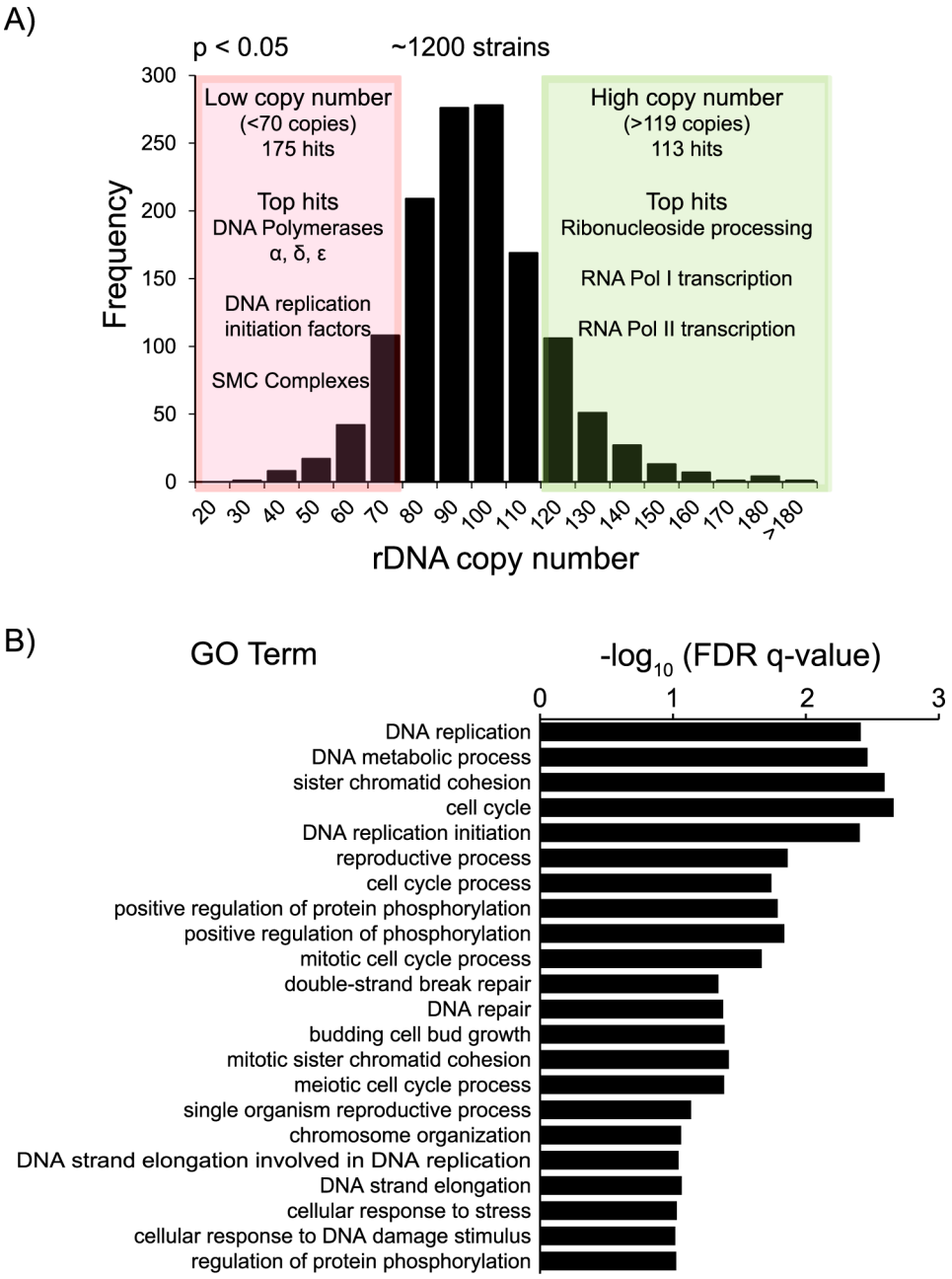

Figure 2.2. Screen for essential genes that maintain rDNA copy number. (A) Distribution of rDNA copy number across the yeast ts mutant collection. 175 and 113 strains had significantly lower (<70 copies) and higher copy number (>119 copies) respectively ($p<0.05$). (B) $-\log_{10}$ transformed FDR q-values for significantly enriched ($p<0.001$) GO terms (sorted in order of increasing p-values from top to bottom) in low copy number hits.

2.6.3 DNA replication stresses cause contraction of the rDNA array independent of Fob1

Recently Kwan et al. (2016) reported that unsolicited, and stably maintained rDNA copy number variations resulting from exposure to lithium acetate were prevalent in yeast mutant collections generated by standard transformation protocols (Kwan et al., 2016). Although it is still unclear whether exposure to lithium acetate induces unsolicited rDNA copy number variations or simply selects for pre-existing copy number variations, it is possible that the copy number changes in at least a subset of our hits are a result of transformation protocols, and unrelated to the gene mutation. As a preliminary validation of the correlation between the gene mutation and the change in rDNA copy number in our hits, we analyzed the copy number changes in mutant strains of genes with multiple ts alleles, or multiple isolates of the same ts allele. We found that for most genes with validated rDNA copy number changes, a majority of the multiple mutant strains had a similar alteration in rDNA copy number (Appendices A.2 and A.3). This is a strong indication that at least for a subset of genes, the mutation itself is likely responsible for the altered rDNA array size. To further validate the findings from our screen, we subcultured yeast cells under two separate conditions of DNA replication stress by a) plating them on medium containing 150mM hydroxyurea (HU), a ribonucleotide reductase inhibitor, or b) depleting Pol1, the largest subunit of DNA polymerase α, using a diploid strain homozygous for the *GAL-POL1* allele, containing galactose inducible Pol1 (Casper et al., 2008). Both of these conditions caused a contraction of the rDNA array after 50-75 generations, independent of Fob1 (Figure 2.3).

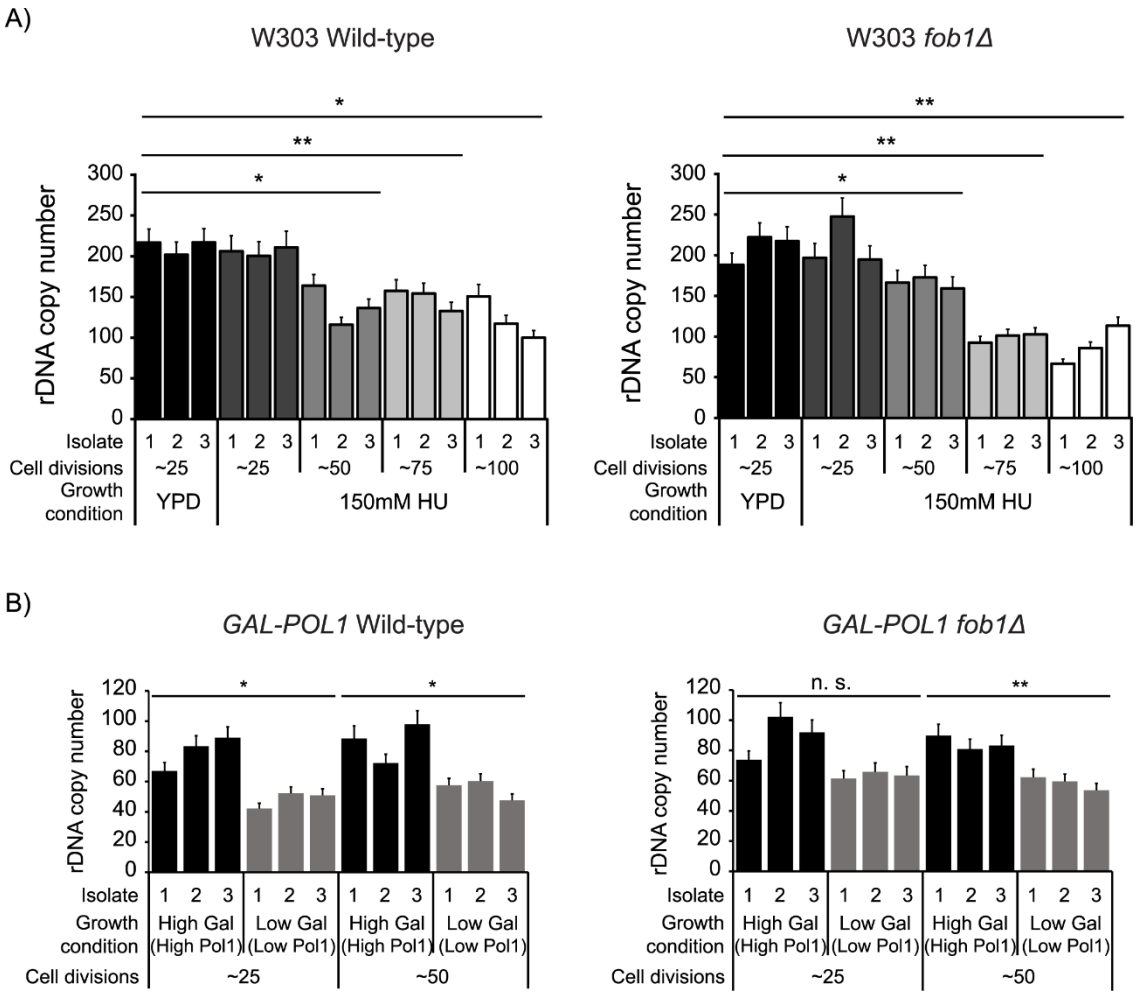

Figure 2.3. DNA replication stresses cause a contraction of the rDNA array independent of Fob1. rDNA copy number in A) WT or *fob1*Δ W303 cells subcultured in 150mM hydroxyurea (HU) for ~100 generations, and B) WT or *fob1*Δ strains with *POL1* driven by galactose inducible *GAL1-10* promoter subcultured in medium containing high or low galactose for ~50 generations. After every 25 generations, 3 independent isolates were used to measure rDNA copy number by ddPCR. Error bars represent standard deviation for each individual reaction. Statistical significance was calculated using a standard 2 tailed t-test. * - $p<0.05$, ** - $p<0.01$, n. s. – not significant.

Additionally, *rnr1*Δ mutants lacking Rnr1, the major isoform of the large subunit of ribonucleotide-diphosphate reductase, also have contracted rDNA arrays (Figure 2.4). These findings led us to hypothesize that since the rDNA is one of the most unstable and hypervariable loci, and difficult to replicate, DNA replication stresses select for smaller rDNA arrays, perhaps because cells with lower copy number can complete DNA replication in a timely manner and continue to propagate. This raised two main questions – 1) What are the consequences of having a contracted array? 2) Does a smaller rDNA array help cells survive and adapt to DNA replication stress, and if so, how?

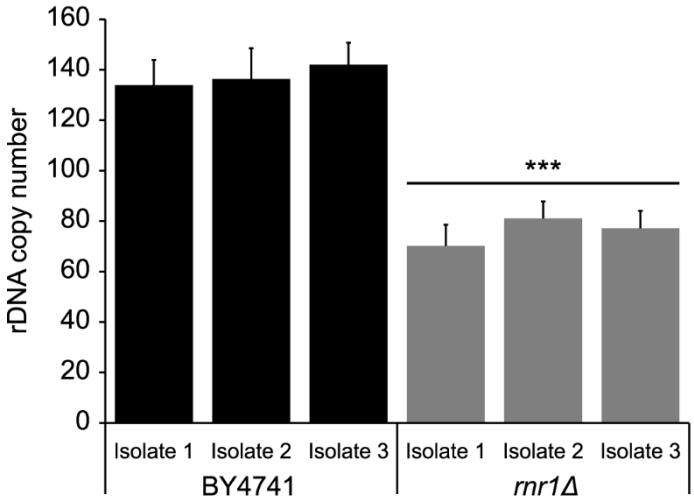

Figure 2.4. rDNA copy number in *rnr1*Δ strains. rDNA copy number in 3 independent isolates each of BY4741 and *rnr1*Δ strains. Error bars represent standard deviation for each individual reaction. Statistical significance was calculated using a standard 2 tailed t-test. *** - p<0.001.

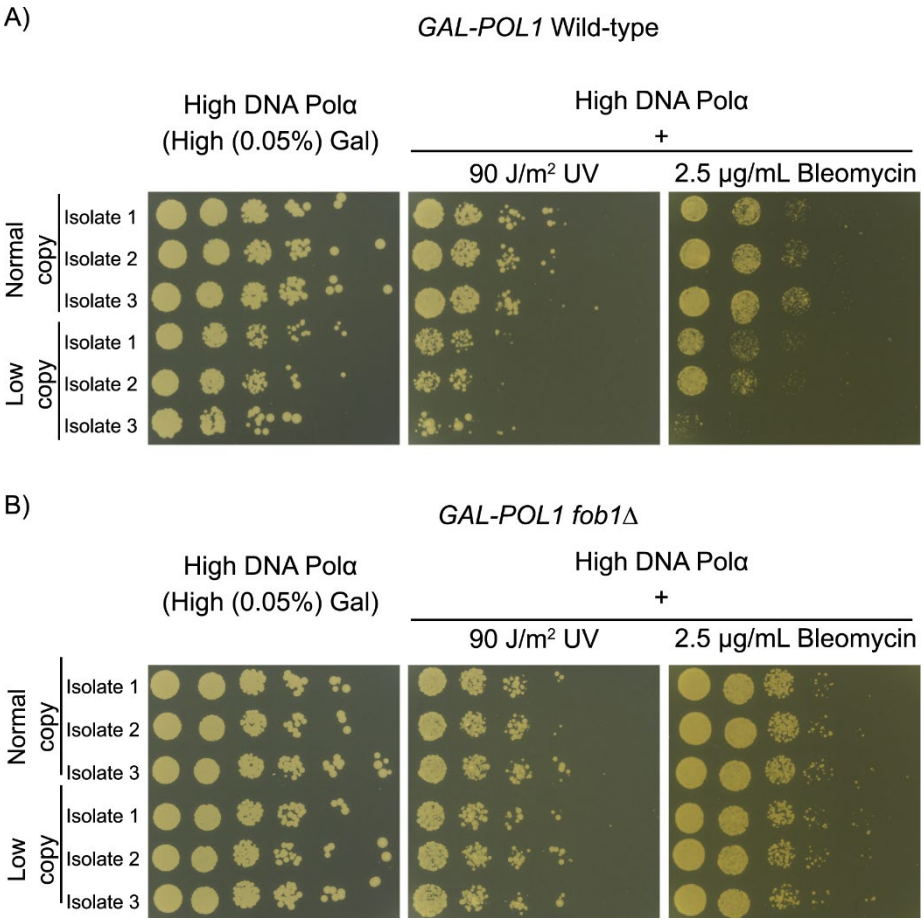

Figure 2.5. Low rDNA copy number makes cells sensitive to DNA damage. A) Wild-type or B) *fob1*Δ *GAL-POL1* cells were subcultured in medium containing high or low levels of galactose for ~50 generations to generate 3 independent isolates each with normal or low rDNA copy number (Table 2.1). 5-fold serial dilutions of these isolates were spotted on to high galactose medium containing bleomycin, or spotted on to high galactose medium followed by irradiation with UV.

To address these questions, we used the strain with galactose inducible Pol1 to generate cells with normal or low rDNA copy number as in Figure 2.3B by growing the strain in medium containing either high or low galactose (high or low DNA polymerase α) respectively. Given the isolate to isolate variability in rDNA copy number, we generated and used 3 independent isolates from each condition for all our studies. Ide et al. (Ide et al., 2010) reported that low rDNA copy number makes cells more sensitive to DNA damaging agents, such as UV and methyl methanesulfonate (MMS). We found that wild-type, but not *fob1*Δ isolates with low rDNA copy number generated by Pol1 depletion also exhibited mild sensitivity to bleomycin and UV (Figure 2.5). Notably, both wild-type and *fob1*Δ isolates with low rDNA copy number grew better than those with normal copy number under conditions of DNA polymerase α depletion (Figure 2.6A). However, selection under altered levels of DNA polymerases is known to induce general genome instability, and often results in mutations that restore normal expression levels (Song et al., 2014; Zheng et al., 2016). Therefore, we wanted to ensure that the survival of the low copy number isolates generated by selection under low levels of DNA polymerase α was not due to chromosomal abnormalities or other mutations which enable expression of normal levels of Pol1. Song et al. (Song et al., 2014) showed that trisomy of Chromosome XIV (on which *POL1* resides) is very rare after 50-75 generations of selection under low levels of DNA polymerase α. Additionally, we tested for deletions in the *GAL1-10* promoter in the normal and low copy number isolates by a PCR-based strategy (Zheng et al., 2016), and found that the *GAL1-10* promoter was intact after 50-75 generations of selection (Figure 2.7). Additionally, strains with low rDNA copy number (20-110 rDNA copies, (Ide et al., 2010)) are also less sensitive to HU than corresponding wild-type cells (~200-250 rDNA copies) (Figure 2.6B) supporting the hypothesis that low rDNA copy number is advantageous to cells under conditions of DNA replication stress.

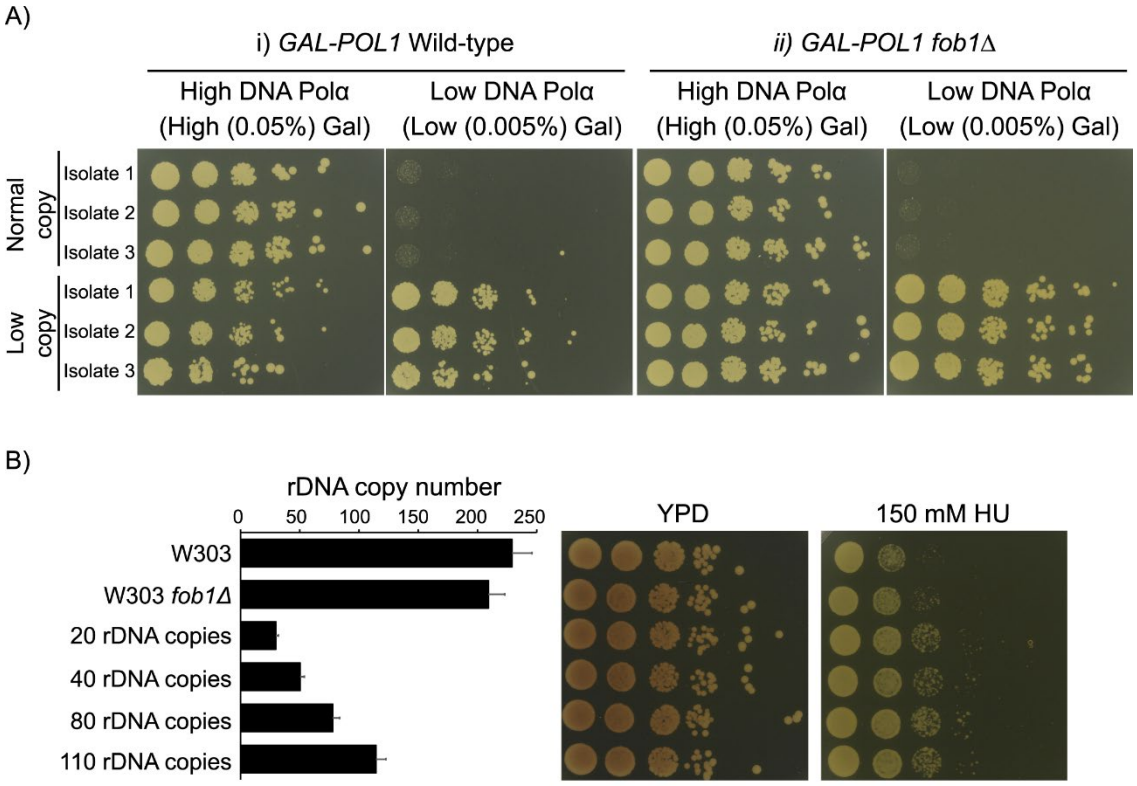

Figure 2.6. Low rDNA copy number confers advantage under DNA replication stress. (A) 3 independent isolates each with normal or low rDNA copy number were generated by subcultuing wild-type or *fob1*Δ *GAL-POL1* cells in medium containing high or low galactose (high or low levels of Pol1 respectively) for ~50-75 generations (Table 2.1) and 5-fold serial dilutions spotted on to medium with DNA replication stress (low Pol1). (B) 10-fold serial dilutions of wild-type and *fob1*Δ cells (~200-250 rDNA copies) along with cells having 20-110 rDNA copies (Ide et al., 2010) were spotted on medium containing hydroxyurea (HU). rDNA copy number was confirmed by ddPCR. Error bars represent standard deviation for each individual reaction.

A)

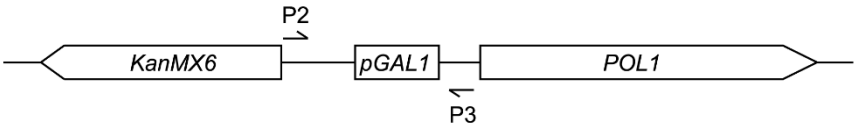

B)

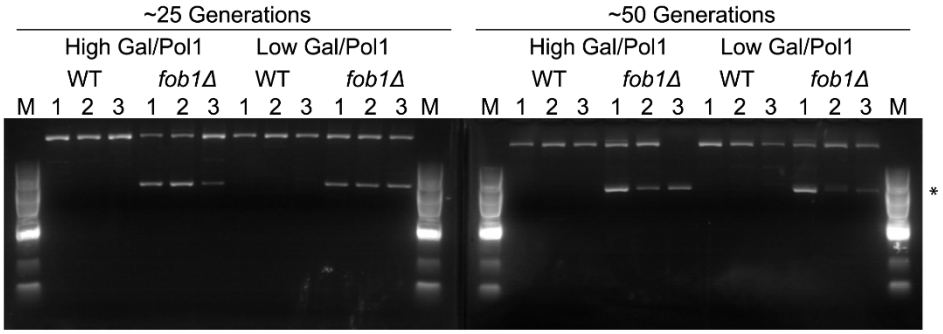

Figure 2.7. *GAL1-10* promoter is intact after 50-75 generations of selection in altered levels of Pol1. A) PCR scheme and relative positions of primers used (Song et al., 2014). B) Wild-type or *fob1*Δ *GAL-POL1* cells were subcultured in either high/low galactose. After ~50 generations, 3 independent isolates from each condition were used to isolate genomic DNA for PCR. PCR products were run on a 1% agarose gel. M – 100bp marker. * - Non-specific band.

2.6.4 Contraction of the rDNA array enables timely completion of DNA replication and cell cycle progression

To further characterize how low rDNA copy number helps cells survive DNA replication stress, we measured the fraction of cells in S-phase in asynchronous cultures of both low and normal copy number isolates under conditions of both high and low levels of DNA polymerase α by flow cytometry. We found that with low levels of DNA polymerase α, the high copy number isolates show a higher fraction of cells in S-phase compared to their low copy number counterparts (Figures 2.8A-B, 2.9A-B). This shows that under conditions of DNA replication stress, cells with smaller rDNA arrays are able to proceed through S-phase and complete DNA replication in a timely manner, allowing them to continue to propagate.

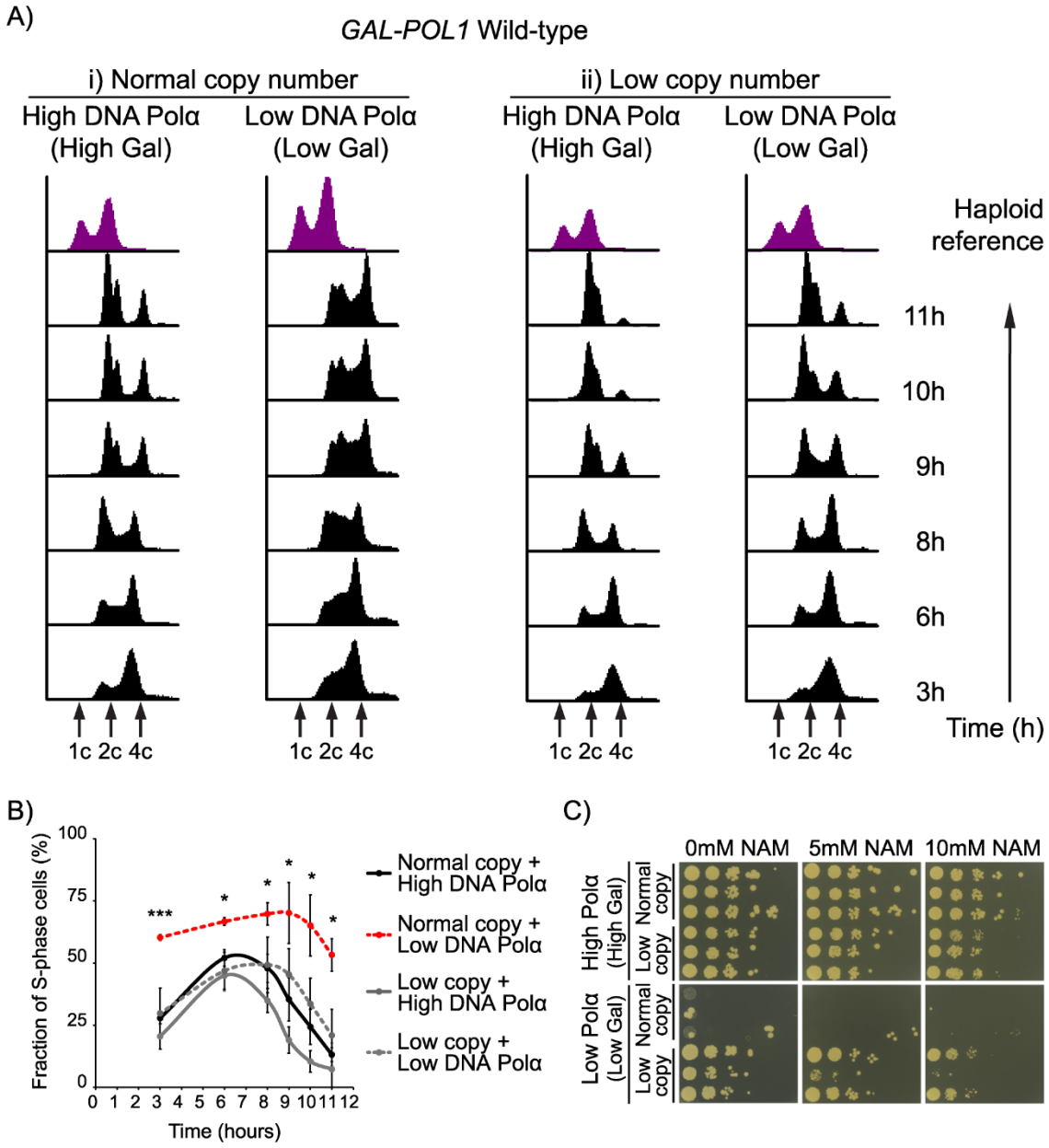

Figure 2.8. Contraction of the rDNA array promotes timely completion of DNA replication and cell cycle progression. Wild-type *GAL-POL1* cells were subcultured in medium containing high or low levels of galactose for ~75 generations to generate 3 independent isolates each with normal or low rDNA copy number (Table 2.1). (A) Representative DNA content profiles over time are shown for asynchronous cultures of isolates with normal (i) and low (ii) rDNA copy number following inoculation into the indicated medium which determines high or low levels of DNA polymerase α. (B) Fraction of cells in S-phase in each of the 4 conditions in (A). Error bars indicate standard deviation based on 3 independent isolates. Statistical significance of differences between fraction of cells in S-phase in high and low levels of DNA polymerase α was calculated using a standard 2-tailed t-test. * - $p<0.05$, *** - $p<0.001$. (C) Increased rARS firing in nicotinamide exacerbates growth defects under conditions of DNA replication stress.

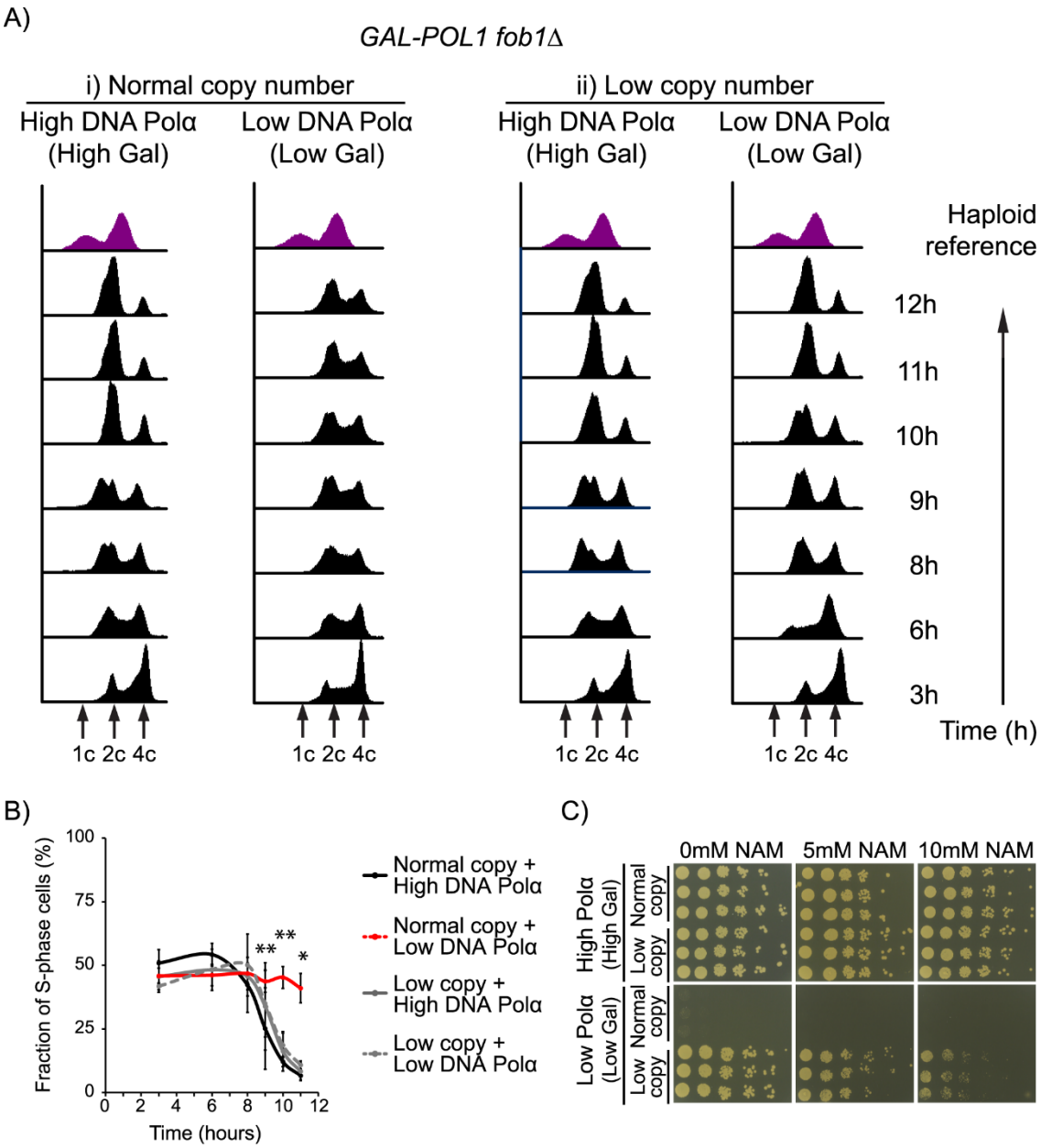

Figure 2.9. Contraction of the rDNA array promotes timely completion of DNA replication and cell cycle progression in *fob1*Δ strains. *fob1*Δ *GAL-POL1* cells were subcultured in medium containing high or low levels of galactose for ~50 generations to generate 3 independent isolates each with normal or low rDNA copy number (Table 2.1). (A) Representative DNA content profiles over time of asynchronous cultures of *fob1*Δ isolates with normal (i) and low (ii) rDNA copy number following inoculation into the indicated medium which determines high or low levels of DNA polymerase α. (B) Fraction of cells in S-phase in each of the 4 conditions in (A). Error bars indicate standard deviation based on 3 independent isolates. Statistical significance of differences between fraction of cells in S-phase in high and low levels of DNA polymerase α was calculated using a standard 2-tailed t-test. * - $p<0.05$, ** - $p<0.01$. (C) Increased rARS firing in nicotinamide exacerbates growth defects under conditions of DNA replication stress.

To test the role of the rDNA array in this rescue, we grew these isolates in high/low galactose (high/low levels of DNA polymerase α respectively) medium containing nicotinamide (NAM), a Sir2 inhibitor. Sir2 represses rARS firing and Sir2 inhibition by NAM will cause more rARS firing (Pasero et al., 2002). One possible effect of increased rARS firing is the titration of replication factors away from the rest of the genome, which could make the normal copy number strain grow poorly, even with high levels of DNA polymerase α. Another consequence of increased rARS firing in NAM is that the distance each replication fork has to travel in the rDNA will be shorter, which might instead rescue the normal copy number strain with low levels of DNA polymerase α. We found that NAM caused the isolates with normal rDNA copy number to grow poorly with low levels of DNA polymerase α (Figures 2.8C, 2.9C). We also observed that the isolates with low rDNA copy number with low levels of DNA polymerase α exhibited mild sensitivity to higher concentrations of NAM (Figures 2.8C, 2.9C). Since higher concentrations of NAM could also inhibit other sirtuins, including Hst3 and Hst4, which are known to participate in DNA replication (Irene et al., 2016), it is possible that the phenotypes observed in NAM are due to a combination of increased rARS firing and additional DNA replication stress imposed by the inhibition of Hst3 and Hst4. Altogether, this suggests that titration of already scarce replication factors by the rDNA is the primary issue faced by the normal copy isolates under conditions of DNA replication stress.

2.6.5 DNA replication stress may be diagnosed by rDNA array size

Our data show that in yeast, under conditions of DNA replication stresses, a smaller rDNA array provides a selective advantage to cells. Since persistent DNA replication stress resulting from mutations that affect DNA replication machinery have been associated with both cancer (Gaillard et al., 2015) and human developmental syndromes (Bicknell et al., 2011), we wondered whether these human conditions would also be associated with genomes containing contracted rDNA arrays. To explore this, we used a previously established MCM2-deficient mouse model of cancer, generated

by integration of a tamoxifen-inducible form of Cre recombinase downstream of the *Mcm2* coding sequence and expression via an internal ribosome entry site (IRES) (Pruitt et al., 2007). In this model, homozygous *Mcm2*$^{IRES\text{-}CreERT2/IRES\text{-}CreERT2}$ (MCM2-deficient) embryos or mouse embryonic fibroblasts have reduced MCM2 expression, approximately one-third of wild-type levels. Although these mice develop normally, MCM2-deficiency results in stem cell deficiencies in multiple tissues, and ultimately, cancer, primarily lymphomas (Pruitt et al., 2007). Moreover, it was also recently reported that the 45S rDNA repeats accumulate high levels of DNA damage in the form of DSBs, both in these MCM2-deficient mice (Pruitt et al., 2017), as well as in mouse hematopoietic stem cells (HSCs) with reduced MCM expression (Flach et al., 2014). Therefore, we used array-based Comparative Genome Hybridization (aCGH) and Next Generation Sequencing (NGS) to study rDNA copy number in thymic lymphoblastic lymphoma (TLL) tumors derived from MCM2-deficient mice. We performed aCGH on 8 TLL tumors derived from *Mcm2*$^{IRES\text{-}CreERT2/IRES\text{-}CreERT2}$ mice on the 129/Sv (6 of 8 tumors) or 129/Sv x C57Bl/6 F1 (2 of 8 tumors) genetic backgrounds using the NimbleGen 720K whole-genome tiling arrays (Rusiniak et al., 2012). All samples were assessed relative to DNA from non-tumorous tissue derived from wild-type littermates of the same genetic background. We also performed NGS on 2 TLL tumor samples derived from *Mcm2*$^{IRES\text{-}CreERT2/IRES\text{-}CreERT2}$ mice on a 129/Sv x C57Bl/6 F1 genetic background and control thymic DNA samples from 2 wild-type littermates. Comparison of aCGH probe $\log_2$ ratios for TLL tumor DNA and DNA from 3 clonally derived neural stem cell cultures along with the NGS data confirmed a loss of approximately half of the 45S rDNA repeats in MCM2-deficient tumors (Figure 2.10). Although the loss of rDNA repeats may simply be a byproduct of tumorigenesis, and not a direct consequence of MCM2 deficiency, these data suggest that under conditions of genotoxic stress, the rDNA may be highly susceptible to DSBs, and while both gain and loss of rDNA repeats may occur frequently in the face of the DNA damage, losses may be selected for under conditions of DNA replication stress. This suggests that rDNA array size may be used as a molecular diagnostic marker for past DNA replication stress.

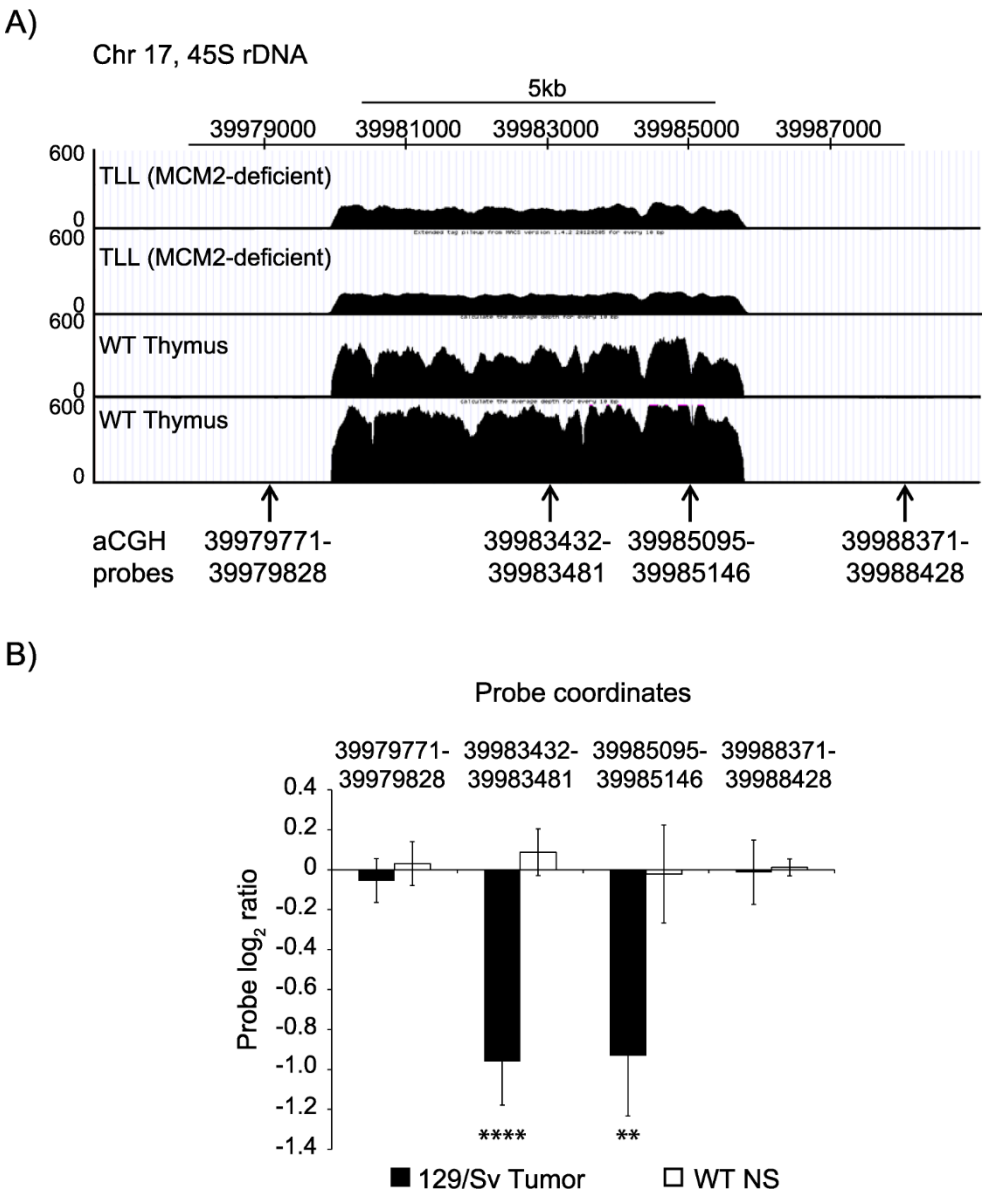

Figure 2.10. 45S rDNA repeats are lost in T-lymphocytic leukemia (TLL) tumors of MCM2-deficient mice. (A) Sequence tag densities (normalized for number of mapped reads) over a portion of the 45S rDNA from 2 TLL tumors arising in *Mcm2*$^{IRES\text{-}CreERT2/IRES\text{-}CreERT2}$ mice on a 129/Sv x C57Bl/6 F1 genetic background and 2 thymuses from wild-type littermates (Kunnev et al., 2015). (B) Average aCGH log_2 values for probes from (A) for 8 TLL tumors arising in *Mcm2*$^{IRES\text{-}CreERT2/IRES\text{-}CreERT2}$ 129/Sv mice (Rusiniak et al., 2012) compared to average aCGH log_2 values for the same probes from 3 clonally derived neural stem cell cultures from wild-type littermates (WT NS). Error bars indicate standard deviation. Statistical significance (129/Sv tumor vs. WT NS) was calculated using a standard 2 tailed t-test. ** - $p<0.01$, **** - $p<0.0001$.

2.7 Discussion

The rDNA array is the most unstable, and hypervariable genetic locus in the yeast genome. It is the most highly transcribed genomic locus, difficult to replicate owing to its repetitive nature, and comprises over 60% of chromosome XII, and ~10% of the yeast genome. This unique locus, therefore, has the potential to act as the “canary in the coalmine”, being particularly sensitive to stresses that disrupt genome integrity, and acting as a source of cellular adaptation, relatively simply, through variation in array size. In wild-type yeast cells, rDNA repeat copy number is maintained at ~150 per haploid cell. However, owing to the tandem arrangement of the repeats, and the associated instability, repeats are lost at a relatively high rate of up to ~1 per cell division (Ganley & Kobayashi, 2011). Therefore, there must be mechanisms in place to a) sense rDNA copy number at each cell division, and b) trigger an appropriate response so that the array size can be maintained at wild-type levels. Studies so far have revealed many pathways that contribute to the maintenance of the rDNA locus, but the fundamental question of what determines normal repeat copy number remains unanswered.

Our screen has identified essential proteins involved in maintenance of the rDNA locus based on screening 45% of essential yeast genes; in the future, we can extend this to nearly 75% by screening additional mutant collections (Ben-Aroya et al., 2008). Our data show that DNA replication stresses select for cells that have a smaller rDNA array, and a smaller array helps cells adapt to replication stress. Data from several studies support our findings – i) contraction of the rDNA array can rescue yeast temperature-sensitive mutants of the Origin Recognition Complex, the key replication initiation complex (Ide et al., 2007), ii) a large deletion of the rDNA array can rescue the synthetic growth defects of *rif1*Δ cells lacking either MRX or Ctf4-Mms22 activity (Shyian et al., 2016), iii) a polymorphism in the rARS that results in a weakly replicating rDNA array causes a contraction of the array and promotes DNA replication in the rest of the genome (Kwan et al., 2013), and iv) coordination of DNA replication and recombination at the rDNA is critical to maintain the integrity and size of the rDNA array (Ii, 2007). Our

data supports the previously reported role of extra, untranscribed rDNA repeats in protecting cells from DNA damaging agents (Ide et al., 2010). In addition, our data suggests that while extra, untranscribed rDNA repeats are essential for allowing co-transcriptional DNA damage repair, they become detrimental to cells under conditions of DNA replication stress.

Each rDNA repeat unit consists of a DNA replication origin, the rARS, and the rDNA array represents roughly one-third of all replication origins in the yeast genome (Foss et al., 2017). At any given time in S-phase, only a fraction of licensed origins are fired, and this is thought to be achieved by limiting the pool of initiation factors available (Mantiero et al., 2011). Recently, Foss et al. (Foss et al., 2017) presented evidence to support the long standing idea that, in yeast, repetitive rDNA compete for origin firing with unique genomic sequences (in yeast, the rest of the genome), and tipping the balance in favor of repetitive rDNA can lead to replication gaps, or underreplicated regions, throughout the rest of the genome. Our data also show that under conditions of DNA replication stress, cells with a smaller rDNA array are able to complete DNA replication and proceed through the cell cycle. This, combined with the growth defects of the cells with normal rDNA copy number in NAM, is in agreement with Foss et al.'s observation that replication gaps produced by deletion of *SIR2* can be suppressed by decreased origin activity within the rDNA. Taken together, these data suggest that the repetitive rDNA array may be particularly sensitive to DNA replication stresses, and while DNA damage repair could result in a gain or loss of repeats, the loss of repeats provides a selective advantage by liberating scarce DNA replication factors for use by the rest of the genome.

Finally, we speculate that the size of the rDNA array may be used as an indicator of past stress. This has interesting implications for human disease. The link between persistent DNA replication stress and tumorigenesis is well established (Gaillard et al., 2015). Additionally, mutations in key components involved in initiation of DNA replication, such as ORC1, ORC4, ORC6, CDT1, CDT6, and CDC45, have been reported to be the cause of Meier-Gorlin syndrome, a primordial dwarfism syndrome

(Bicknell et al., 2011; Fenwick et al., 2016). Our data suggest that these human conditions will be associated with genomes containing contracted 45S rDNA arrays. Xu et al.(Xu et al., 2017) and Wang and Lemos (Wang & Lemos, 2017) recently showed through bioinformatic analyses of whole genome sequencing data from various cancers that 45S arrays are often lost in cancer. These cancer genomes show evidence of a hyperactive mechanistic target of rapamycin (mTOR) pathway (Xu et al., 2017) and p53 mutations (Wang & Lemos, 2017). Xu et al. further discovered that mouse HSCs lacking PTEN, a negative regulator of mTOR, also had contracted 45S rDNA arrays, and these cells were more sensitive to DNA damaging agents such as bleomycin, MMS, and X-rays. Interestingly, this DNA damage sensitivity was independent of mTOR activity, and mainly attributed to low rDNA copy number. Although PTEN is a phosphatase widely known for its role as a tumor suppressor, nuclear PTEN is essential for maintaining genome stability by dephosphorylating MCM2, and modulating replication fork progression under conditions of DNA replication stress (Feng et al., 2015), suggesting that the loss of 45S rDNA repeats observed in the *Pten*$^{-/-}$ mouse HSCs could be attributed to DNA replication stress. DNA replication stress resulting from reduced MCM expression was also shown to drive functional decline in aging mouse HSCs, and caused accumulation of phosphorylated γH2AX at the rDNA (Flach et al., 2014). Our findings on the effect of DNA replication stress on the yeast rDNA predict that persistent DNA replication stress would select for a contraction of the rDNA array in each of these cases, and this is in fact what we observe in the tumors from MCM2-deficient mice. Consistent with previous reports, mouse embryonic fibroblasts derived from our MCM2-deficient mice also show increased levels of DNA damage at the 45S rDNA repeats and sensitivity to UV (Kunnev et al., 2010). This is compelling evidence to suggest that DNA replication stress may be diagnosed by rDNA copy number, and cells with low copy number may be more susceptible to common DNA damaging chemotherapeutic agents. Therefore, rDNA copy number may prove to be an important indicator in human disease. Altogether, these results provide insight into the role of the rDNA locus in acting as a

sensor and source of rapid, reversible adaption to general genomic stress through a plastic array size determined by selective cues from the environment.

2.8 Materials and methods

2.8.1 Yeast strains and growth media

All yeast strains used are listed in Table 2.2. Unless otherwise stated, all growth was carried out in YPD (1% w/v yeast extract, 2% w/v peptone, 2% w/v dextrose) at 30°C. For the experiment in Figure 2.3A, cells were grown in YPD containing 150mM hydroxyurea. The *GAL-POL1* strains were grown in YPR (1% w/v yeast extract, 2% w/v peptone, 3% w/v raffinose) medium containing either high (0.05% w/v) or low (0.005% w/v) levels of galactose as indicated.

2.8.2 rDNA copy number measurement by ddPCR

Genomic DNA was isolated using the YeaStar Genomic DNA Kit (Zymo Research). DNA concentrations were measured on a Qubit Fluorometer using the Qubit dsDNA HS Assay (Invitrogen). For ddPCR, 0.005ng genomic DNA was used per 20µL reaction. Primers and probes used are listed in Table 2.3. Duplexed ddPCR was performed according to the manufacturer's protocol (Bio-Rad). Briefly, master mixes containing primers and probes for rDNA and *TUB1*, genomic DNA, and the restriction endonuclease *Eco*RI-HF (New England Biolabs, Inc.) were prepared and aliquoted into Eppendorf twin.tec plates. Reaction mixtures were incubated at room temperature for 15 minutes to allow restriction digestion of genomic DNA prior to droplet generation. Droplets were cycled to endpoint and subsequently read using the QX200 droplet reader. Quantification was performed using the Quantasoft software.

Standard deviation (SD) for each individual reaction was calculated using the formula

$$\text{Standard deviation} = (CI_{max} - CI_{min}) / (2 \times 1.96) \quad (1)$$

where, (CImax - CImin) is the 95% Confidence Interval for the ratio of absolute copy number of rDNA and *TUB1* in each reaction, with both assays multiplexed in the same well, as generated by Quantasoft.

2.8.3 High-throughput screen for mutants with altered rDNA copy number

2.8.3.1 96-well plate re-array

The *Saccharomyces cerevisiae* ts mutant collection was re-arrayed from its source 384-well format into a 96-well format. This served the purpose of eliminating empty wells, which provided space for control strains (wild-type BY4741 and W303 (2 positions each, 1 fixed position across all plates, and 1 variable position), and the rDNA copy number control strains with 40, 80, and 110 rDNA copies (Ide et al., 2010) (one position each)), and eliminated the need for genomic DNA isolation from numerous empty wells present in the source 384-well format. The re-array was performed using the eight-channel independent liquid handling arm (LiHa) of a Tecan Freedom EVO liquid handling instrument by inoculating 10µL of the yeast ts glycerol stock into 150µL YPD + G418 (200mg/L) in a 96-well microtiter plate (Corning). These plates were incubated for 48 hours at room temperature, and then converted to glycerol stocks by adding 65µL of a 50% v/v mix of glycerol and YPD followed by mixing and freezing down at -80°C.

2.8.3.2 Genomic DNA isolation

Each re-arrayed 96-well plate was thawed and 30µL of each glycerol stock was inoculated into 1.6mL YPD + G418 (200mg/L) in a 96-deepwell plate (Thermo Fisher Scientific) and incubated at room temperature for 48 hours while shaking at 225rpm. The cultures were then incubated at 37°C for 3 hours while shaking at 225rpm. The plates were then spun down and medium was decanted. The cells were then re-suspended in 22µL of 3mg/mL Zymolyase 100T (US Biological) solution and incubated

for an additional hour at 37°C while shaking at 225rpm. The plates were then spun down and the supernatant was decanted. Cell pellets were then processed to isolate genomic DNA using the ReliaPrep 96 genomic DNA MiniPrep HT System (Promega) on the Tecan Freedom EVO liquid handling instrument. The concentrations of genomic DNA in 96-well plates were measured using the QuantiFluor ONE dsDNA System (Promega) and read on a SpectraMax M2e plate reader (Molecular Devices). The genomic DNA was then diluted to 0.5ng/µL using the eight-channel independent LiHa of a Tecan Freedom EVO liquid handling instrument. The genomic DNA was subsequently diluted to 0.005ng/µL for ddPCR.

2.8.3.3 rDNA copy number measurement and hit determination

rDNA copy number across the ts mutant collection was measured using ddPCR as described above. In addition to the control strains on the ts mutant collection plates, an additional 96-well plate containing only the control strains (16 independent isolates per strain in randomized positions across the plate), BY4741, W303, the rDNA copy number control strains with 40, 80, and 110 rDNA copies, and YLR378C (*sec61-2,* the hit with the highest copy number across the ts mutant collection as measured in the initial screen) was also prepared for ddPCR to gauge variability in rDNA copy number between independent isolates, and any effects due to plate position. rDNA copy number measurements for BY4741 were used to set thresholds as follows: Mean rDNA copy number ± 1SD – No change. Mean rDNA copy number + 2SD > rDNA copy number > Mean rDNA copy number + 1SD OR Mean rDNA copy number - 2SD < rDNA copy number < Mean rDNA copy number - 1SD – Moderate change. rDNA copy number > Mean rDNA copy number + 2SD OR rDNA copy number < Mean rDNA copy number - 2SD – Significant change.

2.8.3.4 GO analyses

GO enrichment analyses were performed using Gorilla (Eden et al., 2007; Eden et al., 2009).

2.8.3.5 Karyotyping

The top 89 hits of each category, low and high copy number, were cherry-picked, and genomic DNA was isolated from them in high-throughput format as described above. The genomic DNA was diluted to 0.5ng/µL and 0.01ng used per 20µL reaction for karyotyping. Partial karyotyping to obtain relative number of copies of Chromosomes XII and XIII was done using ddPCR. ddPCR assays for Chromosome XII and XIII were designed and duplexed to determine absolute copy number of each, which was subsequently used to calculate the ratio of chromosome XII relative to chromosome XIII. Primers and probes used, and their relative positions on chromosome arms are listed in Table 2.3.

2.8.4 Subculturing experiments

Strains were streaked out on to appropriate medium from glycerol stocks. Single colonies were picked and re-streaked on to fresh plates every 2-3 days (approximately 25 cell divisions). At each subculture, additional single colonies were also used to isolate genomic DNA for ddPCR. All growth was at 30°C.

2.8.5 Growth assays

Cells were diluted to a starting OD_{600} of 0.1 and 5 more 5-fold serial dilutions (unless otherwise mentioned), following which 4µL of each dilution was spotted on to plates containing the appropriate medium. Plates were incubated at 30°C for 2-3 days and photographed.

2.8.6 Cell cycle analyses

3 isolates each with normal or low rDNA copy number were generated by growing wild-type or *fob1*Δ *GAL-POL1* strains on YPR medium containing either high or low levels of galactose for 50-75 generations. Following confirmation of rDNA array contraction by ddPCR (Table 2.1), the isolates were each inoculated into liquid YPR medium containing either high or low levels of galactose. 100µL culture was collected at various time points. Cells were fixed using 70% v/v ethanol and treated with RNaseA, following which their

DNA was stained using Sytox Green (1µM, at room temperature, in the dark, for at least 30 minutes). In parallel, wild-type haploid yeast cells for use as ploidy reference were also grown, fixed, treated with RNaseA, and stained with CellTrace Violet (1µM, at 37°C, in the dark, for 20 minutes, followed by 2 washes with 1x PBS) prior to staining with Sytox Green to allow distinction between reference and test strains. Before cytometric analysis, 20µL of the fixed and stained reference sample was added to 1mL of each fixed and stained test sample. DNA content analysis was performed on an EC800 Analyzer (Sony Biotechnology). DNA content modeling was performed using FCS Express 6 Plus (De Novo Software).

2.8.7 aCGH and NGS

aCGH, NGS and subsequent data analysis were performed as previously described (Kunnev et al., 2015; Rusiniak et al., 2012).

2.9 Supporting information

Table 2.1. rDNA copy number in *GAL-POL1* isolates used in Figures 2.5 – 2.9.

Wild-type *GAL-POL1*							
Number of cell divisions	Growth condition	Isolate	rDNA copy number	CI max	CI min	Standard deviation	p value
~25 cell divisions	High Gal	Isolate 1	81.958	96	69	6.88776	0.00955
		Isolate 2	90.1439	105	76	7.39796	
		Isolate 3	84.0146	98	70	7.14286	
	Low Gal	Isolate 1	63.1633	74	52	5.61224	
		Isolate 2	47.913	55	40	3.82653	
		Isolate 3	50.3597	53.5	47.2	1.60714	
~50 cell divisions	High Gal	Isolate 1	67.3077	78	57	5.35714	0.04045
		Isolate 2	70.5195	80	61	4.84694	
		Isolate 3	82.4806	95	70	6.37755	
	Low Gal	Isolate 1	62.7907	73	53	5.10204	
		Isolate 2	46.0694	52	40	3.06122	
		Isolate 3	47.3874	55	40	3.82653	
~75 cell divisions	High Gal	Isolate 1	80.0885	87	73	3.57143	0.03501
		Isolate 2	84.115	93	75	4.59184	
		Isolate 3	83.2707	92	75	4.33673	
	Low Gal	Isolate 1	63.5165	71	56	3.82653	
		Isolate 2	58.4892	64	53	2.80612	
		Isolate 3	44.9261	50	40	2.55102	

GAL-POL1 fob1Δ							
Number of cell divisions	Growth condition	Isolate	rDNA copy number	CI max	CI min	Standard deviation	p value
~25 cell divisions	High Gal	Isolate 1	96.281	113	80	8.41837	0.02404
		Isolate 2	80.5426	95	66	7.39796	
		Isolate 3	96.25	114	80	8.67347	
	Low Gal	Isolate 1	60.283	69	51	4.59184	
		Isolate 2	61.6807	72	52	5.10204	
		Isolate 3	58.1967	66	50	4.08163	
~50 cell divisions	High Gal	Isolate 1	90	104	76	7.14286	0.04212
		Isolate 2	89.7727	102	77	6.37755	
		Isolate 3	80.6838	94	68	6.63265	
	Low Gal	Isolate 1	78.5507	90	67	5.86735	
		Isolate 2	74.1007	85	63	5.61224	
		Isolate 3	66.6923	77	57	5.10204	

Table 2.2. List of yeast strains used.

Strain ID	Other ID	Name	Relevant Genotype	References
DSY003		BY4741	*MAT*a *his3Δ1 leu2Δ0 met15Δ0 ura3Δ0*	
DSY018		W303	*MAT*a *{leu2-3,112 trp1-1 can1-100 ura3-1 ade2-1 his3-11,15} [phi$^+$]*	
DSY032	JG1830	W303 *fob1Δ*	W303, except *fob1Δ::NATMX*	
DSY006	YSI102	20 rDNA copies	*MAT*a *ade2-1 ura3-1 his3-11 trp1-1 leu2-3,112 can1-100 fob1Δ::LEU2,* 20 rDNA copies	Ide et al., 2010
DSY007	YSI103	40 rDNA copies	YSI102, except 40 rDNA copies	
DSY008	YSI104	80 rDNA copies	YSI102, except 80 rDNA copies	
DSY009	YSI105	110 rDNA copies	YSI102, except 110 rDNA copies	
DSY021		*rtt109Δ*	BY4741, except *rtt109Δ::KANMX*	Yeast Knockout Collection, *MAT*a haploid
DSY025		*mms22Δ*	BY4741, except *mms22Δ::KANMX*	
DSY030		*rrn10Δ*	BY4741, except *rrn10Δ::KANMX*	
DSY026		*ctf4Δ*	BY4741, except *ctf4Δ::KANMX*	
DSY066		*rnr1 Δ*	BY4742, except *rnr1Δ::KANMX*	Yeast Knockout Collection, *MAT*α haploid
DSY071	AMC20	*GAL-POL1*	a/α *KANMX-GAL1-POL1/KANMX-GAL1-POL1*	Casper et al., 2008
DSY072	AMC160	*GAL-POL1 fob1Δ*	a/α *fob1::NATMX/fob1::NATMX KANMX-GAL1-POL1/KANMX-GAL1-POL1*	

Table 2.3. Sequences of primers used.

ddPCR for rDNA copy number

Gene	Forward primer	Reverse Primer	Probe
TUB1	5'-CCAGTCTTATCCAAATCAAAGG-3'	5'-GGATCACACTTGACCATCT-3'	5'-/56FAM/TCCATGAGT/ZEN/CCAACTCTGTGTCA/3IABkFQ/-3'
25S rDNA	5'-TACCTTCGGTGCCCGAGTTGTAAT-3'	5'-ACCCTCTATGACGTCCTGTTCCAA-3'	5'-/5HEX/AACATAGACAAGGAACGGCCC/3BHQ_1/-3'

ddPCR for karyotyping

Chromosome	Arm	Forward Primer	Reverse Primer	Probe
XII	Right	5'-TATCCAACCACCTGAAGAAG-3'	5'-ACGAGTGCCCAAGTTATAG-3'	5'-/5HEX/AGAACCGAG/ZEN/GAAGAAGTAGCAATC/3IABkFQ/-3'
XIII	Right	5'-CCGTCTTTCGAGCAGTTGA-3'	5'-GCGGGAACTAAGTGCAGAATA-3'	5'-/56FAM/AGGATGAGA/ZEN/GTGAGTGTTAATGAGGG/3IABkFQ/-3'

***pGAL1* PCR**

Primer Name	Sequence
P2	5'-GAAAGAAGAACCTCAGTGG-3'
P3	5'-CCATTTGCGATAGCTCTTGT-3'

2.10 Acknowledgements

We thank William McDowell (Stowers Institute) for assistance with development of the ddPCR assay for rDNA copy number measurement, as well as karyotyping in yeast, and Andrew Box and Jillian Blanck (Stowers Institute) for assistance with cytometry and DNA modeling. We also thank Thomas Petes (Duke University) for the *GAL-POL1* strains and helpful discussions, and Takehiko Kobayashi for the 20-110 rDNA copy strains. This work was done to fulfill, in part, requirements for DS's PhD thesis research as a student registered with the Open University. Original data underlying this manuscript can be accessed from the Stowers Original Data Repository at http://www.stowers.org/research/publications/libpb-1220.

2.11 References

Ben-Aroya, S., Coombes, C., Kwok, T., O'Donnell, K. A., Boeke, J. D., & Hieter, P. (2008). Toward a comprehensive temperature-sensitive mutant repository of the essential genes of Saccharomyces cerevisiae. *Mol Cell, 30*(2), 248-258. doi:10.1016/j.molcel.2008.02.021

Bicknell, L. S., Bongers, E. M., Leitch, A., Brown, S., Schoots, J., Harley, M. E., . . . Jackson, A. P. (2011). Mutations in the pre-replication complex cause Meier-Gorlin syndrome. *Nat Genet, 43*(4), 356-359. doi:10.1038/ng.775

Bose, T., Lee, K. K., Lu, S., Xu, B., Harris, B., Slaughter, B., . . . Gerton, J. L. (2012). Cohesin proteins promote ribosomal RNA production and protein translation in yeast and human cells. *PLoS Genet, 8*(6), e1002749. doi:10.1371/journal.pgen.1002749

Cahyani, I., Cridge, A. G., Engelke, D. R., Ganley, A. R., & O'Sullivan, J. M. (2015). A sequence-specific interaction between the Saccharomyces cerevisiae rRNA gene repeats and a locus encoding an RNA polymerase I subunit affects ribosomal DNA stability. *Mol Cell Biol, 35*(3), 544-554. doi:10.1128/MCB.01249-14

Casper, A. M., Mieczkowski, P. A., Gawel, M., & Petes, T. D. (2008). Low levels of DNA polymerase alpha induce mitotic and meiotic instability in the ribosomal DNA gene cluster of Saccharomyces cerevisiae. *PLoS Genet, 4*(6), e1000105. doi:10.1371/journal.pgen.1000105

Eden, E., Lipson, D., Yogev, S., & Yakhini, Z. (2007). Discovering motifs in ranked lists of DNA sequences. *PLoS Comput Biol, 3*(3), e39. doi:10.1371/journal.pcbi.0030039

Eden, E., Navon, R., Steinfeld, I., Lipson, D., & Yakhini, Z. (2009). GOrilla: a tool for discovery and visualization of enriched GO terms in ranked gene lists. *BMC Bioinformatics, 10*, 48. doi:10.1186/1471-2105-10-48

Feng, J., Liang, J., Li, J., Li, Y., Liang, H., Zhao, X., . . . Yin, Y. (2015). PTEN Controls the DNA Replication Process through MCM2 in Response to Replicative Stress. *Cell Rep, 13*(7), 1295-1303. doi:10.1016/j.celrep.2015.10.016

Fenwick, A. L., Kliszczak, M., Cooper, F., Murray, J., Sanchez-Pulido, L., Twigg, S. R., . . . Bicknell, L. S. (2016). Mutations in CDC45, Encoding an Essential Component of the Pre-initiation Complex, Cause Meier-Gorlin Syndrome and Craniosynostosis. *Am J Hum Genet, 99*(1), 125-138. doi:10.1016/j.ajhg.2016.05.019

Flach, J., Bakker, S. T., Mohrin, M., Conroy, P. C., Pietras, E. M., Reynaud, D., . . . Passegue, E. (2014). Replication stress is a potent driver of functional decline in ageing haematopoietic stem cells. *Nature, 512*(7513), 198-202. doi:10.1038/nature13619

Foss, E. J., Lao, U., Dalrymple, E., Adrianse, R. L., Loe, T., & Bedalov, A. (2017). SIR2 suppresses replication gaps and genome instability by balancing replication between repetitive and unique sequences. *Proc Natl Acad Sci U S A., 114*(3), 552-557. doi:10.1073

French, S. L., Osheim, Y. N., Cioci, F., Nomura, M., & Beyer, A. L. (2003). In exponentially growing Saccharomyces cerevisiae cells, rRNA synthesis is determined by the summed RNA polymerase I loading rate rather than by the number of active genes. *Mol Cell Biol, 23*(5), 1558-1568. doi:10.1128/mcb.23.5.1558-1568.2003

Gaillard, H., Garcia-Muse, T., & Aguilera, A. (2015). Replication stress and cancer. *Nat Rev Cancer, 15*(5), 276-289. doi:10.1038/nrc3916

Ganley, A. R., & Kobayashi, T. (2011). Monitoring the rate and dynamics of concerted evolution in the ribosomal DNA repeats of Saccharomyces cerevisiae using experimental evolution. *Mol Biol Evol, 28*(10), 2883-2891. doi:10.1093/molbev/msr117

Gibbons, J. G., Branco, A. T., Godinho, S. A., Yu, S., & Lemos, B. (2015). Concerted copy number variation balances ribosomal DNA dosage in human and mouse genomes. *Proc Natl Acad Sci U S A, 112*(8), 2485-2490. doi:10.1073/pnas.1416878112

Gibbons, J. G., Branco, A. T., Yu, S., & Lemos, B. (2014). Ribosomal DNA copy number is coupled with gene expression variation and mitochondrial abundance in humans. *Nat Commun, 5*, 4850. doi:10.1038/ncomms5850

Hindson, B. J., Ness, K. D., Masquelier, D. A., Belgrader, P., Heredia, N. J., Makarewicz, A. J., . . . Colston, B. W. (2011). High-throughput droplet digital PCR system for absolute quantitation of DNA copy number. *Anal Chem, 83*(22), 8604-8610. doi:10.1021/ac202028g

Ide, S., Miyazaki, T., Maki, H., & Kobayashi, T. (2010). Abundance of ribosomal RNA gene copies maintains genome integrity. *Science, 327*(5966), 693-696. doi:10.1126/science.1179044

Ide, S., Saka, K., & Kobayashi, T. (2013). Rtt109 Prevents Hyper-Amplification of Ribosomal RNA Genes through Histone Modification in Budding Yeast. *PLoS Genet, 9*(4). doi:10.1371/journal.pgen.1003410.g001

Ide, S., Watanabe, K., Watanabe, H., Shirahige, K., Kobayashi, T., & Maki, H. (2007). Abnormality in initiation program of DNA replication is monitored by the highly repetitive rRNA gene array on chromosome XII in budding yeast. *Mol Cell Biol, 27*(2), 568-578. doi:10.1128/MCB.00731-06

Ii, M., Ii, T., Brill, S. J. (2007). Mus81 functions in the quality control of replication forks at the rDNA and is involved in the maintenance of rDNA repeat number in *Saccharomyces cerevisiae. Mutation Res., 625*(1–2), 1–19.

Irene, C., Theis, J. F., Gresham, D., Soteropoulos, P., & Newlon, C. S. (2016). Hst3p, a histone deacetylase, promotes maintenance of Saccharomyces cerevisiae chromosome III lacking efficient replication origins. *Mol Genet Genomics, 291*(1), 271-283. doi:10.1007/s00438-015-1105-8

Jack, C. V., Cruz, C., Hull, R. M., Keller, M. A., Ralser, M., & Houseley, J. (2015). Regulation of ribosomal DNA amplification by the TOR pathway. *Proc Natl Acad Sci U S A, 112*(31), 9674-9679. doi:10.1073/pnas.1505015112

Kobayashi, T. (2003). The replication fork barrier site forms a unique structure with Fob1p and inhibits the replication fork. *Mol Cell Biol, 23*(24), 9178-9188. doi:10.1128/mcb.23.24.9178-9188.2003

Kobayashi, T. (2006). Strategies to maintain the stability of the ribosomal RNA gene repeats – Collaboration of recombination, cohesion, and condensation–. *Genes Genet. Syst., 81*, 155–161.

Kobayashi, T., Heck, D. J., Nomura, M., & Horiuchi, T. (1998). Expansion and contraction of ribosomal DNA repeats in *Saccharomyces cerevisiae*: requirement of replication fork blocking (Fob1) protein and the role of RNA polymerase I. *Genes Dev, 12*(24), 3821-3830. doi:10.1101/gad.12.24.3821

Kobayashi, T., Horiuchi, T., Tongaonkar, P., Vu, L., & Nomura, M. (2004). SIR2 Regulates Recombination between Different rDNA Repeats, but Not Recombination within Individual rRNA Genes in Yeast. *Cell., 117*(4), 441-453.

Kunnev, D., Freeland, A., Qin, M., Leach, R. W., Wang, J., Shenoy, R. M., & Pruitt, S. C. (2015). Effect of minichromosome maintenance protein 2 deficiency on the locations of DNA replication origins. *Genome Res, 25*(4), 558-569. doi:10.1101/gr.176099.114

Kunnev, D., Rusiniak, M. E., Kudla, A., Freeland, A., Cady, G. K., & Pruitt, S. C. (2010). DNA damage response and tumorigenesis in Mcm2-deficient mice. *Oncogene, 29*(25), 3630-3638. doi:10.1038/onc.2010.125

Kwan, E. X., Foss, E. J., Tsuchiyama, S., Alvino, G. M., Kruglyak, L., Kaeberlein, M., . . . Bedalov, A. (2013). A natural polymorphism in rDNA replication origins links origin activation with calorie restriction and lifespan. *PLoS Genet, 9*(3), e1003329. doi:10.1371/journal.pgen.1003329

Kwan, E. X., Wang, X. S., Amemiya, H. M., Brewer, B. J., & Raghuraman, M. K. (2016). rDNA Copy Number Variants Are Frequent Passenger Mutations in Saccharomyces cerevisiae Deletion Collections and de Novo Transformants. *G3 (Bethesda), 6*(9), 2829-2838. doi:10.1534/g3.116.030296

Li, Z., Vizeacoumar, F. J., Bahr, S., Li, J., Warringer, J., Vizeacoumar, F. S., . . . Boone, C. (2011). Systematic exploration of essential yeast gene function with temperature-sensitive mutants. *Nat Biotechnol, 29*(4), 361-367. doi:10.1038/nbt.1832

Lu, S., Lee, K. K., Harris, B., Xiong, B., Bose, T., Saraf, A., . . . Gerton, J. L. (2014). The cohesin acetyltransferase Eco1 coordinates rDNA replication and transcription. *EMBO Rep, 15*(5), 609-617. doi:10.1002/embr.201337974

Mantiero, D., Mackenzie, A., Donaldson, A., & Zegerman, P. (2011). Limiting replication initiation factors execute the temporal programme of origin firing in budding yeast. *EMBO J, 30*(23), 4805-4814. doi:10.1038/emboj.2011.404

Mayan, M., & Aragon, L. (2010). Cis-interactions between non-coding ribosomal spacers dependent on RNAP-II separate RNAP-I and RNAP-III transcription domains. *Cell Cycle, 9*(21), 4328-4337. doi:10.4161/cc.9.21.13591

Michel, A. H., Kornmann, B., Dubrana, K., Shore, D. (2005). Spontaneous rDNA copy number variation modulates Sir2 levels and epigenetic gene silencing. *Genes Dev. , 19*(10), 1199-1210.

Nasmyth, K., & Haering, C. H. (2009). Cohesin: its roles and mechanisms. *Annu Rev Genet, 43*, 525-558. doi:10.1146/annurev-genet-102108-134233

O'Sullivan, J. M., Sontam, D. M., Grierson, R., & Jones, B. (2009). Repeated elements coordinate the spatial organization of the yeast genome. *Yeast, 26*(2), 125-138. doi:10.1002/yea.1657

Oakes, M., Siddiqi, I., Vu, L., Aris, J., & Nomura, M. (1999). Transcription factor UAF, expansion and contraction of ribosomal DNA (rDNA) repeats, and RNA polymerase switch in transcription of yeast rDNA. *Mol Cell Biol, 19*(12), 8559-8569. doi:10.1128/mcb.19.12.8559

Paredes, S., Branco, A. T., Hartl, D. L., Maggert, K. A., & Lemos, B. (2011). Ribosomal DNA deletions modulate genome-wide gene expression: "rDNA-sensitive" genes and natural variation. *PLoS Genet, 7*(4), e1001376. doi:10.1371/journal.pgen.1001376

Pasero, P., Bensimon, A., & Schwob, E. (2002). Single-molecule analysis reveals clustering and epigenetic regulation of replication origins at the yeast rDNA locus. *Genes Dev, 16*(19), 2479–2484.

Pruitt, S. C., Bailey, K. J., & Freeland, A. (2007). Reduced Mcm2 expression results in severe stem/progenitor cell deficiency and cancer. *Stem Cells, 25*(12), 3121-3132. doi:10.1634/stemcells.2007-0483

Pruitt, S. C., Qin, M., Wang, J., Kunnev, D., & Freeland, A. (2017). A Signature of Genomic Instability Resulting from Deficient Replication Licensing. *PLoS Genet, 13*(1), e1006547. doi:10.1371/journal.pgen.1006547

Rusiniak, M. E., Kunnev, D., Freeland, A., Cady, G. K., & Pruitt, S. C. (2012). Mcm2 deficiency results in short deletions allowing high resolution identification of genes contributing to lymphoblastic lymphoma. *Oncogene, 31*(36), 4034-4044. doi:10.1038/onc.2011.566

Saka, K., Takahashi, A., Sasaki, M., & Kobayashi, T. (2016). More than 10% of yeast genes are related to genome stability and influence cellular senescence via rDNA maintenance. *Nucleic Acids Res, 44*(9), 4211-4221. doi:10.1093/nar/gkw110

Shyian, M., Mattarocci, S., Albert, B., Hafner, L., Lezaja, A., Costanzo, M., . . . Shore, D. (2016). Budding Yeast Rif1 Controls Genome Integrity by Inhibiting rDNA Replication. *PLoS Genet, 12*(11), e1006414. doi:10.1371/journal.pgen.1006414

Song, W., Dominska, M., Greenwell, P. W., & Petes, T. D. (2014). Genome-wide high-resolution mapping of chromosome fragile sites in Saccharomyces cerevisiae. *Proc Natl Acad Sci U S A, 111*(21), E2210-2218. doi:10.1073/pnas.1406847111

Villa, F., Simon, A. C., Ortiz Bazan, M. A., Kilkenny, M. L., Wirthensohn, D., Wightman, M., . . . Labib, K. (2016). Ctf4 Is a Hub in the Eukaryotic Replisome that Links Multiple CIP-Box Proteins to the CMG Helicase. *Mol Cell, 63*(3), 385-396. doi:10.1016/j.molcel.2016.06.009

Wang, M., & Lemos, B. (2017). Genetic context and proliferation determine contrasting patterns of copy number amplification and loss for 5S and 45S ribosomal DNA arrays in cancer. *bioRxiv*. doi:10.1101/154120

Xu, B., Li, H., Perry, J. M., Singh, V. P., Unruh, J., Yu, Z., . . . Gerton, J. L. (2017). Ribosomal DNA copy number loss and sequence variation in cancer. *PLoS Genet, 13*(6), e1006771. doi:10.1371/journal.pgen.1006771

Zheng, D. Q., Zhang, K., Wu, X. C., Mieczkowski, P. A., & Petes, T. D. (2016). Global analysis of genomic instability caused by DNA replication stress in Saccharomyces cerevisiae. *Proc Natl Acad Sci U S A, 113*(50), E8114-E8121. doi:10.1073/pnas.1618129113

CHAPTER 3

Transcription and replication stress facilitate adaptation through inducible copy number variation at tandem repeats

3 CHAPTER 3

3.1 List of Figures

3.2 List of Tables

3.3 Abstract

Tandem repeats are inherently unstable and exhibit extensive copy number variation. Despite increasing evidence linking copy number variations with phenotypic variation, the mechanisms associated with regulation of the two features of tandem repeats that underlie their ability to undergo extensive copy number variation – their inherent instability, and the stable maintenance of normal repeat copy number in unperturbed conditions – remain largely unclear. Here, we used two well-studied repetitive arrays in the yeast genome, the ribosomal DNA (rDNA) locus, and the copper-resistance *CUP1* gene array, to study copy number variation at tandem repeats. We report the development and validation of a quantitative, single cell-based assay to measure repeat instability (qRIN), and demonstrate its use in a quantitative and unbiased high-throughput screen to identify genetic factors that regulate rDNA stability. We identified several pathways that affect rDNA stability; notably, in addition to factors that elevate instability, factors that suppress instability were also identified. This suggests that cells may maintain an "optimal rDNA stability" that promotes genome stability while allowing for rDNA copy number variation in response to genomic stresses. Additionally, to identify factors involved in the maintenance of normal rDNA copy number, we used a droplet digital PCR based assay to measure rDNA copy number in 279 strains of a yeast conditional temperature-sensitive mutant collection of essential genes. Our screens revealed that instability and maintenance of rDNA copy number are regulated by DNA replication, transcription, and histone acetylation. Based on these data, we propose that instability at tandem repeats can be regulated by replication and transcription at these loci. In fact, we find that instability at the *CUP1* array is directly related to *CUP1* copy number, and increased by a) transcription of the locus induced by environmental copper and b) hydroxyurea induced DNA replication stress. Similarly, instability at the constitutively transcribed rDNA array is also affected by perturbed RNA Polymerase I transcription and DNA replication stress. Further, while instability at both rDNA and *CUP1* arrays in response to a variety of stresses is induced rapidly, within a few cell divisions, a change in steady state repeat copy number requires prolonged propagation under selective conditions. We propose that modulation of the fundamental, ubiquitous processes of DNA replication and transcription is a simple, reversible strategy to alter instability at tandem repeats in response to environmental stimuli, which provides cells adaptability through stress and locus-specific copy number variation.

3.4 Introduction

Repetitive DNA sequences constitute large fractions of all eukaryotic genomes and copy number polymorphisms at repetitive regions are now recognized as a significant source of genetic diversity. While large, cytogenetically recognizable structural alterations and single nucleotide polymorphisms (SNPs) have been observed for many decades, the widespread prevalence of copy number variations in eukaryotic genomes is only just beginning to be appreciated. In fact, copy number variations are now recognized as the most significant source of genetic diversity in human populations (Iafrate et al., 2004; Redon et al., 2006; Sebat et al., 2004; Zarrei et al., 2015). Copy number variations have also been associated with many human chromosomal syndromes (Wyandt et al., 2017). However, copy number variations are not always detrimental to cellular and organismal function, and can have a wide range of phenotypic effects ranging from embryonic lethality to adaptation (reviewed in (Beckmann et al., 2007; Hurles et al., 2008)). In fact, a recent genome wide association study of 1011 natural isolates of the budding yeast, *Saccharomyces cerevisiae*, showed that copy number variations not only constituted the most genetic variation, but also had the most significant effect on phenotype (Peter et al., 2018). Recent computational studies estimate that the human genome contains at least 25,000 arrays of tandem repeats between 600 bp and 10 kb in length, with 503 arrays larger than 10 kb (Warburton et al., 2008), and these tandem repeats exhibit extreme variability in copy number (Brahmachary et al., 2014). These data suggest that copy number polymorphisms, particularly at tandem repeats, may significantly contribute to genome function. While the potential functional impact of copy number variations is beginning to be appreciated, the extent of copy number variation in the genomes of higher eukaryotes remains far from fully determined because of technical difficulties in sequencing, assembling, and identifying repetitive genomic regions. As a result, fundamental principles governing the behavior of tandem repeats critical to their ability to undergo copy number variations, and the impact of variation on cellular function remain largely uncharacterized. To elucidate the mechanisms underlying the regulation

of instability and adaptive copy number changes at tandem repeats, we chose to study the two features of tandem repeats that are key to their ability to undergo extensive copy number variation –instability, and copy number maintenance – using two well-studied repetitive arrays in the yeast genome, the ribosomal DNA (rDNA) locus, and the copper-resistance *CUP1* gene array.

The rDNA genes encode ribosomal RNA (rRNA), and are the most well-characterized tandem repeat family. Given their universally conserved function in ribosome biogenesis, and the conservation of the organization of the genes and key regulatory elements from yeast to humans, the budding yeast rDNA locus has been used as a model to study mechanisms of copy number variation at tandem repeats. The budding yeast rDNA locus comprises ~100-200 copies of a 9.1kb repeat unit arranged in tandem on the long arm of Chromosome XII. Each 9.1kb repeat unit contains coding sequences for a pre-35S rRNA, transcribed by RNA Polymerase I (RNAPI), that gives rise to the 18S, 25S, and 5.8S rRNA species, and a 5S rRNA, transcribed by RNA Polymerase III (RNAPIII). The 35S and 5S rRNA coding sequences are separated by two intergenic spacers (IGS), IGS1 and IGS2, which contain important regulatory elements. IGS2 contains an rDNA origin of replication, rARS, and a cohesin associating sequence (CAR). IGS1 contains a replication fork barrier site (RFB) bound by the replication fork blocking protein Fob1, and E-pro, a non-coding, bidirectional, RNA Polymerase II (RNAPII) promoter whose activity is normally suppressed by Sir2, an NAD+-dependent histone deacetylase (Figure 3.1A). The rDNA array is the most highly transcribed locus in the yeast genome, and high rates of transcription from multiple copies of rDNA repeats are essential to support rRNA production in actively growing cells. rDNA repeat units are maintained far in excess of the requirement for ribosome biogenesis, with only about half of the 100-200 repeats transcribed in actively growing yeast cells (French et al., 2003). Additionally, while rDNA copy number can be reduced significantly (up to ~20 copies) without affecting rRNA output or cell growth (French et al., 2003; Kobayashi et al., 1998), extra, untranscribed rDNA repeats are required to

ensure efficient DNA damage repair in the highly transcribed rDNA array (Ide et al., 2010).

Normal rDNA copy number is thought to be maintained by a recombination-mediated amplification of rDNA repeats that depends on RNAPI transcription (Kobayashi et al., 1998). Recent work from Mansisidor et al. (2018) and Iida et al. (2019) suggests that cells depend on multiple RNAPI transcription dependent mechanisms to a) monitor rDNA copy number at every cell division, and b) trigger amplification of the array in cells with critically low rDNA copy number (Iida & Kobayashi, 2019; Mansisidor et al., 2018). During S-phase, the binding of Fob1 to the RFB inhibits DNA replication in the direction opposite to 35S rDNA transcription, preventing the head on collision of transcription and replication machinery (Brewer et al., 1992; Kobayashi, 2003). DNA replication forks stalled at the RFB are processed into double stranded breaks (DSBs), which are repaired by homologous recombination-mediated repair pathways (Kobayashi, 2003; Kobayashi et al., 1998). The presence of multiple identical tandem repeats that can serve as templates for recombination allows unequal sister chromatid exchange (USCE) events to occur, which frequently result in copy number variations. USCE is suppressed by cohesin binding at the CAR (Kobayashi et al., 2004). Recombination is further suppressed by binding of Sir2 to E-pro (Kobayashi & Ganley, 2005; Kobayashi et al., 2004). Despite these known mechanisms to suppress recombination at the rDNA, recombination-mediated repeat loss is relatively high in wild-type cells, even in unperturbed conditions. Additionally, copy number changes at the rDNA have been observed as adaptive responses to mutations and environmental stresses, particularly DNA replication stress (Ide et al., 2007; Kwan et al., 2013; Salim et al., 2017; Shyian et al., 2016) and perturbations in RNAPI transcription (Albert et al., 2011; Kobayashi et al., 1998; Oakes et al., 1993; Oakes et al., 1999). This relatively high instability at the rDNA locus, the paradoxical, stable maintenance of normal repeat copy number, and the apparent lack of correlation between instability and repeat copy number changes have all been areas of active investigation for the last several years.

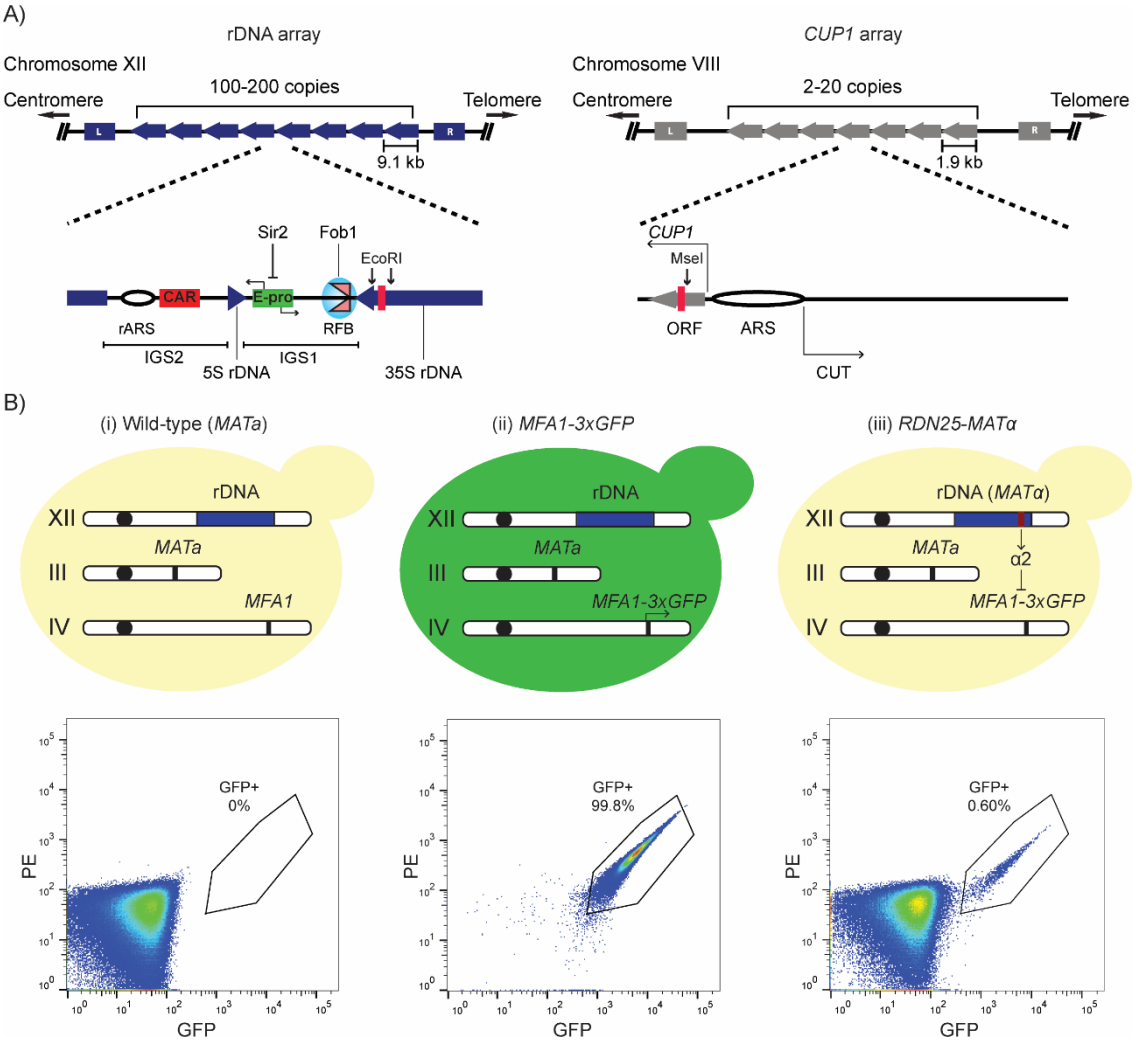

Figure 3.1. Development of a system to study copy number variation at tandem repeats. (A) The rDNA and *CUP1* gene arrays share design features. Cartoons showing the structure of the rDNA and *CUP1* gene arrays in S. cerevisiae along with key regulatory elements in each array. The rDNA array comprises 100-200 ~9.1kb repeat units arranged in tandem at a single locus on Chromosome XII. Direction of blue block arrows indicates direction of rDNA transcription. IGS1 and IGS2, Intergenic spacers 1 and 2; rARS, rDNA origin of replication; CAR, cohesin associating region; E-pro, bidirectional RNAPII promoter whose activity is suppressed by Sir2 binding; RFB, replication fork barrier, bound by Fob1. The *CUP1* array comprises 2-20 ~2kb repeats arranged in tandem at a single locus on Chromosome VIII. Direction of grey block arrows indicates direction of *CUP1* ORF transcription. ARS, origin of replication; CUT, cryptic unstable transcript. Red bars within coding sequences of both arrays indicate target regions for ddPCR assays to measure repeat copy number Relevant restriction sites flanking the ddPCR assay targets are also indicated. (B) Basic principle of the quantitative, single cell assay to measure repeat instability (qRIN). *MFA1* in a haploid, wild-type *MATa* strain (i) is tagged with 3 copies of GFP to generate the *MFA1-3×GFP* strain (ii). A single copy of *MATALPHA* is integrated at the locus of interest, ex., one rDNA repeat (iii). The α2 repressor produced from *MATALPHA* represses GFP expression. GFP-positive cells produced by loss of the *MATALPHA*-containing region can be rapidly counted using flow cytometry as shown in representative flow cytometry analyses of the wild-type *MATa* strain, the *MFA1-3×GFP* strain, and the *RDN25-MATα* strains with GFP-positive cells gated by the black polygon.

While the yeast rDNA array has served as the exclusive model to study the behavior of tandem repeats, rDNA genes are constitutively transcribed, and their transcription is essential for cell viability. Work from Hull et al. (2017) showed that transcription of the *CUP1* gene array induces copy number variation at this locus, suggesting that the inherent instability at the rDNA array is due in part to constitutively high levels of transcription at the array. The requirement of rDNA transcription for cell survival makes it impossible to study transcription-dependent and independent aspects of copy number variation using the rDNA array. The *CUP1* array shares design features with the rDNA array. It comprises 2-20 copies of a ~2kb repeat unit, arranged in tandem at a single locus on chromosome VIII. Each repeat unit contains the *CUP1* coding sequence and an origin of replication (ARS). The *CUP1* promoter has been shown to be bidirectional, with sense and antisense transcription producing *CUP1* mRNA and a cryptic unstable transcript (CUT) respectively (Hull et al., 2017) (Figure 3.1A). *CUP1* encodes a metallothionein that sequesters environmental copper and cadmium. *CUP1* is only transcribed in the presence of copper in the medium, and copy number correlates directly with copper resistance, making the *CUP1* array a powerful, inducible system to study copy number variation and adaptation. Further, work from Hull et al. (2017) showed that *CUP1* copy number variation was regulated by acetylation of the lysine 56 of histone H3 (H3K56), a chromatin mark well known for its role in maintaining rDNA copy number (Ide et al., 2013). These data suggest conservation of the basic principles of copy number variation at the rDNA and *CUP1* arrays.

Here we report the development and validation of a quantitative, single cell-based assay to measure repeat instability (qRIN), and demonstrate its use in a quantitative and unbiased high-throughput screen to identify genetic factors that regulate rDNA stability. We identified several pathways that impact rDNA instability; notably, in addition to factors that elevate instability, factors that suppress instability were also identified. This suggests that rather than minimizing instability, cells may have evolved to maintain an “optimal rDNA stability” that promotes genome stability while

allowing for copy number variations to occur readily in response to genomic stresses. Additionally, to identify factors involved in the maintenance of normal rDNA copy number, we used a droplet digital PCR (ddPCR) based assay to measure rDNA copy number in 279 strains of a yeast conditional temperature-sensitive (yTs) mutant collection of essential genes. Our screens revealed that instability and maintenance of copy number of the rDNA array are regulated by DNA replication, transcription, and histone acetylation. Based on these data, we propose that instability at tandem repeats can be regulated by modulation of replication and transcription at these loci.

Mounting evidence suggests that despite the presence of elaborate mechanisms to avoid them, secondary structures produced by transcription, and the transcription machinery itself could frequently hinder replisome progression and are a major source of genomic instability. At repetitive loci, the availability of multiple identical sequences in a head to tail arrangement for use as template for recombination produces copy number variation. Under conditions of stress, selection can act on this existing copy number variation, and copy number variants that confer a selective advantage continue to propagate, facilitating adaptation. To further analyze the role of DNA replication and transcription in regulating repeat stability and adaptive copy number changes, we utilized the *CUP1* array. Using the qRIN assay, we show that instability at the *CUP1* array is directly related to *CUP1* copy number, and is in fact increased by both, copper-induced transcription of the locus and hydroxyurea induced DNA replication stress in a dose-dependent manner. Similarly, instability at the constitutively transcribed rDNA array is also affected by perturbed RNA Polymerase I transcription and DNA replication stress. Additionally, while changes in instability at both rDNA and *CUP1* arrays in response to a variety of stresses are observed within a few cell divisions, a change in steady state repeat copy number only occurs after prolonged propagation under selective conditions. We propose that modulation of replication and/or transcription is a simple, reversible strategy to alter instability at tandem repeats in response to

environmental stimuli, which provides cells rapid adaptability through copy number variation.

3.5 Results

3.5.1 Development and validation of qRIN, a quantitative, single-cell assay to measure repeat instability

The budding yeast rDNA locus has been used almost exclusively as a model to study copy number variation at tandem repeats for several decades. Since recombination-mediated repeat copy number variation is the major source of instability at the rDNA locus, various measures of rDNA copy number variation and rDNA repeat loss rates have been used as indicators of rDNA stability. In some studies, pulsed-field gel electrophoresis has been used to observe changes in rDNA copy number, and the extent of copy number variation as indicated by the size of chromosome XII has been used to obtain a qualitative estimate of rDNA instability relative to controls (Horigome et al., 2019; Saka et al., 2016). However, this method is labor-intensive, and only provides a qualitative estimate of relative rDNA copy number variation. Studies on recombination at the rDNA in yeast typically involved estimation of rDNA repeat loss rates by marker-loss assays, which involved measuring the frequency of loss of a selectable marker (such as *URA3*, *ADE2, LEU2*) integrated into a single rDNA repeat (Gottlieb & Esposito, 1989; Petes, 1980; Szostak & Wu, 1980; Wagstaff et al., 1985). Loss of the rDNA repeat containing the selectable marker results in changes in color or growth of yeast colonies on selective media, and counting the number of colonies that had lost the marker enabled a semi-quantitative estimation of rDNA repeat loss rates. This method involves plating and counting thousands of colonies, and is therefore not amenable to high-throughput analysis. A variation of the marker-loss assay, the marker-duplication assay, was developed by Johzuka and Horiuchi (2002) to provide a more direct measure of recombination. In this assay, accumulation of recombinant products was monitored by

detecting duplication of the selectable marker by Southern blotting (Johzuka & Horiuchi, 2002). Since marker loss can be affected by a variety of recombination and rearrangement pathways, the marker-duplication assay offered the ability to directly monitor the formation of recombinant products. However, the use of Southern blots makes this assay relatively tedious. Moreover, the marker-duplication assay does not allow for direct calculation of recombination frequencies, making it semi-quantitative at best. A more recent study involved the insertion of a small targeted mutation in the IGS of a single rDNA repeat and monitoring the rate of loss of this single unit and its frequency of duplication over several generations (Ganley & Kobayashi, 2011). While the results from this study revealed many interesting features of the dynamics of repeat loss and duplication at the rDNA array, this method is still not amenable to high-throughput analysis because it involves colony PCR of >200 colonies per time point to estimate the fraction of cells that have lost or gained the tagged repeat. Moreover, the use of different parameters by different groups to represent their estimates of rDNA instability makes direct comparison of data from different studies challenging.

To measure rDNA instability in a quantitative, highly sensitive, and simple manner that is easily amenable to high-throughput studies, we developed a single-cell, fluorescence-based assay that combines the basic principles of traditional marker-loss assays and those of the quantitative, single-cell based assay for measurement of chromosome transmission fidelity (qCTF) in yeast developed by Zhu et al. (2015). The qCTF assay provides a direct readout of a chromosome loss event that can be detected in single cells via irreversible gain of GFP fluorescence soon after the loss of a tester chromosome, which can be detected and quantified in large populations of cells using flow cytometry (Zhu et al., 2015). We call our assay qRIN, or quantitative Repeat Instability. To construct the reporter strain to measure rDNA instability, we first tagged the most highly expressed *MATa*-specific gene, *MFA1* (Ghaemmaghami et al., 2003) with 3 copies of GFP in a haploid S288C yeast strain of *MATa* mating type. The *MATα* locus was then introduced into a single rDNA repeat unit. The α2 transcriptional repressor produced from the *MATα* locus strongly represses *MATa*-specific genes, such

as *MFA1-3×GFP*. Thus, when the *MATα*-containing rDNA repeat is present, the expression of Mfa1-3×GFP is strongly repressed; however, if this repeat is lost, Mfa1-3×GFP will be expressed and the cell will become highly fluorescent within one cell cycle after the loss event due to rapid proteasome degradation of the α2 repressor (Laney et al., 2006) (Figure 3.1B).

To measure rDNA repeat loss rates, single colonies of freshly revived reporter strains are inoculated into Leucine-dropout medium to select for the retention of the *MATα-LEU2* repressor construct, and allowed to grow overnight. The cultures are then diluted into non-selective medium (time t=0) to allow for the loss of the *MATα*-containing rDNA repeat. The cell density and fraction of GFP-positive cells are measured at the start of the experiment. Following growth in non-selective medium for ~24 hours (time t=24h, ~10-12 doublings), cell density and fraction of GFP-positive cells in the culture are measured. Optical density at 600nm (OD_{600}) is used as a measure of cell density, and the fraction of fluorescent cells can be rapidly measured using flow cytometry in low or high-throughput formats, and subsequently used to calculate the rate of loss of rDNA repeats using a simple mathematical formula derived based on the methods in Zhu et al. (Zhu et al., 2015).

Traditional marker-loss assays employed colony sectoring analyses to estimate the fraction of cells that had lost the selectable marker, followed by classical fluctuation test-based models (Luria–Delbrück method (Luria & Delbruck, 1943), extended by others (Capizzi & Jameson, 1973; Lea & Coulson, 1949; Luria, 1951)) to estimate marker loss rates. However, this method requires multiple parallel cultures to estimate marker loss rates in a single sample. Additionally, the relatively small population sizes (a few cells to a few hundred cells at most) increases the likelihood of “jackpot events” (Luria & Delbruck, 1943), which are random mutations that occur early during the course of establishment of the population, and predominate the population. Therefore, we chose to use a mutation accumulation model which allows the estimation of rDNA repeat loss rates for any sample from a single culture using 2 measurements, i) fraction of GFP-positive cells, and ii) OD_{600}, from 2 time points, t=0 and t=24h, the start and end of the

experiment respectively. The use of this model requires starting with, and analyzing population sizes large enough so that the probability of occurrence of the mutation of interest (here, the loss of the *MATα* containing rDNA repeat, which generates a GFP-positive cell) at every generation is nearly 1. The use of flow cytometry to measure the fraction of GFP-positive cells allows us to measure the large numbers of cells required for this type of analysis. Our starting population and the populations of cells analyzed typically contain at least 200,000 cells, which is not only much larger than the population size used in fluctuation tests, but also minimizes the likelihood of jackpot events.

Briefly, consider the reporter strain in which the *MATα*-containing rDNA repeat is lost at a rate of $\boldsymbol{m}$ per cell division, where $\boldsymbol{m}$ represents the fraction of cells, on average, that lose the *MATα*-containing rDNA repeat and become fluorescent, or GFP-positive, at every division. If the number of GFP-positive cells (cells that have lost the *MATα*-containing rDNA repeat) and GFP-negative cells (cells that contain a *MATα*-containing rDNA repeat) in the population at any given generation, $\boldsymbol{n}$ are $\boldsymbol{N_n^+}$ and $\boldsymbol{N_n^-}$ respectively, then the total number of cells at any generation $\boldsymbol{n}$ will be

$$\boldsymbol{N_n = N_n^+ + N_n^-} \qquad \textbf{(1)}$$

At every cell division, the number of GFP-negative cells doubles, but also decreases by a fraction of $\boldsymbol{m}$ as some cells lose *MATα* and become fluorescent. Therefore, at any generation $\boldsymbol{n}$, the number of GFP-negative cells can be represented by the equation

$$\boldsymbol{N_n^- = 2^n(1-m)^n N_0^-} \qquad \textbf{(2)}$$

where $\boldsymbol{N_0^-}$ is the number of GFP-negative cells at t=0, and $\boldsymbol{m}$ is the rate of loss of *MATα* per cell division. Further, the number of GFP-positive cells at any generation $\boldsymbol{n}$ can be obtained from the relation

$$N_n^+ = N_n - N_n^-$$

(3)

Therefore, the ratio of GFP-positive cells to GFP-negative cells at any generation n can be represented by R_n , and,

$$R_n = \frac{N_n^+}{N_n^-}$$

(4)

Substituting the expressions for N_n^+ and N_n^- from equations ***(1-3)***, R_n may be re-written as

$$R_n = \frac{[N_n - N_n^-]}{[2^n(1-m)^n N_0^-]}$$

$$R_n = \frac{[2^n N_0 - 2^n(1-m)^n N_0^-]}{[2^n(1-m)^n N_0^-]}$$

$$R_n = \frac{[N_0^- + N_0^+ - (1-m)^n N_0^-]}{[(1-m)^n N_0^-]}$$

$$R_n = \frac{[1 + (N_0^+/N_0^-)]}{[(1-m)^n]} - 1$$

$$R_n = \frac{[1 + R_0]}{[(1-m)^n]} - 1$$

where R_0 is the ratio of GFP-positive cells to GFP-negative cells at t=0. Further,

$$(1-m)^n = \frac{[1 + R_0]}{[1 + R_n]}$$

$$m = [(1 + R_0)/(1 + R_n)]^{1/n}$$

For cases where repeat loss rates are very small, $\boldsymbol{m} \ll \mathbf{1}$, this equation can be further simplified to

$$\mathbf{1} - \boldsymbol{mn} = (\mathbf{1} + \boldsymbol{R_0})/(\mathbf{1} + \boldsymbol{R_n})$$

$$\boldsymbol{m} = \mathbf{1} - \frac{[\mathbf{1} - \{(\mathbf{1} + \boldsymbol{R_0})/(\mathbf{1} + \boldsymbol{R_n})\}]}{\boldsymbol{n}}$$

$$\boldsymbol{m} = \frac{(\boldsymbol{R_n} - \boldsymbol{R_0})}{\boldsymbol{n}(\mathbf{1} + \boldsymbol{R_n})}$$

(5)

The values for $\boldsymbol{R_0}$ and $\boldsymbol{R_n}$ can be obtained simply from the measurements of fractions or numbers of GFP-positive and GFP-negative cells at t=0 and t=24h respectively. The number of generations, $\boldsymbol{n}$, can be obtained from the change in the total number of cells over $\boldsymbol{n}$ generations as

$$\boldsymbol{n} = \log_2 \frac{\boldsymbol{N_n}}{\boldsymbol{N_0}}$$

where $\boldsymbol{N_0}$ is the total number of cells at t=0. Since OD_{600} at any generation $\boldsymbol{n}$, $\boldsymbol{OD_{600-n}}$, is directly proportionate to the total number of cells at that generation, this relationship can be re-written as

$$\boldsymbol{n} = \log_2 \frac{\boldsymbol{OD_{600-n}}}{\boldsymbol{OD_{600-0}}}$$

(6)

where $\boldsymbol{OD_{600-0}}$ and $\boldsymbol{OD_{600-n}}$ are the OD_{600} measurements at t=0 and t=24h respectively. Therefore, the rate of loss of the *MATα*-containing rDNA repeat unit per cell division can be obtained from equations (5) and (6) with measurements of OD_{600} values and numbers of GFP-positive and GFP-negative cells at the start (t=0) and end (t=24h) of the experiment.

These calculations make the following key assumptions:

1. The rate of loss of the *MATα*-containing rDNA repeat, $\boldsymbol{m}$, is constant.
2. GFP-positive cells are generated predominantly by a complete loss of the *MATα*-containing rDNA repeat unit.
3. GFP-positive cells generated by loss of the *MATα*-containing rDNA repeat unit have similar growth rate and doubling time as the GFP-negative cells that retain *MATα*.
4. Loss of GFP-positive or GFP-negative cells from the population, by cell death, for example, is negligible over the course of the experiment.

To validate the qRIN assay, we first constructed a reporter strain, hereafter referred to as *RDN25-MATα*, where the *MATα-LEU2* repressor construct was integrated near the 3'-end of the 25S rRNA coding sequence of a single rDNA repeat. We grew this strain overnight in Leucine-dropout medium to select for *MATα*, diluted into complete, non-selective medium (t=0) and allowed growth for 10-12 generations (t=24h). We collected and analyzed samples from t=0 and t=24h by flow cytometry. As expected, a vast majority of cells were GFP-negative at both time points (Figure 3.2A). A small fraction of cells (0.436 ± 0.08%, n= 8 experiments) exhibited GFP fluorescence 10-100 fold higher than that of the GFP-negative population at t=24h, and a small, but lower fraction of cells (0.118 ± 0.02%, n= 8 experiments) also exhibited similar GFP fluorescence at t=0. (Figure 3.2A). In contrast, this highly fluorescent GFP-positive population was the predominant population (97.06 ± 2.70% at t=24h and 94.78 ± 3.79% at t=0, n= 8 experiments) in samples collected at both time points from the parent strain, hereafter referred to as *MFA1-3×GFP*, that contains the 3×GFP tagged Mfa1, but lacks the *MATα-LEU2* repressor (Figure 3.2A). Additionally, this highly fluorescent GFP-positive population was absent at both time points in a control strain, BY4741, that does not contain the 3×GFP tagged Mfa1(Figure 3.2A).

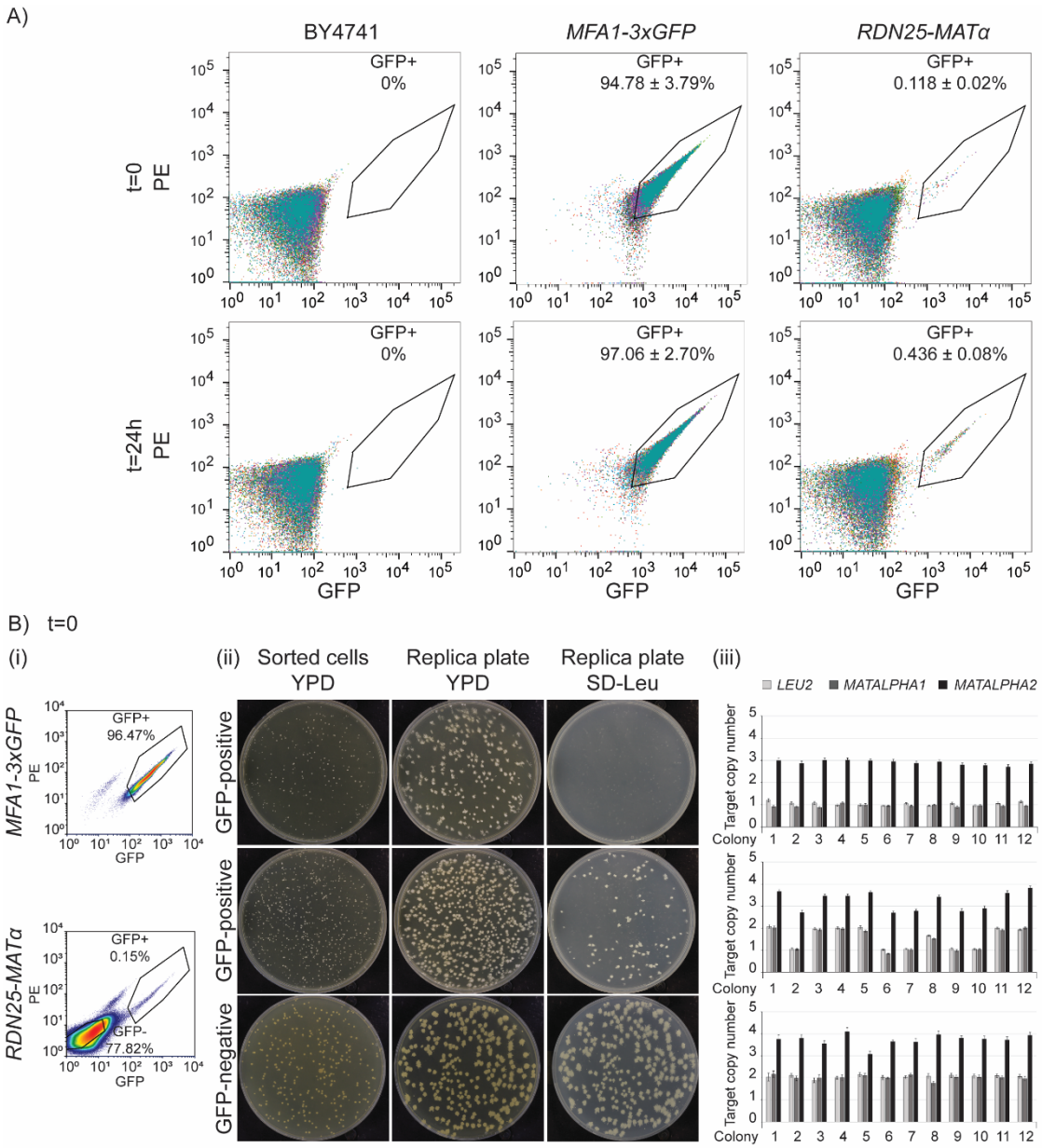

Figure 3.2. Validation of the qRIN assay. A) Flow cytometry analyses showing the fraction of GFP-positive cells at t=0 and t=24h in BY4741, the wild-type, non-fluorescent control strain, and the *MFA1-3×GFP* and the *RDN25-MATα* strains. Data for 8 independent colonies for each strain have been overlaid. GFP-positive cells are gated by the black polygon. B) (i) Flow cytometry data showing GFP-positive and GFP-negative cells sorted from the *MFA1-3×GFP* and *RDN25-MATα* strains at t=0. Sorted cells are gated by black polygons. (ii) Sorted GFP-positive and GFP-negative cells plated on YPD plates, and replica plated on to YPD and SD-Leu plates. 78.25% (331/423 colonies) GFP-positive cells from *RDN25-MATα* strain are Leu-. (iii) Copy number of *MATALPHA-LEU2* in 12 colonies picked from the YPD replica plate for each sorted population measured by ddPCR. Error bars represent standard deviation for each individual reaction. 41.67% (5/12 colonies) GFP-positive cells from the *RDN25-MATα* strain have lost the *MATALPHA-LEU2* construct.

We then used fluorescence-activated cell sorting (FACS) to sort both, the GFP-positive and GFP-negative populations, in the *RDN25-MATα* reporter strain grown in

complete medium to test for the presence of the *MATα-LEU2* repressor construct. To do this we collected samples at t=0 and t=24h from the *RDN25-MATα* strain grown as described above (Figures 3.2B (i), 3.3A (i)). As a control, we also sorted GFP-positive cells from the *MFA1-3×GFP* strain grown in complete medium at both t=0 and t=24h (Figures 3.2B (i) and 3.3A (i)). We then plated the FACS-sorted cells at single-cell density on to rich medium, followed by replica plating on to Leucine-dropout medium. We found that all the sorted GFP-negative cells from the *RDN25-MATα* strain were Leu+ at both time points (Figures 3.2B (ii), 3.3A (ii)). As expected, 100% of the sorted GFP-positive cells from the *MFA1-3×GFP* strain at both time points were Leu- (Figures 3.2B (ii), 3.3A (ii)). Only 78.25% (331/423 colonies) of the GFP-positive cells sorted from *RDN25-MATα* at t=0 were Leu-, likely owing mostly to the imperfect nature of selection in dropout medium (Figure 3.2B (ii)). However, 91% (364/400 colonies) of the GFP-positive cells sorted from *RDN25-MATα* at t=24h were Leu-, suggesting that most of the GFP-positive cells generated during the course of growth in non-selective medium had lost *MATα-LEU2* (Figure 3.3A (ii)).

To confirm that most of the GFP-positive cells had in fact lost *MATα-LEU2*, we picked 12 colonies at random from the different sorted populations that had been plated on rich medium for both, the *MFA1-3×GFP* and the *RDN25-MATα* strains, and measured the copy number of *LEU2* and the two genes that constitute the *MATα* locus, *MATα1* and *MATα2*, using ddPCR assays designed to target these genes. The *MFA1-3×GFP* strain contains 1 copy of *leu2-3,112*, which confers leucine auxotrophy, 1 copy of *MATα1* (at the silenced *HML* locus), and 3 copies of *MATα2* (1 copy of *MATα2* at the silenced *HML* locus, 1 copy of *MATa2* identical in sequence to *MATα2* at the mating type *MAT* locus, and 1 copy of *MATa2* at the silenced *HMR* locus). The *RDN25-MATα* strain derived from this strain contains 1 additional copy each of *LEU2*, *MATα1* and *MATα2*. Therefore, the GFP-positive cells sorted from *MFA1-3×GFP* at t=0 and t=24h should contain 1 copy each of *LEU2* and *MATα1*, and 3 copies of *MATα2*, which is what our ddPCR copy number measurements show (Figures 3.2B (iii), 3.3A (iii)). Similarly,

the GFP-negative cells sorted from *RDN25-MATα* contain 2 copies each of *LEU2* and *MATα1* and 4 copies of *MATα2* as expected (Figures 3.2B (iii), 3.3A (iii)). Finally, 5/12 (41.67%) of the sorted GFP-positive cells from t=0 and 11/12 (91.67%) of the sorted GFP-positive cells from t=24h of the *RDN25-MATα* strain contain only 1 copy each of *LEU2* and *MATα1*, and 3 copies of *MATα2*, which are the expected copy number measurements of *MATα* and *LEU2* for cells that have lost the *MATα-LEU2* repressor (Figures 3.2B (iii), 3.3A (iii)). Some of these GFP-positive cells could be generated by silencing of the *MATα-LEU2* within the rDNA and could account for a small fraction of the GFP-positive cells that still contain the *MATα-LEU2* repressor. Silencing of RNAPII transcribed reporters at the rDNA can be altered by several factors including the integration site within a single repeat and relative location within the array, and levels of silencing factors like Sir2 (Huang & Moazed, 2003; Smith et al., 1998; D. Wang et al., 2016); a significant change in silencing of the *MATα-LEU2* repressor is expected to result in an underestimation of rDNA repeat loss rates. This is a caveat inherent to all marker loss assays, and our validation experiments confirm that GFP-positive cells in the wild-type reporter strain grown in non-selective medium are mostly generated by a complete loss of the *MATα-LEU2* repressor construct.

Figure 3.3. Additional validation of the qRIN assay. (A) GFP-positive cells in the *RDN25-MATα* strain are generated predominantly by a complete loss of *MATALPHA-LEU2*. (i) Flow cytometry data showing GFP-positive and GFP-negative cells sorted from the *MFA1-3×GFP* and *RDN25-MATα* strains grown in non-selective medium(t=24h). (ii) Sorted GFP-positive and GFP-negative cells plated on YPD plates, and replica plated on to YPD and SD-Leu plates. 91% (364/400 colonies) GFP-positive cells from *RDN25-MATα* strain are Leu-. (iii) Copy number of *MATALPHA-LEU2* in 12 colonies picked from the YPD replica plate for each sorted population measured by ddPCR. Error bars represent standard deviation for each individual reaction. 91.67% (11/12 colonies) GFP-positive cells from the *RDN25-MATα* strain have lost the *MATALPHA-LEU2* construct. (B) Loss of *MATALPHA-LEU2* does not confer a growth advantage. Representative growth curves of single colonies (1 each) derived from sorted GFP-positive cells from *RDN25-MATα* and *MFA1-3×GFP* strains and sorted GFP-negative cells from *RDN25-MATα*. Growth curves were plotted based on average of triplicate measurements of OD_{600} taken at 15-minute intervals for 24 hours. Inset: Growth rates for four independent colonies derived from each population. Error bars represent standard deviation. (C) Average repeat loss rates from 3 different genomic regions – *CUP1* gene arrays containing 2, 6, 12, or 17 copies of *CUP1*, the rDNA array, and a "stable" intergenic region downstream of *TUB1*. (D) Similar rDNA repeat loss rates obtained from a variety of reporter strains. (E) Altered rDNA repeat loss rates in mutants known to affect rDNA stability. For (C) – (E) error bars represent standard deviation based on four biological replicates. Statistical significance was calculated using a standard 2-tailed t-test. * - $p<0.05$, ** - $p<0.01$, *** - $p<0.001$, **** - $p<0.0001$, n. s.– not significant.

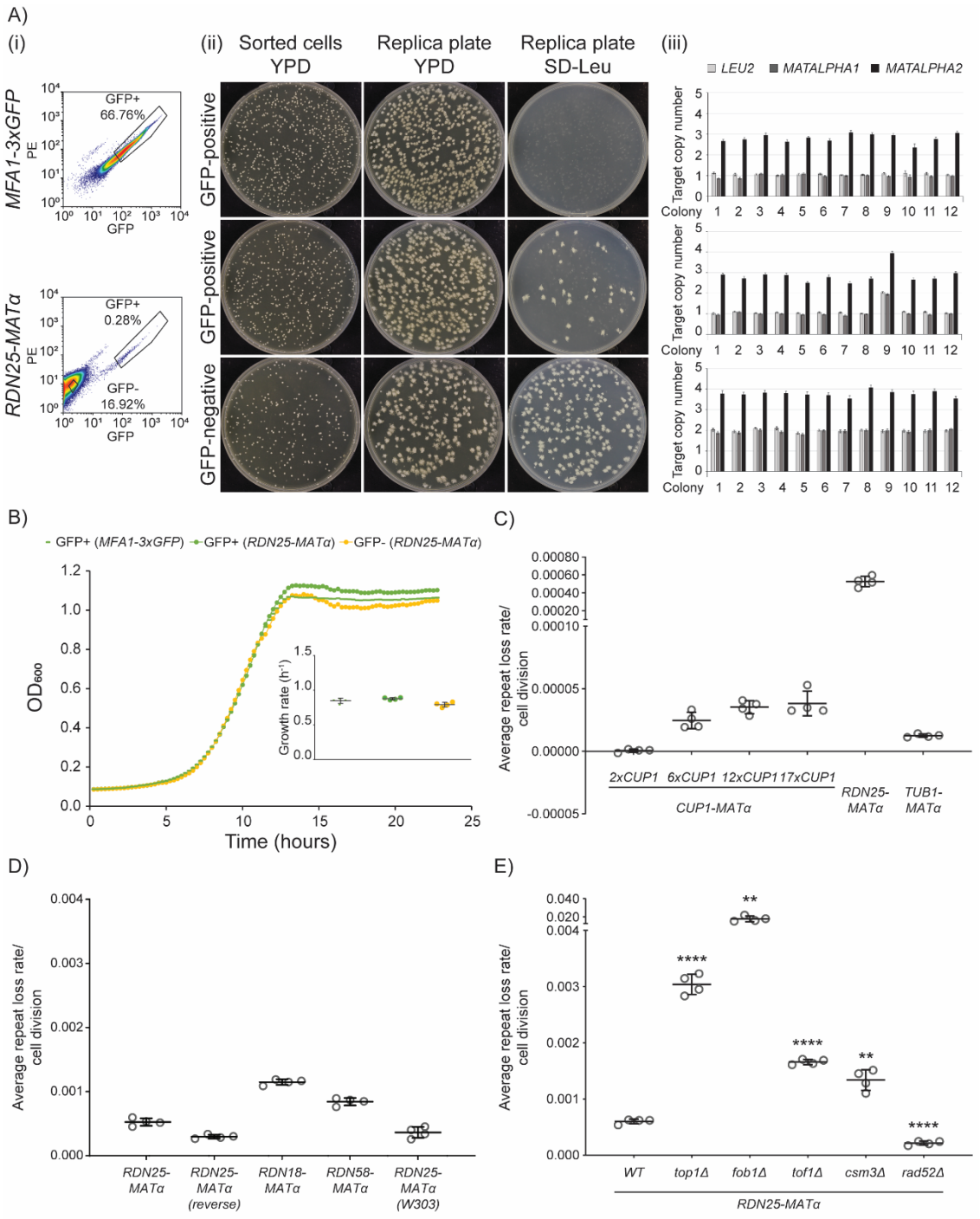
A)
(i)
(ii) Sorted cells YPD
Replica plate YPD
Replica plate SD-Leu
(iii)
MFA1-3xGFP
RDN25-MATα
PE
GFP
GFP+ 66.76%
GFP+ 0.28%
GFP- 16.92%
GFP-positive
GFP-positive
GFP-negative
LEU2
MATALPHA1
MATALPHA2
Target copy number
Colony 1 2 3 4 5 6 7 8 9 10 11 12
B)
GFP+ (MFA1-3xGFP)
GFP+ (RDN25-MATα)
GFP- (RDN25-MATα)
OD600
Time (hours)
Growth rate (h-1)
C)
Average repeat loss rate/ cell division
2xCUP1
6xCUP1
12xCUP1
17xCUP1
CUP1-MATα
RDN25-MATα
TUB1-MATα
D)
Average repeat loss rate/ cell division
RDN25-MATα
RDN25-MATα (reverse)
RDN18-MATα
RDN58-MATα
RDN25-MATα (W303)
E)
Average repeat loss rate/ cell division
WT
top1Δ
fob1Δ
tof1Δ
csm3Δ
rad52Δ
RDN25-MATα

Next, we compared growth rates of cultures derived from GFP-positive and GFP-negative cells sorted from samples collected at t=24h for *RDN25-MATα* and found no significant differences (Figure 3.3B). This validates our assumption that loss of the *MATα-LEU2* repressor does not alter growth rates of the *RDN25-MATα* strain in the "wild-type" reporter strain background in non-selective medium. There may be conditions under which loss of the *MATα-LEU2* repressor may confer a competitive growth advantage/disadvantage to the resulting GFP-positive cells. In these cases, the formula to calculate repeat loss rates can be modified as described in Zhu et al. (2015), and requires the measurement of OD_{600} and the fraction of the GFP-positive cells at an additional time point during the course of growth (Zhu et al., 2015). However, equal growth rates of the GFP-positive and GFP-negative cells is a reasonable assumption that simplifies the experimental design and calculations of rDNA repeat loss rates for most situations, particularly for high-throughput screens.

To test the quantitative performance of our assay, we calculated rDNA repeat loss rates per cell division in the *RDN25-MATα* reporter strain grown in non-selective medium for 10-12 generations as described above. While average repeat loss rates ranged from ~0.0003-0.001 per cell division across all our experiments, biological replicates within any single experiment showed very little variability, as shown in Figure 3.3C. The rates of rDNA repeat loss estimated using our assay are similar to the estimates of mitotic intrachromosomal recombination rates at the rDNA obtained using traditional marker loss assays (Table 3.1).

Table 3.1. Summary of rDNA and *CUP1* instability measurements.

Parameter measured	Assay	Estimate (units)	Reference
Mitotic sister-chromatid recombination at the rDNA	Traditional marker loss assay	0.0012 (/cell/cell division)	(Casper et al., 2008; Gottlieb & Esposito, 1989)
Average loss rate of tagged rDNA unit	Colony PCR for tag	0.0032 (/repeat/cell division)	(Ganley & Kobayashi, 2011)
Average rDNA repeat loss rate	qRIN	0.0003-0.001 (/repeat/cell division)	This study
Mitotic sister-chromatid recombination at the *CUP1* array	Traditional marker loss assay	0.00015 (/cell/cell division)	(Zhao et al., 2017)
CUP1 copy number variation	Gel electrophoresis and Southern blotting	0.00034 (/cell/cell division)	(Andersen et al., 2015)
Average *CUP1* repeat loss rate (transcription-independent)	qRIN	1×10^{-6} (2×*CUP1*) – 5×10^{-5} (17×*CUP1*) (/repeat/cell division)	This study
Base substitutional mutation rate (yeast)	Whole genome sequencing	0.33×10^{-9} (/site/cell division)	(Lynch et al., 2008)

Further, we also constructed three additional reporter strains where the *MATα-LEU2* repressor was integrated into different parts of a single rDNA repeat. *RDN18-MATα* and *RDN58-MATα* contain *MATα-LEU2* integrated into the 18S rRNA and the 5.8S rRNA coding sequences of a single rDNA repeat respectively, and *RDN25-MATα (reverse)* contains *MATα-LEU2* integrated near the 3'-end of the 25S rDNA gene on the non-coding strand. The rDNA repeat loss rates calculated using these different reporter strains were similar to one another in any given experiment, and all within the range of 0.0003-0.001/cell division across all experiments (Figure 3.3D). We constructed a fourth reporter strain, *TUB1-MATα*, where the *MATα-LEU2* repressor was inserted into the intergenic region downstream of the essential gene *TUB1*, a unique genomic region that

should be “stable” relative to the rDNA. As shown in Figure 3.3C, the loss of *MATα* is negligibly low for this region, as expected.

Next, we chose a small set of genes well-known for their effects on rDNA stability – *TOP1*, which encodes Topoisomerase I, *RAD52,* which is required for homologous recombination-mediated DSB repair, and *FOB1*, which encodes the rDNA RFB binding protein. We deleted each of these genes in the *RDN25-MATα* reporter strain to test the ability of our assay to detect changes in rDNA stability. The *top1*Δ mutants showed increased rDNA repeat loss rates (Figure 3.3E). This is consistent with previous reports of increased marker loss rates and extensive copy number variation at the rDNA in *top1* mutants (Andersen et al., 2015; Houseley et al., 2007). The *rad52*Δ mutants showed decreased rDNA repeat loss rates, as expected, supporting the idea that homologous recombination-mediated repeat loss is the major source of instability at the rDNA.

The *RDN25-MATα fob1*Δ mutants, on the other hand, showed a significant increase in rDNA repeat loss rates relative to wild-type controls in our assay (Figure 3.3E), contrary to previous reports of lower marker loss and marker duplication frequencies in these mutants (Johzuka & Horiuchi, 2002; Kobayashi, 2003; Kobayashi et al., 1998). We observed a consistent increase in rDNA repeat loss rates in *fob1*Δ mutants in multiple independent isolates of *fob1*Δ in the *RDN25-MATα* background across multiple experiments. We also did not observe lower repeat loss rates in *fob1*Δ mutants in the *RDN18-MATα* and *RDN58-MATα* backgrounds (Figure 3.4A). To rule out the contribution of the genetic background of our reporter strains to this phenotype, we also generated *fob1*Δ mutants in the *RDN25-MATα* (W303) strain background and measured rDNA repeat loss rates as before. We found that rDNA repeat loss rates in the *fob1*Δ mutants were higher than those in the wild-type *RDN25-MATα* (W303) strain (Figure 3.4A). We confirmed that there were no changes in rDNA copy number, and that there was only one copy of the *MATα-LEU2* repressor in the *fob1*Δ mutants (Figure 3.4B). Given the reported roles of Fob1 in the silencing of RNAPII transcribed genes at the rDNA (Buck et al., 2016; Di Felice et al., 2019) and the lack of clear separation

between GFP-positive and GFP-negative cells in this mutant (Figure 3.5), we considered the possibility that the expression of the *MATα-LEU2* repressor may be altered in a *fob1*Δ mutant background. To test for the presence of the *MATα-LEU2* repressor construct, we sorted GFP-positive and GFP-negative cells from t=0 and t=24h for wild-type and *fob1*Δ *RDN25-MATα* strains grown in complete medium. As described before, we plated the sorted cells at single-cell density on to rich medium, followed by replica plating on to Leucine-dropout medium. We found that 100% of the GFP-positive cells sorted from the *RDN25-MATα fob1*Δ strain were Leu+, suggesting retention of the *MATα-LEU2* repressor and the generation of GFP-positive cells likely through silencing of the repressor (Figure 3.5).

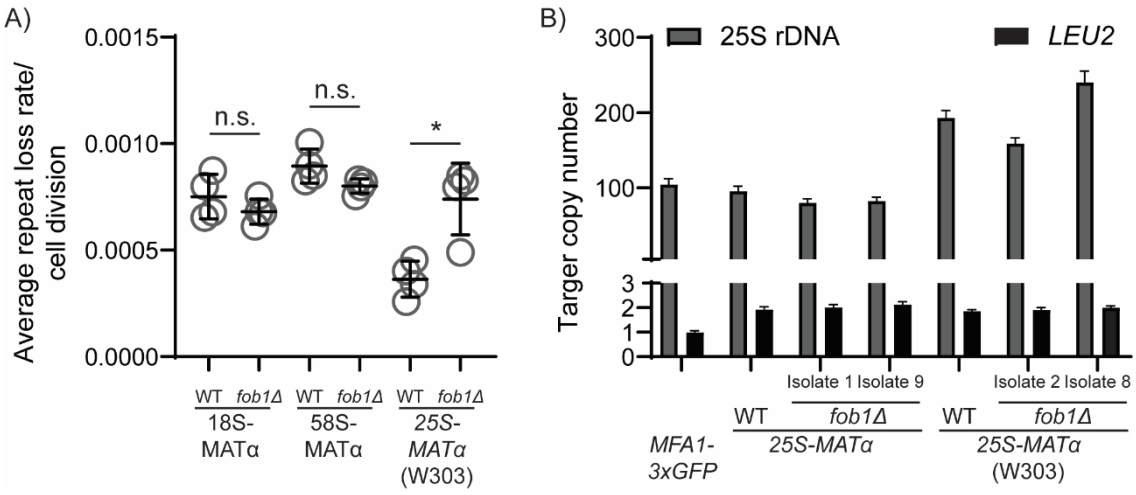

Figure 3.4. Analysis of rDNA stability in *fob1*Δ mutants. A) rDNA repeat loss rates in *fob1*Δ mutants in various reporter strain backgrounds. Error bars represent standard deviation based on 4 biological replicates. Statistical significance was calculated using a standard 2-tailed t-test. * - p<0.05, n. s.– not significant. B) rDNA and *MATALPHA-LEU2* copy number measurements in *fob1*Δ mutants with increased rDNA instability. Error bars represent standard deviation for each individual reaction.

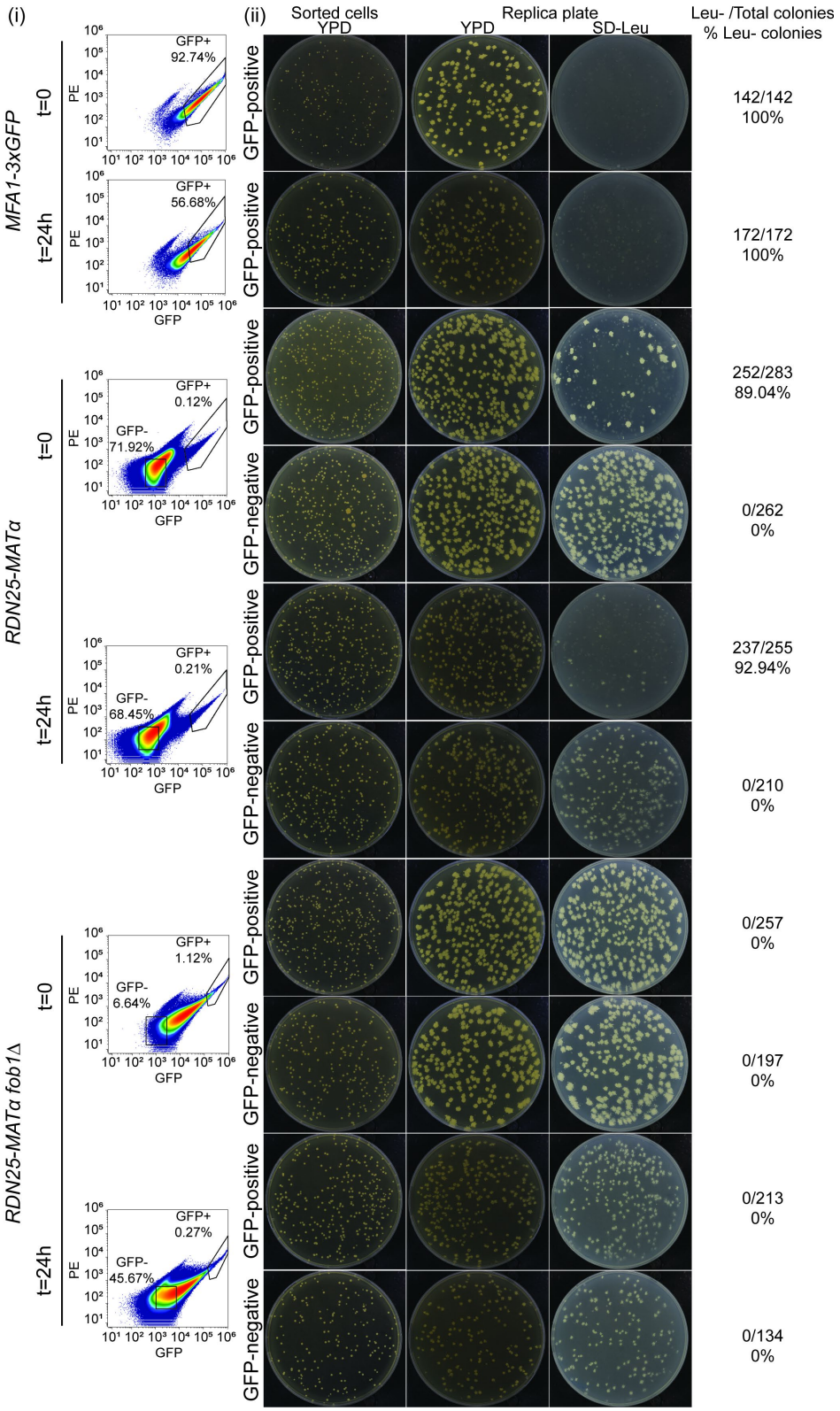

Figure 3.5. Analysis of the loss of *MATALPHA-LEU2* in *fob1*Δ mutants. (i) Flow cytometry data showing GFP-positive and GFP-negative cells sorted from the *MFA1-3×GFP*, and wild-type and *fob1*Δ *RDN25-MATα* strains at t=0 and t=24h. Sorted cells are gated by black polygons. (ii) Sorted GFP-positive and GFP-negative cells plated on YPD plates, and replica plated on to YPD and SD-Leu plates. Fraction of Leu- cells is indicated for each sorted population. 100% of the GFP-positive cells from *RDN25-MATα fob1*Δ strain are Leu+.

Tof1 and Csm3, like Fob1, are required for replication fork pausing within the rDNA and RFB activity, however, loss of these proteins does not affect reporter silencing within the rDNA (Bando et al., 2009; Mohanty et al., 2009). To test the effects of reporter silencing-independent loss of RFB activity on rDNA stability, we deleted *TOF1* and *CSM3* in the *RDN25-MATα* strain, and measured rDNA stability in the mutant strains. We found that both *tof1*Δ and *csm3*Δ mutants had increased rDNA repeat loss rates (Figure 3.3E), suggesting that the loss of RFB activity is detrimental to rDNA stability, presumably because of increased head-on collisions of the replisome with RNAPI transcription machinery.

We did not include *sir2*Δ mutants in these validation experiments despite the well-known role of Sir2 in suppressing recombination at the rDNA array and the subsequent increase in rDNA instability in *sir2*Δ mutants (Gottlieb & Esposito, 1989). This was because Sir2 is also important for silencing of the *HML* and *HMR* loci, which contain full, silenced copies of the *MATα* and *MATa* loci (Rine & Herskowitz, 1987). Our reporter system relies on the native *HML* and *HMR* loci remaining silenced, so that GFP-repression is dependent solely on the *MATα-LEU2* construct inserted in the rDNA. In a *sir2*Δ mutant strain, the *HML* and *HMR* loci may be de-silenced, resulting in constitutive expression of *MATα*, and consequent repression of Mfa1-3×GFP irrespective of the presence of the *MATα-LEU2* repressor construct. To test this, we measured rDNA repeat loss rates in the *RDN25-MATα* reporter strain grown in nicotinamide (NAM), an inhibitor of sirtuins including Sir2. As predicted, in NAM, the fraction of GFP-positive cells at t=0 is lower than that in untreated controls, and remains low even after growth in non-selective medium, and therefore the calculated repeat loss rates were also low (Figure 3.6). While our qRIN assay depends on normal function and silencing of the *HML* and *HMR* loci, the quantitative power and scalability offered by this assay far outweighs this caveat.

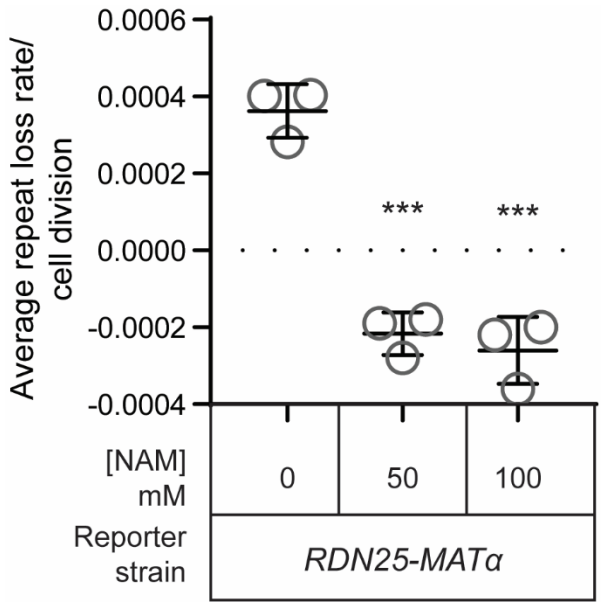

Figure 3.6. Analysis of rDNA stability in nicotinamide. Error bars represent standard deviation based on 3 biological replicates. Statistical significance was calculated using a standard 2-tailed t-test. *** - p<0.001.

Finally, we demonstrate the versatility of the qRIN assay by adapting it to measure repeat loss rates at a second tandem array in the yeast genome, the *CUP1* gene array. Estimates of *CUP1* instability and copy number variation from previous studies are also summarized in Table 3.1. To construct the *CUP1-MATα* reporter strains, we integrated the *MATα-LEU2* repressor construct at the 3'-end of the *CUP1* ORF in a single *CUP1* repeat unit in the *MFA1-3×GFP* strain. This transformation resulted in *CUP1-MATα* isolates that had *CUP1* gene arrays ranging in size from 2-17 repeats. As expected, copper resistance in the reporter strains was directly related to *CUP1* copy number, and required the *CUP1* transcription factor Cup2 (Ace1) (Figure 3.7A).

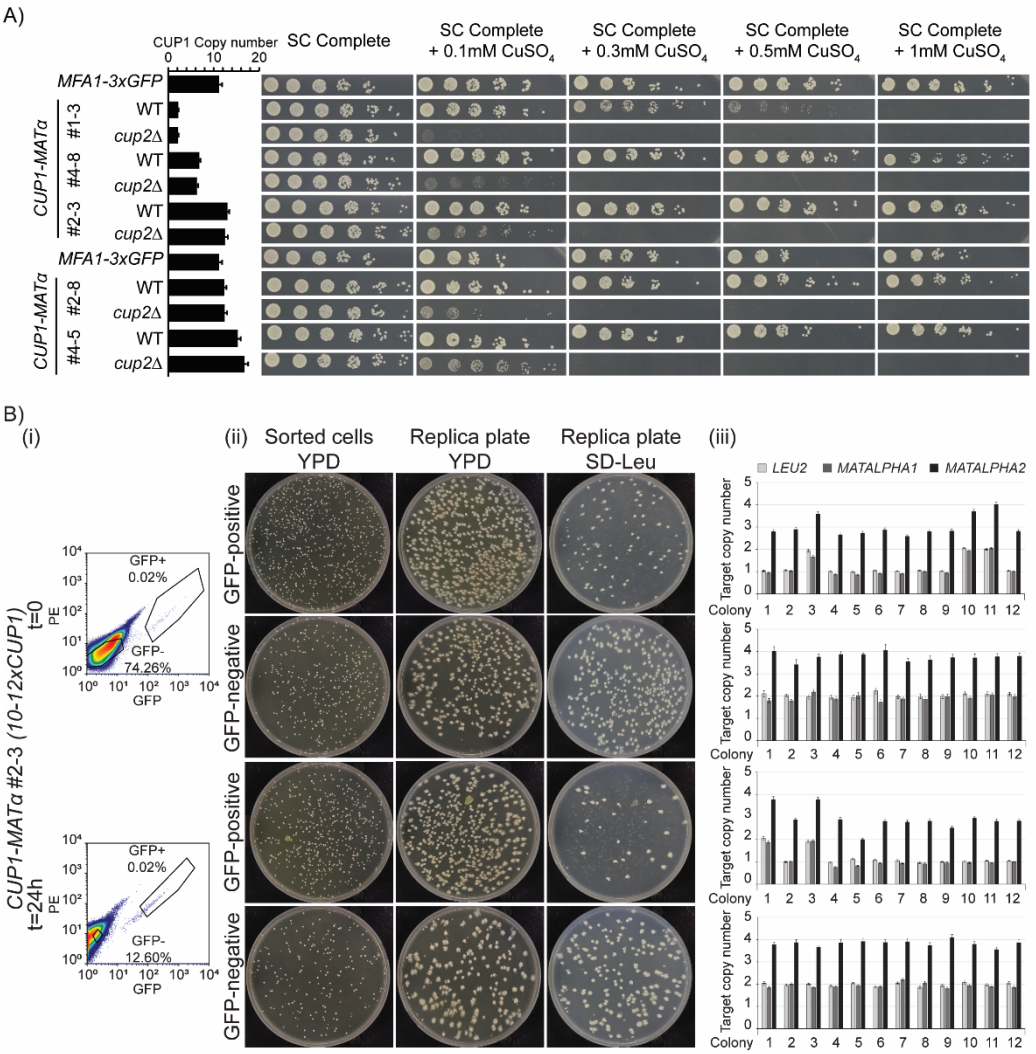

Figure 3.7. Validation of the qRIN assay for the *CUP1-MATα* reporter strains. A) Growth assays showing copper sensitivity of various reporter strains. *CUP1* copy number was measured by ddPCR. Error bars represent standard deviation for each individual reaction. B) GFP-positive cells are generated by loss of *MATα-LEU2* (i) Flow cytometry data showing GFP-positive and GFP-negative cells sorted from a *CUP1-MATα* strain with ~12×*CUP1* at t=0 and t=24h. Sorted cells are gated by black polygons. (ii) Sorted GFP-positive and GFP-negative cells plated on YPD plates, and replica plated on to YPD and SD-Leu plates. At t=0, 82.08% (394/480 colonies) of GFP-positive cells are Leu-. At t=24h, 92.31% (360/390 colonies) of GFP-positive cells are Leu-. At both time points, 100% of GFP-negative cells (303/303 colonies at t=0 and 170/170 colonies at t=24h) are Leu+. (iii) Copy number of *MATALPHA-LEU2* in 12 colonies picked from the YPD replica plate for each sorted population measured by ddPCR. Error bars represent standard deviation for each individual reaction. At t=0, 75% (9/12 colonies) of GFP-positive cells have lost the *MATALPHA-LEU2* construct. At t=24h, 83.33% (10/12 colonies) of GFP-positive cells have lost the *MATALPHA-LEU2* construct. At both time points, 100% of GFP-negative cells (12/12 colonies) have retained the *MATALPHA-LEU2* construct.

As with the *RDN25-MATα* strain, we validated that GFP-positive cells in the *CUP1-MATα* reporter strains were generated mostly by the loss of the *MATα-LEU2* repressor (Figure 3.7B). We then measured transcription-independent *CUP1* repeat loss rates in each of the reporter strains with 2-17 copies of *CUP1.* Strains were grown in non-selective medium, without any copper, and repeat loss rates calculated using the formulae described above. We found that transcription-independent repeat loss rates at the *CUP1* array correlated positively with *CUP1* copy number, and ranged from 1×10^{-6} per cell division in a 2-copy array to 5×10^{-5} per cell division in a 17-copy array (Figure 3.3C). This suggests that transcription-independent repeat instability may be directly related to the size of the tandem array. Further, in the absence of transcription, the instability at the *CUP1* array was at least 10-fold lower than that of the constitutively transcribed rDNA (Figure 3.3C), suggesting that the larger size of the rDNA array and its constitutive transcription are significant sources of rDNA instability. This further affirms the power of using an inducible array in the study of mechanisms involved in the regulation of copy number variation at tandem repeats. Notably, repeat loss rates at both tandem arrays are orders of magnitude higher than the rate of single base substitutions in the yeast genome (Table 3.1), consistent with their potential to have profound impacts on genome diversity and evolution (reviewed in (Press et al., 2019)).

3.5.2 High-throughput screens to identify factors that regulate rDNA copy number variation

Saka et al. (2016) reported the first high-throughput screen to identify non-essential genes involved in the maintenance of rDNA stability in yeast. This group used PFGE to screen a yeast deletion mutant collection of non-essential genes for alterations in the extent of rDNA copy number variation, as indicated by the size of chromosome XII (Saka et al., 2016). This approach is, at best, a qualitative estimate of variability in rDNA copy

number. While marker loss assays have been used to carry out screens, these have been focused on the identification of factors involved in silencing of reporters at the rDNA (Smith et al., 1999). Further, several reports suggest that rDNA copy number is maintained by the fundamental processes of DNA replication and RNAPI transcription, but many components of these processes are essential to cell viability and are missing from high-throughput screens using the yeast knockout collection of non-essential genes. In order to identify pathways that regulate rDNA instability in an unbiased manner, while achieving maximum coverage of the genome, we chose to use our qRIN assay to measure rDNA repeat loss rates in a library of strains in which gene dosage was moderately increased. To achieve this, we used the MoBY-ORF library, which comprises 4,956 uniquely barcoded yeast ORFs, each cloned into a Uracil-selectable plasmid along with their endogenous promoter and 3'-UTR sequences to ensure normal expression patterns (Ho et al., 2009). The plasmids also contain a yeast centromeric sequence, which ensures that the plasmid is maintained at a low copy number (~1-3 copies/cell), thereby only moderately increasing the gene dosage. This library represents ~90% of all non-dubious ORFs annotated in the Saccharomyces Genome Database (SGD) and contains over 250 essential genes. We isolated the individual MoBY-ORF plasmids and transformed them each into the *RDN25-MATα* reporter strain to generate the *RDN25-MATα* (+MoBY-ORF) strain library comprising 4763 strains (representing 96.1% of the 4956 MoBY-ORF plasmids) (Figure 3.8A). Additionally, the MoBY empty vector, p5472, was also transformed into the *RDN25-MATα* reporter strain to generate the *RDN25-MATα* (+p5472) control strain. The *RDN25-MATα* (+MoBY-ORF) strain library was arrayed into 60 96-well plates, with the following control strains added to random empty wells in each plate: BY4741 (wild-type, *MATa* strain with no 3×GFP tag), *MFA1-3×GFP*, *RDN25-MATα*, and *RDN25-MATα* (+p5472) (Appendix B.1).

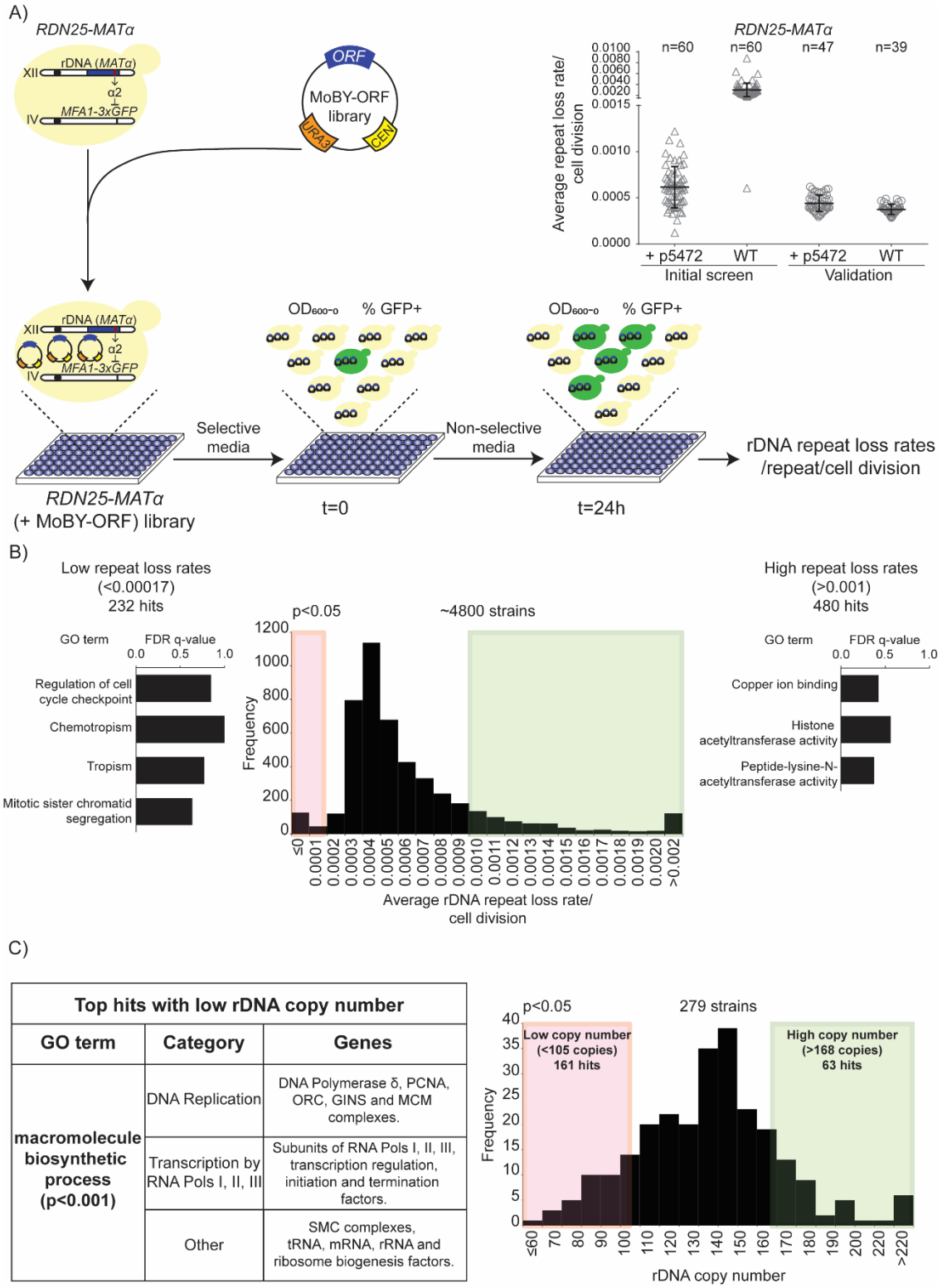

Top hits with low rDNA copy number		
GO term	**Category**	**Genes**
macromolecule biosynthetic process (p<0.001)	DNA Replication	DNA Polymerase δ, PCNA, ORC, GINS and MCM complexes.
	Transcription by RNA Pols I, II, III	Subunits of RNA Pols I, II, III, transcription regulation, initiation and termination factors.
	Other	SMC complexes, tRNA, mRNA, rRNA and ribosome biogenesis factors.

Figure 3.8. Screens to identify genes that regulate copy number variation at the rDNA. (A) Cartoon showing the design of the overexpression screen to identify genes that regulate rDNA stability. Inset, rDNA repeat loss rates in wild-type *RDN25-MATα* and *RDN25-MATα* (+p5472) strains. Error bars represent standard deviation. (B) Distribution of rDNA repeat loss rates across the ~4800 strains of the *RDN25-MATα* (+MoBY-ORF) library. 232 and 480 strains had significantly lower (<0.00017/cell division) and higher rDNA repeat loss rates (>0.001/cell division) respectively (p<0.05). FDR q-values for significantly enriched (p<0.001) GO terms (sorted in order of increasing p-values from top to bottom) for hits with high and low repeat loss rates are also shown. (C) Distribution of rDNA copy number in a second yeast ts mutant collection. 161 and 63 strains had significantly lower (<105 copies) and higher copy number (>168 copies) respectively (p<0.05). The table summarizes the top hits with low rDNA copy number.

We then used our qRIN assay in high-throughput format to measure rDNA repeat loss rates in the *RDN25-MATα* (+MoBY-ORF) strain library as illustrated in Figure 3.8A. As with batch cultures, we first grew the *RDN25-MATα* (+MoBY-ORF) strain library overnight in Leucine and Uracil-dropout medium to select for retention of the *MATα-LEU2* repressor and the MoBY-ORF plasmid. We diluted the cultures into Uracil-dropout medium (t=0) to select for retention of the MoBY-ORF plasmid while allowing for loss of the *MATα-LEU2* repressor, and grew cells for ~24 hours (t=24h, ~10-12 doublings). The control strain *RDN25-MATα* was initially grown in Leucine-dropout medium, followed by dilution into non-selective medium at t=0, whereas the control strains BY4741 and *MFA1-3×GFP* were always grown in non-selective medium. We collected samples at t=0 and t=24h for measuring the fraction of GFP-positive cells by cytometry. We also measured OD_{600} values at both time-points, and calculated rDNA repeat loss rates/cell division for the *RDN25-MATα* (+MoBY-ORF) strain library using the formula described above.

The average of rDNA repeat loss rates/cell division obtained across all 60 96-well plates was 0.0029±0.0012 (n=60) in *RDN25-MATα*, and 0.0006±0.0002 (n=60) in *RDN25-MATα* (+p5472) (Figure 3.8A). Surprisingly, the average rDNA repeat loss rates/ cell division for the *RDN25-MATα* control strain was ~5-fold higher than the rate obtained for the *RDN25-MATα* (+p5472) control strain. However, the rDNA repeat loss rates for the *RDN25-MATα* (+p5472) strain is within the range of 0.0003-0.001/cell division we observed for the *RDN25-MATα* strain in batch cultures. A closer examination of the cytometry data for the *RDN25-MATα* strain revealed that the fraction of GFP-positive cells was higher than usual at both, t=0 and t=24h, suggesting a jackpot event, a loss of the *MATα-LEU2* repressor early in the establishment of the culture that was used to inoculate all 60 plates used in the initial screen. We measured rDNA repeat loss rates in 47 colonies each of freshly revived *RDN25-MATα* and *RDN25-MATα* (+p5472) strains grown in a 96-well plate as in the initial screen. 8/47 colonies of the *RDN25-MATα* strain showed higher fractions of GFP-positive cells at t=0 and t=24h, characteristic of jackpot

events, and data from these colonies were excluded from the analyses. Based on the analysis of rDNA repeat loss rates for the remaining colonies, we found that the two reporter strains had similar rDNA repeat loss rates that were indistinguishable from rates calculated for the *RDN25-MATα* (+p5472) strain in the initial screen (Figure 3.8A).

A distribution of rDNA repeat loss rates/cell division for the entire *RDN25-MATα* (+MoBY-ORF) strain library is shown in Figure 3.8B. rDNA repeat loss rates ranged from -0.003 to +0.01/cell division, with the distribution centered around ~0.0004/cell division. We used the variation in rDNA repeat loss rates for the *RDN25-MATα* (+p5472) strain across all 60 96-well plates from the initial screen to set thresholds to identify *RDN25-MATα* (+MoBY-ORF) strains that had significantly altered rDNA repeat loss rates. Of the ~4800 *RDN25-MATα* (+MoBY-ORF) strains screened, 712 strains had significantly altered rDNA repeat loss rates relative to the empty vector control strain ($p<0.05$). Of these, 480 strains had significantly higher (>0.001/cell division) rDNA repeat loss rates, and 232 strains had significantly lower (<0.0001/cell division) rDNA repeat loss rates than the empty vector control strain. We cherry-picked the top ~200 hits with elevated rDNA repeat loss rates, and the top ~100 hits with reduced rDNA repeat loss rates and subjected them to additional validation. We re-arrayed these hits into 3 96-well plates, along with control strains BY4741, *MFA1-3×GFP*, *RDN25-MATα*, *RDN25-MATα* (+p5472), and *RDN25-MATα top1*Δ (which has elevated rDNA repeat loss rates, Figure 3.3E). We measured rDNA repeat loss rates in high-throughput format in these hits 2 more times to obtain 3 independent measurements of rDNA repeat loss rates (including the initial screen) for each of these strains. The rDNA repeat loss rates from these 3 independent measurements are summarized in Appendix B.2. 65 of the ~200 hits with high instability and 73 of the ~100 hits with low instability showed similarly high or low rDNA instability rates in at least one additional validation run. We also isolated genomic DNA from these cherry-picked hits and measured rDNA copy number as well as *MATα-LEU2* copy number. These copy number measurements are also summarized in Appendix B.2. We wanted to ensure that the reduction in rDNA repeat loss rates were

not due to amplifications of the *MATα-LEU2* repressor. In fact, almost all the hits had only one copy of *MATα-LEU2* repressor, and rDNA copy number similar to that of the *RDN25-MATα* (+p5472) strain. The only exception was *RDN25-MATα* (+MoBY-*YCR035C*), which had reduced rDNA repeat loss rates, and 4 copies of the *MATα-LEU2* repressor, suggesting duplications of the *MATα-LEU2* repressor, likely during strain construction. This strain also had significantly lower rDNA copy number (~69 copies), and so we excluded this strain from further analyses. These data suggest that the results of our screen were not confounded significantly by copy number changes at the rDNA or amplifications of the *MATα-LEU2* repressor.

We then performed a gene-ontology (GO) enrichment analysis on the initial 712 hits to identify pathways involved in regulating rDNA stability. We found that the hits with lower rDNA repeat loss rates were significantly enriched for genes involved in nucleic-acid metabolism and DNA repair and/or recombination pathways (for example, *SGS1*, *HCA4*, *MLH1*, *ADE6*), mitotic cell cycle checkpoint regulation (for example, *MAD1*, *RTT107*, *SLX4*, *CDH1*) and sister chromatid segregation (for example, *SMC4*, *ECO1*, *CIN8*, *NPA3*) ($p<0.001$) (Figure 3.8B, Appendix B.2). In contrast, the hits with elevated rDNA repeat loss rates were significantly enriched for genes involved in acetylation of histones, specifically at lysine residues (for example, *RTT109*, *GCN5*, *SPT10*, *HFI1*, *SAS3*, *SAS4*, *SAS5*, *NAT4*) ($p<0.001$) (Figure 3.8B, Appendix B.2). Interestingly, the hits with elevated rDNA repeat loss rates were also significantly enriched for genes involved in copper transport and/or homeostasis ($p<0.001$) (Figure 3.8B, Appendix B.2). This suggests that rDNA stability could be modulated by environmental stresses such as high concentrations of copper. However, the copper response genes in yeast (ex., *SOD1*) are also known to be activated by DNA damage (Dong et al., 2013), and could regulate rDNA stability through their role in the DNA damage response. Further, the identification of hits with both increased and decreased rDNA repeat loss rates also suggests that cells may have evolved to optimize rDNA instability rather than minimize it so as to allow for rDNA copy number variation in response to genomic stresses.

Finally, to gain a comprehensive understanding of the pathways involved in the regulation of copy number variation at the rDNA, we wanted to supplement our results from the screen for pathways that regulate instability with pathways that are involved in the maintenance of rDNA copy number. We had reported previously, through an unbiased screen of ~45% of essential yeast genes, that mutations in DNA replication machinery were associated with a loss of rDNA repeats (Salim et al., 2017). However, this collection was missing mutants representing RNAPI and RNAPIII transcription, key processes that have the potential to regulate rDNA copy number maintenance. Therefore, in this study we extended this screen to nearly 75% of essential yeast genes by screening an additional yeast temperature sensitive (yTs) mutant collection of 279 strains (Ben-Aroya et al., 2008). We measured rDNA copy number in this yTs mutant collection using established ddPCR based assays (Salim et al., 2017). The mutant strains, along with wild-type controls, were grown at the permissive temperature (room temperature), and then shifted to the restrictive temperature (37˚C) for 3 hours. Following this, genomic DNA was isolated, and copy number measured using ddPCR.

A distribution of rDNA copy number across the 279 strains screened is shown in Figure 3.8C, and also summarized in Appendix B.3. The mean rDNA copy number of wild-type strains was 136.58 ± 15.8 (n=8). Mutants with significantly higher or lower rDNA copy number were identified based on thresholds set by variation in rDNA copy number in wild-type controls. Of the 279 strains screened, 161 strains had significantly lower copy number (<105 copies) and 63 strains had significantly higher copy number (>168 copies) than wild-type controls ($p < 0.05$) (Figure 3.8C). GO enrichment analyses of the 63 hits with high copy number did not yield any significantly enriched GO terms. The hits with low rDNA copy number, however, were significantly enriched for genes involved in macromolecular biosynthesis ($p<0.001$) (Figure 3.8C). A closer look at the genes comprising this significantly enriched GO term revealed that these were genes involved in DNA replication (subunits of DNA polymerase δ, the Origin Recognition Complex, MCM and GINS complexes, PCNA), transcription (subunits of RNAPI, RNAPII

and RNAPIII, transcription initiation, elongation and termination factors), rRNA and tRNA synthesis factors, and SMC complex subunits (cohesin and SMC5/6 complex subunits) (Appendix B.3). Taken together, these data from multiple high-throughput genetic screens revealed that rDNA stability and repeat copy number are regulated by the fundamental processes of DNA replication, transcription, and histone acetylation.

3.5.3 Repeat instability at the rDNA and *CUP1* arrays is induced by DNA replication stress and transcription

Based on the results of our screens, seminal work in bacteria showing that replication-transcription conflicts promote mutagenesis (reviewed in (Lang & Merrikh, 2018)), and elegant work in yeast demonstrating the role of transcription in promoting copy number variation at the *CUP1* array (Hull et al., 2017), we proposed that copy number variation at tandem repeats like the rDNA could be regulated by modulation of replication and/or transcription. Conflicts between the DNA replication machinery and transcription machinery operating on the same DNA template have now been established as a significant source of genomic instability. Despite the presence of elaborate cellular mechanisms to avoid them, these replication-transcription conflicts occur frequently genome-wide and result in stalled or collapsed DNA replication forks. Collapsed replication forks are processed into DSBs, which are repaired by one of many recombination-mediated repair pathways. While this occurs genome-wide, the presence of multiple repeat units that can serve as template for recombination results in copy number variation at tandem repeats at every cell division. While average repeat copy number of a population remains stable in unperturbed conditions, under stress, selection of advantageous copy number variants can facilitate adaptation (reviewed in (Salim & Gerton, 2019)). Based on this model, we hypothesized that instability at tandem repeats like the rDNA and *CUP1* arrays could be regulated by modulation of DNA replication, transcription, or even the downstream processes of recombination-mediated DSB repair.

To test this hypothesis, we first tested the effect of DNA replication stress on instability at both, the rDNA and *CUP1* arrays. We measured rDNA and *CUP1* repeat loss rates in *RDN25-MATα* or *CUP1-MATα* (17×*CUP1*) treated with 0-200mM hydroxyurea (HU), a ribonucleotide reductase inhibitor that depletes cellular dNTP pools. We found that HU induced repeat instability at both the rDNA and *CUP1* gene arrays in a dose dependent manner; importantly, the induction of instability at *CUP1* was transcription-independent (Figure 3.9A). As a control, we also treated the *TUB1-MATα* strains with 0-200mM HU and found that instability at this non-repetitive genomic locus remained low and unchanged irrespective of the dose of HU (Figure 3.9A). Therefore, DNA replication stress can increase instability specifically at tandem repeats.

Next, we perturbed transcription at the rDNA by deleting several genes known to play critical roles in RNAPI transcription. Loss of Rpa34, a subunit of RNAPI involved in transcription elongation, resulted in increased instability at the rDNA (Figure 3.9B). Loss of the Rpa49 subunit of RNAPI also altered rDNA stability, however we observed significant variability in the direction and magnitude of change in rDNA stability between biological replicates (Figure 3.9B). We speculate that this could be due to suppressor mutations that are known to arise in the *rpa49*Δ background that could result in altered RNAPI transcription (Darriere et al., 2019). Loss of Hmo1, an HMG-box protein involved in regulation of RNAPI transcription, induced instability at the rDNA (Figure 3.9B), consistent with a previous report of increased marker loss rates at the rDNA in *hmo1*Δ mutants (Mansisidor et al., 2018). We also generated mutants lacking Rnh1 and Rnh201, subunits of the functionally redundant RNases H1 and H2 respectively, that are required to process R-loops generated at the highly transcribed rDNA genes. Loss of Rnh1 and Rnh201 should result in an accumulation of R-loops at the rDNA and create more replication-transcription conflicts. Our model predicts that this should induce instability at the rDNA, which is exactly what we observed in *rnh1*Δ*rnh201*Δ mutants (Figure 3.9B). *HMO1* and *RNH201* were also validated hits from our screen;

overexpression of each of these genes increased rDNA instability (Appendices B.1 and B.2).

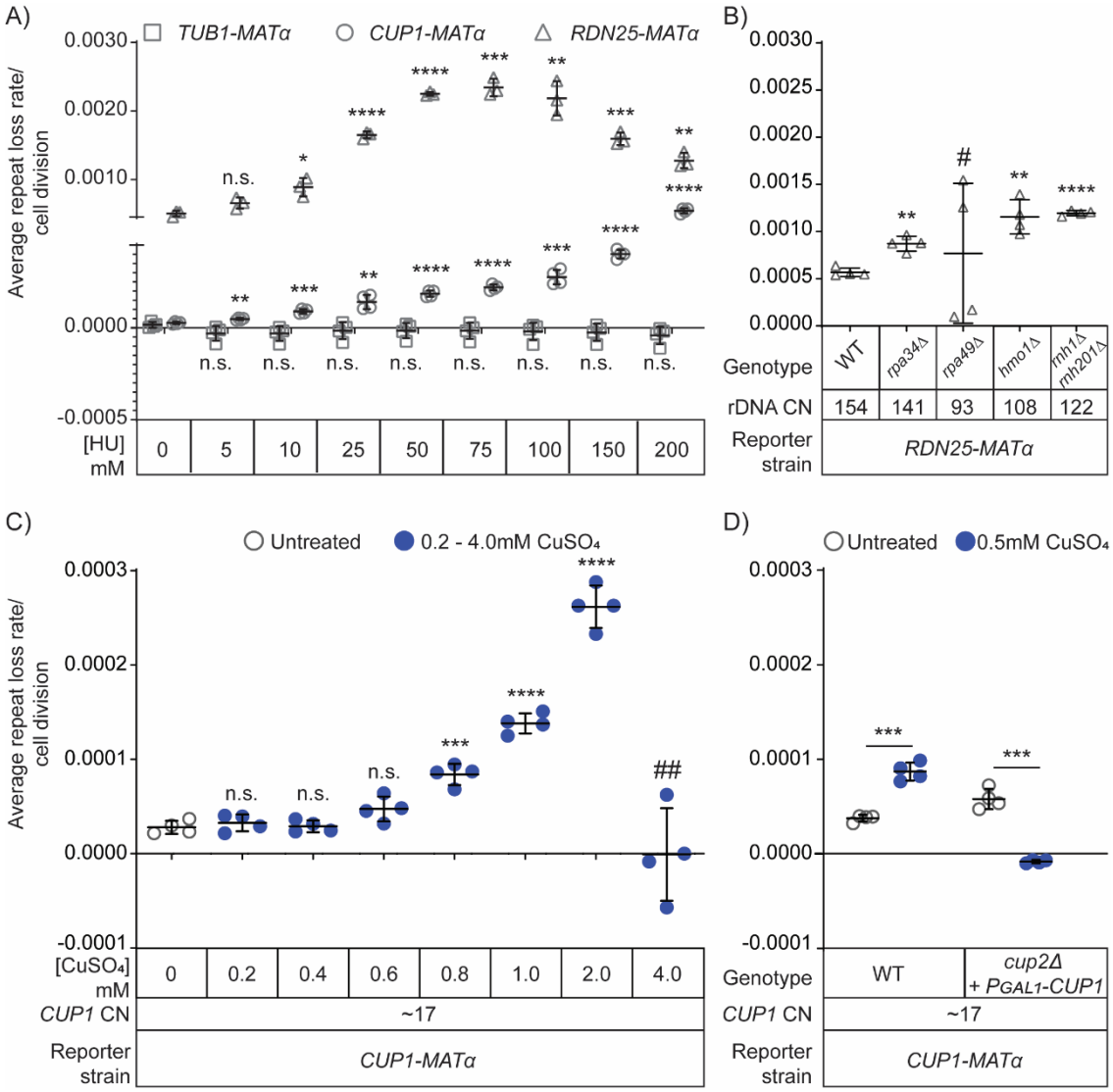

Figure 3.9. Transcription and replication stress induce repeat instability. (A) Repeat instability is induced by Hydroxyurea (HU) induced replication stress in a dose-dependent manner at both, the rDNA and *CUP1* gene arrays, but not at *TUB1*. (B) rDNA repeat loss rates in mutants that affect RNAPI transcription. # High variability in repeat loss rates between biological replicates. (C) Dose-dependent induction of instability at the *CUP1* gene array by copper. ## No growth/ cell divisions in the duration of the experiment. (D) Copper induces instability through Cup2-mediated transcription of *CUP1*. (A)-(D) Error bars represent standard deviation based on 4 biological replicates. Statistical significance was calculated using a standard 2-tailed t-test. * - p<0.05, ** - p<0.01, *** - p<0.001, **** - p<0.0001, n. s.– not significant.

While these results suggest that transcription at the rDNA induces rDNA instability, the requirement of rDNA transcription for cell viability makes it impossible to

test this directly. To complement these data, and directly test the effects of transcription on repeat stability, we used the *CUP1-MATα* reporter strains and measured *CUP1* instability in the presence of copper in the medium. We observed that copper induced *CUP1* instability in a dose dependent manner (Figure 3.9C). Since copper is also known to induce DNA damage, and copper response genes are induced by and involved in the DNA damage response, we wanted to verify that it is the copper-induced transcription of the array that induces *CUP1* instability. To this end, we constructed a strain lacking Cup2, the transcription factor required for copper-induced *CUP1* transcription (Welch et al., 1989). Since *cup2*Δ strains cannot grow in copper, we introduced into this strain a high-copy plasmid containing the *CUP1* ORF under the control of a galactose inducible promoter, resulting in *CUP1-MATα cup2*Δ (+P_{GAL1}-*CUP1*) strains that do not transcribe the native *CUP1* array in the presence of copper in the medium, but are copper resistant when galactose is present in the medium (Figure 3.10A). We found that copper no longer induced *CUP1* instability in this strain (Figures 3.9D, 3.10B), suggesting that it is the copper-induced transcription, and not DNA damage, that induces *CUP1* instability. These data suggest that instability at both the rDNA and *CUP1* gene arrays can be rapidly induced (~5-10 cell divisions) by modulation of replication or transcription.

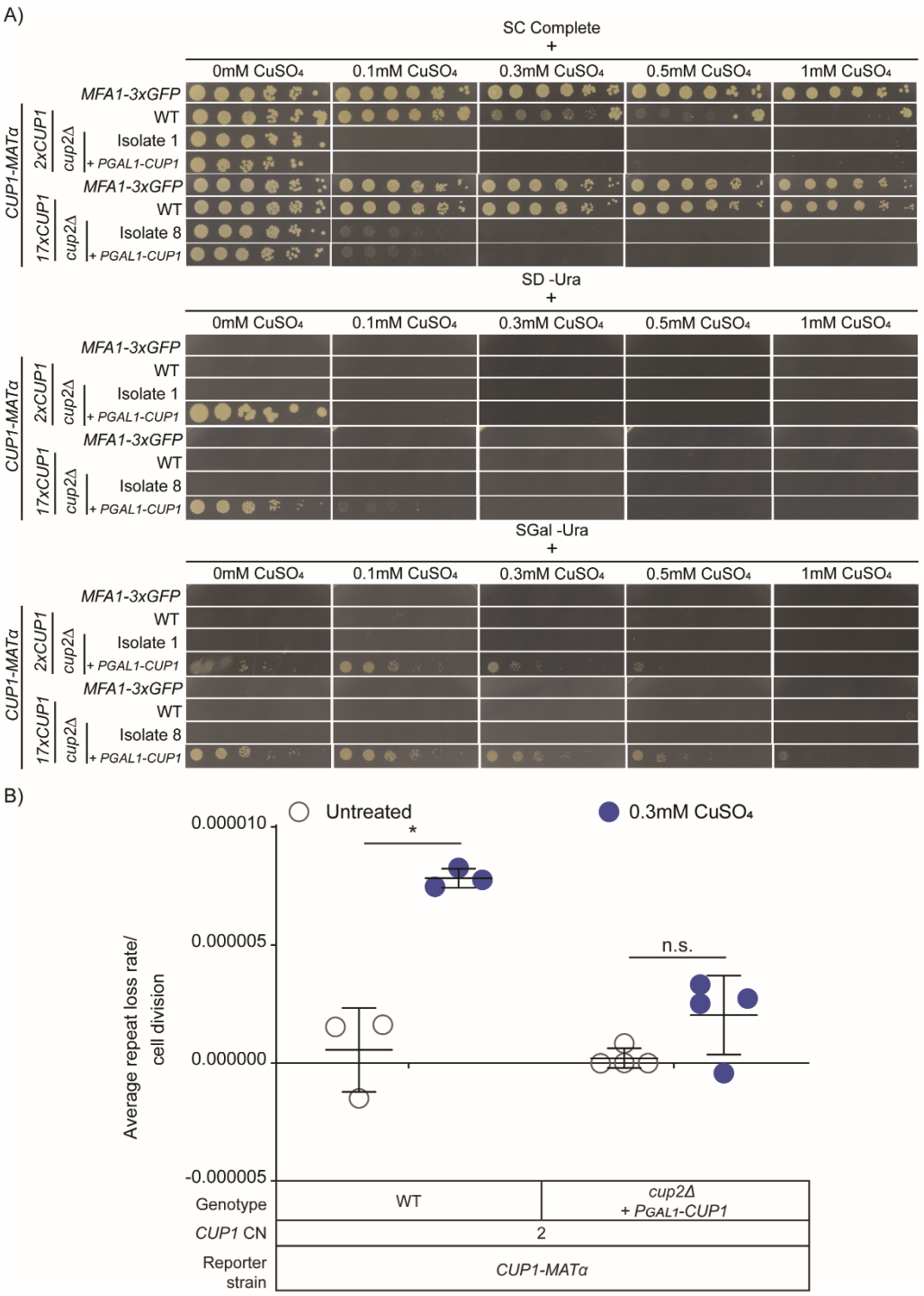

Figure 3.10. Validation of the *CUP1-MATα cup2Δ* (+P$_{GAL1}$-*CUP1*) strains. A) *CUP1-MATα cup2Δ* (+P$_{GAL1}$-*CUP1*) strains are copper-resistant in galactose-containing medium. B) *CUP1* repeat loss rates in *CUP1-MATα cup2Δ* (+P$_{GAL1}$-*CUP1*) strains with 2×*CUP1*. Error bars represent standard deviation based on 3-4 biological replicates. Statistical significance was calculated using a standard 2-tailed t-test. * - p<0.05, n. s. – not significant.

3.5.4 Stress-induced instability facilitates adaptation through environment and locus-specific copy number changes

Since replication stress and transcription induce repeat instability, we wondered if there would be synergy between the effects of DNA replication and transcription on repeat instability. To test this, we grew the *RDN25-MATα rpa34*Δ strain in the presence of HU. Interestingly, HU-induced rDNA instability was lower in the *rpa34*Δ strain relative to the wild-type *RDN25-MATα* strain (Figure 3.11A (i)), suggesting that slowing DNA replication and transcription may reduce instability at the rDNA. At the *CUP1* array, transcription and replication stress had an additive effect on instability (Figure 3.11A (ii)). These data suggest that repeat instability is regulated by the relative balance between DNA replication and transcription at the array. Perturbation of one or both can rapidly induce instability within a few generations, presumably by increasing the frequency of replication-transcription conflicts.

We had previously reported that replication stress induced by high levels of HU selects for a loss of rDNA repeats; cells that had lost rDNA repeats survived better under conditions of replication stress, suggesting that the loss of rDNA repeats facilitated adaptation to DNA replication stress (Salim et al., 2017). However, the loss of repeats required propagation under conditions of DNA replication stress (≥150mM HU) for at least 50 generations (Salim et al., 2017). Repeat instability, as measured by our assay, on the other hand, is rapidly induced within a few generations in a variety of conditions including low doses of HU. Therefore, we wanted to examine changes in steady state copy number in response to prolonged propagation under these stresses.

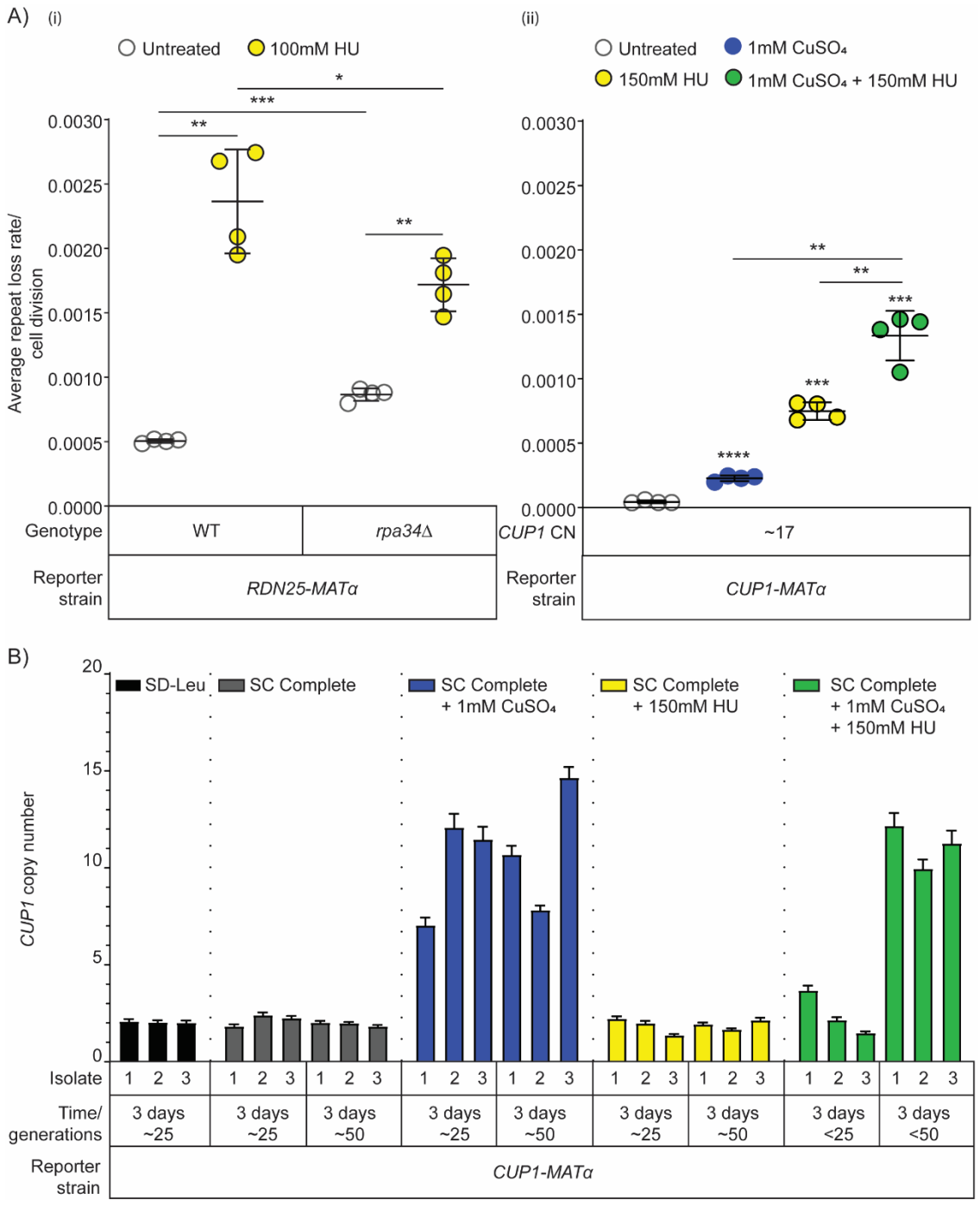

Figure 3.11. Stress-induced instability facilitates adaptation through stress and locus-specific copy number changes. (A) Synergy between transcription and Hydroxyurea (HU) induced replication stress at (i) rDNA and (ii) *CUP1* arrays. Error bars represent standard deviation based on 4 biological replicates. Statistical significance was calculated using a standard 2 tailed t-test. * - p<0.05, ** - p<0.01, *** - p<0.001, **** - p<0.0001. (B) The wild-type *CUP1-MATα* strain (2×*CUP1*) was subcultured in the indicated medium for ~6 days (approximately 50 generations). After every 3 days, 3 independent isolates were used to measure *CUP1* copy number by ddPCR. Error bars represent standard deviation for each individual reaction.

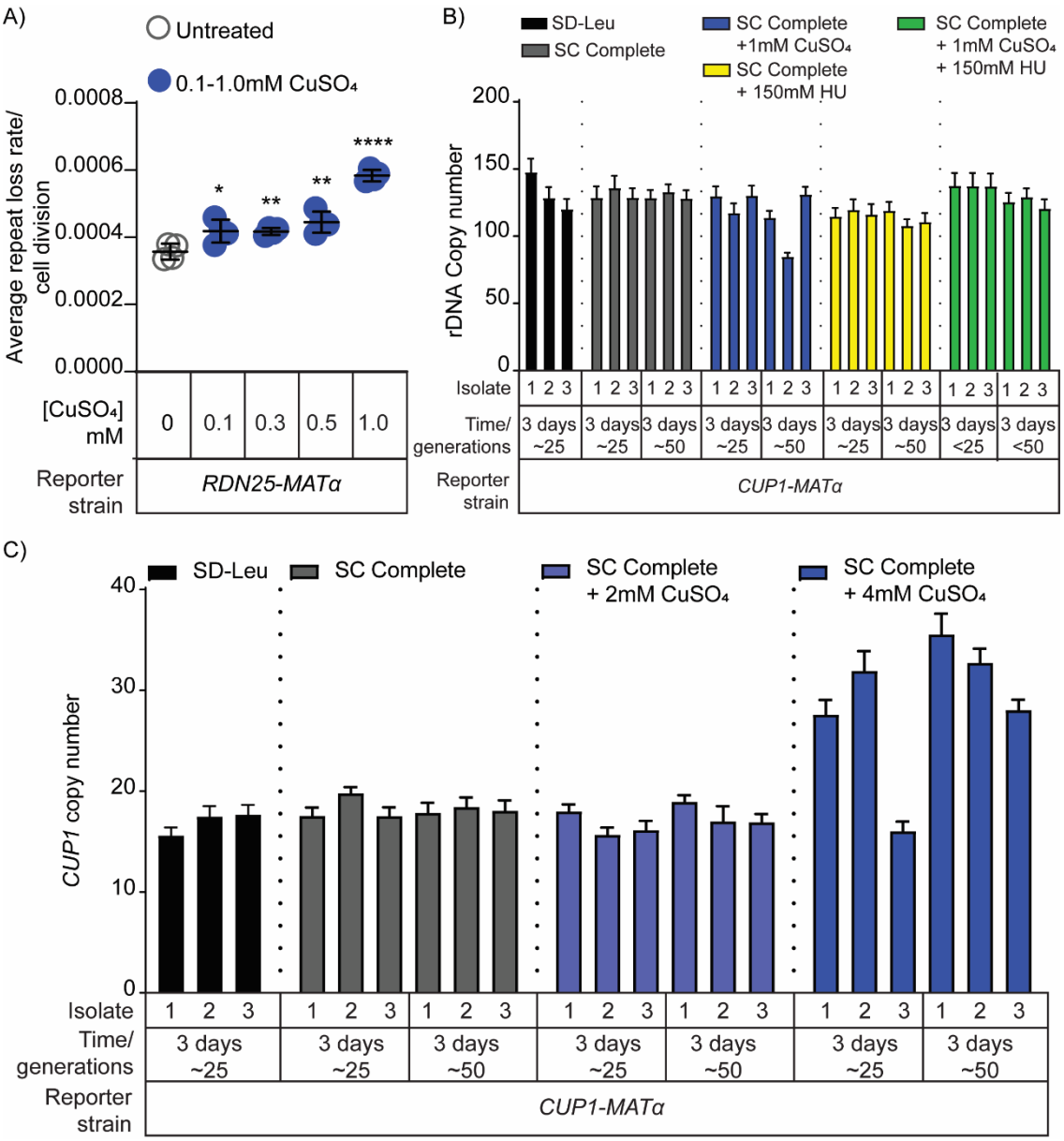

Figure 3.12. Stress and locus-specific copy number changes under selection. A) Copper induces rDNA instability. Error bars represent standard deviation based on 4 biological replicates. Statistical significance was calculated using a standard 2-tailed t-test. * - p<0.05, ** - p<0.01, **** - p<0.0001. B) rDNA copy number measurements in the samples in Figure 3.11B. C) Subculture of the wild-type *CUP1-MATα* (17×*CUP1*) strain in low (non-selective) and high (selective) concentrations of copper for ~6 days (approximately 50 generations). After every 3 days, 3 independent isolates were used to measure *CUP1* copy number by ddPCR. Error bars represent standard deviation for each individual reaction.

To study transcription-dependent adaptation via copy number variation, we chose to monitor *CUP1* copy number in a *CUP1-MATα* reporter strain subcultured for ~50 generations in complete medium, or complete medium containing copper, or HU. We found that copper resistant cells emerged after ~25-50 generations in high concentrations of copper, and these cells had amplified *CUP1* arrays (Figure 3.11B).

High concentrations of copper that select for amplified *CUP1* arrays also induce instability at the rDNA array (Figure 3.12A), however, rDNA copy number remains unaltered in these cells (Figure 3.12B). Importantly, while instability at the *CUP1* array is also induced by low concentrations of copper that cells are resistant to, *CUP1* copy number remains unchanged in these conditions, even after 50 generations of growth (Figure 3.12C). Further, no changes in *CUP1* array size were observed in HU (Figure 3.11B). These experiments highlight the distinction between instability and copy number changes.

Finally, given the synergistic effect of HU and copper on *CUP1* instability, we also subcultured the *CUP1-MATα* reporter strain used in Figure 3.11B in medium containing both copper and HU to test whether the additive effect on instability might accelerate adaptation to high concentrations of copper. We found that copper resistant cells with amplified *CUP1* arrays emerged, however our ability to qualitatively estimate adaptation rates was confounded by the slow growth of cells in medium containing both copper and HU. Altogether, these data strongly support our hypothesis that while repeat instability can be rapidly induced by DNA replication stress and transcription in a dose-dependent manner, a change in steady state repeat copy number requires prolonged exposure to conditions that select for locus-specific advantageous copy number variants that facilitate adaptation.

3.6 Discussion

Tandem repeats are inherently unstable and exhibit extensive copy number variation in natural populations. The tandem array of rDNA repeats in budding yeast has served as a model to study the behavior of tandem repeats for decades. The extensive copy number variation at tandem repeats including the rDNA was thought to be the inevitable consequence of the inherent instability at these repeats. This was confounded by the observation that normal rDNA copy number was stably maintained under

laboratory growth conditions. While mechanisms that are involved in recovery of rDNA copy number to wild-type levels are beginning to be characterized, mechanisms underlying alterations in rDNA copy number and stability under stress, or in mutant genetic backgrounds have remained elusive. A comprehensive understanding of the basic principles of regulation of repeat stability and copy number maintenance required the development of quantitative, sensitive assays to measure repeat stability and copy number in a high-throughput manner. To this end, we developed a quantitative, single-cell assay to measure repeat instability (qRIN) in budding yeast, and used it to screen for genes involved in regulating rDNA stability. We also used previously established ddPCR based assays to measure rDNA copy number in a yTs mutant collection of 279 essential genes and identify additional essential factors involved in rDNA copy number maintenance. Altogether, our screens revealed that rDNA copy number and stability are regulated by the fundamental processes of DNA replication, transcription, and histone acetylation. The role of DNA replication and transcription in modulating repeat stability is the subject of this study; the role of histone acetylation is currently under investigation.

The traditional view of evolution states that adaptive mutations occur at random under stress and are selected for during growth under that stress. However, several studies in bacteria have shown that the genome may be designed to direct mutations to loci that require rapid evolution and tune the rates of mutation at relevant loci in the face of stress (reviewed in (Salim & Gerton, 2019)). Directing mutations to specific genomic regions is not restricted to bacteria; elegant work by Hull et al. (2017) demonstrated that in budding yeast, mutagenesis could be directed to the *CUP1* array in a transcription-dependent manner ((Hull et al., 2017)). We extend our understanding of repeat stability by demonstrating its dependence not only on transcription itself, but also on transcription-associated consequences, such as R-loops. Furthermore, we demonstrate synergy with DNA replication and torsional stress. Selection can act on the variation resulting from induced instability, which can produce a new “adapted” steady state copy number over time. Therefore, stress-induced instability at tandem repeats can accelerate adaptation

through copy number variation. These data support the model that the sensitivity of tandem repeats to transcription and DNA replication stress makes them unstable by design, enabling them to accommodate copy number variation and facilitate rapid, reversible response and adaptation to genomic stresses.

We have identified principles of regulation of copy number variation at two repetitive arrays in the yeast genome. The players we characterized, DNA replication and transcription, are fundamental processes that are universally conserved. Mounting evidence suggests that replication-transcription conflicts are a major source of genomic instability in mammalian genomes as well (reviewed in (Hamperl & Cimprich, 2016)). Significant portions of mammalian genomes are made up of repetitive elements; while many repeats are yet to be identified, it has been established that copy number variation at tandem repeats is a significant source of genetic and phenotypic diversity in populations. The fundamental principles underlying copy number variation at tandem repeats in budding yeast can therefore be used to understand the behavior of other tandem repeats. One interesting application of our findings is in understanding the molecular evolution of cancer genomes because cancer cells are frequently characterized by transcriptional stress and copy number amplifications. Altered transcription may induce copy number variation at tandem repeats, facilitating adaptive copy number changes to occur, both, during the course of disease establishment and in response to therapy. The observations that (a) the rDNA array is highly susceptible to recombination-mediated rearrangements in solid tumors ((Stults et al., 2009)), (b) rRNA transcription is frequently dysregulated in cancers ((Lu et al., 2009; Udugama et al., 2018; Xu et al., 2017)), (c) RNAPI transcription has emerged as an effective therapeutic target in a variety of cancers ((Hannan et al., 2013)), and (d) 45S rDNA repeats were lost in most cancer genomes studied (Udugama et al., 2018; M. Wang & Lemos, 2017; Xu et al., 2017) are in support of this idea. Our studies of the yeast rDNA and *CUP1* repeats may serve as a touchstone for understanding the principles of regulation of other

tandem repeats, which will further our understanding of the important functional and evolutionary roles they play in genome biology.

3.7 Materials and Methods

3.7.1 Yeast strains and media

All yeast strains used are listed in Table 3.2. Strains were grown in non-selective SC complete medium (6.7g/L Yeast Nitrogen Base without amino acids + Ammonium Sulfate, 20g/L Dextrose, 2g/L synthetic complete (SC) supplement), or SD-dropout medium (6.7g/L Yeast Nitrogen Base without amino acids + Ammonium Sulfate, 20g/L Dextrose, CSM-dropout supplement) lacking specific amino acids as indicated. Copper and/or HU treated cells were grown in SC complete medium containing indicated concentrations of $CuSO_4$ and/or HU. Rich medium used was YPD (1% yeast extract, 2% peptone, 2% dextrose). For *CUP1-MATα cup2*Δ (+P_{GAL1}-*CUP1*) strains, selective medium used was SRaff-Leu-Ura (6.7g/L Yeast Nitrogen Base without amino acids + Ammonium Sulfate, 0.67g/L CSM-Leu-Ura supplement, 20g/L Raffinose), and non-selective medium used was SRaff+Gal-Ura (6.7g/L Yeast Nitrogen Base without amino acids + Ammonium Sulfate, 0.77g/L CSM-Ura supplement, 20g/L Raffinose, 20g/L Galactose) containing the indicated concentration of $CuSO_4$. All growth was at 30°C. Strain construction was carried out using standard yeast protocols. All strains were verified by replica-plating and PCR, followed by ddPCR to measure copy numbers of rDNA, *CUP1* as well as the *MATα-LEU2* repressor (Table 3.3). Instability reporter strains were also tested for GFP expression and repression by flow-cytometry. Primers used for strain construction are listed in Table 3.4.

3.7.2 ddPCR

Genomic DNA isolation, quantification, and ddPCR were carried out as previously described (Salim et al., 2017). ddPCR primers, probes and PCR conditions used are listed in Table 3.4.

3.7.3 Measurement of repeat loss rates

3.7.3.1 Growth and sample collection

Single colonies (4 each) of freshly revived reporter strains were inoculated into 5mL SD-Leu medium and grown overnight (up to 24 hours) at 30°C. The next day, each overnight culture was used to inoculate cells into 5mL SC Complete such that the starting cell density of this culture was OD_{600}≥0.05. Actual OD_{600} following inoculation into SC complete medium (t=0), $OD_{600\text{-}0}$, was also measured and recorded, following which cells were allowed to grow in SC complete medium for ~24 hours (~10-12 doublings, t=24h) at 30°C. Additionally, 100-200µL of each overnight culture (SD-Leu) was also harvested and fixed for cytometric analysis of the fraction of GFP-positive cells at t=0. The next day, the cell density of each SC Complete culture (t=24h), $OD_{600\text{-}24,}$ was measured and recorded. Additionally, 100-200µL of each culture was harvested and fixed for cytometric analysis of the fraction of GFP-positive cells at t=24h.

3.7.3.2 Preparing samples for cytometry

To prepare cells for cytometry, cells were harvested from an appropriate volume of the culture by centrifuging at <3000 rpm for 5 min. The medium was aspirated, and cells were washed once in 1xPBS (<3000 rpm, 5 min). Following removal of 1xPBS, cells were resuspended in 100-200µL 4% paraformaldehyde solution (Per 40mL: 10mL 16% paraformaldehyde (Ted Pella), 1.36g sucrose) and incubated at room temperature, in the dark, for 15 minutes. Fixed cells were centrifuged at 3000 rpm for 5 min to remove the paraformaldehyde, washed once with 1xPBS (3000 rpm, 5 min), and resuspended in 1mL 1xPBS. Fixed samples were then stored at 4°C in the dark for up to a week until needed for cytometry.

3.7.3.3 Flow cytometry

Fixed samples were analyzed on a MACSQuant Analyzer (Miltenyi Biotec) or a ZE5 Cell Analyzer (Bio-Rad). At least 200,000 single cells were counted for each sample. Data analysis was performed using FlowJo v10 to obtain the fraction of GFP-positive cells.

3.7.3.4 Calculation of repeat loss rates

The fraction of GFP-positive cells and OD_{600} measurements for each sample at t=0 and t=24h were recorded in Microsoft Excel. Equations (5) and (6) were applied to these data to calculate repeat loss rates using Mathematica 10 (Wolfram Research, 2014).

3.7.4 Testing for loss of the *MATα-LEU2* repressor

Single colonies of freshly revived *MFA1-3×GFP*, *RDN25-MATα*, and *CUP1-MATα* strains were inoculated into 5mL SC Complete and SD-Leu respectively, and allowed to grow to overnight at 30°C. The next day, a small aliquot of each overnight culture (t=0) was used for FACS sorting GFP-positive and GFP-negative cells from each sample. The overnight culture was also diluted into 5mL SC Complete medium, and allowed to grow overnight at 30°C. The following day, an aliquot from this culture (t=24h) was also used for FACS.

Samples from t=0 and t=24h were sorted using an S3 Cell Sorter (Bio-Rad), MoFlo Legacy cell sorter (Beckman Coulter) or an Influx cell sorter (BD Biosciences) depending on instrument availability. 100,000 GFP-negative cells and 1000-100,000 GFP-positive cells (depending on the frequency of GFP-positive cells) were sorted from each sample into ~500µL YPD. The sorted cells were diluted and plated at single cell density on to YPD plates. The plates were incubated at 30°C for ~2 days until colonies appeared. The plates were photographed, following which each plate was replica plated on to both, YPD and SD-Leu plates. The plates were incubated at 30°C for 1 day, until colonies appeared, and photographed.

12 single colonies were then picked at random from the YPD replica plates, resuspended in 200µL ddH_2O, and stored at -80°C prior to genomic DNA isolation for ddPCR. 4 additional single colonies were also picked from the replica plates to generate the growth curves in Figure 3.3B. Single colonies were used to inoculate 175µL SC Complete at a starting OD_{600} of 0.05 in a 96-well plate. Each colony was inoculated in triplicate, and growth curves were generated from average (of 3) measurements of OD_{600} taken every 15 minutes using a TECAN Infinite M200 plate reader for growth at 30 °C for 24 hours.

3.7.5 High-throughput screens

3.7.5.1 Screen to identify factors that regulate rDNA stability

3.7.5.1.1 Plasmid prep and transformation into WT reporter strain

The freshly revived *RDN25-MATα* strain was inoculated into 200mL SD-Leu and incubated overnight, with shaking, at 30°C. The following morning the culture was spun down and the medium decanted. The cell pellet was then washed twice with ddH_2O and once with 0.1M Lithium acetate. The washed pellet was resuspended in 1.5mL 1M Lithium acetate, 0.5mL ddH_2O, and 2mL 2mg/mL sheared salmon sperm DNA. 50µL of this mix was aliquoted into all wells of a 96-well PCR plate. 200ng of each MoBY plasmid was then added to each well of the PCR plate and vortexed prior to the addition of 100µL 50% PEG3350. The plate was sealed, vortexed, and briefly spun down before heat shocking at 42°C for 1 hour. The plate was then spun down and the supernatant was aspirated off. 200µL SD-Leu-Ura was then added to each well and the cultures were transferred to a flat-bottom 96-well plate and incubated overnight, with shaking, at 30°C. Cultures were then spotted onto SD-Leu-Ura PlusPlates and grown for two nights at 30°C. Cells from each spot were then inoculated into 150µL SD-Leu-Ura broth and grown overnight at

30°C. 65µL 50% glycerol was added to each well of the plate, mixed and frozen at -80°C.

3.7.5.1.2 Growth and prep for cytometry

30µL of the glycerol stock of each strain from *RDN25-MATα* + MoBY library was inoculated into 1.5mL SD-Leu-Ura in a 96-deepwell plate. These plates were incubated overnight, with shaking, at 30°C. The next morning, 100µL of the overnight cultures were fixed for cytometric analysis. In parallel, the overnight cultures were also diluted 1:50 into 1.5mL SD-Ura in 96-deepwell plates. OD_{600} following inoculation into non-selective medium (t=0), $OD_{600\text{-}0}$, was measured immediately after inoculation using a TECAN Infinite M200 plate reader and recorded. This set of plates was incubated overnight, with shaking, at 30°C. The following morning, 100µL of the overnight cultures in non-selective media were fixed for cytometric analysis. Additionally, the cultures were diluted 1:10 and used to obtain OD_{600} following growth in non-selective medium (t=24h), $OD_{600\text{-}24}$, using a TECAN Infinite M200 plate reader. Cells were fixed for cytometry as described above, with minor modifications. Briefly, cells were pelleted, resuspended in 100µL 4% paraformaldehyde and incubated at room temperature for 15 minutes. Fixed cells were then washed twice with 200µL 1xPBS and resuspended in 250µL 1xPBS. Flow cytometry to estimate the fraction of GFP-positive cells, and calculation of rDNA repeat loss rates was carried out as described above.

3.7.5.1.3 Hit validation

The top ~200 hits with high rDNA instability and the top ~100 hits with low rDNA instability were cherry-picked and re-arrayed into 96-well plates as previously described (Salim et al., 2017). rDNA repeat loss rates were measured in these strains 2 additional times (3 independent measurements including initial screen) as described above. Genomic

DNA was isolated from these hits for ddPCR as previously described (Salim et al., 2017).

3.7.5.2 Screen to identify genes involved in rDNA copy number maintenance

Genomic DNA isolation from the yTs mutant collection of essential genes (Ben-Aroya et al., 2008) and ddPCR were performed as previously described (Salim et al., 2017). rDNA copy number measurements for 8 colonies of wild-type BY4741 (Appendix B.3) were used to set thresholds as follows: Mean rDNA copy number ± 2SD–No change. rDNA copy number > Mean rDNA copy number + 2SD OR rDNA copy number < Mean rDNA copy number - 2SD–Significant change.

3.7.5.3 GO enrichment analysis

GO enrichment analyses were performed using GOrilla (Eden et al., 2007; Eden et al., 2009).

3.7.6 Subculturing experiments

All subculturing experiments were performed as previously described (Salim et al., 2017).

3.8 Supporting Information

Table 3.2. List of yeast strains used.

Strain ID	Name	Background	Relevant Genotype	References
DSY003	BY4741	BY4741	*MAT*a *his3Δ1 leu2Δ0 met15Δ0 ura3Δ0*	Salim et al. (2017)
DSY018	W303	W303-a	*MAT*a *{leu2-3,112 trp1-1 can1-100 ura3-1 ade2-1 his3-11,15} [phi$^+$]*	Salim et al. (2017)
DSY20.1	*MFA1-3xGFP*	S288C	MATa ura3-52 his3-Δ200 trp1-1 leu2-3,112, MFA1-3xGFP-HIS5(Sp)	RLY8491 from Zhu et al. (2015)
DSY48.7	*RDN25-MATα*	S288C	DSY20.1, *RDN25-MATα-LEU2*	This study
DSY33.2	*RDN25-MATα (reverse)*	S288C	DSY20.1, *RDN25-MATα-LEU2* (reverse orientation)	This study
DSY64.1	*RDN18-MATα*	S288C	DSY20.1, *RDN18-MATα-LEU2*	This study
DSY65.1	*RDN58-MATα*	S288C	DSY20.1, *RDN58-MATα-LEU2*	This study
DSY77.2	*RDN25-MATα (W303)*	S288C	DSY018, *ade2-1::ADE2, MFA1-3xGFP-URA3, RDN25-MATα-LEU2*	This study
DSY99.12	*TUB1-MATα*	S288C	DSY20.1, *TUB1-MATα-LEU2*	This study
DSY75.13	*RDN25-MATα top1Δ*	S288C	DSY48.7, *top1Δ::NatMX*	This study
DSY184.1	*RDN25-MATα rad52Δ*	S288C	DSY48.7, *rad52Δ::KanMX*	This study
DSY185.9	*RDN25-MATα tof1Δ*	S288C	DSY48.7, *tof1Δ::KanMX*	This study
DSY186.17	*RDN25-MATα csm3Δ*	S288C	DSY48.7, *csm3Δ::KanMX*	This study
DSY80.1, DSY80.9	*RDN25-MATα fob1Δ*	S288C	DSY48.7, *fob1Δ::NatMX*	This study
	RDN25-MATα (W303) fob1Δ	S288C	DSY77, *fob1Δ::NatMX*	This study
DSY73	*RDN18-MATα fob1Δ*	S288C	DSY64.1, *fob1Δ::NatMX*	This study
DSY74	*RDN58-MATα fob1Δ*	S288C	DSY65.1, *fob1Δ::NatMX*	This study
DSY131	*CUP1-MATα (2×CUP1)*	S288C	DSY20.1, *CUP1-MATα-LEU2, 2×CUP1*	This study
DSY132	*CUP1-MATα (12×CUP1)*	S288C	DSY20.1, *CUP1-MATα-LEU2, 12×CUP1*	This study
DSY134	*CUP1-MATα (17×CUP1)*	S288C	DSY20.1, *CUP1-MATα-LEU2, 17×CUP1*	This study
DSY135	*CUP1-MATα (6×CUP1)*	S288C	DSY20.1, *CUP1-MATα-LEU2, 6×CUP1*	This study
DSY149.1	*CUP1-MATα (2×CUP1) cup2Δ*	S288C	DSY131, *cup2Δ::KanMX*	This study
DSY150.7	*CUP1-MATα (12×CUP1) cup2Δ*	S288C	DSY132, *cup2Δ::KanMX*	This study
DSY152.8	*CUP1-MATα (17×CUP1) cup2Δ*	S288C	DSY133, *cup2Δ::KanMX*	This study
DSY153.4	*CUP1-MATα (6×CUP1) cup2Δ*	S288C	DSY134, *cup2Δ::KanMX*	This study
DSY155.1	*CUP1-MATα (2×CUP1) cup2Δ (+PGAL1-CUP1)*	S288C	DSY149.1, *PGAL1-YHR055C-URA3*	This study
DSY156.1	*CUP1-MATα (12×CUP1) cup2Δ (+PGAL1-CUP1)*	S288C	DSY150.7, *PGAL1-YHR055C-URA3*	This study
DSY158.1	*CUP1-MATα (17×CUP1) cup2Δ (+PGAL1-CUP1)*	S288C	DSY152.8, *PGAL1-YHR055C-URA3*	This study
DSY159.1	*CUP1-MATα (6×CUP1) cup2Δ (+PGAL1-CUP1)*	S288C	DSY153.4, *PGAL1-YHR055C-URA3*	This study
DSY82.1	*RDN25-MATα rnh1Δrnh201Δ*	S288C	DSY48.7, *rnh1Δ::NatMX rnh201Δ::KanMX*	This study
DSY81	*RDN25-MATα hmo1Δ*	S288C	DSY48.7, *hmo1Δ::KanMX*	This study
DSY101.1	*RDN25-MATα rpa34Δ*	S288C	DSY48.7, *rpa34Δ::KanMX*	This study
DSY102.3	*RDN25-MATα rpa49Δ*	S288C	DSY48.7, *rpa49Δ::KanMX*	This study

Table 3.3. Relevant rDNA, *CUP1* and *MATα-LEU2* copy number measurements in all reporter strains used.

CN – Copy number, SD – Standard deviation for each individual reaction.

Strain ID	Name	25S rDNA		*CUP1*		*LEU2-3*	
		CN	SD	CN	SD	CN	SD
DSY003	BY4741	146.8599	9.6938776	12.079208	0.7142857	0	n/a
DSY018	W303	239.88439	16.581633	9.8865979	0.3061224		
DSY20.1	MFA1-3xGFP	111.89873	7.9081633	9.4362018	0.5612245	0.9580645	0.0714286
DSY48.7	*RDN25-MATα*	109.35252	8.1632653	12.589641	0.7142857	2.0892019	0.1632653
DSY33.2	*RDN25-MATα (reverse)*	158.49057	11.479592	10.440252	0.7397959	2.2799597	0.0357143
DSY64.1	*RDN18-MATα*	271.07438	22.193878	11.510791	0.8418367	2.1268012	0.0331633
DSY65.1	*RDN58-MATα*	165.08876	11.22449	11.610738	0.7908163	2.1052632	0.0306122
DSY77.2	*RDN25-MATα (W303)*	192.70517	9.9489796	10.122511	0.3571429	1.9611307	0.0918367
DSY99.12	*TUB1-MATα*	101.75355	5.6122449	11.225962	0.5102041	2.0448878	0.1147959
DSY75.13	*RDN25-MATα top1Δ*	100.20964	4.0816327	11.364162	0.3316327	1.9487179	0.0816327
DSY184.1	*RDN25-MATα rad52Δ*	132.27273	11.22449	10.83045	0.6377551	1.8469055	0.1122449
DSY185.9	*RDN25-MATα tof1Δ*	123.98773	8.6734694	10.945122	0.5867347	2.0033223	0.125
DSY186.17	*RDN25-MATα csm3Δ*	91.45	6.8877551	11.770492	0.6122449	2.060423	0.1122449
DSY80.1	*RDN25-MATα fob1Δ*	80	5.6122449	11.121495	0.6632653	2.005305	0.1147959
DSY80.9		82.5	5.3571429	10.396825	0.5612245	2.122807	0.122449
	RDN25-MATα (W303) fob1Δ	159.00621	7.3979592	10.767544	0.4336735	1.7722096	0.0943878
DSY131	*CUP1-MATα (2×CUP1)*	136.64596	10.459184	2.0580205	0.1377551	1.9540984	0.127551
DSY132	*CUP1-MATα (12×CUP1)*	112.03704	7.6530612	13.064067	0.6632653	2.111413	0.1122449
DSY134	*CUP1-MATα (17×CUP1)*	116.37931	7.3979592	14.761905	0.7397959	2.0572289	0.122449
DSY135	*CUP1-MATα (6×CUP1)*	114.25	7.6530612	5.9090909	0.255102	2.1560694	0.125
DSY149.1	*CUP1-MATα (2×CUP1) cup2Δ*			2.1345566	0.125	1.9600726	0.0816327
DSY150.7	*CUP1-MATα (12×CUP1) cup2Δ*			12.432432	0.6887755	1.9865169	0.0892857
DSY152.8	*CUP1-MATα (17×CUP1) cup2Δ*			16.678322	0.8163265	1.9964029	0.0816327
DSY153.4	*CUP1-MATα (6×CUP1) cup2Δ*			6.2571429	0.2806122	1.9645733	0.0790816
DSY82.1	*RDN25-MATα rnh1Δrnh201Δ*	121.76591	4.8469388	9.5825243	0.255102	2	0.0790816
DSY81	*RDN25-MATα hmo1Δ*	107.90323	4.3367347	10.358491	0.2806122	1.8446602	0.0688776
DSY101.1	*RDN25-MATα rpa34Δ*	141.13924	7.6530612			2.1686747	0.0994898
DSY102.3	*RDN25-MATα rpa49Δ*	92.703151	3.8265306			2.029703	0.0739796

Table 3.4. List of primers used.

ddPCR assays

	Gene	Forward primer	Reverse Primer	Probe	Restriction enzyme	Tm (°C)	gDNA (ng/20uL rxn)
1	*TUB1*	5'-CCAGTCTTATCCAAATCAAAGG-3'	5'-GGATCACACTTGACCATCT-3'	5'-/56FAM/TCCATGAGT/ZEN/CCAACTCTGTGTCA/3IABkFQ/-3'	*Eco* RI or *Mse* I	57	≥0.005
2	*RDN25*	5'-TACCTTCGGTGCCCGAGTTGTAAT-3'	5'-ACCCTCTATGACGTCCTGTTCCAA-3'	5'-/5HEX/AACATAGACAAGGAACGGCCC/3BHQ_1/-3'	*Eco* RI	57	0.005
3	*CUP1-1*	5'-GAAGGTCATGAGTGCCAATG-3'	5'-GCATTTGTCGTCGCTGTT-3'	5'-/5HEX/AAATCATGTAGCTGCCCAACGG/3BHQ_1/-3'	*Mse* I	57	0.005
4	*MATALPHA2*	5'-CGCTAATTCTGGAGCGATTG-3'	5'-GCAAAGAACATCGAGAACCC-3'	5'-/5HEX/TCATTAGATTCTCTAGGCCCTTGGT/3BHQ_1/-3'	*Mse* I	57	0.01
5	*MATALPHA1*	5'-CAGTTTGGCTCCGGTGTAA-3'	5'-GCGCGAAGTAGTCCCATATT-3'	5'-/5HEX/AATGTCTTGTCTTCTCTGCTCGC/3BHQ_1/-3'	*Mse* I	57	0.01
6	*leu2-3,112*	5'-GACAAGAACACCGCATTTGG-3'	5'-CAGACAAGATAGTGGCGATAGG-3'	5'-/5HEX/CCACGGTTCTGCTCCAGATTT/3BHQ_1/-3'	*Mse* I	57	0.01

Other primers used

Purpose	Forward	Reverse	Comments	Plasmids
MFA1 3xGFP tagging	5'-ATTATCAAAGGTGTCTTCTGGGACCCAGCATGTGTTATTGCTggtgacggtgctggttta-3'	5'-AAGATAAAGGAGGGAGAACAACGTTTTTGTACGCAGAAACTAtcgatgaattcgagctcg-3'	F5 and R3 primers from Sheff et al. (2004) with overhangs homologous to 3' end of MFA1.	pKT128 (3xGFP-HIS5(Sp)) ; pKT209 (3xGFP-URA3(Ca))
MAT α-LEU2 integration	5'-(gene specific sequence)-TTAACCCTCACTAAAGGGAA-3'	5'-(gene specific sequence)-ccgtttctgacagagtaaaatt-3'	Forward and Reverse primers with overhangs homologous to locus of integration.	pRS305 (*MATα-LEU2*)
Gene specific sequences used for *MATα-LEU2* integration	5'-GGCGTCGCTGAACCATAGCAGGCTAGCAACGGTGCACTTG-3'	5'-CATTGCAATTCGCCAGCAAGCACCCAAGGCCTTTCCGC-3'	*RDN25*	
	5'-TTGTAATTATTGCTCTTCAACGAGGAATTCCTAGTAAGCG-3'	5'-AAAGGGCAGGGACGTAATCAACGCAAGCTGATGACTTG-3'	*RDN18*	
	5'-TTCCGTGAATCATCGAATCTTTGAACGCACATTGCGCCCC-3'	5'-AAATGACGCTCAAACAGGCATGCCCCCTGGAATACCAA-3'	*RDN58*	
	5'-CAAGTCTGAAGAAACCAAGAAGTCATGCTGCTCTGGGAAA-3'	5'-AAATAGTTAGATGAATATATTAAAGACTATTCGTTTCA-3'	*CUP1*	
	5'-GTTCACTCTCGCCCCAACCTCCTTATCCTTTCTATATTT-3'	5'-TAACAGTAGGGGGAATTTTTTTTTTTACAATATACTTG-3'	*TUB1*	

3.9 Acknowledgements

We thank Jin Zhu, Dominic Heinecke, and Rong Li (formerly at the Stowers Institute) for generously sharing qCTF strains, plasmids, reagents, and their expertise during the development of our qRIN assay. We also thank Andrew Box, Jungeun Park, and Laura Holmes (Stowers Institute) for assistance with development of methods for cytometric analysis of samples and analysis of cytometry data, and the Cytometry core facility (Stowers Institute), particularly Dustin DeGraffenreid for assistance with FACS sorting cells and analyzing sorting data. We are also grateful to Sue-Jinks Robertson (Duke University) for strains, and the Molecular Biology core facility (Stowers Institute) for access to the TECAN plate reader. This work was done to fulfill, in part, requirements for DS's PhD thesis research as a student registered with the Open University.

3.10 References

Albert, B., Leger-Silvestre, I., Normand, C., Ostermaier, M. K., Perez-Fernandez, J., Panov, K. I., . . . Gadal, O. (2011). RNA polymerase I-specific subunits promote polymerase clustering to enhance the rRNA gene transcription cycle. *J Cell Biol, 192*(2), 277-293. doi:10.1083/jcb.201006040

Andersen, S. L., Sloan, R. S., Petes, T. D., & Jinks-Robertson, S. (2015). Genome-destabilizing effects associated with top1 loss or accumulation of top1 cleavage complexes in yeast. *PLoS Genet, 11*(4), e1005098. doi:10.1371/journal.pgen.1005098

Bando, M., Katou, Y., Komata, M., Tanaka, H., Itoh, T., Sutani, T., & Shirahige, K. (2009). Csm3, Tof1, and Mrc1 form a heterotrimeric mediator complex that associates with DNA replication forks. *J Biol Chem, 284*(49), 34355-34365. doi:10.1074/jbc.M109.065730

Beckmann, J. S., Estivill, X., & Antonarakis, S. E. (2007). Copy number variants and genetic traits: closer to the resolution of phenotypic to genotypic variability. *Nat Rev Genet, 8*(8), 639-646. doi:10.1038/nrg2149

Ben-Aroya, S., Coombes, C., Kwok, T., O'Donnell, K. A., Boeke, J. D., & Hieter, P. (2008). Toward a comprehensive temperature-sensitive mutant repository of the essential genes of Saccharomyces cerevisiae. *Mol Cell, 30*(2), 248-258. doi:10.1016/j.molcel.2008.02.021

Brahmachary, M., Guilmatre, A., Quilez, J., Hasson, D., Borel, C., Warburton, P., & Sharp, A. J. (2014). Digital genotyping of macrosatellites and multicopy genes reveals novel biological functions associated with copy number variation of large tandem repeats. *PLoS Genet, 10*(6), e1004418. doi:10.1371/journal.pgen.1004418

Brewer, B. J., Lockshon, D., & Fangman, W. L. (1992). The arrest of replication forks in the rDNA of yeast occurs independently of transcription. *Cell, 71*(2), 267-276. doi:10.1016/0092-8674(92)90355-g

Buck, S. W., Maqani, N., Matecic, M., Hontz, R. D., Fine, R. D., Li, M., & Smith, J. S. (2016). RNA Polymerase I and Fob1 contributions to transcriptional silencing at the yeast rDNA locus. *Nucleic Acids Res, 44*(13), 6173-6184. doi:10.1093/nar/gkw212

Capizzi, R. L., & Jameson, J. W. (1973). A table for the estimation of the spontaneous mutations rate of cells in culture. *Mutation Research/Fundamental and Molecular Mechanisms of Mutagenesis, 17*(1), 147-148. doi:10.1016/0027-5107(73)90265-0

Casper, A. M., Mieczkowski, P. A., Gawel, M., & Petes, T. D. (2008). Low levels of DNA polymerase alpha induce mitotic and meiotic instability in the ribosomal DNA gene cluster of Saccharomyces cerevisiae. *PLoS Genet, 4*(6), e1000105. doi:10.1371/journal.pgen.1000105

Darriere, T., Pilsl, M., Sarthou, M. K., Chauvier, A., Genty, T., Audibert, S., . . . Gadal, O. (2019). Genetic analyses led to the discovery of a super-active mutant of the RNA polymerase I. *PLoS Genet, 15*(5), e1008157. doi:10.1371/journal.pgen.1008157

Di Felice, F., Egidi, A., D'Alfonso, A., & Camilloni, G. (2019). Fob1p recruits DNA topoisomerase I to ribosomal genes locus and contributes to its transcriptional silencing maintenance. *Int J Biochem Cell Biol, 110*, 143-148. doi:10.1016/j.biocel.2019.03.006

Dong, K., Addinall, S. G., Lydall, D., & Rutherford, J. C. (2013). The yeast copper response is regulated by DNA damage. *Mol Cell Biol, 33*(20), 4041-4050. doi:10.1128/MCB.00116-13

Eden, E., Lipson, D., Yogev, S., & Yakhini, Z. (2007). Discovering motifs in ranked lists of DNA sequences. *PLoS Comput Biol, 3*(3), e39. doi:10.1371/journal.pcbi.0030039

Eden, E., Navon, R., Steinfeld, I., Lipson, D., & Yakhini, Z. (2009). GOrilla: a tool for discovery and visualization of enriched GO terms in ranked gene lists. *BMC Bioinformatics, 10*, 48. doi:10.1186/1471-2105-10-48

French, S. L., Osheim, Y. N., Cioci, F., Nomura, M., & Beyer, A. L. (2003). In exponentially growing Saccharomyces cerevisiae cells, rRNA synthesis is determined by the summed RNA polymerase I loading rate rather than by the number of active genes. *Mol Cell Biol, 23*(5), 1558-1568. doi:10.1128/mcb.23.5.1558-1568.2003

Ganley, A. R., & Kobayashi, T. (2011). Monitoring the rate and dynamics of concerted evolution in the ribosomal DNA repeats of Saccharomyces cerevisiae using experimental evolution. *Mol Biol Evol, 28*(10), 2883-2891. doi:10.1093/molbev/msr117

Ghaemmaghami, S., Huh, W. K., Bower, K., Howson, R. W., Belle, A., Dephoure, N., . . . Weissman, J. S. (2003). Global analysis of protein expression in yeast. *Nature, 425*(6959), 737-741. doi:10.1038/nature02046

Gottlieb, S., & Esposito, R. E. (1989). A new role for a yeast transcriptional silencer gene, SIR2, in regulation of recombination in ribosomal DNA. *Cell, 56*(5), 771-776. doi:10.1016/0092-8674(89)90681-8
Hamperl, S., & Cimprich, K. A. (2016). Conflict Resolution in the Genome: How Transcription and Replication Make It Work. *Cell, 167*(6), 1455-1467. doi:10.1016/j.cell.2016.09.053
Hannan, R. D., Drygin, D., & Pearson, R. B. (2013). Targeting RNA polymerase I transcription and the nucleolus for cancer therapy. *Expert Opin Ther Targets, 17*(8), 873-878. doi:10.1517/14728222.2013.818658
Ho, C. H., Magtanong, L., Barker, S. L., Gresham, D., Nishimura, S., Natarajan, P., . . . Boone, C. (2009). A molecular barcoded yeast ORF library enables mode-of-action analysis of bioactive compounds. *Nat Biotechnol, 27*(4), 369-377. doi:10.1038/nbt.1534
Horigome, C., Unozawa, E., Ooki, T., & Kobayashi, T. (2019). Ribosomal RNA gene repeats associate with the nuclear pore complex for maintenance after DNA damage. *PLoS Genet, 15*(4), e1008103. doi:10.1371/journal.pgen.1008103
Houseley, J., Kotovic, K., El Hage, A., & Tollervey, D. (2007). Trf4 targets ncRNAs from telomeric and rDNA spacer regions and functions in rDNA copy number control. *EMBO J, 26*(24), 4996-5006. doi:10.1038/sj.emboj.7601921
Huang, J., & Moazed, D. (2003). Association of the RENT complex with nontranscribed and coding regions of rDNA and a regional requirement for the replication fork block protein Fob1 in rDNA silencing. *Genes Dev, 17*(17), 2162-2176. doi:10.1101/gad.1108403
Hull, R. M., Cruz, C., Jack, C. V., & Houseley, J. (2017). Environmental change drives accelerated adaptation through stimulated copy number variation. *PLoS Biol, 15*(6), e2001333. doi:10.1371/journal.pbio.2001333
Hurles, M. E., Dermitzakis, E. T., & Tyler-Smith, C. (2008). The functional impact of structural variation in humans. *Trends Genet, 24*(5), 238-245. doi:10.1016/j.tig.2008.03.001
Iafrate, A. J., Feuk, L., Rivera, M. N., Listewnik, M. L., Donahoe, P. K., Qi, Y., . . . Lee, C. (2004). Detection of large-scale variation in the human genome. *Nat Genet, 36*(9), 949-951. doi:10.1038/ng1416
Ide, S., Miyazaki, T., Maki, H., & Kobayashi, T. (2010). Abundance of ribosomal RNA gene copies maintains genome integrity. *Science, 327*(5966), 693-696. doi:10.1126/science.1179044
Ide, S., Saka, K., & Kobayashi, T. (2013). Rtt109 Prevents Hyper-Amplification of Ribosomal RNA Genes through Histone Modification in Budding Yeast. *PLoS Genet, 9*(4). doi:10.1371/journal.pgen.1003410.g001
Ide, S., Watanabe, K., Watanabe, H., Shirahige, K., Kobayashi, T., & Maki, H. (2007). Abnormality in initiation program of DNA replication is monitored by the highly repetitive rRNA gene array on chromosome XII in budding yeast. *Mol Cell Biol, 27*(2), 568-578. doi:10.1128/MCB.00731-06
Iida, T., & Kobayashi, T. (2019). RNA Polymerase I Activators Count and Adjust Ribosomal RNA Gene Copy Number. *Mol Cell, 73*(4), 645-654 e613. doi:10.1016/j.molcel.2018.11.029
Johzuka, K., & Horiuchi, T. (2002). Replication fork block protein, Fob1, acts as an rDNA region specific recombinator in S. cerevisiae. *Genes to Cells, 7*(2), 99-113. doi:10.1046/j.1356-9597.2001.00508.x
Kobayashi, T. (2003). The replication fork barrier site forms a unique structure with Fob1p and inhibits the replication fork. *Mol Cell Biol, 23*(24), 9178-9188. doi:10.1128/mcb.23.24.9178-9188.2003
Kobayashi, T., & Ganley, A. R. (2005). Recombination regulation by transcription-induced cohesin dissociation in rDNA repeats. *Science, 309*(5740), 1581-1584. doi:10.1126/science.1116102
Kobayashi, T., Heck, D. J., Nomura, M., & Horiuchi, T. (1998). Expansion and contraction of ribosomal DNA repeats in *Saccharomyces cerevisiae*: requirement of replication fork blocking (Fob1) protein and the role of RNA polymerase I. *Genes Dev, 12*(24), 3821-3830. doi:10.1101/gad.12.24.3821
Kobayashi, T., Horiuchi, T., Tongaonkar, P., Vu, L., & Nomura, M. (2004). SIR2 Regulates Recombination between Different rDNA Repeats, but Not Recombination within Individual rRNA Genes in Yeast. *Cell., 117*(4), 441-453.
Kwan, E. X., Foss, E. J., Tsuchiyama, S., Alvino, G. M., Kruglyak, L., Kaeberlein, M., . . . Bedalov, A. (2013). A natural polymorphism in rDNA replication origins links origin activation with calorie restriction and lifespan. *PLoS Genet, 9*(3), e1003329. doi:10.1371/journal.pgen.1003329
Laney, J. D., Mobley, E. F., & Hochstrasser, M. (2006). The short-lived Matalpha2 transcriptional repressor is protected from degradation in vivo by interactions with its corepressors Tup1 and Ssn6. *Mol Cell Biol, 26*(1), 371-380. doi:10.1128/MCB.26.1.371-380.2006

Lang, K. S., & Merrikh, H. (2018). The Clash of Macromolecular Titans: Replication-Transcription Conflicts in Bacteria. *Annu Rev Microbiol, 72*, 71-88. doi:10.1146/annurev-micro-090817-062514

Lea, D. E., & Coulson, C. A. (1949). The distribution of the numbers of mutants in bacterial populations. *J Genet, 49*(3), 264-285. doi:10.1007/bf02986080

Lu, Y., Chang, Q., Zhang, Y., Beezhold, K., Rojanasakul, Y., Zhao, H., . . . Chen, F. (2009). Lung cancer-associated JmjC domain protein mdig suppresses formation of tri-methyl lysine 9 of histone H3. *Cell Cycle, 8*(13), 2101-2109. doi:10.4161/cc.8.13.8927

Luria, S. E. (1951). The Frequency Distribution of Spontaneous Bacteriophage Mutants as Evidence for the Exponential Rate of Phage Reproduction. *Cold Spring Harbor Symposia on Quantitative Biology, 16*(0), 463-470. doi:10.1101/SQB.1951.016.01.033

Luria, S. E., & Delbruck, M. (1943). Mutations of Bacteria from Virus Sensitivity to Virus Resistance. *Genetics, 28*(6), 491-511.

Lynch, M., Sung, W., Morris, K., Coffey, N., Landry, C. R., Dopman, E. B., . . . Thomas, W. K. (2008). A genome-wide view of the spectrum of spontaneous mutations in yeast. *Proc Natl Acad Sci U S A, 105*(27), 9272-9277. doi:10.1073/pnas.0803466105

Mansisidor, A., Molinar, T., Jr., Srivastava, P., Dartis, D. D., Pino Delgado, A., Blitzblau, H. G., . . . Hochwagen, A. (2018). Genomic Copy-Number Loss Is Rescued by Self-Limiting Production of DNA Circles. *Mol Cell, 72*(3), 583-593 e584. doi:10.1016/j.molcel.2018.08.036

Mohanty, B. K., Bairwa, N. K., & Bastia, D. (2009). Contrasting roles of checkpoint proteins as recombination modulators at Fob1-Ter complexes with or without fork arrest. *Eukaryot Cell, 8*(4), 487-495. doi:10.1128/EC.00382-08

Oakes, M., Nogi, Y., Clark, M. W., & Nomura, M. (1993). Structural alterations of the nucleolus in mutants of Saccharomyces cerevisiae defective in RNA polymerase I. *Mol Cell Biol, 13*(4), 2441-2455. doi:10.1128/mcb.13.4.2441

Oakes, M., Siddiqi, I., Vu, L., Aris, J., & Nomura, M. (1999). Transcription factor UAF, expansion and contraction of ribosomal DNA (rDNA) repeats, and RNA polymerase switch in transcription of yeast rDNA. *Mol Cell Biol, 19*(12), 8559-8569. doi:10.1128/mcb.19.12.8559

Peter, J., De Chiara, M., Friedrich, A., Yue, J. X., Pflieger, D., Bergstrom, A., . . . Schacherer, J. (2018). Genome evolution across 1,011 Saccharomyces cerevisiae isolates. *Nature, 556*(7701), 339-344. doi:10.1038/s41586-018-0030-5

Petes, T. (1980). Unequal meiotic recombination within tandem arrays of yeast ribosomal DNA genes. *Cell, 19*(3), 765-774. doi:10.1016/s0092-8674(80)80052-3

Press, M. O., Hall, A. N., Morton, E. A., & Queitsch, C. (2019). Substitutions Are Boring: Some Arguments about Parallel Mutations and High Mutation Rates. *Trends Genet, 35*(4), 253-264. doi:10.1016/j.tig.2019.01.002

Redon, R., Ishikawa, S., Fitch, K. R., Feuk, L., Perry, G. H., Andrews, T. D., . . . Hurles, M. E. (2006). Global variation in copy number in the human genome. *Nature, 444*(7118), 444-454. doi:10.1038/nature05329

Rine, J., & Herskowitz, I. (1987). Four genes responsible for a position effect on expression from HML and HMR in *Saccharomyces cerevisiae*. *Genetics, 116*(1), 9-22.

Saka, K., Takahashi, A., Sasaki, M., & Kobayashi, T. (2016). More than 10% of yeast genes are related to genome stability and influence cellular senescence via rDNA maintenance. *Nucleic Acids Res, 44*(9), 4211-4221. doi:10.1093/nar/gkw110

Salim, D., Bradford, W. D., Freeland, A., Cady, G., Wang, J., Pruitt, S. C., & Gerton, J. L. (2017). DNA replication stress restricts ribosomal DNA copy number. *PLoS Genet, 13*(9), e1007006. doi:10.1371/journal.pgen.1007006

Salim, D., & Gerton, J. L. (2019). Ribosomal DNA instability and genome adaptability. *Chromosome Res, 27*(1-2), 73-87. doi:10.1007/s10577-018-9599-7

Sebat, J., Lakshmi, B., Troge, J., Alexander, J., Young, J., Lundin, P., . . . Wigler, M. (2004). Large-scale copy number polymorphism in the human genome. *Science, 305*(5683), 525-528. doi:10.1126/science.1098918

Shyian, M., Mattarocci, S., Albert, B., Hafner, L., Lezaja, A., Costanzo, M., . . . Shore, D. (2016). Budding Yeast Rif1 Controls Genome Integrity by Inhibiting rDNA Replication. *PLoS Genet, 12*(11), e1006414. doi:10.1371/journal.pgen.1006414

Smith, J. S., Brachmann, C. B., Pillus, L., & Boeke, J. D. (1998). Distribution of a limited Sir2 protein pool regulates the strength of yeast rDNA silencing and is modulated by Sir4p. *Genetics, 149*(3), 1205–1219.

Smith, J. S., Caputo, E., & Boeke, J. D. (1999). A genetic screen for ribosomal DNA silencing defects identifies multiple DNA replication and chromatin-modulating factors. *Mol Cell Biol, 19*(4), 3184-3197. doi:10.1128/mcb.19.4.3184

Stults, D. M., Killen, M. W., Williamson, E. P., Hourigan, J. S., Vargas, H. D., Arnold, S. M., . . . Pierce, A. J. (2009). Human rRNA gene clusters are recombinational hotspots in cancer. *Cancer Res, 69*(23), 9096-9104. doi:10.1158/0008-5472.CAN-09-2680

Szostak, J. W., & Wu, R. (1980). Unequal crossing over in the ribosomal DNA of Saccharomyces cerevisiae. *Nature, 284*(5755), 426-430. doi:10.1038/284426a0

Udugama, M., Sanij, E., Voon, H. P. J., Son, J., Hii, L., Henson, J. D., . . . Wong, L. H. (2018). Ribosomal DNA copy loss and repeat instability in ATRX-mutated cancers. *Proc Natl Acad Sci U S A, 115*(18), 4737-4742. doi:10.1073/pnas.1720391115

Wagstaff, J. E., Klapholz, S., Waddell, C. S., Jensen, L., & Esposito, R. E. (1985). Meiotic exchange within and between chromosomes requires a common Rec function in Saccharomyces cerevisiae. *Mol Cell Biol, 5*(12), 3532-3544. doi:10.1128/mcb.5.12.3532

Wang, D., Mansisidor, A., Prabhakar, G., & Hochwagen, A. (2016). Condensin and Hmo1 Mediate a Starvation-Induced Transcriptional Position Effect within the Ribosomal DNA Array. *Cell Rep, 14*(5), 1010-1017. doi:10.1016/j.celrep.2016.01.005

Wang, M., & Lemos, B. (2017). Ribosomal DNA copy number amplification and loss in human cancers is linked to tumor genetic context, nucleolus activity, and proliferation. *PLoS Genet, 13*(9), e1006994. doi:10.1371/journal.pgen.1006994

Warburton, P. E., Hasson, D., Guillem, F., Lescale, C., Jin, X., & Abrusan, G. (2008). Analysis of the largest tandemly repeated DNA families in the human genome. *BMC Genomics, 9*, 533. doi:10.1186/1471-2164-9-533

Welch, J., Fogel, S., Buchman, C., & Karin, M. (1989). The CUP2 gene product regulates the expression of the CUP1 gene, coding for yeast metallothionein. *EMBO J, 8*(1), 255-260.

Wolfram Research, I. (2014). Mathematica. Champaign, IL: Wolfram Research, Inc.

Wyandt, H. E., Wilson, G. N., & Tonk, V. S. (2017). *Human Chromosome Variation: Heteromorphism, Polymorphism and Pathogenesis*.

Xu, B., Li, H., Perry, J. M., Singh, V. P., Unruh, J., Yu, Z., . . . Gerton, J. L. (2017). Ribosomal DNA copy number loss and sequence variation in cancer. *PLoS Genet, 13*(6), e1006771. doi:10.1371/journal.pgen.1006771

Zarrei, M., MacDonald, J. R., Merico, D., & Scherer, S. W. (2015). A copy number variation map of the human genome. *Nat Rev Genet, 16*(3), 172-183. doi:10.1038/nrg3871

Zhao, Y., Dominska, M., Petrova, A., Bagshaw, H., Kokoska, R. J., & Petes, T. D. (2017). Properties of Mitotic and Meiotic Recombination in the Tandemly-Repeated CUP1 Gene Cluster in the Yeast Saccharomyces cerevisiae. *Genetics, 206*(2), 785-800. doi:10.1534/genetics.117.201285

Zhu, J., Heinecke, D., Mulla, W. A., Bradford, W. D., Rubinstein, B., Box, A., . . . Li, R. (2015). Single-Cell Based Quantitative Assay of Chromosome Transmission Fidelity. *G3 (Bethesda), 5*(6), 1043-1056. doi:10.1534/g3.115.017913

CHAPTER 4

H3K56 acetylation and homologous recombination govern an adaptive program at tandem repeats

4 CHAPTER 4

4.1 List of Figures

4.2 List of Tables

4.3 Abstract

Tandem repeats are recognized as a significant genetic source of adaptation to stress, yet the mechanisms that regulate copy number variations at these repeats in response to the environment remain poorly understood. In this study, we use the rDNA locus and the copper-resistance *CUP1* gene array to characterize the role of H3K56 acetylation in regulating copy number variation at tandem repeats in yeast. We found that while instability at the rDNA array was greatly reduced by loss of H3K56 acetylation in *rtt109*Δ mutants, hyper-acetylation of H3K56 in *hst3*Δ*hst4*Δ mutants, and various point mutations in H3K56 (H3K56A, H3K56R, H3K56Q), all increased rDNA instability. Consistent with previous reports, we found that all these mutations were associated with amplifications of the rDNA array. Using the copper-inducible *CUP1* gene array, we found that both *rtt109*Δ and *hst3*Δ*hst4*Δ mutants exhibited decreased transcription-dependent instability at *CUP1*. Despite increased stability, amplification of the *CUP1* array and adaptation to high concentrations of copper still occurred in both *rtt109*Δ and *hst3*Δ*hst4*Δ mutants. Interestingly, in low concentrations of copper, *CUP1* amplification still occurred in the *rtt109*Δ strain, but not in the corresponding wild-type or *hst3*Δ*hst4*Δ strains. Further, disrupting the H3K56 acetylation pathway also affected both, basal and copper-induced *CUP1* transcription. These data suggest that H3K56 acetylation regulates transcription and transcription-induced instability at the *CUP1* array, and importantly, it functions to restrict transcription-induced amplification of the *CUP1* array. Additionally, adaptation to high concentrations of copper is dependent on Rad51 and Rad52, suggesting that *CUP1* amplification is dependent on homologous recombination. Based on these data, we speculate that the loss of Rtt109 may influence recombination events in a manner that results in a bias toward amplification of an array under transcriptional stress. Altogether, this study suggests that the rDNA hyper-amplification phenotype in mutants with disrupted H3K56 acetylation may also be due to constitutive, perturbed transcription and recombination pathway bias at the locus. The ubiquity of H3K56 acetylation and its demonstrated role in the regulation of copy number variation at multiple tandem repeats in yeast suggests that this chromatin mark could play a critical and conserved role in influencing adaptive outcomes by modulating the stability and amplification of repeats in response to transcriptional stress.

4.4 Introduction

Tandem repeats are pervasive in eukaryotic genomes, and are unstable by design. The presence of multiple identical repeat units in a head-to-tail arrangement makes them susceptible to copy number variation resulting from polymerase slippage during DNA replication and/or unequal exchange events during recombination-mediated repair. Copy number variation at tandem repeats is now widely recognized as the most significant source of genotypic and phenotypic diversity in yeast and human populations (Iafrate et al., 2004; Peter et al., 2018; Redon et al., 2006; Sebat et al., 2004; Steenwyk & Rokas, 2018; Zarrei et al., 2015). While the potential functional impact of tandem repeats on adaptation to stress is beginning to be appreciated, repeats are often neglected in genomics studies. Consequently, the molecular mechanisms that regulate copy number variations and their role in cellular adaptation to the environment have remained largely unclear. The identification and characterization of these mechanisms is critical to comprehend genome plasticity.

The most well-studied tandem repeat family are the ribosomal DNA (rDNA) genes in the budding yeast, *Saccharomyces cerevisiae*. The rDNA genes encode ribosomal RNA (rRNA), which are essential structural and catalytic components of ribosomes. The yeast rDNA array is the most highly transcribed genomic locus, and multiple copies of rDNA repeats are essential to support the high cellular demand for rRNA. Budding yeast have 100-200 copies of rDNA genes arranged in tandem at a single locus on Chromosome XII. Only about half of the ~150 repeats are transcribed in actively growing yeast cells and rDNA copy number can be reduced significantly (up to ~20 copies) without affecting rRNA output or cell growth (French et al., 2003; Kobayashi et al., 1998). The extra, untranscribed rDNA repeats are required to ensure efficient DNA damage repair at this highly transcribed locus (Ide et al., 2010). Paradoxically, despite the relatively high instability at the locus, normal rDNA copy number is stably maintained in unperturbed conditions. Further, rDNA copy number changes occur frequently as adaptive responses to a variety of mutations and environmental stresses, usually with

little effect on total rRNA levels (Albert et al., 2011; Ide et al., 2007; Kobayashi et al., 1998; Kwan et al., 2013; Oakes et al., 1993; Oakes et al., 1999; Salim et al., 2017; Shyian et al., 2016). These data suggest that the functions of the rDNA go well beyond ribosome biogenesis. Therefore, characterization of the mechanisms regulating the stability of the rDNA array and its ability to accommodate extensive copy number variation is key to understanding the impact of these variations on genomic adaptation to the environment.

While the last two decades have witnessed the discovery of many genes involved in the regulation of rDNA copy number variation in budding yeast (Ide et al., 2013; Saka et al., 2016; Salim et al., 2017; Smith et al., 1999), the lack of quantitative, sensitive assays to measure rDNA instability in a high-throughput manner has limited our understanding of how instability aids adaptive copy number variation. The lack of a clear distinction between repeat instability and changes in steady state copy number has also resulted in several apparently paradoxical findings. We previously reported the development and validation of qRIN, a quantitative, single-cell, fluorescence-based assay to measure repeat instability in budding yeast as well as droplet digital PCR (ddPCR) assays to measure repeat copy number (Chapter 3, (Salim et al., 2017)). Through multiple high-throughput genetic screens, we found that rDNA stability and copy number are regulated by the fundamental processes of DNA replication, transcription, and histone acetylation. Since constitutive transcription of rDNA genes is essential for cell viability, we used a second array, the tandem array of the copper-inducible *CUP1* genes to characterize the dependence of repeat stability on DNA replication and transcription. Through parallel studies using both, the rDNA and *CUP1* arrays, we demonstrated that transcription and DNA replication stress can rapidly induce repeat instability. However, a change in steady state copy number, or adaptation, requires selection over time. These data demonstrate that replication and transcription create a program of instability and adaptation at tandem repeats in response to stress.

Histone acetylation is a chromatin mark well known for its roles in promoting transcription (Varv et al., 2010; Yang et al., 2008), maintaining DNA replication timing and origin firing (Aparicio et al., 2004; Casas-Delucchi et al., 2012; Unnikrishnan et al., 2010; Vogelauer et al., 2002), and even influencing the choice of break repair pathway (Che et al., 2015; Munoz-Galvan et al., 2013), and therefore has the potential to have profound impacts on rDNA stability and copy number variation. In fact, multiple studies have shown that the acetylation status of various histone residues affects several aspects of rDNA biology. While the role of Sir2 in regulating recombination at the rDNA was first demonstrated in 1989 (Gottlieb & Esposito, 1989), its function as an NAD+-dependent histone deacetylase that specifically targets lysines 9, 14, and 56 of histone H3 (H3K9, H3K14, and H3K56), and lysine 16 of histone H4 (H4K16) was only identified much later. It is now known that H3K14 and H4K16 acetylation regulate non-coding RNA Polymerase II (RNAPII) transcription and silencing at the rDNA (Cesarini et al., 2012; D'Alfonso et al., 2016; F. Xu et al., 2007; H. H. Xu et al., 2016). The subsequent identification of the key global H3K56 deacetylases, Hst3 and Hst4 (Celic et al., 2006; Maas et al., 2006), and the global H3K56 acetyltransferase, Rtt109 (Han et al., 2007a), and the characterization of phenotypes of cells that had hyper- or hypo-acetylated H3K56 established the importance of this post-translational modification in maintaining normal DNA replication timing, replisome stability, appropriate DNA damage response, and genome stability (Hachinohe et al., 2011; Han et al., 2007b; Kadyrova et al., 2013; Luciano, 2015; Maas et al., 2006; Simoneau et al., 2016; Yoshida et al., 2014). The discovery that the target of rapamycin (TOR) signaling pathway regulates rDNA copy number (Jack et al., 2015) and rRNA biogenesis by targeting the H3K56 residue (Chen et al., 2012) established the importance of H3K56 acetylation at the rDNA. Further, loss of Rtt109, or Hst3 and Hst4 were both shown to result in amplification of rDNA repeats (Ide et al., 2013), suggesting a key role for H3K56 acetylation in the regulation of rDNA stability and steady state copy number. Work from Hull et al. (2017) showed that *CUP1* copy number variation was induced by transcription and regulated by H3K56 acetylation

(Hull et al., 2017). These data suggest at least partial conservation of the roles of H3K56 acetylation in regulating repeat stability and adaptation at the two arrays.

In this study, we directly compare the impact of H3K56 acetylation on the normal program of instability and adaptation at these two tandem arrays. We found that while loss of H3K56 acetylation in *rtt109*Δ mutants increased rDNA stability, hyper-acetylation of H3K56 in *hst3*Δ*hst4*Δ mutants, and various point mutations that mimic the unacetylated (H3K56A and H3K56R) or acetylated (H3K56Q) forms of H3K56, all increased rDNA instability. This result suggests that the H3K56 acetylation/deacetylation cycle regulates stability more than any particular state of acetylation. Interestingly, all these mutations were associated with amplifications of the rDNA array. To reconcile the differences between stability and amplification in these mutants, and characterize the contribution of transcription to these phenotypes, we used the inducible *CUP1* gene array. We found that the effects of hypo- and hyper-acetylation of H3K56 on repeat stability were dependent on transcription. Both, *rtt109*Δ and *hst3*Δ*hst4*Δ mutants exhibited decreased transcription-induced *CUP1* instability. Despite repeat stabilization, both *rtt109*Δ and *hst3*Δ*hst4*Δ mutants were able to adapt to high concentrations of copper through amplification of the *CUP1* array. Interestingly, in low concentrations of copper that do not impair growth, *CUP1* amplification still occurred in the *rtt109*Δ strain, but not in the corresponding wild-type or *hst3*Δ*hst4*Δ strains. Disrupting the H3K56 acetylation pathway also affected total *CUP1* mRNA levels in both, copper-treated and untreated conditions. These data suggest that H3K56 acetylation is required for regulating transcription and restricting transcription-induced amplification of the *CUP1* array independent of growth defects.

Given the roles of H3K56 acetylation in affecting the choice of recombination pathway, and low transcription-dependent *CUP1* repeat loss rates in *rtt109*Δ mutants, we hypothesized that the loss of Rtt109 may influence recombination events at the array in a manner that results in overall amplification of the array when it is transcribed. In fact, we find that adaptation to high concentrations of copper is dependent on Rad51 and

Rad52, suggesting that *CUP1* amplification may also be dependent on homologous recombination. Based on these data, we speculate that *CUP1* amplification in the *rtt109*Δ mutants may also be mediated by homologous recombination. Altogether, this data in combination with our observation of decreased rDNA repeat loss rates in *rtt109*Δ mutants suggests that the rDNA hyper-amplification phenotype in these mutants may also be due to a combination of perturbed transcription and recombination pathway bias. Our studies suggest that H3K56 acetylation is essential for the normal stress induced program for adaptation at tandem repeats.

4.5 Results

4.5.1 H3K56 acetylation regulates rDNA stability and copy number

To measure rDNA and *CUP1* instability, we used the *RDN25-MATα* and *CUP1-MATα* reporter strains respectively. The construction and validation of these reporter strains was described in Chapter 3. Briefly, reporter strains were constructed by tagging the constitutively expressed *MATa* specific gene, *MFA1* with 3 copies of GFP to generate the highly fluorescent *MFA1-3×GFP* strain. The *MATα* locus was then integrated at the 3'-end of the 25S rDNA gene, or the the 3'-end of the *CUP1* ORF within a single repeat to generate the *RDN25-MATα* or the *CUP1-MATα* reporter strain respectively. The α2 transcriptional repressor produced from the *MATα* locus strongly represses *MATa*-specific genes, including *MFA1-3×GFP*. When the *MATα*-containing repeat is lost, Mfa1-3×GFP will be expressed and the cell will become highly fluorescent within one cell cycle after the loss event due to rapid proteasome degradation of the α2 repressor (Chapter 3). Loss rates of the *MATα*-containing region per cell division can be calculated by monitoring the change in frequency of GFP-positive cells over the course of growth in non-selective medium using the formula described in Chapter 3.

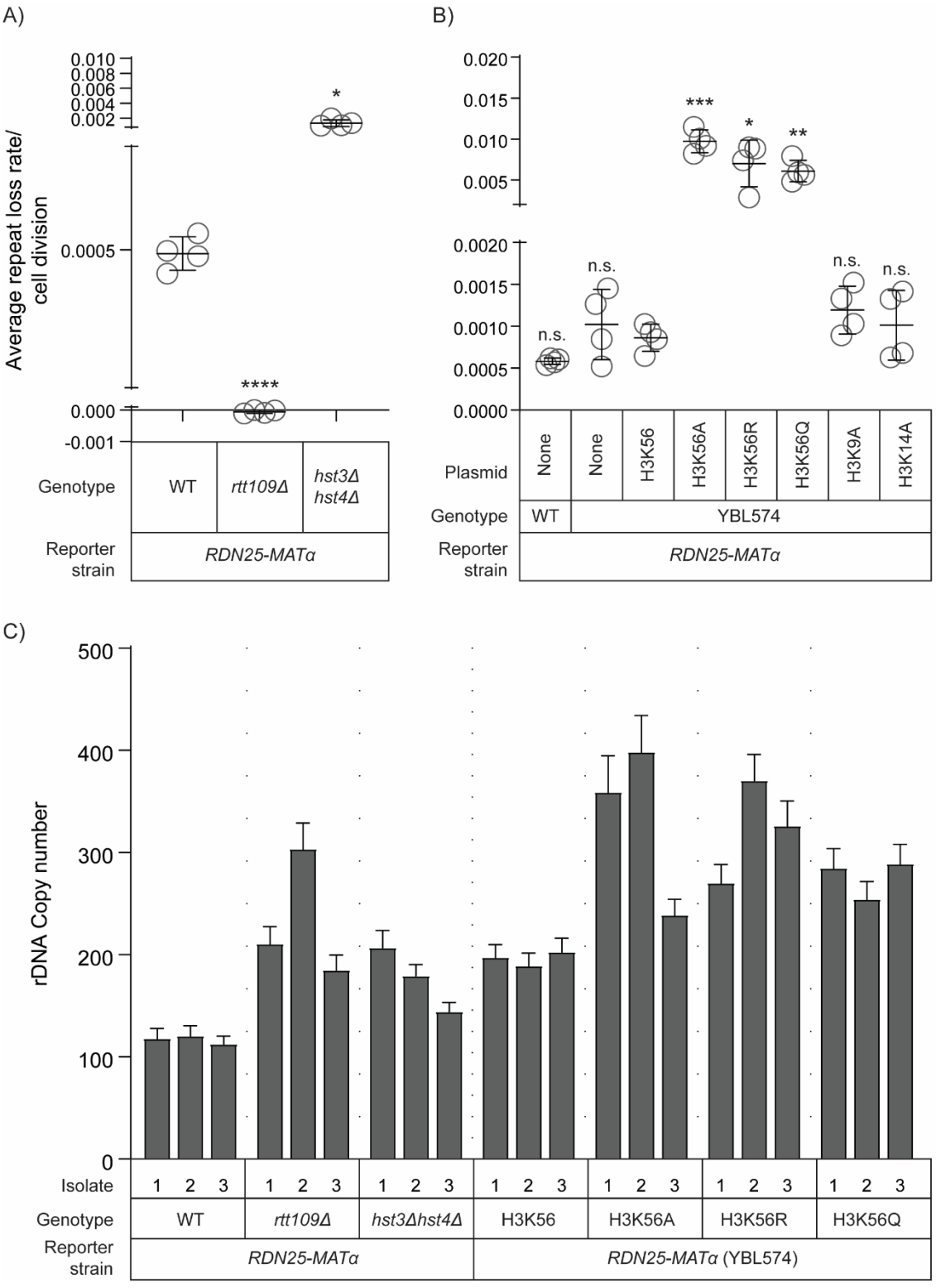

Figure 4.1. H3K56 acetylation regulates rDNA stability and copy number. (A) rDNA repeat loss rates in *rtt109*Δ and *hst3*Δ*hst4*Δ mutants. (B) rDNA repeat loss rates in various H3K56 point mutants. Error bars in (A) and (B) represent standard deviation based on 4 biological replicates. Statistical significance was calculated using a standard 2-tailed t-test. * - p<0.05, ** - p<0.01, *** - p<0.001, **** - p<0.0001, n. s.– not significant. (C) Mutations that affect H3K56 acetylation are associated with expansion of the rDNA array. rDNA copy number was measured in 3 independent isolates of each strain using ddPCR. Error bars represent standard deviation for each individual reaction.

To directly test the role of H3K56 acetylation in the regulation of rDNA stability, we generated *rtt109*Δ mutants and *hst3*Δ*hst4*Δ double mutants in the *RDN25-MATα* background. We first measured rDNA repeat loss rates in these mutants. Interestingly, *rtt109*Δ mutants had significantly lower rDNA repeat loss rates than wild-type *RDN25-MATα* (Figure 4.1A). On the other hand, the *hst3*Δ*hst4*Δ double mutants had higher rDNA repeat loss rates than wild-type *RDN25-MATα* (Figure 4.1A). We also measured the loss of *MATα* from a unique intergenic region downstream of *TUB1*, and found that loss of Rtt109 did not affect the stability of this region (Figure 4.2). This suggests that the effects of perturbed H3K56 acetylation may be specific to transcribed tandem repeats. While Hst3 and Hst4 mainly target acetylated H3K56, Rtt109 acetylates both H3K56 and H3K9 residues. Additionally, given the role of Sir2 in regulating rDNA stability, and the role of its multiple targets, particularly H3K14, in regulating silencing at the rDNA, we sought to identify the key lysine residue of histone H3 involved in regulation of rDNA stability and copy number variation.

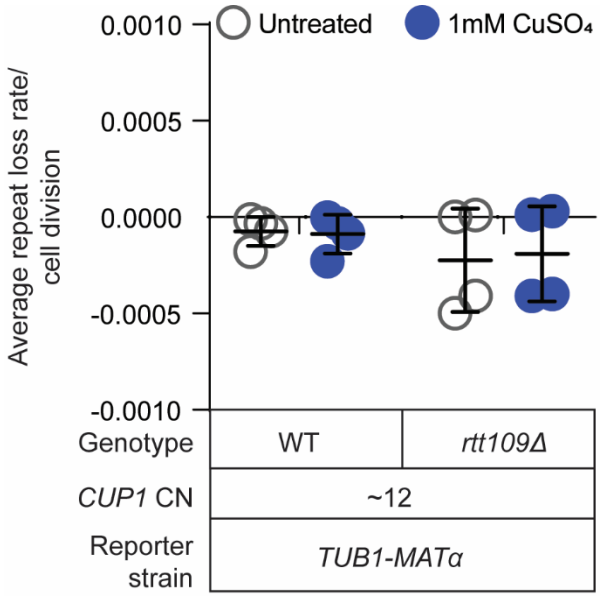

Figure 4.2. Loss of Rtt109 and copper treatment do not affect instability at *TUB1*. *MATα* loss rates from a unique, intergenic region downstream of *TUB1*. Error bars represent standard deviation based on 4 biological replicates.

To characterize the role of the H3K56 residue in regulating rDNA stability, we generated three H3K56 point mutants, an alanine substitution mutant, H3K56A (Nakanishi et al., 2008), and H3K56R (which mimics the unacetylated form of H3K56) and H3K56Q (which mimics the acetylated form of H3K56). We also generated alanine substitution mutants in H3K9 and H3K14, H3K9A and H3K14A (Nakanishi et al., 2008). We transformed each of these plasmids into the *RDN25-MATα* (YBL574) reporter strain, which was constructed exactly as described above in the yeast histone shuffle strain, YBL574 (Nakanishi et al., 2008). YBL574 has the native histone H3/H4 loci (*HHT1-HHF1* and *HHT2-HHF2*) deleted and carries wild-type *HHT2-HHF2* on a Uracil-selectable plasmid. The H3K56A, H3K56R, H3K56Q, H3K9A, and H3K14A mutations were each carried on a Tryptophan-selectable plasmid. We transformed each of the mutant plasmids, as well as a Tryptophan-selectable plasmid carrying wild-type *HHT2-HHF2* into *RDN25-MATα* (YBL574). We grew transformants on Tryptophan-dropout medium containing 5-fluorooroticacid (5-FOA) to select for the Tryptophan-selectable mutant *HHT2-HHF2* plasmids and simultaneously remove the Uracil-selectable wild-type *HHT2-HHF2* plasmids. We then measured rDNA repeat loss rates in the resulting strains.

The “wild-type” *RDN25-MATα* and *RDN25-MATα* (YBL574) reporter strains as well as the *RDN25-MATα* (YBL574) strain containing the wild-type *HHT2-HHF2* plasmid had comparable rDNA repeat loss rates (Figure 4.1B). We found that the H3K9A and H3K14A mutations did not alter rDNA repeat loss rates. All three H3K56 mutations altered rDNA repeat loss rates, however, unexpectedly, H3K56A, H3K56R, and H3K56Q, all increased rDNA repeat loss rates (Figure 4.1B). Next, we measured rDNA copy number in multiple isolates of each of these strains. Despite isolate to isolate variability in rDNA copy number, the *rtt109*Δ and *hst3*Δ*hst4*Δ double mutants, and all three H3K56 mutant strains had amplified rDNA arrays in comparison to the corresponding parent strains as previously reported (Ide et al., 2013) (Figure 4.1C).

These data suggest that the H3K56 acetylation pathway plays a key role in the regulation of rDNA stability and maintenance of normal rDNA copy number.

4.5.2 H3K56 acetylation regulates *CUP1* transcription and stability

H3K56 acetylation has been demonstrated to directly affect rDNA transcription; while total 18S and 25S rRNA levels in H3K56A mutants are comparable to wild-type strains, these mutants have decreased RNA polymerase I (RNAPI) binding at the rDNA and accumulate unprocessed rRNA precursors, both indicative of reduced rDNA transcription efficiency (Chen et al., 2012). Further, the normal H3K56 acetylation/deacetylation cycle has been shown to be important to promote DNA damage repair via homologous recombination with the sister chromatid (Che et al., 2015; Munoz-Galvan et al., 2013). Consistent with this, control of rDNA amplification by the TOR signaling pathway has been shown to be mediated by H3K56 acetylation through break-induced replication (BIR) mediated repair pathways (Chen et al., 2012; Jack et al., 2015). These data suggest that rDNA amplification in mutants with perturbed H3K56 acetylation is due at least in part to constitutive and perturbed transcription at the locus, which may in turn influence the choice of the repair pathways in a manner that results in a net gain of repeats.

High levels of constitutive rDNA transcription are essential for cell viability. This makes it impossible to directly test transcription-dependent and independent functions of H3K56 acetylation in the maintenance of rDNA stability and copy number. We chose to study this in the copper-inducible *CUP1* gene array because Hull et al. (2017) showed that transcription induces copy number variation at the *CUP1* array in an Rtt109 dependent manner (Hull et al., 2017). Based on their observation of low *CUP1* copy number variation in *rtt109*Δ mutants, this group had predicted that adaptation and *CUP1* amplification in response to copper would require Rtt109. This prediction is confounding given the rDNA hyper-amplification observed in *rtt109*Δ mutants. However, their results

are consistent with our observations of decreased rDNA repeat loss rates in *rtt109*Δ mutants, and high rDNA repeat loss rates in *hst3*Δ*hst4*Δ mutants (Figure 4.1A). We also previously showed that instability at both, the rDNA and *CUP1* arrays is regulated by the fundamental processes of DNA replication and transcription (Chapter 3). Taken together, these data suggest that the use of the inducible *CUP1* array can help identify conserved general principles that govern the regulation of these two tandem repeats by H3K56 acetylation.

We found that disrupting the H3K56 acetylation cycle prevented transcription-induced instability at *CUP1*. We showed previously that copper-induced transcription increases *CUP1* instability in a dose-dependent manner in *CUP1-MATα* reporter strains with 2-20 copies of *CUP1* (Chapter 3). In contrast, in strains with at least 6 copies of *CUP1* (≥6×*CUP1*), we find that transcription does not increase instability in the *rtt109*Δ or the *hst3*Δ*hst4*Δ mutants (Figures 4.3A, 4.4A). Further, while transcription-independent *CUP1* instability in the *rtt109*Δ mutants is comparable to that of corresponding wild-type strains, transcription-independent *CUP1* instability in *hst3*Δ*hst4*Δ mutants is significantly elevated (Figures 4.3A, 4.4A).

Interestingly, we also find that a 2-copy *CUP1* gene array (2×*CUP1)* responds differently to transcription when H3K56 acetylation is perturbed. In the 2×*CUP1* strains, copper-induced *CUP1* repeat loss rates in both *rtt109*Δ and *hst3*Δ*hst4*Δ strains are comparable to that in the corresponding wild-type strain. However, as in strains with ≥6×*CUP1*, transcription-independent *CUP1* instability is elevated in *hst3*Δ*hst4*Δ mutants, suggesting that copper-induced transcription does not further increase *CUP1* instability in these mutants (Figure 4.3A). Therefore, while hypo-acetylation of H3K56 may affect the stability of ≥6×*CUP1* repeats differently from 2×*CUP1* repeats, the effects of hyper-acetylation of H3K56 are independent of array size. These data suggest that both transcription-dependent and independent stability at the *CUP1* array are affected by the H3K56 acetylation/deacetylation pathway.

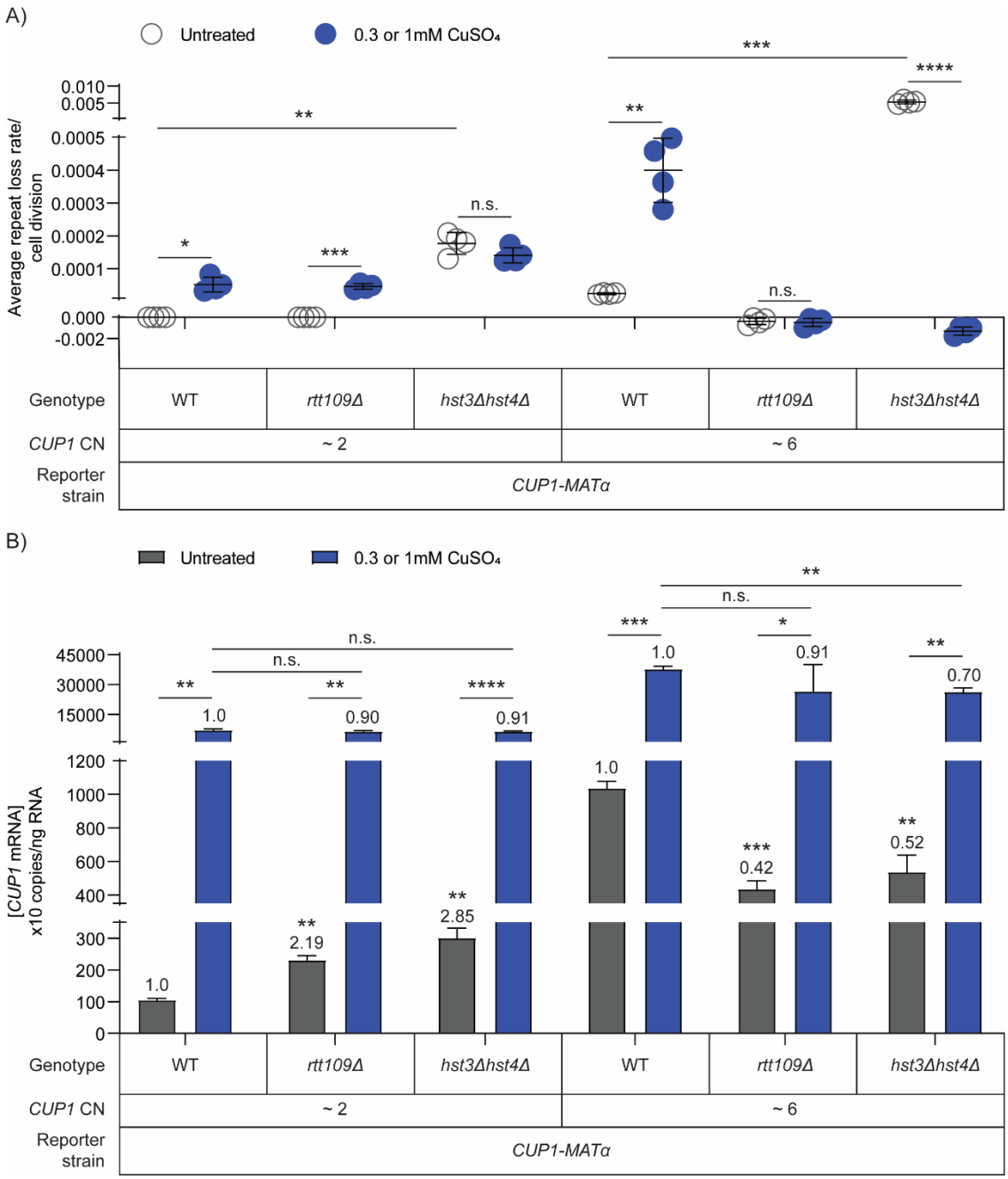

Figure 4.3. H3K56 acetylation regulates *CUP1* instability and transcription. (A) Transcription -dependent and independent *CUP1* repeat loss rates in *rtt109*Δ and *hst3*Δ*hst4*Δ mutants. Error bars represent standard deviation based on 4 biological replicates. (B) Absolute *CUP1* mRNA concentration (×10 copies/ng of total RNA) in *rtt109*Δ and *hst3*Δ*hst4*Δ mutants measured by RT-ddPCR. Error bars represent standard deviation based on 3 technical replicates for cDNA synthesis from the same RNA sample. Fold-change relative to the corresponding wild-type strain is indicated. For (A) and (B), the 2×*CUP1* strains were grown in 0.3mM $CuSO_4$, and the 6×*CUP1* strains were grown in 1mM $CuSO_4$. Statistical significance was calculated using a standard 2-tailed t-test. * - p<0.05, ** - p<0.01, *** - p<0.001, **** - p<0.0001, n. s.– not significant.

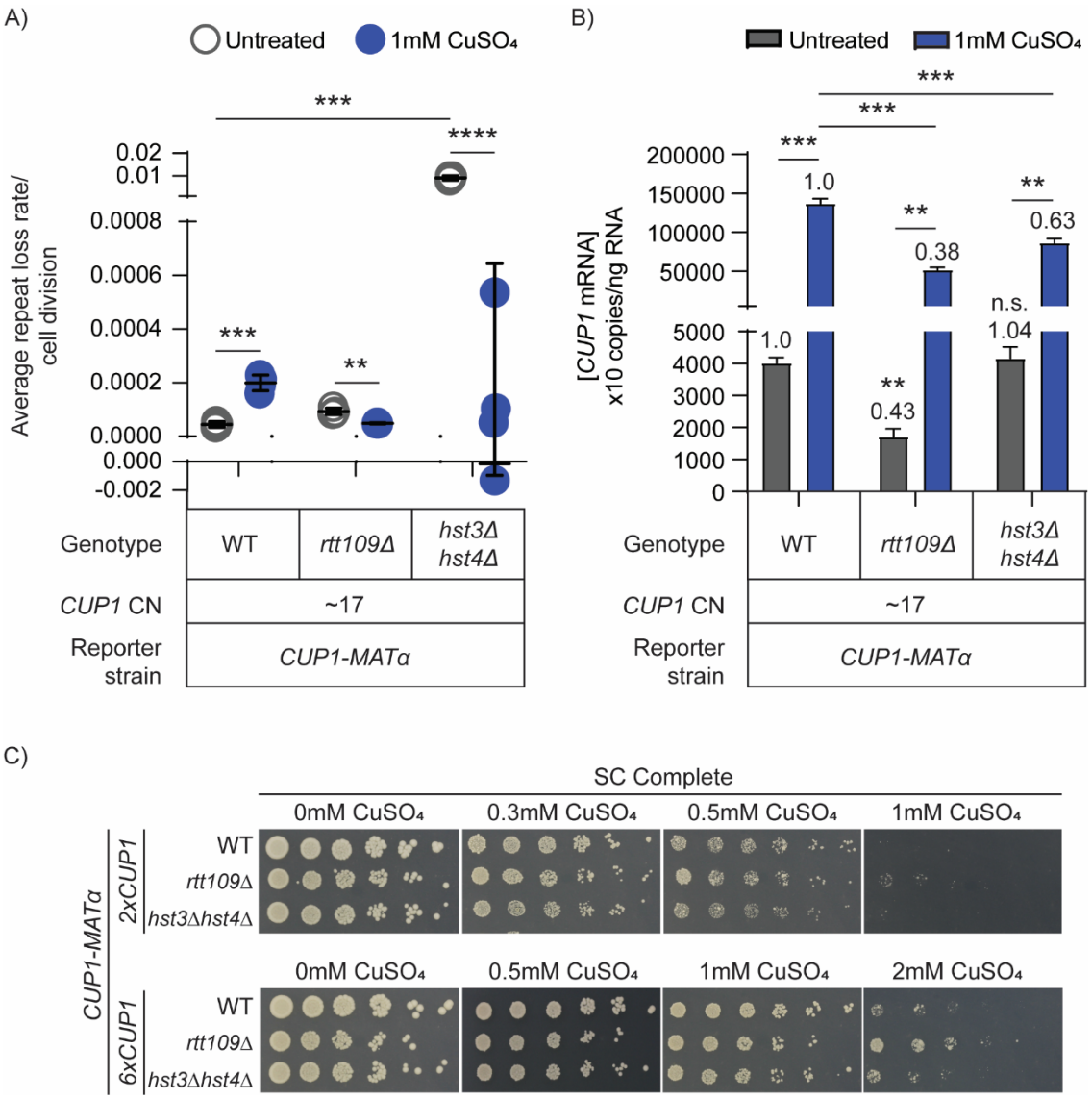

Figure 4.4. Effects of disrupted H3K56 acetylation on *CUP1* instability and transcription in a 17×*CUP1* strain. (A) Transcription-dependent and independent *CUP1* repeat loss rates in 17×*CUP1 rtt109*Δ and *hst3*Δ*hst4*Δ mutants. Error bars represent standard deviation based on 4 biological replicates. (B) Absolute *CUP1* mRNA concentration (×10 copies/ng of total RNA) in 17×*CUP1 rtt109*Δ and *hst3*Δ*hst4*Δ mutants measured by RT-ddPCR. Error bars represent standard deviation based on 3 technical replicates for cDNA synthesis from the same RNA sample. Fold-change relative to the corresponding wild-type strain is indicated. Statistical significance was calculated using a standard 2-tailed t-test. * - p<0.05, ** - p<0.01, *** - p<0.001, **** - p<0.0001, n. s.– not significant. (C) Growth assays showing copper resistance of *rtt109*Δ and *hst3*Δ*hst4*Δ mutants.

Given the role of H3K56 acetylation in promoting transcription at the rDNA, and the induction of instability at the *CUP1* array by transcription in a dose-dependent manner, we wondered whether the changes in *CUP1* instability in the *rtt109*Δ and *hst3*Δ*hst4*Δ mutants were due in part to altered *CUP1* transcription. To test this, we measured basal *CUP1* mRNA levels in wild-type, *rtt109*Δ and *hst3*Δ*hst4*Δ mutant strains

in *CUP1-MATα* reporter strains with 2, 6, or 17 copies of *CUP1*. We also measured *CUP1* mRNA levels in each of these strains following induction of the *CUP1* array with the same concentrations of copper used for the instability measurements in Figures 4.3A and 4.4A. Copper-treated 2×*CUP1 rtt109*Δ and *hst3*Δ*hst4*Δ strains show a small, but statistically insignificant decrease in *CUP1* mRNA levels (90% and 91% of wild-type levels in *rtt109*Δ and *hst3*Δ*hst4*Δ respectively) (Figure 4.3B). The decrease in *CUP1* mRNA levels is modest in the 6×*CUP1* strains (91% and 70% of wild-type levels in *rtt109*Δ and *hst3*Δ*hst4*Δ respectively), and significant in the 17×*CUP1* strains (38% and 63% of wild-type levels in *rtt109*Δ and *hst3*Δ*hst4*Δ respectively) (Figures 4.3B, 4.4B). Nevertheless, the *rtt109*Δ and *hst3*Δ*hst4*Δ strains do not exhibit altered copper sensitivity compared to corresponding wild-type strains (Figure 4.4C). These data suggest that the H3K56 acetylation/deacetylation cycle is important for copper-induced *CUP1* transcription at ≥6×*CUP1* arrays. Given the higher transcriptional output and the more pronounced decrease in *CUP1* transcript levels in the mutant 17×*CUP1* strains, it is tempting to speculate that disruption of H3K56 acetylation/deacetylation becomes increasingly detrimental to transcription as array size and transcriptional load on the array increases.

Basal *CUP1* mRNA levels in untreated cells were also significantly affected in the *rtt109*Δ and *hst3*Δ*hst4*Δ mutants in all three *CUP1-MATα* reporter strains tested. We found that the 2×*CUP1 rtt109*Δ and *hst3*Δ*hst4*Δ strains exhibited a ~2.2-fold and ~2.9-fold increase in basal *CUP1* mRNA levels respectively (Figure 4.3B). On the other hand, the basal transcript abundance was significantly reduced in both *rtt109*Δ and *hst3*Δ*hst4*Δ mutants in strains with ≥6×*CUP1*. The 6×*CUP1 rtt109*Δ and *hst3*Δ*hst4*Δ strains exhibited a ~2.4-fold and ~1.9-fold decrease in basal *CUP1* mRNA levels respectively (Figure 4.3B). While the 17×*CUP1 rtt109*Δ strain exhibited a ~2.3-fold decrease in *CUP1* mRNA levels, transcript levels were unchanged in the 17×*CUP1 hst3*Δ*hst4*Δ strains (Figure 4.4B). These data show that the H3K56

acetylation/deacetylation pathway is critical to maintain normal basal *CUP1* transcription irrespective of array size.

The decrease in both, transcriptional output as well as transcription-dependent instability, particularly in ≥6×*CUP1* repeats suggests that the H3K56 acetylation/deacetylation pathway regulates instability at the *CUP1* array partly through its effects on transcription. The striking differences in the nature of changes in basal *CUP1* transcript levels and *CUP1* instability between the mutant 2×*CUP1* and ≥6×*CUP1* strains also highlights that the size of the tandem array is critical in determining its response to transcription and perturbed H3K56 acetylation. Since transcription-induced *CUP1* instability facilitates adaptation to high concentrations of copper (Chapter 3), the dependence of transcription and stability of the *CUP1* array on the H3K56 acetylation pathway suggests that the typical response of this array to transcription is critically dependent on its H3K56 acetylation status.

4.5.3 H3K56 acetylation restricts transcription-induced *CUP1* amplification

We previously showed that in wild-type *CUP1-MATα* cells, *CUP1* amplification facilitates adaptation to high concentrations of copper after prolonged propagation (25-50 generations) in selective conditions (Chapter 3, Figures 4.5 – 4.7). While all mutations that affect H3K56 acetylation are known to be associated with amplifications of the rDNA array, we noticed that in uninduced conditions, copy number of the *CUP1* array was stably maintained in both, *rtt109*Δ and *hst3*Δ*hst4*Δ mutants irrespective of starting array size (Figures 4.5 – 4.7). Because both *rtt109*Δ and *hst3*Δ*hst4*Δ mutants with ≥6×*CUP1* had low copper-induced instability and *CUP1* mRNA levels, like Hull et al. (2017), we also predicted that these mutants may be defective in adapting to high concentrations of copper. However, when we subcultured various *rtt109*Δ and *hst3*Δ*hst4*Δ reporter strains with ≥6×*CUP1* in high concentrations of copper, we were surprised to find that

copper resistant cells that had amplified *CUP1* arrays readily emerged after 25-50 generations as in the corresponding wild-type strains (Figures 4.5 – 4.7).

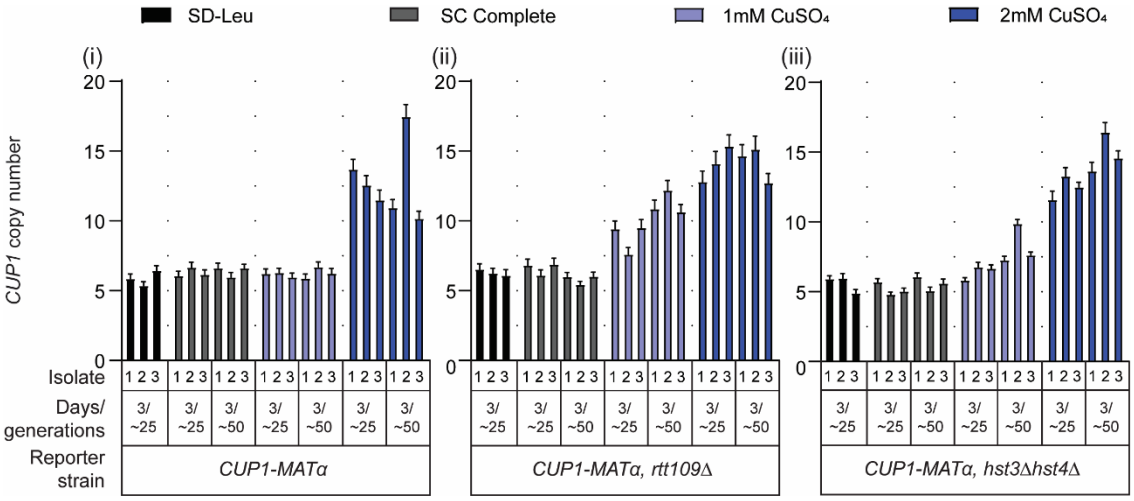

Figure 4.5. H3K56 acetylation restricts transcription-induced amplification of the 6×*CUP1* array. (i) Wild-type, (ii) *rtt109*Δ or (iii) *hst3*Δ*hst4*Δ *CUP1-MATα* strains (6×*CUP1*) were subcultured in the indicated medium for ~6 days (approximately 50 generations). After every 3 days, 3 independent isolates were used to measure *CUP1* copy number by ddPCR. Error bars represent standard deviation for each individual reaction.

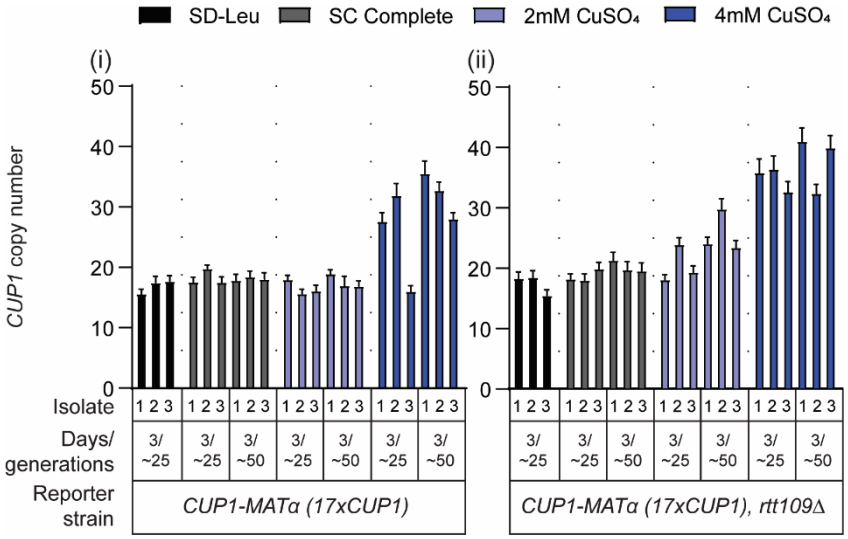

Figure 4.6. H3K56 acetylation restricts transcription-induced amplification of the 17×*CUP1* array. (i) Wild-type or (ii) *rtt109*Δ *CUP1-MATα* strains (17×*CUP1*) were subcultured in the indicated medium for ~6 days (approximately 50 generations). After every 3 days, 3 independent isolates were used to measure *CUP1* copy number by ddPCR. Error bars represent standard deviation for each individual reaction.

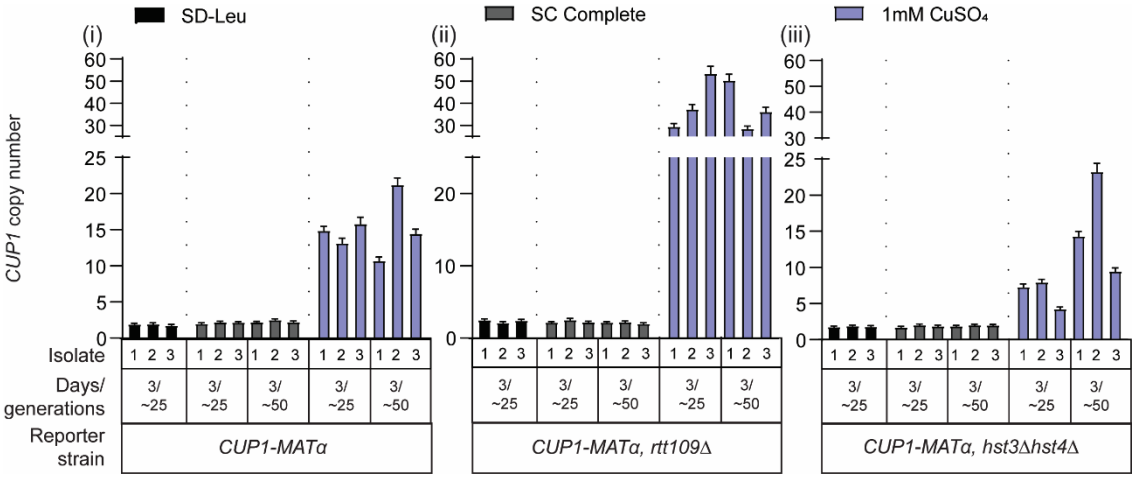

Figure 4.7. H3K56 acetylation restricts transcription-induced amplification of the 2×*CUP1* array. (i) Wild-type, (ii) *rtt109*Δ or (iii) *hst3*Δ*hst4*Δ *CUP1-MATα* strains (2×*CUP1*) were subcultured in the indicated medium for ~6 days (approximately 50 generations). After every 3 days, 3 independent isolates were used to measure *CUP1* copy number by ddPCR. Error bars represent standard deviation for each individual reaction.

Despite having copper-induced *CUP1* instability and *CUP1* mRNA levels similar to wild-type strains, the 2×*CUP1 rtt109*Δ strains exhibited massive *CUP1* amplifications. Copper-resistant isolates contained up to 100×*CUP1* after ~50 generations in high concentrations of copper, while WT cells cultured in the same conditions typically only contained up to ~20×*CUP1* (Figure 4.7). Interestingly, while *CUP1* arrays amplified under selection in the 2×*CUP1 hst3*Δ*hst4*Δ strain, the extent of *CUP1* amplification in these mutants was much lower than that observed in the 2×*CUP1 rtt109*Δ strains (Figure 4.7). Since this was reminiscent of the large rDNA amplifications observed in *rtt109*Δ mutants and the relatively smaller rDNA amplifications in *hst3*Δ*hst4*Δ mutants, we hypothesized that in *rtt109*Δ and *hst3*Δ*hst4*Δ mutants, transcription of the locus may induce amplification of the *CUP1* array independent of growth defects. If this were the case, we would expect *CUP1* amplifications to occur even in low concentrations of copper that do not affect cell growth.

We chose to study the ≥6×*CUP1 rtt109*Δ and *hst3*Δ*hst4*Δ strains to test this hypothesis because, unlike the 2×*CUP1* strains, transcription-induced instability was

low in these strains irrespective of array size, suggesting that ≥6×*CUP1* arrays are better representative of the behavior of the multi-copy repeats like the rDNA array. We subcultured ≥6×*CUP1 rtt109*Δ and *hst3*Δ*hst4*Δ strains in low levels of copper that do not impair growth. Importantly, these concentrations of copper induce instability at the *CUP1* array in wild-type cells, but not in *rtt109*Δ or *hst3*Δ*hst4*Δ mutants (Figures 4.3A, 4.4A). Interestingly, despite low rates of repeat loss, we found that after 25-50 generations, *CUP1* amplification still occurred in all the ≥6×*CUP1 rtt109*Δ strains, but not in the corresponding wild-type strains (Figures 4.5, 4.6). This result demonstrates that stability and copy number maintenance need not be directly correlated, and highlights the importance of distinguishing between changes in instability and steady state copy number.

While the *hst3*Δ*hst4*Δ mutants did not exhibit net *CUP1* amplification after ~50 generations in these non-selective conditions, we found that there was more isolate to isolate variability in *CUP1* copy number in these strains (Figure 4.5 (iii)). Given the high transcription-independent repeat loss rates in this strain, it is possible that *CUP1* amplification is countered by high rates of repeat loss, and requires propagation longer than 50 generations in these conditions, however this remains to be tested. These data suggest that H3K56 acetylation is required for regulating transcription and transcription-induced instability at the *CUP1* array, and importantly, it also functions to restrict transcription-induced amplification. Further, the characteristic adaptive response that occurs in response to transcription at the *CUP1* array depends on the H3K56 acetylation/deacetylation cycle, and disruption of this pathway results in unsolicited changes in repeat stability and copy number in response to transcriptional stress.

4.5.4 The transcription-induced adaptive program at *CUP1* is dependent on homologous recombination

The acetyltransferase activity of Rtt109 requires the histone chaperones Asf1 and Vps75 (Han et al., 2007b, 2007c). While both Asf1 and Vps75 are required for H3K9 acetylation by Rtt109, only Asf1 is required for H3K56 acetylation, and loss of Vps75 only results in a small decrease in global H3K56 acetylation levels (Fillingham et al., 2008; Han et al., 2007c; Selth & Svejstrup, 2007). Houseley and Tollervey (2011) first reported amplification of the rDNA array in both, *asf1*Δ and *rtt109*Δ mutants. Consistent with our observations of reduced rDNA repeat loss rates in *rtt109*Δ mutants, these studies showed that *asf1*Δ mutants also had low rDNA repeat loss rates (Houseley & Tollervey, 2011). Additionally, rDNA amplification in the *asf1*Δ mutants was found to be independent of the canonical homologous recombination proteins, Rad51, Rad52, and Rad59, and occurred through BIR (Houseley et al., 2011).

Our studies of adaptation in *rtt109*Δ and *hst3*Δ*hst4*Δ strains revealed that transcription induces *CUP1* amplifications independent of growth defects, suggesting a defective adaptive response, rather than the lack of it, in the absence of H3K56 acetylation. Therefore, we considered the possibility that, like the rDNA amplifications in the *rtt109*Δ and *asf1*Δ mutants, *CUP1* amplifications in the *rtt109*Δ *and hst3*Δ*hst4*Δ mutants may also be the result of a recombination pathway bias that results in a net gain of repeats in response to transcriptional stress.

Since the deletion of *ASF1* and *RTT109* had similar effects on rDNA stability, we wondered whether loss of Asf1 and Rtt109 would have similar effects on the *CUP1* array. To test this, we deleted *ASF1* and *VPS75* in *CUP1-MATα* strains with 2×*CUP1* and 6×*CUP1*. We also deleted these genes in the *RDN25-MATα* strain to verify their reported effects on rDNA stability. Like *rtt109*Δ mutants, *asf1*Δ mutants also exhibited a) low rDNA repeat loss rates (Figure 4.8A), and b) low transcription-induced *CUP1* instability in the 6×*CUP1* strain (Figure 4.8B). Further, *vps75*Δ mutants only showed a modest decrease in both, rDNA instability, as well as transcription-induced *CUP1*

instability, as expected from its minor contribution to H3K56 acetylation by Rtt109 (Figure 4.8). These data suggest that the recombination pathway bias that results in rDNA amplification may be responsible for transcription-induced *CUP1* amplification in *rtt109*Δ mutants as well. Ide et al. (2013) reported that rDNA amplification in *rtt109*Δ mutants likely occurred through rolling-circle replication initiated by the incorporation of extrachromosomal rDNA circles into chromosomal rDNA, indicating subtle differences between the effects of Asf1 and Rtt109 on rDNA amplification. Further, extrachromosomal *CUP1* circles are known to be at least 3 orders of magnitude rarer than extrachromosomal rDNA circles, suggesting that their contribution to *CUP1* amplification in *rtt109*Δ mutants may be negligible (Moller et al., 2015).

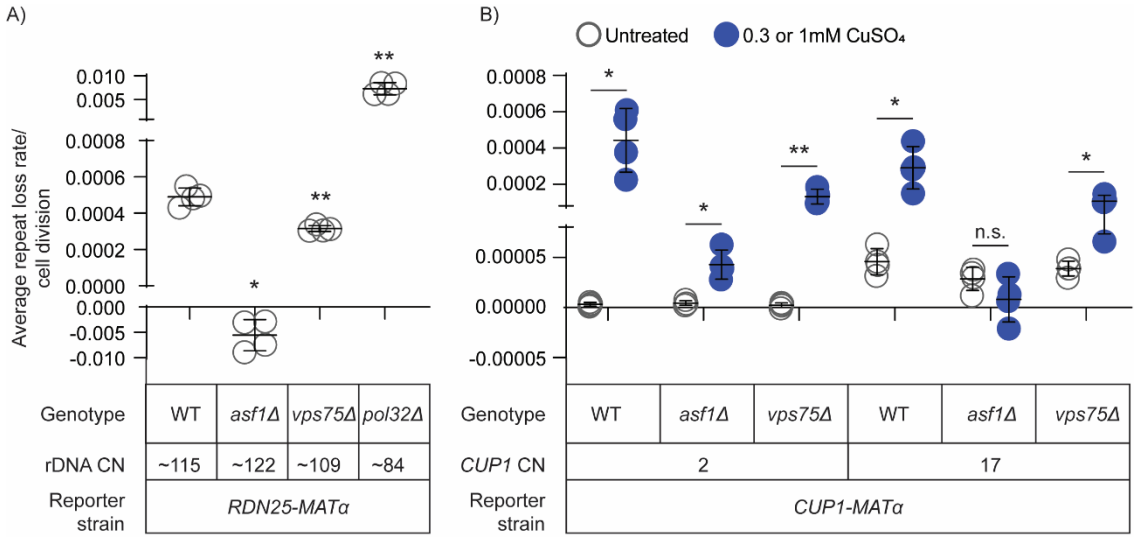

Figure 4.8. Histone chaperones, Asf1 and Vps75, and DNA polymerase δ regulate rDNA and *CUP1* instability. A) rDNA repeat loss rates and B) transcription-dependent and independent *CUP1* repeat loss rates in *asf1*Δ and *vps75*Δ, and *pol32*Δ mutants. Error bars represent standard deviation based on 4 biological replicates. For (B), the 2×*CUP1* strains were grown in 0.3mM $CuSO_4$, and the 6×*CUP1* strains were grown in 1mM $CuSO_4$. Statistical significance was calculated using a standard 2-tailed t-test. * - p<0.05, ** - p<0.01, n. s.– not significant.

To identify the repair pathways that mediate transcription-induced adaptive responses at the *CUP1* array, we deleted genes in key DNA damage repair pathways – non-homologous end joining (NHEJ), canonical homologous recombination (HR), and BIR – in the wild-type and *rtt109*Δ strains. Loss of Yku70, a subunit of the Ku complex

involved in NHEJ, had no effect on transcription-dependent or transcription-independent instability at the *CUP1* array in wild-type or *rtt109*Δ mutant strains (Figure 4.9). Moreover, rDNA copy number in the *yku70*Δ strain was similar to that of the wild-type strain, and *rtt109*Δ*yku70*Δ mutants had amplified rDNA arrays like the parent *rtt109*Δ strain (Figure 4.9). This is consistent with previous reports of reduced NHEJ efficiency in *rtt109*Δ mutants (Jessulat et al., 2008). Based on these data, we suggest that NHEJ is unlikely to be a major mechanism of *CUP1* or rDNA amplification in *rtt109*Δ mutants.

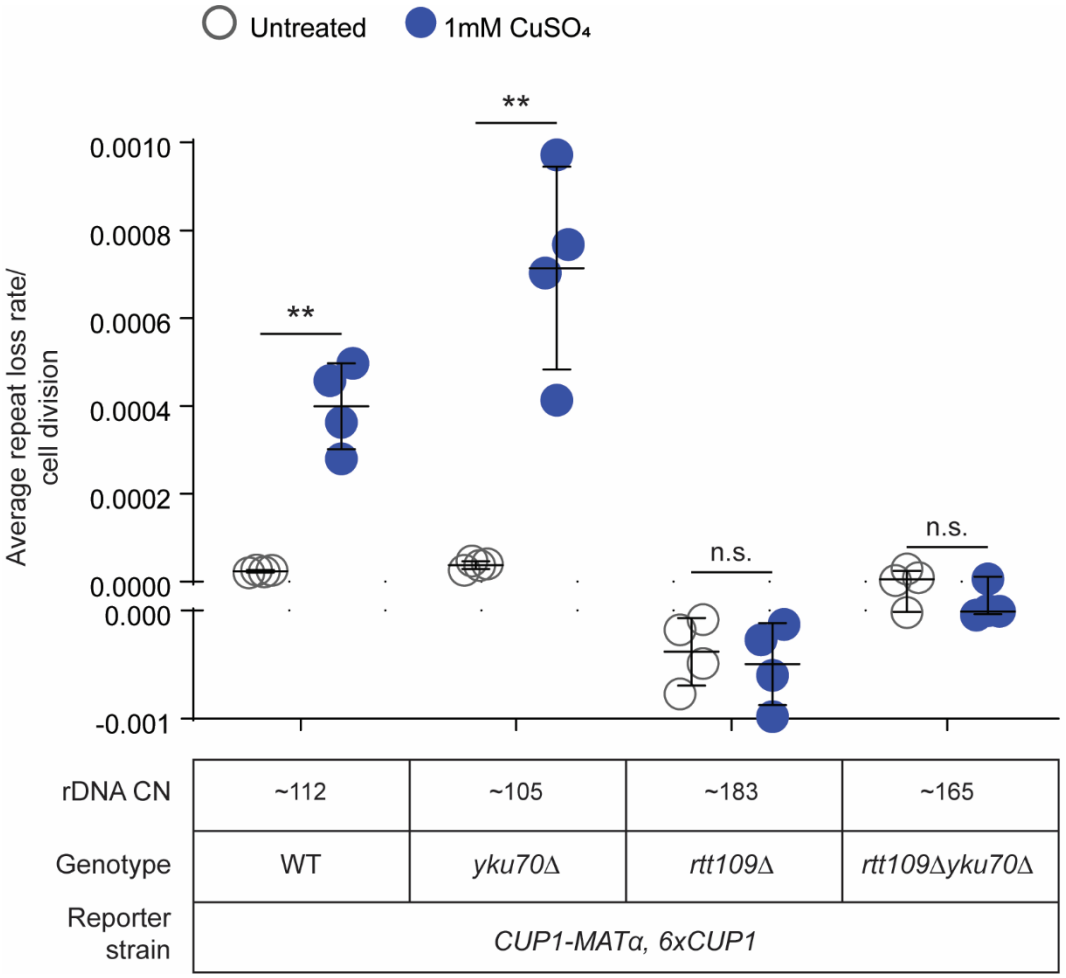

Figure 4.9. *CUP1* instability is not dependent on NHEJ. (A) Transcription-dependent and independent *CUP1* repeat loss rates in *yku70*Δ mutants in wild-type and *rtt109*Δ backgrounds. Error bars represent standard deviation based on 4 biological replicates. Statistical significance was calculated using a standard 2-tailed t-test. ** - p<0.01, n. s.– not significant. rDNA copy number in each mutant is also indicated.

Loss of Rad51 and Rad52, the key HR proteins, and Pol32, the DNA polymerase δ subunit required for efficient BIR, resulted in low transcription-dependent *CUP1* repeat loss rates in wild-type cells (Figure 4.10A). This suggests that HR and/or BIR are

important for the maintenance of the *CUP1* array as well as transcription-induced adaptive responses. However, deletion of these genes did not alter *CUP1* instability in the *rtt109*Δ mutant background (Figure 4.10A). Rad52 is one of the first proteins to be recruited to resected ends at the site of DNA damage, and is required for efficient Rad51-mediated recombination (Symington et al., 2014). Rad52 can also direct repair to DNA replication-dependent BIR, particularly in situations where canonical HR may not be favorable, for example, if high homology only exists on one side of the damage site, or if HR is otherwise suppressed (Symington et al., 2014). Both, hypo- and hyper-acetylation of H3K56 have been shown to suppress sister chromatid recombination (Munoz-Galvan et al., 2013). Further, hyper-acetylation of H3K56 has been shown to inhibit BIR (Che et al., 2015). Taken together with our *CUP1* instability measurements, this led us to predict that amplification of the *CUP1* and rDNA arrays may be dependent on Rad52, and Rad51 and/or Pol32 depending on whether the amplifications occurred via canonical HR and/or BIR.

To test this, we subcultured wild-type and *rtt109*Δ mutants, as well as *rad51*Δ, *rad52*Δ, and *pol32*Δ mutants in both strain backgrounds in high concentrations of copper. We also measured rDNA copy number in these mutant strains to infer common pathways that mediate rDNA and *CUP1* amplification in *rtt109*Δ mutants. We found that adaptation to high concentrations of copper required both, Rad51, and Rad52 in both, wild-type and *rtt109*Δ strains (Figure 4.10B). This suggests that transcription-induced *CUP1* amplification in requires both Rad51 and Rad52. Interestingly, the *rad51*Δ and *rtt109*Δ*rad51*Δ mutants also had rDNA copy number similar to wild-type strains, suggesting that the amplification of the rDNA array in *rtt109*Δ mutants may also be dependent on Rad51. Additionally, the *rad52*Δ and *rtt109*Δ*rad52*Δ mutants had amplified rDNA arrays, that were even larger than the array size in their corresponding parent strains (Figure 4.10A). Since Rad52 acts upstream of Rad51, these data, combined with the requirement of both, Rad52 and Rad51 for adaptation to copper,

suggest that amplification of both, rDNA and *CUP1* arrays is dependent on Rad52-dependent, Rad51-mediated recombination.

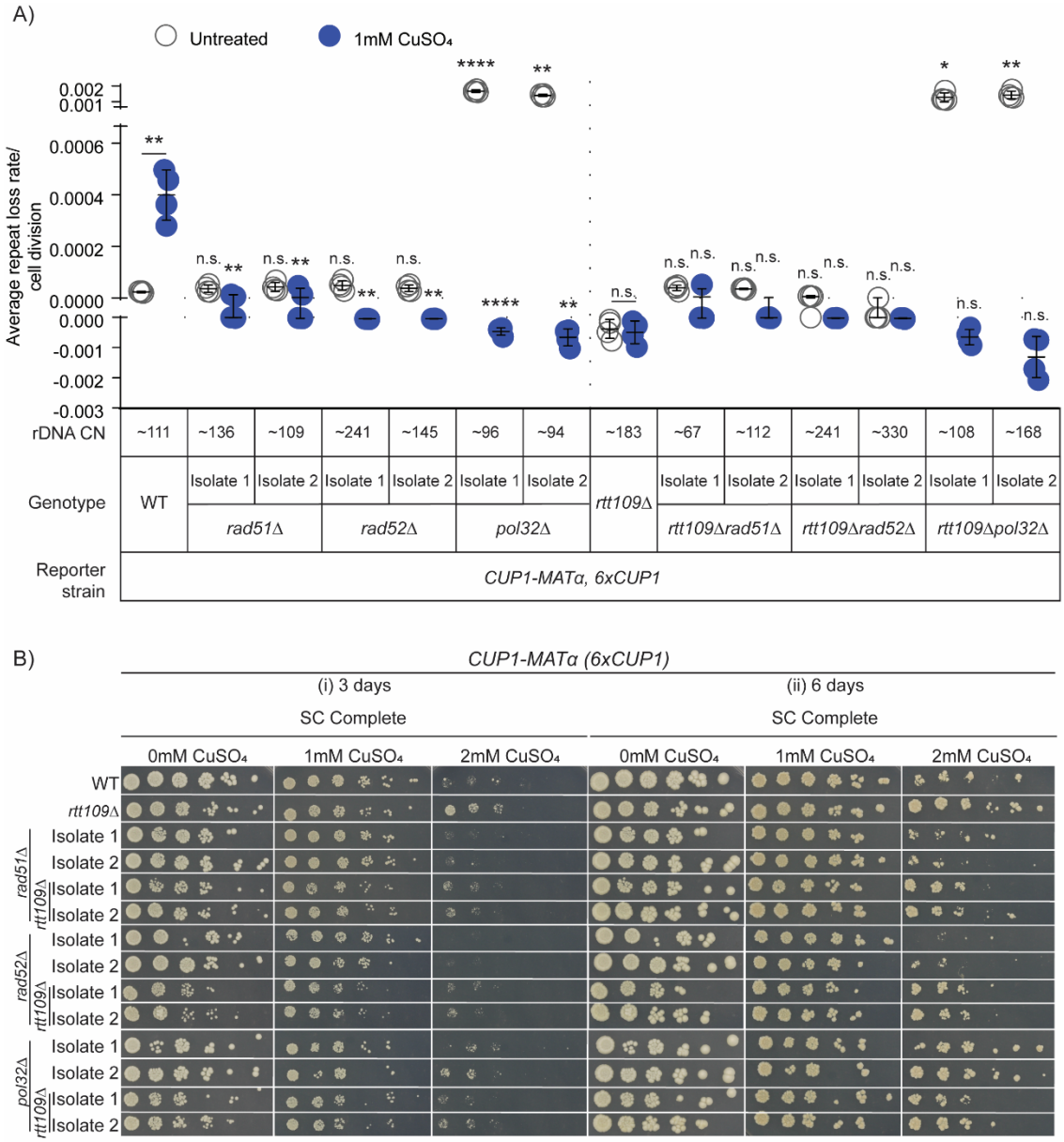

Figure 4.10. Transcription-induced *CUP1* instability and adaptation is dependent on homologous recombination. (A) Transcription-dependent and independent *CUP1* repeat loss rates in *rad51*Δ, *rad52*Δ, and *pol32*Δ mutants in wild-type and *rtt109*Δ backgrounds. Error bars represent standard deviation based on 4 biological replicates. Statistical significance was calculated using a standard 2-tailed t-test. * - p<0.05, ** - p<0.01, *** - p<0.001, **** - p<0.0001, n. s.– not significant. For statistical analysis, the *CUP1* repeat loss rate for each strain was compared to the repeat loss rate of the parent strain in the same growth condition, unless otherwise indicated. (B) Growth assays showing growth defects of *rad51*Δ and *rad52*Δ mutants in high concentrations of copper (2mM $CuSO_4$).

Despite having low transcription-dependent instability, both, *pol32*Δ and *rtt109*Δ*pol32*Δ mutants had no trouble adapting to high concentrations of copper. Interestingly, *pol32*Δ mutants had significantly high levels of transcription-independent *CUP1* instability in both, the wild-type and *rtt109*Δ mutant backgrounds (Figure 4.10A). *pol32*Δ mutants also had elevated rDNA instability (Figure 4.8A). These data suggest DNA replication stress in *pol32*Δ mutants can generate significant instability independent of transcription at both arrays. This is consistent with our model of repeat instability being inducible by transcription and replication stress (described in Chapters 1 and 3). Interestingly, rDNA copy number in the *pol32*Δ and *rtt109*Δ*pol32*Δ mutants also exhibited variability, with some isolates showing array sizes similar to, and lower than wild-type strains (Figures 4.8A, 4.10A). We speculate that amplification in the *rtt109*Δ*pol32*Δ strains may be countered by elevated rates of repeat loss at both, rDNA and *CUP1* arrays. Therefore, in *rtt109*Δ strains, efficient DNA replication in the presence of Rad52 and Pol32 could also result in the low repeat loss rates and net amplification observed at both, the rDNA and *CUP1* arrays.

Further, the effect of the *pol32*Δ mutation on stability at both arrays was identical to that of the *hst3*Δ*hst4*Δ deletion on the two arrays (Compare Figure 4.1A to Figure 4.8A and Figure 4.3A to Figure 4.10A). Hyper-acetylation of H3K56 in *hst3*Δ*hst4*Δ mutants has been previously shown to inhibit extensive DNA synthesis during DNA repair, which inhibits efficient replication fork progression during BIR (Che et al., 2015). Frequent fork stalling and inefficient DNA synthesis can induce instability at tandem repeats independent of transcription. Such a mechanism can result in elevated levels of both losses and gains of repeats. Transcriptional stress selects for cells with amplified arrays over time, however the high repeat loss rates would result in slower adaptation. The relatively smaller rDNA amplifications in *hst3*Δ*hst4*Δ mutants, and the lack of *CUP1* amplification in these mutants in non-selective conditions within 50 generations support this idea. We predict that transcription-induced *CUP1* amplification in *hst3*Δ*hst4*Δ mutants will require longer propagation, an idea we are currently testing. Further, Rad52

has been shown to be essential in *hst3*Δ*hst4*Δ mutants; Rad51 is not essential in these mutants, however in the absence of Rad51, Pol32 becomes essential in the *hst3*Δ*hst4*Δ*rad51*Δ mutants (Munoz-Galvan et al., 2013). Taken together with our findings of the requirement of Rad51 and Rad52 for the normal adaptive responses at the *CUP1* array in *rtt109*Δ mutants, we propose that disruption of the H3K56 acetylation pathway results in a bias towards homologous recombination at the locus, which produces atypical copy number variation and adaptation in response to transcription.

Altogether, our data suggests that Rad52-mediated recombination is required for adaptation to high concentrations of copper in both, wild-type and *rtt109*Δ strains. This suggests the dependence of *CUP1* amplification in response to transcriptional stress on homologous recombination. Moreover, rDNA amplification in *rtt109*Δ mutants is also dependent on Rad51 or Pol32 mediated repair. We speculate that the same pathways that are required for adaptation to high concentrations of copper will be involved in the transcription-induced *CUP1* amplification that we observed in *rtt109*Δ mutants in low concentrations of copper. To test this prediction, we also subcultured *rad51*Δ, *rad52*Δ, and *pol32*Δ mutants in both wild-type and *rtt109*Δ strain backgrounds in low concentrations of copper used in the experiments in Figure 4.10 for ~50 generations. Copy number measurements in the subcultured strains are ongoing. When complete, these data will extend our understanding of the pathways involved in mediating transcription-induced adaptive responses at the *CUP1* array. By measuring rDNA copy number in the same samples, we will also be able to infer pathways responsible for rDNA hyper-amplification in the *rtt109*Δ mutants. These experiments will characterize the contribution of H3K56 acetylation in regulating instability and recombination at tandem repeats to ensure prototypical adaptive responses to perturbed transcription.

4.6 Discussion

Eukaryotic genomes contain large stretches of tandem repeats. These repeats are repositories for copy number variation and can facilitate rapid adaptation to stress. Stress-induced adaptation through copy number variation could facilitate genome evolution in a variety of conditions like cancers, and treatment with anti-cancer drugs or antibiotics. This underscores the need to characterize the program of adaptation at tandem repeats. Here, we used two tandem arrays in budding yeast, the rDNA array and the *CUP1* gene array, to define the program of repeat stability and adaptation in response to transcriptional stress. We previously showed that replication and transcription are key factors involved in the rapid induction of instability and adaptation to stress through changes in repeat copy number. In this work we define the contributions of histone acetylation and recombination to the process of adaptation at tandem repeats.

Through studies using the *CUP1* array, we show that H3K56 acetylation a) regulates transcription, b) supports transcription-dependent repeat instability, and c) restricts transcription-induced repeat amplification. Importantly, we demonstrate that the responses to perturbation of H3K56 acetylation are dependent on the size of the array and its transcriptional status. While Hull et. al (2017) had proposed the importance of H3K56 acetylation in transcription-induced copy number variation, our studies provide experimental evidence for the role of this chromatin mark in governing transcription-induced instability at the *CUP1* array and subsequent adaptation to copper. Our findings also highlight the importance of the characterization of instability and distinguishing it from changes in steady state copy number upon prolonged propagation under transcriptional stress. Further, we show that adaptation is dependent on Rad52-mediated homologous recombination. Our studies suggest that loss of H3K56 acetylation may bias recombination events at the array toward amplification under transcriptional stress, which manifests as low repeat loss rates. Parallel measurements of repeat stability and copy number changes at the rDNA suggest that the rDNA hyper-

amplification phenotype in these mutants may also be due to constitutive, perturbed transcription and homologous recombination at the locus. Altogether, we have demonstrated that under conditions of transcriptional stress, H3K56 acetylation restricts amplification and homologous recombination promotes adaptation.

Our findings have profound impacts for understanding the general principles underlying the evolution of genomes under stress. It was shown several years ago that the TOR pathway regulates rDNA transcription by targeting the H3K56 acetylation pathway. Interestingly, in cells with low rDNA copy number, TOR induced rDNA transcription as well as canonical HR-independent rDNA amplification by inhibiting key H3K56 deacetylates (Chen et al., 2012; Jack et al., 2015). Our data show that the regulation of repeat stability and copy number by transcription and histone acetylation is not limited to recovery or maintenance of normal rDNA copy number. These regulatory principles are broadly applicable to understanding extra-ribosomal, adaptive rDNA copy number changes. Our studies of the *CUP1* array suggest that transcription and histone acetylation may govern the behavior of tandem repeats in general and dictate adaptive outcomes. These data also have implications for understanding the molecular evolution of diseases like cancer, which are characterized by global dysregulation of transcription and histone acetylation, and copy number amplifications (Audia & Campbell, 2016; Santarius et al., 2010). We speculate that altered transcription in the context of perturbed histone acetylation may underlie at least some of these amplifications. Further, because histone acetylation is often a target of anti-cancer drugs, understanding how acetylation impacts the stability and copy number of tandem arrays could be relevant to understanding how cancer cells adapt in response to therapy. Taken together, these data reveal the unifying principles that govern genome plasticity and adaptation.

4.7 Materials and Methods

4.7.1 Yeast strains and media

All yeast strains used are listed in Table 4.1. Strains were grown in non-selective SC complete medium (6.7g/L Yeast Nitrogen Base without amino acids + Ammonium Sulfate, 20g/L Dextrose, 2g/L synthetic complete (SC) supplement), or SD-dropout medium (6.7g/L Yeast Nitrogen Base without amino acids + Ammonium Sulfate, 20g/L Dextrose, 0.69g/L CSM-dropout supplement) lacking specific amino acids as indicated. Rich medium used was YPD (1% yeast extract, 2% peptone, 2% dextrose). Copper treated cells were grown in SC complete medium containing indicated concentrations of $CuSO_4$. Rich medium used was YPD (1% yeast extract, 2% peptone, 2% dextrose). For *CUP1-MATα cup2*Δ (+P_{GAL1}-*CUP1*) strains, selective medium used was SRaff-Leu-Ura (6.7g/L Yeast Nitrogen Base without amino acids + Ammonium Sulfate, 0.67g/L CSM-Leu-Ura supplement, 20g/L Raffinose), and non-selective medium used was SRaff+Gal-Ura (6.7g/L Yeast Nitrogen Base without amino acids + Ammonium Sulfate, 0.77g/L CSM-Ura supplement, 20g/L Raffinose, 20g/L Galactose) containing the indicated concentration of $CuSO_4$. All growth was at 30°C. Strain construction was carried out using standard yeast protocols. All strains were verified by replica-plating and PCR, followed by ddPCR to measure copy numbers of rDNA, *CUP1* as well as the *MATα-LEU2* repressor (Table 4.2). Instability reporter strains were also tested for GFP expression and repression by flow-cytometry. Primers used for strain construction and PCR verification are listed in Table 4.3.

4.7.2 ddPCR

Genomic DNA isolation, quantification, and ddPCR were carried out as previously described (Salim et al., 2017). ddPCR primers, probes and PCR conditions used are listed in Table 4.3.

4.7.3 Measurement of rDNA and *CUP1* repeat loss rates

rDNA and *CUP1* repeat loss rates were measured as described in Chapter 3.

4.7.4 H3 point mutants and plasmid shuffle

Plasmids containing *hht2(*K56A)-*HHF2*, *hht2(*K9A)-*HHF2*, *hht2*(K14A)-*HHF2*, and *HHT2-HHF2* (wild-type) were obtained from the SHIMA library (Nakanishi et al., 2008). Plasmids containing *hht2(*K56R)-*HHF2* and *hht2(*K56Q)-*HHF2* were generated by site-directed mutagenesis as described in (Nakanishi et al., 2008). Each of these plasmids also contain the *TRP1* selectable marker. Each plasmid was transformed into the *RDN25-MATα* (YBL574) reporter strain, and transformants selected by plating on SD-Leu-Trp medium. Cells were subjected to two rounds of selection on to SD-Leu-Trp+5-FOA to eliminate the plasmid containing wild-type *HHT2-HHF2* (*URA3*) to obtain the *RDN25-MATα* (YBL574) + *HHT2-HHF2* or H3K56A or H3K56R or H3K56Q or H3K9A or H3K14A strains. rDNA repeat loss rates in these strains were measured as described above. Selective medium used was SD-Leu-Trp, and non-selective medium used was SD-Trp.

4.7.5 *CUP1* mRNA measurements

Freshly revived *CUP1-MATα* reporter strains were grown overnight at 30°C in 5mL selective medium (SD-Leu). In the morning, 100µL of this overnight culture was diluted into 10mL of SC Complete or SC Complete containing 0.3mM (for 2×*CUP1* strain) or 1mM (for 6×*CUP1* and 17×*CUP1* strains) $CuSO_4$. These cultures were incubated at 30°C and allowed to grow to an OD_{600} of ~0.6-1.0. Cells were harvested, and pellets were flash frozen in liquid nitrogen and stored at −80°C until further use. RNA was isolated from frozen cell pellets using the hot acid phenol method. Briefly, the frozen cell pellet was resuspended in 800µL of cold AE Buffer (50 mM NaOAc (pH 5.2), 10 mM EDTA in RNase free water),

80µL of 10% SDS and 800µL acid phenol (pH 4.3) (Ambion #AM9720) and incubated at 65°C for 10 min. The cell suspension was incubated on ice for 5 min and centrifuged for 20 min at 14,000 rpm, 4°C. The supernatant was transferred to a fresh tube, mixed with 800µL of chloroform and centrifuged for 15 min at 14,000 rpm, 4°C. The chloroform extraction was repeated one more time. The supernatant was transferred to a fresh tube, and 10µg of linear acrylamide, 3M NaOAc, pH 5.2–5.6 ($1/10^{th}$ of total volume) and isopropanol (volume equal to total volume) were added and centrifuged for 20 min at 14,000 rpm, 4°C. The pellet was washed with 1mL 70% ethanol and resuspended in 100µL TE buffer (10 mM Tris (pH 8.0), 0.1 mM EDTA in RNase free water). The RNA was chilled on ice for 5min, then incubated for ~30s at 65°C. It was mixed by gentle vortexing and chilled on ice for 5min before storing at −80°C until further use.

Purity of each RNA sample was analyzed on a NanoDrop ND-1000 spectrophotometer. RNA integrity was analyzed using a 2100 Bioanalyzer (Agilent Technologies). After ensuring purity and integrity, RNA concentration was measured on a Qubit 2.0 Fluorometer using the Qubit RNA BR assay (Invitrogen). For each sample, 1µg total RNA was used to set up DNase treatment reactions (to remove genomic DNA contamination) followed by cDNA synthesis reactions using the iScript gDNA Clear cDNA Synthesis Kit (Bio-rad). All reactions were set up in triplicate. Additionally, a “no-RT control” reaction (identical in composition to the three cDNA synthesis reactions, but lacking reverse transcriptase) was also set up for each sample. Following DNase treatment and cDNA synthesis, the cDNA was serially diluted using RNase free water, and *CUP1* mRNA immediately measured using ddPCR.

ddPCR was performed as described previously (Salim et al., 2017), with some modifications. Primers and conditions used are listed in S2Table. 5µL serially diluted cDNA was used per 20µL reaction. ddPCR was performed according to the manufacturer’s protocol (Bio-Rad). Briefly, master mixes containing the

dsDNA binding dye EvaGreen, primers for *CUP1* or reference genes, cDNA, and the restriction endonuclease MseI (New England Biolabs, Inc.) were prepared and aliquoted into Eppendorf twin.tec plates. Reaction mixtures were incubated at room temperature for 15 minutes to allow restriction digestion of cDNA prior to droplet generation. Droplets were cycled to endpoint and subsequently read using the QX200 droplet reader. Quantification was performed using the Quantasoft software to obtain the absolute concentration of the target of interest (copies/µL). Expression of 8 reference genes (*TUB1*, *ACT1*, *CDC28*, *MUD1*, *SER2*, *SPT15*, *TRP1*, and *ZWF1)* was also measured in each sample, but not used for normalization of *CUP1* mRNA levels owing to changes in their expression in the presence of copper, and in mutant backgrounds. The strains tested carry an auxotrophic mutation in the *TRP1* gene, and do not express *TRP1*. Therefore, *TRP1* expression was used as a control. Average [*CUP1* mRNA] (copies/ng of total RNA) and standard deviation were calculated for each sample based on data from triplicate cDNA samples (at the same dilution) synthesized from the same RNA sample.

4.7.6 Subculturing experiments

All subculturing experiments were performed as previously described (Salim et al., 2017).

4.8 Supporting Information

Table 4.1. List of yeast strains used.

Strain ID	Name	Background	Relevant Genotype	References
DSY20.1	*MFA1-3xGFP*	S288C	*MATa ura3-52 his3-Δ200 trp1-1 leu2-3,112, MFA1-3xGFP-HIS5(Sp)*	RLY8491 from Zhu et al. (2015)
DSY48.7	*RDN25-MATα*	S288C	DSY20.1, *RDN25-MATα-LEU2*	Chapter 3
DSY99.12	*TUB1-MATα*	S288C	DSY20.1, *TUB1-MATα-LEU2*	Chapter 3
DSY131	*CUP1-MATα (2xCUP1)*	S288C	DSY20.1, *CUP1-MATα-LEU2, 2×CUP1*	Chapter 3
DSY132	*CUP1-MATα (12xCUP1)*	S288C	DSY20.1, *CUP1-MATα-LEU2, 12×CUP1*	Chapter 3
DSY134	*CUP1-MATα (17xCUP1)*	S288C	DSY20.1, *CUP1-MATα-LEU2, 17×CUP1*	Chapter 3
DSY135	*CUP1-MATα (6xCUP1)*	S288C	DSY20.1, *CUP1-MATα-LEU2, 6×CUP1*	Chapter 3
DSY143.1	*TUB1-MATα rtt109Δ*	S288C	DSY99.12, *rtt109Δ::KanMX*	This study
DSY90.1	*RDN25-MATα rtt109Δ*	S288C	DSY48.7, *rtt109Δ::KanMX*	This study
DSY93.1	*RDN25-MATα hst3Δhst4Δ*	S288C	DSY48.7, *hst3Δ::KanMX, hst4Δ::NatMX*	This study
DSY87	*YBL574*		*MATa, leu2Δ1, his3Δ200, ura3-52, trp1Δ63, lys2-128δ, (hht1-hhf1)ΔLEU2 (hht2-hhf2)Δ::HIS3 Ty912Δ35-lacZ::his4, {pDM9-HHT1-HHF1-URA3}*	Nakanishi et al., 2008
DSY137	*RDN25-MATα (YBL574)*	YBL574	DSY87, except *his4::HIS4, (hht1-hhf1)ΔNATMX (hht2-hhf2)Δ::KANMX, MFA1-3xGFP-HIS5(Sp), RDN25-MATα-LEU2*	This study
DSY138.1	*RDN25-MATα (YBL574) HHT2-HHF2*	YBL574	DSY137, plasmid shuffle with {p-*HHT2-HHF2-TRP1*}	This study. Plasmids from SHIMA library (Nakanishi et al., 2008).
DSY139.1	*RDN25-MATα (YBL574) H3K56A*	YBL574	DSY137, plasmid shuffle with {p-*hht2(K56A)-HHF2-TRP1*}	
DSY140.1	*RDN25-MATα (YBL574) H3K56R*	YBL574	DSY137, plasmid shuffle with {p-*hht2(K56R)-HHF2-TRP1*}	
DSY141.1	*RDN25-MATα (YBL574) H3K56Q*	YBL574	DSY137, plasmid shuffle with {p-*hht2(K56Q)-HHF2-TRP1*}	
DSY142.1	*RDN25-MATα (YBL574) H3K9A*	YBL574	DSY137, plasmid shuffle with {p-*hht2(K9A)-HHF2-TRP1*}	
	RDN25-MATα (YBL574) H3K14A	YBL574	DSY137, plasmid shuffle with {p-*hht2(K14A)-HHF2-TRP1*}	
DSY200.4	*RDN25-MATα asf1Δ*	S288C	DSY48.7, *asf1Δ::KANMX*	This study
DSY198	*RDN25-MATα vps75Δ*	S288C	DSY48.7, *vps75Δ::KANMX*	This study
DSY199.12	*RDN25-MATα pol32Δ*	S288C	DSY48.7, *pol32Δ::NATMX*	This study
DSY144	*2×CUP1 rtt109Δ*	S288C	DSY131, *rtt109Δ::KanMX*	This study
DSY191	*2×CUP1-MATα hst3Δhst4Δ*	S288C	DSY131, *hst3Δ::KanMX hst4Δ::NatMX*	This study
DSY163.1	*6×CUP1-MATα rtt109Δ*	S288C	DSY135, *rtt109Δ::KanMX*	This study
DSY192	*6×CUP1-MATα hst3Δhst4Δ*	S288C	DSY135, *hst3Δ::KanMX hst4Δ::NatMX*	This study
DSY154.1	*17×CUP1-MATα rtt109Δ*	S288C	DSY134, *rtt109Δ::KanMX*	This study
DSY208	*17×CUP1-MATα hst3Δhst4Δ*	S288C	DSY134, *hst3Δ::KanMX hst4Δ::NatMX*	This study
DSY145	*12×CUP1-MATα rtt109Δ*	S288C	DSY132, *rtt109Δ::KanMX*	This study
DSY187	*6×CUP1 rad51Δ*	S288C	DSY131, *rad51Δ::NatMX*	This study
DSY188	*6×CUP1 rad52Δ*	S288C	DSY131, *rad52Δ::KanMX*	This study
DSY189.18	*6×CUP1 yku70Δ*	S288C	DSY131, *yku70Δ::NatMX*	This study
DSY202	*6×CUP1 pol32Δ*	S288C	DSY131, *pol32Δ::NatMX*	This study
DSY190	*6×CUP1 rtt109Δrad51Δ*	S288C	DSY131, *rtt109Δ::KanMX rad51Δ::NatMX*	This study
DSY207	*6×CUP1 rtt109Δrad52Δ*	S288C	DSY131, *rtt109Δ::NatMX rad52Δ::KanMX*	This study
DSY209.36	*6×CUP1 rtt109Δyku70Δ*	S288C	DSY131, *rtt109Δ::KanMX yku70Δ::NatMX*	This study
DSY205	*6×CUP1 rtt109Δpol32Δ*	S288C	DSY131, *rtt109Δ::KanMX pol32Δ::NatMX*	This study
DSY193	*2×CUP1 asf1Δ*	S288C	DSY131, *asf1Δ::KanMX*	This study
DSY195.37	*2×CUP1 vps75Δ*	S288C	DSY131, *vps75Δ::KanMX*	This study
DSY194	*6×CUP1-MATα asf1Δ*	S288C	DSY135, *asf1Δ::KanMX*	This study
DSY196.43	*6×CUP1-MATα vps75Δ*	S288C	DSY135, *vps75Δ::KanMX*	This study

Table 4.2. Relevant rDNA, *CUP1* and *MATα-LEU2* copy number measurements in all reporter strains used.

Strain ID	Name	25S rDNA		*CUP1*		*LEU2-3*	
		CN	SD	CN	SD	CN	SD
DSY20.1	*MFA1-3xGFP*	117.30769	9.1836735	12.062937	0.6377551	1.0128205	0.0765306
DSY48.7	*RDN25-MATα*	114.52381	8.1632653	11.829268	0.6887755	2	0.130102
DSY99.12	*TUB1-MATα*	101.75355	5.6122449	11.225962	0.5102041	2.0448878	0.1147959
DSY131	*CUP1-MATα (2xCUP1)*	126.20968	7.3979592	1.9956616	0.1071429	2.0970874	0.1020408
DSY134	*CUP1-MATα (17xCUP1)*	122.5625	7.6530612	15.714286	0.9693878	2.0961538	0.0994898
DSY135	*CUP1-MATα (6xCUP1)*	111.09091	8.6734694	5.8974359	0.3571429	1.9084967	0.122449
DSY143.1	*TUB1-MATα rtt109Δ*	150.67385	8.1632653	10.707865	0.3571429	1.9253438	0.0586735
DSY90.1	*RDN25-MATα rtt109Δ*	170.56	14.540816			2.1181102	0.1352041
DSY93.1	*RDN25-MATα hst3Δhst4Δ*	178.02198	13.010204	9.4721408	0.5102041	2.1277372	0.1505102
DSY137	*RDN25-MATα (YBL574)*					2.0778443	0.1147959
DSY138.1	*RDN25-MATα (YBL574) HHT2-HHF2*	197.15302	12.755102	20.647619	0.9438776	2.1090047	0.1760204
DSY139.1	*RDN25-MATα (YBL574) H3K56A*	358.92857	35.714286	20.769231	0.5867347	2.0208333	0.1530612
DSY140.1	*RDN25-MATα (YBL574) H3K56R*	269.869	18.367347	22.067039	0.5867347	2.1472393	0.1964286
DSY141.1	*RDN25-MATα (YBL574) H3K56Q*	284.44444	19.387755	12.319277	0.3061224	1.7988506	0.1505102
DSY142.1	*RDN25-MATα (YBL574) H3K9A*	190.81081	18.112245	21.322314	1.8112245	2.05	0.2091837
DSY200.4	*RDN25-MATα asf1Δ*	121.76471	7.9081633	10.034247	0.5867347	2.322449	0.1581633
DSY198	*RDN25-MATα vps75Δ*	108.02395	6.6326531	10.823529	0.5612245	2.1190476	0.1173469
DSY199.12	*RDN25-MATα pol32Δ*	83.304721	5.3571429	10.021739	0.4591837	2.1990741	0.1147959
DSY144	*2×CUP1 rtt109Δ*	132.58929	8.4183673	2.0188679	0.1147959	2.0949721	0.127551
DSY191.2	*2×CUP1-MATα hst3Δhst4Δ*	174.79675	10.204082	1.7043702	0.0943878	1.8743169	0.1045918
DSY191.4		130.04484	7.3979592	1.8679868	0.119898	2.020339	0.130102
DSY163.1	*6×CUP1-MATα rtt109Δ*	182.6087	12.755102	5.8715596	0.3316327	2.1321839	0.127551
DSY192.9	*6×CUP1-MATα hst3Δhst4Δ*	143.5	8.4183673	5.4571429	0.2806122	2.0636943	0.1403061
DSY192.10		163	10.969388	6.5437788	0.4846939	2.1358025	0.1454082
DSY154.1	*17×CUP1-MATα rtt109Δ*	158.49315	10.204082	19.848485	1.3520408	2.0935484	0.1173469
DSY208.1	*17×CUP1-MATα hst3Δhst4Δ*	128.62595	8.1632653	14.463895	0.6377551	1.827957	0.1020408
DSY208.5		119.45701	8.4183673	14.789082	0.7142857	1.7422434	0.1045918
DSY187.1	*6×CUP1 rad51Δ*	135.7764	9.1836735	6.4795918	0.3826531	1.9746835	0.1122449
DSY187.2		108.78788	6.377551	6.4171123	0.3061224	2.0197044	0.1122449
DSY188.10	*6×CUP1 rad52Δ*	241.17647	15.816327	5.8928571	0.3571429	2.125	0.1403061
DSY188.11		145.50265	8.6734694	5.7894737	0.3061224	2.1847134	0.125
DSY189.18	*6×CUP1 yku70Δ*	104.68571	6.6326531	6.1904762	0.3316327	1.9120235	0.1122449
DSY202.18	*6×CUP1 pol32Δ*	96.029412	6.122449	5.3009259	0.25	2.0481928	0.1096939
DSY202.20		93.703704	5.8673469	6.0054348	0.3061224	2	0.1020408
DSY190.28	*6×CUP1 rtt109Δrad51Δ*	66.797386	4.5918367	5.3963415	0.3061224	1.825	0.1147959
DSY190.33		111.88525	6.122449	6.1744966	0.3061224	1.965812	0.0943878
DSY207.2	*6×CUP1 rtt109Δrad52Δ*	240.90909	21.428571	6.0218978	0.3826531	2.1254753	0.1428571
DSY207.3		328.35821	25.510204	5.220339	0.3316327	2	0.122449
DSY193	*2×CUP1 asf1Δ*	120.2454	7.3979592	2.3367003	0.1428571	2.2168285	0.1326531
DSY195.37	*2×CUP1 vps75Δ*	108.17121	6.122449	1.9365854	0.0994898	1.9730942	0.0994898
DSY194	*6×CUP1-MATα asf1Δ*	114.48864	6.8877551	6.1988304	0.3061224	1.9859944	0.1045918
DSY196.43	*6×CUP1-MATα vps75Δ*	119.81818	7.1428571	6.0703812	0.3061224	2.1117647	0.1173469
DSY209.36	*6×CUP1 rtt109Δyku70Δ*	164.23841	11.989796	5.9861592	0.3316327	2.1182432	0.125
DSY205.37	*6×CUP1 rtt109Δpol32Δ*	107.17131	6.122449	5.9765625	0.3571429	2.1333333	0.1326531
DSY205.38		168.62319	11.734694	5.8666667	0.3571429	2.0137615	0.1326531

Table 4.3. List of primers used.

ddPCR assays for copy number measurements

	Gene	Forward primer	Reverse Primer	Probe	Restriction enzyme	Tm (°C)	gDNA (ng/20uL rxn)
1	*TUB1*	5'-CCAGTCTTATCCAAATCAAAGG-3'	5'-GGATCACACTTGACCATCT-3'	5'-/56FAM/TCCATGAGT/ZEN/CCAACTCTGTGTCA/3IABkFQ/-3'	*Eco* RI or *Mse* I	57	≥0.005
2	*RDN25*	5'-TACCTTCGGTGCCCGAGTTGTAAT-3'	5'-ACCCTCTATGACGTCCTGTTCCAA-3'	5'-/5HEX/AACATAGACAAGGAACGGCCC/3BHQ_1/-3'	*Eco* RI	57	0.005
3	*CUP1-1*	5'-GAAGGTCATGAGTGCCAATG-3'	5'-GCATTTGTCGTCGCTGTT-3'	5'-/5HEX/AAATCATGTAGCTGCCCAACGG/3BHQ_1/-3'	*Mse* I	57	0.005
4	*MATALPHA2*	5'-CGCTAATTCTGGAGCGATTG-3'	5'-GCAAAGAACATCGAGAACCC-3'	5'-/5HEX/TCATTAGATTCTCTAGGCCCTTGGT/3BHQ_1/-3'	*Mse* I	57	0.01
5	*MATALPHA1*	5'-CAGTTTGGCTCCGGTGTAA-3'	5'-GCGCGAAGTAGTCCCATATT-3'	5'-/5HEX/AATGTCTTGTCTTCTCTGCTCGC/3BHQ_1/-3'	*Mse* I	57	0.01
6	*leu2-3,112*	5'-GACAAGAACACCGCATTTGG-3'	5'-CAGACAAGATAGTGGCGATAGG-3'	5'-/5HEX/CCACGGTTCTGCTCCAGATTT/3BHQ_1/-3'	*Mse* I	57	0.01

Primers used for RT-ddPCR

	Gene	Forward primer	Reverse Primer	Assay	Restriction enzyme	Tm (°C)	cDNA (RNA equivalent, ng/20uL rxn)
1	*CUP1-1*	5'-GAAGGTCATGAGTGCCAATG-3'	5'-GCATTTGTCGTCGCTGTT-3'	EvaGreen	*Mse* I	57	0.0005-0.5
2	*TUB1*	5'-CCAGTCTTATCCAAATCAAAGG-3'	5'-GGATCACACTTGACCATCT-3'	EvaGreen	*Mse* I	57	0.5
3	*ACT1*	5'-TCGTTCCAATTTACGCTGGTT-3'	5'-CGGCCAAATCGATTCTCAA-3'	EvaGreen	*Mse* I	57	0.5
4	*CDC28*	5'-GATACATGGTCCATCGGCTGTA-3'	5'-CCACTGAAGATTGGTTTCCTGTT-3'	EvaGreen	*Mse* I	57	0.5
5	*MUD1*	5'-AAATTTGCCAAGCGGCACTA-3'	5'-CAACTAAAGCCTCATTGCCAAGT-3'	EvaGreen	*Mse* I	57	0.5
6	*SER2*	5'-CCAAGAGGTCATCGAATTGATTG-3'	5'-CTGTGATCTCGTGCACTTGTTCT-3'	EvaGreen	*Mse* I	57	0.5
7	*SPT15*	5'-TGCGCTACATGCCCGTAA-3'	5'-CGCATGATGACAGCAGCAA-3'	EvaGreen	*Mse* I	57	0.5
8	*TRP1*	5'-CGGCTTGCAGAGCACAGA-3'	5'-AGCAAGTCAGCATCGGAATCTAG-3'	EvaGreen	*Mse* I	57	0.5
9	*ZWF1*	5'-TCGTGTGTACGCAGAGAATGG-3'	5'-TCGTGGCCGAAAGGTTTC-3'	EvaGreen	*Mse* I	57	0.5

4.9 Acknowledgements

We would like to thank Jerry Workman for the YBL574 strain. We are also grateful to the Molecular biology core facility (Stowers Institute) for construction of H3K56 point mutants and for access to the TECAN plate reader. This work was done to fulfill, in part, requirements for DS's PhD thesis research as a student registered with the Open University.

4.10 References

Albert, B., Leger-Silvestre, I., Normand, C., Ostermaier, M. K., Perez-Fernandez, J., Panov, K. I., . . . Gadal, O. (2011). RNA polymerase I-specific subunits promote polymerase clustering to enhance the rRNA gene transcription cycle. *J Cell Biol, 192*(2), 277-293. doi:10.1083/jcb.201006040

Aparicio, J. G., Viggiani, C. J., Gibson, D. G., & Aparicio, O. M. (2004). The Rpd3-Sin3 histone deacetylase regulates replication timing and enables intra-S origin control in Saccharomyces cerevisiae. *Mol Cell Biol, 24*(11), 4769-4780. doi:10.1128/MCB.24.11.4769-4780.2004

Audia, J. E., & Campbell, R. M. (2016). Histone Modifications and Cancer. *Cold Spring Harb Perspect Biol, 8*(4), a019521. doi:10.1101/cshperspect.a019521

Casas-Delucchi, C. S., van Bemmel, J. G., Haase, S., Herce, H. D., Nowak, D., Meilinger, D., . . . Cardoso, M. C. (2012). Histone hypoacetylation is required to maintain late replication timing of constitutive heterochromatin. *Nucleic Acids Res, 40*(1), 159-169. doi:10.1093/nar/gkr723

Celic, I., Masumoto, H., Griffith, W. P., Meluh, P., Cotter, R. J., Boeke, J. D., & Verreault, A. (2006). The sirtuins hst3 and Hst4p preserve genome integrity by controlling histone h3 lysine 56 deacetylation. *Curr Biol, 16*(13), 1280-1289. doi:10.1016/j.cub.2006.06.023

Cesarini, E., D'Alfonso, A., & Camilloni, G. (2012). H4K16 acetylation affects recombination and ncRNA transcription at rDNA in Saccharomyces cerevisiae. *Mol Biol Cell, 23*(14), 2770-2781. doi:10.1091/mbc.E12-02-0095

Che, J., Smith, S., Kim, Y. J., Shim, E. Y., Myung, K., & Lee, S. E. (2015). Hyper-Acetylation of Histone H3K56 Limits Break-Induced Replication by Inhibiting Extensive Repair Synthesis. *PLoS Genet, 11*(2), e1004990. doi:10.1371/journal.pgen.1004990

Chen, H., Fan, M., Pfeffer, L. M., & Laribee, R. N. (2012). The histone H3 lysine 56 acetylation pathway is regulated by target of rapamycin (TOR) signaling and functions directly in ribosomal RNA biogenesis. *Nucleic Acids Res, 40*(14), 6534-6546. doi:10.1093/nar/gks345

D'Alfonso, A., Di Felice, F., Carlini, V., Wright, C. M., Hertz, M. I., Bjornsti, M. A., & Camilloni, G. (2016). Molecular Mechanism of DNA Topoisomerase I-Dependent rDNA Silencing: Sir2p Recruitment at Ribosomal Genes. *J Mol Biol, 428*(24 Pt B), 4905-4916. doi:10.1016/j.jmb.2016.10.032

Fillingham, J., Recht, J., Silva, A. C., Suter, B., Emili, A., Stagljar, I., . . . Greenblatt, J. F. (2008). Chaperone control of the activity and specificity of the histone H3 acetyltransferase Rtt109. *Mol Cell Biol, 28*(13), 4342-4353. doi:10.1128/MCB.00182-08

French, S. L., Osheim, Y. N., Cioci, F., Nomura, M., & Beyer, A. L. (2003). In exponentially growing Saccharomyces cerevisiae cells, rRNA synthesis is determined by the summed RNA polymerase I loading rate rather than by the number of active genes. *Mol Cell Biol, 23*(5), 1558-1568. doi:10.1128/mcb.23.5.1558-1568.2003

Gottlieb, S., & Esposito, R. E. (1989). A new role for a yeast transcriptional silencer gene, SIR2, in regulation of recombination in ribosomal DNA. *Cell, 56*(5), 771-776. doi:10.1016/0092-8674(89)90681-8

Hachinohe, M., Hanaoka, F., & Masumoto, H. (2011). Hst3 and Hst4 histone deacetylases regulate replicative lifespan by preventing genome instability in Saccharomyces cerevisiae. *Genes Cells, 16*(4), 467-477. doi:10.1111/j.1365-2443.2011.01493.x

Han, J., Zhou, H., Horazdovsky, B., Zhang, K., Xu, R. M., & Zhang, Z. (2007a). Rtt109 acetylates histone H3 lysine 56 and functions in DNA replication. *Science, 315*(5812), 653-655. doi:10.1126/science.1133234

Han, J., Zhou, H., Li, Z., Xu, R. M., & Zhang, Z. (2007b). Acetylation of lysine 56 of histone H3 catalyzed by RTT109 and regulated by ASF1 is required for replisome integrity. *J Biol Chem, 282*(39), 28587-28596. doi:10.1074/jbc.M702496200

Han, J., Zhou, H., Li, Z., Xu, R. M., & Zhang, Z. (2007c). The Rtt109-Vps75 histone acetyltransferase complex acetylates non-nucleosomal histone H3. *J Biol Chem, 282*(19), 14158-14164. doi:10.1074/jbc.M700611200

Houseley, J., & Tollervey, D. (2011). Repeat expansion in the budding yeast ribosomal DNA can occur independently of the canonical homologous recombination machinery. *Nucleic Acids Res, 39*(20), 8778-8791. doi:10.1093/nar/gkr589

Hull, R. M., Cruz, C., Jack, C. V., & Houseley, J. (2017). Environmental change drives accelerated adaptation through stimulated copy number variation. *PLoS Biol, 15*(6), e2001333. doi:10.1371/journal.pbio.2001333

Iafrate, A. J., Feuk, L., Rivera, M. N., Listewnik, M. L., Donahoe, P. K., Qi, Y., . . . Lee, C. (2004). Detection of large-scale variation in the human genome. *Nat Genet, 36*(9), 949-951. doi:10.1038/ng1416

Ide, S., Miyazaki, T., Maki, H., & Kobayashi, T. (2010). Abundance of ribosomal RNA gene copies maintains genome integrity. *Science, 327*(5966), 693-696. doi:10.1126/science.1179044

Ide, S., Saka, K., & Kobayashi, T. (2013). Rtt109 Prevents Hyper-Amplification of Ribosomal RNA Genes through Histone Modification in Budding Yeast. *PLoS Genet, 9*(4). doi:10.1371/journal.pgen.1003410.g001

Ide, S., Watanabe, K., Watanabe, H., Shirahige, K., Kobayashi, T., & Maki, H. (2007). Abnormality in initiation program of DNA replication is monitored by the highly repetitive rRNA gene array on chromosome XII in budding yeast. *Mol Cell Biol, 27*(2), 568-578. doi:10.1128/MCB.00731-06

Jack, C. V., Cruz, C., Hull, R. M., Keller, M. A., Ralser, M., & Houseley, J. (2015). Regulation of ribosomal DNA amplification by the TOR pathway. *Proc Natl Acad Sci U S A, 112*(31), 9674-9679. doi:10.1073/pnas.1505015112

Jessulat, M., Alamgir, M., Salsali, H., Greenblatt, J., Xu, J., & Golshani, A. (2008). Interacting proteins Rtt109 and Vps75 affect the efficiency of non-homologous end-joining in Saccharomyces cerevisiae. *Arch Biochem Biophys, 469*(2), 157-164. doi:10.1016/j.abb.2007.11.001

Kadyrova, L. Y., Mertz, T. M., Zhang, Y., Northam, M. R., Sheng, Z., Lobachev, K. S., . . . Kadyrov, F. A. (2013). A reversible histone H3 acetylation cooperates with mismatch repair and replicative polymerases in maintaining genome stability. *PLoS Genet, 9*(10), e1003899. doi:10.1371/journal.pgen.1003899

Kobayashi, T., Heck, D. J., Nomura, M., & Horiuchi, T. (1998). Expansion and contraction of ribosomal DNA repeats in *Saccharomyces cerevisiae*: requirement of replication fork blocking (Fob1) protein and the role of RNA polymerase I. *Genes Dev, 12*(24), 3821-3830. doi:10.1101/gad.12.24.3821

Kwan, E. X., Foss, E. J., Tsuchiyama, S., Alvino, G. M., Kruglyak, L., Kaeberlein, M., . . . Bedalov, A. (2013). A natural polymorphism in rDNA replication origins links origin activation with calorie restriction and lifespan. *PLoS Genet, 9*(3), e1003329. doi:10.1371/journal.pgen.1003329

Luciano, P., Dehé, P., Audebert, S., Géli, V., Corda, Y. (2015). Replisome Function During Replicative Stress Is Modulated by Histone H3 Lysine 56 Acetylation Through Ctf4. *Genetics*. doi:10.1534/genetics.114.173856/-/DC1

Maas, N. L., Miller, K. M., DeFazio, L. G., & Toczyski, D. P. (2006). Cell cycle and checkpoint regulation of histone H3 K56 acetylation by Hst3 and Hst4. *Mol Cell, 23*(1), 109-119. doi:10.1016/j.molcel.2006.06.006

Moller, H. D., Parsons, L., Jorgensen, T. S., Botstein, D., & Regenberg, B. (2015). Extrachromosomal circular DNA is common in yeast. *Proc Natl Acad Sci U S A, 112*(24), E3114-3122. doi:10.1073/pnas.1508825112

Munoz-Galvan, S., Jimeno, S., Rothstein, R., & Aguilera, A. (2013). Histone H3K56 acetylation, Rad52, and non-DNA repair factors control double-strand break repair choice with the sister chromatid. *PLoS Genet, 9*(1), e1003237. doi:10.1371/journal.pgen.1003237

Nakanishi, S., Sanderson, B. W., Delventhal, K. M., Bradford, W. D., Staehling-Hampton, K., & Shilatifard, A. (2008). A comprehensive library of histone mutants identifies nucleosomal residues required for H3K4 methylation. *Nat Struct Mol Biol, 15*(8), 881-888. doi:10.1038/nsmb.1454

Oakes, M., Nogi, Y., Clark, M. W., & Nomura, M. (1993). Structural alterations of the nucleolus in mutants of Saccharomyces cerevisiae defective in RNA polymerase I. *Mol Cell Biol, 13*(4), 2441-2455. doi:10.1128/mcb.13.4.2441

Oakes, M., Siddiqi, I., Vu, L., Aris, J., & Nomura, M. (1999). Transcription factor UAF, expansion and contraction of ribosomal DNA (rDNA) repeats, and RNA polymerase switch in transcription of yeast rDNA. *Mol Cell Biol, 19*(12), 8559-8569. doi:10.1128/mcb.19.12.8559

Peter, J., De Chiara, M., Friedrich, A., Yue, J. X., Pflieger, D., Bergstrom, A., . . . Schacherer, J. (2018). Genome evolution across 1,011 Saccharomyces cerevisiae isolates. *Nature, 556*(7701), 339-344. doi:10.1038/s41586-018-0030-5

Redon, R., Ishikawa, S., Fitch, K. R., Feuk, L., Perry, G. H., Andrews, T. D., . . . Hurles, M. E. (2006). Global variation in copy number in the human genome. *Nature, 444*(7118), 444-454. doi:10.1038/nature05329

Saka, K., Takahashi, A., Sasaki, M., & Kobayashi, T. (2016). More than 10% of yeast genes are related to genome stability and influence cellular senescence via rDNA maintenance. *Nucleic Acids Res, 44*(9), 4211-4221. doi:10.1093/nar/gkw110

Salim, D., Bradford, W. D., Freeland, A., Cady, G., Wang, J., Pruitt, S. C., & Gerton, J. L. (2017). DNA replication stress restricts ribosomal DNA copy number. *PLoS Genet, 13*(9), e1007006. doi:10.1371/journal.pgen.1007006

Santarius, T., Shipley, J., Brewer, D., Stratton, M. R., & Cooper, C. S. (2010). A census of amplified and overexpressed human cancer genes. *Nat Rev Cancer, 10*(1), 59-64. doi:10.1038/nrc2771

Sebat, J., Lakshmi, B., Troge, J., Alexander, J., Young, J., Lundin, P., . . . Wigler, M. (2004). Large-scale copy number polymorphism in the human genome. *Science, 305*(5683), 525-528. doi:10.1126/science.1098918

Selth, L., & Svejstrup, J. Q. (2007). Vps75, a new yeast member of the NAP histone chaperone family. *J Biol Chem, 282*(17), 12358-12362. doi:10.1074/jbc.C700012200

Shyian, M., Mattarocci, S., Albert, B., Hafner, L., Lezaja, A., Costanzo, M., . . . Shore, D. (2016). Budding Yeast Rif1 Controls Genome Integrity by Inhibiting rDNA Replication. *PLoS Genet, 12*(11), e1006414. doi:10.1371/journal.pgen.1006414

Simoneau, A., Ricard, E., Weber, S., Hammond-Martel, I., Wong, L. H., Sellam, A., . . . Wurtele, H. (2016). Chromosome-wide histone deacetylation by sirtuins prevents hyperactivation of DNA damage-induced signaling upon replicative stress. *Nucleic Acids Res, 44*(6), 2706-2726. doi:10.1093/nar/gkv1537

Smith, J. S., Caputo, E., & Boeke, J. D. (1999). A genetic screen for ribosomal DNA silencing defects identifies multiple DNA replication and chromatin-modulating factors. *Mol Cell Biol, 19*(4), 3184-3197. doi:10.1128/mcb.19.4.3184

Steenwyk, J. L., & Rokas, A. (2018). Copy Number Variation in Fungi and Its Implications for Wine Yeast Genetic Diversity and Adaptation. *Front Microbiol, 9*, 288. doi:10.3389/fmicb.2018.00288

Symington, L. S., Rothstein, R., & Lisby, M. (2014). Mechanisms and regulation of mitotic recombination in Saccharomyces cerevisiae. *Genetics, 198*(3), 795-835. doi:10.1534/genetics.114.166140

Unnikrishnan, A., Gafken, P. R., & Tsukiyama, T. (2010). Dynamic changes in histone acetylation regulate origins of DNA replication. *Nat Struct Mol Biol, 17*(4), 430-437. doi:10.1038/nsmb.1780

Varv, S., Kristjuhan, K., Peil, K., Looke, M., Mahlakoiv, T., Paapsi, K., & Kristjuhan, A. (2010). Acetylation of H3 K56 is required for RNA polymerase II transcript elongation through heterochromatin in yeast. *Mol Cell Biol, 30*(6), 1467-1477. doi:10.1128/MCB.01151-09

Vogelauer, M., Rubbi, L., Lucas, I., Brewer, B. J., & Grunstein, M. (2002). Histone acetylation regulates the time of replication origin firing. *Mol Cell, 10*(5), 1223-1233. doi:10.1016/s1097-2765(02)00702-5

Xu, F., Zhang, Q., Zhang, K., Xie, W., & Grunstein, M. (2007). Sir2 deacetylates histone H3 lysine 56 to regulate telomeric heterochromatin structure in yeast. *Mol Cell, 27*(6), 890-900. doi:10.1016/j.molcel.2007.07.021

Xu, H. H., Su, T., & Xue, Y. (2016). Histone H3 N-terminal acetylation sites especially K14 are important for rDNA silencing and aging. *Sci Rep, 6*, 21900. doi:10.1038/srep21900

Yang, B., Miller, A., & Kirchmaier, A. L. (2008). HST3/HST4-dependent deacetylation of lysine 56 of histone H3 in silent chromatin. *Mol Biol Cell, 19*(11), 4993-5005. doi:10.1091/mbc.E08-05-0524

Yoshida, K., Bacal, J., Desmarais, D., Padioleau, I., Tsaponina, O., Chabes, A., . . . Pasero, P. (2014). The histone deacetylases sir2 and rpd3 act on ribosomal DNA to control the replication program in budding yeast. *Mol Cell, 54*(4), 691-697. doi:10.1016/j.molcel.2014.04.032

Zarrei, M., MacDonald, J. R., Merico, D., & Scherer, S. W. (2015). A copy number variation map of the human genome. *Nat Rev Genet, 16*(3), 172-183. doi:10.1038/nrg3871

CHAPTER 5

Discussion

Some sections of this chapter are excerpts from Salim, D., & Gerton, J. L. (2019). Ribosomal DNA instability and genome adaptability. *Chromosome Res, 27*(1-2), 73-87. doi:10.1007/s10577-018-9599-7

5 CHAPTER 5

5.1 List of Figures

5.2 Key conclusions

Copy number variations at tandem repeats have emerged as the most significant source of phenotypic diversity in natural populations. Despite their potential to have profound impacts on cellular and organismal adaptation, they have remained the most understudied class of mutations. This is because a) they are missing from genome assemblies owing to their repetitive nature, b) the lack of distinction between instability and changes in steady state copy number has resulted in many seemingly paradoxical findings, and c) existing assays to measure repeat stability and copy number lack the sensitivity and quantitative power to identify subtle changes that may be more relevant for adaptation.

My thesis work focused on the identification and characterization of basic principles that regulate copy number variation at tandem repeats in the budding yeast, *Saccharomyces cerevisiae*. I developed sensitive assays that enabled rapid quantification of instability and copy number of tandem repeats. I used these assays to characterize the regulation of copy number variation at two well-studied tandem arrays in the yeast genome, the ribosomal DNA (rDNA) array, and the copper-resistance *CUP1* gene array. In this chapter, I briefly summarize the main findings from my work on tandem repeats in budding yeast, and discuss some key outstanding questions. Finally, I also speculate about the broad relevance and implications of my work in understanding the behavior of other tandem repeats and their contributions to genome plasticity and the molecular evolution of cancer. Some sections of this chapter are excerpts from (Salim & Gerton, 2019).

5.2.1 rDNA copy number variation facilitates adaptation

The tandem array of rDNA repeats in budding yeast has served as a model to study the behavior of tandem repeats for decades. rDNA genes encode the essential RNA components of ribosomes. Despite its critical role in cell viability, the rDNA array is the

most unstable, and hypervariable locus in the yeast genome. It is the most highly transcribed genomic locus, and comprises over 60% of chromosome XII, and ~10% of the yeast genome. Therefore, rDNA stability has the potential to significantly impact genome stability and function. Further, the ability of the rDNA locus to accommodate extensive copy number variation with little to no effect on ribosome biogenesis supports the idea that the functions of the rDNA go well beyond rRNA biogenesis. A dynamic locus that can bind factors involved in DNA replication, recombination, and transcription could produce a wide range of cellular responses by titrating key chromatin modifying factors. Therefore, the rDNA array has the potential to act as the “canary in the coalmine”, being particularly sensitive to stresses that disrupt genome integrity, and acting as a source of cellular adaptation, relatively simply, through variation in array size.

While several factors that affect rDNA copy number had been previously identified, the determination of “normal” rDNA copy number remained unclear. Through a screen of a yeast conditional temperature-sensitive mutant collection of essential genes, I found that low rDNA copy number was associated with compromised DNA replication (Chapter 2, (Salim et al., 2017)). Through serial subculturing experiments, I showed that sustained replication stress causes a contraction of the rDNA array (Chapter 2, (Salim et al., 2017)). Interestingly, under conditions of DNA replication stress, cells with a smaller rDNA array were able to complete DNA replication in a timely manner and continue to propagate (Chapter 2, (Salim et al., 2017)). Therefore, while extra, untranscribed rDNA repeats are essential for allowing co-transcriptional DNA damage repair (Ide et al., 2010), they become detrimental to cells under conditions of DNA replication stress. Work from Foss et al. (2017) provided evidence for the long standing idea that, in yeast, repetitive rDNA compete for origin firing with unique genomic sequences (in yeast, the rest of the genome), and tipping the balance in favor of the rDNA can lead to underreplicated regions throughout the rest of the genome. Importantly, these replication gaps could be suppressed by decreased origin activity within the rDNA (Foss et al., 2017). These data, taken together with my data, suggest

that the rDNA array may be particularly sensitive to DNA replication stresses. Additionally, while DNA damage repair could result in a gain or loss of repeats, the loss of rDNA repeats facilitates adaptation to DNA replication stress, likely by liberating scarce replication factors for use by the rest of the genome. Finally, the loss of 45S rDNA repeats in thymic tumors derived from mice with reduced expression of the MCM2 subunit of the MCM2-7 DNA replicative helicase also suggests that past replication stress may be diagnosed by a contracted rDNA array (Chapter 2, (Salim et al., 2017)). Taken together, these results provide insight into the role of the rDNA locus in acting as a sensor and source of rapid, reversible adaption to general genomic stress through a plastic array size determined by selective cues from the environment.

5.2.2 DNA Replication and transcription modulate copy number variation

The extensive copy number variation at tandem repeats including the rDNA was thought to be the inevitable consequence of the inherent instability at these repeats. However, despite high recombination-mediated repeat loss, normal rDNA copy number is stably maintained under laboratory growth conditions. Therefore, early studies were focused on characterizing the mechanisms involved in recovery of rDNA copy number to wild-type levels following repeat loss. Additionally, while several factors that altered rDNA stability and/or copy number were identified, mechanisms underlying many of these changes remained elusive because of the lack of correlation between changes in stability and copy number. I performed multiple high-throughput genetic screens to identify pathways that regulate rDNA stability and copy number with the aim of distinguishing between changes in rDNA stability and copy number. These screens revealed that rDNA copy number and stability are regulated by the fundamental processes of DNA replication, transcription, and histone acetylation (Chapter 3).

Based on data from my screens, seminal work in bacteria showing that replication-transcription conflicts could promote mutagenesis (Lang & Merrikh, 2018),

and the demonstrated role of transcription in promoting copy number variation at the *CUP1* array (Hull et al., 2017), I hypothesized that instability at tandem repeats could be modulated by replication and transcription at the locus. Conflicts between the DNA replication machinery and transcription machinery operating on the same DNA template occur frequently genome-wide and result in stalled or collapsed DNA replication forks. Collapsed replication forks are processed into double-stranded breaks, which are repaired by one of many recombination-mediated repair pathways. At tandem repeats, the presence of multiple identical repeat units that can serve as template for recombination results in copy number variation. While average repeat copy number of a population remains stable in unperturbed conditions, under stress, selection of advantageous copy number variants can facilitate adaptation (reviewed in (Salim et al., 2019)).

Through parallel studies of the rDNA and copper-inducible *CUP1* array, I demonstrated that repeat instability could be induced by DNA replication stress, transcription, as well as transcription- and replication-associated consequences like R-loops and torsional stress (Chapter 3). More importantly, while repeat instability could be rapidly induced by a variety of stresses, a change in steady state repeat copy number required prolonged exposure to conditions that selected for locus-specific, advantageous copy number variants (Chapter 3). Therefore, stress-induced instability at tandem repeats can accelerate adaptation through copy number variation. The sensitivity of tandem repeats to transcription and DNA replication stress makes them unstable by design, enabling them to accommodate copy number variation and undergo rapid, reversible, and adaptive responses to genomic stresses.

5.2.3 H3K56 acetylation restricts transcription-induced copy number variation

Histone acetylation is well known for its roles in promoting transcription (Varv et al., 2010; Yang et al., 2008), maintaining DNA replication timing and origin firing (Aparicio et al., 2004; Casas-Delucchi et al., 2012; Unnikrishnan et al., 2010; Vogelauer et al., 2002), and even influencing the choice of break repair pathway (Che et al., 2015; Munoz-Galvan et al., 2013). This chromatin mark, therefore, has the potential to have profound impacts on stability and copy number variation of tandem repeats. In fact, histone acetylation has been shown to regulate several aspects of rDNA biology, including suppression of recombination (Gottlieb & Esposito, 1989), silencing of RNAPII transcribed genes and regulation of non-coding RNAPII transcription in the rDNA (Cesarini et al., 2012; D'Alfonso et al., 2016; H. H. Xu et al., 2016).

Acetylation of H3K56 is critical to promote RNAPI transcription, rRNA processing, and to maintain rDNA copy number (Chen et al., 2012; Houseley et al., 2011; Ide et al., 2013; Jack et al., 2015). Further, work from Hull et al. (2017) showed that H3K56 acetylation was required for transcription-induced *CUP1* copy number variation. Through studies using the *CUP1* array, I showed that H3K56 acetylation a) regulates transcription, b) induces transcription-dependent repeat instability, and c) restricts transcription-induced repeat amplification (Chapter 4). Importantly, the responses to perturbation of H3K56 acetylation were dependent on the size of the array and its transcriptional status. Further, adaptation to high concentrations of copper required homologous recombination (Chapter 4). My parallel studies of the rDNA and *CUP1* loci suggest that loss of H3K56 acetylation may influence recombination events at both arrays in a manner that results in a bias toward amplification of the array when it is transcribed, independent of growth defects. These data suggest that H3K56 acetylation, together with homologous recombination, could play a conserved role in modulating the stability of tandem repeats and restricting potentially maladaptive copy number variation in response to transcriptional stress.

5.3 Future Directions

5.3.1 H3K56 acetylation and recombination pathway bias

In *S. cerevisiae*, H3K56 residues of newly synthesized histone H3 molecules are acetylated by Rtt109, facilitating their deposition onto newly replicated DNA during S-phase. The acetyltransferase activity of Rtt109 requires the histone chaperones Asf1 and Vps75 (Han et al., 2007b, 2007c). When cells enter the G2/M phase of the cell cycle, acetylation on H3K56 is rapidly removed by the sirtuins Hst3 and Hst4 (Maas et al., 2006; Masumoto et al., 2005; Recht et al., 2006). The H3K56 acetylation/deacetylation cycle was originally reported to be important to maintain genome stability. Loss of Rtt109, Hst3, or Hst4 has been shown to disrupt DNA replication and transcription(Aparicio et al., 2004; Casas-Delucchi et al., 2012; Unnikrishnan et al., 2010; Varv et al., 2010; Vogelauer et al., 2002; Yang et al., 2008). It also makes cells sensitive to genotoxic agents, and significantly impairs recovery from DNA damaging agents (Celic et al., 2006; Celic et al., 2008; Driscoll et al., 2007; Han et al., 2007a). In the following years, it was shown that the H3K56 acetylation status can also influence the choice of the DNA damage repair pathway (Che et al., 2015; Munoz-Galvan et al., 2013). These data suggest that the normal H3K56 acetylation cycle regulates transcription, maintains normal replication fork dynamics during DNA replication and ensures efficient DNA damage repair.

Since the coordination of replication, transcription and recombination is critical to maintain the stability and copy number of tandem repeats, H3K56 acetylation could play a critical role in the maintenance of repetitive genomic loci. In fact, the role of H3K56 acetylation in regulating the stability and copy number of the rDNA repeats has been known for several years. Loss of Asf1, Rtt109, Hst3 and Hst4, and point mutations in the H3K56 residue, are all associated with amplifications of the rDNA array ((Houseley et al., 2011; Ide et al., 2013), Chapter 4). More recently, loss of Rtt109 and Hst3/Hst4 were also shown to affect copy number variation at the *CUP1* array (Hull et al., 2017).

These data suggest that H3K56 acetylation could govern the behavior of multiple tandem repeats. Interestingly, the loss of Asf1 or Rtt109 results in low repeat loss rates at both, the rDNA and *CUP1* arrays (Chapter 4). On the other hand, loss of Hst3 and Hst4 increased repeat instability at both arrays (Chapter 4). Interestingly, all these mutations resulted in amplifications of the rDNA array, and transcription-dependent amplifications at the *CUP1* array (Chapter 4). How both, hypo- and hyper acetylation of H3K56, produce strikingly similar cellular phenotypes and rDNA amplifications has been a long-standing question in the field.

A large body of work has revealed that H3K56 acetylation can affect DNA repair pathway choice and recombination outcomes. Loss of Rtt109 or Vps75 was shown to decrease the efficiency of non-homologous end joining (NHEJ) (Jessulat et al., 2008). Asf1 and Rtt109 were also shown to be required for both, equal, and unequal sister chromatid exchange (USCE) (Endo et al., 2010; Prado et al., 2004). H3K56 acetylation was also shown to be involved in directing the repair of breaks generated during DNA replication to recombination with the sister chromatid (Munoz-Galvan et al., 2013). Hyperacetylation of H3K56, on the other hand, was shown to inhibit efficient DNA replication during break-induced replication (BIR) (Che et al., 2015). Interestingly, the key homologous recombination protein, Rad52, is essential in *hst3*Δ*hst4*Δ double mutants. Further, Rad51 was only essential in the *hst3*Δ*hst4*Δ mutants when Pol32 was ablated. These data suggest that in the absence of normal H3K56 acetylation, cells are preferentially dependent on specific recombination pathways. Based on these data, several mechanisms have been proposed to explain the rDNA amplification phenotype observed in mutants with disrupted H3K56 acetylation. These mechanisms are illustrated in Figure 5.1.

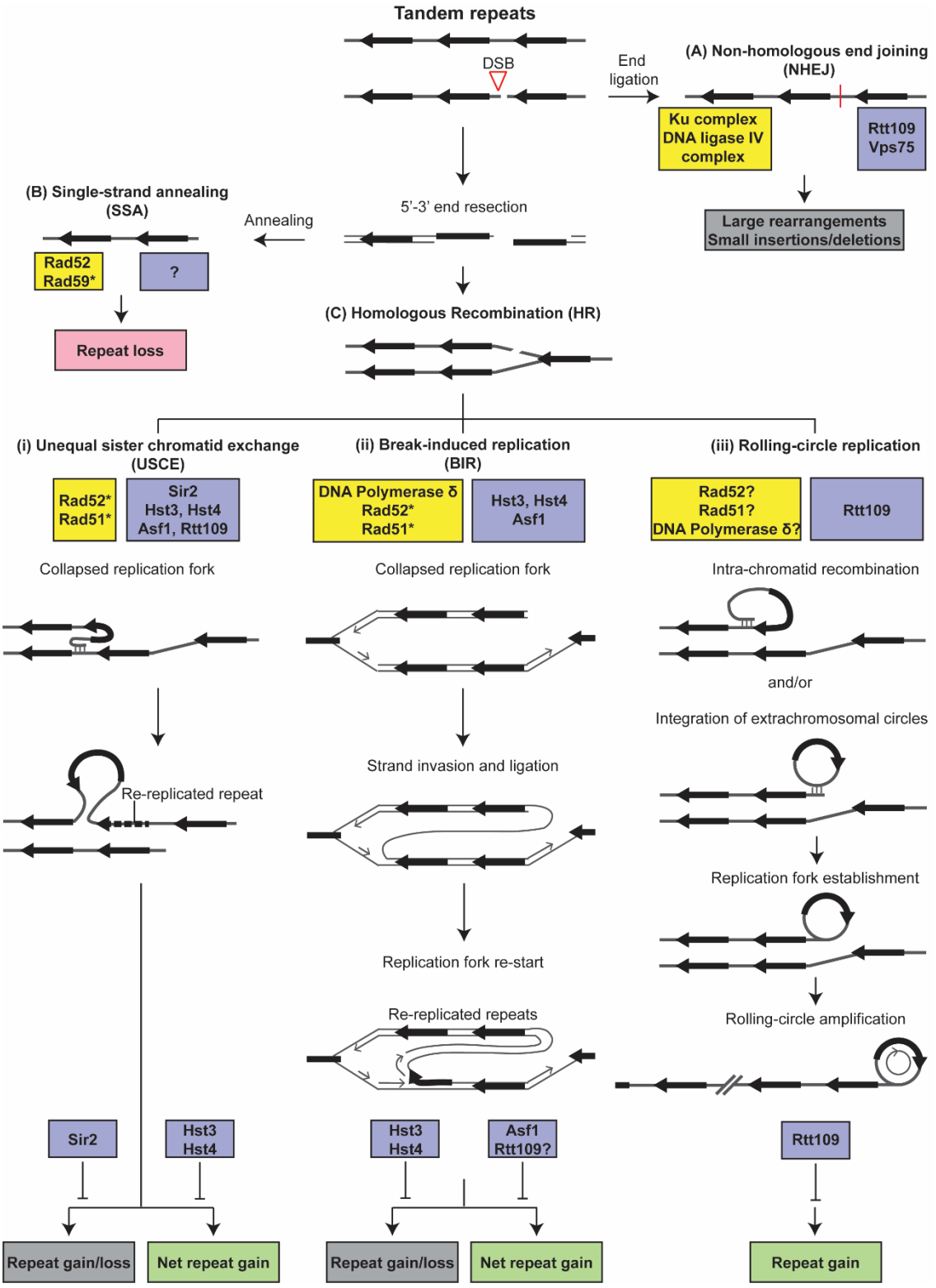
Tandem repeats
DSB
End ligation
(A) Non-homologous end joining (NHEJ)
Ku complex
DNA ligase IV complex
Rtt109
Vps75
Large rearrangements
Small insertions/deletions
5'-3' end resection
Annealing
(B) Single-strand annealing (SSA)
Rad52
Rad59*
?
Repeat loss
(C) Homologous Recombination (HR)
(i) Unequal sister chromatid exchange (USCE)
Rad52*
Rad51*
Sir2
Hst3, Hst4
Asf1, Rtt109
Collapsed replication fork
Re-replicated repeat
Sir2
Hst3
Hst4
Repeat gain/loss
Net repeat gain
(ii) Break-induced replication (BIR)
DNA Polymerase δ
Rad52*
Rad51*
Hst3, Hst4
Asf1
Collapsed replication fork
Strand invasion and ligation
Replication fork re-start
Re-replicated repeats
Hst3
Hst4
Asf1
Rtt109?
Repeat gain/loss
Net repeat gain
(iii) Rolling-circle replication
Rad52?
Rad51?
DNA Polymerase δ?
Rtt109
Intra-chromatid recombination
and/or
Integration of extrachromosomal circles
Replication fork establishment
Rolling-circle amplification
Rtt109
Repeat gain

Figure 5.1. Model for control of copy number by H3K56 acetylation and recombination. Various pathways for repair of double-stranded breaks in a hypothetical tandem array of 3 repeats are shown. Yellow boxes contain key repair proteins involved in each pathway. Purple boxes contain H3K56 acetylation pathway components known to regulate each repair pathway. * indicates that the pathway has been reported to occur independent of this protein. ? indicates unknown or proposed role in repeat copy number maintenance. Potential impact on copy number is indicated in pink (repeat loss), green (repeat gain), or gray (multiple/alternate outcomes) boxes. (A) Non-homologous end joining (NHEJ) involves re-ligation of broken ends. NHEJ is mediated by the Ku complex and a specialized ligase, DNA ligase IV, in a complex with Lif1 and Nej1 (XRCC4 and XLC in mammals, not shown). Resected ends can be annealed at regions of homology surrounding the break by (B) single strand annealing (SSA), which results in repeat loss. Breaks can also be repaired by one of the many forms of (C) homologous recombination (HR). Replication coupled repair typically occurs by sister chromatid recombination (C-i). Recombination between misaligned repeats results in copy number variation, producing losses and gains. HR may also occur by replication-dependent mechanisms like break-induced replication (BIR) or rolling-circle replication (C-ii, iii). BIR results in copy number variation depending on the template used as substrate, whereas rolling-circle replication results in amplifications. This figure is based on the following references (Che et al., 2015; Endo et al., 2010; Haber, 2013; Houseley & Tollervey, 2011; Hull et al., 2017; Ide et al., 2013; Jack et al., 2015; Jessulat et al., 2008; Munoz-Galvan et al., 2013; Prado et al., 2004).

Ide et al. (2013) proposed that in the absence of Rtt109, rolling-circle replication mediates rDNA hyper-amplification (Ide et al., 2013). This type of a mechanism could be initiated by intra-chromosomal recombination, or integration of extrachromosomal rDNA circles into the chromosomal rDNA locus (Figure 5.1, (Ide et al., 2013)). Houseley and Tollervey (2011) suggested that rDNA amplification in *asf1*Δ mutants occurred via USCE and BIR. Jack et al (2015) showed that the TOR pathway can mediate rDNA amplification through its effects on Sir2, Hst3, and Hst4, which in turn control USCE or BIR (Figure 5.1). My studies using the *CUP1* array suggest that transcription-induced copy number variation is dependent on Rad52 and Rad51, suggesting a homologous recombination-mediated mechanism. These studies suggest that the acetylation status of H3K56 residues governs the normal maintenance of tandem repeats by directing repair to different repair pathways. Further, the disruption of copy number maintenance in the absence of this chromatin mark suggests that it could also influence adaptive copy number changes in wild-type cells through a recombination pathway bias.

While the role of H3K56 acetylation in maintaining the normal DNA damage response is clear, exactly how any chromatin mark may direct break repair and copy number variation in response to transcriptional stress in cells is unclear. One way to achieve a recombination pathway bias could be through the recruitment of specific checkpoint or repair proteins by different chromatin marks. Acetylated H3K56 has been shown to be specifically retained at sites of DNA damage through checkpoint-dependent downregulation of Hst3 (Masumoto et al., 2005; Thaminy et al., 2007). Further, acetylated H3K56 recruits cohesin and repair proteins (Thaminy et al., 2007). In the absence of the normal acetylation cycle, cells may be unable to use this modification to properly direct damage response proteins to facilitate replication or repair. Since cohesin plays an important role in suppressing USCE at the rDNA (Kobayashi & Ganley, 2005), decreased cohesin recruitment could direct break repair to this pathway. Increased repeat loss rates and copy number variation at both, rDNA and *CUP1* arrays in *hst3*Δ*hst4*Δ mutants supports this possibility. Interestingly, cohesin binding at the rDNA was shown to be unaffected in *rtt109*Δ mutants (Ide et al., 2013). This argues against a significant role for cohesin recruitment in establishing a recombination pathway bias in *rtt109*Δ mutants. Alternatively, the acetylation status of chromatin could affect accessibility of DNA repair proteins through its known roles in silencing and chromatin condensation (Driscoll et al., 2007; Masumoto et al., 2005; Yang et al., 2008). The decreased efficiency of break repair observed in *hst3*Δ*hst4*Δ mutants supports this idea (Munoz-Galvan et al., 2013).

Another way to achieve specific recombination outcomes is by influencing the choice of the DNA template used as substrate for homologous recombination. Because acetylated histone H3 is incorporated into newly synthesized DNA behind the replication fork, an asymmetry of H3K56 acetylation exists on either side of the replication fork. Several groups have proposed that this asymmetry is critical for template choice. Therefore, in the absence of H3K56 acetylation, or when acetylated H3K56 is distributed throughout the chromatin, the preference for recombination with the sister chromatid

may be lost (Munoz-Galvan et al., 2013). Additionally, when H3K56 acetylation levels are high, the replication fork may stall more frequently, inducing further recombination (Hull et al., 2017). The presence of multiple identical repeat units in tandem arrays increases the likelihood of unequal recombination, which generates copy number variation. These mechanisms are not mutually exclusive and may be synergistic with transcription at the locus, and therefore, are worth investigating in the future.

5.3.2 Regulation of copy number variation through chromatin marks

The role of histone acetylation in the regulation of the stability and copy number of tandem repeats like the rDNA and *CUP1* is now well established. The adverse effects of disruption of histone acetylation pathways, particularly the H3K56 acetylation pathway, on genome stability and transcription are also very well characterized. My work has added to this by revealing a unique role for H3K56 acetylation in suppressing potentially maladaptive transcription-induced amplifications at tandem repeats. However, the regulation of repeat copy number variation by H3K56 acetylation, or any chromatin mark, in wild-type cells in response to the environment is still unclear. How do cells specifically modulate H3K56 acetylation at tandem repeats without affecting global H3K56 acetylation? How can recombination outcomes at specific loci be controlled without affecting genome-wide recombination?

The rDNA repeats are organized in the nucleolus, therefore exclusion of specific proteins from the nucleolus could be one way of achieving rDNA specific modulation of repeat stability and copy number variation. In fact, canonical homologous recombination proteins have been shown to be excluded from nucleoli (Torres-Rosell et al., 2007). Jack et al. (2015) suggest that a moderate decrease in H3K56 deacetylase levels or activity combined with the exclusion of homologous recombination proteins from the nucleolus could drive canonical homologous recombination independent rDNA amplification

without causing global H3K56 hyperacetylation and genomic instability (Jack et al., 2015).

While exclusion of proteins from the nucleoli is a plausible mechanism for regulation of rDNA specific repeat dynamics, other tandem repeats like the RNAPII transcribed *CUP1* array likely depend on different mechanisms to ensure repeat specific regulation of copy number variation by chromatin marks. Locus-specific manipulation of H3K56 acetylation will therefore enable us to begin to understand how H3K56 acetylation directly regulates copy number variation at tandem repeats. To achieve this, the H3K56 acetyltransferase, Rtt109 or the deacetylase, Hst3 (or Hst4) could be fused to a protein that localizes specifically to the rDNA or *CUP1* array. Rtt109 and Hst3/Hst4 could be targeted to the rDNA by fusion to Hmo1. Similarly, these proteins could be targeted to the *CUP1* array by fusion to the Cup2 transcription factor. These constructs can be integrated into the native Rtt109 or Hst3/Hst4 loci, or expressed from their endogenous promoter on a *CEN* vector (1-3 copies/cell). Fusion proteins containing catalytically dead Rtt109 and Hst3/Hst4 will serve as important controls. Addition of a 13×Myc tag to the constructs will enable measurement of expression, localization, and enzymatic activity of the fusion proteins. Localization to the intended target array can be verified using chromatin immunoprecipitation combined with ddPCR to measure enrichment at the rDNA or *CUP1* arrays. The expression and enzymatic activity of the fusion proteins can be tested by expressing them in *rtt109*Δ and *hst3*Δ*hst4*Δ strains and probing for H3K56 acetylation through Western blotting with standard antibodies against acetylated H3K56. These strains can then be used to measure repeat instability and adaptation. Comparison of these results to the instability and adaptive responses in the *rtt109*Δ and *hst3*Δ*hst4*Δ mutants will allow distinction between the effects of local and global acetylation of H3K56 on stability and copy number of tandem repeats. These studies are vital to extend our understanding of how mutagenesis can be directed to relevant loci without compromising general genome stability.

5.3.3 Exceptions to the rule – 2-copy repeats

The inducible *CUP1* array proved to be a powerful system that allowed the evaluation of transcription-dependent and independent mechanisms of regulation of copy number variation. The generation of strains with *CUP1* arrays ranging in size from 2-20 copies also allowed characterization of the effect of array size on repeat stability and copy number variation. When the H3K56 acetylation pathway was disrupted, all the strains with ≥6 copies of *CUP1* exhibited similar repeat dynamics and transcription-induced amplification. The 2-copy array, on the other hand exhibited dramatically different repeat dynamics (Chapter 4). First, the loss of H3K56 acetylation in 2×*CUP1 rtt109*Δ mutants had no effect on repeat stability. Second, both hypo- and hyperacetylation of H3K56 led to increased basal transcription of the 2×*CUP1* array; copper-induced *CUP1* transcription was unaffected. Third, 2×*CUP1 rtt109*Δ mutants exhibited dramatic transcription-induced amplification of the *CUP1* array in high concentrations of copper (2×*CUP1* to ~100×*CUP1* in *rtt109*Δ mutants compared to 2×*CUP1* to ~20×*CUP1* in wild-type or *hst3*Δ*hst4*Δ strains). These observations suggest that 2-copy tandem repeats respond differently to chromatin modifications like H3K56 acetylation, particularly when the array is highly transcribed. Further the massive amplifications in these strains (2×*CUP1* to ~100×*CUP1* in 25-50 generations) cannot be explained simply by recombination pathway biases.

Ide et al. (2013) suggested a rolling-circle replication based amplification mechanism for rDNA repeats in *rtt109*Δ mutants based on their observation of increased incorporation of extrachromosomal rDNA circles into the chromosomal rDNA (Ide et al., 2013) (Figure 5.1). While transcription-induced amplification was observed in the ≥6×*CUP1 rtt109*Δ mutant strains, the degree of amplification was comparable to the corresponding wild-type strains. In these strains a rolling-circle replication mechanism seems unlikely, especially considering that extrachromosomal *CUP1* circles are rare in the yeast genome (Moller et al., 2015). However, in the 2×*CUP1* strains, it is possible that amplification is mediated, at least in part, by incorporation of extrachromosomal

CUP1 circles into the chromosomal locus. This can be tested by measuring the levels of extrachromosomal *CUP1* circles in the genome by Southern blotting. Increased incorporation into the chromosomal locus is expected to result in a decrease in the free extrachromosomal pool of *CUP1* circles. However, given the low levels of extrachromosomal *CUP1* circles, they may be undetectable by Southern blots. Alternatively, incorporation into the chromosomal *CUP1* locus can be tested by following a strategy similar to the one adopted by Ide et al. (2013). A plasmid containing the entire *CUP1* repeat unit and a selectable marker can be constructed and introduced into wild-type and *rtt109*Δ mutant strains with 2×*CUP1*. The strains can be subcultured in high concentrations of copper to produce cells with "hyper-amplified" *CUP1* arrays. Subsequently, chromosomal incorporation of the *CUP1* plasmid can be evaluated by probing for the selectable marker by Southern blotting.

Further, it is tempting to speculate that the behavior of 2-copy repeats may be more similar to that of unique regions of the genome. In fact, the transcript levels of several reference genes used for RT-ddPCR were significantly altered in the *rtt109*Δ mutants (Figure 5.2). However, *rtt109*Δ strains did not exhibit altered instability at a unique intergenic region downstream of *TUB1* (Chapter 4). This region is likely transcriptionally silent, therefore, this result may not be representative of the response of a unique, highly transcribed gene to disrupted H3K56 acetylation. Since 2-5 copy repeats are abundant in the genomes of higher eukaryotes, the characterization of the unique dynamics of the 2×*CUP1 rtt109*Δ strains will provide insights into the response of low copy repeats to transcriptional stress.

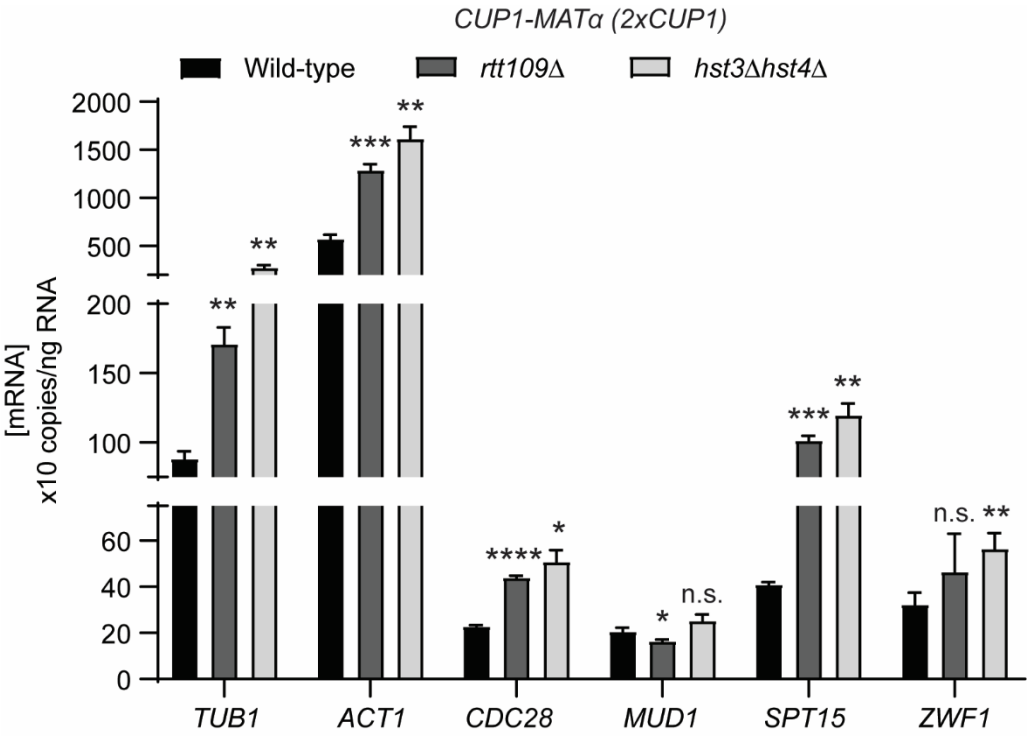

Figure 5.2. Disruption of the H3K56 acetylation pathway affects global gene expression. Absolute mRNA concentration (×10 copies/ng of total RNA) of indicated reference genes in 2×*CUP1* wild-type, *rtt109*Δ and *hst3*Δ*hst4*Δ strains grown in complete medium measured by RT-ddPCR. Statistical significance of the difference between mRNA levels for each gene in the *rtt109*Δ or *hst3*Δ*hst4*Δ mutants and the wild-type strain was calculated using a standard 2-tailed t-test. * - p<0.05, ** - p<0.01, *** - p<0.001, **** - p<0.0001, n. s.– not significant.

5.4 Outlook

5.4.1 Beyond rDNA – other tandem repeats

My thesis work has identified principles of regulation of copy number variation at two repetitive arrays in the yeast genome. The players I characterized, DNA replication and transcription, are fundamental processes that are universally conserved. Mounting evidence suggests that replication-transcription conflicts are a major source of genomic instability in mammalian genomes as well (reviewed in (Hamperl & Cimprich, 2016)). Significant portions of mammalian genomes are made up of repetitive elements; while many repeats are yet to be identified, it has been established that copy number variation at tandem repeats is a significant source of genetic and phenotypic diversity in populations. The fundamental principles underlying copy number variation at tandem repeats in budding yeast can therefore be used to understand the behavior of other tandem repeats.

Mammalian genomes contain many more large stretches of repetitive regions than yeast, and the role of variation at these loci in phenotypic diversity and adaptation is only just beginning to be appreciated. While the rDNA plays a central role in cell physiology, it accounts for <1% of the human genome. However, it may serve as a model for understanding general principles governing copy number variation at other tandem repeats and the functional impact of such variation. For example, relatively little is known about the factors that determine and maintain 5S rDNA copy number. In higher eukaryotes, 5S rDNA genes are organized as one or more tandem clusters of repeats physically separated from the 45S rDNA genes. While there is evidence of mitotic and meiotic recombination within the 5S rDNA arrays in human genomes (Stults et al., 2008), the 5S rDNA has been observed to exhibit relatively low copy number variation in experimental systems. For example, although a modest amplification of the 5S rDNA was found in cancer genomes that exhibited a loss of 45S rDNA repeats, this amplification was found to be mainly due to amplification of the 1q42 chromosomal

segment on which the 5S rDNA repeats reside (Wang & Lemos, 2017). Moreover, analysis of 5S and 45S rDNA repeat copy number in human and mouse whole genome sequencing data suggests that copy number changes at the two loci may be under selection by mechanisms that ensure maintenance of correct rRNA stoichiometry (Gibbons et al., 2015). Work in budding yeast suggests that ribosome biogenesis is regulated at the transcription level, with RNAPI transcription being the key determinant of the biogenesis of other ribosomal components (Laferte et al., 2006). These observations are confounding in light of high copy number variation at the 5S rDNA loci in human populations (Stults et al., 2008). Therefore, the selective pressures acting on the 5S rDNA repeats and the impact of 5S rDNA copy number variation on cellular and organismal adaptation may be different from those of the 45S rDNA repeats and remain largely unknown.

Another example of highly repetitive DNA in the human genome is alpha satellite DNA, the major type of satellite DNA in humans. Alpha satellite DNA is enriched at human centromeres and is known to be essential for several aspects of centromere function, including kinetochore assembly and heterochromatin formation. Despite the essential and universally conserved function of centromeres in chromosome segregation, the presence of several megabases of repetitive satellite DNA has excluded centromeres from human genome sequence assemblies. More recently, it was discovered that centromeric satellite DNA can be transcribed to produce non-coding RNA that plays important roles in maintaining centromeric repeat stability and function (reviewed in (Hall et al., 2012), (McNulty & Sullivan, 2018)). The observation that both centromeric satellite repeat DNA copy number as well as transcription could be altered in cancers (Bersani et al., 2015; Ting et al., 2011) suggests that variation at the centromeric repeats may have important functional consequences in normal physiology and disease. Interestingly, work on the repetitive, regional centromeres in *S. pombe* showed that the coordination of replication and non-coding RNA transcription is critical for the establishment of heterochromatin, which is essential for normal centromere

function (Zaratiegui et al., 2011). Moreover, loss of the RNA interference (RNAi) machinery, which is essential for the maintenance of heterochromatin, also results in instability at centromeric repeats in *S. pombe* (reviewed in (Forsburg & Shen, 2017)). Similarly, mouse embryonic cells lacking Dicer, a key component of RNAi, were also observed to have upregulated pericentromeric RNA transcription and defective centromeric silencing (Kanellopoulou et al., 2005). Based on the similarities between the regulation of stability of the rDNA repeats and centromeric repeats, I speculate that modulation of transcription and/or replication may play critical roles in the maintenance of stability and function of mammalian centromeres. While the role of the centromeric satellite DNA in establishment of centromeric chromatin and kinetochore assembly is clear, the nature and extent of copy number variation at these satellites and their effects on chromosome segregation remain unknown.

5.4.2 Tandem repeats in the molecular evolution of cancer

The fundamental principles that have been shown to influence the copy number of tandem repeats in model systems can be used to consider cancer genomes because a) the rDNA array has been shown to be highly susceptible to recombination-mediated rearrangements in solid tumors (Stults et al., 2009), b) rRNA transcription appears to be frequently dysregulated in cancers (Lu et al., 2009; Udugama et al., 2018; B. Xu et al., 2017), and c) RNAPI transcription has emerged as an effective therapeutic target in a variety of cancers (Hannan et al., 2013). If variation in copy number can be induced by transcription, then instability at rDNA repeats may be induced as rapidly proliferating cancer cells increase transcription to meet the high demand for ribosomes. While increased variation in rDNA copy number could result in loss and gain of repeats, changes in steady state rDNA copy number, and their effects on tumor progression are poorly understood. Data from studies in budding yeast suggest that while an increase in rDNA copy number may facilitate increased rRNA production while reducing RNAPI

transcriptional load on the rDNA loci, amplified rDNA arrays may also hinder faithful genome replication and repair. In fact, several independent studies of human cancer genomes and murine models of cancer have all revealed that rDNA repeats tend to be lost in cancer (Salim et al., 2017; Udugama et al., 2018; Wang et al., 2017; B. Xu et al., 2017). The striking consistency of repeat loss suggests that loss of repeats may be adaptive. I speculate that altered rRNA transcription may initially induce variation in copy number, but a loss of repeats may allow for easier genome replication and faster proliferation, and may thus be selected for.

My studies also suggest that histone acetylation may govern the transcription-induced behavior of multiple tandem repeats and dictate adaptive outcomes. These data also have implications for understanding the molecular evolution of cancer genomes, which are characterized by global dysregulation of transcription and histone acetylation, and copy number amplifications (Audia & Campbell, 2016; Santarius et al., 2010). I speculate that altered transcription in the context of perturbed histone acetylation may underlie at least some of these amplifications. Further, because histone acetylation is often a target of anti-cancer drugs (Eckschlager et al., 2017), understanding how acetylation impacts the stability and copy number of tandem arrays could be relevant to understanding how cancer cells adapt in response to therapy.

Cancer cells often contain an array of mutations, sometimes simplistically divided into driver and passenger mutations. Driver mutations help drive tumor development and progression, while passenger mutations are considered neutral. However, there may be a third class of mutations that could occur in cancer, adaptive mutations, and copy number variation at tandem repeats could be an example of this type of mutation. Adaptive mutations could facilitate proliferation without necessarily acting as independent drivers. Given the prevalence of large stretches of repetitive DNA in the human genome, and the paucity of methods to study these sequences, functionally relevant copy number changes at other repetitive regions of the genome may have gone undetected in cancer.

5.5 Summary

My studies of the rDNA and *CUP1* repeats have revealed how the fundamental processes of DNA replication and transcription can tune rates of adaptation through their effects on copy number variation at these loci. These results have profound impacts for understanding the evolution of genomes under stress and advance our understanding of the principles of regulation of additional tandem repeats and the important functional and evolutionary roles they play in genome biology. Repetitive sequences constitute up to half of the genomes of higher eukaryotes. Repetitive DNA, particularly tandem repeats, are generally thought of as detrimental to faithful propagation of the genome. The ubiquity of tandem repeats and their persistence through evolutionary time suggests that the advantages offered by a repeat-rich, malleable genome far outweighs the risks repeats pose to the fidelity of genome replication. The organization of essential loci like the rDNA repeats in this unstable configuration, and the vast body of work demonstrating the adaptive potential of rDNA copy number variation further supports the idea that genomes may be designed to allow for rapid adaptability of critical genomic regions. Work in bacteria has revealed that key stress response and virulence genes are often encoded on the lagging strand; when these genes are transcribed, their orientation likely makes the more mutagenic head-on collisions between the transcription and replication machineries frequent (H. Merrikh, 2017). Consistent with this, these genes exhibit elevated rates of mutagenesis when transcribed (C. N. Merrikh & Merrikh, 2018; Paul et al., 2013; Sankar et al., 2016). These data provide compelling evidence to support the idea that bacterial genomes may be organized so as to be able to direct mutations to relevant loci to promote rapid adaptation. Therefore, studying different tandem repeat families may be also be critical to understanding the evolution of genome organization and molecular strategies for optimizing genome fitness.

5.6 References

Aparicio, J. G., Viggiani, C. J., Gibson, D. G., & Aparicio, O. M. (2004). The Rpd3-Sin3 histone deacetylase regulates replication timing and enables intra-S origin control in Saccharomyces cerevisiae. *Mol Cell Biol, 24*(11), 4769-4780. doi:10.1128/MCB.24.11.4769-4780.2004

Audia, J. E., & Campbell, R. M. (2016). Histone Modifications and Cancer. *Cold Spring Harb Perspect Biol, 8*(4), a019521. doi:10.1101/cshperspect.a019521

Bersani, F., Lee, E., Kharchenko, P. V., Xu, A. W., Liu, M., Xega, K., . . . Haber, D. A. (2015). Pericentromeric satellite repeat expansions through RNA-derived DNA intermediates in cancer. *Proc Natl Acad Sci U S A, 112*(49), 15148-15153. doi:10.1073/pnas.1518008112

Casas-Delucchi, C. S., van Bemmel, J. G., Haase, S., Herce, H. D., Nowak, D., Meilinger, D., . . . Cardoso, M. C. (2012). Histone hypoacetylation is required to maintain late replication timing of constitutive heterochromatin. *Nucleic Acids Res, 40*(1), 159-169. doi:10.1093/nar/gkr723

Celic, I., Masumoto, H., Griffith, W. P., Meluh, P., Cotter, R. J., Boeke, J. D., & Verreault, A. (2006). The sirtuins hst3 and Hst4p preserve genome integrity by controlling histone h3 lysine 56 deacetylation. *Curr Biol, 16*(13), 1280-1289. doi:10.1016/j.cub.2006.06.023

Celic, I., Verreault, A., & Boeke, J. D. (2008). Histone H3 K56 hyperacetylation perturbs replisomes and causes DNA damage. *Genetics, 179*(4), 1769-1784. doi:10.1534/genetics.108.088914

Cesarini, E., D'Alfonso, A., & Camilloni, G. (2012). H4K16 acetylation affects recombination and ncRNA transcription at rDNA in Saccharomyces cerevisiae. *Mol Biol Cell, 23*(14), 2770-2781. doi:10.1091/mbc.E12-02-0095

Che, J., Smith, S., Kim, Y. J., Shim, E. Y., Myung, K., & Lee, S. E. (2015). Hyper-Acetylation of Histone H3K56 Limits Break-Induced Replication by Inhibiting Extensive Repair Synthesis. *PLoS Genet, 11*(2), e1004990. doi:10.1371/journal.pgen.1004990

Chen, H., Fan, M., Pfeffer, L. M., & Laribee, R. N. (2012). The histone H3 lysine 56 acetylation pathway is regulated by target of rapamycin (TOR) signaling and functions directly in ribosomal RNA biogenesis. *Nucleic Acids Res, 40*(14), 6534-6546. doi:10.1093/nar/gks345

D'Alfonso, A., Di Felice, F., Carlini, V., Wright, C. M., Hertz, M. I., Bjornsti, M. A., & Camilloni, G. (2016). Molecular Mechanism of DNA Topoisomerase I-Dependent rDNA Silencing: Sir2p Recruitment at Ribosomal Genes. *J Mol Biol, 428*(24 Pt B), 4905-4916. doi:10.1016/j.jmb.2016.10.032

Driscoll, R., Hudson, A., & Jackson, S. P. (2007). Yeast Rtt109 promotes genome stability by acetylating histone H3 on lysine 56. *Science, 315*(5812), 649-652. doi:10.1126/science.1135862

Eckschlager, T., Plch, J., Stiborova, M., & Hrabeta, J. (2017). Histone Deacetylase Inhibitors as Anticancer Drugs. *Int J Mol Sci, 18*(7). doi:10.3390/ijms18071414

Endo, H., Kawashima, S., Sato, L., Lai, M. S., Enomoto, T., Seki, M., & Horikoshi, M. (2010). Chromatin dynamics mediated by histone modifiers and histone chaperones in postreplicative recombination. *Genes Cells, 15*(9), 945-958. doi:10.1111/j.1365-2443.2010.01435.x

Forsburg, S. L., & Shen, K. F. (2017). Centromere Stability: The Replication Connection. *Genes (Basel), 8*(1). doi:10.3390/genes8010037

Foss, E. J., Lao, U., Dalrymple, E., Adrianse, R. L., Loe, T., & Bedalov, A. (2017). SIR2 suppresses replication gaps and genome instability by balancing replication between repetitive and unique sequences. *Proc Natl Acad Sci U S A., 114*(3), 552-557. doi:10.1073

Gibbons, J. G., Branco, A. T., Godinho, S. A., Yu, S., & Lemos, B. (2015). Concerted copy number variation balances ribosomal DNA dosage in human and mouse genomes. *Proc Natl Acad Sci U S A, 112*(8), 2485-2490. doi:10.1073/pnas.1416878112

Gottlieb, S., & Esposito, R. E. (1989). A new role for a yeast transcriptional silencer gene, SIR2, in regulation of recombination in ribosomal DNA. *Cell, 56*(5), 771-776. doi:10.1016/0092-8674(89)90681-8

Haber, J. E. (2013). *Genome Stability: DNA Repair and Recombination*: Garland Science, New York.

Hall, L. E., Mitchell, S. E., & O'Neill, R. J. (2012). Pericentric and centromeric transcription: a perfect balance required. *Chromosome Res, 20*(5), 535-546. doi:10.1007/s10577-012-9297-9

Hamperl, S., & Cimprich, K. A. (2016). Conflict Resolution in the Genome: How Transcription and Replication Make It Work. *Cell, 167*(6), 1455-1467. doi:10.1016/j.cell.2016.09.053
Han, J., Zhou, H., Horazdovsky, B., Zhang, K., Xu, R. M., & Zhang, Z. (2007a). Rtt109 acetylates histone H3 lysine 56 and functions in DNA replication. *Science, 315*(5812), 653-655. doi:10.1126/science.1133234
Han, J., Zhou, H., Li, Z., Xu, R. M., & Zhang, Z. (2007b). Acetylation of lysine 56 of histone H3 catalyzed by RTT109 and regulated by ASF1 is required for replisome integrity. *J Biol Chem, 282*(39), 28587-28596. doi:10.1074/jbc.M702496200
Han, J., Zhou, H., Li, Z., Xu, R. M., & Zhang, Z. (2007c). The Rtt109-Vps75 histone acetyltransferase complex acetylates non-nucleosomal histone H3. *J Biol Chem, 282*(19), 14158-14164. doi:10.1074/jbc.M700611200
Hannan, R. D., Drygin, D., & Pearson, R. B. (2013). Targeting RNA polymerase I transcription and the nucleolus for cancer therapy. *Expert Opin Ther Targets, 17*(8), 873-878. doi:10.1517/14728222.2013.818658
Houseley, J., & Tollervey, D. (2011). Repeat expansion in the budding yeast ribosomal DNA can occur independently of the canonical homologous recombination machinery. *Nucleic Acids Res, 39*(20), 8778-8791. doi:10.1093/nar/gkr589
Hull, R. M., Cruz, C., Jack, C. V., & Houseley, J. (2017). Environmental change drives accelerated adaptation through stimulated copy number variation. *PLoS Biol, 15*(6), e2001333. doi:10.1371/journal.pbio.2001333
Ide, S., Miyazaki, T., Maki, H., & Kobayashi, T. (2010). Abundance of ribosomal RNA gene copies maintains genome integrity. *Science, 327*(5966), 693-696. doi:10.1126/science.1179044
Ide, S., Saka, K., & Kobayashi, T. (2013). Rtt109 Prevents Hyper-Amplification of Ribosomal RNA Genes through Histone Modification in Budding Yeast. *PLoS Genet, 9*(4). doi:10.1371/journal.pgen.1003410.g001
Jack, C. V., Cruz, C., Hull, R. M., Keller, M. A., Ralser, M., & Houseley, J. (2015). Regulation of ribosomal DNA amplification by the TOR pathway. *Proc Natl Acad Sci U S A, 112*(31), 9674-9679. doi:10.1073/pnas.1505015112
Jessulat, M., Alamgir, M., Salsali, H., Greenblatt, J., Xu, J., & Golshani, A. (2008). Interacting proteins Rtt109 and Vps75 affect the efficiency of non-homologous end-joining in Saccharomyces cerevisiae. *Arch Biochem Biophys, 469*(2), 157-164. doi:10.1016/j.abb.2007.11.001
Kanellopoulou, C., Muljo, S. A., Kung, A. L., Ganesan, S., Drapkin, R., Jenuwein, T., . . . Rajewsky, K. (2005). Dicer-deficient mouse embryonic stem cells are defective in differentiation and centromeric silencing. *Genes Dev, 19*(4), 489-501. doi:10.1101/gad.1248505
Kobayashi, T., & Ganley, A. R. (2005). Recombination regulation by transcription-induced cohesin dissociation in rDNA repeats. *Science, 309*(5740), 1581-1584. doi:10.1126/science.1116102
Laferte, A., Favry, E., Sentenac, A., Riva, M., Carles, C., & Chedin, S. (2006). The transcriptional activity of RNA polymerase I is a key determinant for the level of all ribosome components. *Genes Dev, 20*(15), 2030-2040. doi:10.1101/gad.386106
Lang, K. S., & Merrikh, H. (2018). The Clash of Macromolecular Titans: Replication-Transcription Conflicts in Bacteria. *Annu Rev Microbiol, 72*, 71-88. doi:10.1146/annurev-micro-090817-062514
Lu, Y., Chang, Q., Zhang, Y., Beezhold, K., Rojanasakul, Y., Zhao, H., . . . Chen, F. (2009). Lung cancer-associated JmjC domain protein mdig suppresses formation of tri-methyl lysine 9 of histone H3. *Cell Cycle, 8*(13), 2101-2109. doi:10.4161/cc.8.13.8927
Maas, N. L., Miller, K. M., DeFazio, L. G., & Toczyski, D. P. (2006). Cell cycle and checkpoint regulation of histone H3 K56 acetylation by Hst3 and Hst4. *Mol Cell, 23*(1), 109-119. doi:10.1016/j.molcel.2006.06.006
Masumoto, H., Hawke, D., Kobayashi, R., & Verreault, A. (2005). A role for cell-cycle-regulated histone H3 lysine 56 acetylation in the DNA damage response. *Nature, 436*(7048), 294-298. doi:10.1038/nature03714
McNulty, S. M., & Sullivan, B. A. (2018). Alpha satellite DNA biology: finding function in the recesses of the genome. *Chromosome Res, 26*(3), 115-138. doi:10.1007/s10577-018-9582-3
Merrikh, C. N., & Merrikh, H. (2018). Gene inversion potentiates bacterial evolvability and virulence. *Nat Commun, 9*(1), 4662. doi:10.1038/s41467-018-07110-3
Merrikh, H. (2017). Spatial and Temporal Control of Evolution through Replication-Transcription Conflicts. *Trends Microbiol, 25*(7), 515-521. doi:10.1016/j.tim.2017.01.008

Moller, H. D., Parsons, L., Jorgensen, T. S., Botstein, D., & Regenberg, B. (2015). Extrachromosomal circular DNA is common in yeast. *Proc Natl Acad Sci U S A, 112*(24), E3114-3122. doi:10.1073/pnas.1508825112

Munoz-Galvan, S., Jimeno, S., Rothstein, R., & Aguilera, A. (2013). Histone H3K56 acetylation, Rad52, and non-DNA repair factors control double-strand break repair choice with the sister chromatid. *PLoS Genet, 9*(1), e1003237. doi:10.1371/journal.pgen.1003237

Paul, S., Million-Weaver, S., Chattopadhyay, S., Sokurenko, E., & Merrikh, H. (2013). Accelerated gene evolution through replication-transcription conflicts. *Nature, 495*(7442), 512-515. doi:10.1038/nature11989

Prado, F., Cortes-Ledesma, F., & Aguilera, A. (2004). The absence of the yeast chromatin assembly factor Asf1 increases genomic instability and sister chromatid exchange. *EMBO Rep, 5*(5), 497-502. doi:10.1038/sj.embor.7400128

Recht, J., Tsubota, T., Tanny, J. C., Diaz, R. L., Berger, J. M., Zhang, X., . . . Allis, C. D. (2006). Histone chaperone Asf1 is required for histone H3 lysine 56 acetylation, a modification associated with S phase in mitosis and meiosis. *Proc Natl Acad Sci U S A, 103*(18), 6988-6993. doi:10.1073/pnas.0601676103

Salim, D., Bradford, W. D., Freeland, A., Cady, G., Wang, J., Pruitt, S. C., & Gerton, J. L. (2017). DNA replication stress restricts ribosomal DNA copy number. *PLoS Genet, 13*(9), e1007006. doi:10.1371/journal.pgen.1007006

Salim, D., & Gerton, J. L. (2019). Ribosomal DNA instability and genome adaptability. *Chromosome Res, 27*(1-2), 73-87. doi:10.1007/s10577-018-9599-7

Sankar, T. S., Wastuwidyaningtyas, B. D., Dong, Y., Lewis, S. A., & Wang, J. D. (2016). The nature of mutations induced by replication-transcription collisions. *Nature, 535*(7610), 178-181. doi:10.1038/nature18316

Santarius, T., Shipley, J., Brewer, D., Stratton, M. R., & Cooper, C. S. (2010). A census of amplified and overexpressed human cancer genes. *Nat Rev Cancer, 10*(1), 59-64. doi:10.1038/nrc2771

Stults, D. M., Killen, M. W., Pierce, H. H., & Pierce, A. J. (2008). Genomic architecture and inheritance of human ribosomal RNA gene clusters. *Genome Res, 18*(1), 13-18. doi:10.1101/gr.6858507

Stults, D. M., Killen, M. W., Williamson, E. P., Hourigan, J. S., Vargas, H. D., Arnold, S. M., . . . Pierce, A. J. (2009). Human rRNA gene clusters are recombinational hotspots in cancer. *Cancer Res, 69*(23), 9096-9104. doi:10.1158/0008-5472.CAN-09-2680

Thaminy, S., Newcomb, B., Kim, J., Gatbonton, T., Foss, E., Simon, J., & Bedalov, A. (2007). Hst3 is regulated by Mec1-dependent proteolysis and controls the S phase checkpoint and sister chromatid cohesion by deacetylating histone H3 at lysine 56. *J Biol Chem, 282*(52), 37805-37814. doi:10.1074/jbc.M706384200

Ting, D. T., Lipson, D., Paul, S., Brannigan, B. W., Akhavanfard, S., Coffman, E. J., . . . Haber, D. A. (2011). Aberrant overexpression of satellite repeats in pancreatic and other epithelial cancers. *Science, 331*(6017), 593-596. doi:10.1126/science.1200801

Torres-Rosell, J., Sunjevaric, I., De Piccoli, G., Sacher, M., Eckert-Boulet, N., Reid, R., . . . Lisby, M. (2007). The Smc5-Smc6 complex and SUMO modification of Rad52 regulates recombinational repair at the ribosomal gene locus. *Nat Cell Biol, 9*(8), 923-931. doi:10.1038/ncb1619

Udugama, M., Sanij, E., Voon, H. P. J., Son, J., Hii, L., Henson, J. D., . . . Wong, L. H. (2018). Ribosomal DNA copy loss and repeat instability in ATRX-mutated cancers. *Proc Natl Acad Sci U S A, 115*(18), 4737-4742. doi:10.1073/pnas.1720391115

Unnikrishnan, A., Gafken, P. R., & Tsukiyama, T. (2010). Dynamic changes in histone acetylation regulate origins of DNA replication. *Nat Struct Mol Biol, 17*(4), 430-437. doi:10.1038/nsmb.1780

Varv, S., Kristjuhan, K., Peil, K., Looke, M., Mahlakoiv, T., Paapsi, K., & Kristjuhan, A. (2010). Acetylation of H3 K56 is required for RNA polymerase II transcript elongation through heterochromatin in yeast. *Mol Cell Biol, 30*(6), 1467-1477. doi:10.1128/MCB.01151-09

Vogelauer, M., Rubbi, L., Lucas, I., Brewer, B. J., & Grunstein, M. (2002). Histone acetylation regulates the time of replication origin firing. *Mol Cell, 10*(5), 1223-1233. doi:10.1016/s1097-2765(02)00702-5

Wang, M., & Lemos, B. (2017). Ribosomal DNA copy number amplification and loss in human cancers is linked to tumor genetic context, nucleolus activity, and proliferation. *PLoS Genet, 13*(9), e1006994. doi:10.1371/journal.pgen.1006994

Xu, B., Li, H., Perry, J. M., Singh, V. P., Unruh, J., Yu, Z., . . . Gerton, J. L. (2017). Ribosomal DNA copy number loss and sequence variation in cancer. *PLoS Genet, 13*(6), e1006771. doi:10.1371/journal.pgen.1006771

Xu, H. H., Su, T., & Xue, Y. (2016). Histone H3 N-terminal acetylation sites especially K14 are important for rDNA silencing and aging. *Sci Rep, 6*, 21900. doi:10.1038/srep21900

Yang, B., Miller, A., & Kirchmaier, A. L. (2008). HST3/HST4-dependent deacetylation of lysine 56 of histone H3 in silent chromatin. *Mol Biol Cell, 19*(11), 4993-5005. doi:10.1091/mbc.E08-05-0524

Zaratiegui, M., Castel, S. E., Irvine, D. V., Kloc, A., Ren, J., Li, F., . . . Martienssen, R. A. (2011). RNAi promotes heterochromatic silencing through replication-coupled release of RNA Pol II. *Nature, 479*(7371), 135-138. doi:10.1038/nature10501

APPENDIX A

rDNA copy number measurements in the yTs mutant collection used in Chapter 2.

Appendix A.1 rDNA copy number in the yTs mutant collection

(Salim et al., 2017)

Key

Mean BY4741 CN (variable position)	94.5
SD	12.2

rDNA CN < Mean WT CN - 2SD	Significant change in copy number
Mean WT CN - 2SD < rDNA CN < Mean WT CN - SD	Moderate change in copy number
rDNA CN > Mean WT CN + 2SD	Significant change in CN
Mean WT CN + SD < rDNA CN < Mean WT CN + 2SD	Moderate change in CN
< 10,000 total droplets	No quantification
< 10 copies/uL TUB1 or rDNA	Less accurate quantification
No or too few FAM and/or HEX negative droplets	No quantification
ChrXII/ChrXIII significantly different from 1.	Unreliable copy number measurement

Control strains	BY4741	Wild-type
	W303	Wild-type
	40C	Strain with 40 rDNA copies
	80C	Strain with 80 rDNA copies
	110C	Strain with 110 rDNA copies

Plate	Row	Column	Strain	rDNA CN	Plate	Row	Column	Strain	rDNA CN
1	A	1	BY4741	76.9481	9	A	1	YLR430W	140
1	B	1	YDR196C	78.5047	9	B	1	YDL147W	96.7033
1	C	1	YKL189W	52.3148	9	C	1	YPR108W	79.40199
1	D	1	YKL018W	65.7955	9	D	1	YHR036W	77.04918
1	E	1	YFL045C	56.9672	9	E	1	YHR036W	84.53947
1	F	1	YNR026C	66.8721	9	F	1	YNR043W	94.02542
1	G	1	YFL039C	97.7316	9	G	1	YLR298C	97.42489
1	H	1	YHR166C	102.985	9	H	1	YDL195W	101.2862
1	A	2	YFL009W	82.438	9	A	2	YOL144W	124.6291
1	B	2	YHR007C	89.5161	9	B	2	YDR212W	91.22137
1	C	2	YLR229C	63.301	9	C	2	YJR006W	74.33333
1	D	2	YIL068C	68.9394	9	D	2	YDR145W	79.13832
1	E	2	YHR107C	67.9245	9	E	2	YPR168W	80.65934
1	F	2	YBR160W	62.259	9	F	2	YOR057W	98.29932
1	G	2	YFL039C	78.2998	9	G	2	YLR298C	98.3165
1	H	2	W303	130.667	9	H	2	W303	148.1081
1	A	3	YMR001C	54.7945	9	A	3	YLR022C	91.45251
1	B	3	YPR165W	68.3742	9	B	3	YDL008W	102.8205
1	C	3	YOR361C	63.8272	9	C	3	YKL165C	98.4472
1	D	3	YJR065C	65	9	D	3	YDR182W	97.4026
1	E	3	YDR166C	69.2683	9	E	3	YPR178W	97.11111
1	F	3	YLR166C	67.9157	9	F	3	YOR116C	98.19005
1	G	3	YBR236C	72.0074	9	G	3	YLR007W	91.75947
1	H	3	YHR166C	82.3776	9	H	3	YLR116W	94.29224
1	A	4	YDL017W	71.9472	9	A	4	YPR161C	104.644
1	B	4	YNL263C	63.747	9	B	4	YDR362C	102.6341
1	C	4	YDR172W	65.4412	9	C	4	YLR145W	100.3953
1	D	4	YGL233W	64.556	9	D	4	YDR228C	76.19048
1	E	4	YLR208W	79.0598	9	E	4	YHR036W	94.90617
1	F	4	YER136W	67.1078	9	F	4	YPR086W	94.7619
1	G	4	YGR140W	68.5363	9	G	4	YLR298C	106.2304
1	H	4	YFR036W	72.6862	9	H	4	YJL085W	117.2174
1	A	5	YDL220C	89.4286	9	A	5	YPR161C	103.1546

1	B	5	YDL102W	59.6447
1	C	5	YLR310C	70.6745
1	D	5	YER157W	65.8854
1	E	5	YMR079W	71.6247
1	F	5	YGR002C	49.3506
1	G	5	YPR025C	65.8667
1	H	5	YBL084C	64.0816
1	A	6	YAR019C	68.8172
1	B	6	YDR364C	98.3333
1	C	6	YHR107C	70.1435
1	D	6	YAL041W	80.4545
1	E	6	YBR080C	65.0655
1	F	6	YDR180W	66.5789
1	G	6	YCR002C	78.1597
1	H	6	YBL084C	78.2667
1	A	7	YKL022C	76.9401
1	B	7	YKL045W	29.9342
1	C	7	YDR182W	91.8884
1	D	7	YER008C	66.3194
1	E	7	YDR498C	75.119
1	F	7	YIL026C	63.2075
1	G	7	YCR002C	66.6667
1	H	7	YBR196C	88.4726
1	A	8	YOR236W	91.1538
1	B	8	YNL262W	48.6475
1	C	8	YJL194W	68.8073
1	D	8	YDR170C	86.8167
1	E	8	YNL272C	71.8
1	F	8	YFL008W	67.3854
1	G	8	YJR076C	66.4275
1	H	8	YDR054C	101.46
1	A	9	YLR314C	103.978
1	B	9	YOR257W	55.9829
1	C	9	YDL164C	80.6533
1	D	9	YBL050W	80.6742
1	E	9	YGR009C	63.4375
1	F	9	YJL097W	55.6484
1	G	9	YCR002C	83.9698
1	H	9	YCR093W	134.025
1	A	10	YDL029W	86.6412
1	B	10	YJR057W	77.1591
1	C	10	YAL038W	80
1	D	10	YNL287W	66.7085
1	E	10	YDR473C	74.6606
1	F	10	YDL003W	67.907
1	G	10	YJR076C	74.065
1	H	10	YGL130W	99.5984
1	A	11	YBR087W	56.2766
1	B	11	YLR310C	85.9155
1	C	11	YGR264C	54.2074
1	D	11	YER157W	53.6017
1	E	11	YMR094W	86.3889
1	F	11	YJL074C	65.8661
1	G	11	YJR076C	93.5443
1	H	11	YDR052C	89.0984

9	B	5	YDR394W	98.28431
9	C	5	YML098W	103.2353
9	D	5	YDR328C	80.68966
9	E	5	YAR019C	82.39437
9	F	5	YML010W	35.59585
9	G	5	YMR168C	87.8553
9	H	5	YKR037C	149.7041
9	A	6	YPR161C	117.3653
9	B	6	YER006W	100.3279
9	C	6	YHR036W	93.29317
9	D	6	YEL026W	73.4715
9	E	6	YBL034C	89.65517
9	F	6	YGR116W	70.73298
9	G	6	YML069W	90.61224
9	H	6	YOL123W	71.00346
9	A	7	YOL021C	109.899
9	B	7	YFL034C-B	118.6667
9	C	7	YMR112C	111.0672
9	D	7	YER093C	97.46835
9	E	7	YFR051C	105.6
9	F	7	YGR156W	81.25
9	G	7	YML069W	101.0345
9	H	7	YDL103C	122.5
9	A	8	YKL024C	126.2525
9	B	8	YFL034C-B	77.16846
9	C	8	YNL138W	87.45763
9	D	8	YER148W	104.8458
9	E	8	YGL093W	110.9375
9	F	8	YIL118W	91.54472
9	G	8	YJL085W	118.4314
9	H	8	YDL103C	117.2388
9	A	9	BY4741	109.2265
9	B	9	YFL039C	94.88491
9	C	9	YLR115W	87.04762
9	D	9	YFL034C-B	95.48936
9	E	9	YBR154C	130.9016
9	F	9	YKL112W	106.3855
9	G	9	YOR149C	96.64179
9	H	9	YPL190C	113.4454
9	A	10	YKL024C	100.5128
9	B	10	YGL022W	64.30108
9	C	10	YCR042C	102.0833
9	D	10	YFL034C-B	79.61165
9	E	10	YHR036W	119.2913
9	F	10	YKL203C	81.01604
9	G	10	YOR260W	113.213
9	H	10	YDR113C	114.955
9	A	11	YKL024C	119.7753
9	B	11	YHR005C	85.13834
9	C	11	YDL014W	123.3333
9	D	11	YPL169C	86.27219
9	E	11	YJR093C	86.94545
9	F	11	YKR037C	133.5088
9	G	11	YDL126C	149.115
9	H	11	YPL255W	89.64646

1	A	12	YIL062C	74.2798	9	A	12	YDL097C	103.9216
1	B	12	YBR102C	81.4118	9	B	12	YIL004C	119.8361
1	C	12	YDR164C	81.9231	9	C	12	YDL140C	124.4792
1	D	12	BY4741	85.7937	9	D	12	BY4741	85.32895
1	E	12	W303	118.222	9	E	12	W303	138.2734
1	F	12	40C	36.5854	9	F	12	40C	32.62136
1	G	12	80C	51.6279	9	G	12	80C	60.24096
1	H	12	110C	86.1386	9	H	12	110C	106.2281
2	A	1	YNL102W	*110.553*	10	A	1	YKL021C	*119.512*
2	B	1	YDL108W	129.831	10	B	1	YDL108W	99.90698
2	C	1	YLR268W	81.8966	10	C	1	YLR268W	80.29979
2	D	1	YGR140W	85.3403	10	D	1	YGR140W	78
2	E	1	YFR028C	89.3204	10	E	1	YFR028C	77.67722
2	F	1	YBR109C	113.122	10	F	1	YBR109C	79.82262
2	G	1	YDL028C	110.829	10	G	1	YDL028C	102.2508
2	H	1	YDR087C	130.549	10	H	1	YDR087C	107.0111
2	A	2	BY4741	115.179	10	A	2	YLR117C	117.4785
2	B	2	YIL150C	106.154	10	B	2	YIL150C	84.68468
2	C	2	YPR055W	104.189	10	C	2	YPR055W	83.57143
2	D	2	YOR181W	95	10	D	2	YBR079C	80.27778
2	E	2	YFR028C	81.2261	10	E	2	YFR028C	33.97554
2	F	2	YGR092W	78.3665	10	F	2	YGR092W	76.41196
2	G	2	YDL028C	80.2956	10	G	2	YDL028C	55.57325
2	H	2	W303	190.291	10	H	2	W303	151.6514
2	A	3	YGL116W	115.743	10	A	3	YFL017C	78.18182
2	B	3	YBL023C	121.083	10	B	3	YBL023C	81.89091
2	C	3	YLR305C	92.7083	10	C	3	YLR305C	92.96875
2	D	3	YDL102W	94.717	10	D	3	YDL102W	70.88525
2	E	3	YOR074C	117.518	10	E	3	YOR074C	92.13592
2	F	3	YGR092W	92.1622	10	F	3	YGR092W	93.59756
2	G	3	YOL094C	64.3629	10	G	3	YOL094C	57.17822
2	H	3	YPR103W	107.216	10	H	3	YER125W	116.7453
2	A	4	YCR002C	104.326	10	A	4	YMR229C	102.4465
2	B	4	YEL032W	68.0282	10	B	4	YEL032W	64.6778
2	C	4	YGL130W	78.7234	10	C	4	YGL130W	82.31707
2	D	4	YFL039C	128.444	10	D	4	YFL039C	114.3137
2	E	4	YAL041W	122.326	10	E	4	YAL041W	96.86275
2	F	4	YGR092W	92.1084	10	F	4	YGR092W	105.7143
2	G	4	YPR103W	97.9592	10	G	4	YDL105W	110.5691
2	H	4	YER133W	133.113	10	H	4	YER133W	133.5689
2	A	5	YPR181C	127.527	10	A	5	YDL132W	90
2	B	5	YKL089W	95.3552	10	B	5	YKL089W	83.82114
2	C	5	YBR202W	93.1611	10	C	5	YBR202W	87.82222
2	D	5	YFL039C	116.997	10	D	5	YFL039C	109.1892
2	E	5	YAL041W	108.214	10	E	5	YAL041W	122.7143
2	F	5	YDR052C	75.9298	10	F	5	YDR052C	62.88321
2	G	5	YKL018W	146.473	10	G	5	YKL018W	121.1111
2	H	5	YER133W	135.658	10	H	5	YER133W	128.6957
2	A	6	YNL222W	109.215	10	A	6	YDL084W	121.608
2	B	6	YPL211W	97.6446	10	B	6	YPL211W	74.71698
2	C	6	YJR076C	129.487	10	C	6	YJR076C	79.88
2	D	6	YFL039C	154.39	10	D	6	YFL039C	111.8692
2	E	6	YBR160W	86.1644	10	E	6	YBR160W	89.71061
2	F	6	YDR052C	111.863	10	F	6	YDR052C	91.25
2	G	6	YBR160W	91.3462	10	G	6	YBR160W	112.3611

2	H	6	YGL048C	116.667
2	A	7	YDR208W	117.903
2	B	7	YNL267W	130.612
2	C	7	YFL039C	111.445
2	D	7	YOR336W	82.7586
2	E	7	YOR257W	97.1557
2	F	7	YDR052C	109.762
2	G	7	YBR160W	86.6207
2	H	7	YGR120C	118.862
2	A	8	YFL039C	136.084
2	B	8	YNL267W	94.715
2	C	8	YDL014W	109.194
2	D	8	YFL039C	121.136
2	E	8	YOR257W	79.602
2	F	8	YDR052C	82.5561
2	G	8	YML031W	93.9219
2	H	8	YIL048W	113.575
2	A	9	YOR335C	132.121
2	B	9	YBR237W	105.466
2	C	9	YDR208W	NO CALL
2	D	9	YFL039C	107.478
2	E	9	YOR048C	79.7753
2	F	9	YPL209C	107.547
2	G	9	YBR110W	109.25
2	H	9	YIL109C	114.884
2	A	10	YGL048C	142.193
2	B	10	YMR235C	128.281
2	C	10	YLR314C	108.046
2	D	10	YFL039C	110.435
2	E	10	YBR109C	100.144
2	F	10	YDL028C	99.4872
2	G	10	YPR103W	94.4444
2	H	10	YKL145W	104.216
2	A	11	YGL048C	116.256
2	B	11	YPL085W	99.8319
2	C	11	YDL017W	102.289
2	D	11	YPR176C	111.481
2	E	11	YBR109C	100.179
2	F	11	YDL028C	56.1176
2	G	11	YDL126C	70.3261
2	H	11	YKL210W	NO CALL
2	A	12	YLR071C	61.5714
2	B	12	YFL039C	89.0909
2	C	12	YFL039C	102.083
2	D	12	BY4741	94.709
2	E	12	W303	154.757
2	F	12	40C	35.9756
2	G	12	80C	76.1111
2	H	12	110C	100
3	A	1	YPR103W	121.369
3	B	1	YPR103W	92.7928
3	C	1	YBR135W	90.3797
3	D	1	YDR510W	74.8
3	E	1	YPR034W	65.3608
3	F	1	YIL126W	63.7037

10	H	6	YGL048C	113.6552
10	A	7	YGR098C	122.5806
10	B	7	YNL267W	126.5179
10	C	7	YDR050C	102.1429
10	D	7	YOR336W	93.05556
10	E	7	YOR257W	92.97125
10	F	7	YDR052C	93.17308
10	G	7	YBR160W	99.82301
10	H	7	YGR120C	119.3264
10	A	8	YGR172C	107.7951
10	B	8	YNL267W	113.6585
10	C	8	YDL014W	79.7973
10	D	8	YFL039C	94.87705
10	E	8	YOR257W	79.80998
10	F	8	YDR052C	69.73995
10	G	8	YML031W	102.2131
10	H	8	YIL048W	119.7802
10	A	9	YGR172C	96.11307
10	B	9	YBR237W	116.4151
10	C	9	YDR208W	100
10	D	9	YFL039C	92.15017
10	E	9	YDL105W	118.7574
10	F	9	YPL209C	110.9816
10	G	9	YBR110W	105.3846
10	H	9	YIL109C	105.5762
10	A	10	BY4741	116.5789
10	B	10	YMR235C	170.3833
10	C	10	YLR314C	124.3262
10	D	10	YFL039C	110.1961
10	E	10	YBR109C	95.69231
10	F	10	YDL028C	106.1184
10	G	10	YDL105W	144.6715
10	H	10	YKL145W	115.698
10	A	11	YML049C	106.2147
10	B	11	YPL085W	94.48
10	C	11	YDL017W	69.87879
10	D	11	YPR176C	98.73239
10	E	11	YBR109C	70.95745
10	F	11	YDL028C	109.5238
10	G	11	YDL126C	113.172
10	H	11	YKL210W	151.9084
10	A	12	YPL266W	84.16422
10	B	12	YAL003W	65.38462
10	C	12	YKL104C	103.4934
10	D	12	BY4741	97.16418
10	E	12	W303	134.1053
10	F	12	40C	41.2
10	G	12	80C	71.57895
10	H	12	110C	90.27778
11	A	1	YML130C	127.7533
11	B	1	YFR037C	103.9409
11	C	1	YIL147C	115.814
11	D	1	YDR437W	61.60714
11	E	1	YDR437W	119.4853
11	F	1	YBL093C	79.26829

3	G	1	YFL034C-B	75.8333	11	G	1	YLR086W	61.09215
3	H	1	YDR356W	100.413	11	H	1	YDR356W	76.0101
3	A	2	YKR002W	NO CALL	11	A	2	YKR002W	137.457
3	B	2	YPL209C	97.6471	11	B	2	YPL209C	90.63444
3	C	2	YFL039C	103.659	11	C	2	YFL039C	118.7311
3	D	2	YOR181W	90.5333	11	D	2	YOR181W	88.53503
3	E	2	YGR113W	80.5195	11	E	2	YGR113W	69.05371
3	F	2	YFL037W	62.8916	11	F	2	YFL037W	80.58252
3	G	2	YLR397C	89.4737	11	G	2	YLR397C	91.99085
3	H	2	W303	142.994	11	H	2	W303	143.8298
3	A	3	BY4741	88.1381	11	A	3	YFR037C	137.5309
3	B	3	YLR088W	82.6923	11	B	3	YLR088W	84.92936
3	C	3	YFL039C	83.3333	11	C	3	YFL039C	89.32886
3	D	3	YJL019W	79.0698	11	D	3	YDL105W	92.64706
3	E	3	YGR113W	98.4259	11	E	3	YGR113W	116.0169
3	F	3	YHR027C	81.7333	11	F	3	YHR027C	92.14286
3	G	3	YNL207W	105.139	11	G	3	YNL207W	77.08649
3	H	3	YFL034C-B	105.376	11	H	3	YOL144W	110.661
3	A	4	YLL031C	97.7778	11	A	4	YLL031C	96.80851
3	B	4	YDL126C	85.5128	11	B	4	YDL126C	92.61214
3	C	4	YFL039C	70.4808	11	C	4	YFL039C	98.51632
3	D	4	YOR122C	75.7292	11	D	4	YOR122C	105.9299
3	E	4	YGR113W	80.6122	11	E	4	YGR113W	99.66825
3	F	4	YOR204W	101.25	11	F	4	YDR188W	119.7309
3	G	4	YOR157C	71.2	11	G	4	YOR157C	87.5
3	H	4	YGR099W	90.5045	11	H	4	YLR022C	102.5547
3	A	5	YLL031C	110.345	11	A	5	YLL031C	130.402
3	B	5	YDL126C	82.0513	11	B	5	YDL126C	95.29086
3	C	5	YGR140W	88.8016	11	C	5	YGR140W	85.33333
3	D	5	YOR122C	91.3386	11	D	5	YOR122C	87.56098
3	E	5	YGR113W	83.4983	11	E	5	YGR113W	82.31707
3	F	5	YBR143C	77.4775	11	F	5	YHR058C	92.33038
3	G	5	YOR326W	71.1735	11	G	5	YOR326W	83.75
3	H	5	YFL034C-B	63.1405	11	H	5	YPR161C	99.80989
3	A	6	YLR026C	73.3509	11	A	6	YLR026C	103.5602
3	B	6	YJL034W	77.6763	11	B	6	YJL034W	86.46739
3	C	6	YLR457C	99.2308	11	C	6	YLR457C	97.60192
3	D	6	YLL050C	86.0465	11	D	6	YLL050C	92.65487
3	E	6	YIL144W	90.0631	11	E	6	YIL144W	85.92593
3	F	6	YDL007W	73.1169	11	F	6	YLR186W	78.54015
3	G	6	YPL228W	77.728	11	G	6	YPL228W	89.83051
3	H	6	YFL034C-B	93.4568	11	H	6	YPR161C	107.4405
3	A	7	YLR078C	96.5517	11	A	7	YLR078C	124.7134
3	B	7	YPL160W	72.2222	11	B	7	YHR088W	82.22222
3	C	7	YFL039C	93.8158	11	C	7	YFL039C	104.7337
3	D	7	YAL034W-A	73.7705	11	D	7	YAL034W-A	104.0964
3	E	7	YLL036C	89.0671	11	E	7	YLL036C	109.5031
3	F	7	YJL074C	58.4867	11	F	7	YJL074C	78.13559
3	G	7	YGL145W	85.2577	11	G	7	YGL145W	83.72093
3	H	7	YNL061W	87.3786	11	H	7	YPR161C	110.6796
3	A	8	YLR459W	86.5385	11	A	8	YLR459W	105.1282
3	B	8	YOR075W	81.1613	11	B	8	YOR075W	94.7205
3	C	8	YOR181W	71.4286	11	C	8	YKL052C	79.87988
3	D	8	YBR156C	84.9576	11	D	8	YBR156C	80.7393
3	E	8	YLL050C	89.3293	11	E	8	YLL050C	95.49839

3	F	8	YOR259C	84.0979
3	G	8	YFR027W	80.8383
3	H	8	YMR005W	48.3019
3	A	9	YLR459W	91.5385
3	B	9	YLR378C	121.673
3	C	9	YML064C	79.6831
3	D	9	YER013W	80.0429
3	E	9	YDR060W	83.8816
3	F	9	YLR086W	56.8889
3	G	9	YAR007C	70
3	H	9	YOL123W	72.9938
3	A	10	YLR459W	88.2895
3	B	10	YFL039C	86.9512
3	C	10	YFR028C	90.3974
3	D	10	YGR113W	87.6056
3	E	10	YDR060W	85.1673
3	F	10	YLR127C	82.8169
3	G	10	YBL034C	83.3811
3	H	10	YOR046C	140.226
3	A	11	YML130C	103.942
3	B	11	YFL039C	98.5663
3	C	11	YGR179C	86.0177
3	D	11	YGL061C	77.5281
3	E	11	YDR189W	77.0283
3	F	11	YOR259C	88.3289
3	G	11	YBL076C	77.8378
3	H	11	YPR033C	87.8049
3	A	12	YOR149C	91.0582
3	B	12	YFL039C	77.6829
3	C	12	YOR074C	57.4809
3	D	12	BY4741	74.7059
3	E	12	W303	141
3	F	12	40C	37.25
3	G	12	80C	54.3333
3	H	12	110C	111.818
4	A	1	YER012W	144.181
4	B	1	YDR356W	94.1026
4	C	1	YLR268W	103.364
4	D	1	YCL059C	89.7172
4	E	1	YOR326W	69.5652
4	F	1	YPR175W	50.1825
4	G	1	YDL030W	103.167
4	H	1	YGL097W	69.5455
4	A	2	YGR185C	97
4	B	2	YJL090C	42.788
4	C	2	YDL165W	98.8636
4	D	2	YCL059C	80.875
4	E	2	YNR011C	72.5974
4	F	2	YDR460W	112.048
4	G	2	YNL102W	56.875
4	H	2	W303	135.735
4	A	3	YHR186C	125.856
4	B	3	YMR117C	81.5982
4	C	3	YDR168W	91.2698
4	D	3	YDL090C	94.3137

11	F	8	YOR259C	93.40659
11	G	8	YFR027W	93.90698
11	H	8	YOL021C	107.4074
11	A	9	YLR459W	112.1655
11	B	9	YLR378C	193.36
11	C	9	YML064C	90.625
11	D	9	YER013W	127.809
11	E	9	YDR060W	89.57854
11	F	9	YLR430W	86.72377
11	G	9	YAR007C	110.2062
11	H	9	YKL024C	109.8592
11	A	10	YLR459W	106.2099
11	B	10	YFL039C	102.965
11	C	10	YKL052C	82.27723
11	D	10	YGR113W	93.57616
11	E	10	YDR060W	80.26316
11	F	10	YLR127C	98.34746
11	G	10	YBL034C	76.5678
11	H	10	YKL024C	113.2597
11	A	11	BY4741	99.66346
11	B	11	YFL039C	115.528
11	C	11	YGR179C	111.8705
11	D	11	YGL061C	80.20654
11	E	11	YDR189W	98.56734
11	F	11	YOR259C	146.0976
11	G	11	YBL076C	88.78788
11	H	11	YKL024C	106.9767
11	A	12	YOR149C	104.3723
11	B	12	YFL039C	96.46302
11	C	12	YPR133C	88.22642
11	D	12	BY4741	89.80263
11	E	12	W303	138.2114
11	F	12	40C	32.83019
11	G	12	80C	66.61972
11	H	12	110C	93.23944
12	A	1	YER012W	94.02597
12	B	1	YDR356W	83.82239
12	C	1	YLR268W	77.77293
12	D	1	YCL059C	85.49849
12	E	1	YOR326W	64.97758
12	F	1	YPR175W	40.24648
12	G	1	YDL030W	105.2434
12	H	1	YHR036W	75.64103
12	A	2	YGR185C	93.45455
12	B	2	YJL090C	39.58106
12	C	2	YDL165W	76.22222
12	D	2	YCL059C	75.71942
12	E	2	YNR011C	86.05442
12	F	2	YHR036W	72.33607
12	G	2	YNL102W	52.33333
12	H	2	W303	155.5066
12	A	3	YHR186C	104.4643
12	B	3	YMR117C	92.60563
12	C	3	YDR168W	80.8046
12	D	3	YDL090C	80.29703

4	E	3	YGL207W	91.3924	12	E	3	YGL207W	86.22642
4	F	3	YLL004W	64.4986	12	F	3	YLL004W	58.64286
4	G	3	YPL082C	93.9467	12	G	3	YPL082C	92
4	H	3	YDR167W	125.882	12	H	3	YLR007W	91.92982
4	A	4	BY4741	80.8511	12	A	4	YJL001W	98.77907
4	B	4	YAL041W	79.9412	12	B	4	YAL041W	83.67347
4	C	4	YIL046W	76.2226	12	C	4	YPR108W	84.5953
4	D	4	YJR045C	80.6667	12	D	4	YJR045C	83.0814
4	E	4	YIR008C	61.8788	12	E	4	YIR008C	55.25547
4	F	4	YHR164C	134.783	12	F	4	YHR164C	101.7483
4	G	4	YPR055W	93.5985	12	G	4	YPR055W	85.65891
4	H	4	YER168C	105.731	12	H	4	YKL021C	79.27273
4	A	5	YMR117C	116.406	12	A	5	YMR117C	102.1667
4	B	5	YNR026C	109.035	12	B	5	YNR026C	110.4545
4	C	5	YDR168W	79.0357	12	C	5	YDR168W	66.91011
4	D	5	YPL093W	75.3351	12	D	5	YPL093W	77.77778
4	E	5	YJR065C	91.1067	12	E	5	YJR065C	#VALUE!
4	F	5	YIR006C	110.14	12	F	5	YIR006C	121.8254
4	G	5	YBL035C	48.3879	12	G	5	YBL035C	33.22785
4	H	5	YLL031C	85.4386	12	H	5	YLR117C	91.70103
4	A	6	YMR168C	106.224	12	A	6	YMR168C	97.7381
4	B	6	YOL139C	95.297	12	B	6	YOL139C	88.77828
4	C	6	YIR022W	82.3322	12	C	6	YIR022W	79.62025
4	D	6	YPR183W	100.276	12	D	6	YPR183W	86.98061
4	E	6	YJR068W	54.9176	12	E	6	YJR068W	58.13896
4	F	6	YJL005W	104.032	12	F	6	YJL005W	93.62869
4	G	6	YOR174W	67.8431	12	G	6	YHR036W	69.08497
4	H	6	YOL123W	74.7742	12	H	6	YFL017C	54.17969
4	A	7	YBR060C	72.7572	12	A	7	YBR060C	#VALUE!
4	B	7	YFL005W	88.2158	12	B	7	YFL005W	88.08333
4	C	7	YKL112W	106.796	12	C	7	YKL112W	106.2016
4	D	7	YBR060C	92.7126	12	D	7	YBR060C	79.42149
4	E	7	YNL102W	49.2509	12	E	7	YNL102W	37.09602
4	F	7	YGL130W	84.7436	12	F	7	YGL130W	72.05882
4	G	7	YBR055C	83.2278	12	G	7	YBR055C	82.7027
4	H	7	YDL132W	115.459	12	H	7	YMR229C	86.47959
4	A	8	YJR065C	103.125	12	A	8	YJR065C	#VALUE!
4	B	8	YDR054C	67.6923	12	B	8	YDR054C	98.83041
4	C	8	YMR220W	98.8095	12	C	8	YMR220W	89.88506
4	D	8	YBR135W	97.4708	12	D	8	YBR135W	96.78363
4	E	8	YNL102W	70.6618	12	E	8	YNL102W	#VALUE!
4	F	8	YJR076C	89.1837	12	F	8	YJR076C	110.9917
4	G	8	YGL116W	81.7552	12	G	8	YGL116W	75.25714
4	H	8	YDL084W	114.685	12	H	8	YDL132W	96.44269
4	A	9	YJR065C	81.0526	12	A	9	YJR065C	100.2451
4	B	9	YBR060C	54.3262	12	B	9	YBR060C	50.17123
4	C	9	YFL008W	97.4504	12	C	9	YFL008W	84.97076
4	D	9	YGL155W	121.136	12	D	9	YGL155W	86.33484
4	E	9	YNL102W	85.0988	12	E	9	YNL102W	57.52809
4	F	9	YBR236C	79.6117	12	F	9	YBR236C	81.90255
4	G	9	YDL043C	91.2069	12	G	9	YDL043C	81.55462
4	H	9	YGR098C	102.202	12	H	9	YDL084W	81.52381
4	A	10	YJR065C	114.815	12	A	10	YJR065C	100.7905
4	B	10	YLR215C	90.7216	12	B	10	YDL097C	88.33922
4	C	10	YHR191C	49.0602	12	C	10	YHR191C	76.97436

4	D	10	YFL009W	70.2413
4	E	10	YNL102W	46.7949
4	F	10	YGL130W	69.2552
4	G	10	YDL064W	93.7662
4	H	10	YGR172C	97.5904
4	A	11	YJR065C	114.34
4	B	11	YBR060C	104.856
4	C	11	YHR191C	76.3462
4	D	11	YKL112W	101.609
4	E	11	YKL049C	86.8966
4	F	11	YLR321C	70.3431
4	G	11	YDR331W	95.1389
4	H	11	YGR172C	104.054
4	A	12	YJL001W	103.416
4	B	12	YIL046W	92.987
4	C	12	YBL034C	77.4105
4	D	12	BY4741	75.8865
4	E	12	W303	127.5
4	F	12	40C	37.8049
4	G	12	80C	74.4
4	H	12	110C	100.246
5	A	1	YGR075C	102.974
5	B	1	YFR037C	95.3723
5	C	1	YIL147C	87.4269
5	D	1	YKL052C	89.172
5	E	1	YLR272C	50.9559
5	F	1	YGL075C	69.1958
5	G	1	YIL109C	73.7931
5	H	1	YNR035C	100.816
5	A	2	YML049C	103.595
5	B	2	YKL203C	75.6774
5	C	2	YAL041W	96.8627
5	D	2	YMR013C	79.0132
5	E	2	YGR006W	87.8571
5	F	2	YGL093W	74.2616
5	G	2	YIL150C	67.1649
5	H	2	W303	158.333
5	A	3	YPL266W	84.7895
5	B	3	YDR373W	84.6377
5	C	3	YKL052C	75.8247
5	D	3	YGL073W	73.4375
5	E	3	YIR010W	84.3434
5	F	3	YGR103W	76.4045
5	G	3	YLL003W	72.1569
5	H	3	YNR035C	105.35
5	A	4	YAL003W	87.3684
5	B	4	YGR091W	77.3788
5	C	4	YAL041W	76.3314
5	D	4	YNL261W	69.4444
5	E	4	YIR010W	73.5897
5	F	4	YDR212W	65.9615
5	G	4	YGR218W	120
5	H	4	YGR091W	88.024
5	A	5	BY4741	92.3214
5	B	5	YJL203W	84.3243

12	D	10	YFL009W	84.74359
12	E	10	YNL102W	38.39357
12	F	10	YGL130W	76.72634
12	G	10	YDL064W	90.51095
12	H	10	YGR098C	85.90909
12	A	11	YJR065C	69.65957
12	B	11	YBR060C	91.27907
12	C	11	YHR191C	72.66667
12	D	11	YKL112W	91.68421
12	E	11	YKL049C	83.04147
12	F	11	YHR036W	103.7681
12	G	11	YDR331W	92.09979
12	H	11	YGR172C	96.91667
12	A	12	BY4741	101.4773
12	B	12	YDL147W	83.77778
12	C	12	YHR036W	101.7857
12	D	12	BY4741	87.85714
12	E	12	W303	121.1765
12	F	12	40C	30.40404
12	G	12	80C	62.59843
12	H	12	110C	86.375
13	A	1	YGR172C	#VALUE!
13	B	1	BY4741	83.33333
13	C	1	YHR088W	83.67347
13	D	1	YIL147C	80.55556
13	E	1	YOR181W	100.5495
13	F	1	YOR181W	83.03571
13	G	1	YFL034C-B	81.02679
13	H	1	YIL046W	103.7975
13	A	2	YML049C	101.2195
13	B	2	YFL009W	92.33577
13	C	2	YDR196C	63.91185
13	D	2	YNL222W	70.66116
13	E	2	YOR048C	58.90411
13	F	2	YFR028C	75.04873
13	G	2	YGR099W	86.48649
13	H	2	W303	156.4767
13	A	3	YPL266W	93.11475
13	B	3	YMR001C	73.60483
13	C	3	YOR257W	67.19764
13	D	3	YDR208W	61.74377
13	E	3	YPR103W	73.42857
13	F	3	YOR074C	69.15709
13	G	3	YFL034C-B	#VALUE!
13	H	3	YDR460W	99.34498
13	A	4	YAL003W	#VALUE!
13	B	4	YDL017W	78.78788
13	C	4	YKL189W	63.27609
13	D	4	YFL039C	68.94737
13	E	4	YPR103W	92.20056
13	F	4	YDR510W	123.1707
13	G	4	YFL034C-B	70.43478
13	H	4	YLR321C	44.31818
13	A	5	YDR050C	96.61972
13	B	5	YDL220C	83.65385

5	C	5	YDR182W	103.226	13	C	5	YKL018W	94.04762
5	D	5	YKR083C	89.3889	13	D	5	YOR335C	82.26601
5	E	5	YJL019W	78.0627	13	E	5	YPR103W	57.32759
5	F	5	YKL042W	94.7059	13	F	5	YJL019W	61.92771
5	G	5	YGL065C	88.75	13	G	5	YNL061W	71.77419
5	H	5	YER018C	98.5227	13	H	5	YOR174W	84.77032
5	A	6	YDR050C	110.519	13	A	6	YKL104C	116.9065
5	B	6	YMR268C	78.0781	13	B	6	YAR019C	78.35165
5	C	6	YDR182W	90.4274	13	C	6	YJR065C	#VALUE!
5	D	6	YMR277W	100.081	13	D	6	YGL048C	94.38202
5	E	6	YJR112W	76.8667	13	E	6	YPR103W	74.50704
5	F	6	YPL233W	74.4141	13	F	6	YPR034W	82.97214
5	G	6	YPL076W	80.3279	13	G	6	YMR005W	85.92814
5	H	6	YPL175W	97.6959	13	H	6	YBL034C	71.47708
5	A	7	YKL104C	96.679	13	A	7	YBR079C	99.07407
5	B	7	YLR274W	77	13	B	7	YKL022C	85.14851
5	C	7	YFL009W	65.4583	13	C	7	YGR002C	61.6179
5	D	7	YOR057W	172.5	13	D	7	YGL048C	83.90411
5	E	7	YJR112W	78.9423	13	E	7	YKL052C	76.14555
5	F	7	YKL042W	80.9583	13	F	7	YIL126W	56.88889
5	G	7	YPL076W	89.6074	13	G	7	YOL123W	73.17744
5	H	7	YLL003W	80.0712	13	H	7	YGL097W	68.72428
5	A	8	YBR079C	99.2063	13	A	8	YDL105W	125.3968
5	B	8	YHR088W	84.8485	13	B	8	YOR236W	62.72727
5	C	8	YFR028C	102.895	13	C	8	YJL097W	67.46988
5	D	8	YPL252C	86.5132	13	D	8	YLR071C	89.18919
5	E	8	YJR112W	102.553	13	E	8	YKL052C	96.36049
5	F	8	YPL233W	72.0144	13	F	8	YOR204W	92.33512
5	G	8	YER125W	84.4488	13	G	8	YOR046C	87.24138
5	H	8	YER148W	95.4683	13	H	8	YOL123W	110.9677
5	A	9	YDL105W	124.142	13	A	9	YDL105W	93.59606
5	B	9	YFR052W	94.8214	13	B	9	YLR314C	83.84146
5	C	9	YGL116W	87.9093	13	C	9	YNL102W	#VALUE!
5	D	9	YOR122C	87.8261	13	D	9	YFL039C	62.06452
5	E	9	YDL058W	81.2016	13	E	9	YPR103W	94.37148
5	F	9	YPR133C	63.4783	13	F	9	YBR143C	115.7143
5	G	9	YER125W	87.1972	13	G	9	YPR033C	101.6854
5	H	9	YGR156W	93.8938	13	H	9	YDR167W	82.22857
5	A	10	YDL105W	121.32	13	A	10	YDL105W	143.865
5	B	10	YDL102W	81.4727	13	B	10	YDL029W	108.2102
5	C	10	YNL258C	46.8033	13	C	10	YGL116W	85.55556
5	D	10	YGR006W	101.333	13	D	10	YFL039C	98.86364
5	E	10	YNL062C	86.9014	13	E	10	YPL160W	81.12245
5	F	10	YBL034C	79.2308	13	F	10	YDL007W	94.76662
5	G	10	YNL006W	113.855	13	G	10	YLR215C	82.22973
5	H	10	YGR246C	90.1734	13	H	10	YER168C	100.7519
5	A	11	YDL105W	108.411	13	A	11	YFR037C	119.3069
5	B	11	YJR057W	79.863	13	B	11	YBR087W	77.39726
5	C	11	YPL228W	85.3922	13	C	11	YCR002C	65.66667
5	D	11	YJL050W	55.9356	13	D	11	YFL039C	104.7727
5	E	11	YGL075C	76.5625	13	E	11	YBR135W	91.22807
5	F	11	YBR055C	95.493	13	F	11	YFL034C-B	72.38095
5	G	11	YNL006W	99.8864	13	G	11	YIL046W	77.06271
5	H	11	YNR053C	138.439	13	H	11	YLL031C	85.14851
5	A	12	YFR037C	92.7778	13	A	12	YFR037C	117.3442

5	B	12	YAL041W	90.6977
5	C	12	YPL228W	127.5
5	D	12	BY4741	78.4791
5	E	12	W303	154.561
5	F	12	40C	32.3077
5	G	12	80C	61.7857
5	H	12	110C	119.565
6	A	1	YPL020C	113.948
6	B	1	YPR161C	104.762
6	C	1	YOR232W	93.8983
6	D	1	YDR145W	86.3636
6	E	1	YKL172W	82.7397
6	F	1	YBL105C	75.3409
6	G	1	YIL115C	77.6471
6	H	1	YOR244W	106.827
6	A	2	YDR437W	88.785
6	B	2	YML046W	90.7042
6	C	2	YGL055W	84.6899
6	D	2	YDR145W	90.2692
6	E	2	YOR341W	94.2017
6	F	2	YBR247C	91.5094
6	G	2	YHR036W	94.0625
6	H	2	W303	151.379
6	A	3	YDL105W	80.4587
6	B	3	YMR033W	78.5
6	C	3	YIL126W	48
6	D	3	YER022W	100.99
6	E	3	YPL028W	97.8622
6	F	3	YBR265W	92.4157
6	G	3	YLR045C	86.4686
6	H	3	YBR155W	80.4938
6	A	4	YDR437W	156.643
6	B	4	YJL039C	93.1122
6	C	4	YAL001C	87.1345
6	D	4	YDL147W	95.9184
6	E	4	YOR341W	97.6898
6	F	4	YHR036W	93.7391
6	G	4	YNL075W	90.6336
6	H	4	YBR123C	120.2
6	A	5	YBL093C	91.0256
6	B	5	YLR163C	82.881
6	C	5	YBR198C	90.9722
6	D	5	YFR004W	72.5606
6	E	5	YEL019C	107.657
6	F	5	YLR045C	92.891
6	G	5	YOR204W	92.3902
6	H	5	YOR329C	102.244
6	A	6	BY4741	96
6	B	6	YKR008W	78.2051
6	C	6	YKL024C	93.5714
6	D	6	YFR031C	66.045
6	E	6	YFR004W	94.5295
6	F	6	YGL137W	85.7934
6	G	6	YNL216W	75.5172
6	H	6	YOR329C	96.7864

13	B	12	YIL062C	73.14949
13	C	12	YPR181C	80.66667
13	D	12	BY4741	90.36199
13	E	12	W303	130.4545
13	F	12	40C	37.81609
13	G	12	80C	55.05747
13	H	12	110C	97.6
14	A	1	YPR133C	#VALUE!
14	B	1	YFL009W	98.16456
14	C	1	YDR196C	92.30769
14	D	1	YNL222W	83.18681
14	E	1	YOR048C	65.01976
14	F	1	YFR028C	78.81356
14	G	1	YGR099W	95.79288
14	H	1	YBL034C	81.05991
14	A	2	YDR437W	82.46154
14	B	2	BY4741	84.3949
14	C	2	YOR257W	59.04908
14	D	2	YDR208W	60.75949
14	E	2	YPR103W	73.69942
14	F	2	YOR074C	68.39187
14	G	2	YFL034C-B	67.34694
14	H	2	W303	152.64
14	A	3	YDL105W	113.1008
14	B	3	YDL017W	71.09929
14	C	3	YKL189W	72.34957
14	D	3	YFL039C	76.81416
14	E	3	YPR103W	83.62832
14	F	3	YDR510W	77.61506
14	G	3	YFL034C-B	63.22581
14	H	3	YLR321C	74.36364
14	A	4	YDR437W	130.8448
14	B	4	YDL220C	77.76316
14	C	4	YKL018W	72.58824
14	D	4	YOR335C	88.21918
14	E	4	YPR103W	71.13924
14	F	4	YJL019W	58.61702
14	G	4	YNL061W	66.1157
14	H	4	YOR174W	78.49206
14	A	5	YBL093C	75.2381
14	B	5	YAR019C	91.96429
14	C	5	YJR065C	69.33702
14	D	5	YGL048C	84.31373
14	E	5	YPR103W	58.42239
14	F	5	YPR034W	77.47126
14	G	5	YMR005W	82.83784
14	H	5	YKL024C	108.8141
14	A	6	YDR188W	158.0071
14	B	6	YKL022C	#VALUE!
14	C	6	YGR002C	67.97235
14	D	6	YGL048C	67.83688
14	E	6	YPR161C	91.9708
14	F	6	YIL126W	66.00362
14	G	6	YOL123W	65
14	H	6	YGL097W	79.67213

6	A	7	YDR188W	95.3125	14	A	7	YHR058C	95.90747
6	B	7	YPR161C	92.1053	14	B	7	YOR236W	82.28814
6	C	7	YKL024C	83.9344	14	C	7	YJL097W	75.22727
6	D	7	YGR245C	89.7747	14	D	7	YLR071C	87.03448
6	E	7	YBL105C	104.833	14	E	7	YOL021C	82.49337
6	F	7	YGR211W	136.25	14	F	7	YOR204W	41.11111
6	G	7	YNL216W	83.8053	14	G	7	YOR046C	98.33333
6	H	7	YBR058C-A	100.632	14	H	7	YDR460W	114.2857
6	A	8	YHR058C	99.422	14	A	8	YLR186W	103.0207
6	B	8	YPR178W	91.0843	14	B	8	YLR314C	77.27273
6	C	8	YBR198C	150.5	14	C	8	YNL102W	58.24847
6	D	8	YGR274C	90.375	14	D	8	YFL039C	65.60606
6	E	8	YPR108W	83.1752	14	E	8	YPR103W	86.30573
6	F	8	YGR216C	94.3254	14	F	8	YBR143C	72.7957
6	G	8	YOR244W	117.986	14	G	8	YPR033C	111.5232
6	H	8	YKL193C	99.3304	14	H	8	YDR167W	112.7083
6	A	9	YLR186W	124.675	14	A	9	YLR430W	112.2137
6	B	9	YPR161C	108.371	14	B	9	YDL029W	84.35277
6	C	9	YBR198C	98.0952	14	C	9	YGL116W	115.4054
6	D	9	YGR274C	94.4488	14	D	9	YFL039C	84.40367
6	E	9	YBL105C	107.926	14	E	9	YPL160W	67.33068
6	F	9	YLR045C	81.875	14	F	9	YDL007W	94.16058
6	G	9	YOR204W	104.172	14	G	9	YLR215C	72.50554
6	H	9	YKL193C	145.424	14	H	9	YER168C	84.27152
6	A	10	YLR430W	102.29	14	A	10	YOL144W	101.0909
6	B	10	YOL021C	74.7664	14	B	10	YBR087W	57.60728
6	C	10	YDR145W	120.169	14	C	10	YCR002C	76.3285
6	D	10	YHR024C	91.0938	14	D	10	YFL039C	82.29508
6	E	10	YBL105C	102.366	14	E	10	YBR135W	130.9859
6	F	10	YLR045C	86.7978	14	F	10	YFL034C-B	71.67139
6	G	10	YHR036W	96.063	14	G	10	YIL046W	72.53521
6	H	10	YDR243C	105.882	14	H	10	YLL031C	73.89937
6	A	11	YOL144W	110.714	14	A	11	YLR022C	124.8889
6	B	11	YDR303C	105.952	14	B	11	YIL062C	68.80952
6	C	11	YDR145W	95.411	14	C	11	YPR181C	86.53846
6	D	11	YKL125W	133.043	14	D	11	YOR181W	100.6
6	E	11	YBL105C	100.838	14	E	11	YOR181W	88.59316
6	F	11	YGL022W	102.743	14	F	11	YFL034C-B	74.10256
6	G	11	YOR244W	112.542	14	G	11	YIL046W	79.56522
6	H	11	YDR062W	140.381	14	H	11	YOL123W	109.5
6	A	12	YLR022C	125.064	14	A	12	YPR161C	110.7759
6	B	12	YKL024C	129.01	14	B	12	YMR001C	45.75243
6	C	12	YDL097C	105.789	14	C	12	YPR161C	113.3333
6	D	12	BY4741	86.7876	14	D	12	BY4741	82.67717
6	E	12	W303	109.535	14	E	12	W303	154.9231
6	F	12	40C	32.5	14	F	12	40C	40.9434
6	G	12	80C	69.0476	14	G	12	80C	56.88525
6	H	12	110C	106.522	14	H	12	110C	96.08333
7	A	1	YDR013W	35.7878	15	A	1	YKL024C	90.19608
7	B	1	YLR007W	110.748	15	B	1	YOR257W	74.41558
7	C	1	YFL017C	44.2601	15	C	1	YKL024C	83.49515
7	D	1	YMR229C	68.3486	15	D	1	YDL097C	92.81346
7	E	1	YNL061W	92.243	15	E	1	YDL147W	68.25397
7	F	1	YML098W	36.7105	15	F	1	YFL034C-B	79.7527
7	G	1	YER125W	86.9792	15	G	1	YIL046W	110.3448

7	H	1	YPL043W	75.2525
7	A	2	YDR325W	86.7089
7	B	2	YKL021C	80.9146
7	C	2	YMR296C	80.4813
7	D	2	YGR158C	57.6389
7	E	2	YNL061W	69.2929
7	F	2	YMR227C	90.9091
7	G	2	YFL029C	96.9869
7	H	2	W303	131.907
7	A	3	YHR036W	95.122
7	B	3	YFL038C	90.4762
7	C	3	YMR296C	112.595
7	D	3	YIL021W	85.9375
7	E	3	YNL061W	81.0976
7	F	3	YMR240C	93.6869
7	G	3	YDL084W	95.3795
7	H	3	YGR172C	75.2306
7	A	4	YDR361C	75.1786
7	B	4	YGL098W	67.9426
7	C	4	YGR099W	75.5618
7	D	4	YFL034C-B	74.1096
7	E	4	YNL061W	89.071
7	F	4	YNR003C	70.6564
7	G	4	YGL044C	90.6154
7	H	4	YGR172C	94.8276
7	A	5	YHR036W	90.407
7	B	5	YLR117C	90.3636
7	C	5	YHR170W	77.4266
7	D	5	YIR012W	73.7736
7	E	5	YML069W	73.494
7	F	5	YOR046C	70.9189
7	G	5	YJL173C	85.0794
7	H	5	YML049C	127.907
7	A	6	YDR002W	76.7778
7	B	6	YEL055C	73.2456
7	C	6	YMR296C	44.1463
7	D	6	YJL081C	72.7447
7	E	6	YNL061W	77.476
7	F	6	YPR110C	73.2222
7	G	6	YIL118W	85.7988
7	H	6	YPL266W	97.6
7	A	7	BY4741	83.1034
7	B	7	YEL055C	80.9574
7	C	7	YGL120C	90
7	D	7	YKL006C-A	91.3966
7	E	7	YDL132W	81.3834
7	F	7	YBL034C	68.917
7	G	7	YGR098C	79.8148
7	H	7	YAL003W	79.9035
7	A	8	YLR249W	89.2929
7	B	8	YEL055C	83.8264
7	C	8	YGL112C	85.2113
7	D	8	YJL125C	63.1034
7	E	8	YLR298C	87.9757
7	F	8	YKR086W	72.4632

15	H	1	YOL123W	121.52
15	A	2	YFL009W	137.4613
15	B	2	YDR196C	77.98165
15	C	2	YNL222W	89.10891
15	D	2	YOR048C	68.27068
15	E	2	YFR028C	94.89362
15	F	2	YGR099W	92.07921
15	G	2	YBL034C	112.6437
15	H	2	W303	146.0674
15	A	3	YMR001C	79.6875
15	B	3	BY4741	87.13911
15	C	3	YDR208W	74.28571
15	D	3	YPR103W	#VALUE!
15	E	3	YOR074C	89.02027
15	F	3	YFL034C-B	70.6422
15	G	3	YDR460W	101.2346
15	H	3	YHR036W	106.0976
15	A	4	YDL017W	96.89119
15	B	4	YKL189W	92.06349
15	C	4	YFL039C	93.27273
15	D	4	YPR103W	74.94253
15	E	4	YDR510W	105.1754
15	F	4	YFL034C-B	177.4359
15	G	4	YLR321C	87.32558
15	H	4	YHR036W	100
15	A	5	YDL220C	114.4444
15	B	5	YKL018W	100
15	C	5	YOR335C	93.68421
15	D	5	YPR103W	82.76316
15	E	5	YJL019W	93.06667
15	F	5	YNL061W	77.41935
15	G	5	YOR174W	91.61392
15	H	5	YHR036W	*141.115*
15	A	6	YAR019C	114.3072
15	B	6	YJR065C	84.92366
15	C	6	YGL048C	115.7025
15	D	6	YPR103W	92.68182
15	E	6	YPR034W	88.08989
15	F	6	YMR005W	77.0017
15	G	6	YPR108W	97.5
15	H	6	YHR036W	123.4401
15	A	7	YKL022C	108.642
15	B	7	YGR002C	81.91489
15	C	7	YGL048C	93.33333
15	D	7	YOR181W	63.1
15	E	7	YIL126W	#VALUE!
15	F	7	YOL123W	72.9682
15	G	7	YGL097W	57.93103
15	H	7	YLR007W	97.67442
15	A	8	YOR236W	101.5068
15	B	8	YJL097W	101.25
15	C	8	YLR071C	70.69307
15	D	8		#VALUE!
15	E	8	YOR204W	#VALUE!
15	F	8	YOR046C	100.7874

7	G	8	YDR088C	93.4028	15	G	8	YHR036W	106.8702
7	H	8	YDR050C	*119.565*	15	H	8	YKL021C	104.6667
7	A	9	YDR062W	110.864	15	A	9	YLR314C	120.2959
7	B	9	YDL030W	80.7775	15	B	9	YNL102W	85.59499
7	C	9	YFL034C-B	82.7523	15	C	9	YFL039C	66.91843
7	D	9	YKL173W	96.4	15	D	9	YPR103W	92.73927
7	E	9	YLR298C	82.5949	15	E	9	YBR143C	106.5719
7	F	9	YML015C	93.3929	15	F	9	YPR033C	112.9973
7	G	9	YDR088C	85.5446	15	G	9	YDR167W	103.2609
7	H	9	YKL104C	98.5202	15	H	9	YLR117C	104.6512
7	A	10	YDR062W	99.434	15	A	10	YDL029W	109.4099
7	B	10	YKR086W	99.789	15	B	10	YGL116W	98.54545
7	C	10	YFL034C-B	95.7944	15	C	10	YFL039C	115.3846
7	D	10	YKL173W	100.561	15	D	10	YPL160W	90.63291
7	E	10	YMR197C	77.1956	15	E	10	YDL007W	110.4816
7	F	10	YIL143C	67.953	15	F	10	YLR215C	88.26531
7	G	10	YER093C	92.2667	15	G	10	YER168C	98.58012
7	H	10	YBR079C	79.2291	15	H	10	YFL017C	60.14625
7	A	11	YDR062W	65.0515	15	A	11	YBR087W	124.1692
7	B	11	YDR082W	106.716	15	B	11	YCR002C	93.29268
7	C	11	YFL034C-B	77.2124	15	C	11	YFL039C	122.3404
7	D	11	YLR066W	73.2432	15	D	11	YBR135W	106.7391
7	E	11	YMR197C	103.004	15	E	11	YFL034C-B	78.97727
7	F	11	YLR298C	97.1119	15	F	11	YIL046W	97.23618
7	G	11	YER093C	81.7204	15	G	11	YLL031C	102.8169
7	H	11	YDL105W	154.583	15	H	11	YMR229C	109.8398
7	A	12	YER171W	103.425	15	A	12	YIL062C	120.4082
7	B	12	YMR296C	110.738	15	B	12	YPR181C	91.73554
7	C	12	YFL034C-B	80.5104	15	C	12	YOR181W	124.3243
7	D	12	BY4741	92	15	D	12	BY4741	87.58621
7	E	12	W303	124.161	15	E	12	W303	199.4186
7	F	12	40C	31.5686	15	F	12	40C	38.77778
7	G	12	80C	49.5	15	G	12	80C	65.43478
7	H	12	110C	110.345	15	H	12	110C	110.339
8	A	1	YMR239C	108	16	A	1	BY4741	122.1884
8	B	1	YDR228C	99.0476	16	B	1	W303	162.3116
8	C	1	YMR028W	84	16	C	1	40C	41.12628
8	D	1	YFR037C	85.5238	16	D	1	80C	53.13559
8	E	1	YDR238C	94.2222	16	E	1	110C	95.77236
8	F	1	YDR292C	92.1053	16	F	1	YLR378C	128.2653
8	G	1	YOR249C	76.8421	16	G	1	BY4741	95.75472
8	H	1	YKL052C	94.6667	16	H	1	W303	173.2026
8	A	2	YMR239C	93.3333	16	A	2	40C	49.01316
8	B	2	YDR228C	65.1064	16	B	2	80C	72.48996
8	C	2	YJR017C	103.023	16	C	2	110C	111.6
8	D	2	YML105C	77.314	16	D	2	YLR378C	110.0437
8	E	2	YDR238C	80.1042	16	E	2	BY4741	90.50279
8	F	2	YOR272W	84.1379	16	F	2	W303	151.5464
8	G	2	YOR249C	108.333	16	G	2	40C	44.32836
8	H	2	W303	156.774	16	H	2	80C	66.66667
8	A	3	YNL138W	120.604	16	A	3	110C	118.75
8	B	3	YOR294W	83.6559	16	B	3	YLR378C	150.6481
8	C	3	YKL028W	97	16	C	3	BY4741	96.64634
8	D	3	YDL087C	93.5484	16	D	3	W303	146.4844
8	E	3	YHR088W	88.6585	16	E	3	40C	35.74661

8	F	3	YJL002C	73.2222
8	G	3	YLR383W	86.8512
8	H	3	YKL052C	81.5789
8	A	4	YLR105C	98
8	B	4	YOR294W	102
8	C	4	YFR005C	93.7186
8	D	4	YDR478W	94.0741
8	E	4	YHR069C	82.6289
8	F	4	YEL034W	71.3008
8	G	4	YGR074W	91.1111
8	H	4	YPR133C	86.9
8	A	5	YGR048W	94.0556
8	B	5	YPL010W	84.8447
8	C	5	YDR311W	57.6374
8	D	5	YHR052W	79.1489
8	E	5	YLR440C	102.96
8	F	5	YEL034W	94.9007
8	G	5	YEL034W	90.1064
8	H	5	YDR437W	87.395
8	A	6	YPL217C	137.982
8	B	6	YLR195C	97.8571
8	C	6	YMR213W	99.2063
8	D	6	YDL217C	103.103
8	E	6	YLR440C	97.0833
8	F	6	YOR174W	63.5714
8	G	6	YEL034W	108.75
8	H	6	YDL105W	75.082
8	A	7	YDR228C	111.099
8	B	7	YPL255W	85.7265
8	C	7	YDL105W	134.043
8	D	7	YDR311W	115.033
8	E	7	YOL034W	86.8519
8	F	7	YOL135C	87.2611
8	G	7	YBR193C	103.784
8	H	7	YDR437W	132.19
8	A	8	BY4741	102.642
8	B	8	YKR062W	90.9746
8	C	8	YDL145C	104.286
8	D	8	YBR211C	107.059
8	E	8	YDR021W	86.8103
8	F	8	YOL135C	105.036
8	G	8	YLR005W	98.3838
8	H	8	YBL093C	80.6557
8	A	9	YOR020C	137.5
8	B	9	YOR151C	136.61
8	C	9	YJR046W	56.3107
8	D	9	YLR212C	174.932
8	E	9	YDL143W	169.487
8	F	9	YBR193C	104.966
8	G	9	YIL147C	91.9231
8	H	9	YDR188W	106.912
8	A	10	YMR308C	111.905
8	B	10	YLR103C	47.0213
8	C	10	YPL124W	87.6
8	D	10	YLR212C	158.478

16	F	3	80C	66.69903
16	G	3	110C	103.3333
16	H	3	YLR378C	142.1176
16	A	4	YLR378C	154.3357
16	B	4	110C	105.493
16	C	4	80C	63.87931
16	D	4	40C	38.30396
16	E	4	W303	142.4286
16	F	4	BY4741	95.9292
16	G	4	YLR378C	130.708
16	H	4	110C	124.812
16	A	5	80C	76.06061
16	B	5	40C	54.7619
16	C	5	W303	168.3673
16	D	5	BY4741	94.93671
16	E	5	YLR378C	131.4504
16	F	5	110C	94.68182
16	G	5	80C	91.02041
16	H	5	40C	39.87603
16	A	6	W303	174.5763
16	B	6	BY4741	102.0231
16	C	6	YLR378C	104.8113
16	D	6	110C	105.3628
16	E	6	80C	66.3964
16	F	6	40C	43.23333
16	G	6	W303	158.011
16	H	6	BY4741	109.9788
16	A	7	W303	179.5041
16	B	7	80C	70.87413
16	C	7	YLR378C	109.8571
16	D	7	BY4741	97.76536
16	E	7	40C	38.75
16	F	7	110C	114.2647
16	G	7	W303	165.5085
16	H	7	80C	74.16357
16	A	8	YLR378C	150.678
16	B	8	BY4741	114.1649
16	C	8	40C	41.70455
16	D	8	110C	112.1512
16	E	8	W303	131.7757
16	F	8	80C	65.13944
16	G	8	YLR378C	139.8148
16	H	8	BY4741	117.1582
16	A	9	40C	46.03922
16	B	9	110C	103.04
16	C	9	W303	150.4
16	D	9	80C	60.93284
16	E	9	YLR378C	119.2
16	F	9	BY4741	99.03288
16	G	9	40C	39.71944
16	H	9	110C	125.4019
16	A	10	BY4741	134.3096
16	B	10	40C	46.30769
16	C	10	110C	96.74242
16	D	10	W303	145.5195

8	E	10	YMR236W	86.5385	16	E	10	80C	64.63687
8	F	10	YGL001C	95.5932	16	F	10	YLR378C	131.5
8	G	10	YNL118C	57.2222	16	G	10	BY4741	113.4694
8	H	10	YHR058C	105.8	16	H	10	40C	42.85171
8	A	11	YMR308C	90	16	A	11	110C	118.4699
8	B	11	YML114C	125.69	16	B	11	W303	148.8688
8	C	11	YPL124W	85.2273	16	C	11	80C	58.44961
8	D	11	YDL008W	127.895	16	D	11	YLR378C	142
8	E	11	YKL154W	56.6667	16	E	11	BY4741	100.2653
8	F	11	YNL118C	91.4286	16	F	11	40C	40.11628
8	G	11	YOL069W	90.2857	16	G	11	110C	121.3636
8	H	11	YLR186W	130.857	16	H	11	W303	192.7273
8	A	12	YDR228C	112.373	16	A	12	80C	70.42194
8	B	12	YDL105W	112.254	16	B	12	YLR378C	133.1897
8	C	12	YFR037C	97.4468	16	C	12	BY4741	116.9643
8	D	12	BY4741	85.2525	16	D	12	40C	42.6087
8	E	12	W303	164.545	16	E	12	110C	109.3023
8	F	12	40C	35.6522	16	F	12	W303	164.8276
8	G	12	80C	53.0208	16	G	12	80C	61.56098
8	H	12	110C	100.984	16	H	12	YLR378C	145.0794

Appendix A.2 rDNA copy number and karyotype in top 89 hits with low rDNA copy number

Key

rDNA CN < Mean WT CN - 2SD	Significant change in copy number
Mean WT CN - 2SD < rDNA CN < Mean WT CN - SD	Moderate change in copy number
< 10,000 total droplets	No quantification
< 10 copies/uL TUB1 or rDNA	Less accurate quantification
No or too few FAM and/or HEX negative droplets	No quantification
ChrXII/ChrXIII significantly different from 1.	Unreliable copy number measurement

Destination Wells	Systematic name	rDNA Copy number				Karyotype	Standard Name
		Initial Screen	Run 2	Run 3	At Permissive temperature	Ratio of ChrXII/ChrXIII	
A1	YKL018W	65.79545455	156.25	118.2572614	108.976378	1.027027027	SWD2
C1	YBR160W	62.25895317	110.5386417	92.71255061	94.26470588	1.046511628	CDC28
D1	YOR361C	63.82716049	99.00199601	#VALUE!	83.4939759	1.026143791	PRT1
E1	YDR172W	65.44117647	99.29078014	106.1445783	89.44723618	1.044534413	SUP35
F1	YDL102W	59.64467005	85.28571429	67.46987952	70.19672131	0.972222222	POL3
G1	YGR002C	49.35064935	83.2	68.41463415	81.56028369	1.039370079	SWC4
H1	YDR180W	66.57894737	119.9203187	#VALUE!	107.4	1.005586592	SCC2
A2	YKL045W	29.93421053	43.81107492	43.66666667	36.73740053	1.050724638	PRI2
B2	YIL026C	63.20754717	116.9072165	91.57608696	92.48366013	1.019277108	IRR1
C2	YNL262W	48.64754098	70.32418953	59.91304348	58.20754717	0.98630137	POL2
D2	YJL194W	68.80733945	108.6956522	95.43010753	93.79844961	0.993736952	CDC6
E2	YFL008W	67.38544474	104.2513863	87.83185841	97.65886288	1.04519774	SMC1
F2	YDL003W	67.90697674	101.7006803	90.32258065	88.59030837	1.105527638	MCD1
G2	YBR087W	56.27659574	#VALUE!	67.68916155	62.01550388	0.910197869	RFC5
H2	YGR264C	54.2074364	88.88888889	88.61471861	85.16949153	0.96641791	MES1
A3	YJL074C	65.86614173	111.1363636	94.72972973	98.36065574	1.052205221	SMC3
B3	YOL094C	64.36285097	64.8	73.54085603	62.72058824	0.993714645	RFC4
C3	YEL032W	68.02816901	62.90322581	60.16771488	57.95698925	0.994007491	MCM3
D3	YPR034W	65.36082474	86.66666667	83.25892857	78.10945274	0.988364972	ARP7
E3	YIL126W	63.7037037	81.9047619	77.10843373	79.76782753	0.700363636	STH1
F3	YJL074C	58.48670757	81.13207547	#VALUE!	67.96178344	1.020100503	SMC3
G3	YLR086W	56.88888889	65.23517382	142.6666667	68.14345992	1.017415215	SMC4
H3	YOR074C	57.48091603	79.58158996	87.21238938	67.47311828	1.040798611	CDC21
B4	YPR175W	50.18248175	60.75268817	#VALUE!	53.5915493	0.996042962	DPB2
C4	YJL090C	42.78801843	61.33928571	58.05343511	46.52173913	0.977808599	DPB11
D4	YNL102W	56.875	66.40625	57.38095238	61.47982063	0.987463838	POL1
E4	YLL004W	64.49856734	72.13114754	61.39240506	64.7752809	1.010322581	ORC3
F4	YIR008C	61.87878788	79.75609756	67.26315789	55.72438163	1	PRI1
G4	YBL035C	48.38790932	59.11439114	57.72020725	48.35443038	0.991002571	POL12
H4	YJR068W	54.91764706	88.56557377	90.5785124	79.41605839	0.992606285	RFC2
A5	YNL102W	49.25093633	#VALUE!	77.53424658	55.18382353	0.998496241	POL1
B5	YBR060C	54.32624113	53.57142857	55.55555556	46.05363985	1.039591315	ORC2
C5	YHR191C	49.06015038	59.08440629	56.42701525	52.24358974	1.017107309	CTF8
D5	YNL102W	46.79487179	62.27272727	52.52365931	51.52505447	0.998445596	POL1
E5	YGL130W	69.25515055	96.08391608	#VALUE!	89.97005988	1.024121657	CEG1
F5	YLR272C	50.95588235	68.24817518	74.22619048	55.94095941	1.08248731	YCS4
H5	YIL150C	67.16494845	98.1233244	97.27272727	87.94117647	1.001319261	MCM10
A6	YNL261W	69.44444444	#VALUE!	133.0136986	104.8387097	1.016842105	ORC5
B6	YJL050W	55.93561368	75.2	69.0821256	71.96610169	1.010116732	MTR4
C6	YIL126W	48	74.28571429	56.29032258	48.42406877	1.006329114	STH1
D6	YFR031C	66.04501608	81.46341463	71.23015873	56.42361111	1.049773756	SMC2
E6	YDR013W	35.78778135	53.13953488	46.15384615	43.17596567	0.997755331	PSF1
F6	YMR229C	68.34862385	96.97542533	88.39590444	81.72284644	1.028639618	RRP5
G6	YGR158C	57.63888889	92.17877095	100.3012048	83.80952381	1.025761124	MTR3
H6	YNL061W	69.29292929	#VALUE!	97.8021978	105.0952381	0.995137763	NOP2
A7	YJL125C	63.10344828	#VALUE!	114.9315068	92.44444444	1.021786492	GCD14
B7	YDR228C	65.10638298	85.54216867	72.43589744	75	1.004175365	PCF11
C7	YDR311W	57.63736264	74.77477477	79.22437673	58.42911877	0.754440154	TFB1
D7	YOR174W	63.57142857	90.68825911	78.28418231	79.56	0.990972919	MED4
E7	YJR046W	56.31067961	72.69230769	70.66666667	72.73224044	1.023744292	TAH11
F7	YLR103C	47.0212766	60.96899225	61.71875	58.06896552	1.037656904	CDC45
G7	YNL118C	57.22222222	185	187.9310345	131.5384615	1.061093248	DCP2
H7	YML010W	35.59585492	52.55411255	43.36787565	40.81081081	1.027667984	SPT5

A8	YFR028C	33.97553517	106.6666667	159.6774194	18.4375	1.046643914	CDC14
B8	YOL094C	57.17821782	#VALUE!	55.92783505	51.53846154	1.014354067	RFC4
C8	YEL032W	64.6778043	77.8125	71.55477032	60.80188679	1.020537125	MCM3
E8	YDR052C	62.88321168	72.71095153	67.5	56.88995215	1.011727079	DBF4
F8	YDR052C	69.73995272	75.51724138	71.39534884	63.2748538	1.012264922	DBF4
G8	YDL017W	69.87878788	78.64197531	75.58139535	84.03100775	1.019607843	CDC7
H8	YLR086W	61.09215017	83.70786517	83.28173375	68.76623377	1.050259965	SMC4
A9	YPR175W	40.24647887	61.15384615	53.36225597	43.60169492	1.132716049	DPB2
B9	YJL090C	39.58105647	54.89614243	47.21845319	42.04255319	1.001759531	DPB11
C9	YNL102W	52.33333333	82.12598425	62.99019608	78.27067669	1.019310345	POL1
D9	YLL004W	58.64285714	84.98293515	82.3015873	77.03910615	1.00921659	ORC3
E9	YIR008C	55.25547445	85.50802139	77.02479339	61.65467626	0.981949458	PRI1
G9	YDR168W	66.91011236	104.2139384	92.88	93.36134454	1.032258065	CDC37
H9	YBL035C	33.2278481	63.5625	60.67307692	52.7826087	1	POL12
A10	YJR068W	58.13895782	80.18867925	81.23076923	#VALUE!	1.012698413	RFC2
B10	YNL102W	37.09601874	52.14876033	47.3255814	53.63402062	1.007831822	POL1
C10	YBR060C	50.17123288	52	48.71794872	54.18918919	1.010638298	ORC2
D10	YNL102W	57.52808989	78.42105263	81.25	72.73858921	1.023360288	POL1
E10	YNL102W	38.3935743	62.56	58.75	50.63492063	1.01027146	POL1
F10	YOR048C	58.90410959	82.9588015	87.60736196	78.43665768	0.977851606	RAT1
G10	YOR074C	69.15708812	106.097561	98.40707965	94.01234568	1.107279693	CDC21
A11	YLR321C	44.31818182	74.41176471	56.49164678	48.74015748	1.041963016	SFH1
B11	YGR002C	61.61790017	82.68292683	80.10526316	82.16606498	0.727106227	SWC4
C11	YIL126W	56.88888889	147	192.5	103.0769231	1.018808777	STH1
D11	YOR048C	65.01976285	81.10465116	78.27476038	64.40729483	0.996555683	RAT1
E11	YOR074C	68.39186691	89.71153846	85.69565217	72.49134948	1.012605042	CDC21
F11	YNL061W	66.11570248	#VALUE!	74.32646593	75.74850299	1.019309538	NOP2
G11	YGR002C	67.97235023	78.27160494	74.58893871	80.61643836	0.989795918	SWC4
H11	YIL126W	66.00361664	87.0604782	87.27272727	78.14814815	1.017799353	STH1
A12	YOL123W	65	115.3284672	102.6728111	120.1351351	1.016	HRP1
B12	YOR204W	41.11111111	175	89.36170213	118.75	1.113879004	DED1
D12	YNL102W	58.24847251	89.96598639	83.18584071	79.375	1	POL1
E12	YPL160W	67.33067729	89.65517241	83.5	83.88429752	1.011235955	CDC60
F12	YBR087W	57.60728218	68.98839138	57.86259542	58	1.014516129	RFC5
G12	YIL062C	68.80952381	90.90909091	85.8056266	94.74820144	1.036684135	ARC15
H12	YOR048C	68.27067669	101.7142857	99.40677966	79.13043478	1.04601227	RAT1

Appendix A.3 rDNA copy number and karyotype of top 89 hits with high rDNA copy number

Key

rDNA CN > Mean WT CN + 2SD	Significant change in CN
Mean WT CN + SD < rDNA CN < Mean WT CN + 2SD	Moderate change in CN
< 10,000 total droplets	No quantification
< 10 copies/uL TUB1 or rDNA	Less accurate quantification
No or too few FAM and/or HEX negative droplets	No quantification
ChrXII/ChrXIII significantly different from 1.	Unreliable copy number measurement

Destination Wells	Systematic name	rDNA Copy number				Karyotype	Standard Name
		Initial Screen	Run 2	Run 3	At Permissive temperature	Ratio of ChrXII/ChrXIII	
A1	YCR093W	134.0248963	144.3010753	184.6715328	132.2413793	1.003571429	CDC39
C1	YDL108W	129.8305085	108.1967213	112.826087	115.3191489	1.033088235	KIN28
D1	YDR087C	130.5494505	105.7553957	124.010989	93.63957597	1.01223491	RRP1
E1	YBL023C	121.0826211	92.81914894	107.8838174	86.09625668	0.931985294	MCM2
F1	YER133W	133.1125828	89.84455959	115.6521739	84.24242424	0.962328767	GLC7
G1	YPR181C	127.5272162	124.7787611	114.7151899	15.92592593	0.975206612	SEC23
H1	YKL018W	146.473029	146.223565	189.8203593	134.529148	0.965753425	SWD2
A2	YER133W	135.6578947	NO CALL	166.3414634	109.6590909	0.971428571	GLC7
B2	YJR076C	129.4871795	122.0657277	132.1285141	106.0869565	1.017891374	CDC11
C2	YOR335C	132.1212121	105.923913	115.6725146	85.65022422	1.003816794	ALA1
D2	YGL048C	142.192691	102.5723473	106.9620253	102.9288703	1.013065327	RPT6
E2	YMR235C	128.28125	101.6025641	109.3814433	83.0455259	1.025641026	RNA1
F2	YPR103W	121.3689482	110.3896104	113.1672598	91.52542373	1.038107753	PRE2
G2	YLR378C	121.6730038	143.7788018	186.4197531	160.6756757	1.026425591	SEC61
H2	YOR046C	140.2255639	141.1111111	159.1111111	117.1919771	1.048	DBP5
A3	YER012W	144.1805226	115.8536585	139.8467433	108.6805556	1.036676218	PRE1
B3	YHR186C	125.8555133	103.5211268	123.8916256	97.08133971	1.202883625	KOG1
C3	YDR167W	125.8823529	93.35329341	91.4516129	79.63917526	0.991511036	TAF10
D3	YHR164C	134.7826087	123.3830846	145.6390977	128.3018868	1.025280899	DNA2
E3	YGL155W	121.1363636	102.9411765	129.8039216	88.0625	0.995121951	CDC43
F3	YGR218W	120	108.4328358	98.46153846	82.76699029	1.023558083	CRM1
G3	YOR057W	172.5	187.4576271	172.8947368	137.7880184	1.004651163	SGT1
H3	YDL105W	124.1420118	109.9242424	133.8181818	101.4124294	1.152979066	NSE4
B4	YDL105W	121.319797	124	NO CALL	90.7480315	1.033939394	NSE4
C4	YNR053C	138.4393064	119.3251534	109.0174966	101.8055556	1.923611111	NOG2
D4	YPL228W	127.5	85.92592593	107.2580645	84.26315789	0.96626506	CET1
E4	YBR123C	120.2	NO CALL	103.9735099	93.6802974	1.014694509	TFC1
F4	YGR211W	136.25	86.9124424	93.0952381	89.07103825	0.996314496	ZPR1
G4	YBR198C	150.5	151.0714286	151.4285714	118.9784946	1.070512821	TAF5
H4	YLR186W	124.6753247	108.1578947	136.7816092	95.72072072	1.008836524	EMG1
A5	YKL193C	145.4237288	153.1791908	188.9108911	131.1163895	1.092198582	SDS22
B5	YDR145W	120.1694915	110	133.9622642	95.10204082	1.00317965	TAF12
C5	YKL125W	133.0434783	118.3064516	141.5286624	84.38735178	1.026694045	RRN3
D5	YLR022C	125.0641026	93.89380531	111.2903226	88.54651163	1.027377522	SDO1
E5	YML049C	127.9069767	108.9605735	134.6516008	119.1964286	0.978930308	RSE1
F5	YDR050C	119.5652174	96.52173913	99.12790698	90.72512648	1.04738676	TPI1
H5	YDL105W	154.5833333	126.8	186.5116279	119.2857143	1.255574614	NSE4
A6	YNL138W	120.6040268	118.9368771	146.8926554	104.0816327	1.025380711	SRV2
B6	YPL217C	137.9824561	227.8571429	170.6481481	103.6111111	1.030832477	BMS1
C6	YDL105W	134.0425532	83.43612335	114.9238579	92.19512195	1.038847118	NSE4
D6	YOR020C	137.5	138.875	121.1594203	101.3157895	1.01285347	HSP10
E6	YOR151C	136.6101695	112.5448029	#VALUE!	107.3529412	NO CALL	RPB2
F6	YDL143W	169.4871795	126.3598326	120.4819277	116.9230769	1.070618557	CCT4
G6	YML114C	125.6896552	102.8813559	124.2	111.2179487	1.005995204	TAF8
H6	YDL008W	127.8947368	104.0298507	140.3333333	106.6914498	0.99537037	APC11
A7	YLR186W	130.8571429	180.620155	196.4516129	155.2631579	1.862934363	EMG1
B7	YLR430W	140	102.6699029	134.6049046	93.64806867	0.987544484	SEN1
C7	YOL144W	124.6290801	99.75903614	125.8426966	85.05319149	1.167128347	NOP8
D7	YKR037C	149.704142	159.6590909	0.018131102	137.9182156	#VALUE!	SPC34
E7	YDL103C	122.5	119.2424242	NO CALL	99.54285714	1.001620746	QRI1
F7	YBR154C	130.9016393	115.3293413	133.6363636	141.71875	1.197038256	RPB5
G7	YHR036W	119.2913386	139.04	169.4630872	128.1786942	1.004552352	BRL1
H7	YDL014W	123.3333333	80.50632911	105.9431525	90.64220183	1.013452915	NOP1

A8	YKR037C	133.5087719	134.9462366	173.5099338	85.55555556	1.033744856	SPC34
B8	YDL126C	149.1150442	108.9058524	115.4639175	101.1377246	0.817701453	CDC48
C8	YIL004C	119.8360656	100.3448276	NO CALL	77.02970297	0.994530538	BET1
E8	YDL140C	124.4791667	147.2392638	143.6754177	117.5	0.998019802	RPO21
F8	YER133W	133.5689046	119.5571956	128.8495575	107.7083333	0.990752972	GLC7
G8	YAL041W	122.7142857	126.8421053	107.4509804	86.35294118	1.036908881	CDC24
H8	YKL018W	121.1111111	147.804878	182.7309237	107.7033493	0.978813559	SWD2
A9	YER133W	128.6956522	136.6666667	155.4216867	111.3084112	0.979508197	GLC7
B9	YDL084W	121.6080402	110.1162791	120.4511278	84.79532164	1.017272727	SUB2
C9	YGR098C	122.5806452	101.4018692	129.3515358	NO CALL	1.050732807	ESP1
D9	YMR235C	170.3832753	171.1904762	109.8333333	87.70226537	0.930930931	RNA1
E9	YLR314C	124.3262411	95.98360656	137.0175439	93.3463035	1.001694915	CDC3
G9	YDL105W	144.6715328	114.4230769	144.1176471	102.6030369	1.063535912	NSE4
H9	YKL210W	151.9083969	130.9468822	NO CALL	135.8885017	1.006633499	UBA1
A10	YKR002W	137.4570447	291.6666667	242.3728814	NO CALL	1.138760407	PAP1
B10	YFR037C	137.5308642	111.4285714	117.027027	95.12195122	1	RSC8
C10	YLR078C	124.7133758	117.6744186	109.75	103.3755274	1.007011394	BOS1
D10	YLR378C	193.36	149.5384615	182.2834646	148.4946237	1.02189781	SEC61
E10	YER013W	127.8089888	127.4311927	148.2889734	118.75	1.009615385	PRP22
F10	YOR259C	146.097561	148.0487805	171.1428571	134.0707965	1	RPT4
G10	YDR510W	123.1707317	170.0847458	187.2037915	140.2555911	1.126865672	SMT3
A11	YDL105W	125.3968254	144.1463415	NO CALL	108.5308057	1.163666121	NSE4
B11	YDL105W	143.8650307	NO CALL	142.9710145	107.0103093	1.077639752	NSE4
C11	YFR037C	119.3069307	127.5609756	126.6972477	93.61702128	0.996677741	RSC8
D11	YDR188W	158.0071174	104.5801527	149.7797357	100.9852217	1.002267574	CCT6
E11	YBR135W	130.9859155	135.5670103	164.171123	142.9347826	1.159090909	CKS1
F11	YLR022C	124.8888889	100.6006006	115.1745068	104.3137255	1.004237288	SDO1
G11	YOL123W	121.52	104.159292	107.3109244	100.8064516	0.983443709	HRP1
H11	YFL009W	137.4613003	NO CALL	149.068323	102.3904382	0.989384289	CDC4
A12	YFL034C-B	177.4358974	NO CALL	218.699187	149.6402878	1.081818182	MOB2
B12	YHR036W	141.1149826	115.4954955	118.3333333	106.9444444	1.007490637	BRL1
D12	YHR036W	123.4401349	116.4705882	#VALUE!	103.562341	1.001548787	BRL1
E12	YLR314C	120.295858	98.71428571	89.6460177	90.25974026	0.989473684	CDC3
F12	YBR087W	124.1691843	101.779661	115.8450704	89.48863636	0.994966443	RFC5
G12	YIL062C	120.4081633	79.22077922	100.2409639	75.88652482	1	ARC15
H12	YOR181W	124.3243243	123.3552632	NO CALL	122	0.972866305	LAS17

APPENDIX B

rDNA repeat loss rates and copy number measurements from screens in Chapter 3.

Appendix B.1 rDNA repeat loss rates in the RDN25-MATα (+MoBY-ORF) library

Data from initial screen.

Data sorted by Plate number NP1-NP47 and EP1-EP13.

Key

	Control strains
BY4741	WT, no GFP tag
GFP+	*MFA1-3xGFP*
DES7	*RDN25-MAT* α
p5472	*RDN25-MAT* α + p5472
	ORF present in MoBY database, but not in our plasmid preps (no band on e-gel).
	Empty well in MoBY database, but growth in our preps.
	Strain moved from its original location to make room for controls and blank for OD measurement.
	"Low instability"; rDNA repeat loss rates < 0.00017
	"High instability"; rDNA repeat loss rates > 0.001

Plate	Well	Sample Name	Loss rate
NP1	A1	YML071C	0.000631
NP1	A2	YML074C	0.000555
NP1	A3	YML094W	0.000949
NP1	A4	YML095C	0.00059
NP1	A5	YML096W	0.000746
NP1	A6	YML097C	0.000702
NP1	A7	YML101C	0.000634
NP1	A8	p5472	0.000605
NP1	A9	YML106W	0.000748
NP1	A10	YML107C	0.00061
NP1	A11	YML108W	0.000707
NP1	A12	YML109W	0.000632
NP1	B1	YML110C	0.000704
NP1	B2	YML111W	0.001946
NP1	B3	YML113W	0.000778
NP1	B4	YML116W	0.00044
NP1	B5	YML117W	0.000614
NP1	B6	YML118W	0.000625
NP1	B7	YML120C	0.000598
NP1	B8	YML121W	0.000767
NP1	B9	YML129C	0.000839
NP1	B10	GFP+	
NP1	B11	YMR095C	0.00068
NP1	B12	YMR096W	0.00072
NP1	C1	YMR097C	0.000618
NP1	C2	YMR099C	0.000583
NP1	C3	YMR100W	0.000729
NP1	C4	YMR106C	0.000554
NP1	C5	YMR107W	0.000709
NP1	C6	YMR108W	0.000754
NP1	C7	YMR109W	0.000632
NP1	C8	YMR110C	0.000848
NP1	C9	YMR115W	0.000619
NP1	C10	YMR120C	0.001298
NP1	C11	YMR124W	0.001104
NP1	C12	YMR125W	0.000733
NP1	D1	YMR126C	0.000669
NP1	D2	YMR127C	0.000655
NP1	D3	YMR129W	0.000266
NP1	D4	YMR130W	0.000764
NP1	D5	YMR132C	0.000811
NP1	D6	YMR133W	0.000719
NP1	D7	YMR135C	0.000616
NP1	D8	BY4741	0
NP1	D9	YCL038C	0.00092
NP1	D10	YGL235W	0.000736
NP1	D11	YJR070C	0.00082
NP1	D12	YJR074W	0.000852
NP1	E1	YJR077C	0.000482
NP1	E2	YJR080C	0.000837
NP1	E3	YJR084W	0.00069
NP1	E4	YJR094W-A	0.000888
NP1	E5	YJR095W	0.000838
NP1	E6	YJR096W	0.000853
NP1	E7	DES7	0.002179
NP1	E8	YJR098C	0.000729
NP1	E9	YJR099W	0.000522
NP1	E10	YJR100C	0.000983
NP1	E11	YJR116W	0.000424
NP1	E12	YJR117W	0.000788
NP1	F1	YJR118C	0.000857
NP1	F2	YJR119C	0.0006
NP1	F3	YJR120W	0.000727
NP1	F4		
NP1	F5	YJR133W	0.000663
NP1	F6	YJR139C	
NP1	F7	YJR140C	0.000312
NP1	F8	YJR142W	0.000804
NP1	F9	YJR144W	0.000555
NP1	F10	YKL005C	0.001208
NP1	F11	YLR146C	0.000944
NP1	F12	YLR286C	0.000928
NP1	G1	YLR343W	0.000713
NP1	G2		
NP1	G3		
NP1	G4		
NP1	G5	NP1-1	0.000438
NP1	G6		
NP1	G7		
NP1	G8		
NP1	G9		
NP1	G10	NP1-2	0.00048
NP1	G11		
NP1	G12		
NP1	H1		
NP1	H2		
NP1	H3		
NP1	H4		
NP1	H5		
NP1	H6		
NP1	H7		
NP1	H8		
NP1	H9		
NP1	H10		
NP1	H11		
NP1	H12		
NP2	A1	YAL064C-A	0.000585
NP2	A2	YBL091C-A	0.000705
NP2	A3	YBR269C	0.006156
NP2	A4	YBR271W	0.000462
NP2	A5	YBR191W	0.000885
NP2	A6	YCL035C	0.00059
NP2	A7	YDR074W	0.000759
NP2	A8	YER027C	0.001098
NP2	A9	YER037W	0.000483
NP2	A10	YGR155W	0.000753
NP2	A11	YLR192C	0.000677
NP2	A12	YLR237W	0.000799
NP2	B1	YLR246W	0.0007
NP2	B2	YLR346C	0.000663
NP2	B3	YLR361C	0.000757
NP2	B4	YLR370C	0.000321
NP2	B5	YLR394W	0.000541
NP2	B6	YLR406C	0.000915
NP2	B7	YML022W	0.000593
NP2	B8	YML036W	0.000883
NP2	B9	YML041C	0.000786
NP2	B10	YML047C	0.0007
NP2	B11	YML075C	
NP2	B12	YML076C	0.000714
NP2	C1	YML086C	0.00121
NP2	C2	YMR048W	0.000851
NP2	C3	YMR137C	0.000528
NP2	C4	YMR138W	0.000741
NP2	C5	YMR139W	0.000509
NP2	C6	YMR160W	0.000578

NP2	C7	YMR173W	0.000857
NP2	C8	YMR198W	0.000907
NP2	C9	YOR298C-A	0.000737
NP2	C10	YPL148C	
NP2	C11	YPL183C	0.000729
NP2	C12	YPL183W-A	0.000889
NP2	D1	YPL189W	0.000639
NP2	D2	YPL224C	0.001912
NP2	D3	YDR245W	0.000688
NP2	D4	YDR247W	0.000292
NP2	D5	YDR248C	0.000689
NP2	D6	YDR249C	0.000232
NP2	D7	YDR251W	0.000665
NP2	D8	YDR252W	0.000998
NP2	D9	YDR253C	0.000883
NP2	D10	YDR254W	0.00118
NP2	D11	YDR255C	0.00056
NP2	D12	YDR256C	0.000526
NP2	E1	YDR257C	0.000481
NP2	E2	p5472	0.000454
NP2	E3	YDR259C	0.000424
NP2	E4	GFP+	
NP2	E5	YDR261C	0.000326
NP2	E6	YDR262W	0.000706
NP2	E7	YDR263C	0.000354
NP2	E8	YDR264C	0.000475
NP2	E9	YDR265W	
NP2	E10	YDR266C	0.000747
NP2	E11	YDR268W	0.001196
NP2	E12	YDR270W	0.000654
NP2	F1	YDR272W	0.00097
NP2	F2	YDR273W	0.000806
NP2	F3	YDR275W	0.000574
NP2	F4	YDR276C	0.000745
NP2	F5	YDR277C	0.000782
NP2	F6	YDR279W	0.000852
NP2	F7	YDR284C	0.000313
NP2	F8	YDR286C	0.001667
NP2	F9	YDR287W	0.000566
NP2	F10	YDR289C	0.001068
NP2	F11	BY4741	0
NP2	F12	YDR294C	0.00123
NP2	G1	YDR295C	0.000621
NP2	G2	YDR296W	0.001164
NP2	G3	YDR297W	0.000298
NP2	G4	YDR300C	0.000453
NP2	G5	YDR304C	0.000676
NP2	G6	YDR305C	0.001418
NP2	G7	YDR306C	0.001052
NP2	G8	YDR307W	0.001051
NP2	G9	YDR309C	0.000312
NP2	G10	YDR310C	0.001146
NP2	G11	YDR312W	0.000277
NP2	G12	YDR314C	0.000859
NP2	H1	YDR316W	0.000662
NP2	H2	YDR317W	0.001205
NP2	H3	YDR318W	0.000786

NP2	H4	YDR320C	0.000707
NP2	H5	YDR321W	0.000653
NP2	H6	YDR322W	0.000815
NP2	H7	YDR323C	0.000662
NP2	H8	DES7	0.002405
NP2	H9	YDR330W	0.00031
NP2	H10	YDR332W	0.000277
NP2	H11		
NP2	H12	YDR337W	0.00335
NP3	A1	YBR273C	0.000258
NP3	A2	YBR281C	0.000609
NP3	A3	YBR282W	0.000453
NP3	A4	YBR284W	
NP3	A5	YBR285W	0.000233
NP3	A6	YBR297W	0.000297
NP3	A7	YCR026C	0.00022
NP3	A8	YCR028C	0.000599
NP3	A9	YCR037C	0.000312
NP3	A10	YCR051W	0.000527
NP3	A11	YCR059C	0.001778
NP3	A12	YCR065W	0.000312
NP3	B1	YCR068W	0.000257
NP3	B2	YCR077C	0.000256
NP3	B3	YCR081W	
NP3	B4	YCR087C-A	0.000289
NP3	B5	YEL012W	0.000738
NP3	B6	YER031C	0.000184
NP3	B7	YER046W	0.00039
NP3	B8	YER063W	0.000276
NP3	B9	YER066W	0.000395
NP3	B10	YGR188C	0.000631
NP3	B11	YGR201C	0.000319
NP3	B12	YGR204W	0.000985
NP3	C1	YHL002W	
NP3	C2	YHL011C	0.000254
NP3	C3	YHL039W	0.000838
NP3	C4	YHR003C	0.000234
NP3	C5	YHR004C	0.000203
NP3	C6	YHR005C	0.000106
NP3	C7	YHR006W	0.001032
NP3	C8	YHR008C	0.000348
NP3	C9	YHR009C	0.000458
NP3	C10	YHR025W	0.000281
NP3	C11	YHR059W	0.001112
NP3	C12	YHR067W	0.000233
NP3	D1	YHR127W	0.00057
NP3	D2	YHR131C	0.000151
NP3	D3	YHR185C	0.000483
NP3	D4	p5472	0.000705
NP3	D5	YLL007C	0.000761
NP3	D6	YMR154C	0.000341
NP3	D7	YNL274C	0.003191
NP3	D8	YOL141W	0.000255
NP3	D9	YOL143C	0.00044
NP3	D10	YOL158C	0.000404
NP3	D11	YOL159C	0.000307
NP3	D12	YOL162W	0.000633

NP3	E1	YOL163W	0.000448
NP3	E2	YOR008C-A	0.000304
NP3	E3	YFL060C	0.000472
NP3	E4	YJL103C	0.000294
NP3	E5	YML073C	0.000476
NP3	E6	YNL018C	0.000447
NP3	E7	YNL047C	0.000309
NP3	E8	YNL053W	0.000374
NP3	E9	YNL055C	0.000458
NP3	E10	YNL059C	0.00044
NP3	E11	YNL069C	0.000242
NP3	E12	YNL086W	0.000534
NP3	F1	YNL096C	0.000779
NP3	F2	YNL111C	0.000563
NP3	F3	YNL147W	0.000501
NP3	F4	YNL220W	0.000579
NP3	F5	GFP+	
NP3	F6	YNL284C	0.00049
NP3	F7	YNR033W	0.001031
NP3	F8	YPL158C	0.000282
NP3	F9	YPL194W	0.000244
NP3	F10	YPR011C	0.00055
NP3	F11	YPR021C	0.002493
NP3	F12	YPR083W	0.000443
NP3	G1	YPR118W	0.000902
NP3	G2	YPR133W-A	0.000562
NP3	G3	YPR151C	0.0004
NP3	G4	BY4741	0
NP3	G5	YDR347W	0.000462
NP3	G6	YDR348C	0.000665
NP3	G7	YDR349C	0.001711
NP3	G8	YDR350C	0.000679
NP3	G9	DES7	0.001889
NP3	G10	YDR352W	0.000228
NP3	G11	YDR354W	0.000231
NP3	G12	YDR358W	0.000214
NP3	H1	YDR359C	0.000345
NP3	H2		
NP3	H3	YDR368W	
NP3	H4	YDR370C	0.001314
NP3	H5	YDR371W	0.000439
NP3	H6	YDR372C	0.00059
NP3	H7	YDR377W	0.000291
NP3	H8	YDR378C	0.000257
NP3	H9	YDR379W	0.000242
NP3	H10		
NP3	H11	YDR382W	
NP3	H12	YDR383C	
NP4	A1	YDR384C	0.000356
NP4	A2	YDR385W	0.000329
NP4	A3	YDR386W	-0.00029
NP4	A4	YDR387C	0.000272
NP4	A5	YDR388W	0.000317
NP4	A6	YDR389W	0.000203
NP4	A7	YDR391C	0.00038
NP4	A8	YDR393W	0.000409
NP4	A9	YDR395W	0.000495

NP4	A10	YDR399W	0.000297
NP4	A11	YDR400W	0.000335
NP4	A12	p5472	0.000469
NP4	B1	YDR405W	0.000293
NP4	B2	YDR409W	0.000317
NP4	B3	YDR410C	0.000409
NP4	B4	YDR411C	0.000317
NP4	B5	YDR418W	0.000272
NP4	B6	GFP+	
NP4	B7	YDR421W	0.000303
NP4	B8	YDR422C	0.000223
NP4	B9	YDR423C	0.000669
NP4	B10	YDR425W	0.000321
NP4	B11	YDR428C	0.000442
NP4	B12	YDR430C	0.000296
NP4	C1	YDR432W	0.000277
NP4	C2	YDR435C	0.000369
NP4	C3	YDR436W	0.00032
NP4	C4	YHR142W	0.000315
NP4	C5	YHR143W	0.001995
NP4	C6	YHR147C	0.000703
NP4	C7	YHR151C	0.000586
NP4	C8	YHR152W	0.000826
NP4	C9	YHR153C	0.000425
NP4	C10	YHR156C	0.00041
NP4	C11	YHR157W	0.000354
NP4	C12	YHR159W	0.000316
NP4	D1	YHR160C	0.00018
NP4	D2	YHR161C	0.000209
NP4	D3	YHR163W	0.001251
NP4	D4	YHR167W	0.000413
NP4	D5	YHR176W	6.8E-05
NP4	D6	YHR177W	0.00031
NP4	D7	BY4741	0
NP4	D8	YHR182W	0.000385
NP4	D9	YHR183W	0.000367
NP4	D10	YHR184W	0.000382
NP4	D11	YHR189W	0.000378
NP4	D12	YHR195W	0.000309
NP4	E1	YHR198C	0.000295
NP4	E2	YHR199C	0.000484
NP4	E3	YHR200W	0.000398
NP4	E4	YHR202W	
NP4	E5	YHR203C	0.001393
NP4	E6	YHR204W	0.00036
NP4	E7	YHR206W	0.000276
NP4	E8	YHR209W	0.000365
NP4	E9	YHR210C	0.000603
NP4	E10		
NP4	E11	YIL005W	
NP4	E12	YIL011W	
NP4	F1	DES7	0.001776
NP4	F2	YIL015W	0.000233
NP4	F3	YIL016W	0.000349
NP4	F4	YIL017C	0.000919
NP4	F5	YIL020C	0.0003
NP4	F6	YIL024C	0.000282
NP4	F7	YIL027C	0.000365
NP4	F8	YIL029C	0.000544
NP4	F9	YIL034C	0.000507
NP4	F10	YIL035C	0.000333
NP4	F11	YIL036W	0.000327
NP4	F12	YIL037C	0.000255
NP4	G1	YIL039W	0.000263
NP4	G2	YIL040W	0.000322
NP4	G3	YIL043C	0.000534
NP4	G4	YIL044C	0.000869
NP4	G5	YIL045W	0.000279
NP4	G6	YIL049W	0.000536
NP4	G7	YIL050W	0.000933
NP4	G8	YIL053W	
NP4	G9	YIL057C	0.000398
NP4	G10	YIL064W	0.000304
NP4	G11	YIL065C	0.000266
NP4	G12	YIL072W	
NP4	H1	YIL073C	
NP4	H2	YIL076W	0.00024
NP4	H3	YIL077C	0.000247
NP4	H4	YIL084C	0.000735
NP4	H5	YIL087C	0.000253
NP4	H6	YIL088C	0.000733
NP4	H7	YIL090W	0.000629
NP4	H8	YIL093C	0.000453
NP4	H9	YIL095W	0.000601
NP4	H10	YIL096C	
NP4	H11	YIL097W	
NP4	H12		
NP5	A1	YIL006W	0.00058
NP5	A2	YIL007C	0.000286
NP5	A3	YIL008W	0.000418
NP5	A4	YIL009W	0.000454
NP5	A5	YIL010W	0.001029
NP5	A6	p5472	0.00091
NP5	A7	YIL038C	0.000466
NP5	A8	YIL042C	0.000815
NP5	A9	YIL052C	0.000586
NP5	A10	YIL055C	
NP5	A11	YIL056W	0.000399
NP5	A12	YIL060W	0.001143
NP5	B1	YIL066C	0.000387
NP5	B2	YIL067C	0.000439
NP5	B3	YIL069C	0.00076
NP5	B4	YIL070C	0.000341
NP5	B5	YIL071C	0.000344
NP5	B6	YIL074C	0.000348
NP5	B7	YIL085C	0.00145
NP5	B8	YIL089W	0.000394
NP5	B9	YIL094C	0.000967
NP5	B10	YIL098C	0.000612
NP5	B11	YIL099W	0.000327
NP5	B12	YIL101C	0.000266
NP5	C1	YIL102C	0.000419
NP5	C2	YIL103W	0.000792
NP5	C3	YIL108W	0.00037
NP5	C4	YIL110W	0.000562
NP5	C5	YIL111W	0.000447
NP5	C6	YIL114C	0.00036
NP5	C7	YIL116W	0.000874
NP5	C8	YIL117C	0.000318
NP5	C9	GFP+	
NP5	C10	YIL120W	0.00102
NP5	C11	YIL121W	0.001139
NP5	C12	YIL122W	0.000452
NP5	D1	YIL123W	0.000402
NP5	D2	YIL124W	0.000529
NP5	D3	YIL128W	0.000462
NP5	D4	BY4741	0
NP5	D5	YIL132C	0.000515
NP5	D6	YIL133C	0.000408
NP5	D7	YIL135C	
NP5	D8	YIL136W	0.00036
NP5	D9		
NP5	D10	YIL138C	0.000782
NP5	D11	YIL139C	0.00164
NP5	D12	YIL140W	0.000325
NP5	E1	YIL145C	0.000612
NP5	E2	YIL146C	0.000378
NP5	E3	YIL148W	0.00044
NP5	E4	YIL149C	0.000378
NP5	E5	YIL152W	0.000649
NP5	E6	YIL153W	0.000413
NP5	E7	YIL154C	0.000371
NP5	E8	YIL155C	0.000329
NP5	E9	YIL157C	0.00046
NP5	E10	YIL159W	0.00109
NP5	E11	YIL160C	0.000249
NP5	E12	YIL161W	0.000554
NP5	F1	YIL162W	0.00055
NP5	F2	YIL164C	0.000267
NP5	F3	YIL165C	0.001532
NP5	F4	YIL166C	0.00084
NP5	F5	YIL173W	0.000838
NP5	F6	YIR001C	0.000887
NP5	F7	YIR003W	0.000362
NP5	F8	YIR004W	0.000688
NP5	F9	YIR005W	0.000615
NP5	F10	YIR009W	0.000329
NP5	F11	YIR013C	0.000487
NP5	F12	YIR014W	0.000358
NP5	G1	YIR016W	0.000543
NP5	G2	YJL218W	0.000653
NP5	G3	YJL217W	0.000769
NP5	G4	DES7	0.002303
NP5	G5	YJL214W	0.00036
NP5	G6	YJL210W	0.00069
NP5	G7	YJL208C	0.00067
NP5	G8	YJL204C	0.000594
NP5	G9	YJL201W	0.000671
NP5	G10	YJL192C	0.000884
NP5	G11	YJL190C	0.000322
NP5	G12	YJL187C	0.0003

NP5	H1	YJL185C	0.000255971
NP5	H2	YJL183W	0.000362157
NP5	H3	YJL180C	0.000438025
NP5	H4	YJL179W	0.000348734
NP5	H5	YJL178C	0.000339486
NP5	H6	YJL176C	0.000570573
NP5	H7	YJL171C	0.000788421
NP5	H8	YJL166W	0.000536973
NP5	H9		
NP5	H10	YJL159W	0.000631685
NP5	H11	YJL158C	0.000285094
NP5	H12	YJL155C	0.000332606
NP6	A1	YJL148W	0.00030756
NP6	A2	YJL146W	0.000155124
NP6	A3	YJL145W	7.84362E-05
NP6	A4	YJL144W	0.000301434
NP6	A5	YJL133W	0.00059261
NP6	A6	YJL131C	0.000708017
NP6	A7	YDR049W	0.000197484
NP6	A8	YDR051C	0.000421937
NP6	A9	YDR056C	0.000311722
NP6	A10	YDR057W	0.001110892
NP6	A11	YDR059C	0.000336886
NP6	A12	YDR061W	0.000330517
NP6	B1	YDR063W	0.000351533
NP6	B2	YDR065W	0.000387797
NP6	B3	YDR066C	0.000422945
NP6	B4	YDR067C	0.000536062
NP6	B5	YDR068W	0.000528113
NP6	B6	YDR070C	0.000443479
NP6	B7	YDR072C	0.000386627
NP6	B8	YDR073W	0.000376391
NP6	B9	YDR076W	0.000436499
NP6	B10	YDR077W	0.000679151
NP6	B11	YDR078C	0.00048311
NP6	B12	YDR079W	0.000613064
NP6	C1	YDR080W	0.000237283
NP6	C2	YDR083W	0.000410857
NP6	C3	YDR084C	0.000401455
NP6	C4	YDR085C	0.000336209
NP6	C5	YDR090C	0.000462513
NP6	C6		
NP6	C7	YDR096W	0.000556834
NP6	C8	YDR098C	
NP6	C9	YDR099W	0.000901383
NP6	C10	YDR100W	0.001504859
NP6	C11	YDR101C	0.000389027
NP6	C12	YDR103W	
NP6	D1	YDR104C	0.000259562
NP6	D2	p5472	0.000439109
NP6	D3	YDR107C	0.000363823
NP6	D4	YDR108W	0.000383221
NP6	D5	YDR109C	0.000302443
NP6	D6	YDR110W	0.000301166
NP6	D7	GFP+	
NP6	D8	YDR115W	0.000378816
NP6	D9	YDR116C	0.000359799
NP6	D10	YDR117C	0.000552954
NP6	D11	BY4741	0
NP6	D12	YDR120C	0.00040692
NP6	E1	YDR121W	0.000298205
NP6	E2		
NP6	E3	YDR123C	-0.000133491
NP6	E4	YDR124W	0.000351859
NP6	E5	YDR125C	0.000300277
NP6	E6		
NP6	E7	YDR128W	0.000390471
NP6	E8	YDR130C	0.000389348
NP6	E9	YDR131C	0.000369394
NP6	E10		
NP6	E11		
NP6	E12	YDR137W	0.00026738
NP6	F1	YDR138W	0.00029102
NP6	F2	YDR139C	0.000289881
NP6	F3	YDR142C	4.90024E-05
NP6	F4	YDR143C	0.000444999
NP6	F5	YDR146C	0.000277347
NP6	F6	DES7	0.001986312
NP6	F7	YFL028C	0.000179844
NP6	F8	YFL030W	0.000494062
NP6	F9		
NP6	F10		
NP6	F11	YFL046W	0.000436151
NP6	F12	YFL047W	0.000457144
NP6	G1	YFL049W	0.000354762
NP6	G2	YFL050C	0.000361679
NP6	G3	YFL051C	0.000383742
NP6	G4	YFL052W	0.000397457
NP6	G5	YFL053W	0.000612719
NP6	G6	YFL054C	0.000347816
NP6	G7	YFL055W	0.000387624
NP6	G8	YFL056C	0.000285272
NP6	G9	YFR001W	
NP6	G10	YFR006W	0.000243682
NP6	G11	YFR009W	-9.3328E-05
NP6	G12	YFR015C	0.000352545
NP6	H1	YFR016C	
NP6	H2	YFR017C	0.000360549
NP6	H3	YFR022W	0.000272458
NP6	H4	YFR023W	0.0002688
NP6	H5	YFR031C-A	0.000397588
NP6	H6		
NP6	H7		
NP6	H8		
NP6	H9		
NP6	H10		
NP6	H11		
NP6	H12		
NP7	A1	YJR073C	0.000512804
NP7	A2	YJR075W	0.000417161
NP7	A3	YJR078W	0.000421804
NP7	A4	YJR079W	0.000610329
NP7	A5	YJR082C	0.000310092
NP7	A6	YJR083C	0.000343804
NP7	A7	YJR088C	0.00025634
NP7	A8	YJR092W	0.000243757
NP7	A9	YJR102C	0.000658861
NP7	A10	YJR103W	0.000455486
NP7	A11	YJR105W	0.000481279
NP7	A12	YJR108W	0.000336587
NP7	B1	YJR110W	0.000378793
NP7	B2	p5472	0.000520085
NP7	B3	YJR115W	0.000456959
NP7	B4	YJR127C	0.000503463
NP7	B5	YJR129C	0.000580776
NP7	B6	YJR130C	0.000613751
NP7	B7	YJR135C	0.000351586
NP7	B8	YJR137C	0.000487667
NP7	B9	YJR147W	0.000619424
NP7	B10		
NP7	B11	YJR152W	2.28173E-05
NP7	B12	YJR154W	0.000389889
NP7	C1	YKL002W	0.000529003
NP7	C2	YKL006W	0.000327674
NP7	C3	YKL008C	0.000827063
NP7	C4	YKL010C	0.000526114
NP7	C5	YKL011C	0.000961269
NP7	C6	YKL016C	0.000507522
NP7	C7	YKL017C	0.00050249
NP7	C8	YKL020C	0.000455679
NP7	C9	YKL023W	0.000316038
NP7	C10	YKL025C	0.000500218
NP7	C11	YKL026C	0.000275175
NP7	C12	YKL027W	0.000517619
NP7	D1	GFP+	
NP7	D2	YKL037W	0.000641611
NP7	D3	YKL039W	0.000393357
NP7	D4	YKL040C	0.000462366
NP7	D5	YKL041W	-4.22145E-05
NP7	D6	YKL043W	0.000690356
NP7	D7	YKL046C	0.000450476
NP7	D8	YKL047W	0.000566145
NP7	D9	YKL048C	0.000401338
NP7	D10	YKL050C	0.000437872
NP7	D11	YKL051W	0.000434569
NP7	D12	BY4741	0
NP7	E1	YKL056C	0.000344531
NP7	E2	YKL057C	0.000753784
NP7	E3	YKL061W	0.000225
NP7	E4	YKL062W	0.000433358
NP7	E5	YKL063C	0.000341775
NP7	E6	YKL064W	0.000461312
NP7	E7	YKL067W	0.000700474
NP7	E8	YKL068W	0.000487204
NP7	E9	YKL069W	0.000453246
NP7	E10	YKL070W	0.000484817
NP7	E11	YKL071W	0.00018261
NP7	E12	YKL072W	0.000387505
NP7	F1	YKL074C	0.000414701
NP7	F2	YKL075C	0.000390244
NP7	F3	YKL077W	0.000486695

NP7	F4	YKL079W	0.000753
NP7	F5	YKL080W	0.000258
NP7	F6	YKL081W	0.000369
NP7	F7	YKL084W	0.000493
NP7	F8	YKL085W	0.000975
NP7	F9	YKL086W	0.000491
NP7	F10	DES7	0.002071
NP7	F11	YKL093W	0.000382
NP7	F12	YKL094W	0.000603
NP7	G1	YKL096W	0.000333
NP7	G2	YKL098W	0.000417
NP7	G3	YKL100C	0.000396
NP7	G4	YKL101W	0.000513
NP7	G5	YKL103C	0.000445
NP7	G6	YKL107W	0.000737
NP7	G7	YKL109W	0.001722
NP7	G8	YKL110C	0.000415
NP7	G9	YKL113C	0.000424
NP7	G10	YKL116C	0.000334
NP7	G11	YKL117W	0.000773
NP7	G12	YKL119C	0.000338
NP7	H1	YKL120W	0.000504
NP7	H2	YKL124W	0.000229
NP7	H3	YKL126W	0.000384
NP7	H4	YKL130C	0.000454
NP7	H5	YKL132C	0.000668
NP7	H6	YKL133C	0.000466
NP7	H7	YKL134C	0.000796
NP7	H8	YKL135C	0.000773
NP7	H9	YKL138C	0.000371
NP7	H10	YKL140W	0.000516
NP7	H11	YKL142W	
NP7	H12	YKL143W	0.000367
NP8	A1	YKL146W	0.000206
NP8	A2	YKL149C	0.000363
NP8	A3	YKL155C	0.000362
NP8	A4	YKL156W	0.000462
NP8	A5	YKL160W	0.000444
NP8	A6	YKL162C	0.00038
NP8	A7	YKL167C	0.000857
NP8	A8	YKL170W	0.000696
NP8	A9	YKL190W	0.000383
NP8	A10	YKL198C	0.000366
NP8	A11	YKL206C	0.000344
NP8	A12	YKL207W	0.000446
NP8	B1	YKL208W	0.000314
NP8	B2	YKL211C	0.000415
NP8	B3	p5472	0.000428
NP8	B4	YKL214C	0.000399
NP8	B5	YKL216W	0.000448
NP8	B6	YKL217W	0.000369
NP8	B7	YKL221W	0.00061
NP8	B8	YKL222C	0.000422
NP8	B9	GFP+	
NP8	B10	YKR003W	0.000439
NP8	B11	YKR005C	0.00059
NP8	B12		

NP8	C1	YKR007W	0.000369759
NP8	C2	YKR011C	0.000406839
NP8	C3	YKR013W	0.000430648
NP8	C4	YKR015C	0.000342026
NP8	C5	YKR016W	0.000589568
NP8	C6	YKR018C	0.000642996
NP8	C7	YKR020W	0.000620244
NP8	C8	YKR024C	0.000416928
NP8	C9	YKR030W	0.000564896
NP8	C10	YKR043C	0.000458856
NP8	C11	BY4741	0
NP8	C12	YKR045C	0.000435074
NP8	D1	YKR048C	0.000270218
NP8	D2	YKR049C	0.000322575
NP8	D3	YKR051W	0.000200222
NP8	D4	YKR052C	0.000364243
NP8	D5	YKR055W	0.000333421
NP8	D6	YKR058W	0.000620691
NP8	D7	YKR059W	0.000368289
NP8	D8	YKR061W	0.001146752
NP8	D9	YKR065C	0.000466979
NP8	D10	YLR420W	0.000452758
NP8	D11	YLR126C	0.000352277
NP8	D12	YLR128W	0.000447404
NP8	E1	YLR130C	0.000525204
NP8	E2	YLR133W	0.000339383
NP8	E3	YLR136C	0.00054275
NP8	E4	YLR137W	0.000326084
NP8	E5	DES7	0.002404122
NP8	E6	YLR142W	0.000473355
NP8	E7	YLR150W	0.000214051
NP8	E8	YLR151C	0.000518107
NP8	E9	YLR152C	0.00033747
NP8	E10	YLR154C	0.000287506
NP8	E11	YLR164W	0.000365637
NP8	E12	YLR165C	0.000673286
NP8	F1	YLR168C	0.000309665
NP8	F2	YLR170C	0.000288747
NP8	F3	YLR172C	0.00045493
NP8	F4	YLR173W	0.000315965
NP8	F5	YLR177W	0.000282843
NP8	F6	YLR179C	0.000276868
NP8	F7	YLR180W	0.000252391
NP8	F8	YLR181C	0.000288309
NP8	F9	YLR183C	0.000202419
NP8	F10	YLR185W	0.000200155
NP8	F11	YLR188W	0.000283494
NP8	F12	YLR190W	0.000318739
NP8	G1	YLR191W	0.000474573
NP8	G2	YLR193C	0.000275706
NP8	G3	YLR199C	0.000349717
NP8	G4	YLR200W	0.000311734
NP8	G5	YLR201C	0.000307603
NP8	G6	YLR203C	0.000340727
NP8	G7	YLR204W	
NP8	G8	YLR205C	0.000278823
NP8	G9	YLR206W	0.000250824

NP8	G10	YLR209C	0.000251
NP8	G11	YLR211C	
NP8	G12	YLR213C	0.000312
NP8	H1	YLR214W	0.000258
NP8	H2	YLR216C	0.000411
NP8	H3	YLR218C	0.00037
NP8	H4	YLR220W	0.000401
NP8	H5	YLR221C	0.000261
NP8	H6	YLR224W	0.000394
NP8	H7	YLR225C	0.000396
NP8	H8	YLR226W	0.000456
NP8	H9		
NP8	H10	YLR231C	
NP8	H11	YLR234W	0.000599
NP8	H12	YLR238W	
NP9	A1	p5472	0.000328
NP9	A2	YLR241W	0.000297
NP9	A3	YLR242C	0.000531
NP9	A4	YLR244C	0.000241
NP9	A5	YLR247C	0.000329
NP9	A6	YLR248W	0.000692
NP9	A7	YLR250W	0.000373
NP9	A8	YLR253W	0.000596
NP9	A9	YLR254C	0.000341
NP9	A10	YLR257W	0.000399
NP9	A11	YLR258W	0.002564
NP9	A12	YLR260W	0.000316
NP9	B1	YLR262C	0.000276
NP9	B2	YLR264W	0.00033
NP9	B3	YLR265C	0.000415
NP9	B4	GFP+	
NP9	B5	YLR267W	0.000528
NP9	B6	BY4741	0
NP9	B7	YLR273C	0.000494
NP9	B8	DES7	0.002308
NP9	B9	YLR281C	0.000344
NP9	B10	YLR283W	
NP9	B11	YLR284C	
NP9	B12	YLR285W	
NP9	C1	YLR287C	0.00022
NP9	C2	YLR287C-A	0.000512
NP9	C3	YLR288C	0.000302
NP9	C4	YLR289W	0.000258
NP9	C5	YLR290C	0.000384
NP9	C6	YLR292C	0.000243
NP9	C7	YLR293C	0.000386
NP9	C8	YLR297W	0.000263
NP9	C9	YLR299W	0.000341
NP9	C10	YLR300W	0.000237
NP9	C11	YLR304C	0.000345
NP9	C12	YLR308W	0.000199
NP9	D1	YLR312C	0.00026
NP9	D2	YLR312W-A	0.000261
NP9	D3	YLR313C	0.000607
NP9	D4	YLR315W	0.000216
NP9	D5	YLR320W	0.000277
NP9	D6	YHL047C	0.00028

NP9	D7	YHL046C	
NP9	D8	YHL044W	0.000372
NP9	D9	YHL043W	0.000255
NP9	D10	YHL042W	0.000313
NP9	D11	YHL040C	0.000647
NP9	D12	YHL038C	0.000212
NP9	E1	YHL036W	0.000264
NP9	E2		
NP9	E3	YHL034C	0.000252
NP9	E4	YHL033C	0.000295
NP9	E5	YHL032C	0.000312
NP9	E6	YHL031C	
NP9	E7	YHL030W	0.000352
NP9	E8	YHL029C	0.00024
NP9	E9	YHL028W	0.00033
NP9	E10		
NP9	E11		
NP9	E12		
NP9	F1	YHL022C	
NP9	F2	YHL021C	0.000329
NP9	F3	YHL020C	0.00046
NP9	F4	YHL019C	
NP9	F5	YHL017W	0.00029
NP9	F6	YHL014C	
NP9	F7	YHL013C	0.00026
NP9	F8	YHL012W	0.000284
NP9	F9	YHL010C	0.000328
NP9	F10	YHL009C	0.000181
NP9	F11	YHL008C	0.001075
NP9	F12	YHL007C	
NP9	G1	YHL006C	0.000258
NP9	G2	YHL003C	
NP9	G3	YHR001W-A	0.000883
NP9	G4	YHR010W	0.00029
NP9	G5	YHR011W	0.000298
NP9	G6	YHR012W	0.00056
NP9	G7	YHR013C	0.000282
NP9	G8	YHR014W	0.000261
NP9	G9	YHR015W	0.00026
NP9	G10	YHR018C	0.002636
NP9	G11	YHR021C	
NP9	G12	YHR022C	0.000328
NP9	H1	YHR028C	0.00052
NP9	H2	YHR029C	0.000297
NP9	H3	YHR030C	0.000194
NP9	H4	YHR031C	0.000316
NP9	H5	YHR033W	
NP9	H6	YHR034C	0.000263
NP9	H7	YHR035W	0.000216
NP9	H8	YHR037W	
NP9	H9	YHR038W	
NP9	H10	YHR039C	
NP9	H11	YHR044C	0.000223
NP9	H12		
NP10	A1	YOR001W	0.000672
NP10	A2	YOR002W	0.000276
NP10	A3	YOR003W	0.000391

NP10	A4	YOR005C	0.000315
NP10	A5	YOR006C	0.00041
NP10	A6	YOR007C	0.000324
NP10	A7		
NP10	A8	YOR009W	0.000429
NP10	A9	YOR010C	0.00041
NP10	A10	YOR011W	0.000317
NP10	A11	YOR012W	0.000324
NP10	A12	YOR014W	0.000369
NP10	B1	YOR016C	0.000362
NP10	B2	YOR022C	0.000394
NP10	B3	YOR023C	0.000349
NP10	B4	YOR025W	0.000341
NP10	B5	YOR026W	0.000316
NP10	B6	YOR027W	0.001183
NP10	B7	YOR028C	0.000375
NP10	B8	YOR030W	0.000654
NP10	B9	YOR031W	0.000526
NP10	B10	YOR033C	0.000363
NP10	B11	YOR034C	0.000501
NP10	B12	YOR035C	0.000558
NP10	C1	YOR036W	0.000336
NP10	C2	YOR037W	0.000374
NP10	C3	p5472	0.000478
NP10	C4	YOR039W	0.000424
NP10	C5	YOR040W	0.000466
NP10	C6	YOR042W	0.000591
NP10	C7	YOR043W	0.000459
NP10	C8	YOR044W	0.000625
NP10	C9	YOR045W	0.000335
NP10	C10	YOR047C	0.000395
NP10	C11	YOR049C	0.000487
NP10	C12	YOR051C	0.000485
NP10	D1	YOR052C	0.000235
NP10	D2	YOR054C	0.000645
NP10	D3	YOR058C	0.000356
NP10	D4	YOR059C	0.000419
NP10	D5	GFP+	
NP10	D6	YOR062C	0.0003
NP10	D7	YOR064C	0.000466
NP10	D8	YOR065W	0.000762
NP10	D9	YOR066W	0.00033
NP10	D10	BY4741	0
NP10	D11	YOR068C	0.000478
NP10	D12	YOR069W	0.000679
NP10	E1	YOR070C	0.00035
NP10	E2	YOR071C	0.000353
NP10	E3	YOR073W	0.00025
NP10	E4	YOR078W	0.000618
NP10	E5	YOR079C	0.000443
NP10	E6	YOR080W	0.000373
NP10	E7	YOR081C	0.000242
NP10	E8	DES7	0.001981
NP10	E9	YOR084W	0.000535
NP10	E10	YOR085W	0.000232
NP10	E11	YOR086C	0.000402
NP10	E12	YOR087W	0.000291

NP10	F1	YOR089C	0.00031
NP10	F2	YOR090C	0.000288
NP10	F3	YOR092W	0.000309
NP10	F4	YOR093C	0.000466
NP10	F5	YOR094W	0.000273
NP10	F6	YOR097C	0.000288
NP10	F7	YOR099W	0.000961
NP10	F8	YOR100C	0.000376
NP10	F9	YOR101W	0.000578
NP10	F10	YOR104W	0.000351
NP10	F11	YOR106W	0.000244
NP10	F12	YOR107W	0.000321
NP10	G1	YOR108W	0.000433
NP10	G2		
NP10	G3	YOR111W	0.000538
NP10	G4	YOR113W	0.001361
NP10	G5	YOR115C	0.00032
NP10	G6	YOR118W	0.000265
NP10	G7	YOR125C	0.000526
NP10	G8	YOR126C	0.000257
NP10	G9	YOR128C	0.000509
NP10	G10	YOR129C	0.00032
NP10	G11	YOR130C	0.000485
NP10	G12	YOR131C	0.000613
NP10	H1	YOR132W	0.001013
NP10	H2	YOR133W	0.000331
NP10	H3	YOR134W	0.000279
NP10	H4	YOR136W	0.000401
NP10	H5	YOR137C	0.000474
NP10	H6	YOR138C	0.000207
NP10	H7	YOR140W	0.000266
NP10	H8	YOR142W	0.000315
NP10	H9	YOR144C	0.000854
NP10	H10	YOR147W	0.00034
NP10	H11	YOR150W	0.000602
NP10	H12	YOR152C	0.000585
NP11	A1		
NP11	A2	YOR155C	0.000316
NP11	A3	YOR156C	0.000308
NP11	A4	YOR158W	0.000341
NP11	A5	YOR161C	0.000324
NP11	A6	YOR163W	0.000339
NP11	A7	YOR164C	0.000372
NP11	A8	YOR165W	0.000297
NP11	A9	YOR166C	0.000424
NP11	A10	YOR167C	0.000318
NP11	A11	YOR171C	0.000392
NP11	A12	YOR172W	
NP11	B1	YOR173W	0.000344
NP11	B2	p5472	0.000401
NP11	B3	YOR177C	0.000373
NP11	B4	YOR178C	0.000217
NP11	B5	YOR179C	0.000615
NP11	B6	YOR180C	0.00039
NP11	B7	YOR182C	0.000397
NP11	B8	YOR183W	0.000401
NP11	B9	YOR184W	0.000298

NP11	B10	YOR185C	0.000399
NP11	B11	YOR188W	0.000291
NP11	B12	YOR189W	0.000305
NP11	C1	YOR190W	0.000353
NP11	C2	GFP+	
NP11	C3	YOR192C	0.000878
NP11	C4	YOR289W	0.000483
NP11	C5	BY4741	0
NP11	C6	DES7	0.002789
NP11	C7	YOR295W	0.000456
NP11	C8	YOR296W	0.000364
NP11	C9	YOR297C	0.000439
NP11	C10	YOR298W	0.000472
NP11	C11	YOR299W	0.000332
NP11	C12	YOR301W	0.000289
NP11	D1	YOR304C-A	0.000256
NP11	D2	YOR304W	0.000359
NP11	D3	YOR307C	0.000446
NP11	D4	YOR308C	0.000658
NP11	D5	YOR311C	0.000361
NP11	D6	YOR313C	0.000453
NP11	D7	YOR315W	0.000397
NP11	D8	YOR316C	0.000472
NP11	D9	YOR322C	0.000532
NP11	D10	YOR323C	0.000303
NP11	D11	YOR324C	0.000352
NP11	D12		
NP11	E1	YOR332W	0.000302
NP11	E2	YOR334W	0.000441
NP11	E3	YOR337W	0.000245
NP11	E4	YOR338W	0.000529
NP11	E5	YOR339C	0.000375
NP11	E6		
NP11	E7	YOR344C	0.000287
NP11	E8	YOR346W	0.000372
NP11	E9	YOR347C	0.000281
NP11	E10	YOR348C	0.000346
NP11	E11	YOR349W	0.000565
NP11	E12	YOR350C	0.000342
NP11	F1	YOR369C	0.000281
NP11	F2	YOR371C	0.000321
NP11	F3	YOR374W	0.000305
NP11	F4	YOR351C	0.000547
NP11	F5	YOR354C	0.00024
NP11	F6	YOR355W	0.000518
NP11	F7	YOR356W	0.000439
NP11	F8	YOR357C	0.000511
NP11	F9	YOR358W	0.000757
NP11	F10	YOR359W	0.000259
NP11	F11	YOR360C	0.00053
NP11	F12	YOR363C	0.000267
NP11	G1	YOR375C	0.000331
NP11	G2	YOR377W	0.000301
NP11	G3	YOR378W	0.000377
NP11	G4	YOR380W	0.000368
NP11	G5	YOR381W	0.000244
NP11	G6	YOR382W	0.000359
NP11	G7	YHR046C	0.000734
NP11	G8	YHR047C	0.000611
NP11	G9	YHR048W	0.000514
NP11	G10	YHR049W	0.000274
NP11	G11	YHR050W	0.000314
NP11	G12	YHR051W	0.000357
NP11	H1	YHR057C	0.000265
NP11	H2	YHR060W	0.000443
NP11	H3	YHR061C	0.000441
NP11	H4	YHR066W	0.000385
NP11	H5	YHR075C	0.000392
NP11	H6	YHR076W	0.000467
NP11	H7	YHR077C	0.000425
NP11	H8	YHR080C	
NP11	H9	YHR081W	0.000431
NP11	H10	YHR082C	0.000473
NP11	H11	YHR084W	0.000272
NP11	H12	YHR086W	
NP12	A1	YHR087W	0.000485
NP12	A2	YHR092C	0.000384
NP12	A3	YHR094C	0.000549
NP12	A4	YHR096C	0.000334
NP12	A5	YHR100C	0.000817
NP12	A6	YHR103W	0.000686
NP12	A7	YHR104W	0.000432
NP12	A8	YHR105W	0.000304
NP12	A9	YHR108W	0.000497
NP12	A10	YHR109W	0.000678
NP12	A11	YHR110W	0.000424
NP12	A12	YHR111W	0.000524
NP12	B1	YHR112C	0.000361
NP12	B2	YHR113W	0.000452
NP12	B3	YHR114W	0.000566
NP12	B4	YHR115C	0.000653
NP12	B5	YHR116W	0.000493
NP12	B6	YHR117W	0.000597
NP12	B7	YHR120W	0.00076
NP12	B8	YHR121W	0.00062
NP12	B9	YHR123W	0.000599
NP12	B10	YHR124W	0.000766
NP12	B11	YHR126C	0.000414
NP12	B12	YHR129C	0.000541
NP12	C1	YHR132C	0.000379
NP12	C2	YHR133C	0.000458
NP12	C3	YHR134W	0.000605
NP12	C4	YHR135C	0.000437
NP12	C5	YHR136C	0.000904
NP12	C6	YHR137W	0.000731
NP12	C7	YHR138C	0.000458
NP12	C8	YHR139C	0.000565
NP12	C9	YMR140W	0.000606
NP12	C10	YMR143W	0.00056
NP12	C11	YMR144W	0.000697
NP12	C12	YMR145C	0.000481
NP12	D1	YMR147W	0.000394
NP12	D2	YMR148W	0.000501
NP12	D3	YMR152W	0.00066
NP12	D4	YMR153W	0.000685
NP12	D5	YMR155W	0.000593
NP12	D6	YMR156C	0.00071
NP12	D7	YMR157C	0.000528
NP12	D8	YMR161W	0.000441
NP12	D9	p5472	0.000616
NP12	D10	YMR165C	0.000439
NP12	D11	YMR170C	0.000462
NP12	D12	YMR177W	0.000552
NP12	E1	YMR178W	0.000381
NP12	E2	YMR179W	0.000455
NP12	E3	YMR180C	0.000386
NP12	E4	YMR182C	0.000614
NP12	E5	YMR183C	0.00047
NP12	E6	YMR184W	0.000426
NP12	E7	YMR186W	0.00061
NP12	E8	YMR187C	0.000387
NP12	E9	YMR188C	0.000457
NP12	E10	YMR189W	0.000428
NP12	E11	YMR193W	0.000492
NP12	E12	YMR194W	0.000408
NP12	F1	YMR195W	0.000402
NP12	F2	BY4741	0
NP12	F3	YMR199W	0.000434
NP12	F4	YMR201C	0.000456
NP12	F5	YMR202W	0.000485
NP12	F6	YMR204C	0.000422
NP12	F7	YMR205C	0.000581
NP12	F8	YMR210W	0.000396
NP12	F9	YMR214W	0.000541
NP12	F10	YMR217W	0.000415
NP12	F11	YMR223W	0.000406
NP12	F12	YMR224C	0.000442
NP12	G1	YMR228W	0.000495
NP12	G2	YMR230W	0.00044
NP12	G3	YOR384W	0.000458
NP12	G4	YOR385W	0.000406
NP12	G5	YOL001W	0.000583
NP12	G6	YOL003C	0.000727
NP12	G7	YOL006C	0.000541
NP12	G8	YOL008W	0.000587
NP12	G9	YOL009C	0.000472
NP12	G10	YOL011W	0.000491
NP12	G11	YOL012C	0.000589
NP12	G12	YOL013C	0.000344
NP12	H1	DES7	0.002319
NP12	H2	YOL018C	0.000435
NP12	H3	YOL019W	0.000476
NP12	H4	YOL020W	0.000526
NP12	H5	YOL023W	0.000582
NP12	H6	YOL024W	0.0005
NP12	H7	YOL025W	0.000476
NP12	H8	YOL027C	0.000592
NP12	H9	GFP+	
NP12	H10	YOL029C	0.000406
NP12	H11	YOL030W	0.00042
NP12	H12	YOL031C	0.000394

NP13	A1	YOL032W	0.000885
NP13	A2	YOL033W	0.000373
NP13	A3	YOL036W	0.000623
NP13	A4	YOL039W	0.000446
NP13	A5	YOL041C	0.000375
NP13	A6	YOL042W	0.000434
NP13	A7	YOL043C	0.000521
NP13	A8	YOL044W	0.001114
NP13	A9	YOL047C	0.001343
NP13	A10	YOL048C	0.000926
NP13	A11	YOL049W	0.000364
NP13	A12	YOL051W	0.000621
NP13	B1	YOL052C	0.000484
NP13	B2	YOL053W	0.000541
NP13	B3	YOL054W	0.000391
NP13	B4	YOL055C	0.000549
NP13	B5	YOL056W	0.000538
NP13	B6	YOL057W	0.000312
NP13	B7	YOL058W	0.00043
NP13	B8	YOL059W	0.000379
NP13	B9	YOL062C	0.000392
NP13	B10	YOL063C	0.000436
NP13	B11	p5472	0.00072
NP13	B12	YOL065C	0.000428
NP13	C1	BY4741	0
NP13	C2	YOL070C	0.00071
NP13	C3	YOL071W	0.000539
NP13	C4	YOL072W	0.000403
NP13	C5	YOL076W	0.00079
NP13	C6	YOL080C	0.000742
NP13	C7	GFP+	
NP13	C8	YOL082W	0.000408
NP13	C9	YPL274W	0.000395
NP13	C10	YPL273W	0.000365
NP13	C11	YPL272C	0.000721
NP13	C12	YPL270W	0.000314
NP13	D1	YPL269W	0.00078
NP13	D2	YPL267W	0.000481
NP13	D3	YPL265W	0.000372
NP13	D4	YPL264C	0.000695
NP13	D5	YPL263C	0.000475
NP13	D6	YPL262W	0.000483
NP13	D7	YPL260W	0.000437
NP13	D8	YPL259C	0.0004
NP13	D9	YPL258C	0.000507
NP13	D10	YPL257W	0.00045
NP13	D11	YPL256C	0.00042
NP13	D12	YPL254W	0.001829
NP13	E1	YPL253C	0.000708
NP13	E2	YPL250C	0.000511
NP13	E3	YPL249C	0.000514
NP13	E4	YPL248C	0.002849
NP13	E5	YPL247C	0.000959
NP13	E6	YPL246C	0.000402
NP13	E7	YPL245W	0.000794
NP13	E8	YPL241C	0.00113
NP13	E9	YPL240C	0.000438

NP13	E10	YPL239W	0.000585
NP13	E11	YPL236C	0.000613
NP13	E12	YPL230W	0.000373
NP13	F1	YPL229W	0.00057
NP13	F2	YPL227C	0.000378
NP13	F3	YPL225W	0.000631
NP13	F4	YPL223C	0.000635
NP13	F5	YPL222W	0.000391
NP13	F6	YPL221W	0.000543
NP13	F7	YPL220W	0.000466
NP13	F8	YPL219W	0.000386
NP13	F9	YPL215W	0.000739
NP13	F10	YPL214C	0.000853
NP13	F11	YPL213W	0.000431
NP13	F12	YPL212C	0.000842
NP13	G1	YPL207W	0.000464
NP13	G2	YPL206C	0.000402
NP13	G3	YPL203W	0.000397
NP13	G4	YPL202C	0.000306
NP13	G5	YPL201C	0.000506
NP13	G6	YPL200W	0.000495
NP13	G7	YPL199C	0.002128
NP13	G8	YPL198W	0.000763
NP13	G9	YPL196W	0.001276
NP13	G10	YPL193W	0.001914
NP13	G11	YPL192C	0.000826
NP13	G12	DES7	0.000606
NP13	H1	YOL015W	0.000588
NP13	H2	YGR256W	0.000621
NP13	H3	YGR260W	0.000543
NP13	H4	YGR261C	0.001178
NP13	H5	YGR262C	0.000469
NP13	H6	YGR263C	0.00034
NP13	H7	YGR266W	0.000441
NP13	H8	YGR268C	0.000608
NP13	H9	YGR270W	0.000421
NP13	H10	YGR279C	0.000361
NP13	H11	YGR281W	0.000338
NP13	H12	YGR282C	
NP14	A1	p5472	0.000617
NP14	A2	YGR284C	0.000244
NP14	A3	YGR285C	0.001003
NP14	A4	YGR286C	0.000523
NP14	A5	YGR287C	0.000539
NP14	A6	YGR288W	0.001004
NP14	A7	YIL009C-A	0.000754
NP14	A8	YIR017C	0.00077
NP14	A9		
NP14	A10	YIR021W	0.000641
NP14	A11	YIR024C	0.00055
NP14	A12	YIR026C	0.000574
NP14	B1	YIR027C	0.003239
NP14	B2	YIR029W	0.00023
NP14	B3	YIR031C	0.002917
NP14	B4	YIR033W	0.000326
NP14	B5	YIR034C	0.000954
NP14	B6	YIR035C	0.000273

NP14	B7	YIR037W	0.000324
NP14	B8	YIR038C	0.00095
NP14	B9	YIR039C	0.000738
NP14	B10	YIR042C	0.00094
NP14	B11	YKL033W-A	0.000804
NP14	B12	YKR035W-A	0.000449
NP14	C1	YKR066C	0.000315
NP14	C2	YKR067W	0.00279
NP14	C3	YKR069W	0.000299
NP14	C4	YKR070W	0.000279
NP14	C5	YKR072C	
NP14	C6	YKR074W	0.000367
NP14	C7	YKR075C	0.000309
NP14	C8	YKR076W	0.000374
NP14	C9	YKR078W	0.000538
NP14	C10	YKR080W	0.001222
NP14	C11	YKR084C	0.000285
NP14	C12	YKR087C	0.000529
NP14	D1	YKR088C	0.000191
NP14	D2	YKR089C	0.000381
NP14	D3	YKR090W	0.001937
NP14	D4	YKR091W	0.000293
NP14	D5	YKR092C	0.000751
NP14	D6	YKR097W	0.001964
NP14	D7	YKR100C	
NP14	D8	YKR103W	0.001942
NP14	D9	YKR104W	0.000379
NP14	D10	YLR262C-A	0.000321
NP14	D11	YLR422W	0.000262
NP14	D12	YLR426W	0.000833
NP14	E1	YLR427W	0.00068
NP14	E2	YLR435W	0.000232
NP14	E3	YLR436C	0.001224
NP14	E4	YLR437C	0.000363
NP14	E5	YLR438W	0.000289
NP14	E6	YLR441C	
NP14	E7	YLR443W	0.000551
NP14	E8	YLR445W	0.00034
NP14	E9	YLR447C	0.000402
NP14	E10	YLR449W	0.002602
NP14	E11	YLR452C	0.001713
NP14	E12	YLR453C	0.000512
NP14	F1	BY4741	0
NP14	F2	YLR456W	0.000393
NP14	F3	YLR460C	0.001332
NP14	F4	YLR461W	0.000575
NP14	F5	YML021C	0.002492
NP14	F6	YML081C-A	0.000299
NP14	F7	YMR060C	0.000644
NP14	F8	GFP+	
NP14	F9	YMR174C	0.000378
NP14	F10	YMR175W	0.000336
NP14	F11	YNR032C-A	
NP14	F12	YNR051C	0.000271
NP14	G1	DES7	0.002831
NP14	G2	YNR057C	0.000654
NP14	G3	YNR058W	0.000815

NP14	G4	YNR059W	0.000809
NP14	G5	YNR060W	0.000307
NP14	G6	YNR061C	0.000336
NP14	G7	YNR062C	0.000749
NP14	G8	YNR063W	0.002284
NP14	G9	YNR064C	0.000341
NP14	G10	YNR065C	0.000277
NP14	G11	YNR066C	0.000273
NP14	G12	YNR067C	0.000292
NP14	H1	YNR068C	
NP14	H2	YPL187W	0.000243
NP14	H3	YPL186C	0.001175
NP14	H4	YPL184C	
NP14	H5	YPL179W	0.000302
NP14	H6	YPL177C	0.000414
NP14	H7	YPL176C	0.000313
NP14	H8	YPL172C	0.000385
NP14	H9	YPL171C	0.000365
NP14	H10	YPL170W	0.000244
NP14	H11	YPL168W	0.000303
NP14	H12		
NP15	A1	YPL174C	0.005896
NP15	A2	YPL173W	0.001277
NP15	A3	YPL166W	0.000792
NP15	A4	YPL165C	0.000916
NP15	A5	YPL164C	0.00051
NP15	A6	YPL163C	0.000331
NP15	A7	p5472	0.000934
NP15	A8	BY4741	0
NP15	A9	YPL159C	0.001006
NP15	A10	YPL157W	0.000422
NP15	A11	YPL156C	0.000398
NP15	A12	YPL155C	0.000319
NP15	B1	YPL154C	0.001363
NP15	B2	YPL152W	0.000853
NP15	B3	YPL150W	0.000636
NP15	B4	YPL147W	0.000365
NP15	B5	YPL145C	0.0039
NP15	B6	YPL144W	0.000639
NP15	B7	YPL141C	0.000391
NP15	B8	YPL140C	0.001099
NP15	B9	YPL139C	0.000609
NP15	B10	YPL138C	0.000588
NP15	B11	YPL135W	0.000691
NP15	B12	YPL133C	0.000803
NP15	C1	YPL130W	0.000783
NP15	C2	YPL129W	0.000764
NP15	C3	YPL127C	0.000406
NP15	C4	YPL125W	0.000423
NP15	C5	YPL123C	0.000254
NP15	C6	YPL121C	0.002346
NP15	C7	YPL120W	0.00096
NP15	C8	YPL119C	0.000351
NP15	C9	YPL118W	0.000709
NP15	C10	YPL116W	0.000729
NP15	C11	GFP+	
NP15	C12	YPL113C	0.001036

NP15	D1	YPL112C	0.001326
NP15	D2	YPL111W	0.000303
NP15	D3	YPL110C	0.001545
NP15	D4	YPL109C	0.000335
NP15	D5	YPL108W	0.000682
NP15	D6	YPL107W	0.001097
NP15	D7	YPL106C	0.000702
NP15	D8	YPL103C	0.001197
NP15	D9	YPL100W	0.000545
NP15	D10	YPL099C	0.000903
NP15	D11	DES7	0.003114
NP15	D12	YPL097W	0.000917
NP15	E1	YPL096W	
NP15	E2	YPL095C	
NP15	E3	YPL092W	0.00195
NP15	E4	YPL090C	0.000739
NP15	E5	YPL089C	0.000917
NP15	E6	YPL088W	0.000334
NP15	E7	YPL086C	0.000287
NP15	E8	YPL081W	0.000495
NP15	E9	YPL079W	0.004827
NP15	E10	YPL077C	0.000611
NP15	E11	YPL074W	0.000961
NP15	E12	YPL072W	0.000508
NP15	F1	YPL071C	0.000328
NP15	F2	YPL070W	0.000919
NP15	F3	YPL069C	0.000253
NP15	F4	YPL066W	0.002271
NP15	F5	YPL064C	0.000456
NP15	F6	YPL059W	0.00033
NP15	F7		
NP15	F8	YPL057C	0.000918
NP15	F9	YPL056C	0.000603
NP15	F10	YPL055C	0.00051
NP15	F11	YPL054W	0.000736
NP15	F12	YPL053C	0.000538
NP15	G1	YPL052W	0.000269
NP15	G2	YPL051W	0.000686
NP15	G3	YPL050C	0.002051
NP15	G4	YPL049C	0.000464
NP15	G5	YPL048W	0.000623
NP15	G6	YPL047W	0.000713
NP15	G7	YPL046C	0.000838
NP15	G8	YPL045W	0.000277
NP15	G9	YPL042C	0.000757
NP15	G10	YPL041C	0.000654
NP15	G11		
NP15	G12		
NP15	H1	YPL038W	0.001896
NP15	H2		
NP15	H3	YPL033C	0.000979
NP15	H4	YPL032C	0.000483
NP15	H5	YPL030W	0.000767
NP15	H6	YPL029W	0.000649
NP15	H7	YPL026C	0.001078
NP15	H8	YPL023C	0.000488
NP15	H9	YPL021W	0.001004

NP15	H10	YPL019C	
NP15	H11	YPL018W	0.000783
NP15	H12	YPL015C	0.000563
NP16	A1	YPL014W	0.00072
NP16	A2	YPL013C	0.000534
NP16	A3	YPL009C	0.000459
NP16	A4	YPL006W	0.000453
NP16	A5	YPL005W	0.001309
NP16	A6	YPL003W	0.001449
NP16	A7	YPL002C	0.000945
NP16	A8	YPL001W	
NP16	A9	YPR001W	0.000933
NP16	A10	YPR002W	0.000618
NP16	A11	YPR003C	0.009012
NP16	A12	BY4741	0
NP16	B1	YPR005C	0.000842
NP16	B2	YPR106W	0.000704
NP16	B3	p5472	0.000595
NP16	B4	YPR116W	0.00029
NP16	B5	GFP+	
NP16	B6	YPR119W	0.000494
NP16	B7	YPR122W	0.002632
NP16	B8	YPR124W	0.00044
NP16	B9	YPR125W	
NP16	B10	YPR127W	0.002702
NP16	B11	YPR128C	0.000852
NP16	B12	YPR129W	0.000363
NP16	C1	YPR131C	0.000428
NP16	C2	YPR132W	0.002131
NP16	C3	YPR135W	0.002391
NP16	C4	YPR138C	0.004806
NP16	C5	YPR139C	0.003042
NP16	C6	YPR140W	0.000695
NP16	C7	YPR141C	0.000406
NP16	C8	YPR145W	0.000196
NP16	C9	YPR147C	0.000489
NP16	C10	YPR148C	0.001347
NP16	C11	YPR149W	0.001481
NP16	C12	YPR152C	0.000449
NP16	D1	YPR153W	0.000845
NP16	D2	YPR154W	0.000322
NP16	D3	YPR155C	0.000456
NP16	D4	YPR156C	0.000635
NP16	D5	YPR158W	0.000484
NP16	D6	YPR159W	0.000338
NP16	D7	YPR160W	0.000793
NP16	D8	YPR163C	0.000419
NP16	D9	DES7	0.003037
NP16	D10	YPR166C	0.001724
NP16	D11	YPR167C	0.000581
NP16	D12	YPR171W	0.001257
NP16	E1		
NP16	E2	YPR174C	0.000191
NP16	E3		
NP16	E4	YPR185W	0.00091
NP16	E5	YPR188C	0.000654
NP16	E6		

NP16	E7	YPR191W	0.000297
NP16	E8	YPR192W	0.000328
NP16	E9		
NP16	E10	YPR196W	0.00103
NP16	E11	YPR199C	0.00038
NP16	E12	YPR200C	0.000436
NP16	F1	YPR201W	0.000182
NP16	F2	YJL006C	0.000622
NP16	F3	YJL020C	0.000259
NP16	F4	YJL023C	0.000358
NP16	F5	YJL024C	0.000503
NP16	F6	YJL027C	0.000288
NP16	F7	YJR001W	
NP16	F8	YJR004C	0.000364
NP16	F9	YJR005W	0.000414
NP16	F10	YJR009C	0.000432
NP16	F11	YJR011C	0.000568
NP16	F12	YJR014W	0.000443
NP16	G1	YJR019C	0.000569
NP16	G2	YJR024C	0.00074
NP16	G3	YJR025C	0.002183
NP16	G4	YJR032W	0.001109
NP16	G5	YJR033C	0.000367
NP16	G6	YJR034W	0.00077
NP16	G7	YJR035W	0.000533
NP16	G8	YJR036C	0.000921
NP16	G9	YJR039W	0.000406
NP16	G10	YJR043C	0.003103
NP16	G11	YJR048W	0.000274
NP16	G12	YJR049C	0.001574
NP16	H1	YJR050W	0.001281
NP16	H2	YJR051W	0.000583
NP16	H3	YJR053W	0.000239
NP16	H4	YJR054W	0.002936
NP16	H5	YJR055W	0.001216
NP16	H6	YJR056C	0.000444
NP16	H7	YJR058C	0.000444
NP16	H8	YJR060W	0.001299
NP16	H9	YJR061W	0.001387
NP16	H10		
NP16	H11	YDL133C-A	
NP16	H12	YDR058C	0.000384
NP17	A1	YDR202C	0.000431
NP17	A2	YDR205W	0.000829
NP17	A3	YFR039C	0.000341
NP17	A4	YGL219C	0.000552
NP17	A5	YGR028W	0.000731
NP17	A6	YGR032W	0.000296
NP17	A7	YGR038W	0.000795
NP17	A8	YGR040W	0.000597
NP17	A9	YGR053C	0.000879
NP17	A10	YGR063C	0.000401
NP17	A11	YGR089W	0.000643
NP17	A12	p5472	0.000585
NP17	B1	YGR106C	0.00054
NP17	B2	YGR110W	0.000633
NP17	B3	YGR238C	0.000492
NP17	B4	YGR248W	0.000341
NP17	B5	YGR250C	0.000685
NP17	B6	YJL137C	0.000423
NP17	B7	YJL139C	0.000418
NP17	B8	YJL140W	0.000664
NP17	B9	YJL141C	0.000212
NP17	B10	YJL151C	0.000314
NP17	B11	YJL160C	0.000869
NP17	B12	BY4741	0
NP17	C1	YJL165C	0.000296
NP17	C2	YJL177W	0.000495
NP17	C3	YJL184W	0.000624
NP17	C4	YJL189W	0.000397
NP17	C5	YJL191W	0.000468
NP17	C6	YJL200C	0.000919
NP17	C7	YJL206C	0.000606
NP17	C8	YJL213W	0.000627
NP17	C9	YKL096W-A	0.000637
NP17	C10	YKL194C	0.000483
NP17	C11	YKL201C	0.003038
NP17	C12	YKL204W	0.000823
NP17	D1	YKL209C	0.000422
NP17	D2	YKL215C	0.000435
NP17	D3	YKL220C	0.000664
NP17	D4	YKR019C	0.000622
NP17	D5	YKR023W	0.000738
NP17	D6	GFP+	
NP17	D7	YKR028W	0.000315
NP17	D8	YKR029C	0.000307
NP17	D9	YKR039W	0.000712
NP17	D10	DES7	0.002919
NP17	D11	YML035C	0.000416
NP17	D12	YFL014W	0.000394
NP17	E1	YFL042C	0.000319
NP17	E2	YFR025C	0.000579
NP17	E3	YFR030W	0.000262
NP17	E4	YHR146W	0.000294
NP17	E5	YHR171W	0.000457
NP17	E6	YJL070C	0.000384
NP17	E7	YJL078C	0.000474
NP17	E8	YJL094C	0.000367
NP17	E9	YJL101C	0.000455
NP17	E10	YJL128C	0.000501
NP17	E11	YKR094C	0.000268
NP17	E12	YKR096W	
NP17	F1		
NP17	F2	YLR110C	0.00045
NP17	F3	YLR390W-A	0.000398
NP17	F4	YLR439W	0.000409
NP17	F5	YLR455W	0.00031
NP17	F6	YML066C	0.00053
NP17	F7	YML115C	0.000465
NP17	F8	YMR037C	0.000676
NP17	F9		
NP17	F10	YMR104C	0.000472
NP17	F11	YMR118C	0.000679
NP17	F12	YMR119W	0.000449
NP17	G1		
NP17	G2	YNR055C	0.000304
NP17	G3	YNR069C	0.000831
NP17	G4	YOL125W	0.000469
NP17	G5	YOL147C	0.000506
NP17	G6	YPL268W	0.000303
NP17	G7		
NP17	G8	YPR008W	0.000222
NP17	G9	YPR013C	0.000343
NP17	G10	YPR023C	0.000435
NP17	G11	YPR024W	0.000663
NP17	G12	YPR026W	
NP17	H1	YPR031W	0.000528
NP17	H2	YPR037C	0.000625
NP17	H3	YPR043W	0.000366
NP17	H4	YPR067W	0.000491
NP17	H5	YPR078C	0.000492
NP17	H6	YAR002C-A	0.000799
NP17	H7	YBR083W	0.000795
NP17	H8	YBR084C-A	0.000561
NP17	H9	YBR090C	0.000556
NP17	H10	YBR125C	0.000318
NP17	H11	YBR131W	0.000392
NP17	H12	YBR168W	
NP18	A1	YBR169C	0.000718
NP18	A2	YBR270C	0.000482
NP18	A3	YBR272C	0.000469
NP18	A4	YBR276C	0.000411
NP18	A5	YBR287W	0.000806
NP18	A6	YBR288C	0.000582
NP18	A7	YBR289W	0.000945
NP18	A8	YBR294W	0.001047
NP18	A9	YBR301W	0.001432
NP18	A10	p5472	0.000637
NP18	A11	BY4741	0
NP18	A12	GFP+	
NP18	B1	YCR046C	0.00072
NP18	B2	YCR047C	0.000322
NP18	B3	YCR060W	0.000937
NP18	B4	DES7	0.003055
NP18	B5	YCR069W	0.000124
NP18	B6	YCR083W	0.000631
NP18	B7	YCR084C	0.000648
NP18	B8	YCR088W	0.002222
NP18	B9	YDR007W	0.00091
NP18	B10	YFL026W	0.001336
NP18	B11	YFR011C	0.000923
NP18	B12	YFR013W	0.001124
NP18	C1	YNL052W	0.000305
NP18	C2	YNL056W	2.04E-05
NP18	C3	YNL065W	0.000539
NP18	C4	YNL066W	0.000705
NP18	C5	YNL070W	0.001042
NP18	C6	YNL072W	0.001226
NP18	C7	YNL073W	0.001518
NP18	C8	YNL074C	0.002095
NP18	C9	YNL076W	0.000809

NP18	C10	YNL078W	0.000884
NP18	C11	YNL079C	0.004095
NP18	C12	YNL080C	
NP18	D1		
NP18	D2	YNL085W	0.00027
NP18	D3	YNL090W	0.000403
NP18	D4	YNL093W	0.000565
NP18	D5	YNL095C	0.000445
NP18	D6	YNL097C	0.000853
NP18	D7	YNL099C	0.000569
NP18	D8	YNL104C	0.00066
NP18	D9	YNL107W	0.000757
NP18	D10	YNL115C	0.000529
NP18	D11	YNL119W	
NP18	D12	YNL125C	
NP18	E1	YNL130C	0.000164
NP18	E2	YEL001C	0.00045
NP18	E3	YEL003W	0.000559
NP18	E4	YEL004W	0.000726
NP18	E5		
NP18	E6	YEL006W	0.000744
NP18	E7	YEL009C	0.000455
NP18	E8	YEL013W	0.000784
NP18	E9	YEL015W	0.000665
NP18	E10	YEL016C	
NP18	E11	YEL017C-A	
NP18	E12	YEL017W	
NP18	F1	YEL018W	0.000333
NP18	F2	YEL020C	0.000172
NP18	F3		
NP18	F4		
NP18	F5	YEL027W	2.08E-05
NP18	F6	YEL029C	0.000594
NP18	F7	YEL031W	0.000698
NP18	F8	YEL036C	0.000746
NP18	F9	YEL037C	0.000777
NP18	F10	YEL039C	
NP18	F11	YEL040W	
NP18	F12		
NP18	G1		
NP18	G2	YEL044W	0.000322
NP18	G3		
NP18	G4	YEL048C	0.000529
NP18	G5	YEL049W	0.000493
NP18	G6	YEL050C	0.000433
NP18	G7	YEL051W	0.000892
NP18	G8	YEL052W	0.000663
NP18	G9	YEL053C	0.000406
NP18	G10	YEL054C	0.000268
NP18	G11	YEL056W	
NP18	G12	YEL057C	0.000522
NP18	H1	YEL060C	0
NP18	H2	YEL062W	0.000386
NP18	H3	YEL063C	0.000542
NP18	H4	YEL064C	0.000269
NP18	H5	YEL065W	0.000288
NP18	H6	YEL066W	
NP18	H7		
NP18	H8	YEL072W	
NP18	H9	YER001W	0.0002
NP18	H10	YER005W	0.000156
NP18	H11	YER007C-A	
NP18	H12	YER007W	
NP19	A1	YER010C	0.001136
NP19	A2	YER011W	0.001525
NP19	A3	YGR027C	0.000403
NP19	A4	YGR031W	0.001341
NP19	A5	YGR033C	0.001178
NP19	A6	YGR034W	0.001055
NP19	A7	YGR035C	0.000508
NP19	A8	YGR036C	0.001167
NP19	A9	YGR037C	0.001156
NP19	A10	p5472	0.000763
NP19	A11	BY4741	0
NP19	A12	GFP+	
NP19	B1	YGR045C	0.000586
NP19	B2	YGR052W	0.002799
NP19	B3	YGR054W	0.00112
NP19	B4	YGR055W	0.000565
NP19	B5	YGR056W	0.001191
NP19	B6	YGR057C	0.000292
NP19	B7	YGR058W	0.001051
NP19	B8	YGR059W	0.000311
NP19	B9	YGR066C	0.000491
NP19	B10	YGR067C	0.00023
NP19	B11	YGR068C	0.000661
NP19	B12	DES7	0.005957
NP19	C1	YGR071C	0.001725
NP19	C2	YGR076C	0.000886
NP19	C3	YGR077C	0.00352
NP19	C4	YGR078C	0.001626
NP19	C5	YGR080W	0.000786
NP19	C6	YGR084C	0.00137
NP19	C7	YGR087C	0.004173
NP19	C8	YGR088W	0.000382
NP19	C9	YGR097W	0.000882
NP19	C10	YGR100W	0.000352
NP19	C11	YGR101W	0.001798
NP19	C12	YGR102C	
NP19	D1	YGR104C	0.000656
NP19	D2	YGR105W	0.001063
NP19	D3	YGR108W	0.001688
NP19	D4	YGR109C	0.000503
NP19	D5	YGR112W	0.001844
NP19	D6	YGR118W	0.00163
NP19	D7	YGR121C	0.001005
NP19	D8	YGR122W	0.000471
NP19	D9	YJL127C	0.001419
NP19	D10	YJL124C	0.000781
NP19	D11	YJL123C	0.000929
NP19	D12	YJL122W	
NP19	E1	YJL121C	0.000371
NP19	E2	YJL118W	0.000889
NP19	E3	YJL117W	0.000332
NP19	E4	YJL116C	0.000463433
NP19	E5	YJL112W	0.000950168
NP19	E6	YJL110C	0.000820204
NP19	E7	YJL108C	0.000863107
NP19	E8	YJL106W	0.000935088
NP19	E9	YJL100W	0.000952275
NP19	E10	YJL099W	0.00038088
NP19	E11	YJL098W	
NP19	E12		
NP19	F1	YJL092W	0.000473473
NP19	F2		
NP19	F3	YJL088W	0.000777219
NP19	F4	YJL083W	0.001362383
NP19	F5	YJL082W	0.000769568
NP19	F6	YJL079C	0.001515346
NP19	F7	YJL077C	0.000880341
NP19	F8	YJL073W	0.00106654
NP19	F9	YJL071W	
NP19	F10	YJL068C	0.000833067
NP19	F11	YJL066C	0.000613845
NP19	F12	YJL065C	0.000836083
NP19	G1	YJL063C	0.00089825
NP19	G2	YJL062W	0.001114232
NP19	G3	YJL060W	0.001606817
NP19	G4	YJL059W	0.000366758
NP19	G5	YJL058C	0.00078296
NP19	G6		
NP19	G7	YJL056C	0.000655064
NP19	G8	YJL055W	0.000385696
NP19	G9	YJL053W	0.001018012
NP19	G10	YJL052W	0.000315835
NP19	G11	YJL051W	0.000456141
NP19	G12	YJL049W	0.0007432
NP19	H1	YJL048C	0.000896781
NP19	H2	YJL047C	0.000870922
NP19	H3	YJL046W	
NP19	H4	YJL044C	
NP19	H5	YJL043W	0.001004373
NP19	H6	YJL038C	0.000961013
NP19	H7	YJL037W	0.000533048
NP19	H8	YJL036W	0.001064277
NP19	H9	YER114C	0.000751864
NP19	H10	YER115C	0.000595508
NP19	H11	YER116C	0.000434675
NP19	H12		
NP20	A1	YBL001C	0.007666554
NP20	A2	YBL003C	0.00084999
NP20	A3	YBL005W	0.001124549
NP20	A4	YBL006C	0.001312103
NP20	A5	YBL007C	0.001031768
NP20	A6	YBL008W	0.000483209
NP20	A7	YBL009W	0.000826165
NP20	A8	YBL010C	0.00137863
NP20	A9	YBL011W	0.000429341
NP20	A10	YBL013W	0.000849284
NP20	A11	YBL015W	0.000966976
NP20	A12	YBL016W	0.001004843

NP20	B1	YBL017C	0.001035
NP20	B2	YBL019W	0.001219
NP20	B3	YBL021C	0.001312
NP20	B4	YBL024W	0.001724
NP20	B5	YBL025W	0.000599
NP20	B6	YBL027W	0.000634
NP20	B7	YBL028C	0.000723
NP20	B8	YBL029W	0.001426
NP20	B9	YBL031W	0.00063
NP20	B10	YBL032W	0.000817
NP20	B11	YBL033C	0.000447
NP20	B12	YBL036C	0.001141
NP20	C1	YBL037W	0.000903
NP20	C2	YBL038W	0.000537
NP20	C3	YBL039C	0.00157
NP20	C4	YBL042C	0.000925
NP20	C5	YBL045C	0.001133
NP20	C6	YBL046W	0.001291
NP20	C7	YBL047C	0.000855
NP20	C8	YBL049W	0.001411
NP20	C9	YBL052C	0.012417
NP20	C10	YBL054W	0.001496
NP20	C11	YBL056W	0.0025
NP20	C12	YBL057C	0.000895
NP20	D1	YBL058W	0.001155
NP20	D2	YBL059W	0.001503
NP20	D3	YBL061C	0.000861
NP20	D4	YBL063W	0.000534
NP20	D5	YBL064C	0.001868
NP20	D6	YBL066C	0.000711
NP20	D7	p5472	0.001125
NP20	D8	YBL068W	0.001472
NP20	D9	YBL069W	0.001092
NP20	D10	YBL072C	0.000867
NP20	D11	YBL075C	0.000763
NP20	D12	YBL078C	0.001202
NP20	E1	YBL079W	0.001474
NP20	E2	YBL080C	0.000644
NP20	E3	YBL081W	0.00172
NP20	E4	YBL085W	0.001243
NP20	E5	YBL086C	0.000894
NP20	E6	YBL087C	0.000723
NP20	E7	YBL089W	0.001671
NP20	E8	YBL090W	0.001006
NP20	E9	YBL091C	0.001125
NP20	E10	YBL093C	0.000747
NP20	E11	YAL068C	0.001072
NP20	E12	YAL067C	0.000879
NP20	F1	BY4741	6.74E-07
NP20	F2	YAL062W	0.004266
NP20	F3	GFP+	
NP20	F4	YAL060W	0.001148
NP20	F5	YAL059W	0.000732
NP20	F6	YAL058W	0.000977
NP20	F7	YAL056W	0.000871
NP20	F8	YAL055W	0.000896
NP20	F9	YAL053W	0.001296
NP20	F10	YAL051W	0.001081
NP20	F11	YAL049C	0.001295
NP20	F12	YAL048C	0.000903
NP20	G1	YAL046C	0.00074
NP20	G2	YAL044C	0.000921
NP20	G3	YAL042W	0.000485
NP20	G4	YAL040C	0.001967
NP20	G5	YAL039C	0.00043
NP20	G6	DES7	0.003338
NP20	G7		
NP20	G8		
NP20	G9	YAL034C	0.001264
NP20	G10	YAL031C	0.001538
NP20	G11	YAL030W	0.001104
NP20	G12	YAL029C	0.001248
NP20	H1	YAL028W	0.001283
NP20	H2	YAL027W	0.000839
NP20	H3	YAL026C	0.001052
NP20	H4	YAL023C	0.001205
NP20	H5	YAL022C	0.000973
NP20	H6	YAL021C	0.001273
NP20	H7	YAL020C	0.000758
NP20	H8	YAL019W	0.000972
NP20	H9	YAL018C	0.000926
NP20	H10	YAL017W	0.00107
NP20	H11	YAL015C	0.000674
NP20	H12		
NP21	A1	YAL013W	0.001164
NP21	A2	YAL011W	0.000263
NP21	A3	YAL010C	0.001566
NP21	A4	YAL009W	0.001153
NP21	A5	YAL008W	0.00097
NP21	A6	YAL007C	0.001874
NP21	A7	YAL005C	0.000447
NP21	A8	YAL002W	0.000834
NP21	A9	YAR002W	0.00938
NP21	A10	YAR003W	0.000911
NP21	A11	p5472	0.000346
NP21	A12	YAR015W	0.000611
NP21	B1	YAR018C	0.001111
NP21	B2	YAR020C	0.001145
NP21	B3	YAR023C	0.00082
NP21	B4	YAR027W	0.000763
NP21	B5	YAR028W	0.001049
NP21	B6	YAR029W	0.000923
NP21	B7	YAR031W	0.001081
NP21	B8	YAR035W	0.000971
NP21	B9	YMR062C	0.000614
NP21	B10	YMR063W	0.001859
NP21	B11	YMR064W	0.000782
NP21	B12	YMR065W	0.000841
NP21	C1	BY4741	6.43E-07
NP21	C2	YMR069W	0.001321
NP21	C3	YMR070W	0.000894
NP21	C4	YMR071C	0.000709
NP21	C5	YMR072W	0.001865
NP21	C6	YMR073C	0.001295
NP21	C7	YMR075W	0.001242
NP21	C8	YMR077C	0.000595
NP21	C9	YMR078C	0.000685
NP21	C10	YMR080C	0.000617
NP21	C11	YMR081C	0.00088
NP21	C12	YMR083W	0.000841
NP21	D1	YMR084W	0.000587
NP21	D2	YMR085W	0.000769
NP21	D3	YMR086W	0.00091
NP21	D4	YMR087W	0.000971
NP21	D5	YMR089C	0.000914
NP21	D6	YMR090W	0.001378
NP21	D7	YMR091C	0.000704
NP21	D8	YMR092C	0.00105
NP21	D9	YNR072W	0.00095
NP21	D10	YNR073C	0.000967
NP21	D11	YNR074C	0.000837
NP21	D12	YNR075W	0.000514
NP21	E1	YOL013W-A	0.000936
NP21	E2	YOL086C	0.001169
NP21	E3	YOL087C	0.001296
NP21	E4	YOL088C	0.000843
NP21	E5	YOL089C	0.001026
NP21	E6	YOL090W	0.000892
NP21	E7	YOL091W	0.00067
NP21	E8	YOL092W	0.000797
NP21	E9	YOL093W	0.000889
NP21	E10	YOL095C	0.000796
NP21	E11	YOL096C	0.001091
NP21	E12	YOL098C	0.001023
NP21	F1	YOL100W	0.00093
NP21	F2	YOL103W	0.001306
NP21	F3	YOL104C	0.000796
NP21	F4	YOL105C	0.000643
NP21	F5	YOL107W	0.000926
NP21	F6	YOL108C	0.000866
NP21	F7	YOL109W	0.000863
NP21	F8	YOL111C	0.000689
NP21	F9	YOL112W	0.000793
NP21	F10	YOL113W	0.000957
NP21	F11	YOL114C	0.000831
NP21	F12	YOL115W	0.000517
NP21	G1	YOL116W	0.000872
NP21	G2	YOL117W	0.001005
NP21	G3	YOL119C	0.001318
NP21	G4	YOL121C	0.00066
NP21	G5	YOL122C	0.000749
NP21	G6	YOL124C	0.000308
NP21	G7	YOL126C	0.001043
NP21	G8	YOL128C	0.001126
NP21	G9	YOL129W	0.000913
NP21	G10	YOL131W	0.001238
NP21	G11	YOL132W	0.001376
NP21	G12	YOL136C	0.000969
NP21	H1	YOL137W	0.000929
NP21	H2	YOL138C	0.000959
NP21	H3	YER101C	0.001119

NP21	H4	YER103W	0.000912908
NP21	H5	YER106W	0.000816358
NP21	H6	YER107C	0.001107807
NP21	H7	YER109C	0.001443001
NP21	H8	YER110C	0.000763905
NP21	H9	YER113C	0.006815097
NP21	H10	GFP+	
NP21	H11	DES7	0.008815007
NP21	H12		
NP22	A1	YER117W	0.000486474
NP22	A2	YER118C	0.000327622
NP22	A3	YER119C	0.000279106
NP22	A4	YER120W	0.000441435
NP22	A5	YER122C	0.000683791
NP22	A6	YER123W	0.000455361
NP22	A7	YER124C	0.00029287
NP22	A8	YER128W	0.000483702
NP22	A9		
NP22	A10	YER130C	0.00040471
NP22	A11	YER131W	0.000290212
NP22	A12	YER132C	0.000313804
NP22	B1	YER134C	0.001164546
NP22	B2	YER137C	0.000397385
NP22	B3	YER140W	0.004390195
NP22	B4	YER141W	0.006335312
NP22	B5	YER142C	0.000768542
NP22	B6	YER143W	0.001021873
NP22	B7	YER145C	0.000322857
NP22	B8	YER149C	0.000400211
NP22	B9	YER150W	0.000324111
NP22	B10	YER151C	0.000390397
NP22	B11	YER152C	0.000347811
NP22	B12	YER153C	0.000939421
NP22	C1	YER154W	0.000345441
NP22	C2	BY4741	0
NP22	C3	YER156C	0.000368312
NP22	C4	YER158C	0.001912212
NP22	C5	YER161C	0.00289558
NP22	C6	GFP+	
NP22	C7	YER163C	0.000347177
NP22	C8	YER164W	0.000416204
NP22	C9		
NP22	C10	YER167W	0.002925689
NP22	C11	YER169W	0.000250809
NP22	C12	YER170W	0.000745685
NP22	D1	YER173W	0.000373272
NP22	D2	YER174C	0.00037042
NP22	D3	YER175C	0.000723369
NP22	D4	p5472	0.001092771
NP22	D5	YER177W	0.00051146
NP22	D6	YER178W	7.91873E-05
NP22	D7	YER179W	0.001736871
NP22	D8	YER180C	0.00062782
NP22	D9	YER182W	0.001152792
NP22	D10	YER183C	0.000350188
NP22	D11	YER184C	0.000590991
NP22	D12	YER185W	0.001413996

NP22	E1	YER186C	0.002101519
NP22	E2	YER187W	0.000400779
NP22	E3	YMR052W	0.000382197
NP22	E4	YMR053C	0.001356796
NP22	E5	DES7	0.004174516
NP22	E6	YMR055C	0.000313849
NP22	E7	YMR056C	0.000340746
NP22	E8	YMR058W	0.000245785
NP22	E9	YCR092C	0.001254567
NP22	E10	YCR094W	0.000342507
NP22	E11	YCR098C	0.00080014
NP22	E12	YCR099C	0.000355246
NP22	F1	YCR100C	0.000459847
NP22	F2	YCR101C	0.001126756
NP22	F3	YCR102C	0.000891627
NP22	F4	YCR105W	0.000634998
NP22	F5	YCR106W	0.000310226
NP22	F6	YDL130W-A	0.000955459
NP22	F7	YDR363W-A	0.000505689
NP22	F8	YDR525W-A	0.000372185
NP22	F9	YDR536W	0.000279455
NP22	F10	YDR538W	0.000617598
NP22	F11	YDR539W	0.000270194
NP22	F12	YDR541C	0.000664303
NP22	G1	YER039C-A	0.001083709
NP22	G2	YER144C	
NP22	G3	YFL034C-A	0.000377762
NP22	G4	YFR032C	0.000386083
NP22	G5	YFR032C-A	0.000456228
NP22	G6	YFR033C	0.00031766
NP22	G7	YFR034C	0.001350309
NP22	G8	YFR035C	0.000504036
NP22	G9	YFR036W	0.002523856
NP22	G10	YFR040W	0.000641577
NP22	G11	YFR041C	0.000264585
NP22	G12	YFR043C	0.001087065
NP22	H1	YFR044C	0.00047761
NP22	H2	YFR045W	0.000354135
NP22	H3	YFR046C	0.000209046
NP22	H4	YFR047C	0.000768137
NP22	H5	YFR048W	0.000770137
NP22	H6	YFR049W	0.000968117
NP22	H7	YFR053C	0.000242387
NP22	H8	YFR055W	0.000434509
NP22	H9		
NP22	H10	YGR220C	0.000674105
NP22	H11	YGR221C	0.000752663
NP22	H12	YGR222W	0.000546858
NP23	A1	YGR223C	0.000315874
NP23	A2	YGR224W	0.000783171
NP23	A3	YGR225W	0.000826885
NP23	A4	YGR226C	0.000422171
NP23	A5	YGR227W	0.000686795
NP23	A6	YGR229C	0.000608
NP23	A7	YGR230W	0.000309173
NP23	A8	YGR231C	0.000680729
NP23	A9	p5472	0.000856727

NP23	A10	YGR233C	0.000469
NP23	A11	YGR234W	0.000523
NP23	A12	YGR235C	0.000422
NP23	B1	YGR236C	0.000685
NP23	B2	YGR240C	0.000531
NP23	B3	YGR241C	0.001228
NP23	B4	YGR243W	0.000877
NP23	B5		
NP23	B6	YGR247W	0.001216
NP23	B7	YAL024C	0.000484
NP23	B8	YCR107W	0.001329
NP23	B9		
NP23	B10	YDR493W	0.000452
NP23	B11	YDR500C	0.001384
NP23	B12	YDR502C	0.001511
NP23	C1	YDR506C	0.001603
NP23	C2	BY4741	0
NP23	C3		
NP23	C4		
NP23	C5	YFL010C	0.001872
NP23	C6	GFP+	
NP23	C7	YFL012W	0.000506
NP23	C8	YFL013C	0.000708
NP23	C9		
NP23	C10	YGR252W	0.001633
NP23	C11	YGR254W	0.002519
NP23	C12	YGR257C	0.001969
NP23	D1	YGR271W	0.000999
NP23	D2		
NP23	D3	YGR273C	0.000664
NP23	D4		
NP23	D5	YGR295C	0.000562
NP23	D6	YHR132W-A	0.001045
NP23	D7	YIL092W	0.000659
NP23	D8	YIR030C	0.000595
NP23	D9	YIR032C	0.000657
NP23	D10	YJR003C	0.0014
NP23	D11	YKL053C-A	0.000413
NP23	D12	YMR322C	0.003743
NP23	E1	YNL138W	0.000797
NP23	E2	YOL152W	0.000847
NP23	E3	YOR265W	0.000571
NP23	E4	YOR268C	0.000663
NP23	E5	YOR271C	0.000463
NP23	E6	YOR273C	0.000333
NP23	E7	YOR274W	0.001625
NP23	E8	YOR275C	0.002029
NP23	E9	YOR276W	0.000742
NP23	E10	YOR302W	0.000764
NP23	E11	YOR303W	0.000952
NP23	E12	YPL004C	0.000604
NP23	F1	YPL027W	0.000407
NP23	F2	YPL034W	0.000686
NP23	F3	YPL078C	0.00068
NP23	F4	YBL095W	0.000452
NP23	F5	YBL102W	0.00107
NP23	F6	YBL103C	0.000344

NP23	F7	YBL107C	0.00120484
NP23	F8	YBR001C	0.000577886
NP23	F9	YBR003W	0.000797455
NP23	F10	YBR005W	0.000376157
NP23	F11	YBR006W	0.0003996
NP23	F12	YBR007C	0.000756068
NP23	G1		
NP23	G2	YBR009C	0.00105861
NP23	G3	YBR010W	0.000749632
NP23	G4	YBR013C	0.000866566
NP23	G5	YBR014C	0.00087121
NP23	G6	YBR015C	0.000374603
NP23	G7	YBR019C	0.000586938
NP23	G8	YBR021W	0.000436529
NP23	G9	YBR022W	0.001022754
NP23	G10	YBR024W	0.001304142
NP23	G11	YBR025C	0.002192142
NP23	G12	YBR026C	0.000732338
NP23	H1	YBR028C	0.00052133
NP23	H2	YBR031W	0.000725642
NP23	H3	YBR035C	0.000864399
NP23	H4	YBR036C	0.000876015
NP23	H5	YBR037C	0.001225098
NP23	H6	YBR039W	0.001006231
NP23	H7	YBR040W	0.000539104
NP23	H8	YBR042C	0.000759125
NP23	H9	DES7	0.003860643
NP23	H10	YBR045C	0.000958195
NP23	H11	YBR046C	0.000561819
NP23	H12		
NP24	A1	YBR048W	0.00057133
NP24	A2	YBR050C	0.000589588
NP24	A3	YBR052C	0.001366621
NP24	A4	YBR053C	0.000471526
NP24	A5		
NP24	A6	YBR056W	0.000689318
NP24	A7	YBR057C	0.000984236
NP24	A8		
NP24	A9	YBR047W	0.00078399
NP24	A10	YBR061C	0.000527942
NP24	A11	YBR062C	0.002817493
NP24	A12	YBR063C	0.001867758
NP24	B1	YBR065C	0.000517135
NP24	B2	YBR066C	0.000491938
NP24	B3	YBR067C	0.003364844
NP24	B4	YBR068C	0.000421667
NP24	B5	YBR069C	0.001149039
NP24	B6	YBR071W	0.001189708
NP24	B7	YBR072W	0.00045344
NP24	B8	YBR076W	0.001086698
NP24	B9	YBR077C	0.001182336
NP24	B10	YBR078W	0.004692777
NP24	B11	YDR148C	0.001366276
NP24	B12	YDR150W	0.000782348
NP24	C1	YDR151C	0.000572807
NP24	C2	YDR152W	0.001436367
NP24	C3	YDR155C	0.000777829
NP24	C4	YDR156W	0.000373
NP24	C5	YDR162C	0.00062
NP24	C6	YDR163W	0.001302
NP24	C7	YDR165W	0.000728
NP24	C8	YDR169C	0.000451
NP24	C9	YDR171W	0.001945
NP24	C10	YDR175C	0.000504
NP24	C11	YDR176W	0.000444
NP24	C12	YDR178W	0.001461
NP24	D1	YDR179C	0.000513
NP24	D2	YDR179W-A	0.000387
NP24	D3	YDR181C	0.001563
NP24	D4	YDR184C	0.000581
NP24	D5	p5472	0.00122
NP24	D6	YDR186C	0.00141
NP24	D7	YDR191W	0.000419
NP24	D8	YDR192C	0.000522
NP24	D9	YDR194C	0.001479
NP24	D10	YDR195W	0.001091
NP24	D11	YDR197W	0.000529
NP24	D12	YDR198C	0.000612
NP24	E1	YDR200C	0.001969
NP24	E2	YDR204W	0.001675
NP24	E3	BY4741	0
NP24	E4	YDR213W	0.000502
NP24	E5	YDR214W	0.000683
NP24	E6	YDR218C	0.000638
NP24	E7	YDR219C	0.000928
NP24	E8	YDR221W	0.001044
NP24	E9	YDR222W	0.001044
NP24	E10	YDR223W	0.000981
NP24	E11	YDR225W	0.000568
NP24	E12	YDR226W	0.000763
NP24	F1	GFP+	
NP24	F2	YDR229W	0.000421
NP24	F3	YDR231C	0.001532
NP24	F4	YDR233C	0.00066
NP24	F5	YDR234W	0.000671
NP24	F6	YDR237W	0.001584
NP24	F7		
NP24	F8	YGL002W	0.000669
NP24	F9	YGL004C	0.001073
NP24	F10	YGL010W	0.001051
NP24	F11	YGL013C	0.00062
NP24	F12	YGL014W	0.000458
NP24	G1	YGL039W	0.000577
NP24	G2	YGL096W	0.000902
NP24	G3	YGL015C	0.000962
NP24	G4	DES7	0.003704
NP24	G5	YGL017W	0.000885
NP24	G6	YGL019W	0.000729
NP24	G7		
NP24	G8	YGL021W	0.000562
NP24	G9	YGL023C	0.00054
NP24	G10	YGL027C	0.000665
NP24	G11	YGL028C	0.000533
NP24	G12	YGL029W	0.00053
NP24	H1	YGL031C	0.000834
NP24	H2	YGL038C	0.000805
NP24	H3	YGL043W	0.001088
NP24	H4	YGL045W	0.000586
NP24	H5	YGL049C	0.001694
NP24	H6	YGL051W	0.00089
NP24	H7	YGL053W	0.000894
NP24	H8	YGL054C	0.000946
NP24	H9	YGL056C	0.000575
NP24	H10	YGL057C	0.000779
NP24	H11	YGL058W	0.000684
NP24	H12	YGL059W	0.001122
NP25	A1	YGL063W	0.000334
NP25	A2	YGL064C	0.000317
NP25	A3	YGL066W	0.0003
NP25	A4	YGL067W	0.000345
NP25	A5	YGL070C	0.000488
NP25	A6	YGL071W	0.000433
NP25	A7	YGL077C	0.001284
NP25	A8	YGL078C	0.00065
NP25	A9	YGL079W	0.000452
NP25	A10	YGL080W	0.000393
NP25	A11	YGL081W	0.000408
NP25	A12	YGL082W	0.000372
NP25	B1	YGL083W	0.000329
NP25	B2	YGL084C	0.000295
NP25	B3	YGL087C	0.000323
NP25	B4	YGL089C	0.000321
NP25	B5	YGL090W	0.000638
NP25	B6	p5472	0.000679
NP25	B7	YGL105W	0.000261
NP25	B8	YGL107C	0.000632
NP25	B9	BY4741	0
NP25	B10	YGL108C	0.000445
NP25	B11	YGL110C	0.000349
NP25	B12	YGL114W	0.000343
NP25	C1	YGL115W	0.000336
NP25	C2	YGL117W	0.000289
NP25	C3	YGL121C	0.000342
NP25	C4	YGL124C	0.000523
NP25	C5	YGL126W	0.00061
NP25	C6	YGL127C	0.00052
NP25	C7	YGL129C	0.000423
NP25	C8	YGL131C	0.000634
NP25	C9	YGL135W	0.001453
NP25	C10	GFP+	
NP25	C11	YGL138C	0.00041
NP25	C12	YGL139W	0.000247
NP25	D1	YGL140C	0.000373
NP25	D2	YGL141W	0.000487
NP25	D3	YGL143C	0.000707
NP25	D4	YGL146C	0.000523
NP25	D5	YGL147C	0.000351
NP25	D6	YGL148W	0.000475
NP25	D7	YGL151W	0.000332
NP25	D8	YGL153W	0.000351
NP25	D9	YGL154C	0.001986

NP25	D10	YGL156W	0.000776
NP25	D11	YGL157W	0.00038
NP25	D12	YGL158W	0.000385
NP25	E1	YGL159W	0.000372
NP25	E2	YGL161C	0.000244
NP25	E3	YGL162W	0.000394
NP25	E4	YGL163C	0.000195
NP25	E5	YGL164C	0.000258
NP25	E6	YGL166W	0.000372
NP25	E7	YGL167C	0.000318
NP25	E8	YGL168W	0.000199
NP25	E9	YGL170C	0.000457
NP25	E10	YGL173C	0.000215
NP25	E11	YGL174W	0.000315
NP25	E12	YGL175C	0.000428
NP25	F1	YGL176C	0.000383
NP25	F2	YGL179C	0.000408
NP25	F3	YGL180W	0.000804
NP25	F4	DES7	0.002677
NP25	F5	YBR173C	0.000155
NP25	F6	YBR176W	0.000321
NP25	F7	YBR177C	0.000169
NP25	F8	YBR183W	0.000276
NP25	F9	YBR185C	0.000338
NP25	F10	YBR186W	0.000428
NP25	F11	YBR187W	0.000272
NP25	F12	YBR188C	0.000324
NP25	G1	YBR194W	0.00044
NP25	G2	YBR195C	0.000245
NP25	G3	YBR197C	0.0003
NP25	G4	YBR199W	0.000303
NP25	G5	YBR200W	0.000506
NP25	G6	YBR201W	0.000358
NP25	G7	YBR204C	0.000335
NP25	G8	YBR205W	0.00044
NP25	G9	YBR207W	0.000346
NP25	G10	YBR210W	0.000379
NP25	G11	YBR212W	0.000268
NP25	G12	YBR213W	0.00036
NP25	H1	YBR214W	0.000295
NP25	H2	YBR215W	0.000437
NP25	H3	YBR216C	0.00036
NP25	H4	YBR217W	0.00041
NP25	H5	YBR218C	0.000378
NP25	H6	YBR219C	0.000387
NP25	H7	YBR220C	0.000282
NP25	H8	YBR221C	0.000273
NP25	H9	YBR222C	0.000319
NP25	H10	YBR225W	0.000276
NP25	H11	YBR227C	0.000389
NP25	H12	YBR228W	
NP26	A1	YBR229C	0.000398
NP26	A2	YBR230C	0.000329
NP26	A3	YBR231C	0.000538
NP26	A4	YBR233W	0.000417
NP26	A5	YBR238C	0.000357
NP26	A6	YBR239C	0.00035
NP26	A7	YBR241C	0.000304
NP26	A8	YBR242W	0.000306
NP26	A9	YBR244W	0.00039
NP26	A10	YBR246W	0.000246
NP26	A11	YBR248C	0.000277
NP26	A12	YBR249C	0.000207
NP26	B1	YBR250W	0.000416
NP26	B2	YBR251W	0.000456
NP26	B3	p5472	0.000511
NP26	B4	YBR258C	0.000395
NP26	B5	YBR259W	0.000387
NP26	B6	YBR261C	0.000496
NP26	B7	YBR263W	0.000427
NP26	B8	YBR264C	0.000335
NP26	B9	YBR267W	0.000302
NP26	B10	YDL099W	0.000266
NP26	B11	YDL100C	0.000303
NP26	B12	YDL101C	0.000234
NP26	C1	YDL104C	0.000329
NP26	C2	YDL106C	0.000335
NP26	C3	YDL107W	0.000369
NP26	C4	YDL109C	0.000358
NP26	C5	YDL110C	0.00033
NP26	C6		
NP26	C7	YDL114W	0.000552
NP26	C8	YDL115C	0.000283
NP26	C9	YDL116W	0.000309
NP26	C10	YDL117W	0.000343
NP26	C11	YDL119C	0.000304
NP26	C12	YDL121C	0.000368
NP26	D1	YDL122W	0.000422
NP26	D2	YDL123W	0.000334
NP26	D3	YDL124W	0.000391
NP26	D4	YDL125C	0.000327
NP26	D5	YDL127W	0.000316
NP26	D6	YDL128W	0.000526
NP26	D7	YDL129W	0.000257
NP26	D8	YDL130W	0.000388
NP26	D9	YDL133W	0.000241
NP26	D10	YDL134C	0.000287
NP26	D11	YDL135C	0.000238
NP26	D12	YDL136W	0.000269
NP26	E1	YDL137W	0.000326
NP26	E2	YDL138W	0.000282
NP26	E3	YDL142C	0.000295
NP26	E4	YDL144C	0.000166
NP26	E5	YDL146W	0.000164
NP26	E6	YDL149W	0.000385
NP26	E7	YDL154W	0.00031
NP26	E8	YDL155W	0.00033
NP26	E9	YDL156W	0.000235
NP26	E10	YDL157C	0.00022
NP26	E11	YDL159W	0.000219
NP26	E12	YDL160C	0.000227
NP26	F1	YDL161W	0.000303
NP26	F2	YDL167C	0.000281
NP26	F3	YDL168W	0.000494
NP26	F4	YDL169C	0.000498
NP26	F5	YDL170W	0.000816
NP26	F6	BY4741	0
NP26	F7	YDL174C	0.000427
NP26	F8	YDL175C	0.000432
NP26	F9	YDL176W	0.00036
NP26	F10	YDL177C	0.000281
NP26	F11	YDL178W	0.000265
NP26	F12	YDL179W	0.000373
NP26	G1	YDL180W	0.000336
NP26	G2	YDL181W	0.000274
NP26	G3	YDL182W	0.000287
NP26	G4	YDL183C	0.00034
NP26	G5	YDL184C	0.000309
NP26	G6	YDL185W	0.000502
NP26	G7	YDL186W	0.000323
NP26	G8	YDL188C	0.000353
NP26	G9	YDL189W	0.000349
NP26	G10	YDL190C	0.000313
NP26	G11	YDL191W	0.0003
NP26	G12	YDL192W	0.000341
NP26	H1	YDL197C	0.000372
NP26	H2	YDL199C	0.00042
NP26	H3	YDL200C	0.000319
NP26	H4	YDL201W	0.001325
NP26	H5	GFP+	
NP26	H6	YDL203C	0.000431
NP26	H7	YDL204W	0.00068
NP26	H8	DES7	0.002826
NP26	H9	YDL210W	0.000287
NP26	H10	YDL211C	0.000346
NP26	H11	YDL214C	0.000245
NP26	H12	YDL215C	
NP27	A1	YDL216C	0.000311
NP27	A2	YDL218W	0.000286
NP27	A3	YDL219W	0.000352
NP27	A4	YDL222C	0.000296
NP27	A5	YDL224C	0.000255
NP27	A6	p5472	0.000673
NP27	A7	YDL226C	0.000332
NP27	A8	YDL227C	0.000444
NP27	A9	YDL229W	0.000315
NP27	A10	YDL230W	0.000367
NP27	A11	YDL231C	0.000353
NP27	A12	BY4741	0
NP27	B1	YDL233W	0.000367
NP27	B2	YDL234C	0.000338
NP27	B3	YDL236W	0.000204
NP27	B4	YDL237W	0.001109
NP27	B5	GFP+	
NP27	B6	YDL240W	0.000337
NP27	B7	YDL241W	0.000293
NP27	B8	YDL243C	0.000332
NP27	B9	DES7	0.002866
NP27	B10	YDR003W	0.000377
NP27	B11	YDR004W	0.000308
NP27	B12	YDR005C	0.000802

NP27	C1	YDR006C	0.000292
NP27	C2	YDR009W	0.000344
NP27	C3	YDR011W	0.000324
NP27	C4	YDR014W	0.000829
NP27	C5	YDR017C	0.000982
NP27	C6	YDR018C	0.000221
NP27	C7	YDR019C	0.000269
NP27	C8	YDR020C	0.000442
NP27	C9	YDR022C	0.000579
NP27	C10	YDR025W	0.000407
NP27	C11	YDR026C	0.000343
NP27	C12	YDR027C	0.000346
NP27	D1	YDR028C	0.000299
NP27	D2	YDR031W	0.000335
NP27	D3	YDR032C	0.000252
NP27	D4	YDR033W	0.000342
NP27	D5	YDR035W	0.000302
NP27	D6	YDR036C	0.000314
NP27	D7	YDR042C	0.000401
NP27	D8		
NP27	D9	YDR046C	0.000429
NP27	D10	YDR438W	0.000352
NP27	D11	YDR439W	0.000331
NP27	D12	YDR440W	0.000301
NP27	E1		
NP27	E2	YDR446W	0.000326
NP27	E3	YDR447C	0.000357
NP27	E4	YDR450W	0.000282
NP27	E5	YDR451C	0.00037
NP27	E6	YDR452W	0.000288
NP27	E7	YDR453C	0.000318
NP27	E8	YDR456W	0.000354
NP27	E9		
NP27	E10	YDR458C	0.000278
NP27	E11	YDR459C	0.000303
NP27	E12	YDR462W	0.000365
NP27	F1	YDR463W	0.00031
NP27	F2	YDR465C	0.000326
NP27	F3	YDR466W	0.000348
NP27	F4	YDR469W	0.000193
NP27	F5	YDR470C	0.000243
NP27	F6	YDR471W	0.000236
NP27	F7	YDR475C	0.000581
NP27	F8	YDR476C	0.000303
NP27	F9	YDR477W	0.000345
NP27	F10	YDR479C	0.000437
NP27	F11	YDR480W	0.000273
NP27	F12	YDR481C	0.000328
NP27	G1	YDR482C	0.000284
NP27	G2	YDR483W	0.000213
NP27	G3	YDR484W	0.00032
NP27	G4	YDR485C	0.000359
NP27	G5	YDR486C	0.000365
NP27	G6	YDR488C	0.000259
NP27	G7	YDR490C	0.000332
NP27	G8	YDR492W	0.000352
NP27	G9	YDR494W	0.000288
NP27	G10	YDR495C	0.000239
NP27	G11	YDR496C	0.000339
NP27	G12		
NP27	H1		
NP27	H2	YDR504C	0.000332
NP27	H3	YDR505C	0.000421
NP27	H4		
NP27	H5	YDR508C	0.000306
NP27	H6	YDR511W	0.00022
NP27	H7	YDR513W	0.000176
NP27	H8	YDR514C	0.000139
NP27	H9	YDR517W	0.000285
NP27	H10		
NP27	H11	YDR519W	
NP27	H12	YDR520C	0.000169
NP28	A1	YDR522C	0.000388
NP28	A2	YDR523C	0.000268
NP28	A3	YDR524C	0.000346
NP28	A4	YDR528W	0.000407
NP28	A5	YDR529C	0.000375
NP28	A6	YDR532C	0.000326
NP28	A7	YDR533C	0.00053
NP28	A8	YDR534C	0.000404
NP28	A9	YER019C-A	0.000256
NP28	A10	YER024W	0.000338
NP28	A11	YER028C	0.000444
NP28	A12	YER030W	0.000353
NP28	B1	YER032W	0.00038
NP28	B2	YER033C	0.000331
NP28	B3	YER034W	0.000328
NP28	B4	YER035W	0.000379
NP28	B5	YER039C	0.000474
NP28	B6	YER040W	0.000474
NP28	B7	YER041W	0.00044
NP28	B8	YER042W	0.000389
NP28	B9	YER044C	0.000367
NP28	B10	YER044C-A	0.00036
NP28	B11	YER045C	0.000363
NP28	B12	YER047C	0.000409
NP28	C1	YER048C	0.000574
NP28	C2	p5472	0.0006
NP28	C3	YER050C	0.000312
NP28	C4	YER051W	0.000365
NP28	C5	YER052C	0.000436
NP28	C6	YER053C	0.000558
NP28	C7	YER054C	0.000691
NP28	C8	YER055C	0.000411
NP28	C9	BY4741	0
NP28	C10	YER056C-A	0.000538
NP28	C11	YER057C	0.000316
NP28	C12	YER058W	0.000337
NP28	D1	YER059W	0.000473
NP28	D2	YER060W	0.000314
NP28	D3	YER060W-A	0.000324
NP28	D4	YER061C	0.000392
NP28	D5	YER062C	0.000476
NP28	D6	YER065C	0.00024
NP28	D7	YER067W	0.000417
NP28	D8	YER068W	0.000311
NP28	D9	YER069W	0.000369
NP28	D10	YER070W	0.000227
NP28	D11	YER071C	0.000234
NP28	D12	YER072W	0.000363
NP28	E1	YER073W	0.000364
NP28	E2	YER074W	0.000334
NP28	E3	YER075C	0.000383
NP28	E4	YER079W	0.000371
NP28	E5	YER080W	0.000553
NP28	E6	YER081W	0.000564
NP28	E7	YER083C	0.000579
NP28	E8	YER085C	0.000295
NP28	E9	YER086W	0.000425
NP28	E10	YER087W	0.000391
NP28	E11	YGL194C	0.00039
NP28	E12	DES7	0.002734
NP28	F1	YGL197W	0.000417
NP28	F2	YGL198W	0.000405
NP28	F3	YGL202W	0.0004
NP28	F4	YGL205W	0.002157
NP28	F5	GFP+	
NP28	F6	YGL208W	0.000441
NP28	F7	YGL209W	0.0003
NP28	F8	YGL211W	0.000411
NP28	F9	YGL212W	0.000491
NP28	F10	YGL213C	0.000282
NP28	F11	YGL216W	0.000303
NP28	F12	YGL220W	0.000709
NP28	G1	YGL221C	0.000252
NP28	G2	YGL222C	0.00017
NP28	G3	YGL226C-A	0.00028
NP28	G4	YGL227W	0.000243
NP28	G5	YGL228W	0.000312
NP28	G6	YGL230C	0.00033
NP28	G7	YGL231C	0.000396
NP28	G8	YGL232W	0.000313
NP28	G9	YGL234W	0.00031
NP28	G10	YGL237C	0.000323
NP28	G11	YGL240W	0.000336
NP28	G12	YGL241W	0.0004
NP28	H1	YGL242C	0.000335
NP28	H2	YGL243W	0.000413
NP28	H3	YGL246C	0.000359
NP28	H4	YGL248W	0.000383
NP28	H5	YGL249W	0.000331
NP28	H6	YGL251C	0.000286
NP28	H7	YGL252C	0.000363
NP28	H8	YGL253W	0.000307
NP28	H9	YGL254W	0.000347
NP28	H10		
NP28	H11	YGL256W	0.000262
NP28	H12	YGL257C	0.000357
NP29	A1	YGL258W	0.000321
NP29	A2	YGL259W	0.000448
NP29	A3	YGL261C	0.000379

NP29	A4	YGL262W	0.000635248
NP29	A5	YGL263W	0.000652122
NP29	A6	YGR001C	0.000337069
NP29	A7	YGR003W	0.000538752
NP29	A8	YGR004W	0.000584599
NP29	A9	YGR006W	0.000557923
NP29	A10	YGR007W	0.000443751
NP29	A11	YGR008C	0.000445764
NP29	A12	p5472	0.000573638
NP29	B1	YGR014W	0.000349644
NP29	B2	YGR016W	0.000384167
NP29	B3	YGR017W	0.000871224
NP29	B4	YGR021W	0.000292849
NP29	B5	YGR023W	0.001627301
NP29	B6	YPR006C	0.000729975
NP29	B7	YPR009W	0.000672191
NP29	B8	YPR015C	0.000497545
NP29	B9	YPR017C	0.000682013
NP29	B10	DES7	0.002792043
NP29	B11	YPR020W	0.00039899
NP29	B12	YPR028W	0.00048692
NP29	C1	YPR029C	0.000334561
NP29	C2	YPR030W	0.00051896
NP29	C3	YPR032W	0.000516553
NP29	C4	YPR046W	0.000728682
NP29	C5	YPR051W	0.000533293
NP29	C6	YPR052C	0.000979294
NP29	C7	YPR057W	0.00105289
NP29	C8	YPR058W	0.000707224
NP29	C9	YPR060C	0.000496157
NP29	C10	YPR061C	0.000692454
NP29	C11	YPR062W	0.000573762
NP29	C12	GFP+	
NP29	D1	YPR065W	0.000444458
NP29	D2	YPR066W	0.000435201
NP29	D3	YPR068C	0.000520789
NP29	D4	YPR069C	0.000477497
NP29	D5	YPR070W	0.000334825
NP29	D6	YPR072W	0.000397863
NP29	D7	YPR073C	0.000411964
NP29	D8	YPR074C	0.000786584
NP29	D9	YPR075C	0.000387535
NP29	D10	YPR079W	0.001009461
NP29	D11	BY4741	0
NP29	D12	YPR093C	7.47481E-05
NP29	E1	YPR100W	0.000415622
NP29	E2	YPR101W	0.000305975
NP29	E3	YBR082C	0.00069763
NP29	E4		
NP29	E5	YBR085W	0.000296197
NP29	E6	YBR092C	0.000759157
NP29	E7	YBR093C	0.000379957
NP29	E8	YBR094W	0.001378521
NP29	E9	YBR095C	0.000748136
NP29	E10		
NP29	E11	YBR098W	0.000363555
NP29	E12	YBR103W	0.000422334

NP29	F1	YBR104W	0.000387
NP29	F2		
NP29	F3	YBR106W	0.000461
NP29	F4	YBR107C	0.00059
NP29	F5	YBR108W	0.000452
NP29	F6	YBR111C	0.000403
NP29	F7	YBR114W	0.000443
NP29	F8		
NP29	F9	YBR117C	0.000684
NP29	F10	YBR118W	0.000852
NP29	F11	YBR119W	0.00049
NP29	F12	YBR120C	0.000449
NP29	G1	YBR126C	0.000412
NP29	G2	YBR127C	0.000424
NP29	G3	YBR128C	0.00044
NP29	G4	YBR129C	0.000432
NP29	G5	YBR130C	0.000521
NP29	G6	YBR132C	0.000523
NP29	G7	YBR133C	0.000398
NP29	G8	YBR137W	0.000359
NP29	G9	YBR138C	0.000428
NP29	G10	YBR139W	0.000499
NP29	G11	YBR141C	0.000403
NP29	G12	YBR145W	0.000432
NP29	H1	YBR146W	0.000681
NP29	H2	YBR147W	0.000361
NP29	H3	YBR148W	0.000553
NP29	H4	YBR149W	0.000494
NP29	H5	YBR151W	0.000616
NP29	H6	YBR156C	0.000472
NP29	H7	YBR157C	0.000544
NP29	H8	YBR158W	0.000537
NP29	H9		
NP29	H10		
NP29	H11	YBR162W-A	0.000395
NP29	H12	YBR164C	0.000526
NP30	A1	YBR165W	0.000499
NP30	A2	YBR166C	0.000354
NP30	A3	YBR170C	0.000633
NP30	A4	YBR171W	0.000888
NP30	A5	YBR172C	0.001127
NP30	A6	YCL002C	0.000691
NP30	A7		
NP30	A8	YCL008C	0.000611
NP30	A9	YCL009C	0.000677
NP30	A10	YCL010C	0.000584
NP30	A11	YCL011C	0.000635
NP30	A12		
NP30	B1	YCL016C	0.0006
NP30	B2	YCL025C	0.000646
NP30	B3	YCL027W	0.000655
NP30	B4	YCL028W	0.000668
NP30	B5	p5472	0.0007
NP30	B6	YCL030C	0.000754
NP30	B7	YCL033C	0.000705
NP30	B8	YCL034W	0.000584
NP30	B9	YCL036W	0.000776

NP30	B10	DES7	0.002359
NP30	B11	YCL042W	0.000479
NP30	B12		
NP30	C1	YCL047C	0.000397
NP30	C2	YCL048W	0.00189
NP30	C3	GFP+	
NP30	C4	YCL050C	0.000749
NP30	C5	YCL051W	0.000956
NP30	C6	YCL055W	0.00083
NP30	C7	YCL056C	0.000812
NP30	C8	YCL057W	0.000505
NP30	C9	BY4741	0
NP30	C10	YCL063W	0.000561
NP30	C11	YCL064C	0.000614
NP30	C12	YCL069W	0.000551
NP30	D1	YCR002C	0.000558
NP30	D2	YCR003W	0.000516
NP30	D3	YCR004C	0.000459
NP30	D4	YCR005C	0.000799
NP30	D5	YCR007C	0.000574
NP30	D6	YCR008W	0.000629
NP30	D7	YCR009C	0.000802
NP30	D8	YCR010C	0.00064
NP30	D9	YCR014C	0.000602
NP30	D10	YCR015C	0.000753
NP30	D11	YCR016W	0.000588
NP30	D12	YCR019W	0.000632
NP30	E1	YCR020C	
NP30	E2	YCR020C-A	0.000471
NP30	E3	YCR021C	0.000802
NP30	E4	YCR023C	0.000539
NP30	E5	YDL001W	0.000694
NP30	E6	YDL002C	0.000721
NP30	E7	YDL005C	0.000538
NP30	E8	YDL006W	0.000751
NP30	E9	YDL010W	0.000607
NP30	E10	YDL012C	0.000663
NP30	E11	YDL013W	0.00045
NP30	E12	YDL018C	0.00059
NP30	F1	YDL019C	0.000517
NP30	F2	YDL020C	0.000508
NP30	F3		
NP30	F4	YDL022W	0.000698
NP30	F5	YDL024C	0.000586
NP30	F6	YDL027C	0.000751
NP30	F7	YDL033C	0.000312
NP30	F8		
NP30	F9	YDL036C	0.000678
NP30	F10	YDL037C	0.000448
NP30	F11		
NP30	F12	YDL040C	0.000569
NP30	G1		
NP30	G2	YDL046W	0.0005
NP30	G3	YDL047W	0.000564
NP30	G4	YDL048C	0.00065
NP30	G5	YDL051W	0.000571
NP30	G6	YDL052C	0.000575

NP30	G7	YDL053C	
NP30	G8	YDL054C	0.000630304
NP30	G9	YDL056W	0.000550422
NP30	G10	YDL059C	0.001026994
NP30	G11	YDL061C	0.000548937
NP30	G12	YDL063C	0.000575646
NP30	H1	YDL065C	0.000618348
NP30	H2	YDL066W	0.000552362
NP30	H3	YDL067C	0.000630766
NP30	H4		
NP30	H5	YDL070W	0.00062479
NP30	H6	YDL072C	0.000469934
NP30	H7	YDL074C	
NP30	H8	YDL075W	0.000632167
NP30	H9	YDL076C	0.000389013
NP30	H10	YDL077C	0.000376036
NP30	H11	YDL078C	0.000529943
NP30	H12	YDL079C	0.000329913
NP31	A1	p5472	0.000515198
NP31	A2	YDL082W	0.000390802
NP31	A3	YDL083C	0.000510119
NP31	A4	YDL085W	0.000472505
NP31	A5	YDL086W	0.000558933
NP31	A6	YDL088C	0.000618871
NP31	A7	YDL089W	0.000510031
NP31	A8	YDL090C	0.000483897
NP31	A9	YDL091C	0.000594859
NP31	A10	YDL093W	0.000801707
NP31	A11	DES7	0.002184309
NP31	A12	YEL011W	0.000454648
NP31	B1	YER077C	0.000525179
NP31	B2	YER078C	0.000576773
NP31	B3	YER088C	0.000622222
NP31	B4	GFP+	
NP31	B5	YER092W	0.00062191
NP31	B6	YER095W	0.000707293
NP31	B7	YER096W	0.000671318
NP31	B8	YER098W	0.000831191
NP31	B9	YGR210C	0.000652764
NP31	B10	BY4741	0
NP31	B11	YHR032W	0.000725871
NP31	B12	YHR045W	0.000668336
NP31	C1	YHR064C	0.000580145
NP31	C2	YHR140W	0.000632529
NP31	C3	YHR162W	0.000573036
NP31	C4	YHR168W	0.000405914
NP31	C5	YHR181W	0.000784567
NP31	C6	YHR191C	0.000647083
NP31	C7	YHR193C	0.000950621
NP31	C8		
NP31	C9		
NP31	C10	YLR030W	0.000732625
NP31	C11	YLR032W	0.000640426
NP31	C12	YLR034C	0.000642758
NP31	D1	YLR035C	0.000382355
NP31	D2	YLR036C	0.000406826
NP31	D3	YLR038C	0.000479674

NP31	D4	YLR039C	0.001243
NP31	D5	YLR040C	0.000385
NP31	D6	YLR050C	0.000514
NP31	D7	YMR142C	0.000638
NP31	D8	YMR158W	0.000537
NP31	D9	YMR171C	0.000527
NP31	D10	YMR181C	0.000309
NP31	D11	YMR209C	0.000453
NP31	D12	YMR271C	0.000502
NP31	E1	YMR279C	0.000418
NP31	E2	YMR306W	0.000353
NP31	E3	YMR311C	0.000473
NP31	E4	YMR312W	0.000399
NP31	E5	YMR313C	0.000379
NP31	E6	YMR315W	0.000587
NP31	E7		
NP31	E8	YMR318C	0.000577
NP31	E9	YNL252C	0.000343
NP31	E10	YNL279W	0.000531
NP31	E11	YNL316C	0.000335
NP31	E12	YOL016C	0.000443
NP31	F1	YOR096W	0.000445
NP31	F2	YOR306C	0.000396
NP31	F3	YOR317W	0.000413
NP31	F4	YPL132W	0.000463
NP31	F5	YPL134C	0.000548
NP31	F6	YGR124W	0.000442
NP31	F7	YGR125W	0.000565
NP31	F8	YGR126W	0.000479
NP31	F9	YGR127W	0.00053
NP31	F10	YGR129W	0.000246
NP31	F11	YGR130C	0.000489
NP31	F12	YGR131W	0.000432
NP31	G1	YGR133W	0.000455
NP31	G2	YGR135W	0.000377
NP31	G3	YGR136W	0.000437
NP31	G4	YGR138C	0.000481
NP31	G5	YGR142W	0.000481
NP31	G6	YGR143W	0.000698
NP31	G7	YGR144W	0.000675
NP31	G8	YGR146C	0.00056
NP31	G9	YGR148C	0.000504
NP31	G10	YGR149W	
NP31	G11	YGR154C	0.000315
NP31	G12	YGR157W	0.000461
NP31	H1	YGR161C	0.000286
NP31	H2	YGR163W	0.000433
NP31	H3	YGR165W	0.00038
NP31	H4	YGR166W	0.000491
NP31	H5	YGR167W	0.000511
NP31	H6	YGR168C	0.000509
NP31	H7	YGR169C	0.000655
NP31	H8	YGR170W	0.000409
NP31	H9	YGR171C	0.000628
NP31	H10	YGR173W	0.000586
NP31	H11	YGR174C	0.000521
NP31	H12		

NP32	A1	YGR177C	0.000266
NP32	A2	YGR178C	0.000313
NP32	A3	YGR180C	0.000736
NP32	A4	YGR181W	0.000858
NP32	A5	YGR183C	0.000468
NP32	A6		
NP32	A7	YGR187C	0.000908
NP32	A8	YGR189C	0.000327
NP32	A9	YGR192C	0.000339
NP32	A10	YGR193C	0.000456
NP32	A11	YGR194C	0.0015
NP32	A12	YGR196C	0.000607
NP32	B1	YGR197C	0.000634
NP32	B2	YGR199W	0.000378
NP32	B3	YGR202C	0.000268
NP32	B4	YGR203W	0.000299
NP32	B5	YGR205W	0.000343
NP32	B6	YGR206W	0.000943
NP32	B7	YGR207C	0.000316
NP32	B8	YGR208W	0.001869
NP32	B9	YGR209C	0.000419
NP32	B10	YGR212W	0.000599
NP32	B11	YGR213C	0.000345
NP32	B12	YGR214W	0.000582
NP32	C1	YGR215W	0.000213
NP32	C2	p5472	0.00058
NP32	C3	YLL001W	0.000243
NP32	C4	YLL005C	0.00102
NP32	C5	YLL006W	0.000352
NP32	C6	YLL010C	0.000333
NP32	C7	DES7	0.003322
NP32	C8	YLL013C	0.000359
NP32	C9	YLL014W	0.000292
NP32	C10	YLL015W	0.000407
NP32	C11	YLL019C	0.000617
NP32	C12	YLL023C	0.00033
NP32	D1	YLL024C	0.000266
NP32	D2	YLL025W	0.000283
NP32	D3	YLL026W	
NP32	D4	GFP+	
NP32	D5	YLL028W	0.000249
NP32	D6	YLL029W	0.000368
NP32	D7	YLL032C	0.000242
NP32	D8	YLL039C	0.000293
NP32	D9	YLL040C	0.000373
NP32	D10	YLL041C	0.000321
NP32	D11	YLL042C	0.000314
NP32	D12	YLL043W	0.000179
NP32	E1	YLL045C	0.000335
NP32	E2	YLL046C	0.002089
NP32	E3	YLL051C	0.001301
NP32	E4	YLL052C	0.000391
NP32	E5	YLL053C	0.003204
NP32	E6	YLL054C	0.00037
NP32	E7	BY4741	0
NP32	E8	YLL056C	0.000318
NP32	E9	YLL057C	0.000295

NP32	E10	YLL058W	0.000296223
NP32	E11	YLL060C	0.000236382
NP32	E12	YLL061W	0.000329076
NP32	F1	YLL062C	0.000883123
NP32	F2	YLL063C	0.000394647
NP32	F3	YLR003C	0.000240275
NP32	F4	YLR004C	0.000251958
NP32	F5	YLR006C	7.15817E-05
NP32	F6	YLR011W	0.000280911
NP32	F7	YLR012C	0.001576406
NP32	F8	YLR013W	
NP32	F9	YLR014C	0.000468803
NP32	F10	YLR015W	0.000304015
NP32	F11	YLR016C	0.000271915
NP32	F12	YLR017W	0.00070003
NP32	G1	YLR018C	0.000317174
NP32	G2	YLR019W	0.000263616
NP32	G3	YLR020C	0.000411847
NP32	G4	YLR021W	0.000893647
NP32	G5	YLR023C	0.000705575
NP32	G6		
NP32	G7	YLR025W	0.000879935
NP32	G8	YLR027C	0.000241134
NP32	G9	YLR042C	0.000407097
NP32	G10	YLR043C	0.001191366
NP32	G11	YLR044C	0.000317274
NP32	G12	YLR046C	0.004194133
NP32	H1	YLR047C	0.000367887
NP32	H2	YLR048W	0.00033829
NP32	H3	YLR053C	0.001299984
NP32	H4	YLR055C	0.000294236
NP32	H5	YLR056W	
NP32	H6	YLR057W	0.00257206
NP32	H7	YLR058C	0.000229911
NP32	H8	YLR059C	0.000772255
NP32	H9	YLR061W	0.000484945
NP32	H10	YLR067C	0.00041786
NP32	H11	YLR068W	0.00028991
NP32	H12	YLR069C	0.005236761
NP33	A1	YLR070C	0.000233864
NP33	A2	YLR072W	0.000285604
NP33	A3	YLR074C	0.00055505
NP33	A4	YLR077W	0.000330004
NP33	A5	YLR079W	0.001080809
NP33	A6	YLR080W	0.000340119
NP33	A7	p5472	0.000780869
NP33	A8	YLR082C	0.001415836
NP33	A9	YLR083C	0.000338626
NP33	A10	YLR085C	0.001720223
NP33	A11	YLR087C	0.001837401
NP33	A12	YLR090W	0.000424815
NP33	B1	YLR091W	0.001453859
NP33	B2	YLR092W	0.000498818
NP33	B3	YLR093C	0.000637857
NP33	B4	YLR094C	0.001481809
NP33	B5	YLR095C	0.000872168
NP33	B6	YLR096W	0.000646692
NP33	B7	YLR097C	0.001041
NP33	B8	YLR098C	0.000849
NP33	B9	YLR099C	0.000813
NP33	B10	GFP+	
NP33	B11	YLR104W	0.000687
NP33	B12	YLR107W	0.001024
NP33	C1	YLR108C	0.000403
NP33	C2	YLR109W	0.000671
NP33	C3	YLR113W	0.000774
NP33	C4	YLR114C	0.0004
NP33	C5	YLR118C	0.000409
NP33	C6	DES7	0.004116
NP33	C7	YLR120C	0.000313
NP33	C8	BY4741	0
NP33	C9	YLR324W	0.002225
NP33	C10	YLR325C	0.000348
NP33	C11	YLR328W	0.000619
NP33	C12	YLR326W	0.000326
NP33	D1	YLR330W	0.000902
NP33	D2	YLR335W	0.000285
NP33	D3	YLR337C	0.000944
NP33	D4	YLR341W	0.001687
NP33	D5	YLR342W	0.000486
NP33	D6	YLR344W	0.00244
NP33	D7	YLR345W	0.000894
NP33	D8	YLR348C	0.002507
NP33	D9	YLR360W	0.000271
NP33	D10	YLR368W	
NP33	D11	YLR369W	
NP33	D12	YLR371W	0.000338
NP33	E1	YLR372W	0.00032
NP33	E2	YLR373C	0.001307
NP33	E3	YLR375W	0.000642
NP33	E4	YLR376C	0.000268
NP33	E5	YLR380W	0.000525
NP33	E6		
NP33	E7	YLR386W	0.000983
NP33	E8	YLR387C	0.000329
NP33	E9	YLR388W	0.000336
NP33	E10	YLR389C	0.000942
NP33	E11	YLR390W	0.000313
NP33	E12	YLR392C	0.000487
NP33	F1	YLR395C	0.00048
NP33	F2	YLR396C	0.000496
NP33	F3	YLR398C	0.000271
NP33	F4	YLR399C	0.000529
NP33	F5	YLR403W	0.000553
NP33	F6	YLR404W	0.003042
NP33	F7	YLR405W	0.000523
NP33	F8		
NP33	F9	YLR408C	0.000337
NP33	F10	YLR410W	0.001039
NP33	F11	YLR412W	0.000295
NP33	F12	YLR417W	0.000311
NP33	G1		
NP33	G2	YMR232W	0.00054
NP33	G3	YMR233W	0.000289
NP33	G4	YMR234W	0.000808
NP33	G5	YMR237W	0.000466
NP33	G6	YMR238W	
NP33	G7	YMR244W	0.001316
NP33	G8	YMR244C-A	
NP33	G9	YMR246W	0.000433
NP33	G10	YMR247C	0.000341
NP33	G11	YMR250W	0.000914
NP33	G12	YMR251W	0.000426
NP33	H1	YMR251W-A	0.000265
NP33	H2	YMR252C	0.000531
NP33	H3	YMR253C	0.000265
NP33	H4	YMR255W	0.000298
NP33	H5	YMR256C	0.001298
NP33	H6	YMR257C	0.000315
NP33	H7	YMR258C	0.000782
NP33	H8		
NP33	H9	YMR261C	0.00023
NP33	H10	YMR262W	0.000617
NP33	H11	YMR263W	0.00044
NP33	H12	YMR264W	0.00047
NP34	A1	YMR265C	0.000315
NP34	A2	YMR266W	0.001394
NP34	A3	YMR267W	0.000245
NP34	A4	YMR269W	0.000402
NP34	A5	YMR272C	0.00026
NP34	A6	YMR273C	0.002936
NP34	A7	YMR274C	0.000333
NP34	A8	YMR275C	0.005526
NP34	A9	YMR276W	0.000283
NP34	A10	YMR278W	0.00027
NP34	A11	YMR280C	0.000275
NP34	A12	p5472	0.000635
NP34	B1	YMR283C	0.000187
NP34	B2	YMR284W	0.000418
NP34	B3	YMR285C	0.000256
NP34	B4	YMR286W	0.000276
NP34	B5	YMR287C	0.000769
NP34	B6	GFP+	
NP34	B7	YMR291W	0.000325
NP34	B8	YLR350W	0.000368
NP34	B9	YLR351C	0.000406
NP34	B10	YLR352W	0.000321
NP34	B11	YLR353W	0.000431
NP34	B12	YLR354C	0.000281
NP34	C1	YLR356W	0.000224
NP34	C2	YLR357W	0.000464
NP34	C3	YMR292W	0.004713
NP34	C4	DES7	0.003918
NP34	C5	YMR294W	0.000342
NP34	C6	YMR295C	0.000369
NP34	C7	YMR297W	0.011418
NP34	C8	YMR299C	0.000343
NP34	C9	BY4741	0
NP34	C10	YMR302C	0.000288
NP34	C11	YMR303C	0.00136
NP34	C12	YMR304W	0.000265

NP34	D1	YMR305C	0.000276324
NP34	D2	YMR307W	0.000221008
NP34	D3	YMR310C	0.000256003
NP34	D4		
NP34	D5	YNL336W	
NP34	D6	YNL335W	0.00398227
NP34	D7	YNL334C	
NP34	D8	YNL333W	0.000401592
NP34	D9		
NP34	D10	YNL329C	0.000338218
NP34	D11	YNL327W	0.000302904
NP34	D12	YNL326C	
NP34	E1	YNL322C	0.000570242
NP34	E2	YNL321W	0.004637932
NP34	E3	YNL320W	0.000542607
NP34	E4	YNL318C	0.000346854
NP34	E5	YNL314W	0.000373176
NP34	E6	YNL311C	0.000224617
NP34	E7	YNL304W	0.000353437
NP34	E8	YNL302C	0.000293576
NP34	E9	YNL301C	0.000518284
NP34	E10	YNL299W	0.000209602
NP34	E11	YNL298W	
NP34	E12		
NP34	F1	YNL294C	0.000257564
NP34	F2	YNL293W	0.000354277
NP34	F3	YNL292W	0.00029591
NP34	F4	YNL291C	0.000349866
NP34	F5	YNL288W	0.000322872
NP34	F6	YNL281W	0.000361489
NP34	F7	YNL280C	0.006645923
NP34	F8	YNL278W	0.00036705
NP34	F9	YNL277W	0.000290619
NP34	F10	YNL275W	0.000320642
NP34	F11	YNL273W	0.000374314
NP34	F12	YNL271C	0.000807586
NP34	G1	YNL270C	0.000377247
NP34	G2	YNL269W	0.000326591
NP34	G3	YNL265C	0.000297018
NP34	G4	YNL264C	0.000252238
NP34	G5	YNL259C	0.003125726
NP34	G6	YNL257C	0.000264144
NP34	G7	YNL246W	0.00030067
NP34	G8		
NP34	G9		
NP34	G10	YNL241C	0.000296567
NP34	G11	YNL239W	0.000285023
NP34	G12	YNL238W	0.000270784
NP34	H1	YNL237W	0.000258709
NP34	H2		
NP34	H3	YNL233W	0.001347573
NP34	H4	YNL230C	0.000279916
NP34	H5	YNL229C	0.000698609
NP34	H6	YNL225C	0.000364083
NP34	H7	YNL224C	0.000375905
NP34	H8	YNL223W	0.001277155
NP34	H9	YNL218W	0.000275101
NP34	H10	YNL217W	0.000330082
NP34	H11	YNL215W	0.000333964
NP34	H12	YNL214W	
NP35	A1	YNL213C	0.000617702
NP35	A2	YNL212W	0.000226883
NP35	A3	YNL211C	0.001321002
NP35	A4	YNL210W	0.000317423
NP35	A5	YNL206C	0.000339086
NP35	A6	YNL204C	0.000428385
NP35	A7	YNL202W	0.000242554
NP35	A8	YNL201C	0.000371663
NP35	A9	YNL200C	0.000347653
NP35	A10	YNL199C	0.000220358
NP35	A11	p5472	0.000456677
NP35	A12	YNL196C	0.000477802
NP35	B1	YNL195C	0.00156837
NP35	B2	YNL194C	0.00032146
NP35	B3	GFP+	
NP35	B4	YNL191W	0.000300917
NP35	B5	YNL190W	0.001402515
NP35	B6	YNL187W	0.000352768
NP35	B7	YNL185C	0.008750338
NP35	B8	DES7	0.003306531
NP35	B9	YNL180C	0.000252847
NP35	B10	YNL177C	0.002524752
NP35	B11	YNL176C	0.000158167
NP35	B12	YNL175C	0.000232849
NP35	C1	BY4741	0
NP35	C2	YNL168C	0.000284224
NP35	C3	YNL167C	0.000364159
NP35	C4		
NP35	C5	YNL164C	0.000266168
NP35	C6	YNL160W	0.004906983
NP35	C7	YNL159C	
NP35	C8	YNL157W	0.000322761
NP35	C9	YNL156C	0.000330925
NP35	C10	YNL155W	0.000300393
NP35	C11	YNL154C	0.000480756
NP35	C12	YNL153C	0.000271113
NP35	D1	YNL148C	0.000386712
NP35	D2	YNL145W	0.000306903
NP35	D3	YNL139C	0.000305553
NP35	D4		
NP35	D5	YNL135C	0.000309241
NP35	D6	YNL134C	0.000246109
NP35	D7	YNL129W	0.00031453
NP35	D8	YNL128W	0.000336282
NP35	D9	YNL127W	
NP35	D10	YNL123W	
NP35	D11	YNL122C	0.000344045
NP35	D12	YNL116W	0.000311181
NP35	E1	YNL108C	0.00046464
NP35	E2	YNL101W	0.000268999
NP35	E3	YNL098C	0.000380849
NP35	E4	YNL092W	0.000770892
NP35	E5	YNL084C	0.000354445
NP35	E6	YNL081C	0.000280587
NP35	E7	YNL077W	0.000191
NP35	E8	YNL063W	0.000366
NP35	E9	YNL058C	0.000345
NP35	E10		
NP35	E11	YNL010W	0.000921
NP35	E12	YNL015W	0.00023
NP35	F1	YNL016W	0.000599
NP35	F2	YNL020C	0.000285
NP35	F3	YNL021W	0.001228
NP35	F4	YNL022C	0.000349
NP35	F5	YNL023C	0.000308
NP35	F6	YNL024C	0.00045
NP35	F7	YNL025C	0.000369
NP35	F8	YNL027W	0.000422
NP35	F9	YNL029C	0.000326
NP35	F10	YNL030W	0.000302
NP35	F11	YNL031C	0.000385
NP35	F12	YNL034W	0.000295
NP35	G1	YNL035C	0.000362
NP35	G2	YNL037C	0.000732
NP35	G3	YNL040W	0.000587
NP35	G4	YNL041C	0.000306
NP35	G5	YNL044W	0.001679
NP35	G6	YNL045W	0.000261
NP35	G7	YNL046W	0.003657
NP35	G8	YNL049C	0.000705
NP35	G9	YNL050C	0.000314
NP35	G10	YNR001C	0.000287
NP35	G11	YNR002C	0.000514
NP35	G12	YNR004W	0.000842
NP35	H1	YNR006W	0.000283
NP35	H2	NP35 H02	0.000375
NP35	H3	YNR008W	0.003329
NP35	H4	YNR009W	0.001013
NP35	H5	YNR010W	0.000268
NP35	H6	YNR012W	
NP35	H7	YNR013C	0.000273
NP35	H8	YNR015W	0.000405
NP35	H9	YNR018W	
NP35	H10	YNR019W	0.000354
NP35	H11	YNR020C	0.000743
NP35	H12	YNR022C	0.000344
NP36	A1	YNR023W	0.000374
NP36	A2	YNR024W	0.000973
NP36	A3	p5472	0.000417
NP36	A4	YNR028W	0.000244
NP36	A5	YNR029C	0.000236
NP36	A6	YNR030W	0.000475
NP36	A7	GFP+	
NP36	A8	DES7	0.002249
NP36	A9	YNR034W	0.001791
NP36	A10	YNR036C	0.000599
NP36	A11	YNR037C	0.00029
NP36	A12	YNR039C	0.000274
NP36	B1	YNR040W	0.000713
NP36	B2	BY4741	0
NP36	B3	YNR047W	0.000282

NP36	B4	YNR048W	0.000198614
NP36	B5	YOR193W	0.002399638
NP36	B6	YOR195W	0.000344413
NP36	B7	YOR196C	0.001101986
NP36	B8	YOR197W	0.000793615
NP36	B9	YOR198C	0.003316999
NP36	B10	YOR209C	0.000332713
NP36	B11	YOR211C	0.000400623
NP36	B12	YOR212W	7.20913E-05
NP36	C1	YOR213C	0.00141804
NP36	C2	YOR214C	0.000239861
NP36	C3	YOR215C	0.000498132
NP36	C4	YOR216C	0.000346398
NP36	C5	YOR220W	0.000252018
NP36	C6	YOR221C	0.000412136
NP36	C7	YOR223W	0.000233213
NP36	C8	YOR226C	0.000290889
NP36	C9	YOR228C	0.000298608
NP36	C10	YOR229W	0.000294145
NP36	C11	YOR230W	0.000109506
NP36	C12		
NP36	D1	YOR237W	0.000298467
NP36	D2	YOR239W	0.000278607
NP36	D3	YOR253W	0.000288042
NP36	D4	YOR255W	0.000223907
NP36	D5	YOR258W	0.00034972
NP36	D6	YOR264W	0.000433329
NP36	D7	YOR279C	0.000342018
NP36	D8	YOR280C	0.000313017
NP36	D9	YOR283W	0.000246811
NP36	D10	YOR285W	0.000263071
NP36	D11	YOR286W	0.000269607
NP36	D12	YOR288C	0.0002423
NP36	E1	YOR208W	0.000454051
NP36	E2		
NP36	E3	YML034W	0.00024899
NP36	E4	YML032C	0.000331986
NP36	E5	YML030W	0.000290489
NP36	E6	YML029W	0.000239339
NP36	E7	YML028W	0.000401415
NP36	E8	YML026C	0.000351201
NP36	E9	YML024W	0.000271221
NP36	E10	YML020W	0.000279917
NP36	E11	YML019W	0.000275583
NP36	E12	YML018C	0.00068759
NP36	F1	YML017W	0.002276905
NP36	F2	YML016C	0.001247961
NP36	F3	YML014W	0.000301814
NP36	F4	YML013W	0.000260453
NP36	F5	YML012W	0.000652812
NP36	F6	YML011C	0.000775705
NP36	F7	YMR014W	0.000252893
NP36	F8	YMR015C	0.000271794
NP36	F9	YMR016C	
NP36	F10	YMR017W	0.000327342
NP36	F11	YMR018W	0.000274963
NP36	F12	YMR019W	0.000280725

NP36	G1	YMR020W	0.000228205
NP36	G2	YMR021C	0.00031522
NP36	G3	YMR022W	0.000332589
NP36	G4	YMR023C	0.000308775
NP36	G5	YMR026C	5.63057E-05
NP36	G6		
NP36	G7	YMR029C	0.005340824
NP36	G8	YMR030W	0.000329003
NP36	G9	YMR031C	0.00029528
NP36	G10	YMR032W	0.000283302
NP36	G11	YMR034C	0.000276068
NP36	G12	YMR035W	0.00028974
NP36	H1	YMR036C	0.000310241
NP36	H2	YMR039C	0.000275468
NP36	H3	YMR040W	0.000252439
NP36	H4	YMR041C	0.001157945
NP36	H5	YMR042W	0.000451637
NP36	H6	YMR044W	0.000315772
NP36	H7	YML088W	0.000282789
NP36	H8	YML087C	0.001164332
NP36	H9	YML083C	0.000256402
NP36	H10	YML082W	0.000268383
NP36	H11	YML081W	0.000207327
NP36	H12	YML080W	0.000281021
NP37	A1	YML079W	0.001754629
NP37	A2	YML078W	0.001348347
NP37	A3	YML063W	0.000960244
NP37	A4	YML062C	0.000602901
NP37	A5	YML061C	0.000364348
NP37	A6	YML060W	0.000709915
NP37	A7	p5472	0.000907588
NP37	A8	YML058W	0.000367395
NP37	A9	YML057W	0.001685046
NP37	A10	YBR278W	0.00055835
NP37	A11	YBR283C	0.000433532
NP37	A12	YBR286W	0.002610889
NP37	B1	YBR290W	0.000844817
NP37	B2	YBR291C	0.000315703
NP37	B3	YBR293W	0.00038604
NP37	B4	YBR298C	0.000346062
NP37	B5	YCR031C	0.001381452
NP37	B6	GFP+	
NP37	B7	YCR036W	0.00231977
NP37	B8	DES7	0.003688477
NP37	B9	BY4741	0
NP37	B10	YCR076C	0.000405224
NP37	B11	YCR091W	0.001474248
NP37	B12		
NP37	C1	YGR237C	0.000678827
NP37	C2	YIR018W	0.00070771
NP37	C3	YIR036C	0.000511752
NP37	C4	YKR077W	0.000404194
NP37	C5	YKR098C	0.000394484
NP37	C6		
NP37	C7	YLL018C-A	0.001880531
NP37	C8	YLR429W	0.000452085
NP37	C9	YLR431C	0.007835143

NP37	C10	YLR432W	0.000622
NP37	C11	YLR442C	0.000312
NP37	C12	YLR446W	0.00054
NP37	D1	YLR448W	0.000459
NP37	D2	YML009C	0.000478
NP37	D3		
NP37	D4		
NP37	D5		
NP37	D6		
NP37	D7		
NP37	D8		
NP37	D9	YHR017W	0.002645
NP37	D10		
NP37	D11		
NP37	D12		
NP37	E1		
NP37	E2	YML119W	0.001209
NP37	E3		
NP37	E4	YMR102C	0.000766
NP37	E5		
NP37	E6	YAL054C	0.000176
NP37	E7	YJR069C	0.00054
NP37	E8		
NP37	E9	YJR107W	0.000321
NP37	E10		
NP37	E11	YJR113C	0.00029
NP37	E12	YJR124C	0.000356
NP37	F1		
NP37	F2	YJR126C	0.000383
NP37	F3		
NP37	F4		
NP37	F5		
NP37	F6		
NP37	F7		
NP37	F8		
NP37	F9	YDL239C	0.000486
NP37	F10	YDR030C	0.001978
NP37	F11		
NP37	F12	YDR144C	0.001355
NP37	G1	YDR153C	0.002055
NP37	G2		
NP37	G3	YDR283C	0.001301
NP37	G4	YDR285W	0.000288
NP37	G5		
NP37	G6	YDR319C	0.001925
NP37	G7	YDR333C	0.00037
NP37	G8	YDR336W	0.000514
NP37	G9		
NP37	G10	YDR357C	0.000434
NP37	G11	YDR364C	0.001002
NP37	G12	YDR419W	0.000718
NP37	H1		
NP37	H2	YDR516C	0.000939
NP37	H3	YDR530C	0.000328
NP37	H4	YEL042W	0.000894
NP37	H5	YER014C-A	0.001799
NP37	H6	YER016W	0.000824

NP37	H7	YER017C	0.000754
NP37	H8	YER019W	0.002321
NP37	H9	YER020W	0.001119
NP37	H10	YFL018C	0.00059
NP37	H11	YFL021W	0.000311
NP37	H12	YFL036W	0.000283
NP38	A1	YFL044C	0.000492
NP38	A2	YFL048C	0.000975
NP38	A3	p5472	0.000785
NP38	A4	YFR024C-A	0.000914
NP38	A5	YFR026C	0.000608
NP38	A6	YGL025C	0.001587
NP38	A7	GFP+	
NP38	A8	YGL037C	0.000577
NP38	A9	YGL060W	0.000769
NP38	A10	YGL076C	0.000611
NP38	A11	YGL095C	0.000736
NP38	A12	YGL125W	0.000589
NP38	B1	YGL203C	0.000832
NP38	B2	YGL236C	0.000653
NP38	B3	YGR015C	0.000489
NP38	B4	YGR062C	0.000356
NP38	B5	YGR079W	0.000362
NP38	B6	YGR111W	0.000907
NP38	B7	YGR141W	0.002307
NP38	B8	YGR152C	0.000556
NP38	B9	YGR200C	0.00128
NP38	B10	YHR097C	0.000609
NP38	B11	YHR106W	0.00054
NP38	B12	YHR150W	0.000923
NP38	C1	YHR179W	0.001153
NP38	C2	YIL023C	0.000702
NP38	C3	YIL041W	0.000481
NP38	C4	YIL079C	0.001341
NP38	C5	YIL105C	0.000833
NP38	C6	YIL134W	0.001193
NP38	C7	DES7	0.002971
NP38	C8	YJL170C	0.001637
NP38	C9	YJL126W	0.000642
NP38	C10	YJL107C	0.001471
NP38	C11	YJL096W	0.001044
NP38	C12	YKL001C	0.000802
NP38	D1	YKL003C	0.001313
NP38	D2	YKL007W	0.000515
NP38	D3	YKL054C	0.000251
NP38	D4	YKL090W	0.000824
NP38	D5	YKL091C	0.000899
NP38	D6	YKL106W	0.00053
NP38	D7	YKL114C	0.001105
NP38	D8	YKL127W	0.001486
NP38	D9	YKL137W	0.001252
NP38	D10	YKL148C	0.000698
NP38	D11	YKL161C	0.000608
NP38	D12	YKL164C	0.000384
NP38	E1	YKL191W	0.001182
NP38	E2	YKR031C	0.000291
NP38	E3	BY4741	0
NP38	E4	YKR044W	0.000748
NP38	E5		
NP38	E6	YKR057W	0.000438
NP38	E7	YKR060W	0.001853
NP38	E8		
NP38	E9	YLL002W	0.001081
NP38	E10	YLL009C	0.000521
NP38	E11	YLL033W	0.000648
NP38	E12	YLR001C	0.000863
NP38	F1	YLR028C	0.000368
NP38	F2	YLR049C	0.00071
NP38	F3	YLR054C	0.001216
NP38	F4	YLR064W	0.00144
NP38	F5	YLR073C	0.000642
NP38	F6	YLR084C	0.000623
NP38	F7		
NP38	F8	YLR174W	0.000729
NP38	F9	YLR210W	0.000589
NP38	F10	YLR227C	0.0006
NP38	F11		
NP38	F12	YLR268W	0.001002
NP38	G1	YLR270W	0.00052
NP38	G2	YLR306W	0.000858
NP38	G3	YLR307W	0.001299
NP38	G4	YLR332W	0.001306
NP38	G5		
NP38	G6	YLR362W	0.000705
NP38	G7	YLR364W	0.001007
NP38	G8	YMR206W	0.000308
NP38	G9	YMR221C	0.001001
NP38	G10	YMR222C	0.000689
NP38	G11	YMR225C	0.000581
NP38	G12	YMR226C	0.001203
NP38	H1	YNL331C	0.000626
NP38	H2	YNL328C	0.000998
NP38	H3	YNL325C	0.000882
NP38	H4	YNL323W	0.00068
NP38	H5	YNL309W	0.000615
NP38	H6	YNL295W	0.000816
NP38	H7	YNL289W	0.000834
NP38	H8	YNL286W	0.001398
NP38	H9	YNL283C	0.000695
NP38	H10	YNL255C	0.000839
NP38	H11	YNL253W	0.00068
NP38	H12	YNL249C	0.000457
NP39	A1	YNL248C	0.000571
NP39	A2	YNL173C	0.000623
NP39	A3	p5472	0.000869
NP39	A4	YNL005C	0.001267
NP39	A5	YNL008C	0.000279
NP39	A6	YNL009W	0.000363
NP39	A7	YNL012W	0.000255
NP39	A8	YNL032W	0.000376
NP39	A9	YOR205C	0.000342
NP39	A10	YOR293W	0.000383
NP39	A11	YOL002C	0.000199
NP39	A12	YOL014W	0.000347
NP39	B1	YOL061W	0.001341054
NP39	B2	YOL084W	0.000867301
NP39	B3	GFP+	
NP39	B4	YPL178W	0.000469718
NP39	B5	YPL101W	0.00057491
NP39	B6	YGR249W	0.000682982
NP39	B7	YKR082W	0.000265247
NP39	B8	YLR425W	0.006850517
NP39	B9	YLR450W	0.000262121
NP39	B10	YER111C	0.00049594
NP39	B11	YMR088C	0.000436767
NP39	B12	DES7	0.002595529
NP39	C1	BY4741	0
NP39	C2		
NP39	C3		
NP39	C4		
NP39	C5	YML102W	0.000276282
NP39	C6	YML112W	0.000245585
NP39	C7	YML123C	0.004077682
NP39	C8	YML124C	0.00021558
NP39	C9	YMR121C	0.000410452
NP39	C10	YJR090C	0.000841613
NP39	C11	YJR091C	0.000217424
NP39	C12	YJR134C	0.000444215
NP39	D1		
NP39	D2	YJL129C	0.000293381
NP39	D3	YJL132W	-7.95881E-05
NP39	D4	YJL042W	0.000274445
NP39	D5	YKR095W	0.001279705
NP39	D6		
NP39	D7		
NP39	D8	YCR048W	0.000379115
NP39	D9	YCR053W	0.000419994
NP39	D10		
NP39	D11	YCR075C	
NP39	D12		
NP39	E1		
NP39	E2		
NP39	E3	YDL194W	0.000349881
NP39	E4	YNL071W	0.000281326
NP39	E5	YNL082W	0.00026339
NP39	E6	YNL087W	0.000296524
NP39	E7	YNL121C	0.000462093
NP39	E8	YDR242W	0.000286925
NP39	E9	YDR515W	0.000374738
NP39	E10	YFL001W	
NP39	E11	YFL004W	0.000477098
NP39	E12		
NP39	F1		
NP39	F2	YGR255C	0.000504828
NP39	F3	YGR258C	0.000333767
NP39	F4		
NP39	F5	YIR023W	0.000314819
NP39	F6	YKR106W	0.003450519
NP39	F7	YNL142W	0.000366311
NP39	F8	YNL315C	0.000322741
NP39	F9	YOL151W	0.000219184

NP39	F10	YOL155C	0.00024999
NP39	F11		
NP39	F12	YOR270C	0.000260295
NP39	G1	YPL137C	0.000381442
NP39	G2	YBL060W	0.000617427
NP39	G3	YBL106C	0.000253376
NP39	G4	YBR081C	0.000484299
NP39	G5	YBR179C	0.000251997
NP39	G6	YBR180W	0.000320306
NP39	G7		
NP39	G8	YBR245C	0.000331119
NP39	G9	YBR268W	0.000221012
NP39	G10		
NP39	G11	YDL080C	0.000341272
NP39	G12	YDR069C	0.000421214
NP39	H1	YDR075W	0.000329611
NP39	H2		
NP39	H3	YDR159W	0.000455247
NP39	H4	YDR244W	0.000501406
NP39	H5		
NP39	H6	YDR369C	0.000324894
NP39	H7	YEL023C	0.0002702
NP39	H8	YFL040W	0.000260536
NP39	H9	YGL006W	0.002578048
NP39	H10	YGL026C	0.000230806
NP39	H11	YGL050W	0.000512292
NP39	H12	YGL062W	0.000280644
NP40	A1	YGL086W	-0.000323359
NP40	A2	YGL094C	-0.000825261
NP40	A3	YGL133W	-0.000746832
NP40	A4	YGR061C	0.000120762
NP40	A5	YHL027W	-0.000587841
NP40	A6	YHL026C	-0.000323057
NP40	A7	YHR073W	-0.000433247
NP40	A8	YHR078W	-0.000542845
NP40	A9	YHR079C	-0.000352875
NP40	A10	YHR154W	-0.000216561
NP40	A11	YHR155W	-0.000290982
NP40	A12	YHR158C	-4.899E-05
NP40	B1	YIL047C	-0.000108983
NP40	B2	YJL212C	0
NP40	B3	YJL209W	-0.000124013
NP40	B4	YJL198W	-0.000229101
NP40	B5	YJL197W	-0.000813613
NP40	B6	YJL193W	-0.000283551
NP40	B7	YJL186W	-0.000808126
NP40	B8	YJL181W	-0.000271761
NP40	B9	YJL168C	-0.000150455
NP40	B10	YJL157C	-0.000211835
NP40	B11	YJL154C	-0.000181624
NP40	B12	YJL153C	-0.000116801
NP40	C1	YJL149W	-0.000285733
NP40	C2	YJL147C	-0.000828295
NP40	C3	YJL138C	-0.000345867
NP40	C4	YJL134W	-0.000279404
NP40	C5	p5472	0.000406561
NP40	C6	YJL102W	0.000295968
NP40	C7	YJL084C	-0.000345012
NP40	C8	YJL080C	-0.001416462
NP40	C9	YKL015W	-0.000343477
NP40	C10	YKL105C	-0.000308257
NP40	C11	YKL157W	-0.000432352
NP40	C12	YKL174C	-0.000363198
NP40	D1	YKL175W	-0.000352028
NP40	D2	YKL179C	-0.00070018
NP40	D3	YKL181W	-0.000498707
NP40	D4	YKL183W	0.000317861
NP40	D5	YKL184W	-0.000461345
NP40	D6	YKL185W	-0.00059076
NP40	D7	YKL187C	0.000119792
NP40	D8	YKL197C	-0.000106871
NP40	D9	YKL205W	-0.000404567
NP40	D10	YKR009C	-0.000250392
NP40	D11	YKR021W	-0.000288192
NP40	D12	YKR026C	-0.00011086
NP40	E1	YKR056W	-0.00037856
NP40	E2	YKR064W	-0.000345608
NP40	E3	YLL038C	-0.000256216
NP40	E4	YLR089C	0.000178005
NP40	E5	YLR451W	-8.0909E-05
NP40	E6	YLR131C	1.62977E-05
NP40	E7	YLR135W	-0.000517036
NP40	E8	YLR138W	-0.000243095
NP40	E9	YLR143W	-0.000590229
NP40	E10	YLR144C	-0.000288855
NP40	E11	BY4741	0
NP40	E12	YLR176C	-0.000207305
NP40	F1	YLR182W	-0.000159586
NP40	F2	YLR187W	-0.000610552
NP40	F3	YLR189C	-0.000434731
NP40	F4	YLR207W	-0.000295162
NP40	F5	YLR219W	3.03988E-05
NP40	F6	YLR233C	0.000180415
NP40	F7	YLR240W	-0.000468967
NP40	F8	YLR263W	9.85725E-05
NP40	F9	GFP+	
NP40	F10	YLR318W	-0.000230277
NP40	F11	YLR319C	-0.000452243
NP40	F12	YLR367W	-0.000545954
NP40	G1	YLR413W	-0.000234314
NP40	G2	YLR414C	-0.000456088
NP40	G3	YLR415C	-0.000328979
NP40	G4	YMR159C	-0.000567752
NP40	G5	YMR166C	-0.000294715
NP40	G6	YMR167W	-0.000611858
NP40	G7	YMR176W	-0.000357597
NP40	G8	YMR190C	-0.000367348
NP40	G9	DES7	0.002258521
NP40	G10	YMR215W	-0.000171105
NP40	G11	YMR216C	-0.000155718
NP40	G12	YNL305C	-0.000363291
NP40	H1	YNL236W	-0.000179827
NP40	H2	YNL219C	-0.000433224
NP40	H3	YNL064C	-0.0009283
NP40	H4	YNL054W	-5.83966E-05
NP40	H5	YOR076C	-0.000491415
NP40	H6	YOR241W	-0.00043013
NP40	H7	YOR242C	-9.95257E-05
NP40	H8	YOR243C	-0.000732227
NP40	H9	YOR245C	-0.000184473
NP40	H10	YOR246C	-0.00057878
NP40	H11	YOR247W	-0.000103532
NP40	H12		
NP41	A1	p5472	0.000858907
NP41	A2	YOR386W	0.001358366
NP41	A3	YOL045W	0.000984248
NP41	A4	YOL075C	0.000807019
NP41	A5	YPL226W	0.000979688
NP41	A6	YPL216W	0.000617622
NP41	A7	YPL022W	0.000832992
NP41	A8	YPR049C	0.000914452
NP41	A9	YPR071W	0.001368153
NP41	A10	YML056C	0.001066358
NP41	A11	YML055W	0.00063877
NP41	A12	YML054C	0.001027208
NP41	B1	GFP+	
NP41	B2	YJR145C	0.001163938
NP41	B3	YJR148W	0.001343009
NP41	B4	YJR150C	0.001018722
NP41	B5	YJR153W	0.001060647
NP41	B6	YML068W	0.002391293
NP41	B7	YMR172W	0.001154692
NP41	B8	YJL003W	0.001297371
NP41	B9	YJL004C	0.001445392
NP41	B10	YML053C	0.00160032
NP41	B11	YML052W	0.00070439
NP41	B12	YJR044C	
NP41	C1	YJR052W	0.001162828
NP41	C2	YJR059W	0.001079484
NP41	C3	YJR062C	0.001377718
NP41	C4	YJR063W	0.000701638
NP41	C5	YCR095C	0.000736657
NP41	C6	YDR174W	0.00221742
NP41	C7	YGR093W	0.000980428
NP41	C8	YGR239C	0.000937464
NP41	C9	YJL196C	0.000369092
NP41	C10	YKR010C	0.000669309
NP41	C11	YKR034W	0.000781945
NP41	C12	YKR036C	0.000804578
NP41	D1	YKR041W	0.001041974
NP41	D2	YPR022C	0.000946621
NP41	D3	YBL051C	
NP41	D4	YBR086C	0.00112919
NP41	D5	YBR262C	0.001633628
NP41	D6	YCL001W	0.001659412
NP41	D7	YCL032W	0.000895607
NP41	D8	YCL045C	0.001088539
NP41	D9	YBR295W	0.002070751
NP41	D10	YCR043C	0.000847028
NP41	D11	YCR073W-A	0.000889044
NP41	D12	YCR086W	0.001047438

NP41	E1	YHR021W-A	0.000539747
NP41	E2	YIR025W	0.001065643
NP41	E3	YKR101W	0.001455207
NP41	E4	YKR105C	0.000804273
NP41	E5	YLR423C	0.000925441
NP41	E6	YMR067C	0.001087753
NP41	E7	YOL101C	0.001239268
NP41	E8	YOL110W	0.001162079
NP41	E9	YLR052W	0.000270761
NP41	E10	YML070W	0.001094216
NP41	E11	YML100W-A	0.000965516
NP41	E12	YMR004W	0.001122718
NP41	F1	YMR101C	0.001197593
NP41	F2	YMR105C	0.001114151
NP41	F3	YMR114C	0.00102665
NP41	F4	YMR116C	0.000731133
NP41	F5	YMR123W	0.000280771
NP41	F6	YML027W	0.001129967
NP41	F7	YML042W	0.001439733
NP41	F8	YAL012W	0.001635955
NP41	F9	YAL016W	0.000931819
NP41	F10	YAL047C	0.000939777
NP41	F11	YJR094C	0.001247881
NP41	F12	YJR104C	0.001336634
NP41	G1	YJR106W	0.000840726
NP41	G2	YJR109C	0.000880239
NP41	G3	YJR122W	0.001170171
NP41	G4	YJR125C	0.001398836
NP41	G5	YML050W	0.001103935
NP41	G6	YML048W	0.000409508
NP41	G7	YMR202W	0.000703862
NP41	G8	BY4741	0
NP41	G9		
NP41	G10	YJL012C	0.000942224
NP41	G11	YJL013C	0.000914767
NP41	G12	YJL016W	0.001016324
NP41	H1	YJL029C	0.000800324
NP41	H2	YJR008W	0.001178343
NP41	H3	YJR010C-A	0.000984354
NP41	H4	YJR015W	0.001070592
NP41	H5	YJR030C	0.001219547
NP41	H6	DES7	0.002076568
NP41	H7	YOR026W	0.001470488
NP41	H8		
NP41	H9	YOR087W	0.001115909
NP41	H10	YOR251C	0.000816557
NP41	H11	YBR189W	0.001459543
NP41	H12		
NP42	A1	YJL163C	-0.000129
NP42	A2	YKR046C	0.000216561
NP42	A3	YKR053C	6.02914E-05
NP42	A4	YJL105W	-0.000132963
NP42	A5	YKR085C	0.000110257
NP42	A6	YNL067W	8.20087E-05
NP42	A7	p5472	0.00064153
NP42	A8	YNL100W	0.000597319
NP42	A9	GFP+	

NP42	A10	YOR266W	-0.000805451
NP42	A11	YOR269W	-0.000131869
NP42	A12	YPR091C	-0.000155383
NP42	B1	YBL043W	0.000269551
NP42	B2	DES7	0.002220995
NP42	B3	YBR016W	0.000361864
NP42	B4	YBR034C	0.000332455
NP42	B5	YBR041W	-0.000560715
NP42	B6	YBR096W	0.000276502
NP42	B7	YBR101C	-0.000639678
NP42	B8	YBR163W	-0.000101027
NP42	B9	YBR175W	0.000300903
NP42	B10	YBR223C	0.000261263
NP42	B11	YDL025C	-0.000293873
NP42	B12	YDL057W	-0.000321485
NP42	C1	YDL173W	7.72381E-05
NP42	C2	BY4741	0
NP42	C3	YDR092W	-0.000510751
NP42	C4	YDR158W	-0.000147833
NP42	C5	YDR173C	-0.000609882
NP42	C6	YDR282C	0.000252808
NP42	C7	YDR315C	-0.00023994
NP42	C8	YDR374C	-0.000227126
NP42	C9	YDR375C	0
NP42	C10	YDR392W	0.000133608
NP42	C11	YDR408C	0.000237261
NP42	C12	YDR414C	5.80436E-05
NP42	D1		
NP42	D2	YFL034W	-0.000515789
NP42	D3	YFR010W	0.000220901
NP42	D4	YFR014C	-0.000125424
NP42	D5	YFR018C	0.000305121
NP42	D6	YGL003C	0.000111233
NP42	D7	YGL196W	0.000293417
NP42	D8	YGL210W	0.000288631
NP42	D9	YGL226W	0.000124683
NP42	D10	YGL229C	0.000290331
NP42	D11	YGL250W	-0.000926441
NP42	D12	YGR026W	-0.000261611
NP42	E1	YGR041W	0.000131589
NP42	E2	YGR085C	9.19283E-05
NP42	E3	YGR096W	3.5465E-05
NP42	E4		
NP42	E5		
NP42	E6		
NP42	E7		
NP42	E8		
NP42	E9		
NP42	E10		
NP42	E11		
NP42	E12		
NP42	F1		
NP42	F2		
NP42	F3		
NP42	F4		
NP42	F5		
NP42	F6		

NP42	F7	YLR063W	0.000340232
NP42	F8	YLR065C	-1.29546E-05
NP42	F9	YLR134W	0.00030708
NP42	F10	YLR295C	-0.000159267
NP42	F11	YLR327C	-0.000697074
NP42	F12	YLR363C	0.000184237
NP42	G1	YLR385C	7.34984E-05
NP42	G2		
NP42	G3	YMR241W	0.000222209
NP42	G4	YMR242C	-0.000107591
NP42	G5	YMR243C	-0.000384814
NP42	G6	YNL332W	-0.00012308
NP42	G7	YNL307C	1.36257E-05
NP42	G8	YNL254C	5.43076E-05
NP42	G9	YNL231C	4.14259E-05
NP42	G10	YNL146W	0.000246517
NP42	G11	YNL144C	0.000279481
NP42	G12	YNL141W	7.14335E-05
NP42	H1	YNL133C	0.000275171
NP42	H2	YNL117W	0.000136425
NP42	H3	YNL094W	4.422E-05
NP42	H4	YNL001W	-0.003108057
NP42	H5	YNL003C	0.000126725
NP42	H6	YNR014W	2.81987E-05
NP42	H7	YNR021W	0.000158422
NP42	H8	YNR045W	7.44462E-05
NP42	H9		
NP42	H10		
NP42	H11		
NP42	H12		
NP43	A1	YAL016C-B	0.000478688
NP43	A2	YAL037C-A	0.000394843
NP43	A3	YAL044W-A	0.000375732
NP43	A4	YAR035C-A	0.000403233
NP43	A5	YBL008W-A	0.000415355
NP43	A6	YBL029C-A	0.000366673
NP43	A7	YBL071C-B	0.000527208
NP43	A8	YBL071W-A	0.00036383
NP43	A9	YBR056W-A	
NP43	A10	YBR058C-A	0.000434573
NP43	A11	YBR072C-A	0.000698639
NP43	A12	YBR085C-A	0.000497062
NP43	B1	YBR111W-A	0.000348962
NP43	B2	YBR182C-A	0.00066866
NP43	B3	YBR196C-B	0.000908395
NP43	B4	YBR200W-A	0.00039346
NP43	B5	YBR221W-A	0.000667661
NP43	B6	YBR230W-A	0.001312734
NP43	B7	YBR296C-A	0.000482181
NP43	B8	YCL001W-B	0.00041979
NP43	B9	YCL005W-A	0.000294592
NP43	B10	YCL026C-B	0.000301754
NP43	B11	YCL057C-A	0.000639791
NP43	B12	YCR075W-A	0.000818524
NP43	C1	YCR095W-A	0.000338763
NP43	C2	YDL085C-A	0.000466407
NP43	C3	YDL159W-A	0.000402992

NP43	C4	YDL160C-A	0.001092
NP43	C5	YDR003W-A	0.000383
NP43	C6	YDR034W-B	0.00072
NP43	C7	YDR079C-A	0.000761
NP43	C8	YDR169C-A	0.000409
NP43	C9	YDR194W-A	0.000502
NP43	C10	YDR246W-A	0.000351
NP43	C11	YDR379C-A	0.001319
NP43	C12	YEL059C-A	0.000354
NP43	D1	YER026C	0.000409
NP43	D2	p5472	0.000628
NP43	D3	YER053C-A	0.000402
NP43	D4	DES7	0.003595
NP43	D5	YER076C	0.001412
NP43	D6	GFP+	0.117717
NP43	D7	YER087C-B	0.000362
NP43	D8	YER099C	0.000429
NP43	D9	YER175W-A	0.000704
NP43	D10	YER180C-A	0.000457
NP43	D11	YFL041W-A	0.000618
NP43	D12		
NP43	E1	YFR012W-A	0.00031
NP43	E2	YFR032C-B	0.00041
NP43	E3	YGL006W-A	0.000377
NP43	E4	YGL041C-B	0.000458
NP43	E5	YGL100W	0.000387
NP43	E6	YGL119W	0.001071
NP43	E7	YGL134W	0.000329
NP43	E8	YGL178W	0.000603
NP43	E9	YGL185C	0.001825
NP43	E10		
NP43	E11	YGL188C-A	0.00062
NP43	E12	YGL191W	0.000476
NP43	F1	YGL192W	0.000409
NP43	F2	YGR035W-A	0.000527
NP43	F3	YGR121W-A	0.00056
NP43	F4	YGR146C-A	0.000413
NP43	F5	YGR161W-C	0.000324
NP43	F6	YGR169C-A	0.000413
NP43	F7	YGR174W-A	0.000336
NP43	F8	YGR204C-A	0.000296
NP43	F9	YGR271C-A	0.000336
NP43	F10	YHL001W	0.000561
NP43	F11	YHL004W	0.000424
NP43	F12	YHL015W-A	0.000372
NP43	G1		
NP43	G2	YHR007C-A	0.000299
NP43	G3	YHR022C-A	0.000459
NP43	G4	YHR050W-A	0.000531
NP43	G5	YHR071W	0.000369
NP43	G6	YHR086W-A	0.000582
NP43	G7	YHR090C	0.000898
NP43	G8	BY4741	0
NP43	G9	YHR141C	0.000465
NP43	G10	YHR149C	0.000514
NP43	G11	YHR175W-A	0.000355
NP43	G12	YHR187W	0.000256
NP43	H1	YHR192W	0.000350314
NP43	H2		
NP43	H3	YHR205W	0.000436097
NP43	H4	YIL002W-A	0.001110667
NP43	H5	YIL046W-A	0.000375761
NP43	H6	YIL127C	0.000707831
NP43	H7	YIL134C-A	0.00065256
NP43	H8		
NP43	H9	YJL047C-A	0.000571357
NP43	H10	YJL062W-A	0.000533223
NP43	H11	YJL077W-B	0.000463367
NP43	H12	YJL127C-B	0.000455662
NP44	A1	YBR274W	0.000857344
NP44	A2		
NP44	A3	YCR061W	0.000368855
NP44	A4		
NP44	A5	YFR038W	0.000500049
NP44	A6	YFR045W	0.000346017
NP44	A7	p5472	0.000761117
NP44	A8	YGR244C	0.000242472
NP44	A9		
NP44	A10	DES7	0.006335993
NP44	A11	GFP+	0.096200905
NP44	A12	BY4741	0
NP44	B1	YER109C	0.00019653
NP44	B2		
NP44	B3	YML104C	7.55061E-05
NP44	B4		
NP44	B5		
NP44	B6		
NP44	B7		
NP44	B8	YKL201C	0.00041362
NP44	B9		
NP44	B10	YNR052C	0.00030723
NP44	B11	YNL090W	0.001333314
NP44	B12	YFL010W-A	0.000294559
NP44	C1	YNL147W	0.000210556
NP44	C2	YAL049C	0.00018396
NP44	C3	YAL021C	0.000757539
NP44	C4		
NP44	C5	YBL104C	0.001054466
NP44	C6	YBR062C	0.000266497
NP44	C7	YBR074W	0.000897238
NP44	C8	YBR098W	0.000478816
NP44	C9	YBR105C	0.000554822
NP44	C10	YBR133C	0.000288935
NP44	C11		
NP44	C12	YBR201W	0.000399081
NP44	D1		
NP44	D2		
NP44	D3	YCL061C	0.000287972
NP44	D4		
NP44	D5	YDL069C	0.000300678
NP44	D6	YDL077C	0.000684573
NP44	D7		
NP44	D8	YDR092W	0.000257297
NP44	D9	YDR147W	0.000563198
NP44	D10		
NP44	D11	YDR315C	0.000927
NP44	D12		
NP44	E1		
NP44	E2		
NP44	E3	YDR485C	0.000244
NP44	E4	YDR501W	0.000278
NP44	E5	YDR518W	
NP44	E6	YEL041W	0.000295
NP44	E7	YER007W	0.000568
NP44	E8	YER016W	0.002021
NP44	E9		
NP44	E10	YGL023C	0.000146
NP44	E11	YGL032C	0.000553
NP44	E12	YGL033W	0.00076
NP44	F1		
NP44	F2	YGL081W	0.000172
NP44	F3	YGL101W	0.001202
NP44	F4	YGL104C	0.000735
NP44	F5	YGL196W	0.00191
NP44	F6	YGL202W	0.002114
NP44	F7	YGL216W	0.000973
NP44	F8	YGL211W	0.000436
NP44	F9		
NP44	F10	YGL237C	0.00025
NP44	F11	YGR037C	0.000295
NP44	F12	YGR062C	0.00084
NP44	G1	YGR180C	
NP44	G2	YHR091C	0
NP44	G3	YIL041W	0.000931
NP44	G4		
NP44	G5		
NP44	G6	YJL059W	0.000316
NP44	G7	YKL002W	0.001012
NP44	G8		
NP44	G9	YKL137W	0.000317
NP44	G10	YKL157W	0.000381
NP44	G11	YKL198C	
NP44	G12		
NP44	H1		
NP44	H2	YLR084C	0.000121
NP44	H3	YLR118C	0.00055
NP44	H4	YLR125W	0.000649
NP44	H5	YLR211C	
NP44	H6	YLR251W	0.000521
NP44	H7	YLR329W	0.000363
NP44	H8	YLR332W	0.000679
NP44	H9		
NP44	H10		
NP44	H11		
NP44	H12	YMR143W	0.0003
NP45	A1		
NP45	A2	YJR085C	0.000282
NP45	A3	YJR086W	0.000509
NP45	A4	YJR101W	0.000302
NP45	A5	YJR112W-A	0.000296
NP45	A6	YJR114W	0.000252

NP45	A7	YJR143C	0.00029
NP45	A8		
NP45	A9	YLL006W-A	0.000403
NP45	A10	YLR264C-A	0.000401
NP45	A11	YLR285C-A	0.000378
NP45	A12	YLR342W-A	0.000322
NP45	B1	YLR361C-A	0.000237
NP45	B2	YLR363W-A	0.000144
NP45	B3	YLR406C-A	0.000289
NP45	B4	YLR412C-A	0.000254
NP45	B5	YLR419W	0.000251
NP45	B6	YML007C-A	0.000431
NP45	B7	YML054C-A	0.00036
NP45	B8	YML058W-A	0.000396
NP45	B9	YMR001C-A	0.00029
NP45	B10	YMR013W-A	0.000371
NP45	B11	YMR105W-A	0.00038
NP45	B12	YMR175W-A	0.000277
NP45	C1	YMR182W-A	0.000248
NP45	C2	YMR194C-B	0.000339
NP45	C3	YMR230W-A	0.000325
NP45	C4	YMR247W-A	0.000331
NP45	C5	YMR272W-B	0.000247
NP45	C6	YMR315W-A	0.00031
NP45	C7	YNL042W-B	0.000231
NP45	C8	YNL067W-B	0.00039
NP45	C9	YNL130C-A	0.000403
NP45	C10	YNL146C-A	0.000394
NP45	C11	YNL162W-A	0.000368
NP45	C12	YNL209W	0.000319
NP45	D1	YNL277W-A	0.000339
NP45	D2	YOL019W-A	0.000313
NP45	D3	YOL038C-A	0.000252
NP45	D4	YOL073C	0.000397
NP45	D5	YOL077W-A	0.000317
NP45	D6	YOL086W-A	0.000351
NP45	D7	YOL097W-A	0.000411
NP45	D8	YOL140W	0.000254
NP45	D9	YOL145C	0.000296
NP45	D10	YOL154W	0.000269
NP45	D11	YOL159C-A	0.000345
NP45	D12	YOL164W	0.000352
NP45	E1	YOL164W-A	0.000284
NP45	E2	YOR020W-A	0.000357
NP45	E3	YOR034C-A	0.000451
NP45	E4	YOR161C-C	0.000329
NP45	E5	YOR293C-A	0.000256
NP45	E6	YOR316C-A	0.000261
NP45	E7	YOR376W-A	0.000292
NP45	E8	YPL038W-A	0.00023
NP45	E9	YPL096C-A	0.000297
NP45	E10	YPL119C-A	0.000277
NP45	E11	YPL152W-A	0.00032
NP45	E12	YPL189C-A	0.000454
NP45	F1	YPL249C-A	0.00067
NP45	F2	YPL277C	0.000274
NP45	F3	YPR108W-A	0.00031

NP45	F4	YPR159C-A	0.000418792
NP45	F5	BY4741	1.77249E-05
NP45	F6	YPL165C	0.000185815
NP45	F7		
NP45	F8		
NP45	F9	YPR141C	0.000390153
NP45	F10	YAR042W	0.000317691
NP45	F11	YCL001W-A	0.000294309
NP45	F12	YCR020W-B	0.000222671
NP45	G1	YCR024C	0.000249802
NP45	G2	YCR027C	0.000371287
NP45	G3	YCR044C	0.000578975
NP45	G4	YCR045C	0.000406477
NP45	G5	YCR063W	0.000459775
NP45	G6		
NP45	G7	YCR071C	0.000330265
NP45	G8	YCR079W	0.000250651
NP45	G9		
NP45	G10		
NP45	G11	YER129W	0.000330787
NP45	G12	YER091C	0.000378811
NP45	H1	p5472	0.000670836
NP45	H2	GFP+	0.071955954
NP45	H3	DES7	0.004838209
NP45	H4	YJR097W	0.0005656
NP45	H5	YKR102W	0.000515719
NP45	H6	YPR007C	0.000346368
NP45	H7	YCR067C	0.000354017
NP45	H8		
NP45	H9	YER089C	0.000347865
NP45	H10	YFL016C	0.000308118
NP45	H11	YBL067C	0.000250565
NP45	H12		
NP46	A1	YBR059C	0.000250264
NP46	A2	YBR084W	0.000247487
NP46	A3		
NP46	A4		
NP46	A5	YCL044C	0.000250532
NP46	A6	YCL061C	0.000265704
NP46	A7	p5472	0.000968985
NP46	A8	DES7	0.003306349
NP46	A9	YDL202W	0.000737053
NP46	A10	YDL206W	
NP46	A11	GFP+	0.104273649
NP46	A12	BY4741	0
NP46	B1	YDR119W	0.000936076
NP46	B2	YDR122W	0.000212862
NP46	B3		
NP46	B4		
NP46	B5	YDR258C	
NP46	B6		
NP46	B7		
NP46	B8		
NP46	B9		
NP46	B10	YDR497C	
NP46	B11	YDR503C	0.000400146
NP46	B12	YER049W	0.003741485

NP46	C1	YFL027C	0.000566397
NP46	C2		
NP46	C3		
NP46	C4		
NP46	C5		
NP46	C6		
NP46	C7		
NP46	C8	YIL002C	0.000227552
NP46	C9		
NP46	C10		
NP46	C11		
NP46	C12	YLR228C	0.000245832
NP46	D1		
NP46	D2	YMR196W	
NP46	D3		
NP46	D4		
NP46	D5	YMR300C	0.000265023
NP46	D6	YNL330C	0.000410257
NP46	D7		
NP46	D8	YNL243W	0.000303903
NP46	D9		
NP46	D10	YNL004W	0.004297956
NP46	D11	YNR007C	0.000884483
NP46	D12	YOR038C	0.000224456
NP46	E1	YOR083W	
NP46	E2		
NP46	E3		
NP46	E4		
NP46	E5		
NP46	E6		
NP46	E7		
NP46	E8	YPL115C	
NP46	E9	YPL098C	0.000419239
NP46	E10		
NP46	E11	YPL040C	0.000304002
NP46	E12	YPL037C	0.003929907
NP46	F1	YPR018W	0.000258667
NP46	F2	YPR111W	0.000739578
NP46	F3		
NP46	F4		
NP46	F5		
NP46	F6	YPL271W	0.001660979
NP46	F7	YPL244C	
NP46	F8	YPL208W	0.000293263
NP46	F9	YPL195W	0.0002397
NP46	F10	YOR120W	0.000396152
NP46	F11	YPL181W	0.000269409
NP46	F12	YOR127W	
NP46	G1	YOR154W	0.000477671
NP46	G2	YOR186W	0.000427436
NP46	G3	YOR187W	7.56527E-05
NP46	G4	YOR201C	0.000282948
NP46	G5	YOR202W	0.000294159
NP46	G6	YOR219C	0.000304373
NP46	G7	YOR222W	0.001428922
NP46	G8	YOR227W	0.001790803
NP46	G9	YOR233W	0.002141517

NP46	G10	YOR234C	0.000257
NP46	G11	YOR238W	0.0003
NP46	G12	YOR284W	
NP46	H1	YOR292C	0.000295
NP46	H2	YOR305W	0.001399
NP46	H3	YOR312C	0.007019
NP46	H4	YOR321W	0.000311
NP46	H5	YOR327C	0.000304
NP46	H6	YOR368W	0.003205
NP46	H7	YOR365C	0.001487
NP46	H8	YOR367W	0.000288
NP46	H9	YOL007C	0.000369
NP46	H10	YOL017W	0.000222
NP46	H11	YOL060C	0.000294
NP46	H12	YOL068C	0.000409
NP47	A1	YBR274W	0.000239
NP47	A2	YBR279W	0.000473
NP47	A3		
NP47	A4	YCR090C	0.000272
NP47	A5	YFR038W	0.000543
NP47	A6	YIR028W	0.000358
NP47	A7	YKR099W	0.000544
NP47	A8		
NP47	A9		
NP47	A10	YNR050C	0.000573
NP47	A11	YMR066W	0.000285
NP47	A12	YNR071C	0.000332
NP47	B1	YMR098C	0.000368
NP47	B2	YHR026W	0.000368
NP47	B3	YHR041C	0.000642
NP47	B4	YDR071C	0.000278
NP47	B5	YML038C	0.000585
NP47	B6		
NP47	B7		
NP47	B8	YGR086C	0.000403
NP47	B9	YGR117C	0.000199
NP47	B10	YJL136C	0.000457
NP47	B11	YKL139W	0.000342
NP47	B12		
NP47	C1	YBR299W	0.000635
NP47	C2	YDR461W	0.000533
NP47	C3	YIL033C	0.000367
NP47	C4	YBR020W	0.000371
NP47	C5	YNL011C	0.000526
NP47	C6	YBL002W	0.000318
NP47	C7	YBL022C	0.00042
NP47	C8	YBL055C	0.000318
NP47	C9	YBR018C	0.000302
NP47	C10	YBR030W	0.000694
NP47	C11	YBR043C	0.000492
NP47	C12	YBR161W	0.000341
NP47	D1	YBR181C	0.000355
NP47	D2	YBR182C	0.0005
NP47	D3	YDL042C	0.000603
NP47	D4	YDL044C	0.000342
NP47	D5	YDL049C	0.000312
NP47	D6	YDL113C	0.000428

NP47	D7	YDL198C	0.000279
NP47	D8	YDL213C	0.000204
NP47	D9	YDR055W	0.000377
NP47	D10	YDR183W	0.000294
NP47	D11	YDR346C	0.000302
NP47	D12	YDR402C	0.000287
NP47	E1		
NP47	E2		
NP47	E3	YDR448W	0.000293
NP47	E4		
NP47	E5		
NP47	E6	YEL046C	0.000321
NP47	E7	YEL061C	0.000163
NP47	E8	YER004W	0.000274
NP47	E9	p5472	0.000375
NP47	E10	GFP+	0.073253
NP47	E11	DES7	0.002582
NP47	E12	YFR008W	0.000548
NP47	F1		
NP47	F2	YGL005C	0.000436
NP47	F3	YGL009C	0.000148
NP47	F4	YGL012W	0.000398
NP47	F5		
NP47	F6		
NP47	F7		
NP47	F8	YGL144C	0.000211
NP47	F9		
NP47	F10	BY4741	0.000583
NP47	F11	YGR020C	0.000334
NP47	F12	YGR049W	0.000341
NP47	G1	YGR072W	0.000285
NP47	G2		
NP47	G3	YGR132C	0.000548
NP47	G4	YGR150C	0.000396
NP47	G5	YGR153W	0.000364
NP47	G6	YHL016C	0.000481
NP47	G7		
NP47	G8	YIL014W	0.000647
NP47	G9	YIL113W	0.000432
NP47	G10		
NP47	G11	YIL158W	0.000327
NP47	G12	YJL164C	0.000238
NP47	H1	YJL115W	0.000389
NP47	H2	YKL009W	0.000385
NP47	H3	YKL065C	0.000406
NP47	H4		
NP47	H5	YKL128C	0.000327
NP47	H6	YKL150W	0.000313
NP47	H7	YKL159C	0.00072
NP47	H8	YKL163W	0.000324
NP47	H9	YKL218C	0.000686
NP47	H10		
NP47	H11		
NP47	H12		
EP1	A1	YAL001C	0.002148
EP1	A2		
EP1	A3		

EP1	A4		
EP1	A5		
EP1	A6		
EP1	A7		
EP1	A8	p5472	0.000696087
EP1	A9	YAL043C	0.000238609
EP1	A10	GFP+	0.103042611
EP1	A11	DES7	0.003448712
EP1	A12	BY4741	2.01876E-08
EP1	B1		
EP1	B2		
EP1	B3	YBL018C	0.000311376
EP1	B4	YBL020W	0.000318659
EP1	B5	YBL023C	0.000380688
EP1	B6	YBL026W	
EP1	B7	YBL030C	0.00032846
EP1	B8	YBL034C	0.000245196
EP1	B9	YBL035C	
EP1	B10	YBL040C	
EP1	B11	YBL041W	0.000253642
EP1	B12	YBL050W	0.002387891
EP1	C1	YBL074C	0.005430748
EP1	C2	YBL076C	
EP1	C3		
EP1	C4	YBL092W	0.00035016
EP1	C5		
EP1	C6	YBL105C	0.000283056
EP1	C7	YBR002C	0.000251422
EP1	C8	YBR004C	0.000324969
EP1	C9	YBR011C	0.000231919
EP1	C10	YBR029C	0.000310614
EP1	C11	YBR038W	0.000270281
EP1	C12	YBR049C	
EP1	D1	YBR055C	0.000265402
EP1	D2	YBR060C	
EP1	D3	YBR070C	0.000315074
EP1	D4	YBR079C	
EP1	D5		
EP1	D6	YBR087W	0.000261531
EP1	D7	YBR088C	0.000327944
EP1	D8	YBR091C	0.000294463
EP1	D9	YBR102C	0.000281489
EP1	D10	YBR109C	0.000337614
EP1	D11		
EP1	D12	YBR121C	
EP1	E1	YBR123C	0.005207983
EP1	E2		
EP1	E3		
EP1	E4	YBR140C	
EP1	E5	YBR142W	0.000309036
EP1	E6	YBR143C	7.054E-05
EP1	E7	YBR152W	0.005634116
EP1	E8	YBR153W	0.000268567
EP1	E9	YBR154C	0.000357938
EP1	E10	YBR155W	0.000278846
EP1	E11	YBR160W	0.000330961
EP1	E12	YBR167C	0.000276013

EP1	F1	YBR192W	0.000246
EP1	F2	YBR193C	0.000303
EP1	F3	YBR196C	0.000279
EP1	F4	YBR198C	0.000636
EP1	F5	YBR202W	0.00028
EP1	F6	YBR211C	0.000325
EP1	F7	YBR234C	0.000122
EP1	F8	YBR236C	0.000275
EP1	F9	YBR237W	0.000293
EP1	F10	YBR243C	0.000165
EP1	F11	YBR247C	0.000235
EP1	F12	YBR252W	
EP1	G1	YBR253W	0.000299
EP1	G2	YBR254C	0.000303
EP1	G3	YBR256C	0.000374
EP1	G4	YBR257W	0.000318
EP1	G5	YBR265W	0.000924
EP1	G6	YCL004W	0.000346
EP1	G7	YCL017C	
EP1	G8	YCL031C	
EP1	G9	YCL043C	0.000259
EP1	G10	YCL052C	0.00029
EP1	G11	YCL054W	0.000333
EP1	G12	YCL059C	0.000274
EP1	H1	YCR012W	0.000355
EP1	H2	YCR035C	0.000162
EP1	H3	YCR052W	0.000315
EP1	H4	YCR054C	0.005236
EP1	H5	YCR057C	
EP1	H6	YCR072C	
EP1	H7		
EP1	H8	YDL003W	0.000268
EP1	H9	YDL004W	
EP1	H10	YDL007W	0.000479
EP1	H11	YDL008W	0.000281
EP1	H12	YDL014W	
EP2	A1		
EP2	A2	YDL017W	0.000273
EP2	A3	YDL028C	0.000221
EP2	A4	YDL029W	0.00026
EP2	A5	YDL030W	0.00025
EP2	A6	YDL031W	0.002953
EP2	A7	YDL043C	0.000177
EP2	A8	YDL045C	0.000217
EP2	A9	YDL055C	0.000377
EP2	A10		
EP2	A11	YDL060W	0.000423
EP2	A12	YDL064W	0.000252
EP2	B1	YDL084W	0.000287
EP2	B2	YDL087C	0.001066
EP2	B3	YDL092W	0.000357
EP2	B4	YDL097C	
EP2	B5	YDL098C	0.00027
EP2	B6		
EP2	B7	YDL103C	
EP2	B8	YDL105W	
EP2	B9	YDL108W	0.000278
EP2	B10		
EP2	B11	YDL120W	0.000343079
EP2	B12	YDL126C	0.000160393
EP2	C1		
EP2	C2	YDL139C	0.000248976
EP2	C3		
EP2	C4	YDL141W	0.000283343
EP2	C5	YDL143W	0.000119496
EP2	C6	YDL145C	0.000283394
EP2	C7	YDL147W	0.000318251
EP2	C8	YDL148C	0.000288013
EP2	C9	YDL150W	
EP2	C10	YDL153C	0.0002727
EP2	C11	YDL164C	0.00028995
EP2	C12	YDL165W	0.000249676
EP2	D1		
EP2	D2	YDL193W	0.000239074
EP2	D3	YDL195W	0.0002377
EP2	D4	YDL205C	0.000389957
EP2	D5	YDL207W	0.000310259
EP2	D6	YDL208W	0.000245755
EP2	D7	YDL209C	0.000330273
EP2	D8	YDL212W	0.000335304
EP2	D9	YDL217C	0.000318213
EP2	D10	YDL220C	0.000344899
EP2	D11	YDL235C	0.000550497
EP2	D12	YDR002W	0.00026252
EP2	E1	YDR013W	0.000303779
EP2	E2	YDR016C	
EP2	E3	YDR021W	0.000392419
EP2	E4	YDR023W	0.000274875
EP2	E5	YDR037W	0.000331388
EP2	E6	YDR041W	0.000206063
EP2	E7	YDR044W	0.000303718
EP2	E8	YDR045C	0.000282514
EP2	E9	YDR047W	0.000303882
EP2	E10		
EP2	E11	YDR052C	0.00175017
EP2	E12	YDR054C	0.000288294
EP2	F1	YDR060W	0.000238608
EP2	F2	YDR062W	0.000236697
EP2	F3	YDR064W	0.000362093
EP2	F4	YDR081C	5.91476E-05
EP2	F5	YDR082W	0.002447553
EP2	F6	YDR086C	
EP2	F7	YDR087C	
EP2	F8	YDR088C	0.000311167
EP2	F9	YDR091C	0.000451777
EP2	F10	YDR113C	0.00033824
EP2	F11	YDR118W	0.000234926
EP2	F12	YDR141C	
EP2	G1	p5472	0.000394573
EP2	G2	GFP+	0.100622281
EP2	G3	YDR164C	0.00022827
EP2	G4	YDR166C	
EP2	G5	YDR167W	0.00024047
EP2	G6	YDR168W	0.005235012
EP2	G7	BY4741	9.10131E-06
EP2	G8	YDR172W	
EP2	G9	YDR177W	1.84549E-05
EP2	G10	YDR180W	
EP2	G11	YDR182W	0.005338637
EP2	G12	YDR188W	0.000268583
EP2	H1	YDR189W	0.000248123
EP2	H2	DES7	0.002883928
EP2	H3	YDR196C	0.000227098
EP2	H4	YDR201W	0.000523647
EP2	H5	YDR208W	0.000319352
EP2	H6		
EP2	H7		
EP2	H8	YDR224C	0.003017266
EP2	H9	YDR228C	0.000221582
EP2	H10	YDR232W	0.000261843
EP2	H11	YDR235W	0.000268819
EP2	H12	YDR236C	0.000265292
EP3	A1	YDR238C	
EP3	A2	YDR240C	0.000310512
EP3	A3	YDR243C	0.000222216
EP3	A4	YDR246W	0.000420387
EP3	A5	YDR280W	0.000279391
EP3	A6	YDR288W	0.000472318
EP3	A7	YDR292C	0.001644434
EP3	A8	YDR299W	0.000468598
EP3	A9	YDR301W	0.000318186
EP3	A10	p5472	0.00063158
EP3	A11	YDR303C	0.000873543
EP3	A12	YDR308C	
EP3	B1	YDR311W	0.000264134
EP3	B2	YDR324C	0.001233296
EP3	B3	YDR325W	0.000276097
EP3	B4	YDR328C	0.00026956
EP3	B5	YDR331W	0.000394657
EP3	B6	YDR339C	0.000718686
EP3	B7	YDR341C	0.000316736
EP3	B8	YDR353W	0.000444673
EP3	B9	YDR356W	0.000476548
EP3	B10	YDR361C	0.001382288
EP3	B11	YDR362C	0.000378702
EP3	B12	YDR365C	0.000251067
EP3	C1	YDR367W	0.000404345
EP3	C2	YDR373W	0.00025341
EP3	C3	YDR376W	0.000681082
EP3	C4	YDR381W	0.000580394
EP3	C5	YDR390C	0.001929982
EP3	C6	YDR394W	0.000718138
EP3	C7	YDR397C	0.000419975
EP3	C8	GFP+	0.123407999
EP3	C9	YDR404C	0.00057862
EP3	C10	YDR407C	0.000155467
EP3	C11	YDR412W	0.000644578
EP3	C12	YDR416W	0.00055779
EP3	D1	YDR427W	
EP3	D2	YDR429C	0.000344567
EP3	D3	YDR434W	0.000263682

EP3	D4	YDR437W	
EP3	D5	YDR449C	
EP3	D6	YDR454C	
EP3	D7	YDR460W	
EP3	D8	YDR464W	
EP3	D9	YDR468C	
EP3	D10	YDR472W	0.000864
EP3	D11	YDR473C	0.000393
EP3	D12	YDR478W	
EP3	E1	YDR487C	0.000591
EP3	E2	YDR489W	0.000539
EP3	E3	YDR498C	0.000352
EP3	E4	YDR499W	0.000752
EP3	E5	YDR510W	0.000327
EP3	E6	YDR527W	0.000877
EP3	E7	YDR531W	0.000397
EP3	E8	YEL002C	0.000933
EP3	E9	YEL019C	0.000483
EP3	E10	YEL026W	0.000546
EP3	E11	YEL032W	0.000259
EP3	E12	YEL034W	
EP3	F1	YEL035C	0.000272
EP3	F2	YEL055C	0.001009
EP3	F3	YEL058W	0.001402
EP3	F4	YER003C	0.000902
EP3	F5	YER006W	0.000851
EP3	F6	YER008C	0.00022
EP3	F7	YER009W	0.000606
EP3	F8	YER012W	0.000816
EP3	F9	YER013W	0.000752
EP3	F10	YER018C	0.00477
EP3	F11	YER021W	0.000495
EP3	F12	YER022W	
EP3	G1	YER023W	0.000396
EP3	G2	YER025W	0.00077
EP3	G3	YER036C	0.000305
EP3	G4	YER038C	0.000454
EP3	G5	YER043C	0.000591
EP3	G6	YER048W-A	0.00054
EP3	G7	YER082C	0.000267
EP3	G8	DES7	0.002791
EP3	G9	YER094C	0.001235
EP3	G10	YER104W	0.000943
EP3	G11	YER112W	0.000499
EP3	G12	BY4741	0
EP3	H1	YER126C	
EP3	H2	YER127W	0.000374
EP3	H3	YER133W	0.001378
EP3	H4	YER136W	0.000389
EP3	H5	YER146W	0.00033
EP3	H6	YER147C	0.000627
EP3	H7	YER148W	0.000683
EP3	H8	YER157W	0.00129
EP3	H9	YER159C	0.000386
EP3	H10	YER165W	0.000723
EP3	H11	YER168C	0.000316
EP3	H12		

EP4	A1	YER172C	0.000129492
EP4	A2	YFL002C	7.2648E-05
EP4	A3	YFL005W	0.000120364
EP4	A4	YFL008W	0.00017172
EP4	A5	YFL009W	0.000215792
EP4	A6	YFL017C	0.000175797
EP4	A7	YFL022C	0.000205402
EP4	A8	YFL024C	0.00014595
EP4	A9	YFL029C	9.04267E-05
EP4	A10	YFL037W	-0.000123156
EP4	A11	YFL038C	0.000149204
EP4	A12	p5472	0.000983538
EP4	B1	YFL045C	0.000132778
EP4	B2	YFR002W	9.95675E-05
EP4	B3	YFR003C	0.000179324
EP4	B4	YFR004W	0.000170754
EP4	B5	YFR005C	7.22687E-05
EP4	B6	YFR027W	-8.58565E-05
EP4	B7	YFR028C	0.000145511
EP4	B8	YFR029W	0.000222754
EP4	B9	YFR031C	0.000201617
EP4	B10	YFR037C	0.000198529
EP4	B11	YFR042W	0.000186832
EP4	B12	YFR050C	0.000205536
EP4	C1	YFR051C	-1.4821E-05
EP4	C2	YFR052W	0.00014396
EP4	C3	YGL001C	
EP4	C4	YGL008C	0.000184887
EP4	C5	YGL011C	-0.000202984
EP4	C6	YGL018C	-0.000435218
EP4	C7	GFP+	0.092143758
EP4	C8	YGL030W	0.000716025
EP4	C9	DES7	0.002205762
EP4	C10	YGL044C	0.000225017
EP4	C11	YGL047W	0.000190433
EP4	C12	YGL048C	8.5684E-05
EP4	D1	BY4741	
EP4	D2	YGL061C	
EP4	D3	YGL065C	0.000155593
EP4	D4	YGL068W	0.000160607
EP4	D5	YGL073W	0.000226228
EP4	D6	YGL075C	-0.00033173
EP4	D7	YGL091C	0.000274086
EP4	D8		
EP4	D9		
EP4	D10	YGL097W	0.000226542
EP4	D11	YGL098W	0.000217953
EP4	D12	YGL099W	
EP4	E1	YGL103W	0.000277922
EP4	E2		
EP4	E3		
EP4	E4	YGL113W	0.000211774
EP4	E5	YGL116W	0.000277338
EP4	E6	YGL120C	0.000238353
EP4	E7	YGL122C	0.000200648
EP4	E8	YGL123W	-0.000620677
EP4	E9	YGL128C	0.000267797

EP4	E10	YGL130W	1.39282E-05
EP4	E11	YGL137W	0.00015675
EP4	E12	YGL142C	0.000267586
EP4	F1	YGL145W	0.000137454
EP4	F2		
EP4	F3	YGL155W	0.000201828
EP4	F4	YGL169W	0.000254191
EP4	F5	YGL171W	0.000198413
EP4	F6	YGL172W	8.396E-05
EP4	F7	YGL201C	0.000381226
EP4	F8	YGL207W	0.000238536
EP4	F9	YGL225W	0.000348309
EP4	F10	YGL233W	0.000261072
EP4	F11		
EP4	F12	YGL245W	0.000104326
EP4	G1	YGL247W	0.000145509
EP4	G2	YGR002C	0.000183884
EP4	G3	YGR005C	7.11886E-05
EP4	G4	YGR009C	0.000216175
EP4	G5	YGR013W	-0.001640187
EP4	G6		
EP4	G7	YGR029W	0.000168427
EP4	G8	YGR030C	0.00024563
EP4	G9	YGR046W	0.000244768
EP4	G10	YGR047C	0.000304784
EP4	G11	YGR048W	0.000199843
EP4	G12	YGR060W	-0.000133367
EP4	H1	YGR065C	0.000252115
EP4	H2	YGR074W	1.38181E-05
EP4	H3	YGR075C	0.000142181
EP4	H4		
EP4	H5		
EP4	H6	YGR090W	
EP4	H7		
EP4	H8		
EP4	H9	YGR095C	0.000314636
EP4	H10	YGR098C	0.00015679
EP4	H11	YGR099W	0.000156309
EP4	H12		
EP5	A1	YGR113W	
EP5	A2	YGR116W	
EP5	A3	YGR119C	
EP5	A4	YGR120C	0.00039971
EP5	A5	YGR128C	
EP5	A6	YGR140W	0.000240533
EP5	A7	YGR145W	0.000330067
EP5	A8	YGR147C	0.000396269
EP5	A9	YGR156W	0.000317651
EP5	A10	YGR158C	0.000366055
EP5	A11	YGR172C	0.000347145
EP5	A12	YGR175C	
EP5	B1	YGR179C	
EP5	B2	YGR185C	0.000283701
EP5	B3	YGR186W	0.000364214
EP5	B4	YGR191W	0.000597737
EP5	B5	YGR195W	0.000348322
EP5	B6	YGR198W	0.000587045

EP5	B7	YGR211W	0.000288329
EP5	B8	YGR216C	0.00037128
EP5	B9	YGR218W	
EP5	B10	YGR245C	0.000253319
EP5	B11	YGR246C	0.000239475
EP5	B12	YGR251W	0.000305529
EP5	C1	YGR253C	0.000391532
EP5	C2	YGR264C	0.000290103
EP5	C3	YGR267C	0.00032494
EP5	C4	GFP+	0.096337036
EP5	C5	YGR277C	0.000820929
EP5	C6	DES7	0.002182178
EP5	C7	BY4741	6.83067E-06
EP5	C8	YHL015W	0.000465064
EP5	C9	YHR005C-A	0.000338338
EP5	C10	YHR007C	0.000290301
EP5	C11	YHR019C	0.000324191
EP5	C12	YHR020W	
EP5	D1	YHR023W	0.000329343
EP5	D2	YHR024C	0.00030961
EP5	D3	YHR036W	0.000911744
EP5	D4	YHR040W	0.000321799
EP5	D5		
EP5	D6	YHR058C	0.000316643
EP5	D7	YHR062C	0.00031405
EP5	D8	YHR065C	
EP5	D9	YHR068W	
EP5	D10	YHR069C	0.000357798
EP5	D11	YHR070W	0.000267139
EP5	D12		
EP5	E1	YHR074W	
EP5	E2	p5472	0.00045704
EP5	E3		
EP5	E4	YHR088W	0.000322338
EP5	E5	YHR101C	0.000575988
EP5	E6	YHR107C	0.000310298
EP5	E7	YHR118C	0.000435167
EP5	E8	YHR122W	0.000660027
EP5	E9	YHR143W-A	
EP5	E10	YHR148W	0.000248213
EP5	E11		
EP5	E12	YHR166C	0.000233591
EP5	F1	YHR170W	0.001249124
EP5	F2	YHR172W	0.000738073
EP5	F3	YHR186C	0.000239108
EP5	F4	YHR188C	0.000343075
EP5	F5	YHR190W	0.000334336
EP5	F6	YHR196W	
EP5	F7		
EP5	F8	YIL003W	0.000347642
EP5	F9	YIL004C	0.000341
EP5	F10	YIL019W	0.000165424
EP5	F11		
EP5	F12	YIL022W	0.000377831
EP5	G1	YIL026C	0.000295025
EP5	G2	YIL031W	0.000266723
EP5	G3	YIL046W	0.000310356
EP5	G4	YIL048W	0.000341515
EP5	G5	YIL051C	0.000415464
EP5	G6	YIL061C	0.000295728
EP5	G7	YIL062C	0.00037406
EP5	G8	YIL063C	0.000308247
EP5	G9	YIL068C	0.000340189
EP5	G10	YIL075C	0.000325824
EP5	G11	YIL078W	
EP5	G12		
EP5	H1	YIL091C	0.000340293
EP5	H2	YIL104C	0.000400883
EP5	H3	YIL106W	0.000378466
EP5	H4	YIL109C	0.000401772
EP5	H5		
EP5	H6	YIL118W	0.000537211
EP5	H7	YIL126W	0.00177668
EP5	H8		
EP5	H9	YIL142W	0.000407378
EP5	H10	YIL143C	0.000398842
EP5	H11	YIL144W	0.000205244
EP5	H12	YIL147C	
EP6	A1	YIL150C	
EP6	A2	YIR006C	0.000179796
EP6	A3	YIR008C	0.000291485
EP6	A4	YIR010W	0.000383484
EP6	A5	YIR011C	0.000430888
EP6	A6	YIR012W	0.00025931
EP6	A7	p5472	0.000122832
EP6	A8	GFP+	0.075653984
EP6	A9	YJL001W	0.0003355
EP6	A10	YJL002C	0.000394065
EP6	A11	DES7	0.002015756
EP6	A12	BY4741	1.71408E-05
EP6	B1	YJL010C	0.000321105
EP6	B2	YJL011C	0.000220067
EP6	B3	YJL014W	0.000303348
EP6	B4	YJL019W	0.00027584
EP6	B5	YJL025W	0.000236207
EP6	B6	YJL026W	0.000206885
EP6	B7	YJL031C	0.000300979
EP6	B8	YJL033W	0.00015055
EP6	B9	YJL034W	0.000337003
EP6	B10	YJL035C	
EP6	B11	YJL039C	0.000309298
EP6	B12	YJL041W	0.00032813
EP6	C1	YJL050W	0.000307195
EP6	C2	YJL054W	0.000304244
EP6	C3	YJL061W	0.000394079
EP6	C4		
EP6	C5	YJL072C	0.000311565
EP6	C6	YJL074C	0.000271012
EP6	C7		
EP6	C8		
EP6	C9	YJL085W	0.000408569
EP6	C10	YJL087C	0.000265777
EP6	C11	YJL090C	0.000333159
EP6	C12	YJL091C	0.000281636
EP6	D1	YJL097W	0.000296
EP6	D2	YJL104W	0.000258
EP6	D3	YJL109C	0.000247
EP6	D4	YJL111W	0.000342
EP6	D5	YJL125C	0.000234
EP6	D6	YJL143W	0.00029
EP6	D7	YJL156C	0.000332
EP6	D8	YJL167W	0.000279
EP6	D9	YJL173C	0.00013
EP6	D10	YJL174W	0.000312
EP6	D11	YJL194W	
EP6	D12	YJL203W	0.000309
EP6	E1	YJR002W	0.000417
EP6	E2	YJR006W	0.000263
EP6	E3	YJR007W	0.000267
EP6	E4		
EP6	E5	YJR016C	0.000262
EP6	E6	YJR017C	-0.000389
EP6	E7	YJR022W	0.000376
EP6	E8	YJR041C	0.000312
EP6	E9	YJR042W	0.000276
EP6	E10	YJR045C	0.000406
EP6	E11		
EP6	E12	YJR057W	0.000272
EP6	F1	YJR064W	0.000231
EP6	F2	YJR065C	0.000354
EP6	F3	YJR067C	
EP6	F4	YJR068W	0.000335
EP6	F5	YJR072C	0.000146
EP6	F6	YJR076C	0.000463
EP6	F7	YJR093C	0.000408
EP6	F8	YJR112W	0.000376
EP6	F9	YJR123W	0.000226
EP6	F10	YJR141W	0.000411
EP6	F11	YKL004W	0.000289
EP6	F12	YKL006C-A	0.000318
EP6	G1	YKL012W	0.000333
EP6	G2	YKL013C	0.000366
EP6	G3	YKL014C	0.000313
EP6	G4	YKL018W	0.000365
EP6	G5	YKL019W	0.000231
EP6	G6	YKL021C	0.000115
EP6	G7	YKL022C	0.00032
EP6	G8	YKL024C	0.000293
EP6	G9		
EP6	G10		
EP6	G11	YKL035W	0.000361
EP6	G12	YKL042W	0.000235
EP6	H1	YKL045W	0.000338
EP6	H2	YKL049C	0.000263
EP6	H3		
EP6	H4	YKL058W	0.000385
EP6	H5	YKL059C	0.000313
EP6	H6	YKL060C	0.00026
EP6	H7		
EP6	H8	YKL082C	0.00019
EP6	H9		

EP6	H10	YKL089W	0.00033549
EP6	H11	YKL095W	0.00028794
EP6	H12	YKL099C	0.0002838
EP7	A1	YKL104C	0.000646723
EP7	A2	YKL108W	0.000368114
EP7	A3	YKL112W	0.000443685
EP7	A4	YKL122C	0.000309392
EP7	A5	YKL125W	0.000372872
EP7	A6	YKL141W	0.000420117
EP7	A7	YKL144C	0.00038346
EP7	A8	YKL145W	0.000396316
EP7	A9	YKL152C	0.000402999
EP7	A10	YKL154W	0.000217678
EP7	A11	YKL165C	0.000372813
EP7	A12	YKL172W	0.000431688
EP7	B1	YKL173W	0.000294794
EP7	B2	YKL180W	0.000312041
EP7	B3	YKL182W	0.001670733
EP7	B4	YKL186C	0.000408439
EP7	B5	YKL189W	0.000272023
EP7	B6	YKL192C	0.000366076
EP7	B7	YKL193C	0.000392653
EP7	B8	YKL195W	0.000354911
EP7	B9	YKL196C	
EP7	B10	p5472	0.000257207
EP7	B11	YKL210W	0.000482264
EP7	B12	YKR002W	0.00030804
EP7	C1	YKR004C	0.000426926
EP7	C2	YKR008W	0.000495735
EP7	C3	GFP+	0.104741891
EP7	C4	YKR025W	0.000844946
EP7	C5	YKR037C	0.000193307
EP7	C6	YKR038C	0.000463658
EP7	C7	YKR062W	0.000509438
EP7	C8	YKR063C	0.000383565
EP7	C9	YKR068C	0.000271104
EP7	C10	YKR071C	0.000332918
EP7	C11	YKR079C	0.000381829
EP7	C12	YKR081C	0.000255778
EP7	D1	YKR083C	0.000342243
EP7	D2	YKR086W	0.000418535
EP7	D3	YLL003W	0.000282955
EP7	D4	YLL004W	0.000528473
EP7	D5	YLL008W	0.000104019
EP7	D6	YLL011W	0.000296371
EP7	D7	DES7	0.002223928
EP7	D8	BY4741	8.32093E-06
EP7	D9	YLL034C	0.000406204
EP7	D10	YLL035W	0.00034133
EP7	D11	YLL036C	0.000354988
EP7	D12		
EP7	E1	YLR002C	0.000423005
EP7	E2	YLR005W	0.000369339
EP7	E3	YLR007W	0.000359857
EP7	E4	YLR008C	0.000262439
EP7	E5	YLR009W	0.000333875
EP7	E6	YLR010C	0.000452593

EP7	E7	YLR022C	0.000340202
EP7	E8	YLR026C	0.000422053
EP7	E9	YLR029C	0.000349776
EP7	E10	YLR033W	0.00044372
EP7	E11	YLR045C	0.000291809
EP7	E12	YLR051C	0.000325121
EP7	F1	YLR060W	0.000402485
EP7	F2	YLR066W	
EP7	F3		
EP7	F4	YLR075W	0.000387756
EP7	F5	YLR078C	0.000470244
EP7	F6		
EP7	F7	YLR088W	2.58094E-05
EP7	F8	YLR100W	0.000356412
EP7	F9	YLR103C	0.000387551
EP7	F10		
EP7	F11		
EP7	F12	YLR115W	0.000382806
EP7	G1	YLR116W	0.000378548
EP7	G2	YLR117C	0.000315407
EP7	G3	YLR127C	0.000262066
EP7	G4	YLR129W	0.000246075
EP7	G5	YLR132C	0.000347057
EP7	G6	YLR141W	0.000403553
EP7	G7	YLR145W	0.00028552
EP7	G8	YLR147C	0.00037415
EP7	G9	YLR153C	0.000296065
EP7	G10	YLR163C	0.000200901
EP7	G11	YLR166C	0.000379645
EP7	G12	YLR167W	0.000374417
EP7	H1	YLR175W	0.00048222
EP7	H2	YLR186W	0.000475163
EP7	H3	YLR195C	0.000329657
EP7	H4	YLR196W	0.000298819
EP7	H5	YLR197W	0.000289656
EP7	H6	YLR208W	0.000495163
EP7	H7	YLR212C	0.00021608
EP7	H8	YLR215C	0.000369158
EP7	H9	YLR222C	0.000421432
EP7	H10	YLR223C	0.000643867
EP7	H11		
EP7	H12	YLR243W	0.000360583
EP8	A1	YLR249W	0.000128293
EP8	A2	YLR259C	0.000262702
EP8	A3	YLR272C	0.000452708
EP8	A4	YLR274W	0.000308305
EP8	A5	YLR275W	0.000244973
EP8	A6	YLR276C	0.000270435
EP8	A7	YLR277C	0.000342347
EP8	A8	YLR291C	0.00016893
EP8	A9	YLR298C	0.000378057
EP8	A10	YLR305C	0.000287651
EP8	A11	p5472	0.000455933
EP8	A12	YLR314C	0.000292609
EP8	B1	YLR316C	0.000418956
EP8	B2	GFP+	0.074201108
EP8	B3	YLR323C	0.00029181

EP8	B4	YLR336C	0.00027707
EP8	B5	YLR340W	0.00031863
EP8	B6	YLR347C	0.000231595
EP8	B7	YLR355C	0.000297355
EP8	B8		
EP8	B9	YLR378C	-0.000301079
EP8	B10	YLR397C	0.000214181
EP8	B11	YLR409C	0.00034179
EP8	B12	YLR424W	0.00027708
EP8	C1	DES7	0.002490439
EP8	C2	YLR438C-A	0.000335685
EP8	C3	YLR440C	0.000301153
EP8	C4	BY4741	6.04375E-07
EP8	C5	YLR459W	0.000400461
EP8	C6		
EP8	C7	YML015C	0.000373507
EP8	C8	YML023C	0.000289418
EP8	C9	YML025C	0.000402945
EP8	C10	YML031W	0.000200454
EP8	C11		
EP8	C12	YML046W	0.000316972
EP8	D1	YML049C	0.00025476
EP8	D2		
EP8	D3	YML065W	0.000270969
EP8	D4	YML069W	0.000375243
EP8	D5	YML077W	0.000288478
EP8	D6	YML085C	0.000502884
EP8	D7		
EP8	D8		
EP8	D9	YML093W	0.000370218
EP8	D10	YML098W	0.000275517
EP8	D11	YML105C	0.000275578
EP8	D12	YML114C	0.000232872
EP8	E1	YML125C	0.00023655
EP8	E2	YML126C	0.00035748
EP8	E3	YML127W	0.000309831
EP8	E4	YML130C	0.000375193
EP8	E5		
EP8	E6		
EP8	E7		
EP8	E8		
EP8	E9		
EP8	E10		
EP8	E11		
EP8	E12	YMR049C	0.000378018
EP8	F1	YMR061W	0.000224921
EP8	F2	YMR076C	0.000333735
EP8	F3	YMR079W	0.000181716
EP8	F4	YMR093W	0.000226419
EP8	F5	YMR094W	0.000199101
EP8	F6	YMR112C	0.000129706
EP8	F7		
EP8	F8	YMR117C	0.00041802
EP8	F9	YMR128W	0.00060635
EP8	F10		
EP8	F11	YMR134W	0.000301854
EP8	F12	YMR146C	0.000331706

EP8	G1		
EP8	G2	YMR168C	0.000277322
EP8	G3	YMR185W	0.000264761
EP8	G4	YMR197C	0.000376545
EP8	G5	YMR200W	0.000327554
EP8	G6	YMR203W	0.000363228
EP8	G7	YMR208W	-8.04688E-05
EP8	G8	YMR211W	0.000325116
EP8	G9	YMR213W	0.000255776
EP8	G10	YMR218C	0.000326849
EP8	G11	YMR220W	0.000237587
EP8	G12	YMR227C	0.00012428
EP8	H1		
EP8	H2	YMR235C	0.000266974
EP8	H3	YMR236W	0.00035835
EP8	H4	YMR239C	0.000257703
EP8	H5	YMR240C	0.000232418
EP8	H6	YMR260C	0.000331769
EP8	H7	YMR268C	1.49008E-05
EP8	H8	YMR270C	0.000302249
EP8	H9	YMR277W	0.000290345
EP8	H10	YMR281W	0.000319388
EP8	H11	YMR288W	0.000246285
EP8	H12	YMR290C	0.000325437
EP9	A1	YMR296C	0.00044518
EP9	A2	YMR298W	0.000341459
EP9	A3	YMR301C	0.000329404
EP9	A4	p5472	0.000342422
EP9	A5	YMR309C	0.000358588
EP9	A6	YMR314W	0.000414097
EP9	A7	DES7	0.00292664
EP9	A8	YNL006W	0.001452646
EP9	A9	YNL007C	0.000426419
EP9	A10	YNL026W	0.000294821
EP9	A11	YNL038W	0.000314017
EP9	A12	YNL039W	0.000252466
EP9	B1	YNL061W	0.000308603
EP9	B2	YNL062C	0.000511404
EP9	B3	YNL075W	0.000388817
EP9	B4	YNL088W	0.000637306
EP9	B5	YNL102W	0.000754119
EP9	B6	YNL103W	0.000489464
EP9	B7	YNL110C	0.000501566
EP9	B8	GFP+	
EP9	B9	YNL113W	0.000519548
EP9	B10	YNL118C	0.000545901
EP9	B11	YNL124W	0.000604848
EP9	B12	YNL126W	0.000495656
EP9	C1	YNL131W	0.000438443
EP9	C2	YNL132W	0.000393599
EP9	C3	YNL137C	0.000433717
EP9	C4	YNL149C	0.00047484
EP9	C5	YNL151C	0.000592208
EP9	C6	YNL152W	0.000716349
EP9	C7	YNL158W	0.000939474
EP9	C8	YNL161W	0.00069321
EP9	C9	YNL162W	0.000551078
EP9	C10	YNL163C	0.000878
EP9	C11	YNL172W	0.000686
EP9	C12	BY4741	0
EP9	D1	YNL181W	0.000424
EP9	D2	YNL182C	0.000503
EP9	D3	YNL188W	0.000595
EP9	D4	YNL189W	0.00053
EP9	D5	YNL207W	0.000564
EP9	D6	YNL216W	
EP9	D7	YNL221C	0.000532
EP9	D8	YNL222W	0.000367
EP9	D9	YNL232W	
EP9	D10	YNL240C	0.000401
EP9	D11	YNL244C	0.000402
EP9	D12	YNL245C	0.000441
EP9	E1		
EP9	E2		
EP9	E3	YNL256W	0.00018
EP9	E4	YNL258C	0.000398
EP9	E5	YNL260C	0.00048
EP9	E6	YNL261W	0.000564
EP9	E7	YNL262W	0.00033
EP9	E8	YNL263C	0.000261
EP9	E9	YNL267W	0.000504
EP9	E10	YNL272C	0.000483
EP9	E11		
EP9	E12	YNL287W	0.000377
EP9	F1	YNL290W	0.000384
EP9	F2	YNL306W	0.000403
EP9	F3	YNL308C	0.000363
EP9	F4	YNL310C	0.000484
EP9	F5	YNL312W	0.000345
EP9	F6	YNL313C	0.000485
EP9	F7	YNL317W	0.000426
EP9	F8	YNR003C	0.000371
EP9	F9	YNR011C	0.000482
EP9	F10	YNR016C	0.000429
EP9	F11	YNR017W	0.000378
EP9	F12	YNR026C	0.000573
EP9	G1	YNR035C	0.000399
EP9	G2	YNR038W	0.000744
EP9	G3	YNR043W	0.000303
EP9	G4	YNR046W	0.00057
EP9	G5	YNR053C	0.001274
EP9	G6	YNR054C	0.000444
EP9	G7	YOL005C	0.000655
EP9	G8	YOL010W	0.000419
EP9	G9	YOL021C	0.000419
EP9	G10	YOL022C	0.000333
EP9	G11	YOL026C	0.000352
EP9	G12	YOL034W	0.000439
EP9	H1	YOL038W	0.000404
EP9	H2	YOL040C	0.000359
EP9	H3	YOL066C	0.000423
EP9	H4		
EP9	H5	YOL077C	0.000455
EP9	H6	YOL078W	0.001201
EP9	H7	YOL094C	0.000596
EP9	H8	YOL097C	0.00062
EP9	H9	YOL102C	0.000575
EP9	H10	YOL120C	0.000928
EP9	H11	YOL123W	0.00041
EP9	H12	YOL127W	0.000335
EP10	A1	p5472	0.000334
EP10	A2	YOL133W	
EP10	A3	YOL135C	0.001127
EP10	A4	YOL139C	0.000305
EP10	A5	YOL144W	0.00028
EP10	A6	YOL146W	0.000639
EP10	A7	DES7	0.003068
EP10	A8	YOR004W	0.002327
EP10	A9	YOR020C	0.000589
EP10	A10	YOR046C	0.000196
EP10	A11	YOR048C	0.000283
EP10	A12	YOR056C	0.0003
EP10	B1	YOR057W	0.000174
EP10	B2	YOR060C	0.0002
EP10	B3	YOR063W	0.000286
EP10	B4	GFP+	
EP10	B5	YOR075W	0.000612
EP10	B6	YOR077W	0.000688
EP10	B7	YOR095C	
EP10	B8	YOR098C	0.000319
EP10	B9	YOR103C	
EP10	B10	YOR110W	
EP10	B11	YOR116C	0.000263
EP10	B12	YOR117W	0.000272
EP10	C1	YOR119C	0.000397
EP10	C2	YOR122C	0.000352
EP10	C3	YOR143C	0.000402
EP10	C4	YOR145C	0.000307
EP10	C5	YOR148C	0.000267
EP10	C6	YOR149C	0.000564
EP10	C7	YOR151C	0.000226
EP10	C8	YOR157C	0.000291
EP10	C9	YOR159C	0.000768
EP10	C10	YOR160W	0.000237
EP10	C11	YOR168W	
EP10	C12	YOR174W	0.000366
EP10	D1	YOR176W	0.000384
EP10	D2	BY4741	0
EP10	D3	YOR194C	0.00039
EP10	D4	YOR204W	0.000436
EP10	D5	YOR206W	0.002801
EP10	D6		
EP10	D7	YOR210W	
EP10	D8	YOR217W	0.000276
EP10	D9	YOR224C	0.00027
EP10	D10	YOR232W	0.000646
EP10	D11	YOR236W	0.000333
EP10	D12	YOR244W	0.000749
EP10	E1	YOR249C	0.000233
EP10	E2	YOR250C	0.000231
EP10	E3		

EP10	E4		
EP10	E5		
EP10	E6	YOR259C	0.000277
EP10	E7	YOR260W	0.000253
EP10	E8	YOR261C	0.00034
EP10	E9	YOR262W	0.000303
EP10	E10	YOR272W	0.000464
EP10	E11	YOR278W	
EP10	E12	YOR281C	0.000904
EP10	F1		
EP10	F2	YOR294W	
EP10	F3	YOR310C	0.000378
EP10	F4	YOR319W	0.004356
EP10	F5	YOR326W	0.003574
EP10	F6	YOR329C	0.000226
EP10	F7	YOR335C	0.000396
EP10	F8	YOR336W	0.000215
EP10	F9	YOR340C	0.000266
EP10	F10	YOR341W	0.000198
EP10	F11	YOR353C	0.002539
EP10	F12	YOR361C	
EP10	G1	YOR362C	0.000281
EP10	G2	YOR370C	0.000208
EP10	G3		
EP10	G4		
EP10	G5	YPL007C	
EP10	G6	YPL010W	0.000296
EP10	G7	YPL011C	
EP10	G8	YPL012W	0.000201
EP10	G9		
EP10	G10	YPL020C	0.000175
EP10	G11	YPL028W	0.000216
EP10	G12	YPL043W	0.000247
EP10	H1		
EP10	H2	YPL075W	0.000234
EP10	H3	YPL076W	0.000335
EP10	H4		
EP10	H5	YPL083C	
EP10	H6	YPL085W	
EP10	H7		
EP10	H8		
EP10	H9	YPL117C	0.000282
EP10	H10	YPL122C	0.001101
EP10	H11	YPL124W	
EP10	H12	YPL126W	
EP11	A1	YPL128C	0.000302
EP11	A2	p5472	0.00039
EP11	A3	YPL143W	0.000303
EP11	A4	YPL146C	0.000513
EP11	A5	YPL151C	0.000364
EP11	A6	YPL153C	0.000215
EP11	A7	YPL160W	0.000369
EP11	A8	YPL169C	0.000359
EP11	A9	YPL175W	0.00047
EP11	A10	DES7	0.002664
EP11	A11	YPL204W	0.000401
EP11	A12	YPL209C	0.000322

EP11	B1	YPL210C	0.000481
EP11	B2	YPL211W	0.000375
EP11	B3	YPL217C	0.000474
EP11	B4	YPL218W	0.000572
EP11	B5	YPL228W	0.000653
EP11	B6	YPL231W	0.000793
EP11	B7	YPL233W	0.00043
EP11	B8	YPL235W	0.000248
EP11	B9	YPL237W	0.000447
EP11	B10	YPL242C	0.000351
EP11	B11	YPL243W	0.000476
EP11	B12	YPL252C	0.0004
EP11	C1	YPL255W	0.000253
EP11	C2	YPL266W	0.000387
EP11	C3	YPR010C	0.000317
EP11	C4	YPR016C	0.00049
EP11	C5	YPR019W	0.000467
EP11	C6	YPR025C	0.000801
EP11	C7	YPR033C	0.000862
EP11	C8	YPR034W	0.000577
EP11	C9	YPR035W	0.000521
EP11	C10	YPR041W	0.000442
EP11	C11	YPR048W	0.000525
EP11	C12	YPR055W	0.000751
EP11	D1	YPR056W	0.000506
EP11	D2	GFP+	
EP11	D3	YPR085C	0.000529
EP11	D4	YPR086W	0.000358
EP11	D5	YPR088C	0.000249
EP11	D6		
EP11	D7	YPR103W	0.00079
EP11	D8	YPR104C	0.000271
EP11	D9	YPR105C	0.000633
EP11	D10	YPR107C	0.000259
EP11	D11	YPR108W	0.000343
EP11	D12	YPR110C	0.000271
EP11	E1		
EP11	E2	YPR113W	0.000613
EP11	E3	YPR133C	0.000355
EP11	E4	YPR137W	0.000299
EP11	E5	YPR143W	0.00034
EP11	E6	YPR144C	0.000369
EP11	E7	BY4741	0
EP11	E8	YPR162C	0.001541
EP11	E9	YPR165W	0.000423
EP11	E10	YPR168W	0.000322
EP11	E11	YPR169W	0.000346
EP11	E12	YPR175W	0.000655
EP11	F1	YPR176C	0.000438
EP11	F2	YPR178W	0.000327
EP11	F3	YPR180W	0.000492
EP11	F4	YPR181C	0.000391
EP11	F5	YPR182W	0.000325
EP11	F6	YPR183W	0.000251
EP11	F7	YPR186C	0.00032
EP11	F8	YPR187W	0.000611
EP11	F9	YPR190C	0.00026

EP11	F10		
EP11	F11	YER029C	0.000378
EP11	F12	YER074W-A	0.000471
EP11	G1	YHR072W-A	0.000371
EP11	G2	YHR089C	0.00036
EP11	G3	YHR102W	0.000431
EP11	G4	YHR128W	0.000444
EP11	G5	YHR169W	0.000414
EP11	G6	YHR199C-A	0.000508
EP11	G7	YLR099W-A	0.000496
EP11	G8	YLR383W	0.000308
EP11	G9	YNL024C-A	0.000456
EP11	G10	YNL036W	0.000397
EP11	G11	YNL138W-A	0.000393
EP11	G12	YOL142W	0.00034
EP11	H1		
EP11	H2		
EP11	H3		
EP11	H4		
EP11	H5		
EP11	H6		
EP11	H7		
EP11	H8		
EP11	H9		
EP11	H10		
EP11	H11		
EP11	H12		
EP12	A1	YAR019C	0.000194
EP12	A2	p5472	0.000522
EP12	A3	DES7	0.00479
EP12	A4	GFP+	
EP12	A5	YER093C	0.001147
EP12	A6	YHR085W	0.000481
EP12	A7	YHR197W	0.000264
EP12	A8	YIL115C	0.001065
EP12	A9	YJL005W	0.000442
EP12	A10	YJL069C	0.000695
EP12	A11	YJL081C	0.000301
EP12	A12	YJR046W	0.000244
EP12	B1	BY4741	0
EP12	B2	YLR086W	0.00016
EP12	B3	YLR229C	0.000461
EP12	B4	YLR321C	0.000631
EP12	B5		
EP12	B6		
EP12	B7	YML064C	0.000287
EP12	B8	YOR373W	0.00024
EP12	B9	YPL016W	0.000274
EP12	B10		
EP12	B11		
EP12	B12		
EP12	C1		
EP12	C2	YBR080C	0.00035
EP12	C3	YBR110W	0.000253
EP12	C4		
EP12	C5	YDL102W	0.000622
EP12	C6		

EP12	C7	YDL166C	0.000584
EP12	C8	YDR050C	
EP12	C9	YDR145W	0.000336
EP12	C10		
EP12	C11	YDR211W	
EP12	C12	YDR212W	0.000394
EP12	D1		
EP12	D2		
EP12	D3		
EP12	D4	YER125W	0.000246
EP12	D5	YGL092W	0.000229
EP12	D6	YGL093W	
EP12	D7	YGL112C	0.000276
EP12	D8		
EP12	D9	YGL238W	
EP12	D10		
EP12	D11	YGR278W	
EP12	D12	YGR280C	0.001277
EP12	E1	YHR042W	0.000239
EP12	E2		
EP12	E3	YHR083W	0.000424
EP12	E4		
EP12	E5	YIL083C	0.000262
EP12	E6		
EP12	E7	YIR015W	0.000974
EP12	E8	YIR022W	0.000251
EP12	E9		
EP12	E10		
EP12	E11	YJL076W	0.001033
EP12	E12	YJR013W	0.000261
EP12	F1	YKL028W	0.000734
EP12	F2	YKL033W	0.00026
EP12	F3	YKL052C	0.000329
EP12	F4	YKL078W	0.000639
EP12	F5	YKL088W	0.000493
EP12	F6	YKR022C	0.000407
EP12	F7	YLL018C	0.000553
EP12	F8	YLL031C	0.000205
EP12	F9	YLR071C	0.00172
EP12	F10	YLR105C	0.000426
EP12	F11		
EP12	F12	YLR310C	0.000265
EP12	G1	YLR359W	0.000138
EP12	G2	YLR457C	0.000316
EP12	G3	YMR047C	0.000473
EP12	G4		
EP12	G5	YMR229C	0.000294
EP12	G6	YMR308C	0.000223
EP12	G7	YNL002C	0.000628
EP12	G8		
EP12	G9	YNL178W	0.000976
EP12	G10		
EP12	G11	YNL251C	0.001598
EP12	G12	YNL282W	0.000269
EP12	H1	YOL069W	0.000287
EP12	H2	YOR074C	0.000652
EP12	H3		
EP12	H4		
EP12	H5		
EP12	H6		
EP12	H7		
EP12	H8		
EP12	H9		
EP12	H10	YPR094W	0.000498
EP12	H11	YPR161C	0.000439
EP12	H12		
EP13	A1	YAL003W	0.000414
EP13	A2	YAL025C	0.00041
EP13	A3	YAL032C	0.000445
EP13	A4	YAL033W	0.000436
EP13	A5	YAL034W-A	0.000218
EP13	A6	YAL038W	0.000646
EP13	A7	YAL041W	0.000517
EP13	A8	GFP+	0.099094
EP13	A9	YAR007C	0.000919
EP13	A10	YAR008W	0.000554
EP13	A11	p5472	0.000513
EP13	A12	YML015C	0.000477
EP13	B1	DES7	0.002099
EP13	B2	YML043C	0.000833
EP13	B3	BY4741	0
EP13	B4		
EP13	B5	YMR001C	0.000618
EP13	B6	YMR005W	0.000368
EP13	B7	YMR013C	0.000355
EP13	B8	YMR028W	0.000757
EP13	B9	YMR033W	0.000525
EP13	B10	YMR043W	0.000496
EP13	B11		
EP13	B12		
EP13	C1	YCL031C	
EP13	C2	YDR224C	0.000548
EP13	C3	YGL044C	0.000599
EP13	C4	YGL145W	0.000599
EP13	C5		
EP13	C6	YHR088W	0.000538
EP13	C7	YHR188C	0.000561
EP13	C8		
EP13	C9		
EP13	C10		
EP13	C11		
EP13	C12	YKL049C	0.000692
EP13	D1	YKL172W	0.000623
EP13	D2	YLR316C	0.000443
EP13	D3		
EP13	D4	YNL112W	0.000566

Appendix B.2 Validation of the top hits with altered rDNA instability

Validation plate key

BY4741	Control strains WT, no GFP tag
GFP+	*MFA1-3xGFP*
DES7	*RDN25-MAT* α
p5472	*RDN25-MAT* α + p5472
DES7 *top1Δ*	*RDN25-MAT α top1Δ*
	ORF present in MoBY database, but not in our plasmid preps (no band on e-gel).
	"Low instability"; rDNA repeat loss rates < 0.00017
	"High instability"; rDNA repeat loss rates > 0.001

ddPCR QC key

<10,000 droplets

Too few negative droplets

<10copies/ uL TUB1

Plate	Well	Sample Name	rDNA repeat loss rate		Copy number	
			Prep 1	Prep 2	rDNA	*LEU2*
High Hit 1	A1	p5472	0.000547	0.0004688	142.29508	#VALUE!
High Hit 1	A2	GFP+	0.1090322	0.1329912	170.33639	1.0113636
High Hit 1	A3	DES7	0.0137721	0.0105878	187.5	2.511811
High Hit 1	A4	YPL066W	0.001099	0.0008964	139.60784	2.1639344
High Hit 1	A5	YPR132W	0.0007042	0.0013219	138.52814	#VALUE!
High Hit 1	A6	YGR071C	0.0006775	0.0006155	126.47059	2.3395445
High Hit 1	A7	YBR123C	0.0015557	0.0047095	93.956044	#VALUE!
High Hit 1	A8	YBL054W	0.0004716	0.0005776	142.52033	2.3836066
High Hit 1	A9	YAR002W	0.0020671	0.0021987	101.07143	2.5304878
High Hit 1	A10	YER161C	0.0004356	0.0004442	156.14173	2.0695364
High Hit 1	A11	YDR506C	0.0006642	0.0007815	127.22772	2.14
High Hit 1	A12	YDR163W	0.000432	0.0003534	144.09091	2.4641148
High Hit 1	B1	YOR319W	0.0049032	0.0033468	#VALUE!	2.3474178
High Hit 1	B2	YPR162C	0.001097	0.0006029	134.90305	2.1017403
High Hit 1	B3	YGR261C	0.0017957	0.0007968	130.16304	2.1195652
High Hit 1	B4	YPL038W	0.0023658	0.0017192	147.21088	2.0273349
High Hit 1	B5	YJR060W	0.0006014	0.0005931	148.01802	2.1693291
High Hit 1	B6	YGR118W	0.0006191	0.0006667	134.57447	2.2453222
High Hit 1	B7	YAL001C	0.0033749	0.004112	120.56738	2.1533742
High Hit 1	B8	YBL079W	0.0004732	0.0006989	133.65854	2.0921305
High Hit 1	B9	YER113C	0.0008996	0.0010178	132.17647	2.2402089
High Hit 1	B10	YER179W	0.0006259	0.0007056	144.05941	2.2355289
High Hit 1	B11	YDR500C	0.0004914	0.0007549	124.90566	2.2467772
High Hit 1	B12	YDR195W	0.0002922	0.00056	131.04712	2.3753501
High Hit 1	C1	YOR206W	0.0008275	0.0017082	122	2.1410256
High Hit 1	C2	YLR071C	0.0005547	0.0009433	121.12299	2.0744681
High Hit 1	C3	YLR449W	0.0026448	0.0023242	123	2.1969697
High Hit 1	C4	YPL110C	0.0005935	0.0007647	123.21429	2.1588595
High Hit 1	C5	YJR050W	0.000859	0.0009402	128.29268	2.1256039
High Hit 1	C6	YGR078C	0.0006558	0.0008563	120.57613	2.4413146
High Hit 1	C7	YML111W	0.0009703	0.0016378	117.19298	2.3065903
High Hit 1	C8	YBL006C	0.0002963	0.0006554	126.13065	2.0121065

High Hit 1	C9	YMR072W	0.0005231	0.0007044	124.60674	2.3134328
High Hit 1	C10	YMR053C	0.0005552	0.0007008	137.65432	2.0078329
High Hit 1	C11	YBR024W	0.00038	0.0004424	130	2.4252874
High Hit 1	C12	YGL043W	0.0003322	0.0005029	148.80383	2.1485944
High Hit 1	D1	YOR004W	0.000937	0.0013399	120.06369	2
High Hit 1	D2	YNL251C	0.0018616	0.0013656	149.06542	2.2787611
High Hit 1	D3	YML021C	0.001983	0.0014847	130.96927	2.2159091
High Hit 1	D4	YPL103C	0.0007465	0.0006953	142.4812	1.967655
High Hit 1	D5	YJR055W	0.0008006	0.0007157	121.40625	2.2689076
High Hit 1	D6	YJL060W	0.0009595	0.0008658	92.916667	2.201005
High Hit 1	D7	YKL005C	0.0008793	0.0008444	145.21277	2.5
High Hit 1	D8	YBL046W	0.0009456	0.0009694	137.12644	2.0153846
High Hit 1	D9	YMR069W	0.0005758	0.0006185	143.07018	2.1019608
High Hit 1	D10	YCR092C	0.000615	0.0005561	138.42365	2.1731844
High Hit 1	D11	YBR037C	0.0005377	0.000825	140.35088	2
High Hit 1	D12	YGL135W	0.0003531	0.0003037	141.17647	2.4703947
High Hit 1	E1	YOL135C	0.0005409	0.0006722	138.69347	2.2601279
High Hit 1	E2	YGR280C	0.0011525	0.000729	131.25	2.1238938
High Hit 1	E3	YLR452C	0.0018826	0.0011233	117.85714	2.7892562
High Hit 1	E4	YPL026C	0.0004408	0.000503	120.4	2.4525547
High Hit 1	E5	YCR088W	0.0005547	0.000811	134.43396	2.3876221
High Hit 1	E6	YJL127C	0.0011655	0.0006504	136.70886	2.2393822
High Hit 1	E7	YBL052C	0.0024332	0.0032769	110.72289	2.1
High Hit 1	E8	YAL021C	0.0005907	0.0008054	125.33333	2.0934844
High Hit 1	E9	YMR075W	0.0007066	0.0006404	154.08537	2.3452381
High Hit 1	E10	YMR322C	0.0003669	-0.00181	146.07843	2.1868787
High Hit 1	E11	YGR247W	0.0005819	0.0007088	144.72727	2.071535
High Hit 1	E12	YDL201W	0.0003713	0.0004032	155.85034	2.2222222
High Hit 1	F1	YPL122C	0.0007007	0.000844	127.41935	2.1202003
High Hit 1	F2	YPL193W	0.0011858	0.0014975	143.77483	2.1707989
High Hit 1	F3	YPL079W	0.0016166	0.003611	117.90393	2.2641509
High Hit 1	F4	YJR043C	0.0009423	0.001909	125.56338	2.25387
High Hit 1	F5	YNL073W	0.0006623	0.0005886	147.30435	2.2203857
High Hit 1	F6	YGR056W	0.0005152	0.00064	75	2.3527273
High Hit 1	F7	YBL001C	0.0032679	0.002888	130.38961	2.1074766
High Hit 1	F8	YAL034C	0.0006091	0.0004244	152.14724	2.1729958
High Hit 1	F9	YAL013W	0.0010369	0.0006954	128.9899	2.2583732
High Hit 1	F10	YBR025C	0.001341	0.0006445	144.90066	2.2762148
High Hit 1	F11	YDR171W	0.0007737	0.0006936	160.44776	2.0588235
High Hit 1	F12	YDL237W	0.0003901	0.0004181	160.91371	2.0786802
High Hit 1	G1	YOR027W	0.0015285	0.0009021	158.44156	2.412523
High Hit 1	G2	YPL254W	0.0020121	0.0008898	131.2253	2.0819672
High Hit 1	G3	YPL121C	0.0022707	0.0014972	141.9214	2.528363
High Hit 1	G4	YPR135W	0.0015212	0.0015476	115.50898	2.3556851
High Hit 1	G5	YNL072W	0.0012126	0.0006304	124.77987	2.1098901
High Hit 1	G6	YBR152W	0.0015703	0.0028183	98.874459	2.3992995
High Hit 1	G7	YBL056W	0.0009579	0.0006877	141.03896	2.1129032

High Hit 1	G8	YAL029C	0.0006277	0.0004623	154.13043	2.1026895
High Hit 1	G9	YER107C	0.0008352	0.0006604	153.37079	2.4378109
High Hit 1	G10	YGR252W	0.0010137	0.0007865	148.03922	2.0618557
High Hit 1	G11	YGL049C	0.0006407	0.0004478	153.52113	2.3020258
High Hit 1	G12	YGR023W	0.0006719	0.0004558	147.22222	2.2037037
High Hit 1	H1	p5472	0.0005185	0.0003893	151.81818	2.3044397
High Hit 1	H2	BY4741	3.253E-05	1.998E-06	158.23529	#VALUE!
High Hit 1	H3	DES7 top1Δ	0.0065101	0.0018248	141.70732	2.3452381
High Hit 1	H4	YJR025C	0.0020148	0.0010481	140.65934	2.0563847
High Hit 1	H5	YFR013W	0.0008491	0.0010589	132.03463	2.2012579
High Hit 1	H6	YBL074C	0.0030411	0.0020727	106.25	1.954023
High Hit 1	H7	YBL024W	0.0009508	0.0005617	139.1453	#VALUE!
High Hit 1	H8	YBL019W	0.0003321	0.0006225	140.89286	2.07
High Hit 1	H9	YER141W	0.0019842	0.0019201	#VALUE!	0.3703704
High Hit 1	H10	YOR274W	0.0006623	0.0007573	131.57895	2.1681416
High Hit 1	H11	YDR181C	0.0005336	0.0004499	145.16129	2.3703704
High Hit 1	H12	YDR168W	0.0042249	0.0024876	149.2891	2.2007722
High Hit 2	A1	p5472	0.0010044	0.0006013	118.95833	2.4072948
High Hit 2	A2	GFP+	0.1385312	0.1496674	99.866667	0.9302326
High Hit 2	A3	DES7	0.0021275	0.0028693	128.64865	2.3422619
High Hit 2	A4	YDR052C	0.0005556	0.0004735	117.67123	2.1935484
High Hit 2	A5	YLR344W	0.0012086	0.0010992	#VALUE!	2.3590909
High Hit 2	A6	YNL185C	0.0002282	0.0041506	83.112245	2.4346734
High Hit 2	A7	YCR036W	0.0004909	0.0006197	106.82731	2.1440536
High Hit 2	A8	YJL170C	0.0003762	0.0007382	127.91667	2.0363985
High Hit 2	A9	YKR095W	0.0004126	0.0010723	124.69388	2.2032258
High Hit 2	A10	YDR174W	0.0012107	0.0006365	123.63636	2.1985816
High Hit 2	A11	YJR052W	0.000478	0.0004486	138.50932	2.1408451
High Hit 2	A12	YOR233W	0.001591	0.0011184	134.38596	2.1126761
High Hit 2	B1	YGR098C	0.0005245	0.000265	128.63636	2.1989664
High Hit 2	B2	YJR072C	0.0007615	0.0004801	99.027778	2.313253
High Hit 2	B3	YMR227C	0.0005704	0.0004138	123.04348	2.163522
High Hit 2	B4	YDR305C	0.0005706	0.0006479	100.66667	2.5800712
High Hit 2	B5	YLR085C	0.0004403	0.0010493	83.898305	2.058011
High Hit 2	B6	YNL021W	0.0014107	0.0012866	78.622047	3.067591
High Hit 2	B7	YDR030C	0.0005396	0.0006318	129.06667	2.3308271
High Hit 2	B8	YGL025C	0.0005157	0.000529	112.6506	2.5085714
High Hit 2	B9	YDR390C	0.0008036	0.0007712	110.25641	2.2047619
High Hit 2	B10	YBR295W	0.000604	0.0006451	140.9375	2.4023256
High Hit 2	B11	YML070W	0.0002361	0.0004844	115.88785	2.2048364
High Hit 2	B12	YHR203C	0.0008007	0.0010391	139.40887	2.1369863
High Hit 2	C1	YDR386W	0.000657	0.0008798	129.85075	2.1538462
High Hit 2	C2	YJL033W	0.0002741	0.0003905	107.06186	2.0906977
High Hit 2	C3	YLR249W	0.0004559	0.0011646	90.637255	2.096475
High Hit 2	C4	YDR317W	0.0008866	0.000627	85.68	2.187234
High Hit 2	C5	YMR297W	0.0039324	0.0060403	60.569395	2.1904762
High Hit 2	C6	YOR198C	0.0021096	0.0014501	81.158798	2.2017937

High Hit 2	C7	YLL018C-A	0.0008073	0.0006499	97.586207	2.3
High Hit 2	C8	YNL286W	0.0003832	0.0007362	109.42623	2.5762712
High Hit 2	C9	YDR292C	0.0006184	0.001185	89.5	2.2435897
High Hit 2	C10	YAL012W	0.0005453	0.0008338	101.88172	2.2190612
High Hit 2	C11	YDL160C-A	0.0003303	0.0007096	98.473282	2.1578947
High Hit 2	C12	YIL126W	0.0027204	0.0052605	78.789238	2.5962963
High Hit 2	D1	YIL019W	0.0003362	0.0007218	110.89494	2.3214286
High Hit 2	D2	YFR009W	0.0004919	0.000561	95.153846	2.3339658
High Hit 2	D3	YMR112C	0.0005194	0.0005842	103.68932	2.4831933
High Hit 2	D4	YDR310C	0.0006087	0.0006956	85.555556	2.3879518
High Hit 2	D5	YNL280C	0.0030464	0.0039683	86.410256	1.9903846
High Hit 2	D6	YML017W	0.0020299	0.0013788	77.172996	2.053719
High Hit 2	D7	YML057W	0.000576	0.0005493	94.87395	2.1775
High Hit 2	D8	YGR200C	0.0007566	0.0006857	105.60976	2.2444444
High Hit 2	D9	YDR324C	0.0005531	0.000683	103.5443	2.2270742
High Hit 2	D10	YBR189W	0.0005725	0.0008368	116.21359	2.0253165
High Hit 2	D11	YOR312C	0.0028521	0.0068505	90.609756	2.6171875
High Hit 2	D12	YHR170W	0.0004812	0.0015127	108.33333	3.2277778
High Hit 2	E1	YJR017C	0.0001812	0.0005229	112.03008	2.7140784
High Hit 2	E2	YLL008W	0.0002394	0.0005903	107.52336	2.1888112
High Hit 2	E3	YDR224C	0.0004433	0.0005707	97.586207	2.4672131
High Hit 2	E4	YER027C	0.0007593	0.0007316	88.527607	2.3762058
High Hit 2	E5	YMR275C	0.0033214	0.0032406	94.795918	2.2102564
High Hit 2	E6	YNR034W	0.0007803	0.0013343	105.80838	2.3705882
High Hit 2	E7	YCR031C	0.0002766	0.0003294	117.109	2.2631579
High Hit 2	E8	YKL137W	0.0006805	0.0007017	97.925311	2.3761682
High Hit 2	E9	YCR059C	0.0012246	0.0017231	106.2069	2.2395833
High Hit 2	E10	YKR101W	0.0009286	0.000664	110.68249	2.1639344
High Hit 2	E11	YNL004W	0.001182	0.0027402	79.680511	2.3493976
High Hit 2	E12	YIL139C	0.0005754	0.0007326	116.78322	2.3180077
High Hit 2	F1	YKL021C	0.0003656	0.0006914	128.92157	2.2397094
High Hit 2	F2	YMR208W	0.0007792	0.0009805	127.84	2.3208333
High Hit 2	F3	YDL031W	0.0005556	0.0006441	99.183673	2.321519
High Hit 2	F4	YDR289C	0.0004789	0.0005997	115.9434	2.1238095
High Hit 2	F5	YNL335W	0.0008608	0.0017326	94.07767	2.4971098
High Hit 2	F6	YOR213C	0.0004201	0.0010567	87.194245	2.3539095
High Hit 2	F7	YDR283C	0.000438	0.0005185	94.590164	2.3496144
High Hit 2	F8	YKL114C	0.000478	0.000466	120.50725	2.5235849
High Hit 2	F9	YDR349C	0.0005719	0.0011864	115.41667	2.2083333
High Hit 2	F10	YOR386W	0.0006192	0.0004669	111.24424	2.2237762
High Hit 2	F11	YPL037C	0.0017661	0.0017148	90.877193	2.2200393
High Hit 2	F12	YKL109W	0.0004719	0.0010111	122.22222	2.0375587
High Hit 2	G1	YJL173C	0.0007291	0.000694	106.09375	2.3486239
High Hit 2	G2	YMR268C	0.0017647	0.0009257	120.12579	2.3548387
High Hit 2	G3	YDR082W	0.0007635	0.0005265	127.55906	2.463035
High Hit 2	G4	YLL046C	0.0009814	0.0016336	94.278351	2.6744868
High Hit 2	G5	YNL259C	0.0017125	0.0021408	161.78571	2.5086705

High Hit 2	G6	YLR431C	0.0012614	0.0014876	91.713147	2.2567288
High Hit 2	G7	YGR141W	0.0014402	0.0012486	98.793103	2.1698113
High Hit 2	G8	YLL002W	0.0004704	0.0005947	104.1958	2.1652174
High Hit 2	G9	YDR370C	0.0008089	0.0009942	112.9717	2.3255269
High Hit 2	G10	YJR104C	0.0004404	0.0006512	115.67944	2.0655738
High Hit 2	G11	YER049W	0.0013959	0.0020622	110.86957	2.2030238
High Hit 2	G12	YNR053C	0.0009413	0.0005908	125.95745	2.0792079
High Hit 2	H1	p5472	0.0007057	0.0004603	121.62651	2.2178478
High Hit 2	H2	BY4741	1.853E-05	0	163.52564	#VALUE!
High Hit 2	H3	DES7 top1Δ	0.0023713	0.0033369	143.58108	2.5446686
High Hit 2	H4	YGR208W	0.0009527	0.0006385	113.3125	2.4210526
High Hit 2	H5	YMR273C	0.0006196	0.0018814	101.8543	2.2683706
High Hit 2	H6	YER019W	0.000716	0.0006219	116.38655	2.4159292
High Hit 2	H7	YKR060W	0.0007907	0.0005644	118.44444	2.3183391
High Hit 2	H8	YLR425W	0.0051665	0.0046688	114.8125	2.4171429
High Hit 2	H9	YML068W	0.0006032	0.0008893	143.11927	2.1956088
High Hit 2	H10	YJR145C	0.0002012	0.0004643	124.03101	2.1825397
High Hit 2	H11	YOR368W	0.0009166	0.0009966	116.46707	2.2815534
High Hit 2	H12	YOL078W	0.0006026	0.0008485	139.15254	2.4615385
Low Hit	A1	p5472	0.0005448	0.000464	112.01299	1.101983
Low Hit	A2	GFP+	-0.002922	0.1372882	#VALUE!	0.9357664
Low Hit	A3	DES7	0.0235596	0.0087344	101.65138	2.3976945
Low Hit	A4	YOR243C	0.0002038	0.0004933	102.35808	#VALUE!
Low Hit	A5	YLR240W	9.081E-05	0.0005759	103.57143	2.195122
Low Hit	A6	YJL138C	4.689E-05	0.0006111	90.816327	1.9318182
Low Hit	A7	YJL168C	6.272E-05	0.000547	179.61538	2.2987805
Low Hit	A8	YLR327C	1.604E-05	0.0004562	130.54348	1.8957746
Low Hit	A9	YBR163W	5.506E-05	0.0004333	95.920398	2.5786164
Low Hit	A10	YOR187W	9.734E-05	0.0002398	146.45669	2.0802377
Low Hit	A11	YGR005C	5.864E-05	0.0004414	112.66968	2.1471173
Low Hit	A12	YFL005W	4.804E-05	0.0004614	121.10526	2.1811927
Low Hit	B1	YLR359W	0.0001725	0.0003323	112.22707	1.9852941
Low Hit	B2	YDL143W	0.0001999	0.0001414	123.74429	2.5934579
Low Hit	B3	YNL064C	0.001562	0.0004811	125.33937	2.4873096
Low Hit	B4	YMR167W	0.0004669	0.0005492	85.493827	2.0367279
Low Hit	B5	YKL184W	5.661E-05	0.0005476	100.59113	1.9464789
Low Hit	B6	YGL086W	0.0001395	0.0004853	83.632653	#VALUE!
Low Hit	B7	YKR026C	2.906E-05	0.0004888	88.181818	2.2292994
Low Hit	B8	YBR101C	-3.01E-05	0.0004802	90.837696	2.0223464
Low Hit	B9	YDR375C	0.0001471	0.000355	139.9359	2.1059783
Low Hit	B10	YEL061C	0.0001971	0.0002992	109.38272	2.2987805
Low Hit	B11	YFR005C	0.000177	0.0004515	109.01786	2.302439
Low Hit	B12	YER172C	6.89E-05	0.0004596	116.74074	2.2927757
Low Hit	C1	YLR086W	6.315E-05	0.0001726	119.92366	2.5106383
Low Hit	C2	YDL126C	0.0001679	0.0003219	132.14815	2.3178295
Low Hit	C3	YJL147C	0.0001314	0.0008272	107.89116	2.1215686
Low Hit	C4	YKL185W	9.763E-05	0.0005284	113.40206	2.2670455

Low Hit	C5	YOR241W	8.072E-05	0.0005952	100.66225	2.0038911
Low Hit	C6	YLR318W	1.576E-05	0.0005492	105.82822	2.0327869
Low Hit	C7	YKL197C	1.531E-05	0.0006358	91.052632	2.3521127
Low Hit	C8	YDR173C	-0.000168	0.000575	113.46847	2.234192
Low Hit	C9	YNL307C	0.0001481	0.0005396	96.470588	2.1631206
Low Hit	C10	YGR013W	-0.000854	0.0031753	100.38314	2.1892393
Low Hit	C11	YFL002C	0.0001233	0.0007909	120.42553	2.2634508
Low Hit	C12	YGR075C	0.0001707	0.0004332	154.84848	2.092233
Low Hit	D1	YER005W	0.0001321	0.0004153	105.80247	2.6532258
Low Hit	D2	YNL176C	0.0001768	0.0003398	106.63594	#VALUE!
Low Hit	D3	YGL094C	1.542E-05	0.0004045	96.491228	2.392638
Low Hit	D4	YLR143W	5.812E-05	0.0005103	94.127907	1.9578947
Low Hit	D5	YKL205W	0.0001574	0.0004377	112.44898	2.4080717
Low Hit	D6	YHR154W	5.684E-05	0.0005807	97.575758	2.1444201
Low Hit	D7	YLR219W	0.0001394	0.0004272	94.785276	2.2201835
Low Hit	D8	YDR092W	0.0001286	0.000445	113.46591	2.1295547
Low Hit	D9	YLR385C	5.831E-05	0.0004357	104.29043	2.1850394
Low Hit	D10	YGL123W	-0.000175	0.0013094	110.97436	2.2159624
Low Hit	D11	YGL172W	0.0001052	0.0004061	104.22222	2.1604938
Low Hit	D12	YGL247W	5.538E-05	0.0004804	119.52381	2.1073986
Low Hit	E1	YBR143C	4.445E-05	0.0004174	131.96581	2.1841004
Low Hit	E2	YOR230W	0.0001025	0.0003667	114.09524	2.1004566
Low Hit	E3	YJL197W	5.69E-05	0.0005372	104.73282	2.3691589
Low Hit	E4	YLR367W	0.0001752	0.0004702	101.57303	2.3180593
Low Hit	E5	YKR056W	0.000139	0.0005432	98.618785	2.432
Low Hit	E6	YLR176C	0.0001101	0.000526	118.79433	2.3693694
Low Hit	E7	YGR061C	0.0002113	0.0003373	93.4375	2.5205479
Low Hit	E8	YDL025C	9.65E-05	0.000516	109.6	2.0249221
Low Hit	E9	YNL067W	0.0001317	0.0003402	112.91667	2.2403259
Low Hit	E10	YFL037W	6.388E-05	2.931E-05	96.866841	1.6359164
Low Hit	E11	YGL048C	0.0001412	0.0005139	125.92593	2.2125436
Low Hit	E12	YFR028C	0.0002061	0.0007528	114.13428	2.124183
Low Hit	F1	YCR035C	5.923E-05	0.0001209	68.841463	5.2380952
Low Hit	F2	YHR005C	0.0001114	0.0004296	149.40476	2.4013158
Low Hit	F3	YJL186W	4.689E-05	0.0007045	124.69565	2.3091787
Low Hit	F4	YLR135W	7.676E-05	0.0005092	122.88136	2.1576577
Low Hit	F5	YMR190C	9.953E-05	0.0004891	119.83051	2.5838509
Low Hit	F6	YNL236W	0.0001074	0.0004674	109.17355	2.2419355
Low Hit	F7	YNL001W	0.000134	0.0006237	108.08333	2.2200957
Low Hit	F8	YDR315C	0.000166	0.0003475	109.96016	2.2263451
Low Hit	F9	YGR085C	0.0001324	0.0003861	137.95455	2.451087
Low Hit	F10	YFR027W	0	0.0004783	107.16846	2.0386643
Low Hit	F11	YFL029C	0.0001415	0.0004929	127.125	2.1967742
Low Hit	F12	YFL024C	0.0001307	0.0002833	142.4581	2.2318059
Low Hit	G1	YDR177W	0.0001053	0.0002601	119.4898	2.32
Low Hit	G2	YJL080C	0.0001063	0.0003676	111.90789	2.0825688
Low Hit	G3	YGL133W	0.0001258	0.0004913	113.77193	2.3666667

Low Hit	G4	YKL181W	0.0001466	0.0004892	165.69767	2.2574257
Low Hit	G5	YMR176W	8.586E-05	0.0004559	119.0625	2.2083333
Low Hit	G6	YLR182W	0.0001609	0.000445	95.167286	2.1775899
Low Hit	G7	YGL250W	7.783E-05	0.0004869	89.669421	2.2532189
Low Hit	G8	YFR014C	0.0001377	0.0004542	112.12121	2.039801
Low Hit	G9	YDR392W	0.0001004	0.0004058	114.375	2.0201005
Low Hit	G10	YGR074W	4.178E-05	0.0006269	113.11377	2.1165312
Low Hit	G11	YFR002W	4.636E-05	0.000819	117.61658	2.1945946
Low Hit	G12	YFL038C	0.0001739	0.0003758	125.4902	2.0348028
Low Hit	H1	p5472	0.0001581	0.0004448	133.81579	2.5449102
Low Hit	H2	BY4741	1.438E-05	6.76E-07	152.20588	0.1098039
Low Hit	H3	DES7 top1Δ	0.0005264	0.001766	126.5625	2.2245763
Low Hit	H4	YOR076C	0.0001584	0.0003816	111.23596	2.2942207
Low Hit	H5	YHR079C	0.0001395	0.0005115	110.37433	2.2622108
Low Hit	H6	YMR216C	0.0001865	0.0003905	125.94059	2.2663551
Low Hit	H7	YOR266W	6.561E-05	0.0005081	115.46053	2.092219
Low Hit	H8	YMR242C	0.0001522	0.000415	98.828125	2.1966527
Low Hit	H9	YHR091C	0.0001172	0.0003854	114.61187	2.2352941
Low Hit	H10	YGL130W	0.0001008	0.0004003	93.590734	2.2052402
Low Hit	H11	YGL245W	0.0001565	0.0004089	103.69128	2.1292776
Low Hit	H12	YGR099W	0.0001536	0.0003282	129.89324	2.4193548

Appendix B.3 rDNA repeat copy number in a second yTs mutant collection (Ben-Aroya et al., 2008)

Plate Key

		Mean CN	SD
	controls	136.58	15.80377
	HIGH copy number	>	168.1878
	LOW copy number	<	104.9727

ddPCR QC key

<10,000 droplets

Too few negative droplets

<10copies/uL TUB1

ORF	Plate	Well		25S rDNA Copy number (37°C)		Systematic name	Standard name	Gene summary
		Row	Column	Prep 1	Prep 2			
YBL026W	1	B	1	108.3333	182.63636	YBL026W	LSM2	Like SM
YBR154C	1	C	1	58.91089	119.41176	YBR154C	RPB5	RNA Polymerase B
YDL147W	1	D	1	#VALUE!	157.91855	YDL147W	RPN5	Regulatory Particle Non-ATPase
YDL045C	1	E	1	73.213	168.87755	YDL045C	FAD1	FAD synthetase
YGL247W	1	F	1	81.3	144.62366	YGL247W	BRR6	Bad Response to Refrigeration
YKR025W	1	G	1	54.79381	185.36585	YKR025W	RPC37	RNA Polymerase C
YMR211W	1	A	2	71.92308	181.06796	YMR211W	DML1	Drosophila melanogaster Misato-Like protein
YAL025C	1	B	2	81.90476	122.97297	YAL025C	MAK16	MAintenance of Killer
YBR153W	1	C	2	69.78723	143.3121	YBR153W	RIB7	RIBoflavin biosynthesis
YDR472W	1	D	2	#VALUE!	140.16393	YDR472W	TRS31	TRapp Subunit
YDR235W	1	E	2	86.37584	156.47668	YDR235W	PRP42	Pre-mRNA Processing
YKL196C	1	F	2	81.52542	115.31532	YKL196C	YKT6	
YNL310C	1	G	2	89.39394	187.21739	YNL310C	ZIM17	ZInc finger Motif protein of 17 kDa
YMR049C	1	H	2	85.75758	184.32203	YMR049C	ERB1	Eukaryotic Ribosome Biogenesis
YOR004W	1	A	3	27.1831	156.58065	YOR004W	UTP23	U Three-associated Protein
YBL074C	1	B	3	72.40964	155.31915	YBL074C	AAR2	A1-Alpha2 Repression
YBR167C	1	C	3	94.03614	177.23214	YBR167C	POP7	Processing Of Precursor RNAs
YDR487C	1	D	3	70.3871	153.36634	YDR487C	RIB3	RIBoflavin biosynthesis
YDL209C	1	E	3	105.0943	218.88112	YDL209C	CWC2	Complexed With Cef1p
YKL195W	1	F	3	65.85492	218.60465	YKL195W	MIA40	Mitochondrial intermembrane space Import and A
YDL103C	1	G	3	75.63265	176.91589	YDL103C	QRI1	
YMR200W	1	H	3	71.70213	157.5641	YMR200W	ROT1	Reversal Of Tor2 lethality
YDR489W	1	A	4	79.95595	117.05882	YDR489W	SLD5	Synthetic Lethality with Dpb11-1
YHR040W	1	B	4	69.89362	124.55621	YHR040W	BCD1	Box C/D snoRNA accumulation
YBR152W	1	C	4	75.90909	148.72727	YBR152W	SPP381	Suppressor of PrP38-1
YER003C	1	D	4	58.19209	141.03704	YER003C	PMI40	PhosphoMannose Isomerase
YDR341C	1	E	4	48.77483	136.50794	YDR341C		
YGR029W	1	F	4	85.41667	151.68539	YGR029W	ERV1	Essential for Respiration and Viability
YHR058C	1	G	4	63.16832	175.15924	YHR058C	MED6	MEDiator complex
YHR101C	1	H	4	91.37466	142.22222	YHR101C	BIG1	Bad In Glucose
YMR298W	1	A	5	24.84375	167.19577	YMR298W	LIP1	Lag1p/Lac1p Interacting Protein
YBR256C	1	B	5	#VALUE!	214.86486	YBR256C	RIB5	RIBoflavin biosynthesis
YDR044W	1	C	5	98.38028	157.07317	YDR044W	HEM13	HEMe biosynthesis
YER023W	1	D	5	70.46512	217.35537	YER023W	PRO3	PROline requiring
YDR280W	1	E	5	50.77922	132.03883	YDR280W	RRP45	Ribosomal RNA Processing
YKL144C	1	F	5	53.379	109.42857	YKL144C	RPC25	RNA Polymerase C
YHR088W	1	G	5	103.5714	174.03846	YHR088W	RPF1	Ribosome Production Factor
YJL025W	1	H	5	97.62533	185.21127	YJL025W	RRN7	Regulation of RNA polymerase I
YHR197W	1	A	6	99.29577	228.76712	YHR197W	RIX1	RIbosome eXport
YBR253W	1	B	6	70.69853	192.13974	YBR253W	SRB6	Suppressor of RNA polymerase B
YDR016C	1	C	6	84.28571	186.6242	YDR016C	DAD1	Duo1 And Dam1 interacting
YER168C	1	D	6	44.16667	153.17073	YER168C	CCA1	tRNA CCA-pyrophosphorylase
YGL113W	1	E	6	37.84314	74.574468	YGL113W	SLD3	Synthetically Lethal with Dpb11-1
YKR068C	1	F	6	#VALUE!	93.72549	YKR068C	BET3	Blocked Early in Transport
YJR093C	1	G	6	79.18871	144.3787	YJR093C	FIP1	Factor Interacting with Poly(A) polymerase
YML092C	1	H	6	62.60274	183.52941	YML092C	PRE8	PRoteinase yscE
YBR079C	1	A	7	87.82609	152.9697	YBR079C	RPG1	
YCL052C	1	B	7	97.8	192.01681	YCL052C	PBN1	Protease B Non-derepressible
YDR045C	1	C	7	77.51634	164.10256	YDR045C	RPC11	RNA Polymerase C
YFL022C	1	D	7	68.47826	167.08333	YFL022C	FRS2	phenylalanyl (F)-tRNA Synthetase
YGL091C	1	E	7	84.13043	155.05618	YGL091C	NBP35	Nucleotide Binding Protein
YGR172C	1	F	7	90.20833	157.19512	YGR172C	YIP1	Ypt-Interacting Protein
YKL021C	1	G	7	74.4186	154.70852	YKL021C	MAK11	MAintenance of Killer
YML126C	1	H	7	#VALUE!	170.09524	YML126C	ERG13	ERGosterol biosynthesis

YBR070C	1	A	8	75.2	200	YBR070C	ALG14	Asparagine Linked Glycosylation
YBR142W	1	B	8	58	168.91892	YBR142W	MAK5	MAintenance of Killer
YDR064W	1	C	8	116.6412	259.2233	YDR064W	RPS13	Ribosomal Protein of the Small subunit
YGL011C	1	D	8	73.82114	158.06452	YGL011C	SCL1	Suppressor of Crl3 ts Lethality
YGR046W	1	E	8	57.93814	150.1626	YGR046W	TAM41	Translocator Assembly and Maintenance
YGR195W	1	F	8	89.56835	155.41985	YGR195W	SKI6	SuperKIller
YKR081C	1	G	8	102.6316	179.62963	YKR081C	RPF2	Ribosome Production Factor
YML077W	1	H	8	113.7157	217.12707	YML077W	BET5	Blocked Early in Transport
YBR049C	1	A	9	68.66142	122.87234	YBR049C	REB1	RNA polymerase I Enhancer Binding protein
YBR234C	1	B	9	#VALUE!	138.36957	YBR234C	ARC40	ARp2/3 Complex subunit
YDR086C	1	C	9	118.3051	196.42857	YDR086C	SSS1	Sec Sixty-one Suppressor
YGR128C	1	D	9	78.18533	148.69888	YGR128C	UTP8	U Three Protein
YEL026W	1	E	9	77.3913	149.72067	YEL026W	SNU13	Small NUclear ribonucleoprotein associated
YHR019C	1	F	9	46.76471	99.329268	YHR019C	DED81	Defines Essential Domain
YJL035C	1	G	9	77.70701	150.12821	YJL035C	TAD2	tRNA-specific Adenosine Deaminase
YLR005W	1	H	9	36.06667	170.15504	YLR005W	SSL1	Suppressor of Stem-Loop mutation
YBR011C	1	A	10	#VALUE!	162.96296	YBR011C	IPP1	Inorganic PyroPhosphatase
YAL043C	1	B	10	68.78307	135.57312	YAL043C	PTA1	Pre-Trna Accumulation
YDL015C	1	C	10	110.473	199.2	YDL015C	TSC13	Temperature-sensitive Suppressors of Csg2 mutar
YGR119C	1	D	10	47.54386	190.61728	YGR119C	NUP57	NUclear Pore
YGR013W	1	E	10	60.3	137.18821	YGR013W	SNU71	Small NUclear ribonucleoprotein associated
YDR091C	1	F	10	60.5	135.69231	YDR091C	RLI1	RNase L Inhibitor
YHR190W	1	G	10	75.30612	176.42586	YHR190W	ERG9	ERGosterol biosynthesis
YIR011C	1	H	10	86.82353	155.66802	YIR011C	STS1	Sec Twenty-three Suppressor 1
YBR029C	1	A	11	36.14583	144.33498	YBR029C	CDS1	CDP-Diacylglycerol Synthase
YBR121C	1	B	11	58.21429	144.42308	YBR121C	GRS1	Glycyl-tRNA Synthase
YDL098C	1	C	11	81	148.80952	YDL098C	SNU23	Small NUclear ribonucleoprotein associated
YER009W	1	D	11	55.27778	141.74757	YER009W	NTF2	Nuclear Transport Factor
YDR118W	1	E	11	108.1188	128.84615	YDR118W	APC4	Anaphase Promoting Complex
YDL111C	1	F	11	52.85714	161.50442	YDL111C	RRP42	Ribosomal RNA Processing
YIL104C	1	G	11	49.49367	119.48882	YIL104C	SHQ1	Small nucleolar RNAs of the box H/ACA family Qua
YMR061W	1	H	11	129.0735	96.206897	YMR061W	RNA14	poly(A) mRNA metabolism
YBL041W	1	A	12	52.05479	172.43402	YBL041W	PRE7	PRoteinase yscE
YBL040C	1	B	12	47.84615	169.81132	YBL040C	ERD2	Endoplasmic reticulum Retention Defective
YDL105W	1	C	12	115.9281	155.68627	YDL105W	NSE4	Non-SMC Element
YER012W	1	D	12	51.53846	170.29703	YER012W	PRE1	PRoteinase yscE
YDR201W	1	E	12	92.02479	151.6129	YDR201W	SPC19	Spindle Pole Component
YGR278W	1	F	12	131.3953	160.62176	YGR278W	CWC22	Complexed With Cef1p
YLL011W	1	G	12	69.55882	99.435028	YLL011W	SOF1	Suppressor Of Fibrillarin
YGL142C	2	A	1	#VALUE!	133.19444	YGL142C	GPI10	GlycosylPhosphatidylInositol anchor biosynthesis
YLR145W	2	B	1	70.28302	82.95082	YLR145W	RMP1	RNase MRP Protein
YDL097C	2	C	1	104.1121	97.25	YDL097C	RPN6	Regulatory Particle Non-ATPase
YOR056C	2	D	1	96.30872	177.35849	YOR056C	NOB1	Nin1 (One) Binding protein
YJR002W	2	E	1	97.5	160.28571	YJR002W	MPP10	M Phase Phosphoproteins
YLR002C	2	F	1	105.5303	144.10774	YLR002C	NOC3	NucleOlar Complex associated
YBR254C	2	G	1	121.3889	176.21212	YBR254C	TRS20	TRapp Subunit
YLR147C	2	B	2	85.0625	122.93578	YLR147C	SMD3	
YGR253C	2	C	2	83.60882	146.91358	YGR253C	PUP2	PUtative Proteasome subunit
YKL035W	2	D	2	105.9211	190.55556	YKL035W	UGP1	UDP-glucose pyrophosphorylase
YHR070W	2	E	2	81.85185	186.89655	YHR070W	TRM5	tRNA Methyltransferase
YNR038W	2	F	2	100.7958	202.85714	YNR038W	DBP6	Dead Box Protein
YBR257W	2	G	2	106.044	86.623377	YBR257W	POP4	Processing Of Precursor RNAs
YLL008W	2	H	2	111.3793	160.91954	YLL008W	DRS1	Deficiency of Ribosomal Subunits
YMR043W	2	A	3	104.9875	120.66667	YMR043W	MCM1	MiniChromosome Maintenance
YLR175W	2	B	3	115.1376	160.38647	YLR175W	CBF5	Centromere Binding Factor
YCR072C	2	C	3	149.4624	278.68852	YCR072C	RSA4	RiboSome Assembly
YMR149W	2	D	3	104.7143	151.36364	YMR149W	SWP1	Suppressor of a WbP1 mutation
YMR208W	2	E	3	116.1644	160.9589	YMR208W	ERG12	ERGosterol biosynthesis
YOL021C	2	F	3	123.9362	145.92857	YOL021C	DIS3	homolog of S. pombe dis3 (chromosome DISjunct
YDL208W	2	G	3	79.72222	145.76923	YDL208W	NHP2	Non-Histone Protein
YOR194C	2	H	3	103.2634	161.72131	YOR194C	TOA1	
YHR196W	2	A	4	111.1864	86.646341	YHR196W	UTP9	U Three Protein
YLR197W	2	B	4	96.82353	101.32075	YLR197W	NOP56	NucleOlar Protein of 56.8 kDa
YLR276C	2	C	4	96.84211	86.99115	YLR276C	DBP9	Dead Box Protein
YNL232W	2	D	4	104.7872	111.63462	YNL232W	CSL4	Cep1 Synthetic Lethal
YMR260C	2	E	4	82.14286	135	YMR260C	TIF11	Translation Initiation Factor

YHR188C	2	F	4	90.09524	120.67797	YHR188C	GPI16	GlycosylPhosphatidylInositol anchor biosynthesis
YDR302W	2	G	4	107.5676	93.653846	YDR302W	GPI11	GlycosylPhosphatidylInositol anchor biosynthesis
YOR206W	2	H	4	113.5802	148.94366	YOR206W	NOC2	NucleOlar Complex associated
YFL002C	2	A	5	#VALUE!	108.43972	YFL002C	SPB4	Suppressor of PAB1
YLR186W	2	B	5	119.1176	150.54545	YLR186W	EMG1	Essential for Mitotic Growth
YLR291C	2	C	5	77.07424	112.9771	YLR291C	GCD7	General Control Derepressed
YNL244C	2	D	5	65.60748	115.29851	YNL244C	SUI1	SUppressor of Initiator codon
YMR288W	2	E	5	104.4	124.53704	YMR288W	HSH155	Human Sap Homolog
YLL035W	2	F	5	76.25899	136.90141	YLL035W	GRC3	
YDR434W	2	G	5	103.4211	154.06897	YDR434W	GPI17	GlycosylPhosphatidylInositol anchor biosynthesis
YOR250C	2	H	5	147.3684	185.02994	YOR250C	CLP1	CLeavage/Polyadenylation factor Ia subunit
YLR007W	2	A	6	140.5556	160.85106	YLR007W	NSE1	Non-SMC Element
YLR196W	2	B	6	103.1169	161.67883	YLR196W	PWP1	Periodic tryptophan (W) Protein
YLR316C	2	C	6	91.57566	149.24623	YLR316C	TAD3	tRNA-specific Adenosine Deaminase
YNL007C	2	D	6	141.9075	260.78431	YNL007C	SIS1	SIt4 Suppressor
YNL002C	2	E	6	105.8824	169.02655	YNL002C	RLP7	Ribosomal-Like Protein
YNR017W	2	F	6	88.02993	148.97959	YNR017W	TIM23	Translocase of the Inner Mitochondrial membrane
YDR437W	2	G	6	112.5397	122.82609	YDR437W	GPI19	Glycosyl PhosphatidylInositol anchor biosynthesis
YNL126W	2	H	6	52.06186	134.57627	YNL126W	SPC98	Spindle Pole Component
YHR118C	2	A	7	87.5	75.878378	YHR118C	ORC6	Origin Recognition Complex
YLR115W	2	B	7	107.6647	141.96429	YLR115W	CFT2	Cleavage Factor Two
YLR317W	2	C	7	116.0606	181.68317	YLR317W		
YNL131W	2	D	7	96.04743	124.18478	YNL131W	TOM22	Translocase of the Outer Mitochondrial membran
YML127W	2	E	7	83.18408	151.37615	YML127W	RSC9	Remodel the Structure of Chromatin
YNL282W	2	F	7	110.9551	217.72727	YNL282W	POP3	Processing Of Precursor RNAs
YNL312W	2	G	7	103.662	145.34884	YNL312W	RFA2	Replication Factor A
YOR160W	2	H	7	115.8696	166.51515	YOR160W	MTR10	Mrna TRansport defective
YHR036W	2	A	8	152.9167	185.75851	YHR036W	BRL1	BRr6 Like protein
YLR116W	2	B	8	115.9649	143.63636	YLR116W	MSL5	Mud Synthetic-Lethal
YLR340W	2	C	8	90.84507	135.08287	YLR340W	RPP0	Ribosomal Protein P0
YMR314W	2	D	8	79.8995	126.11276	YMR314W	PRE5	PRoteinase yscE
YMR218C	2	E	8	88.95105	203.26923	YMR218C	TRS130	TRapp Subunit
YML065W	2	F	8	59.6875	104.33498	YML065W	ORC1	Origin Recognition Complex
YOL066C	2	G	8	98.94737	146.80851	YOL066C	RIB2	RIBoflavin biosynthesis
YPR133C	2	H	8	134.5283	133.33333	YPR133C	SPN1	Suppresses Postrecruitment functions gene Numb
YGR005C	2	A	9	108	150.85714	YGR005C	TFG2	Transcription Factor G
YLR129W	2	B	9	211.626	404.7619	YLR129W	DIP2	DOM34 Interacting Protein
YLR424W	2	C	9	242.5333	310.60606	YLR424W	SPP382	Suppressor of PrP38 #2
YNR043W	2	D	9	109.0984	187.36111	YNR043W	MVD1	MeValonate pyrophosphate Decarboxylase
YMR290C	2	E	9	141.5385	177.3399	YMR290C	HAS1	Helicase Associated with Set1
YOL077C	2	F	9	#VALUE!	158.08581	YOL077C	BRX1	Xenopus laevis Brix (Biogenesis of Ribosomes in Xe
YNL189W	2	G	9	110.8	142.96578	YNL189W	SRP1	Suppressor of Rna Polymerase I
YPR144C	2	H	9	229.4521	197.5	YPR144C	NOC4	NucleOlar Complex associated
YER094C	2	A	10	133.0097	209.01639	YER094C	PUP3	PUtative Proteasome subunit
YLR033W	2	B	10	57.84211	80.666667	YLR033W	RSC58	Remodel the Structure of Chromatin
YOL038W	2	C	10	82.18182	108.41026	YOL038W	PRE6	PRoteinase yscE
YNL038W	2	D	10	109.3939	128.15029	YNL038W	GPI15	GlycosylPhosphatidylInositol anchor biosynthesis
YMR281W	2	E	10	132.037	129.58621	YMR281W	GPI12	GlycosylPhosphatidylInositol anchor biosynthesis
YOR063W	2	F	10	105.6738	151.85185	YOR063W	RPL3	Ribosomal Protein of the Large subunit
YDR454C	2	G	10	83.33333	147.84483	YDR454C	GUK1	GUanylate Kinase
YPR161C	2	H	10	127.191	173.04	YPR161C	SGV1	Suppressor of Gpa1-Val50 mutation
YFR050C	2	A	11	86.06218	171.22642	YFR050C	PRE4	PRoteinase yscE
YLR141W	2	B	11	107.9532	117.87402	YLR141W	RRN5	Regulation of RNA polymerase I
YOL069W	2	C	11	98.54167	148.45815	YOL069W	NUF2	NUclear Filament-containing protein
YOR103C	2	D	11	71.51515	172.36181	YOR103C	OST2	OligoSaccharylTransferase
YOL146W	2	E	11	38.97196	67.132867	YOL146W	PSF3	Partner of Sld Five
YLR100W	2	F	11	122.3214	230.87719	YLR100W	ERG27	ERGosterol biosynthesis
YDR478W	2	G	11	94.53488	117.35537	YDR478W	SNM1	Suppressor of Nuclear Mitochondrial endoribonu
YMR146C	2	H	11	94.26087	103.65517	YMR146C	TIF34	Translation Initiation Factor
YKR063C	2	A	12	90	125.18293	YKR063C	LAS1	Lethal in the Absence of SSD1-v
YIL022W	2	B	12	123.25	144.01575	YIL022W	TIM44	Translocase of the Inner Mitochondrial membrane
YOL144W	2	C	12	131.3636	151.15108	YOL144W	NOP8	NucleOlar Protein
YKL012W	2	D	12	152.9412	121.875	YKL012W	PRP40	Pre-mRNA Processing
YJR006W	2	E	12	102.8571	84.761905	YJR006W	POL31	POLymerase
YOR143C	2	F	12	104.5455	140.68627	YOR143C	THI80	THIamine metabolism
YLR275W	2	G	12	125.3571	139.42308	YLR275W	SMD2	

YDR339C	3	A	1	101.4577	117.36111	YDR339C	FCF1	Faf1p Copurifying Factor
YPL204W	3	B	1	22.98701	127.34584	YPL204W	HRR25	HO and Radiation Repair
YJL069C	3	C	1	130.6034	171.31783	YJL069C	UTP18	U Three Protein
YNL260C	3	D	1	40.74074	156.77966	YNL260C	LTO1	required for biogenesis of the Large ribosomal sub
YCR054C	3	E	1	106.25	242.4	YCR054C	CTR86	Copper TRansport protein
YDR531W	3	F	1	31.40411	152.26131	YDR531W	CAB1	Coenzyme A Biosynthesis
YDL148C	3	G	1	82.17593	93.162393	YDL148C	NOP14	NucleOlar Protein
YPL063W	3	A	2	55.49505	152.70936	YPL063W	TIM50	Translocase of the Inner Mitochondrial membrane
YGL047W	3	B	2	48.04348	127.50929	YGL047W	ALG13	Asparagine-Linked Glycosylation
YKL033W	3	C	2	55.77778	161.49425	YKL033W	TTI1	Two Tel2-Interacting protein
YIL083C	3	D	2	#VALUE!	117.11712	YIL083C	CAB2	Coenzyme A Biosynthesis
YDR299W	3	E	2	55.97403	159.85915	YDR299W	BFR2	BreFeldin A Resistance
YLR060W	3	F	2	73.16667	173.89937	YLR060W	FRS1	phenylalanyl (F)-tRNA Synthetase
YDR240C	3	G	2	71.89573	86.180556	YDR240C	SNU56	Small NUclear ribonucleoprotein associated
YDL141W	3	H	2	#VALUE!	128.48485	YDL141W	BPL1	Biotin:apoProtein Ligase
YOR168W	3	B	3	94.22222	160.11561	YOR168W	GLN4	GLutamiNe metabolism
YKL088W	3	C	3	#VALUE!	153.2646	YKL088W	CAB3	Coenzyme A Biosynthesis
YNL181W	3	D	3	118.0124	140.9375	YNL181W	PBR1	Potentiates Bioactive compound Response
YDR288W	3	E	3	80.67164	158.68852	YDR288W	NSE3	Non SMC Element
YJL072C	3	F	3	45.67308	76.582278	YJL072C	PSF2	Partner of Sld Five
YDR416W	3	G	3	82.53846	88.084112	YDR416W	SYF1	SYnthetic lethal with cdcForty
YDR398W	3	H	3	36.46617	178.51563	YDR398W	UTP5	U Three Protein
YNL158W	3	A	4	#VALUE!	106.81481	YNL158W	PGA1	Processing of Gas1p and ALP
YPL128C	3	B	4	107.7739	77.580645	YPL128C	TBF1	TTAGGG repeat-Binding Factor
YDR367W	3	C	4	100.9852	147.9845	YDR367W	KEI1	Kex2-cleavable protein Essential for Inositol phosp
YNL313C	3	D	4	80.71217	118.75	YNL313C	EMW1	Essential for Maintenance of the cell Wall
YDR246W	3	E	4	91.45985	129.93056	YDR246W	TRS23	TRapp Subunit
YFL009W	3	F	4	61.04762	146.15385	YFL009W	CDC4	Cell Division Cycle
YGL238W	3	G	4	96.01626	151.28049	YGL238W	CSE1	Chromosome SEgregation
YBR004C	3	H	4	87.29097	111.11111	YBR004C	GPI18	GlycosylPhosphatidylInositol
YCR052W	3	A	5	97.21739	125.51471	YCR052W	RSC6	Remodel the Structure of Chromatin
YOR260W	3	B	5	62.89474	117.59563	YOR260W	GCD1	General Control Derepressed
YLR022C	3	C	5	71.05263	132.05374	YLR022C	SDO1	
YOL022C	3	D	5	67.7451	152.06897	YOL022C	TSR4	Twenty S rRNA accumulation
YDR267C	3	E	5	66.69604	114.61165	YDR267C	CIA1	Cytosolic Iron-sulfur protein Assembly
YBR088C	3	F	5	90.19608	161.40351	YBR088C	POL30	POLymerase
YPR082C	3	G	5	89.57816	145.21277	YPR082C	DIB1	S. pombe DIm1+ in Budding yeast
YFL017C	3	H	5	87.66234	151.16279	YFL017C	GNA1	GlucosamiNe-6-phosphate Acetyltransferase
YKL078W	3	A	6	87.31343	132.96089	YKL078W	DHR2	DEAH-box RNA helicase
YOR310C	3	B	6	77.16814	104.81928	YOR310C	NOP58	NucleOlar Protein of 58 kDa
YJL097W	3	C	6	162.9969	252.97619	YJL097W	PHS1	PTPLA Homolog involved in Sphingolipid biosynth
YGR145W	3	D	6	103.0211	#VALUE!	YGR145W	ENP2	Essential Nuclear Protein
YGL111W	3	E	6	75.94142	94.321767	YGL111W	NSA1	Nop Seven Associated
YDL003W	3	F	6	58.60113	90.48583	YDL003W	MCD1	Mitotic Chromosome Determinant
YPR190C	3	G	6	67.44731	97.700535	YPR190C	RPC82	RNA Polymerase C
YDR236C	3	H	6	44.79412	156.917	YDR236C	FMN1	FMN biosynthesis
YNL182C	3	A	7	48	162.22826	YNL182C	IPI3	Involved in Processing ITS2
YPL007C	3	B	7	62.76596	195.32164	YPL007C	TFC8	Transcription Factor C
YHR122W	3	C	7	50.39604	102.91262	YHR122W	CIA2	Cytosolic Iron-sulfur protein Assembly
YLR440C	3	D	7	43.125	114.59854	YLR440C	SEC39	SECretory
YOR060C	3	E	7	33.63636	56.893204	YOR060C	SLD7	Synthetic Lethality with Dpb11-24
YDR331W	3	F	7	32.68156	84.565217	YDR331W	GPI8	GlycosylPhosphatidylInositol anchor biosynthesis
YCR057C	3	G	7	96.26308	79.238095	YCR057C	PWP2	Periodic tryptophan (W) Protein
YMR093W	3	H	7	65.38251	122.8972	YMR093W	UTP15	U Three Protein
YGL245W	3	A	8	25.69038	146.09053	YGL245W	GUS1	GlUtamyl-tRNA Synthetase
YPL235W	3	B	8	34.21569	65.684932	YPL235W	RVB2	RuVB-like
YKR071C	3	C	8	96.23188	136.19403	YKR071C	DRE2	Derepressed for Ribosomal protein S14 Expression
YML023C	3	D	8	90.44776	155.95855	YML023C	NSE5	Non-SMC Element 5
YJL010C	3	E	8	30.06211	105.55556	YJL010C	NOP9	NucleOlar Protein
YKR022C	3	F	8	43.31288	108.43373	YKR022C	NTR2	NineTeen complex Related protein
YDR081C	3	G	8	94.84536	139.7191	YDR081C	PDC2	Pyruvate DeCarboxylase
YPR180W	3	H	8	46.34146	121.39738	YPR180W	AOS1	Activation Of Smt3p
YLR277C	3	A	9	75.03788	134.78261	YLR277C	YSH1	Yeast Seventy-three Homolog
YPR019W	3	B	9	57.97872	102.12766	YPR019W	MCM4	MiniChromosome Maintenance
YLR132C	3	C	9	110.4094	151.35952	YLR132C	USB1	U Six Biogenesis
YOR262W	3	D	9	53.35766	163.84977	YOR262W	GPN2	Gly-Pro-Asn (N) motif

YHR020W	3	E	9	56.7619	115.27094	YHR020W		
YDR180w	3	F	9	34.64481	133.22034	YDR180W	SCC2	Sister Chromatid Cohesion
YGL008C	3	G	9	65.97701	270.56277	YGL008C	PMA1	Plasma Membrane ATPase
YPR162C	3	H	9	#VALUE!	131.09244	YPR162C	ORC4	Origin Recognition Complex
YOR224C	3	A	10	24.63366	157.33788	YOR224C	RPB8	RNA Polymerase B
YDR196C	3	B	10	5	9.3814433	YDR196C	CAB5	
YMR134W	3	C	10	62.72727	103.05825	YMR134W	ERG29	ERGosterol biosynthesis
YDR527W	3	D	10	64.15869	125.79618	YDR527W	RBA50	RNA polymerase II (B) Associated protein
YKL095W	3	E	10	60.84906	113.82514	YKL095W	YJU2	
YPR085C	3	F	10	118.8912	180.88235	YPR085C	ASA1	AStra Associated protein
YGL201C	3	G	10	60.96552	65.375723	YGL201C	MCM6	MiniChromosome Maintenance
YPR035W	3	H	10	67.71879	164.10256	YPR035W	GLN1	GLutamiNe metabolism
YPL131W	3	A	11	36.06509	139.37198	YPL131W	RPL5	Ribosomal Protein of the Large subunit
YFR042W	3	B	11	25.57895	133.33333	YFR042W	KEG1	Kre6-binding ER protein responsible for Glucan sy
YML125C	3	C	11	33.391	102.61438	YML125C	PGA3	Processing of Gas1p and ALP
YNL152W	3	D	11	112.8266	141.66667	YNL152W	INN1	required for INgressioN
YDL193W	3	E	11	93.09463	166.92308	YDL193W	NUS1	Nuclear Undecaprenyl pyrophosphate Synthase
YPR088C	3	F	11	#VALUE!	133.68421	YPR088C	SRP54	Signal Recognition Particle 54-kD subunit
YGR047C	3	G	11	25.66038	127.30627	YGR047C	TFC4	Transcription Factor class C
YJR141W	3	H	11	122.8769	170	YJR141W	IPA1	Important for cleavage and PolyAdenylation
YPL151C	3	A	12	72.69327	81.717172	YPL151C	PRP46	Pre-mRNA Processing
YGR277C	3	B	12	105.32	119.80676	YGR277C	CAB4	Coenzyme A Biosynthesis
YNL247W	3	C	12	97.71987	146.91943	YNL247W		
YHR085W	3	D	12	114.3603	#VALUE!	YHR085W	IPI1	Involved in Processing ITS2
YJR072C	3	E	12	22.69136	141.25874	YJR072C	NPA3	Nucleolar Preribosomal Associated
YDL132W	3	F	12	49.24623	110.41009	YDL132W	CDC53	Cell Division Cycle
YGR094W	3	G	12	29.95157	117.80822	YGR094W	VAS1	VAlyl-tRNA Synthetase
BY4741	Controls plate. 8 colonies of BY4741.				171.65992			
BY4741					122.58065			
BY4741					127.11268			
BY4741					137.72455			
BY4741					142.68775			
BY4741					129.6319			
BY4741					117.89474			
BY4741					143.34975			